NEUROTECHNOLOGIES FOR HUMAN AUGMENTATION

EDITED BY: Davide Valeriani, Hasan Ayaz, Pattie Maes, Riccardo Poli and Nataliya Kosmyna

PUBLISHED IN: Frontiers in Neuroscience

frontiers Research Topics

frontiers

ISSN 1664-8714
ISBN 978-2-88971-973-0
DOI 10.3389/978-2-88971-973-0

About Frontiers

Frontiers is more than just an open-access publisher of scholarly articles: it is a pioneering approach to the world of academia, radically improving the way scholarly research is managed. The grand vision of Frontiers is a world where all people have an equal opportunity to seek, share and generate knowledge. Frontiers provides immediate and permanent online open access to all its publications, but this alone is not enough to realize our grand goals.

Frontiers Journal Series

The Frontiers Journal Series is a multi-tier and interdisciplinary set of open-access, online journals, promising a paradigm shift from the current review, selection and dissemination processes in academic publishing. All Frontiers journals are driven by researchers for researchers; therefore, they constitute a service to the scholarly community. At the same time, the Frontiers Journal Series operates on a revolutionary invention, the tiered publishing system, initially addressing specific communities of scholars, and gradually climbing up to broader public understanding, thus serving the interests of the lay society, too.

Dedication to Quality

Each Frontiers article is a landmark of the highest quality, thanks to genuinely collaborative interactions between authors and review editors, who include some of the world's best academicians. Research must be certified by peers before entering a stream of knowledge that may eventually reach the public - and shape society; therefore, Frontiers only applies the most rigorous and unbiased reviews.
Frontiers revolutionizes research publishing by freely delivering the most outstanding research, evaluated with no bias from both the academic and social point of view. By applying the most advanced information technologies, Frontiers is catapulting scholarly publishing into a new generation.

What are Frontiers Research Topics?

Frontiers Research Topics are very popular trademarks of the Frontiers Journals Series: they are collections of at least ten articles, all centered on a particular subject. With their unique mix of varied contributions from Original Research to Review Articles, Frontiers Research Topics unify the most influential researchers, the latest key findings and historical advances in a hot research area! Find out more on how to host your own Frontiers Research Topic or contribute to one as an author by contacting the Frontiers Editorial Office: frontiersin.org/about/contact

NEUROTECHNOLOGIES FOR HUMAN AUGMENTATION

Topic Editors:
Davide Valeriani, Neurable Inc., United States
Hasan Ayaz, Drexel University, United States
Pattie Maes, Massachusetts Institute of Technology, United States
Riccardo Poli, University of Essex, United Kingdom
Nataliya Kosmyna, Media Lab, Massachusetts Institute of Technology, United States

Citation: Valeriani, D., Ayaz, H., Maes, P., Poli, R., Kosmyna, N., eds. (2021). Neurotechnologies for Human Augmentation. Lausanne: Frontiers Media SA. doi: 10.3389/978-2-88971-973-0

Table of Contents

frontiers in Neuroscience

EDITORIAL
published: 11 November 2021
doi: 10.3389/fnins.2021.789868

Editorial: Neurotechnologies for Human Augmentation

Davide Valeriani[1], Hasan Ayaz[2], Nataliya Kosmyna[3], Riccardo Poli[4] and Pattie Maes[3]*

[1] Neurable Inc., Boston, MA, United States, [2] School of Biomedical Engineering, Science and Health Systems, Drexel University, Philadelphia, PA, United States, [3] Media Lab, Massachusetts Institute of Technology, Cambridge, MA, United States, [4] School of Computer Science and Electronic Engineering, University of Essex, Colchester, United Kingdom

Keywords: brain-computer interface, neuroergonomics, human augmentation, neural decoding, brain stimulation, neurotechnology

Editorial on the Research Topic

Neurotechnologies for Human Augmentation

Neurotechnologies combine neuroscience and engineering to create tools for studying, repairing, and enhancing brain function. Traditionally, researchers have used neurotechnologies, such as Brain-Computer Interfaces (BCIs), as assistive devices, for example to allow locked-in patients to communicate. In the last few decades, non-invasive brain imaging devices, such as electroencephalography (EEG) and functional near-infrared spectroscopy (fNIRS), have become more portable and inexpensive, paving the way to innovative applications of neurotechnologies (Ayaz and Dehais, 2018). Recent trends in neuroergonomics and neural engineering have used neurotechnologies to enhance various human capabilities, including (but not limited to) communication, emotion, perception, memory, attention, engagement, situation awareness, problem-solving, and decision making (Cinel et al., 2019; Kosmyna and Maes, 2019).

This Research Topic provides a collection of 12 contributions on recent advances in the development of non-invasive BCIs for human augmentation, with a particular emphasis on brain stimulation and neural decoding.

To introduce the topic of human augmentation, Dehais and colleagues propose a two-dimensional framework that incorporates arousal and task engagement to characterize different variables typically used in human augmentation, such as mental workload and human performance (Dehais et al., 2020). Specifically, poor task engagement leads to mind wandering or effort withdrawal depending on arousal level, while a too high arousal could lead to perseveration or in attentional blindness and deafness. Neurotechnologies could, therefore, be used to guide the brain to an optimal position in the arousal-engagement space to maximize performance, a position characterized by medium levels of arousal and high task engagement, which could be achieved, for example, by using brain stimulation or neurofeedback.

A few studies in this Research Topic investigated the use of non-invasive brain stimulation to augment human performance: a very popular topic in the area of neurotechnologies (Kadosh, 2014; Santarnecchi et al., 2015). Pilly and colleagues propose a novel paradigm based on virtual reality to use transcranial electrical stimulation (tES) to extend long-term metamemory (Pilly et al.). By applying periodic brief pulses while participants were asleep, they improved memory recall of one-shot viewing of naturalistic episodes over 48 h by 10–20%. Patel and colleagues performed a systematic meta-analysis to review the use of transcranial direct-current stimulation (tDCS) for improving motor performance in upper limbs (Patel et al.). Brain stimulation significantly reduces reaction time, task execution time, and increases force and accuracy in elbow flexion tasks. Wang and colleagues reported that combining brain stimulation with physical training increases motor-evoked potential (MEP) amplitude and muscle strength, and decreases the dynamic posture

Edited and reviewed by:
Michele Giugliano, International School for Advanced Studies (SISSA), Italy

****Correspondence:***
Davide Valeriani
davide.valeriani@gmail.com

Specialty section:
This article was submitted to Neural Technology, a section of the journal Frontiers in Neuroscience

Received: *05 October 2021*
Accepted: *18 October 2021*
Published: *11 November 2021*

Citation:
Valeriani D, Ayaz H, Kosmyna N, Poli R and Maes P (2021) Editorial: Neurotechnologies for Human Augmentation. Front. Neurosci. 15:789868. doi: 10.3389/fnins.2021.789868

stability index, reaction time, and error rate in motor learning tasks (Wang et al.). Similarly, Hollis and colleagues explored the use of transcranial static magnetic field stimulation (tSMS) to facilitate motor learning in healthy children. They found that tSMS did not increase MEP amplitude in children (as found by Wang and colleagues in adults), suggesting that age is a critical factor for the effectiveness of brain stimulation. Yet, they found tSMS inhibited early motor learning and facilitated later stage motor learning in the non-dominant hand, which motivated future investigations of tSMS as a potential non-invasive therapy for children with cerebral palsy (Hollis et al.).

Another set of studies focused on using non-invasive neuroimaging to decode specific mental states, which could provide further insights into brain activity. Asgher and colleagues used fNIRS and deep learning to estimate four different levels of mental workload in human participants (Asgher et al.). While traditional machine learning algorithms reached accuracies below 70%, convolutional neural networks with long short-term memory layers achieved significantly better performance of almost 90% accuracy across the four classes. These results exemplify the potential of deep learning in neural decoding for human augmentation. In another contribution, Klaproth and colleagues used passive BCIs to track perception and auditory processing of pilots during operations (Klaproth et al.). In particular, they found that a passive BCI could use EEG to distinguish between task-relevant and irrelevant alerts received by the pilot, hence improving situation awareness. This work demonstrates how passive BCIs could work as monitoring devices in a practical scenario without disrupting the main task.

Another neural decoding problem with direct applications in BCI research is mental imagery. Wairagkar and colleagues showed that temporal patterns extracted from EEG activity are sufficient to achieve single-trial classification of five different mental imagery tasks (Wairagkar et al.). These patterns can, therefore, be used as control signals of non-invasive BCIs, which could translate them into commands for external devices. Also in the area of neural decoding, Li and colleagues have shown the possibility of using advanced machine learning and signal processing techniques to decode emotions from EEG signals (Li et al.). In this domain, other work has tackled this challenge using more invasive recordings (Sani et al., 2018). Yet, to enable broadly-applicable human augmentation, similar results have to be achieved with non-invasive devices, such as the EEG used by Li and colleagues, which pose fewer ethical and socio-economic barriers than invasive devices.

Another study tackles the exciting area of speech decoding, which aims at translating brain activity into meaningful speech. This problem has been extensively tackled using invasive recordings, such as electrocorticography (Herff et al., 2015; Herff and Schultz, 2016; Angrick et al., 2019; Anumanchipalli et al., 2019). Here, Dash and colleagues demonstrated that this is possible even with non-invasive and, therefore, more practical neural recording devices, such as MEG (Dash et al.).

The transition to non-invasive, real-world BCIs for human augmentation would require strategies to enhance the limited signal quality recorded from the brain. As such, multimodal BCIs depending on a combination of physiological signals will be increasingly important. In that domain, Stuldreher and colleagues determined the synchrony between EEG, heart rate, and electrodermal activity while participants were engaged in an auditory task (Stuldreher et al.). They found that each modality works well in certain scenarios, and that merging all modalities into a unique metric seems most robust across a broad range of applications.

Finally, the development of new non-invasive neurotechnologies presents many opportunities for clinical and field applications as well as multifaceted new challenges (Dehais et al., 2020). In a review paper of this Research Topic, Gaudry and colleagues delve into the neuroethical issues that we might face in the upcoming decades as neurotechnologies transition from research to practice, and even home and office settings (Gaudry et al.).

We hope this Research Topic provides the reader with updates on recent advances in the area of non-invasive neurotechnologies for human augmentation. We would like to thank all authors who contributed, the reviewers who provided invaluable and timely feedback to the authors, and Dr. Eleonora Adami for designing the cover picture of this Research Topic.

AUTHOR CONTRIBUTIONS

DV wrote the first draft of the manuscript. All authors contributed to manuscript revision, read, and approved the submitted version.

ACKNOWLEDGMENTS

The authors would like to thank Dr. Eleonora Adami for creating the cover image of the Research Topic.

REFERENCES

Angrick, M., Herff, C., Mugler, E., Tate, M. C., Slutzky, M. W., Krusienski, D. J., et al. (2019). Speech synthesis from ECoG using densely connected 3D convolutional neural networks. *J. Neural Eng.* 16:036019. doi: 10.1088/1741-2552/ab0c59

Anumanchipalli, G. K., Chartier, J., and Chang, E. F. (2019). Speech synthesis from neural decoding of spoken sentences. *Nature* 568, 493–498. doi: 10.1038/s41586-019-1119-1

Ayaz, H., and Dehais, F. (2018). *Neuroergonomics: The Brain at Work and in Everyday Life*. Academic Press. London, UK.

Cinel, C., Valeriani, D., and Poli, R. (2019). Neurotechnologies for human cognitive augmentation: current state of the art and future prospects. *Front. Human Neurosci.* 13:13. doi: 10.3389/fnhum.2019.00013

Dehais, F., Karwowski, W., and Ayaz, H. (2020). Brain at work and in everyday life as the next frontier: grand field challenges for neuroergonomics. *Front. Neuroergonom.* 1:583733. doi: 10.3389/fnrgo.2020.583733

Herff, C., Heger, D., de Pesters, A., Telaar, D., Brunner, P., Schalk, G., et al. (2015). Brain-to-text: decoding spoken phrases from phone representations in the brain. *Front. Neurosci.* 9:217. doi: 10.3389/fnins.2015.00217

Herff, C., and Schultz, T. (2016). Automatic speech recognition from neural signals: a focused review. *Front. Neurosci.* 10:429. doi: 10.3389/fnins.2016.00429

Kadosh, R. C. (2014). *The Stimulated Brain: Cognitive Enhancement Using Non-Invasive Brain Stimulation.* Elsevier. London, UK.

Kosmyna, N., and Maes, P. (2019). AttentivU: an EEG-based closed-loop biofeedback system for real-time monitoring and improvement of engagement for personalized learning. *Sensors* 19:5200. doi: 10.3390/s19235200

Sani, O. G., Yang, Y., Lee, M. B., Dawes, H. E., Chang, E. F., and Shanechi, M. M. (2018). Mood variations decoded from multi-site intracranial human brain activity. *Nat. Biotechnol.* 36, 954–961. doi: 10.1038/nbt.4200

Santarnecchi, E., Brem, A.-K., Levenbaum, E., Thompson, T., Kadosh, R. C., and Pascual-Leone, A. (2015). Enhancing cognition using transcranial electrical stimulation. *Curr. Opin. Behav. Sci.* 4, 171–178. doi: 10.1016/j.cobeha.2015.06.003

Conflict of Interest: DV is an employee of Neurable Inc.

The remaining authors declare that the research was conducted in the absence of any commercial or financial relationships that could be construed as a potential conflict of interest.

Publisher's Note: All claims expressed in this article are solely those of the authors and do not necessarily represent those of their affiliated organizations, or those of the publisher, the editors and the reviewers. Any product that may be evaluated in this article, or claim that may be made by its manufacturer, is not guaranteed or endorsed by the publisher.

frontiers in Neuroscience

SYSTEMATIC REVIEW
published: 15 November 2019
doi: 10.3389/fnins.2019.01213

The Impact of Transcranial Direct Current Stimulation on Upper-Limb Motor Performance in Healthy Adults: A Systematic Review and Meta-Analysis

Ronak Patel[1], James Ashcroft[1], Ashish Patel[1], Hutan Ashrafian[1], Adam J. Woods[2], Harsimrat Singh[1], Ara Darzi[1] and Daniel Richard Leff[1]*

[1] Department of Surgery & Cancer, Imperial College London, London, United Kingdom, [2] Department of Clinical and Health Psychology, Center for Cognitive Aging and Memory, McKnight Brain Institute, University of Florida, Gainesville, FL, United States

OPEN ACCESS

Edited by:
Hasan Ayaz,
Drexel University, United States

Reviewed by:
Brent Winslow,
Design Interactive, United States
Solaiman Shokur,
Alberto Santos Dumont Association for Research Support, Brazil

****Correspondence:***
Ronak Patel
ronak.patel@imperial.ac.uk

Specialty section:
This article was submitted to Neural Technology, a section of the journal Frontiers in Neuroscience

Received: *27 August 2019*
Accepted: *28 October 2019*
Published: *15 November 2019*

Citation:
Patel R, Ashcroft J, Patel A, Ashrafian H, Woods AJ, Singh H, Darzi A and Leff DR (2019) The Impact of Transcranial Direct Current Stimulation on Upper-Limb Motor Performance in Healthy Adults: A Systematic Review and Meta-Analysis. Front. Neurosci. 13:1213. doi: 10.3389/fnins.2019.01213

Background: Transcranial direct current stimulation (tDCS) has previously been reported to improve facets of upper limb motor performance such as accuracy and strength. However, the magnitude of motor performance improvement has not been reviewed by contemporaneous systematic review or meta-analysis of sham vs. active tDCS.

Objective: To systematically review and meta-analyse the existing evidence regarding the benefits of tDCS on upper limb motor performance in healthy adults.

Methods: A systematic search was conducted to obtain relevant articles from three databases (MEDLINE, EMBASE, and PsycINFO) yielding 3,200 abstracts. Following independent assessment by two reviewers, a total of 86 articles were included for review, of which 37 were deemed suitable for meta-analysis.

Results: Meta-analyses were performed for four outcome measures, namely: reaction time (RT), execution time (ET), time to task failure (TTF), and force. Further qualitative review was performed for accuracy and error. Statistically significant improvements in RT (effect size −0.01; 95% CI −0.02 to 0.001, $p = 0.03$) and ET (effect size −0.03; 95% CI −0.05 to −0.01, $p = 0.017$) were demonstrated compared to sham. In exercise tasks, increased force (effect size 0.10; 95% CI 0.08 to 0.13, $p < 0.001$) and a trend towards improved TTF was also observed.

Conclusions: This meta-analysis provides evidence attesting to the impact of tDCS on upper limb motor performance in healthy adults. Improved performance is demonstrable in reaction time, task completion time, elbow flexion tasks and accuracy. Considerable heterogeneity exists amongst the literature, further confirming the need for a standardised approach to reporting tDCS studies.

Keywords: transcranial direct-current stimulation (tDCS), systematic review, meta-analysis, motor, healthy, performance

INTRODUCTION

Transcranial Direct Current Stimulation (tDCS) is a non-invasive method of brain stimulation proposed to have beneficial effects in both cognitive and motor domains. Benefits have been demonstrated in patients with chronic pain syndromes (Fregni et al., 2006; Fenton et al., 2009; Fagerlund et al., 2015) and neuropsychiatric conditions (Baker et al., 2010; Loo et al., 2012; Palm et al., 2012; Kaski et al., 2014; Bandeira et al., 2016; Breitling et al., 2016), whilst in the healthy population, there is increasing scientific interest in the motor enhancing properties of the technology. Aligning with this trend, an increasing number of commercial companies (Edwards et al., 2017) promote the augmentation of motor abilities with tDCS including greater muscular power output (Okano et al., 2015; Huang et al., 2019), longer athletic endurance (Vitor-Costa et al., 2015; Park et al., 2019) and improved posture and balance (Kaminski et al., 2016; Saruco et al., 2017). This arena is most commonly explored through anodal tDCS to the primary motor cortex (M1), although the precise mechanism of action remains a matter of debate (Giordano et al., 2017). Excitability changes within M1 have been demonstrated, as evidenced through an increase in size of motor evoked potentials within the small muscles of the hand (Nitsche and Paulus, 2000, 2001). Similarly, tDCS transiently modulates cortical activation by raising the resting membrane potential of neurons closer to the activation threshold, thus increasing neuronal excitability (Bindman et al., 1964; Nitsche and Paulus, 2000). These neurophysiological changes persist after stimulation and are suggested to be associated with upregulation in N-methyl-d-aspartate receptor activation (Liebetanz et al., 2002). Regardless of these neurophysiological findings, there is a lack of consensus on the impact of tDCS on motor function in healthy individuals.

Despite a recent surge in meta-analyses on the effect of tDCS on aspects of cognitive function (Medina and Cason, 2017; Nilsson et al., 2017; Westwood and Romani, 2017; Simonsmeier et al., 2018), efforts to quantify the impact on motor function in healthy individuals are few in number (Bastani and Jaberzadeh, 2012; Hashemirad et al., 2016; Machado et al., 2019). Notably, Bastani and Jaberzadeh (2012) performed a meta-analysis focusing on motor cortex excitability and motor function but only included two studies involving healthy participants. Subsequently, Hashemirad et al. (2016) observed that multiple tDCS sessions over M1 induced significant task improvement but this review was limited to motor sequence learning. Other narrative reviews have summarized the effects of tDCS on motor tasks in healthy individuals with enhancing effects demonstrated in bimanual motor skills (Pixa and Pollok, 2018), motor learning (Reis and Fritsch, 2011; Buch et al., 2017), and exercise performance (Angius et al., 2017).

Whilst prior reviews (Reis and Fritsch, 2011; Angius et al., 2017; Buch et al., 2017; Pixa and Pollok, 2018) provide valuable summaries of tDCS studies, a meta-analysis would confer more critical and robust assessment of the impact of tDCS on motor function. Firstly, meta-analysis better estimates the effects that exist within the target population rather than limited to individual studies. Secondly, precision and accuracy of effect sizes is improved through pooled data offering greater statistical power than smaller separate sample sizes. Furthermore, it facilitates identification of methodological patterns or variables that could contribute to conclusions or, similarly, identify inconsistencies that lead to discrepancies within findings.

To date, there has been no systematic evaluation and meta-analysis of the overall impact of tDCS on upper limb motor performance in healthy adults and this paper aims to provide an up-to-date comprehensive analysis of available literature in this regard.

METHODS

Search Strategy

A comprehensive electronic search (**Appendix 1**), of three databases was conducted, namely: (a) MEDLINE (1946—August 2018), (b) PsycINFO (1806—August 2018), and (c) EMBASE (1947—August 2018). Due to variability in motor tasks and outcomes in tDCS literature, the search initially identified all randomised-controlled trials involving tDCS. Additional studies were gathered from cross-referencing bibliographies of included papers and from Google Scholar. The date of the last search conducted was 01 August 2018.

Eligibility Criteria

Retrieved articles were only included if they met the following inclusion criteria:

1. Studies performed on healthy subjects.
2. Studies requiring subjects to perform a motor task involving the upper limbs
3. Studies with published outcome variable data (raw or summary statistics)
4. Sham-controlled studies.

Reviews, case reports, letters, opinions, and conference abstracts were not included. Studies were limited to those carried out on adult human subjects and reported in English language. Any studies using subjects with prior expertise in tasks were not included e.g., pianists in finger tapping tasks or strength-trained athletes in elbow flexion tasks. Any studies which utilized additional interventions alongside tDCS, including pharmacological or other neuro-interventions (e.g., Transcranial Magnetic Stimulation), were also excluded.

Data Extraction

Titles and abstracts of all retrieved articles were screened by three of the reviewers (RP, JA, and AP) to identify relevant studies. Relevant articles that met inclusion criteria were obtained in full text and further assessed for eligibility by the same authors. Any disagreements during the selection process were resolved by discussion with a fourth, senior author (HA). Final selected studies are summarized in **Table 1**.

A data extraction form was generated in Microsoft Excel for Mac Version 16.19 (Microsoft Corporation, Redmond, WA, USA), and the following data were recorded: author, sample size, anode/cathode location, current intensity, experimental task, and performance outcome measure. Where possible, the first motor

TABLE 1 | Characteristics of studies selected for pooled statistical analysis.

References	Sample size	Stimulation	Reference	Current (mA)	Current Density (mA/cm^2)	Duration (min)	Task	Outcome measure used in pooled analysis
Apšvalka et al. (2018)	50	R M1	C-SOR	1	0.029	20	Finger sequence	RT and ET (s)
Arias et al. (2016)	13	L M1	R M1	1	0.029	10	Visuomotor adaptation	RT (ms)
Carlsen et al. (2015)	17	SMA (A+C)	Forehead	1	0.123	10	Simple reaction time task	RT (ms)
Dumel et al. (2016)	23	L M1	C-SOR	2	0.044	20	Serial reaction time task	RT (ms)
Ehsani et al. (2016)	39	L M1; cerebellum	R SOR; R arm	2	0.080	20	Serial reaction time task	RT (s)
Focke et al. (2017)	36	L PMC (A+C)	C-SOR	0.25	0.029	10	Serial reaction time task	RT (ms)
Galea et al. (2011)	40	L M1; R cerebellum	C-SOR; R Buccinator	2	0.080	15	Visuomotor adaptation	RT (ms)
Heise et al. (2014)	32	L M1	C-SOR	1	0.040	20	Serial reaction time task	RT (ms)
Horvath et al. (2016)	230	L M1 (A+C)	C-SOR; R M1, R wrist	1; 2	0.029; 0.057	20	Serial reaction time task	RT (ms)
Kang and Paik (2011)	11	L M1	C-SOR, R M1	2	0.080	20	Serial reaction time task	RT (ms)
Kantak et al. (2012)	13	R M1, PMC	C-SOR	1	0.125	15	Finger sequence	RT (s)
Karok and Witney (2013)	20	R M1	C-SOR; L M1	1.5	0.060	10	Serial finger tapping	RT (s)
Samaei et al. (2017)	30	Cerebellum	R Shoulder	2	0.080	20	Serial reaction time task	RT (s)
Shimizu et al. (2017)	45	Cerebellum (A+C)	Buccinator	2	0.057	20	Serial reaction time task	RT (s)
Waters-Metenier et al. (2014)	52	R M1	L M1	2	0.057	25	Configuration task	RT and ET (s)
Boggio et al. (2006)	8	R M1; L M1	C-SOR	1	0.029	20	JHFT	ET (s)
Convento et al. (2014)	12	R M1; L M1; R PPC; L PPC	C-SOR	2	0.080	10	JHFT	ET (s)
Doppelmayr et al. (2016)	83	L M1; cerebellum; R parietal	HD montage	1	0.318	21	Visuo-motor task	ET (s)
Hummel et al. (2010)	10	R M1	C-SOR	1	0.040	20	JHFT	ET (s)
Karok et al. (2017)	30	R M1	L M1, C-SOR	1.5	0.060	15	Purdue pegboard Test	ET (s)
Kidgell et al. (2013)	11	R M1	C-SOR; L M1	1	0.040	13	Purdue pegboard test	ET (s)
Marquez et al. (2015)	34	R M1; L M1	C-SOR	1	0.029	20	JHFT	ET (s)
Parikh and Cole (2014)	8	L M1	C-SOR	1	0.040	20	Key slot task	ET (ms)
Sohn et al. (2012)	28	R M1 (A+C); L M1	C-SOR	1	0.040	15	JHFT	ET (s)
Tecchio et al. (2010)	44	R M1	R arm	1	0.029	15	Finger tapping	ET (ms)
Waters et al. (2017)	64	Contralateral M1; Ipsilateral M1	Ipsilateral SOR/M1; contralateral M1	2	0.057	25	Finger sequence	ET (s)
Williams et al. (2010)	20	R M1	L M1	1	0.029	40	JHFT	ET (s)
Abdelmoula et al. (2016)	11	L M1	R Shoulder	1.5	0.043	10	Elbow flexion	TTF at 35% of MIVC (Nm)
Kan et al. (2013)	15	R M1	L shoulder	2	0.083	10	Elbow flexion	TTF at 30% of MIVC (Nm)
Oki et al. (2016)	13	R M1	L SOR	1.5	0.043	20	Elbow flexion	TTF at 20% of MIVC
Radel et al. (2017)	22	R PMC; P PFC	HD montage	2	NS	NS	Elbow flexion	TTF at 35% of MIVC (N)
Williams et al. (2013)	18	R M1	C-SOR	1.5	0.043	20	Elbow flexion	TTF at 20% of MIVC (Nm)
Frazer et al. (2016)	14	L M1	C-SOR	2	0.080	20	Wrist flexion	MIVC (Nm)
Frazer et al. (2017)	13	R M1	C-SOR	2	0.080	20	Elbow flexion	1 RM (kg)
Hendy and Kidgell (2013)	20	L M1	C-SOR	2	0.080	20	Wrist extension	1 RM (kg)
Hendy and Kidgell (2014)	10	R M1	C-SOR	2	0.080	20	Wrist extension	1 RM (kg)
Hendy et al. (2015)	16	R M1	C-SOR	1.5	0.060	15	Elbow flexion	1 RM (kg)

R, right; L, left; A+C, anodal and cathodal montages used; M1, Primary Motor Cortex; C-SOR, Contralateral Supraorbital Region; SMA, Supplementary Motor Area; PMC, Pre-motor Cortex; PFC, Prefrontal Cortex; RT, reaction time; ET, execution time; TTF, time to failure; MIVC, maximal isometric voluntary contraction; 1 RM, 1 repetition maximum; JHFT, Jebsen Hand Function Test.

assessment following the first single session of stimulation was used as the post-stimulation measurement. Moreover, significant efforts were made to obtain relevant missing data. Specifically, 19 authors were emailed to request further data, of which six responded.

Quality and Risk of Bias Assessment

Three bias assessment tools were employed to ensure robust evaluation. The quality and the risk of bias of selected articles were independently assessed by two authors (RP and JA). Quality was assessed using the Jadad score (Jadad et al., 1996) and the van Tulder scale (van Tulder et al., 2003). The Cochrane risk of bias tool (Higgins and Green, 2011) was additionally applied to RCTs with assessment of its seven key components. Any disagreement regarding quality or bias assessment was resolved through discussion with a senior author (HA).

Data Analysis

Outcome measures including reaction time, task completion time, time to failure, and force, were identified to allow statistical pooling of results. For each outcome measure, individual meta-analyses were performed using all relevant data sources regardless of stimulation protocol. However, where comparative studies used a variety of stimulation sites, further subgroup analyses were performed to examine the change in effect size using only anodal motor cortex stimulation (with variable cathodal placement). Pooled incidence and outcome measures were calculated through a random effects model employing an inverse variance Der Simonian Laird meta-analytical methodology (Tan et al., 2016). Study heterogeneity was appraised through the I^2 statistic and meta-analysis was performed in Microsoft Excel for Mac Version 16.19 (Microsoft Corporation, Redmond, WA, USA) and Stata Version 15 (Stata Corp LP, College

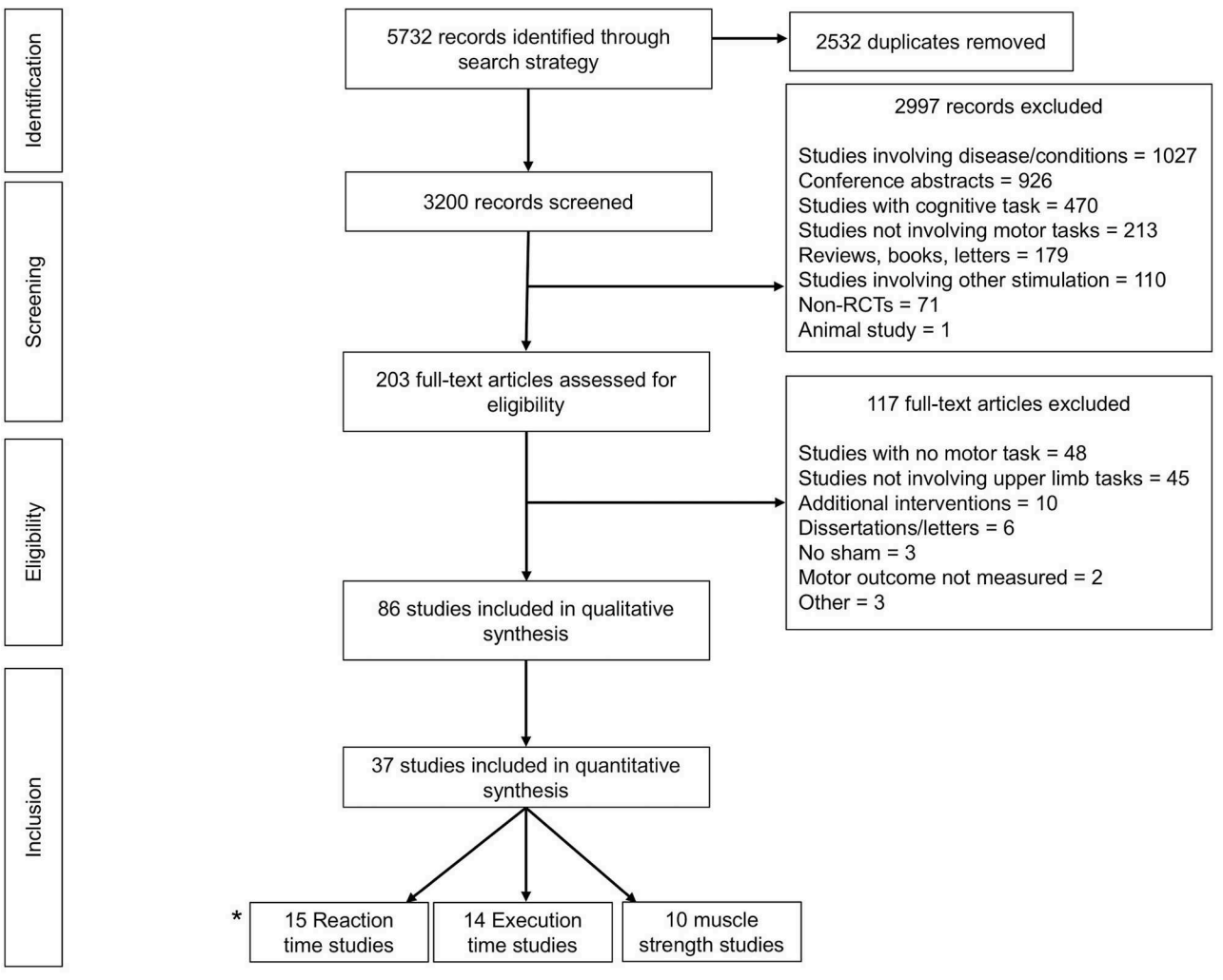

FIGURE 1 | Prisma Flow diagram detailing exclusions throughout each stage of study selection to yield a total of 86 articles for systematic review, 37 of which were meta-analysable. *2 studies (Waters-Metenier et al., 2014; Apšvalka et al., 2018) provided data for both reaction time and execution time.

Station, TX, USA). Where meta-analysis was not possible, narrative review was performed for additional evaluation of relevant literature.

RESULTS

Selected Articles

The flow of articles through the selection process is depicted in **Figure 1**. Following de-duplication, the literature search yielded 3,200 articles. Following exclusions, 86 relevant articles remained for detailed review. Articles were then subcategorized based on availability of performance outcome data suitable for pooled meta-analysis. These included the following outcome variables: reaction time (RT), execution time (ET), time to task failure (TTF), and force in muscle strength tasks. In total, 37 articles remained for final meta-analysis.

Overview of Literature

A total of 86 articles yielded 184 individual montage experiments investigating the impact of tDCS on upper limb motor tasks and there was demonstrable methodological heterogeneity amongst these, as illustrated in **Figure 2**. The typical stimulation protocol utilized 1 mA with 35 cm^2 electrodes pads delivering a currently density of 0.029 mA/cm^2 (30%). Of the total, 43% ($n = 79$) applied stimulation for 20 min and 70% ($n = 130$) used an online approach with motor tasks carried out during the stimulation period. As further illustrated in **Figure 2C**, motor cortex stimulation was the most frequent target area of choice (67%). There was variability with regard to the montage arrangement within each target area. During motor stimulation, the supraorbital region was the most common (67%) location for the reference electrode.

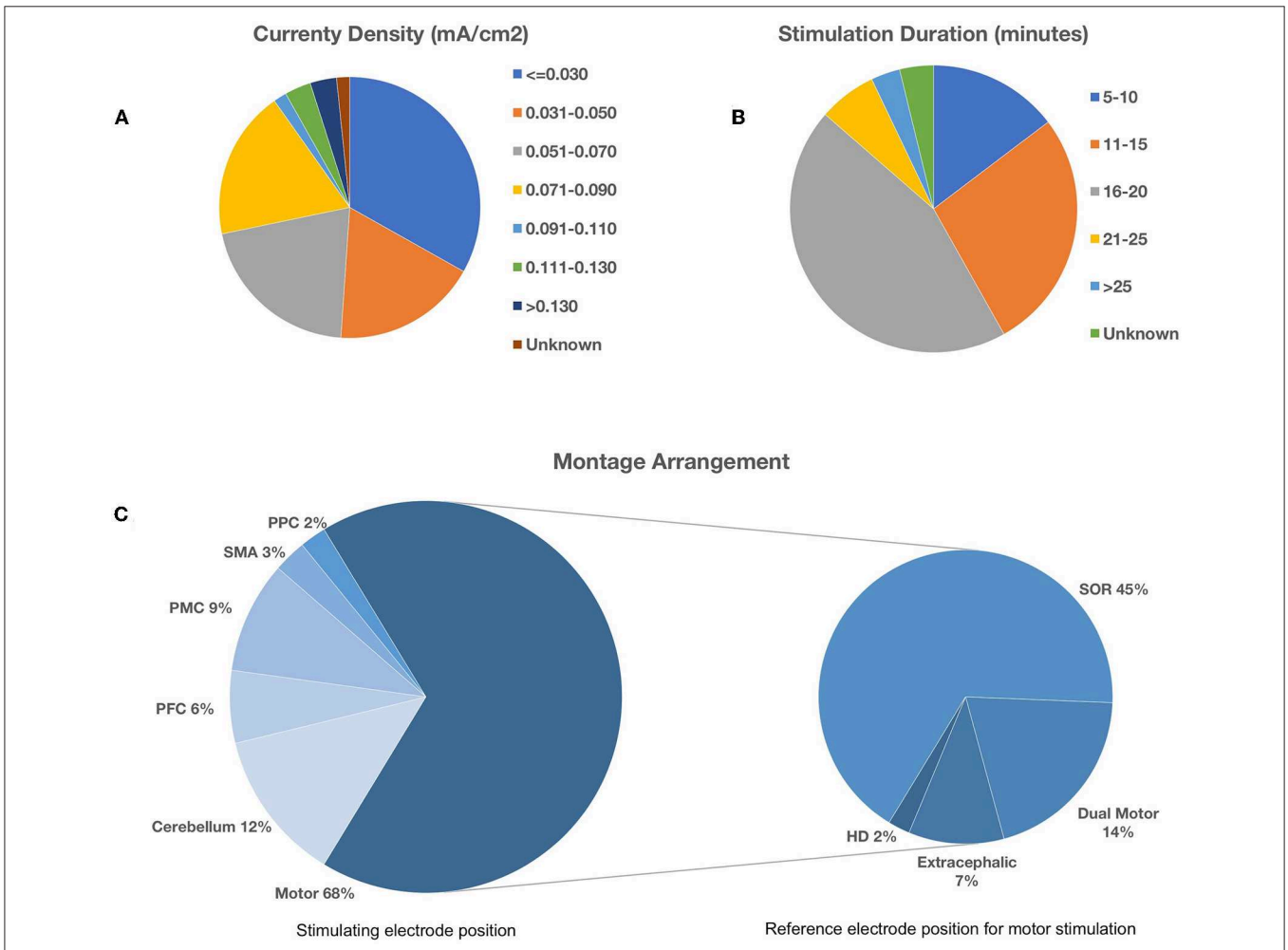

FIGURE 2 | Methodological heterogeneity of selected studies showing variability in **(A)** current density, **(B)** stimulation duration, and **(C)** montage arrangement. Bottom left pie chart illustrates the spread of the target area for stimulation. Bottom right pie chart illustrates the corresponding reference electrode location during motor cortex stimulation. PPC, Posterior Parietal Cortex; SMA, Supplementary Motor Area; PMC, Pre-motor Cortex; PFC, Prefrontal Cortex; SOR, Supraorbital Region; HD, High-Definition.

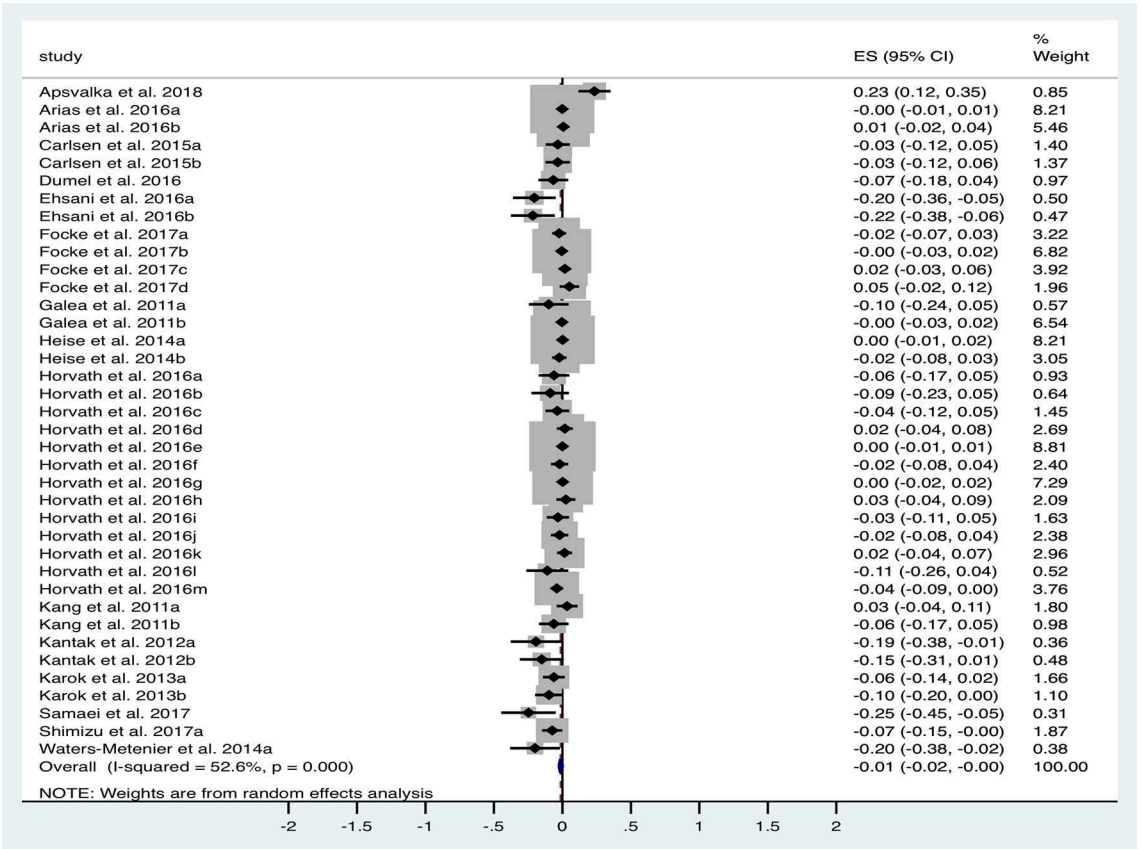

FIGURE 3 | Forest Plot illustrating effect sizes from the comparison in reaction time between tDCS vs. sham. Positive values indicate an increase in reaction time following anodal tDCS whilst negative values indicate a decrease in reaction time. Grey boxes represent the weight given to each study. Error bars represent 95% confidence intervals.

TABLE 2 | Stimulation protocols and outcomes of additional studies investigating the effect of tDCS on reaction time in an upper limb motor task.

References	Sample size	Stimulation	Reference	Current (mA)	Current density (mA/cm^2)	Duration (min)	Task	Significant effect vs. Sham
Ambrus et al. (2016)	17	L M1 (A+C)	C-SOR	1	0.029	12–14	SRTT	Nil
Dumel et al. (2018)	32	L M1	C-SOR	2	0.044	20	SRTT	↑
Ferrucci et al. (2013)	21	Cerebellum	R arm	2	0.057	20	SRTT	↑
Herzfeld et al. (2014)	51	L M1; Cerebellum (A+C)	C-SOR; R Buccinator	2	0.080	25	Hand reaching	Nil
Leite et al. (2011)	30	L M1, L DLPFC (all A+C)	Right SOR	1	0.029	15	SFTT	Nil
Lindenberg et al. (2013)	20	L M1	C-SOR; R M1	1	0.029	30	Choice RTT	Nil
Lindenberg et al. (2016)	24	L M1	C-SOR; R M1	1	0.029	30	RTT	Nil
Nitsche et al. (2003b)	80	L M1; PMC; L lateral PFC; L medial PFC (all A+C)	C-SOR; R M1	1	0.029	15	SRTT	↑ in L M1
Nitsche et al. (2010)	44	L PMC (A+C)	C-SOR	1	0.029	15	SFTT; SRTT	↑ with A stimulation in REM sleep
Stagg et al. (2011)	22	L M1 (A+C)	C-SOR	1	0.029	15	RTT; SRTT	↑ in A online stimulation; ↓ in A/C offline stimulation

Stimulation sites are anodal unless otherwise specified. R, right; L, left; A, anodal, C, cathodal; M1, Primary Motor Cortex; C-SOR, Contralateral Supraorbital Region; PMC, Pre-motor Cortex; PFC, Prefrontal Cortex; DLPFC, Dorsolateral Prefrontal Cortex; SRTT, Serial Reaction Time Task; SFTT, Serial Finger Tapping Task; ↑, denotes improvement in performance with stimulation; ↓, denotes worse performance with stimulation; Nil, no significant effect of tDCS on performance compared to sham stimulation.

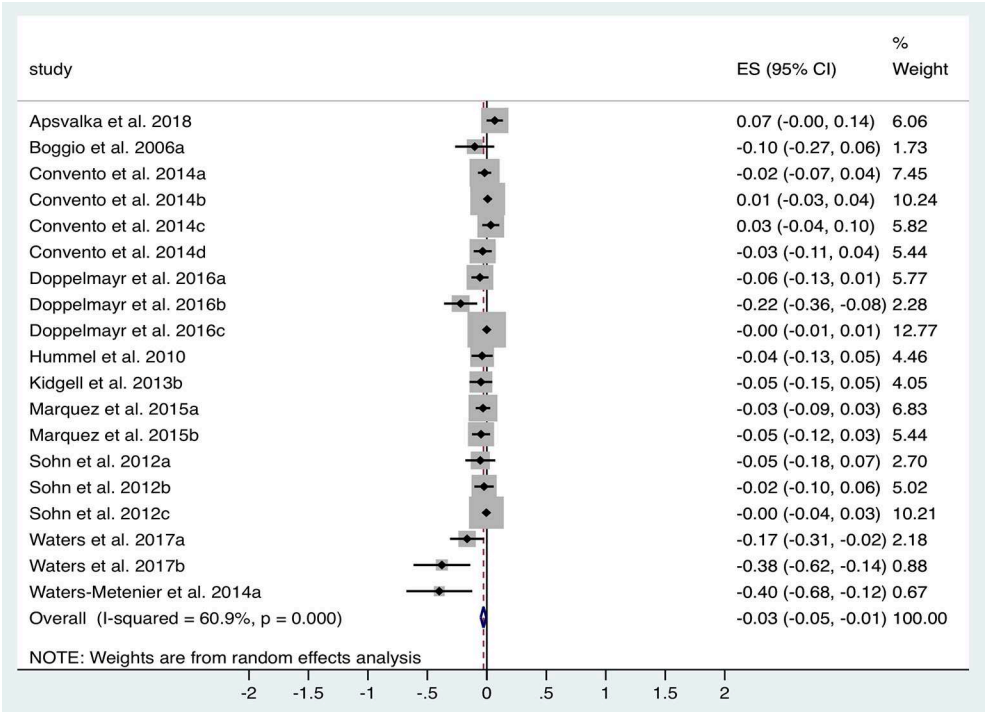

FIGURE 4 | Forest Plot illustrating effect sizes from the comparison in total task time between tDCS vs. sham. Positive values indicate an increase in time taken following anodal tDCS whilst negative values indicate a decrease in time taken. Grey boxes represent the weight given to each study. Error bars represent 95% confidence intervals.

Upper Limb Dexterity Tasks—Reaction Time

A total of 15 studies ($n = 618$ subjects) were suitable for quantitative analysis of the effect of tDCS vs. sham on RT. As illustrated in **Figure 3**, tDCS significantly reduced RT, albeit with a small effect size (ES 0.01, 95% CI −0.02 to 0.001, $p = 0.03$). Significant heterogeneity was observed when comparing tDCS to sham ($I^2 = 53\%$; $\chi^2 = 78.09$, $p < 0.001$). Subgroup analysis of anodal motor stimulation did not alter these results (ES −0.01, 95% CI −0.03 to −0.00, $p = 0.049$). Additional within-group analyses for tDCS and sham groups did not achieve statistical significance. Numerous other studies (summarized in **Table 2**) investigated the impact of tDCS on RT in a motor task but could not be included in the meta-analysis due to a lack of published raw data. Of these studies, 50% reported improvement with tDCS (80% motor stimulation), which is consistent with the observed marginally beneficial statistical effect size.

Upper Limb Dexterity Tasks—Execution Time

A total of 10 studies ($n = 344$ subjects) were suitable for analysis of the impact of tDCS vs. sham on ET. **Figure 4** illustrates the significant reduction in time taken to complete dexterity tasks following tDCS compared to sham with an effect size of −0.03 (95% CI −0.05 to −0.01, $p = 0.017$). Significant heterogeneity was observed ($I^2 = 61\%$; $\chi^2 = 46.03$, $p < 0.001$). Subgroup analysis of anodal motor montages marginally increased the effect size to −0.04 (95% CI −0.07 to −0.01, $p = 0.002$).

Additional within-group analyses was performed on 11 studies for both tDCS and sham compared to baseline. Overall effect size for tDCS was −0.09 (95% CI −0.13 to −0.05, $p < 0.001$) compared to −0.03 (95% CI −0.05 to −0.004, $p = 0.02$) for sham. Subgroup analysis of anodal motor stimulation confirmed these results for both tDCS (ES −0.09) and in sham (ES −0.02). Additional studies without available data for pooled analysis support overall findings with improved ET in a Purdue Pegboard Test (Karok et al., 2017) and a sport cup stacking task (Pixa et al., 2017a).

Upper Limb Dexterity Tasks—Accuracy/Error

Numerous studies have explored the impact of tDCS on a series of motor tasks with accuracy and error as outcome measures (**Table 3**). There is widespread heterogeneity amongst these studies not only in methodological design but also with regard to the task and the definition of the accuracy and error outcome measure. Therefore, we summarize the various montages these and subcategorize them according to the type of outcome measure, namely: correct responses, distance error, degree of error, error count, "skill" (calculated from error

TABLE 3 | Stimulation protocols and outcomes of studies investigating the effect of tDCS on different accuracy and error measurements in motor tasks.

References	Sample size	Stimulation	Reference	Current (mA)	Current density (mA/cm^2)	Duration (min)	Task	Significant effect vs. Sham
Accuracy: correct responses								
Dumel et al. (2016)	23	L M1	C-SOR	2	0.044	20	SRRT	Nil
Gomes-Osman and Field-Fote (2013)	28	Bilateral M1	Bilateral SOR	1	0.036	20	SFTT	↑
Karok and Witney (2013)	20	R M1	C-SOR; L M1	1.5	0.060	10	SFTT	Nil
Vines et al. (2008a)	16	R M1	C-SOR; L M1	1	0.061	20	SFTT	↑ in dual motor
Vines et al. (2008b)	17	L M1, R M1 (all A+C)	C-SOR	1	0.061	20	SFTT	↑ L hand in L M1 (C)
Zimerman et al. (2013)	53	L M1	C-SOR	1	NS	20	SFTT	↑ in older subjects
Zimerman et al. (2014)	23	R M1 (C only)	C-SOR	1	0.040	20	SFTT	↓
Error: distance								
Doppelmayr et al. (2016)	83	L M1, Cerebellum, R parietal	HD	1	0.318	21	Mirror tracing	Nil
Hardwick and Celnik (2014)	22	L cerebellum	Buccinator	2	0.080	15	Reaching task	↑ in older subjects
Lopez-Alonso et al. (2018)	14	L M1	C-SOR	1	0.040	20	SVIPT	Nil
Matsuo et al. (2011)	14	R M1	C- SOR	1	0.029	20	Circle drawing	↑
Mizuguchi et al. (2018)	24	R Cerebellum (A+C)	R Buccinator	2	0.080	20	Dart throwing	↑ in low performers (C)
Prichard et al. (2014)	54	R M1	C-SOR; L M1	1	0.063	20	Tracing task	↑ in both montages
Taubert et al. (2016)	41	R cerebellum(A+C)	R Buccinator	2	0.080	20	Reaching task	↓ in anodal
Vollmann et al. (2013)	36	L M1, L SMA, L pre-SMA	Forehead	0.75 mA	0.070	20	VPFT	↑ in L M1 + L SMA
Error: degrees								
Block and Celnik (2013)	79	L M1; R M1; L cerebellum; R cerebellum	C-SOR; Buccinator	2	0.080	25	VAT	Nil
Galea et al. (2011)	30	L M1; R cerebellum	C-SOR; R Buccinator	2	0.080	15	VAT	↑ in cerebellar
Panouilieres et al. (2015)	80	L M1; R cerebellum	R SOR	2	0.057	17	VAT	↑ in M1
Error count								
Apšvalka et al. (2018)	50	R M1	C-SOR	1	0.029	20	SFTT	Nil
Ehsani et al. (2016)	59	L M1; cerebellum	R SOR; R arm	2	0.080	20	SRTT	↑ in both montages
Horvath et al. (2016)	210	L M1 (A+C)	C-SOR, R M1, R arm	1; 2	0.029; 0.057	20	SRTT	Nil
Leite et al. (2011)	30	L M1, L DLPFC (all A+C)	Right SOR	1	0.029	15	SFTT	Nil
Lindenberg et al. (2013)	20	L M1	C-SOR; R M1	1	0.029	30	Choice RTT	Nil
Lindenberg et al. (2016)	24	L M1	C-SOR; R M1	1	0.029	30	RTT	Nil
Parikh and Cole (2014)	8	L M1	C-SOR	1	0.040	20	Groove pegboard	Nil
Samaei et al. (2017)	30	Cerebellum	R shoulder	2	0.080	20	SRTT	Nil
Shimizu et al. (2017)	45	Cerebellum (A+C)	Buccinator	2	0.057	20	SRTT	Nil
Tecchio et al. (2010)	44	R M1	R arm	1	0.029	15	SFTT	Nil
Vergallito et al. (2018)	24	L PFC; R PFC	C-SOR	1.5	0.060	20	SFTT	↑in L PFC ↑in R PFC in low demand
Waters et al. (2017)	64	Contralateral M1; Ipsilateral M1	Ipsilateral SOR/M1; Contralateral M1	2	0.057	25	SFTT	↑ in both bilateral montages
Waters-Metenier et al. (2014)	52	R M1	L M1	2	0.057	25	SFTT	↑
Skill: calculated from error and speed								
Cantarero et al. (2015)	33	Cerebellum (A+C)	R Buccinator	2	0.080	20	SVIPT	↑ in A
Cuypers et al. (2013)	13	L M1	R SOR	1; 1.5	0.040; 0.060	20	SFTT	↑ with 1.5 mA

(Continued)

TABLE 3 | Continued

References	Sample size	Stimulation	Reference	Current (mA)	Current density (mA/cm^2)	Duration (min)	Task	Significant effect vs. Sham
Hashemirad et al. (2017)	48	L M1; L DLPFC; L PPC	C-SOR	0.3	0.100	20	SVIPT	Nil
Naros et al. (2016)	50	R M1; L M1 (C); R M1; Bilateral M1	C-SOR, C-SOR; L M1; Bilateral SOR	1	0.029	20	Exoskeleton tracing	↑ in all, greatest in bilateral motor
Reis et al. (2009)	36	L M1 (A+C)	C-SOR	1	0.040	20	SVIPT	↑ in both
Rumpf et al. (2017)	47	L M1 (A+C); L PPC	C-SOR	1	0.029	15	SFTT	↑ in L M1 (A)
Saucedo Marquez et al. (2013)	27	R M1	Ipsilateral Shoulder	1	0.040	20	SFTT; SVIPT	↑
Schambra et al. (2011)	87	L M1; R M1	Ipsilateral Shoulder	1	0.040	20	SVIPT	↑ in both. Only L M1 significant
Miscellaneous								
Carter et al. (2017)	10	SMA	Forehead	1	0.128	10	Bimanual coordination	↑
Chothia et al. (2016)	12	L Cerebellum	L Buccinator	2	0.125	15	Rotor pursuit	Nil
Ciechanski et al. (2017)	22	L M1	C-SOR	1	0.040	20	Virtual surgical resection	↑
Dumel et al. (2018)	32	L M1	C-SOR	2	0.044	20	Purdue Pegboard	↑
Furuya et al. (2014)	13	R M1; L M1	L M1; R M1	2	0.057	15	SFTT	↑ in both
Goodwill et al. (2013)	11	R M1	C-SOR; L M1	1	0.040	15	VAT	↑
Karok et al. (2017)	30	R M1	C-SOR; L M1	1.5	0.060	15	VPFT	↑ in both montages
Koyama et al. (2015)	28	R M1	L M1	1	0.040	25	Ballistic thumb movements	↑
Lang et al. (2005)	16	L M1 (A+C)	C-SOR	1	0.029	10	SFTT	Nil
Mccambridge et al. (2016)	16	R M1	L M1	1	0.333	15	Circle tracing	Nil
Pixa et al. (2017b)	31	Bilateral M1	HD	1	0.318	15	Purdue pegboard	↑
Rroji et al. (2015)	14	R M1	Ipsilateral shoulder	1	0.040	20	Thumb flexion	↑
Schmidt et al. (2013)	16	Left M1 (C)	C-SOR	0.7	0.020	10	SFTT	↑
Summers et al. (2018)	14	Cerebellum	R buccinator	2	0.029	30	VAT	Nil
Zhu et al. (2015)	27	L DLPFC (C)	C-SOR	1.5	0.060	15-20	Golf putting	↑

M1, Primary Motor Cortex; SOR, Supraorbital Region; DLPFC, Dorsolateral Prefrontal Cortex; PPC, Posterior Parietal Cortex; HD, High definition; SRTT, Serial Reaction Time Task; SFTT, Serial Finger Tapping Task; SVIPT, Sequential Visual Isometric Pinch Task; VAT, Visuomotor Adaptation Task; VPFT, Visuomotor Pinch Force Task; ↑, denotes improvement in performance with stimulation; ↓, denotes worse performance with stimulation; Nil, no significant effect of tDCS on performance compared to sham stimulation.

and speed measurements of a motor task) and miscellaneous outcome measures.

Dual (Vines et al., 2008a; Gomes-Osman and Field-Fote, 2013; Karok and Witney, 2013) and unilateral dominant (Zimerman et al., 2013) motor cortex stimulation increased the *number of correct responses* in a sequential finger tapping task (SFTT), but was not replicated in other studies (Vines et al., 2008b; Dumel et al., 2016). Cathodal stimulation to the non-dominant (Zimerman et al., 2014) motor cortex decreased the number of correct responses in SFTT. tDCS led to improved *skill outcomes*, in the majority of studies applying motor cortex stimulation (Reis et al., 2009; Schambra et al., 2011; Cuypers et al., 2013; Saucedo Marquez et al., 2013; Naros et al., 2016; Rumpf et al., 2017). Similarly, motor stimulation also demonstrated improvements in a variety of miscellaneous tasks (**Table 3**). Only cerebellar stimulation in this context failed to confer any improvements in motor performance.

Drawing task *distance error* improvements were less consistent with benefits in non-dominant and dual (Matsuo et al., 2011; Prichard et al., 2014), but not dominant motor cortex stimulation (Doppelmayr et al., 2016). Other distance error tasks benefitted with motor (Vollmann et al., 2013) and cerebellar (Hardwick and Celnik, 2014; Mizuguchi et al., 2018) stimulation, but not consistently amongst the literature (Taubert et al., 2016; Lopez-Alonso et al., 2018). Although improvements were demonstrated in visuomotor adaptation tasks (error in degrees) with motor (Panouilìeres et al., 2015) and cerebellar (Galea et al., 2011) stimulation, this was inconsistent (Galea et al., 2011; Block and Celnik, 2013; Panouilìeres et al., 2015). Only a

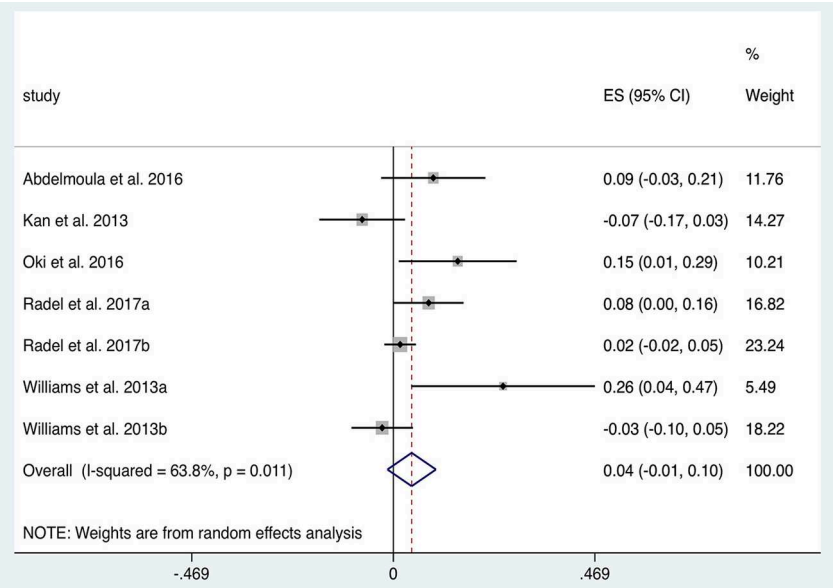

FIGURE 5 | Forest Plot illustrating effect sizes from the comparison in time to elbow flexion task failure between anodal tDCS vs. sham tDCS. Positive values indicate an increase in time to failure following tDCS whilst negative values indicate a decrease in time. Grey boxes represent the weight given to each study. Error bars represent 95% confidence intervals.

minority of studies (Waters-Metenier et al., 2014; Ehsani et al., 2016; Waters et al., 2017; Vergallito et al., 2018) investigating *error count* in a SRTT and SFTT demonstrated improved performance with tDCS, all of which had substantial variation in stimulation montages.

Upper Limb Exercise Tasks: Fatigue

In total five studies with $n = 79$ subjects were suitable for quantitative analysis of the effect of tDCS on TTF in elbow flexion tasks. **Figure 5** illustrates a tendency towards prolonged TTF with tDCS compared to sham (ES 0.04, 95% CI −0.01 to 0.10, $p = 0.139$). Heterogeneity was observed when comparing anodal tDCS to sham in this cohort of studies ($I^2 = 64\%$; $\chi^2 = 16.59$, $p = 0.01$). Subgroup analysis of anodal motor montages increased the effect size to 0.06 (95% CI −0.04 to 0.16, $p = 0.269$).

Upper Limb Exercise Tasks: Strength

Studies investigating the impact of tDCS on strength of contraction in upper limb flexion/extension tasks were divided into four studies with a fatiguing contraction between pre- and post- measurements (therefore causing a decrease in strength) and five studies without such a contraction. The five studies without a fatiguing contraction ($n = 73$ subjects) provided data for within-group analysis of change in strength from baseline in tDCS and sham groups. Anodal motor tDCS increased strength (ES 0.10, 95% CI 0.08 to 0.13, $p < 0.001$; **Figure 6A**) twice as much as sham (ES 0.05, 95% CI 0.03 to 0.08, $p < 0.001$; **Figure 6B**). Both of these analyses exhibited significant heterogeneity ($p < 0.001$). A repeated stimulation protocol was utilized in three studies and stimulation was combined alongside strength training (ST) in four studies. An additional study (Lampropoulou and Nowicky, 2013), not included due to lack of data, showed no effect of tDCS on strength.

Elbow flexion strength was examined either side of a fatiguing contraction in four studies. Within-group analyses revealed similar reductions in strength effect size from baseline in intervention (ES −0.26, 95% CI −0.32 to −0.19, $p < 0.001$) and sham groups (ES −0.22, 95% CI −0.28 to −0.17, $p < 0.001$). Subgroup analysis of anodal motor stimulation was comparable.

Quality Scoring and Risk of Bias Assessment

Summary risk of bias graph is illustrated in **Figure 7** and Results of Jadad Score and Van Tulder quality assessment scores are summarized in **Table 4**. Randomization was utilized in 78% of studies but only 14% were deemed to sufficiently explain methods used for random sequence generation. A double-blind approach was used in 65% of studies with the remaining 16% reporting only single-blinding and 19% did not mention blinding at all. Generally, studies performed well in terms of selective reporting, avoiding co-interventions, retaining acceptable compliance and assessing outcomes at similar time-points.

DISCUSSION

This study provides a comprehensive and contemporaneous review and quantitative analysis of the effect of tDCS on in healthy adults. In regard to dexterity tasks, the present analysis has demonstrated a modest improvement in reaction time and significant improvements in execution time and other performance domains of accuracy and error with tDCS. Analysis of muscle strength studies revealed significant strength

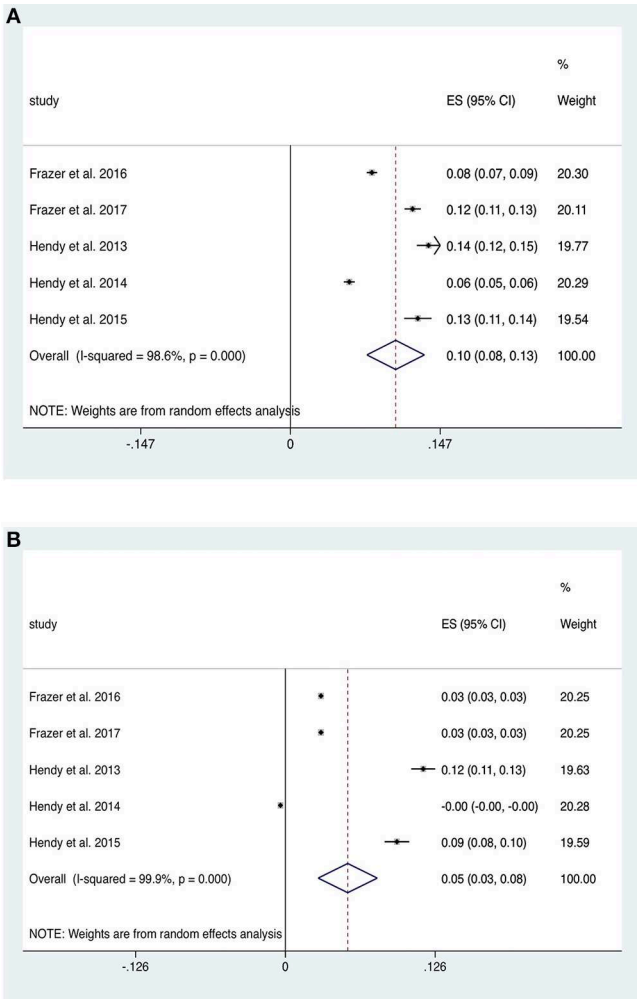

FIGURE 6 | Forest Plot illustrating effect sizes from the comparison in strength between **(A)** anodal tDCS and **(B)** sham tDCS vs. baseline. Positive values indicate an increase strength following each intervention whilst negative values indicate a decrease in strength. Grey boxes represent the weight given to each study. Error bars represent 95% confidence intervals.

improvement with training along with a tendency towards reduced fatigue with tDCS.

Upper Limb Dexterity Tasks

Reduction in motor RT is frequently used as a representation of motor learning, and, numerous studies demonstrate significant reduction in reaction time with tDCS compared to sham. This was commonly observed in unilateral (Nitsche et al., 2003b; Kantak et al., 2012; Karok and Witney, 2013; Heise et al., 2014; Dumel et al., 2016, 2018; Ehsani et al., 2016) and dual (Karok and Witney, 2013; Waters-Metenier et al., 2014) anodal motor stimulation or anodal cerebellar stimulation (Ferrucci et al., 2013; Ehsani et al., 2016; Samaei et al., 2017) with benefits consistent at 24 h retention tests as well (Shimizu et al., 2017). However, improvements were not universal throughout the literature with similar stimulation protocols (Nitsche et al., 2003b; Galea et al., 2011; Stagg et al., 2011; Lindenberg et al., 2013, 2016; Heise et al., 2014; Ambrus et al., 2016; Arias et al., 2016; Horvath et al., 2016; Focke et al., 2017; Apšvalka et al., 2018). Interestingly, RT worsened with cathodal stimulation regardless of site (Leite et al., 2011; Stagg et al., 2011; Carlsen et al., 2015; Shimizu et al., 2017), potentially due to reduced motor cortex excitability with cathodal tDCS (Nitsche et al., 2003a). Further benefits of tDCS in motor tasks was demonstrable with improvements in ET three times greater than sham, a difference made even more apparent when isolating anodal motor stimulation only. All studies with single session anodal stimulation of the non-dominant motor cortex demonstrated improved performance (Boggio et al., 2006; Williams et al., 2010; Sohn et al., 2012; Kidgell et al., 2013; Convento et al., 2014; Parikh and Cole, 2014; Karok et al., 2017). This was not demonstrated with stimulation of the dominant cortex (Boggio et al., 2006; Sohn et al., 2012; Convento et al., 2014) and it is possible that the comparative lack of observed effect on the dominant hand could be due to a ceiling-effect with little room for improvement. However, it could still be beneficial in this context with motor training (Dumel et al., 2018) or in older adults (Hummel et al., 2010). An additional study (Marquez et al., 2015) demonstrated improved performance of the non-dominant hand regardless of laterality of motor cortex stimulation. Amongst other measures of motor performance in dexterity tasks, there is demonstrable and reliable (85% of studies) improvement with dual motor stimulation (Vines et al., 2008a; Gomes-Osman and Field-Fote, 2013; Goodwill et al., 2013; Karok and Witney, 2013; Furuya et al., 2014; Prichard et al., 2014; Waters-Metenier et al., 2014; Koyama et al., 2015; Naros et al., 2016; Karok et al., 2017; Pixa et al., 2017b; Waters et al., 2017). Unilateral motor stimulation was less consistent with as many studies documenting improvement (Matsuo et al., 2011; Reis and Fritsch, 2011; Schambra et al., 2011; Cuypers et al., 2013; Goodwill et al., 2013; Karok and Witney, 2013; Saucedo Marquez et al., 2013; Schmidt et al., 2013; Vollmann et al., 2013; Zimerman et al., 2013; Prichard et al., 2014; Panouilìeres et al., 2015; Rroji et al., 2015; Ehsani et al., 2016; Naros et al., 2016; Rumpf et al., 2017; Dumel et al., 2018) as no effect (Lang et al., 2005; Vines et al., 2008a,b; Tecchio et al., 2010; Leite et al., 2011; Block and Celnik, 2013; Lindenberg et al., 2013, 2016; Parikh and Cole, 2014; Doppelmayr et al., 2016; Dumel et al., 2016; Horvath et al., 2016; Hashemirad et al., 2017; Apšvalka et al., 2018; Lopez-Alonso et al., 2018).

Upper Limb Exercise Performance

A trend towards increased time to task failure (TTF) with anodal tDCS compared to sham, which was demonstrated in both online and offline stimulation protocols of elbow flexion tasks. The impact of offline tDCS between two fatiguing contractions 1 h apart was examined in three studies (Cogiamanian et al., 2007; Kan et al., 2013; Abdelmoula et al., 2016), two of which (Cogiamanian et al., 2007; Abdelmoula et al., 2016) resulted in improved TTF suggesting potential to help reduce neuromuscular fatigue. Interestingly, all three studies showed no difference between strength (as measured by force) between stimulation and sham. The remaining three studies (Williams et al., 2013; Oki et al., 2016; Radel et al., 2017) utilized an online

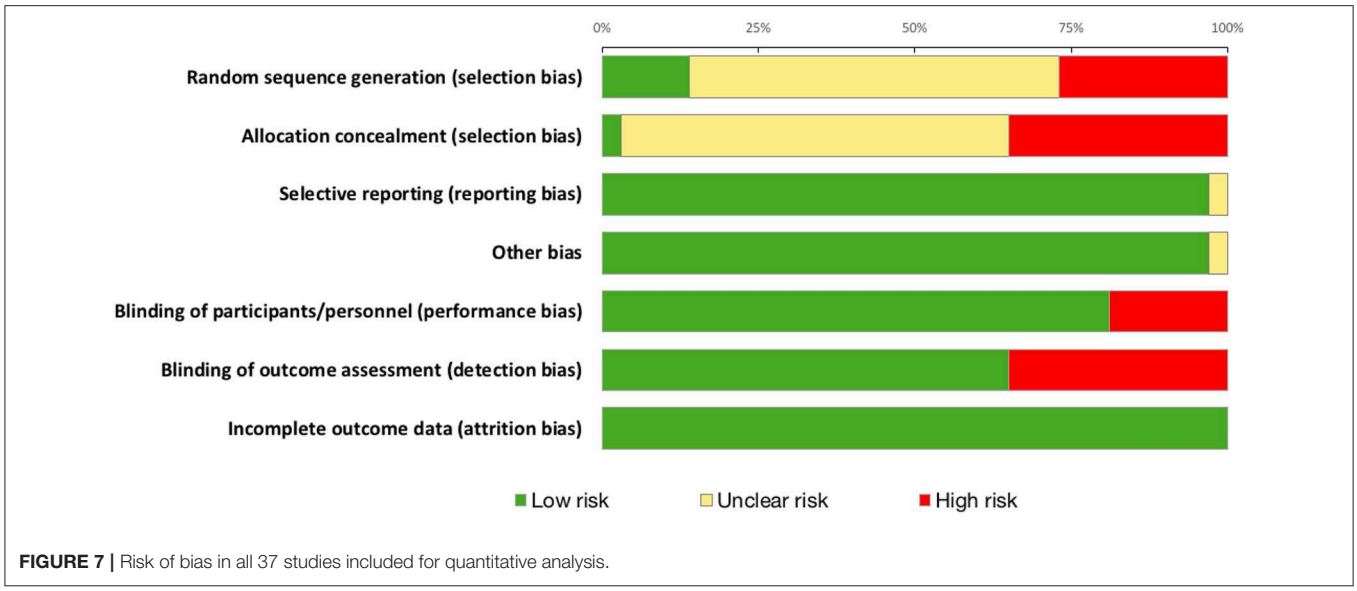

FIGURE 7 | Risk of bias in all 37 studies included for quantitative analysis.

stimulation protocol, two of which (Williams et al., 2013; Oki et al., 2016) demonstrated an improved TTF. Of note, Williams et al. (2013) performed a subgroup analysis which revealed significantly increased TTF in subjects who had stimulation throughout the task against those who had stimulation for part of the task duration. The former was also found to have worsening strength performance. Although overall there seems to be no consistent effect of tDCS on contraction force when separated by a fatiguing contraction, there does appear to be significantly increased force without such contraction. Indeed, tDCS was found to increase by strength twice as much than sham although it must be noted that this is not a direct comparative analysis. Although methodological variability exists within this pool of studies, separate within-group analyses facilitates a robust comparison of tDCS against sham.

These findings align with a recent meta-analysis by Lattari et al. (2018) on effects of tDCS on upper and lower limb muscle strength which demonstrated improved overall improved muscular endurance (TTF) and strength (force of MVC). More recently, Machado et al. (2019) revealed improved TTF with anodal M1 tDCS in cycling but unlike the present study did not analyse TTF in upper limb tasks. They failed to observe an effect of tDCS on strength in upper limb tasks, although they separated isometric, isokinetic and dynamic upper and lower limb exercises and do not report on three studies (Hendy and Kidgell, 2013; Hendy et al., 2015; Frazer et al., 2017) we included. The current analysis further strengthens the case for the potential of tDCS as an ergogenic aid in tasks requiring muscular endurance and strength, with a potentially more profound impact with training and repeated stimulation.

Neural Mechanisms

The vast majority of electrode montages in these experiments performed motor cortex stimulation. The mechanism underlying motor learning through tDCS has been postulated as a result of increased excitability of the motor cortex augmenting successful and active synaptic connections between the neuronal structures activated by tDCS (Bindman et al., 1964). This is supported by neurophysiological studies which demonstrate the importance of M1 in early learning (Karni et al., 1995) and also consolidation of learning (Ungerleider et al., 2002; Doyon et al., 2009). However, despite the overall trends for improved motor performance, the evidence is inconsistent. There may be several explanations for these divergent findings. Firstly, there is considerable experimental variation with regard to tDCS parameters (stimulation intensity, duration, anode and cathode placement; see **Figure 2**), experimental design (e.g., online/offline protocols, timing of motor performance, variable washout periods) and motor tasks and their outcome measures. Secondly, with regards to mechanistic effects, some studies have revealed either minimal change or a decrease in M1 excitability (Jenkins et al., 1994; Toni et al., 1998; Floyer-Lea and Matthews, 2005) suggesting that modulation of this area may not be as influential as previously thought, especially given the large influence of other brain structures in facilitating voluntary movement. Similarly, it is maybe a too simplistic a view to suggest that altering M1 excitability alone will impact on motor learning. Given the well-documented roles of other cortical regions and their interconnections (Doyon et al., 2002; Ungerleider et al., 2002; Hardwick et al., 2013) in performing motor skills, it is perhaps unsurprising that there is such variation in the brain region targeted for stimulation with tDCS. Therefore, it is conceivable that to observe significant gains in motor learning tasks, the reliance on other motor brain areas must be accounted for and augmented as well—a notion which may account for our findings of more consistent improvement with dual motor stimulation (see **Table 3**). Finally, disparate effects of tDCS may be related to the combination of tasks implemented as slight changes in task can not only affect performance, but also learning processes (Nitsche et al., 2003b; Saucedo Marquez et al., 2013).

Underlying neural mechanisms regarding exercise performance are unclear and a number of factors have been

TABLE 4 | Total Jadad and Van Tulder studies for each study included in quantitative analysis.

References	Jadad score	Van Tulder score
Apšvalka et al. (2018)	1	7
Arias et al. (2016)	1	5
Carlsen et al. (2015)	0	6
Dumel et al. (2016)	1	6
Ehsani et al. (2016)	5	10
Focke et al. (2017)	3	9
Galea et al. (2011)	3	9
Heise et al. (2014)	3	8
Horvath et al. (2016)	1	5
Kang and Paik (2011)	3	8
Kantak et al. (2012)	1	5
Karok and Witney (2013)	2	6
Samaei et al. (2017)	4	9
Shimizu et al. (2017)	1	6
Waters-Metenier et al. (2014)	3	8
Boggio et al. (2006)	4	9
Convento et al. (2014)	3	8
Doppelmayr et al. (2016)	4	9
Hummel et al. (2010)	3	7
Karok et al. (2017)	2	6
Kidgell et al. (2013)	4	8
Marquez et al. (2015)	5	10
Parikh and Cole (2014)	1	7
Sohn et al. (2012)	3	8
Tecchio et al. (2010)	1	6
Waters et al. (2017)	5	10
Williams et al. (2010)	4	8
Abdelmoula et al. (2016)	1	6
Kan et al. (2013)	1	6
Oki et al. (2016)	3	8
Radel et al. (2017)	4	8
Williams et al. (2013)	4	9
Frazer et al. (2016)	3	8
Frazer et al. (2017)	3	8
Hendy and Kidgell (2013)	4	8
Hendy and Kidgell (2014)	3	8
Hendy et al. (2015)	3	8

Higher scores represent higher quality.

postulated (Cogiamanian et al., 2007). Increases in motor cortex excitability with tDCS (Nitsche and Paulus, 2000, 2001) were not seen in sustained contractions of 20% (Cogiamanian et al., 2007; Williams et al., 2013) and 35% (Abdelmoula et al., 2016) of maximal isometric voluntary contraction (MIVC). However, one of these studies (Williams et al., 2013) did find significant increases in MEPs during a slight contraction following tDCS suggestive of increased cortical excitability. Furthermore, Krishnan et al. (2014) demonstrated increase in EMG magnitude during elbow flexion in higher force levels at 37.5 and 50% of maximum, but not in lower levels. Improvements in force were additionally associated with increased cortical excitability as seen in studies with (Hendy and Kidgell, 2013, 2014; Hendy et al., 2015; Frazer et al., 2017) or without (Frazer et al., 2016) strength training and with (Hendy and Kidgell, 2013; Hendy et al., 2015; Frazer et al., 2016) or without (Hendy and Kidgell, 2014; Frazer et al., 2017) repeated stimulation. These studies also indicate an increase in cross-activation and decrease in short-interval intracortical inhibition as contributory factors. Conversely, other studies have failed to demonstrate MIVC improvement theorized to be due to ceiling effects of maximal muscle contractility (Kan et al., 2013) but also membrane excitability (Williams et al., 2013) as suggested by a lack of difference in MEPs (Lampropoulou and Nowicky, 2013) during elbow flexion.

Safety Considerations

Given the promising findings in improving upper limb motor performance discussed above, it is important to evaluate the safety aspects neurostimulation technology. Several literature reviews suggest tDCS is safe (Brunoni et al., 2011, 2012; Bikson et al., 2016; Fregni et al., 2016; Woods et al., 2016; Matsumoto and Ugawa, 2017). In an extensive review of tDCS safety (Bikson et al., 2016), no serious adverse events or irreversible injuries were documented in 33,200 sessions in 1,000 subjects including certain potentially vulnerable populations. Common minor side effects include "tingling" and "itching," which are typically transient and subside following stimulation, and redness, which tends to disappear after 1–2 h. For cumulative exposure, a systematic review (Nikolin et al., 2018) concluded no additional risks to subjects with repeated sessions of tDCS. Healthy subjects have received up to 30 sessions of tDCS without any serious adverse events (Paneri et al., 2015) and some neuropsychiatric patients have received over 100 sessions without any serious adverse events (Andrade, 2013). tDCS has also been shown to be safe in children with over 2,800 sessions on nearly 500 subjects showing no serious adverse effects (Bikson et al., 2016). Two additional reviews also supported these findings with no serious adverse effects observed with tDCS in children (Krishnan et al., 2015; Palm et al., 2016). On a cellular level, Nitsche et al. (2003a) examined neuron specific enolase, a protein associated with neuronal death, in subjects undergoing tDCS and revealed no change in enolase concentration following treatment. In cortical imaging studies, MRI was used to examine subjects for brain oedema, disturbance of the blood-brain barrier and structural alterations of the brain following tDCS and demonstrated no such concerns in any of their subjects (Nitsche et al., 2004). Similarly, Tadini et al. (2011) have confirmed no significant abnormal effects of tDCS on EEG. Furthermore, tDCS is recognised by the National Institute for Health and Care Excellence (NICE) as a safe option in the treatment of depression in adults. It is important to note that this safety profile is assumed only for experiments within certain stimulation protocol limits (e.g., stimulation current up to 2 mA). Although these parameters are being extended (e.g., current up to 4 mA) in ongoing research (Chhatbar et al., 2017), further work is required to ascertain the exact protocol limits for physiological safety.

CONCLUSIONS

The current meta-analysis suggests that tDCS confers immediate performance benefits in dexterity tasks and exercise tasks. Importantly, these results must be interpreted with caution owing to the widespread methodological differences in the experimental domain of tDCS highlighted within this review. Whilst it is appropriate to vary methodology according to the proposed scientific question of the study and also to better appraise the physiological mechanisms of tDCS, the sheer range of methodologies currently utilised has rendered it challenging to group studies for meta-analysis. Additional research is required to delineate neural mechanisms contributing to the effect of tDCS on motor performance which will further our understanding of individual, task and study variability. As the field progresses, narrower stimulation protocols and approaching future work with an emerging standardized manner (Buch et al., 2017) will help to derive more reliable conclusions.

LIMITATIONS

The main limitation of this review lies in the considerable methodological heterogeneity of stimulation protocols, task type and reporting of outcomes. Antal and colleagues (Antal et al., 2015) accurately highlight significant limitations of meta-analysis within the field, some of which are unavoidable due to methodological variability. Accordingly, studies were restricted to those which reported data for the same outcome variable at the same post-stimulation time-point; long-term/retention effects were not within the remit of this study. Similarly, although initial analysis included all protocols to provide an overview of the effect of tDCS, further subgroup analyses of anodal motor stimulation was performed to draw more precise conclusions. Further restricting studies to the same montage, current density and duration would limit available data to an extent that statistical analysis would not be possible or appropriate. Although the present analysis combined single- and multi-session experiments, we deemed this to represent the overall impact of tDCS and where possible, data was extracted after the first session only. Although different tasks were combined for RT and ET analyses, this approach is similar to other published tDCS-related meta-analysis (Dedoncker et al., 2016) and a random-effects model analysis was performed to account for heterogeneity. Finally, individual studies included in the meta-analyses had a small sample size which could potentially reduce the power of analysis.

AUTHOR CONTRIBUTIONS

RP, HS, HA, and DL designed the structure and scope of the review. RP, JA, and AP collected review articles. RP prepared the manuscript draft. All authors reviewed and revised the manuscript.

FUNDING

This research was funded by the NIHR Imperial Biomedical Research Centre (BRC; grant 1215-20013). The views expressed are those of the authors and not necessarily those of the NIHR of the Department of Health and Social Care.

REFERENCES

Abdelmoula, A., Baudry, S., and Duchateau, J. (2016). Anodal transcranial direct current stimulation enhances time to task failure of a submaximal contraction of elbow flexors without changing corticospinal excitability. *Neuroscience* 322, 94–103. doi: 10.1016/j.neuroscience.2016.02.025

Ambrus, G. G., Chaieb, L., Stilling, R., Rothkegel, H., Antal, A., and Paulus, W. (2016). Monitoring transcranial direct current stimulation induced changes in cortical excitability during the serial reaction time task. *Neurosci. Lett*. 616, 98–104. doi: 10.1016/j.neulet.2016.01.039

Andrade, C. (2013). Once- to twice-daily, 3-year domiciliary maintenance transcranial direct current stimulation for severe, disabling, clozapine-refractory continuous auditory hallucinations in schizophrenia. *J. ECT* 29, 239–242. doi: 10.1097/YCT.0b013e3182843866

Angius, L., Hopker, J., and Mauger, A. R. (2017). The ergogenic effects of transcranial direct current stimulation on exercise performance. *Front. Physiol.* 8:90. doi: 10.3389/fphys.2017.00090

Antal, A., Keeser, D., Priori, A., Padberg, F., and Nitsche, M. A. (2015). Conceptual and procedural shortcomings of the systematic review "Evidence That Transcranial Direct Current Stimulation (tDCS) generates little-to-no reliable neurophysiologic effect beyond MEP amplitude modulation in healthy human subjects: a systematic review." *Brain Stimul*. 8, 846–849. doi: 10.1016/j.brs.2015.05.010

Apšvalka, D., Ramsey, R., and Cross, E. S. (2018). Anodal tDCS over primary motor cortex provides no advantage to learning motor sequences via observation. *Neural Plast*. 2018:1237962. doi: 10.1155/2018/1237962

Arias, P., Corral-Bergantiños, Y., Robles-García, V., Madrid, A., Oliviero, A., and Cudeiro, J. (2016). Bilateral tDCS on primary motor cortex: effects on fast arm reaching tasks. *PLoS ONE* 11:e0160063. doi: 10.1371/journal.pone.0160063

Baker, J. M., Rorden, C., and Fridriksson, J. (2010). Using transcranial direct-current stimulation to treat stroke patients with Aphasia. *Stroke* 41, 1229–1236. doi: 10.1161/STROKEAHA.109.576785

Bandeira, I. D., Guimarães, R. S. Q., Jagersbacher, J. G., Barretto, T. L., de Jesus-Silva, J. R., Santos, S. N., et al. (2016). Transcranial direct current stimulation in children and adolescents with attention-deficit/hyperactivity disorder (ADHD). *J. Child Neurol*. 31, 918–924. doi: 10.1177/0883073816630083

Bastani, A., and Jaberzadeh, S. (2012). Does anodal transcranial direct current stimulation enhance excitability of the motor cortex and motor function in healthy individuals and subjects with stroke: a systematic review and meta-analysis. *Clin. Neurophysiol*. 123, 644–657. doi: 10.1016/j.clinph.2011.08.029

Bikson, M., Grossman, P., Thomas, C., Zannou, A. L., Jiang, J., Adnan, T., et al. (2016). Safety of transcranial direct current stimulation: evidence based update 2016. *Brain Stimul*. 9, 641–661. doi: 10.1016/j.brs.2016.06.004

Bindman, L. J., Lippold, O. C. J., and Redfearn, J. W. T. (1964). The action of brief polarizing currents on the cerebral cortex of the rat (1) during current flow and (2) in the production of long-lasting after-effects. *J. Physiol*. 172, 369–382. doi: 10.1113/jphysiol.1964.sp007425

Block, H., and Celnik, P. (2013). Stimulating the cerebellum affects visuomotor adaptation but not intermanual transfer of learning. *Cerebllleum* 12, 781–793. doi: 10.1007/s12311-013-0486-7

Boggio, P. S., Castro, L. O., Savagim, E. A., Braite, R., Cruz, V. C., Rocha, R. R., et al. (2006). Enhancement of non-dominant hand motor function by anodal transcranial direct current stimulation. *Neurosci. Lett*. 404, 232–236. doi: 10.1016/j.neulet.2006.05.051

Breitling, C., Zaehle, T., Dannhauer, M., Bonath, B., Tegelbeckers, J., Flechtner, H. H., et al. (2016). Improving interference control in ADHD patients with transcranial direct current stimulation (tDCS). *Front. Cell. Neurosci*. 10:72. doi: 10.3389/fncel.2016.00072

Brunoni, A. R., Amadera, J., Berbel, B., Volz, M. S., Rizzerio, B. G., and Fregni, F. (2011). A systematic review on reporting and assessment of adverse effects associated with transcranial direct current stimulation. *Int. J. Neuropsychopharmacol.* 14, 1133–1145. doi: 10.1017/S1461145710001690

Brunoni, A. R., Nitsche, M. A., Bolognini, N., Bikson, M., Wagner, T., Merabet, L., et al. (2012). Clinical research with transcranial direct current stimulation (tDCS): challenges and future directions. *Brain Stimul.* 5, 175–195. doi: 10.1016/j.brs.2011.03.002

Buch, E. R., Santarnecchi, E., Antal, A., Born, J., Celnik, P. A., Classen, J., et al. (2017). Effects of tDCS on motor learning and memory formation: a consensus and critical position paper. *Clin. Neurophysiol.* 128, 589–603. doi: 10.1016/j.clinph.2017.01.004

Cantarero, G., Spampinato, D., Reis, J., Ajagbe, L., Thompson, T., Kulkarni, K., et al. (2015). Cerebellar direct current stimulation enhances on-line motor skill acquisition through an effect on accuracy. *J. Neurosci.* 35, 3285–3290. doi: 10.1523/JNEUROSCI.2885-14.2015

Carlsen, A. N., Eagles, J. S., and MacKinnon, C. D. (2015). Transcranial direct current stimulation over the supplementary motor area modulates the preparatory activation level in the human motor system. *Behav. Brain Res.* 279, 68–75. doi: 10.1016/j.bbr.2014.11.009

Carter, M. J., Maslovat, D., and Carlsen, A. N. (2017). Intentional switches between coordination patterns are faster following anodal-tDCS applied over the supplementary motor area. *Brain Stimul.* 10, 162–164. doi: 10.1016/j.brs.2016.11.002

Chhatbar, P. Y., Chen, R., Deardorff, R., Dellenbach, B., Kautz, S. A., George, M. S., et al. (2017). Safety and tolerability of transcranial direct current stimulation to stroke patients - A phase I current escalation study. *Brain Stimul.* 10, 553–559. doi: 10.1016/j.brs.2017.02.007

Chothia, M., Doeltgen, S., and Bradnam, L. V. (2016). Anodal cerebellar direct current stimulation reduces facilitation of propriospinal neurons in healthy humans. *Brain Stimul.* 9, 364–371. doi: 10.1016/j.brs.2016.01.002

Ciechanski, P., Cheng, A., Lopushinsky, S., Hecker, K., Gan, L. S., Lang, S., et al. (2017). Effects of transcranial direct-current stimulation on neurosurgical skill acquisition: a randomized controlled trial. *World Neurosurg.* 108, 876–884.e4. doi: 10.1016/j.wneu.2017.08.123

Cogiamanian, F., Marceglia, S., Ardolino, G., Barbieri, S., and Priori, A. (2007). Improved isometric force endurance after transcranial direct current stimulation over the human motor cortical areas. *Eur. J. Neurosci.* 26, 242–249. doi: 10.1111/j.1460-9568.2007.05633.x

Convento, S., Bolognini, N., Fusaro, M., Lollo, F., and Vallar, G. (2014). Neuromodulation of parietal and motor activity affects motor planning and execution. *CORTEX* 57, 51–59. doi: 10.1016/j.cortex.2014.03.006

Cuypers, K., Leenus, D. J. F., van den Berg, F. E., Nitsche, M. A., Thijs, H., Wenderoth, N., et al. (2013). Is motor learning mediated by tDCS intensity? *PLoS ONE* 8:e67344. doi: 10.1371/journal.pone.0067344

Dedoncker, J., Brunoni, A. R., Baeken, C., and Vanderhasselt, M. A. (2016). A systematic review and meta-analysis of the effects of transcranial direct current stimulation (tDCS) over the dorsolateral prefrontal cortex in healthy and neuropsychiatric samples: influence of stimulation parameters. *Brain Stimul.* 9, 501–517. doi: 10.1016/j.brs.2016.04.006

Doppelmayr, M., Pixa, N. H., and Steinberg, F. (2016). Cerebellar, but not motor or parietal, high-density anodal transcranial direct current stimulation facilitates motor adaptation. *J. Int. Neuropsychol. Soc.* 22, 928–936. doi: 10.1017/S1355617716000345

Doyon, J., Bellec, P., Amsel, R., Penhune, V., Monchi, O., Carrier, J., et al. (2009). Contributions of the basal ganglia and functionally related brain structures to motor learning. *Behav. Brain Res.* 199, 61–75. doi: 10.1016/j.bbr.2008.11.012

Doyon, J., Song, A. W., Karni, A., Lalonde, F., Adams, M. M., and Ungerleider, L. G. (2002). Experience-dependent changes in cerebellar contributions to motor sequence learning. *Proc. Natl. Acad. Sci. U.S.A.* 99, 1017–1022. doi: 10.1073/pnas.022615199

Dumel, G., Bourassa, M.-È., Charlebois-Plante, C., Desjardins, M., Doyon, J., Saint-Amour, D., et al. (2018). Multisession anodal transcranial direct current stimulation induces motor cortex plasticity enhancement and motor learning generalization in an aging population. *Clin. Neurophysiol.* 129, 494–502. doi: 10.1016/j.clinph.2017.10.041

Dumel, G., Bourassa, M. E., Desjardins, M., Voarino, N., Charlebois-Plante, C., Doyon, J., et al. (2016). Multisession anodal tDCS protocol improves motor system function in an aging population. *Neural Plast.* 2016, 15–18. doi: 10.1155/2016/5961362

Edwards, D. J., Cortes, M., Wortman-Jutt, S., Putrino, D., Bikson, M., Thickbroom, G., et al. (2017). Transcranial direct current stimulation and sports performance. *Front. Hum. Neurosci.* 11:243. doi: 10.3389/fnhum.2017.00243

Ehsani, F., Bakhtiary, A. H., Jaberzadeh, S., Talimkhani, A., and Hajihasani, A. (2016). Differential effects of primary motor cortex and cerebellar transcranial direct current stimulation on motor learning in healthy individuals: a randomized double-blind sham-controlled study. *Neurosci. Res.* 112, 10–19. doi: 10.1016/j.neures.2016.06.003

Fagerlund, A. J., Hansen, O. A., and Aslaksen, P. M. (2015). Transcranial direct current stimulation as a treatment for patients with fibromyalgia. *Pain* 156, 62–71. doi: 10.1016/j.pain.0000000000000006

Fenton, B. W., Palmieri, P. A., Boggio, P., Fanning, J., and Fregni, F. (2009). A preliminary study of transcranial direct current stimulation for the treatment of refractory chronic pelvic pain. *Brain Stimul.* 2, 103–107. doi: 10.1016/j.brs.2008.09.009

Ferrucci, R., Brunoni, A. R., Parazzini, M., Vergari, M., Rossi, E., Fumagalli, M., et al. (2013). Modulating human procedural learning by cerebellar transcranial direct current stimulation centro clinico per la neurostimolazione, le neurotecnologie ed i disordini del movimento, fondazione IRCCS Ca' granda. *Cerebellum* 12, 485–492. doi: 10.1007/s12311-012-0436-9

Floyer-Lea, A., and Matthews, P. M. (2005). Distinguishable brain activation networks for short- and long-term motor skill learning. *J. Neurophysiol.* 94, 512–518. doi: 10.1152/jn.00717.2004

Focke, J., Kemmet, S., Krause, V., Keitel, A., and Pollok, B. (2017). Cathodal transcranial direct current stimulation (tDCS) applied to the left premotor cortex (PMC) stabilizes a newly learned motor sequence. *Behav. Brain Res.* 316, 87–93. doi: 10.1016/j.bbr.2016.08.032

Frazer, A., Williams, J., Spittles, M., Rantalainen, T., and Kidgell, D. (2016). Anodal transcranial direct current stimulation of the motor cortex increases cortical voluntary activation and neural plasticity. *Muscle Nerve* 54, 903–913. doi: 10.1002/mus.25143

Frazer, A. K., Williams, J., Spittle, M., and Kidgell, D. J. (2017). Cross-education of muscular strength is facilitated by homeostatic plasticity. *Eur. J. Appl. Physiol.* 117, 665–677. doi: 10.1007/s00421-017-3538-8

Fregni, F., Boggio, P. S., Lima, M. C., Ferreira, M. J. L., Wagner, T., Rigonatti, S. P., et al. (2006). A sham-controlled, phase II trial of transcranial direct current stimulation for the treatment of central pain in traumatic spinal cord injury. *Pain* 122, 197–209. doi: 10.1016/j.pain.2006.02.023

Fregni, F., Nitsche, M., Loo, C., Brunoni, A., Marangolo, P., Leite, J., et al. (2016). Regulatory considerations for the clinical and research use of transcranial direct current stimulation (tDCS): review and recommendations from an expert panel. *Clin. Res. Regul. Aff.* 32, 22–35. doi: 10.3109/10601333.2015.980944

Furuya, S., Klaus, M., Nitsche, M. A., Paulus, W., and Altenmüller, E. (2014). Ceiling effects prevent further improvement of transcranial stimulation in skilled musicians. *J. Neurosci.* 34, 13834–13839. doi: 10.1523/JNEUROSCI.1170-14.2014

Galea, J. M., Vazquez, A., Pasricha, N., de Xivry, J.-J. O., and Celnik, P. (2011). Dissociating the roles of the cerebellum and motor cortex during adaptive learning: the motor cortex retains what the cerebellum learns. *Cereb. Cortex* 21, 1761–1770. doi: 10.1093/cercor/bhq246

Giordano, J., Bikson, M., Kappenman, E. S., Clark, V. P., Branch Coslett, H., Hamblin, M. R., et al. (2017). Mechanisms and effects of transcranial direct current stimulation. *Dose-Response* 15:1559325816685467. doi: 10.1177/1559325816685467

Gomes-Osman, J., and Field-Fote, E. C. (2013). Bihemispheric anodal corticomotor stimulation using transcranial direct current stimulation improves bimanual typing task performance. *J. Mot. Behav.* 45, 361–367. doi: 10.1080/00222895.2013.808604

Goodwill, A. M., Reynolds, J., Daly, R. M., and Kidgell, D. J. (2013). Formation of cortical plasticity in older adults following tDCS and motor training. *Front. Aging Neurosci.* 5:87. doi: 10.3389/fnagi.2013.00087

Hardwick, R. M., and Celnik, P. A. (2014). Cerebellar direct current stimulation enhances motor learning in older adults. *Neurobiol. Aging* 35, 2217–2221. doi: 10.1016/j.neurobiolaging.2014.03.030

Hardwick, R. M., Rottschy, C., Miall, R. C., and Eickhoff, S. B. (2013). A quantitative meta-analysis and review of motor learning in the human brain. *Neuroimage* 67, 283–297. doi: 10.1016/j.neuroimage.2012.11.020

Hashemirad, F., Fitzgerald, P. B., Zoghi, M., and Jaberzadeh, S. (2017). Single-session anodal tDCS with small-size stimulating electrodes over frontoparietal superficial sites does not affect motor sequence learning. *Front. Hum. Neurosci.* 11:153. doi: 10.3389/fnhum.2017.00153

Hashemirad, F., Zoghi, M., Fitzgerald, P. B., and Jaberzadeh, S. (2016). The effect of anodal transcranial direct current stimulation on motor sequence learning in healthy individuals: a systematic review and meta-analysis. *Brain Cogn.* 102, 1–12. doi: 10.1016/j.bandc.2015.11.005

Heise, K.-F., Niehoff, M., Feldheim, J.-F., Liuzzi, G., Gerloff, C., and Hummel, F. C. (2014). Differential behavioral and physiological effects of anodal transcranial direct current stimulation in healthy adults of younger and older age. *Front. Aging Neurosci.* 6:146. doi: 10.3389/fnagi.2014.00146

Hendy, A. M., and Kidgell, D. J. (2013). Anodal tDCS applied during strength training enhances motor cortical plasticity. *Med. Sci. Sport. Exerc.* 45, 1721–1729. doi: 10.1249/MSS.0b013e31828d2923

Hendy, A. M., and Kidgell, D. J. (2014). Anodal-tDCS applied during unilateral strength training increases strength and corticospinal excitability in the untrained homologous muscle. *Exp. Brain Res.* 232:3243. doi: 10.1007/s00221-014-4016-8

Hendy, A. M., Teo, W., and Kidgell, D. J. (2015). Anodal transcranial direct current stimulation prolongs the cross-education of strength and corticomotor plasticity. *Med. Sci. Sport. Exerc.* 47, 1788–1797. doi: 10.1249/MSS.0000000000000600

Herzfeld, D. J., Pastor, D., Haith, A. M., Rossetti, Y., Shadmehr, R., and O'Shea, J. (2014). Contributions of the cerebellum and the motor cortex to acquisition and retention of motor memories. *Neuroimage* 98, 147–158. doi: 10.1016/j.neuroimage.2014.04.076

Higgins, J. P. T., and Green, S. (eds). (2011). *Cochrane Handbook for Systematic Reviews of Interventions Version 5.1.0 [updated March 2011]*. The Cochrane Collaboration. Available online at: www.handbook.cochrane.org

Horvath, J. C., Carter, O., and Forte, J. D. (2016). No significant effect of transcranial direct current stimulation (tDCS) found on simple motor reaction time comparing 15 different simulation protocols. *Neuropsychologia* 91, 544–552. doi: 10.1016/j.neuropsychologia.2016.09.017

Huang, L., Deng, Y., Zheng, X., and Liu, Y. (2019). Transcranial direct current stimulation with halo sport enhances repeated sprint cycling and cognitive performance. *Front. Physiol.* 10:118. doi: 10.3389/fphys.2019.00118

Hummel, F. C., Heise, K., Celnik, P., Floel, A., Gerloff, C., and Cohen, L. G. (2010). Facilitating skilled right hand motor function in older subjects by anodal polarization over the left primary motor cortex. *Neurobiol. Aging* 31, 2160–2168. doi: 10.1016/j.neurobiolaging.2008.12.008

Jadad, A., Moore, R., Carroll, D., Jenkinson, C., Reynolds, J., Gavaghan, D., et al. (1996). Assessing the quality of reports of randomized clinical trials: is blinding necessary? *Control. Clin. Trials* 17, 1–12. doi: 10.1016/0197-2456(95)00134-4

Jenkins, I. H., Brooks, D. J., Nixon, P. D., Frackowiak, R. S. J., and Passingham, F. E. (1994). Motor sequence learning: a study with positron emission tomography. *J. Neurosci.* 14, 3775–3790. doi: 10.1523/JNEUROSCI.14-06-03775.1994

Kaminski, E., Steele, C. J., Hoff, M., Gundlach, C., Rjosk, V., Sehm, B., et al. (2016). Transcranial direct current stimulation (tDCS) over primary motor cortex leg area promotes dynamic balance task performance. *Clin. Neurophysiol.* 127, 2455–2462. doi: 10.1016/j.clinph.2016.03.018

Kan, B., Dundas, J. E., and Nosaka, K. (2013). Effect of transcranial direct current stimulation on elbow flexor maximal voluntary isometric strength and endurance. *Appl. Physiol. Nutr. Metab.* 38, 734–739. doi: 10.1139/apnm-2012-0412

Kang, E. K., and Paik, N.-J. (2011). Effect of a tDCS electrode montage on implicit motor sequence learning in healthy subjects. *Exp. Transl. Stroke Med.* 3:4. doi: 10.1186/2040-7378-3-4

Kantak, S. S., Mummidisetty, C. K., and Stinear, J. W. (2012). Primary motor and premotor cortex in implicit sequence learning - evidence for competition between implicit and explicit human motor memory systems. *Eur. J. Neurosci.* 36, 2710–2715. doi: 10.1111/j.1460-9568.2012.08175.x

Karni, A., Meyer, G., Jezzard, P., Adams, M. M., Turner, R., and Ungerleider, L. G. (1995). Functional MRI evidence for adult motor cortex plasticity during motor skill learning. *Nature* 377, 155–158. doi: 10.1038/377155a0

Karok, S., Fletcher, D., and Witney, A. G. (2017). Task-specificity of unilateral anodal and dual-M1 tDCS effects on motor learning. *Neuropsychologia* 94, 84–95. doi: 10.1016/j.neuropsychologia.2016.12.002

Karok, S., and Witney, A. G. (2013). Enhanced motor learning following task-concurrent dual transcranial direct current stimulation. *PLoS ONE* 8:e85693. doi: 10.1371/journal.pone.0085693

Kaski, D., Dominguez, R., Allum, J., Islam, A., and Bronstein, A. (2014). Combining physical training with transcranial direct current stimulation to improve gait in Parkinson's disease: a pilot randomized controlled study. *Clin. Rehabil.* 28, 1115–1124. doi: 10.1177/0269215514534277

Kidgell, D. J., Goodwill, A. M., Frazer, A. K., and Daly, R. M. (2013). Induction of cortical plasticity and improved motor performance following unilateral and bilateral transcranial direct current stimulation of the primary motor cortex. *BMC Neurosci.* 14:64. doi: 10.1186/1471-2202-14-64

Koyama, S., Tanaka, S., Tanabe, S., and Sadato, N. (2015). Dual-hemisphere transcranial direct current stimulation over primary motor cortex enhances consolidation of a ballistic thumb movement. *Neurosci. Lett.* 588, 49–53. doi: 10.1016/j.neulet.2014.11.043

Krishnan, C., Ranganathan, R., Kantak, S. S., Dhaher, Y. Y., and Rymer, W. Z. (2014). Anodal transcranial direct current stimulation alters elbow flexor muscle recruitment strategies. *Brain Stimul.* 7, 443–450. doi: 10.1016/j.brs.2014.01.057

Krishnan, C., Santos, L., Peterson, M. D., and Ehinger, M. (2015). Safety of noninvasive brain stimulation in children and adolescents. *Brain Stimul.* 8, 76–87. doi: 10.1016/j.brs.2014.10.012

Lampropoulou, S. I., and Nowicky, A. V. (2013). The effect of transcranial direct current stimulation on perception of effort in an isolated isometric elbow flexion task. *Motor Control* 17, 412–426. doi: 10.1123/mcj.17.4.412

Lang, N., Siebner, H. R., Ward, N. S., Lee, L., Nitsche, M. A., Paulus, W., et al. (2005). How does transcranial DC stimulation of the primary motor cortex alter regional neuronal activity in the human brain? Europe PMC funders group. *Eur. J. Neurosci.* 22, 495–504. doi: 10.1111/j.1460-9568.2005.04233.x

Lattari, E., Oliveira, B. R. R., Monteiro Júnior, R. S., Marques Neto, S. R., Oliveira, A. J., Maranhão Neto, G. A., et al. (2018). Acute effects of single dose transcranial direct current stimulation on muscle strength: a systematic review and meta-analysis. *PLoS ONE* 13:e0209513. doi: 10.1371/journal.pone.0209513

Leite, J., Carvalho, S., Fregni, F., and Gonçalves, Ó. F. (2011). Task-specific effects of tDCS-induced cortical excitability changes on cognitive and motor sequence set shifting performance. *PLoS ONE* 6:e24140. doi: 10.1371/journal.pone.0024140

Liebetanz, D., Nitsche, M. A., Tergau, F., and Paulus, W. (2002). Pharmacological approach to the mechanisms of transcranial DC-stimulation-induced after-effects of human motor cortex excitability. *Brain* 125, 2238–2247. doi: 10.1093/brain/awf238

Lindenberg, R., Nachtigall, L., Meinzer, M., Sieg, M. M., and Flöel, A. (2013). Differential effects of dual and unihemispheric motor cortex stimulation in older adults. *J. Neurosci.* 33, 9176–9183. doi: 10.1523/JNEUROSCI.0055-13.2013

Lindenberg, R., Sieg, M. M., Meinzer, M., Nachtigall, L., and Flöel, A. (2016). Neural correlates of unihemispheric and bihemispheric motor cortex stimulation in healthy young adults. *Neuroimage* 140, 141–149. doi: 10.1016/j.neuroimage.2016.01.057

Loo, C. K., Alonzo, A., Martin, D., Mitchell, P. B., Galvez, V., and Sachdev, P. (2012). Transcranial direct current stimulation for depression: 3-week, randomised, sham-controlled trial. *Br. J. Psychiatry* 200, 52–59. doi: 10.1192/bjp.bp.111.097634

Lopez-Alonso, V., del Olmo, F. M., Liew, S.-L., Fernández del Olmo, M., and Cheeran, B. (2018). A preliminary comparison of motor learning across different non-invasive brain stimulation paradigms shows no consistent modulations. *Front. Neurosci.* 1:253. doi: 10.3389/fnins.2018.00253

Machado, D. G. D. S., Unal, G., Andrade, S. M., Moreira, A., and Altimari, L. R. (2019). Effect of transcranial direct current stimulation on exercise performance: a systematic review and meta-analysis. *Brain Stimul.* 12:593–605. doi: 10.1016/j.brs.2018.12.227

Marquez, J., Conley, A., Karayanidis, F., Lagopoulos, J., and Parsons, M. (2015). Anodal direct current stimulation in the healthy aged: effects determined by the hemisphere stimulated. *Restor. Neurol. Neurosci.* 33, 509–519. doi: 10.3233/RNN-140490

Matsumoto, H., and Ugawa, Y. (2017). Adverse events of tDCS and tACS: a review. *Clin. Neurophysiol. Pract.* 2, 19–25. doi: 10.1016/j.cnp.2016.12.003

Matsuo, A., Maeoka, H., Hiyamizu, M., Shomoto, K., Morioka, S., and Seki, K. (2011). Enhancement of precise hand movement by transcranial direct current stimulation. *Neuroreport* 22, 78–82. doi: 10.1097/WNR.0b013e32834298b3

Mccambridge, A. B., Stinear, J. W., and Byblow, W. D. (2016). Neurophysiological and behavioural effects of dual-hemisphere transcranial direct current stimulation on the proximal upper limb. *Exp. Brain Res.* 234, 1419–1428. doi: 10.1007/s00221-015-4547-7

Medina, J., and Cason, S. (2017). No evidential value in samples of transcranial direct current stimulation (tDCS) studies of cognition and working memory in healthy populations. *Cortex* 94, 131–141. doi: 10.1016/j.cortex.2017.06.021

Mizuguchi, N., Katayama, T., and Kanosue, K. (2018). The effect of cerebellar transcranial direct current stimulation on a throwing task depends on individual level of task performance. *Neuroscience* 371:119–125. doi: 10.1016/j.neuroscience.2017.11.048

Naros, G., Geyer, M., Koch, S., Mayr, L., Ellinger, T., Grimm, F., et al. (2016). Enhanced motor learning with bilateral transcranial direct current stimulation: impact of polarity or current flow direction? *Clin. Neurophysiol.* 127, 2119–2126. doi: 10.1016/j.clinph.2015.12.020

Nikolin, S., Huggins, C., Martin, D., Alonzo, A., and Loo, C. K. (2018). Safety of repeated sessions of transcranial direct current stimulation: a systematic review. *Brain Stimul.* 11, 278–288. doi: 10.1016/j.brs.2017.10.020

Nilsson, J., Lebedev, A. V., Rydström, A., and Lövdén, M. (2017). Direct-current stimulation does little to improve the outcome of working memory training in older adults. *Psychol. Sci.* 28, 907–920. doi: 10.1177/0956797617698139

Nitsche, M. A., Jakoubkova, M., Thirugnanasambandam, N., Schmalfuss, L., Hullemann, S., Sonka, K., et al. (2010). Contribution of the premotor cortex to consolidation of motor sequence learning in humans during sleep. *J. Neurophysiol.* 104, 2603–2614. doi: 10.1152/jn.00611.2010

Nitsche, M. A., Niehaus, L., Hoffmann, K. T., Hengst, S., Liebetanz, D., Paulus, W., et al. (2004). MRI study of human brain exposed to weak direct current stimulation of the frontal cortex. *Clin. Neurophysiol.* 115, 2419–2423. doi: 10.1016/j.clinph.2004.05.001

Nitsche, M. A., Nitsche, M. S., Klein, C. C., Tergau, F., Rothwell, J. C., and Paulus, W. (2003a). Level of action of cathodal DC polarisation induced inhibition of the human motor cortex. *Clin. Neurophysiol.* 114, 600–604. doi: 10.1016/S1388-2457(02)00412-1

Nitsche, M. A., and Paulus, W. (2000). Excitability changes induced in the human motor cortex by weak transcranial direct current stimulation. *J. Physiol.* 527, 633–639. doi: 10.1111/j.1469-7793.2000.t01-1-00633.x

Nitsche, M. A., and Paulus, W. (2001). Sustained excitability elevations induced by transcranial DC motor cortex stimulation in humans. *Neurology* 57, 1899–1901. doi: 10.1212/WNL.57.10.1899

Nitsche, M. A., Schauenburg, A., Lang, N., Liebetanz, D., Exner, C., Paulus, W., et al. (2003b). Facilitation of implicit motor learning by weak transcranial direct current stimulation of the primary motor cortex in the human facilitation of implicit motor learning by weak transcranial direct current stimulation of the primary motor cortex in the human. *J. Cogn. Neurosci.* 15, 619–626. doi: 10.1162/089892903321662994

Okano, A. H., Fontes, E. B., Montenegro, R. A., Farinatti, P., de, T. V., Cyrino, E. S., et al. (2015). Brain stimulation modulates the autonomic nervous system, rating of perceived exertion and performance during maximal exercise. *Br. J. Sports Med.* 49, 1213–1218. doi: 10.1136/bjsports-2012-091658

Oki, K., Mahato, N. K., Nakazawa, M., Amano, S., France, C. R., Russ, D. W., et al. (2016). Preliminary evidence that excitatory transcranial direct current stimulation extends time to task failure of a sustained, submaximal muscular contraction in older adults. *J. Gerontol. Biol. Sci. Med. Sci.* 71, 1109–1112. doi: 10.1093/gerona/glw011

Palm, U., Schiller, C., Fintescu, Z., Obermeier, M., Keeser, D., Reisinger, E., et al. (2012). Transcranial direct current stimulation in treatment resistant depression: a randomized double-blind, placebo-controlled study. *Brain Stimul.* 5, 242–251. doi: 10.1016/j.brs.2011.08.005

Palm, U., Segmiller, F. M., Epple, A. N., Freisleder, F.-J., Koutsouleris, N., Schulte-Körne, G., et al. (2016). Transcranial direct current stimulation in children and adolescents: a comprehensive review. *J. Neural Transm.* 123, 1219–1234. doi: 10.1007/s00702-016-1572-z

Paneri, B., Khadka, N., Patel, V., Thomas, C., Tyler, W., Parra, L. C., et al. (2015). The tolerability of transcranial electrical stimulation used across extended periods in a naturalistic context by healthy individuals. *PeerJ.* 3:e1097v2. doi: 10.7287/peerj.preprints.1097v2

Panouilieres, M. T. N., Joundi, R. A., Brittain, J.-S., and Jenkinson, N. (2015). The journal of physiology neuroscience C 2015 the authors. *J. Physiol.* 593, 3645–3655. doi: 10.1113/JP270484

Parikh, P. J., and Cole, K. J. (2014). Effects of transcranial direct current stimulation in combination with motor practice on dexterous grasping and manipulation in healthy older adults. *Physiol. Rep.* 2:e00255. doi: 10.1002/phy2.255

Park, S.-B., Sung, D. J., Kim, B., Kim, S., and Han, J.-K. (2019). Transcranial direct current Stimulation of motor cortex enhances running performance. *PLoS ONE* 14:e0211902. doi: 10.1371/journal.pone.0211902

Pixa, N. H., and Pollok, B. (2018). Effects of tDCS on bimanual motor skills: a brief review. *Front. Behav. Neurosci.* 12:63. doi: 10.3389/fnbeh.2018.00063

Pixa, N. H., Steinberg, F., and Doppelmayr, M. (2017a). Effects of high-definition anodal transcranial direct current stimulation applied simultaneously to both primary motor cortices on bimanual sensorimotor performance. *Front. Behav. Neurosci.* 11:130. doi: 10.3389/fnbeh.2017.00130

Pixa, N. H., Steinberg, F., and Doppelmayr, M. (2017b). High-definition transcranial direct current stimulation to both primary motor cortices improves unimanual and bimanual dexterity. *Neurosci. Lett.* 643, 84–88. doi: 10.1016/j.neulet.2017.02.033

Prichard, G., Weiller, C., Fritsch, B., and Reis, J. (2014). Effects of different electrical brain stimulation protocols on subcomponents of motor skill learning. *Brain Stimul.* 7, 532–540. doi: 10.1016/j.brs.2014.04.005

Radel, R., Tempest, G., Denis, G., Besson, P., and Zory, R. (2017). Extending the limits of force endurance: stimulation of the motor or the frontal cortex? *Cortex* 97, 96–108. doi: 10.1016/j.cortex.2017.09.026

Reis, J., and Fritsch, B. (2011). Modulation of motor performance and motor learning by transcranial direct current stimulation. *Curr. Opin. Neurol.* 24, 590–596. doi: 10.1097/WCO.0b013e32834c3db0

Reis, J., Schambra, H. M., Cohen, L. G., Buch, E. R., Fritsch, B., Zarahn, E., et al. (2009). Noninvasive cortical stimulation enhances motor skill acquisition over multiple days through an effect on consolidation. *Proc. Natl. Acad. Sci. U.S.A.* 106, 1590–1595. doi: 10.1073/pnas.0805413106

Rroji, O., van Kuyck, K., Nuttin, B., and Wenderoth, N. (2015). Anodal tDCS over the primary motor cortex facilitates long-term memory formation reflecting use-dependent plasticity. *PLoS ONE* 10:e0127270. doi: 10.1371/journal.pone.0127270

Rumpf, J.-J., Wegscheider, M., Hinselmann, K., Fricke, C., King, B. R., Weise, D., et al. (2017). Enhancement of motor consolidation by post-training transcranial direct current stimulation in older people. *Neurobiol. Aging* 49, 1–8. doi: 10.1016/j.neurobiolaging.2016.09.003

Samaei, A., Ehsani, F., Zoghi, M., Hafez Yosephi, M., and Jaberzadeh, S. (2017). Online and offline effects of cerebellar transcranial direct current stimulation on motor learning in healthy older adults: a randomized double-blind sham-controlled study. *Eur. J. Neurosci.* 45, 1177–1185. doi: 10.1111/ejn.13559

Saruco, E., Di Rienzo, F., Nunez-Nagy, S., Rubio-Gonzalez, M. A., Jackson, P. L., Collet, C., et al. (2017). Anodal tDCS over the primary motor cortex improves motor imagery benefits on postural control: a pilot study. *Sci. Rep.* 7:480. doi: 10.1038/s41598-017-00509-w

Saucedo Marquez, C. M., Zhang, X., Swinnen, S. P., Meesen, R., and Wenderoth, N. (2013). Task-specific effect of transcranial direct current stimulation on motor learning. *Front. Hum. Neurosci.* 7:333. doi: 10.3389/fnhum.2013.00333

Schambra, H. M., Abe, M., Luckenbaugh, D. A., Reis, J., Krakauer, J. W., and Cohen, L. G. (2011). Probing for hemispheric specialization for motor skill learning: a transcranial direct current stimulation study. *J. Neurophysiol.* 106, 652–661. doi: 10.1152/jn.00210.2011

Schmidt, S., Fleischmann, R., Bathe-Peters, R., Irlbacher, K., and Brandt, S. A. (2013). Evolution of premotor cortical excitability after cathodal inhibition of the primary motor cortex: a sham-controlled serial navigated TMS study. *PLoS ONE* 8:e57425. doi: 10.1371/journal.pone.0057425

Shimizu, R. E., Wu, A. D., Samra, J. K., and Knowlton, B. J. (2017). The impact of cerebellar transcranial direct current stimulation (tDCS) on learning fine-motor sequences. *Philos. Trans. R. Soc. Lond. Ser. B Biol. Sci.* 372:20160050. doi: 10.1098/rstb.2016.0050

Simonsmeier, B. A., Grabner, R. H., Hein, J., Krenz, U., and Schneider, M. (2018). Electrical brain stimulation (tES) improves learning more than performance: a meta-analysis. *Neurosci. Biobehav. Rev.* 84, 171–181. doi: 10.1016/j.neubiorev.2017.11.001

Sohn, M. K., Kim, B. O., and Song, H. T. (2012). Effect of stimulation polarity of transcranial direct current stimulation on non-dominant hand function. *Ann. Rehabil. Med.* 36, 1–7. doi: 10.5535/arm.2012.36.1.1

Stagg, C. J., Jayaram, G., Pastor, D., Kincses, Z. T., Matthews, P. M., and Johansen-Berg, H. (2011). Polarity and timing-dependent effects of transcranial direct current stimulation in explicit motor learning. *Neuropsychologia* 49, 800–804. doi: 10.1016/j.neuropsychologia.2011.02.009

Summers, R. L. S., Chen, M., Hatch, A., Kimberley, T. J., Perrey, S., Brighina, F., et al. (2018). Cerebellar transcranial direct current stimulation modulates corticospinal excitability during motor training. *Front. Hum. Neurosci.* 12:118. doi: 10.3389/fnhum.2018.00118

Tadini, L., El-Nazer, R., Brunoni, A. R., Williams, J., Carvas, M., Boggio, P., et al. (2011). Cognitive, mood, and electroencephalographic effects of noninvasive cortical stimulation with weak electrical currents. *J. ECT* 27, 134–140. doi: 10.1097/YCT.0b013e3181e631a8

Tan, A., Ashrafian, H., Scott, A. J., Mason, S. E., Harling, L., Athanasiou, T., et al. (2016). Robotic surgery: disruptive innovation or unfulfilled promise? A systematic review and meta-analysis of the first 30 years. *Surg. Endosc.* 30, 4330–52. doi: 10.1007/s00464-016-4752-x

Taubert, M., Stein, T., Kreutzberg, T., Stockinger, C., Hecker, L., Focke, A., et al. (2016). Remote effects of non-invasive cerebellar stimulation on error processing in motor re-learning. *Brain Stimul.* 9, 692–699. doi: 10.1016/j.brs.2016.04.007

Tecchio, F., Zappasodi, F., Assenza, G., Tombini, M., Vollaro, S., Barbati, G., et al. (2010). Anodal transcranial direct current stimulation enhances procedural consolidation. *J. Neurophysiol.* 104, 1134–1140. doi: 10.1152/jn.00661.2009

Toni, I., Krams, M., Turner, R., and Passingham, R. (1998). The time course of changes during motor sequence learning: a whole-brain fMRI study. *Neuroimage* 8, 50–61. doi: 10.1006/nimg.1998.0349

Ungerleider, L. G., Doyon, J., and Karni, A. (2002). Imaging brain plasticity during motor skill learning. *Neurobiol. Learn. Mem.* 78, 553–564. doi: 10.1006/nlme.2002.4091

van Tulder, M., Furlan, A., Bombardier, C., and Bouter, L. (2003) Editorial Board of the Cochrane Collaboration Back Review G. Updated Method Guidelines for Systematic Reviews in the Cochrane Collaboration Back Review Group. *Spine* 28, 1290–1299. doi: 10.1097/01.BRS.0000065484.95996.AF

Vergallito, A., Romero Lauro, L. J., Bonandrini, R., Zapparoli, L., Danelli, L., and Berlingeri, M. (2018). What is difficult for you can be easy for me. Effects of increasing individual task demand on prefrontal lateralization: a tDCS study. *Neuropsychologia* 109, 283–294. doi: 10.1016/j.neuropsychologia.2017.12.038

Vines, B. W., Cerruti, C., and Schlaug, G. (2008a). Dual-hemisphere tDCS facilitates greater improvements for healthy subjects' non-dominant hand compared to uni-hemisphere stimulation. *BMC Neurosci.* 9:103. doi: 10.1186/1471-2202-9-103

Vines, B. W., Nair, D., and Schlaug, G. (2008b). Modulating activity in the motor cortex affects performance for the two hands differently depending upon which hemisphere is stimulated. *Eur. J. Neurosci.* 28, 1667–1673. doi: 10.1111/j.1460-9568.2008.06459.x

Vitor-Costa, M., Okuno, N. M., Bortolotti, H., Bertollo, M., Boggio, P. S., Fregni, F., et al. (2015). Improving cycling performance: transcranial direct current stimulation increases time to exhaustion in cycling. *PLoS ONE* 10:e0144916. doi: 10.1371/journal.pone.0144916

Vollmann, H., Conde, V., Sewerin, S., Taubert, M., Sehm, B., Witte, O. W., et al. (2013). Anodal transcranial direct current stimulation (tDCS) over supplementary motor area (SMA) but not pre-SMA promotes short-term visuomotor learning. *Brain Stimul.* 6, 101–107. doi: 10.1016/j.brs.2012.03.018

Waters, S., Wiestler, T., and Diedrichsen, J. (2017). Cooperation not competition: bihemispheric tDCS and fMRI show role for ipsilateral hemisphere in motor learning. *J. Neurosci.* 37, 7500–7512. doi: 10.1523/JNEUROSCI.3414-16.2017

Waters-Metenier, S., Husain, M., Wiestler, T., and Diedrichsen, J. (2014). Bihemispheric transcranial direct current stimulation enhances effector-independent representations of motor synergy and sequence learning. *J. Neurosci.* 34, 1037–1050. doi: 10.1523/JNEUROSCI.2282-13.2014

Westwood, S. J., and Romani, C. (2017). Transcranial direct current stimulation (tDCS) modulation of picture naming and word reading: a meta-analysis of single session tDCS applied to healthy participants. *Neuropsychologia* 104, 234–249. doi: 10.1016/j.neuropsychologia.2017.07.031

Williams, J. A., Pascual-Leone, A., and Fregni, F. (2010). Interhemispheric modulation induced by cortical stimulation and motor training. *Phys. Ther.* 90, 398–410. doi: 10.2522/ptj.20090075

Williams, P. S., Hoffman, R. L., and Clark, B. C. (2013). Preliminary evidence that anodal transcranial direct current stimulation enhances time to task failure of a sustained submaximal contraction. *PLoS ONE* 8:e81418. doi: 10.1371/journal.pone.0081418

Woods, A. J., Antal, A., Bikson, M., Boggio, P. S., Brunoni, A. R., Celnik, P., et al. (2016). A technical guide to tDCS, and related non-invasive brain stimulation tools. *Clin. Neurophysiol.* 127, 1031–1048. doi: 10.1016/j.clinph.2015.11.012

Zhu, F. F., Yeung, A. Y., Poolton, J. M., Lee, T. M. C., Leung, G. K. K., and Masters, R. S. W. (2015). Cathodal transcranial direct current stimulation over left dorsolateral prefrontal cortex area promotes implicit motor learning in a golf putting task. *Brain Stimul.* 8, 784–786. doi: 10.1016/j.brs.2015.02.005

Zimerman, M., Heise, K. F., Gerloff, C., Cohen, L. G., and Hummel, F. C. (2014). Disrupting the ipsilateral motor cortex interferes with training of a complex motor task in older adults. *Cereb. Cortex* 24, 1030–1036. doi: 10.1093/cercor/bhs385

Zimerman, M., Nitsch, M., Giraux, P., Gerloff, C., Cohen, L. G., and Hummel, F. C. (2013). Neuroenhancement of the aging brain: restoring skill acquisition in old subjects. *Ann. Neurol.* 73, 10–15. doi: 10.1002/ana.23761

Conflict of Interest: The authors declare that the research was conducted in the absence of any commercial or financial relationships that could be construed as a potential conflict of interest.

APPENDIX 1

Search Strategy

1. exp transcranial direct current stimulation/
2. (transcranial adj5 electric$ adj5 stimulation).mp. [mp=ti, ab, hw, tn, ot, dm, mf, dv, kw, fx, dq, nm, kf, px, rx, ui, sy, tc, id, tm]
3. (transcranial adj5 DC adj5 stimulation).mp. [mp=ti, ab, hw, tn, ot, dm, mf, dv, kw, fx, dq, nm, kf, px, rx, ui, sy, tc, id, tm]
4. (transcranial adj5 direct current adj5 stimulation).mp. [mp=ti, ab, hw, tn, ot, dm, mf, dv, kw, fx, dq, nm, kf, px, rx, ui, sy, tc, id, tm]
5. tdcs.mp. [mp=ti, ab, hw, tn, ot, dm, mf, dv, kw, fx, dq, nm, kf, px, rx, ui, sy, tc, id, tm]
6. or/1-5
7. Pragmatic Clinical Trial.pt.
8. Randomized Controlled Trial.pt.
9. exp Randomized Controlled Trials as Topic/
10. "Randomized Controlled Trial (topic)"/
11. Randomized Controlled Trial/
12. Randomization/
13. Random Allocation/
14. Double-Blind Method/
15. Double Blind Procedure/
16. Double-Blind Studies/
17. Single-Blind Method/
18. Single Blind Procedure/
19. Single-Blind Studies/
20. Placebos/
21. Placebo/
22. (random∗ or sham or placebo∗).mp.
23. ((singl∗ or doubl∗) adj (blind∗ or dumm∗ or mask∗)).mp.
24. or/7-23
25. 6 and 24
26. limit 25 to "all adult (18 plus years)"
27. limit 26 to english language
28. limit 27 to human
29. remove duplicates from 28

frontiers in Neuroscience

ORIGINAL RESEARCH
published: 10 January 2020
doi: 10.3389/fnins.2019.01416

One-Shot Tagging During Wake and Cueing During Sleep With Spatiotemporal Patterns of Transcranial Electrical Stimulation Can Boost Long-Term Metamemory of Individual Episodes in Humans

Praveen K. Pilly[1], Steven W. Skorheim[1†], Ryan J. Hubbard[1†], Nicholas A. Ketz[1], Shane M. Roach[1], Itamar Lerner[2,3], Aaron P. Jones[4], Bradley Robert[4], Natalie B. Bryant[4], Arno Hartholt[5], Teagan S. Mullins[4], Jaehoon Choe[1], Vincent P. Clark[4] and Michael D. Howard[1]*

[1] Center for Human-Machine Collaboration, Information and Systems Sciences Laboratory, HRL Laboratories, LLC, Malibu, CA, United States, [2] Center of Molecular and Behavior Neuroscience, Rutgers University Newark, Newark, NJ, United States, [3] Department of Psychology, The University of Texas at San Antonio, San Antonio, TX, United States, [4] Psychology Clinical Neuroscience Center, Department of Psychology, University of New Mexico, Albuquerque, NM, United States, [5] Institute for Creative Technologies, University of Southern California, Los Angeles, CA, United States

Targeted memory reactivation (TMR) during slow-wave oscillations (SWOs) in sleep has been demonstrated with sensory cues to achieve about 5–12% improvement in post-nap memory performance on simple laboratory tasks. But prior work has not yet addressed the one-shot aspect of episodic memory acquisition, or dealt with the presence of interference from ambient environmental cues in real-world settings. Further, TMR with sensory cues may not be scalable to the multitude of experiences over one's lifetime. We designed a novel non-invasive non-sensory paradigm that tags one-shot experiences of minute-long naturalistic episodes in immersive virtual reality (VR) with unique spatiotemporal amplitude-modulated patterns (STAMPs) of transcranial electrical stimulation (tES). In particular, we demonstrated that these STAMPs can be re-applied as brief pulses during SWOs in sleep to achieve about 10–20% improvement in the metamemory of targeted episodes compared to the control episodes at 48 hours after initial viewing. We found that STAMPs can not only facilitate but also impair metamemory for the targeted episodes based on an interaction between pre-sleep metamemory and the number of STAMP applications during sleep. Overnight metamemory improvements were mediated by spectral power increases following the offset of STAMPs in the slow-spindle band (8–12 Hz) for left temporal areas in the scalp electroencephalography (EEG) during sleep. These results prescribe an optimal strategy to leverage STAMPs for boosting metamemory and suggest that real-world episodic memories can be modulated in a targeted manner even with coarser, non-invasive spatiotemporal stimulation.

Keywords: memory consolidation, non-invasive stimulation, learning and memory, metamemory, targeted memory reactivation

OPEN ACCESS

Edited by:
Hasan Ayaz,
Drexel University, United States

Reviewed by:
Kazumasa Uehara,
National Institute for Physiological Sciences, Japan
Sankaraleengam Alagapan,
Georgia Institute of Technology, United States
Hasan Onur Keles,
University of Houston, United States

****Correspondence:***
Praveen K. Pilly
pkpilly@hrl.com

[†] These authors have contributed equally to this work

Specialty section:
This article was submitted to Neural Technology, a section of the journal Frontiers in Neuroscience

Received: *15 September 2019*
Accepted: *16 December 2019*
Published: *10 January 2020*

Citation:
Pilly PK, Skorheim SW, Hubbard RJ, Ketz NA, Roach SM, Lerner I, Jones AP, Robert B, Bryant NB, Hartholt A, Mullins TS, Choe J, Clark VP and Howard MD (2020) One-Shot Tagging During Wake and Cueing During Sleep With Spatiotemporal Patterns of Transcranial Electrical Stimulation Can Boost Long-Term Metamemory of Individual Episodes in Humans. Front. Neurosci. 13:1416. doi: 10.3389/fnins.2019.01416

INTRODUCTION

The ability to recall previously experienced events and to introspect about them are important aspects of our daily living. However, a mechanistic understanding of how memories of one-shot experiences of real-world episodes are formed, recalled, and monitored in the human brain is still lacking. Metamemory is an executive function that monitors and judges the ability to recall memories accurately (Nelson and Narens, 1990), such as when providing eyewitness testimony in a criminal case or deciding when study material has been sufficiently learned. One is said to have higher metamemory when recall accuracy is proportional to subjective confidence (i.e., more confident when correct and less confident when wrong). In other words, metamemory measures the ability to introspect and discriminate between correct and incorrect memory recalls, avoiding either over- or under-confidence (Galvin et al., 2003; Fleming and Lau, 2014). The neural mechanisms underlying memory monitoring and control have been suggested to work in concert with those involved in the encoding, consolidation, and recall of the memory content (Nelson and Narens, 1990).

Hippocampus is known to play an important role in the online rapid encoding of episodic memories for short-term storage, which subsequently drives offline consolidation for long-term storage in distributed neocortical areas (McClelland et al., 1995; Buzsáki, 1996). But it is also possible for neocortical activations during offline periods to trigger memory replays in the hippocampus (Ji and Wilson, 2007; Rothschild et al., 2017). Consistent with this latter view, there have been a number of demonstrations of offline targeted memory reactivation (TMR) in animals and humans using olfactory and auditory cues to modulate the ability to learn contexts and individual memories (e.g., Rasch et al., 2007; Rudoy et al., 2009; Antony et al., 2012; Bendor and Wilson, 2012). However, these studies have not yet addressed the one-shot aspect of episodic memory acquisition, or dealt with the presence of interference from ambient environmental cues in real-world settings. And a majority of these studies assessed memory performance over less than a day, with about 5–12% improvement in post-nap memory performance on simple laboratory tasks (e.g., Rudoy et al., 2009; Antony et al., 2012), and employed fixed-dose cueing during offline periods. Further, TMR with sensory cues may not be scalable to the multitude of experiences over one's lifetime. Our study overcomes these limitations by investigating long-term behavioral and physiological effects of non-sensory transcranial electrical stimulation (tES) for TMR of naturalistic episodic memories with one-shot acquisition.

Prior work on non-sensory cueing showed that transcranial magnetic stimulation can reactivate the experience of a visual stimulus after repeated pairing with it (Liao et al., 2013). And transcranial alternating current stimulation (tACS) of prefrontal cortex (PFC) at a given frequency (60 or 90 Hz) during encoding can boost subsequent performance for old vs. new recognition of learned words when reapplied at the same frequency during either retrieval (Javadi et al., 2017) or slow-wave (SW) sleep (Crowley and Javadi, 2019). Employing intracranial recordings in awake non-human primates, we showed that transcranial direct current stimulation (tDCS) of PFC alters functional connectivity between brain areas in a frequency-specific manner (Krause et al., 2017). Recently, we showed that tACS can reliably entrain the spiking activity of single neurons in deep structures such as the hippocampus and basal ganglia in a spatially-localized and frequency-dependent manner (Krause et al., 2019b). Building on these prior results, we postulated that spatiotemporal amplitude-modulated patterns (STAMPs) of tES could alter the functional connectivity as well as the spike timing within the brain in unique ways and thereby be leveraged for TMR in more potent ways than sensory cues. In particular, we investigated whether STAMPs of tES could be used to tag specific naturalistic episodes during one-shot viewing in immersive virtual reality (VR) and subsequently cue them during sleep to boost their memory recall over 48 hours in a targeted manner. The overarching goal of this study was to assess if coarser, non-invasive stimulation is sufficient to effectively modulate complex episodic memories in humans.

MATERIALS AND METHODS

STAMPs

Each STAMP is defined as an array of currents across 32 stimulation electrodes located in the 64-channel layout according to the international 10-10 system (see **Supplementary Figure S1**). A library of 256 spatial stimulation patterns was computed based on the criterion that the induced electric fields in the 3D brain volume of a realistic adult human head template (with a cortical mesh of 190,521 dimensions) are as mutually orthogonal as possible. Gradient descent optimization was used to minimize the norm of the cross-correlation function for electric fields across the library. The optimization procedure penalized both correlations and anti-correlations for the electric fields induced across solutions to accommodate both tDCS and tACS STAMPs with the solved spatial patterns as amplitudes. The total injected current was set to 2.5 mA, with maximum 1.5 mA and minimal 150 μA current at any electrode (to avoid impedance issues). Different initializations of the gradient descent search, in terms of the number of starting non-zero current electrodes, yielded STAMP solutions with different sparseness amounts. Solutions using more initial non-zero current electrodes led to STAMP sets with lower overall cross-correlation and lower currents across the montages. STAMPs used in the current study were solved based on initialization of 18 non-zero current electrodes. Of the 256 computed amplitude patterns, 14 were randomly chosen for use in the current study as tDCS and 40 Hz tACS STAMPs.

Subjects

Subjects were 18–40 years of age, used English as a first language, completed high school, and had no history of head injury with loss of consciousness for longer than 5 min. They were right-handed according to the Edinburgh Handedness Inventory (Oldfield, 1971), had no history of neurological or psychiatric disorder, had no history of alcohol or drug abuse, were non-smoking, had no excessive alcohol or caffeine consumption, were not currently taking any medication significantly affecting the central nervous system, had no implanted metal, had no

sensitivity or allergy to latex, had good or corrected hearing and vision, and reported no sleep disturbances. Women who were pregnant, or thought they might be, were also excluded.

A total of 30 healthy subjects completed the experiment. They were recruited using flyers placed around campus of the University of New Mexico and surrounding community, and received monetary compensation upon completion of the study. Of these, six subjects were excluded from the analyses due to either equipment failure during an "Active" night, or non-compliance in following task instructions. All subjects provided signed informed consent to participate in the study, which was approved by the Chesapeake Institutional Review Board. The remaining $N = 24$ subjects (15 female) had a mean age of 23.96 years with a standard deviation of 6.08 years.

Behavioral Paradigm

We employed immersive VR to produce simulated realistic environments for the purpose of systematically investigating the modulation of human episodic memories with STAMPs. VR-derived results have greater predictive validity and relevance for real-world applications when compared to results from standard training and testing tools on a personal computer. In addition, on a more pragmatic level, rather than relying on costly physical mock-ups of functional environments, VR offers the option to produce and distribute identical standard simulation environments.

Subjects were able to freely look around a fully rendered 3D environment on the HTC Vive® platform. Their virtual vantage point was situated on a balcony across from an apartment building set in a non-descript Middle Eastern town. **Supplementary Movie S1**, "Fire Response", is an illustrative episode. The task was to actively surveil the inhabitants of the building and the passers-by so that they would be able to later recall the events. We designed 28 distinct memorable episodes in the VR, each about a minute long. The series of events in an episode generally centered around two main characters, often with one or two less involved characters. Ten declarative statements were composed for each episode to test the ability of the subjects to recall facts about the experienced events. Subjects were instructed to respond to salient events in each episode as they happened by orienting a reticle in the head-mounted display (HMD) toward those events and taking pictures with a virtual camera triggered by a hand-held controller.

In preparation for the experiment, the episodes and questions (i.e., declarative statements) were gradually improved using feedback from 12 pilot subjects (who are different from the subjects for the main experiment). They watched one episode at a time and immediately rated the difficulty of each of the 10 questions on a scale from 1 (easy) to 10 (difficult), and the overall memorability of the episode on a scale from 1 (least memorable) to 10 (most memorable). Average difficulty rating in the subjects' responses tended to covary with the accuracy of their responses across the episodes. We employed an iterative process aimed at subjectively equalizing the overall memorability and question difficulty across the episodes. Each iteration involved getting responses from four pilot subjects, after which the less memorable episodes were altered to increase memorability by adding more salient events. Questions that were answered incorrectly and rated as difficult, across the subjects, were made easier, and those that were answered correctly and rated as easy were increased in difficulty. After three iterations, the 28 episodes were of similar memorability, and the questions were of similar difficulty (see **Supplementary Note**). Using data from one final cohort of four pilot subjects, the set of 28 finalized episodes was curated into four subgroups with the constraints that the average difficulty of the questions and the average memorability of the episodes in each subgroup were similar, and the themes of the events occurring in the episodes were roughly matched. Two groups of 14 episodes each (namely, A and B) were created by randomly choosing among these four subgroups. Episodes were given names but were not presented to the subjects and were used only for reference by the experimenters (see **Supplementary Table S1**).

The experiment was conducted over the course of seven days and included five nights in our sleep laboratory that comprised an acclimation night and four experimental nights (see **Figure 1A**). Two experimental nights followed the acclimation night, whereas the other two took place about 8 days (mean = 8.25, standard deviation = 4.92) later. $N = 24$ subjects were randomly assigned to one of four groups in a within-subjects, counterbalanced, single-blind design based on which episode group ("A," "B") and which stimulation condition ("Active," "Sham") were employed in the first week. For the "Active" stimulation condition, each of the 14 episodes was stimulated with a unique STAMP once during viewing (see **Figure 1B**). The pairing between the 14 STAMPs and episodes was arbitrary and randomly chosen for each subject. Only the STAMPs that were employed for tagging one of the two episode subgroups were re-applied during slow-wave oscillations (SWOs) through the subsequent two experimental nights (see **Figure 1C**). The corresponding half of episodes were termed "Tag & Cue," and the other half of the episodes were termed "Tag & No Cue." For the "Sham" stimulation condition, the 14 episodes were neither tagged during waking nor cued during sleep. Note that subjects were also counterbalanced in terms of which of the four episode subgroups was tagged and cued. See **Figure 2** for an illustration of the STAMP intervention and the scalp topography of the 14 STAMPs.

For each stimulation condition, memory performance was assessed across 3 days over the course of 48 h: immediately following initial viewing of the episodes (termed "Day 1"), following Night 1 and prior to Night 2 (termed "Day 2"), and following Night 2 and prior to Night 3 (termed "Day 3"). To assess memory recall, subjects determined the veracity of two to four declarative statements for each of the 14 episodes by recalling the underlying story (see **Figure 1B**), and also rated their confidence in the correctness of their responses on a scale from 1 to 10. Textual prompts and pictures of characters were the only cues available to recall the pertinent episodes. Subjects were instructed to respond as quickly as possible without sacrificing accuracy. The presentation order of questions within each day of testing was pre-randomized such that a subject would answer one question for all 14 episodes before they would see the next question for a given episode. The pre-randomization

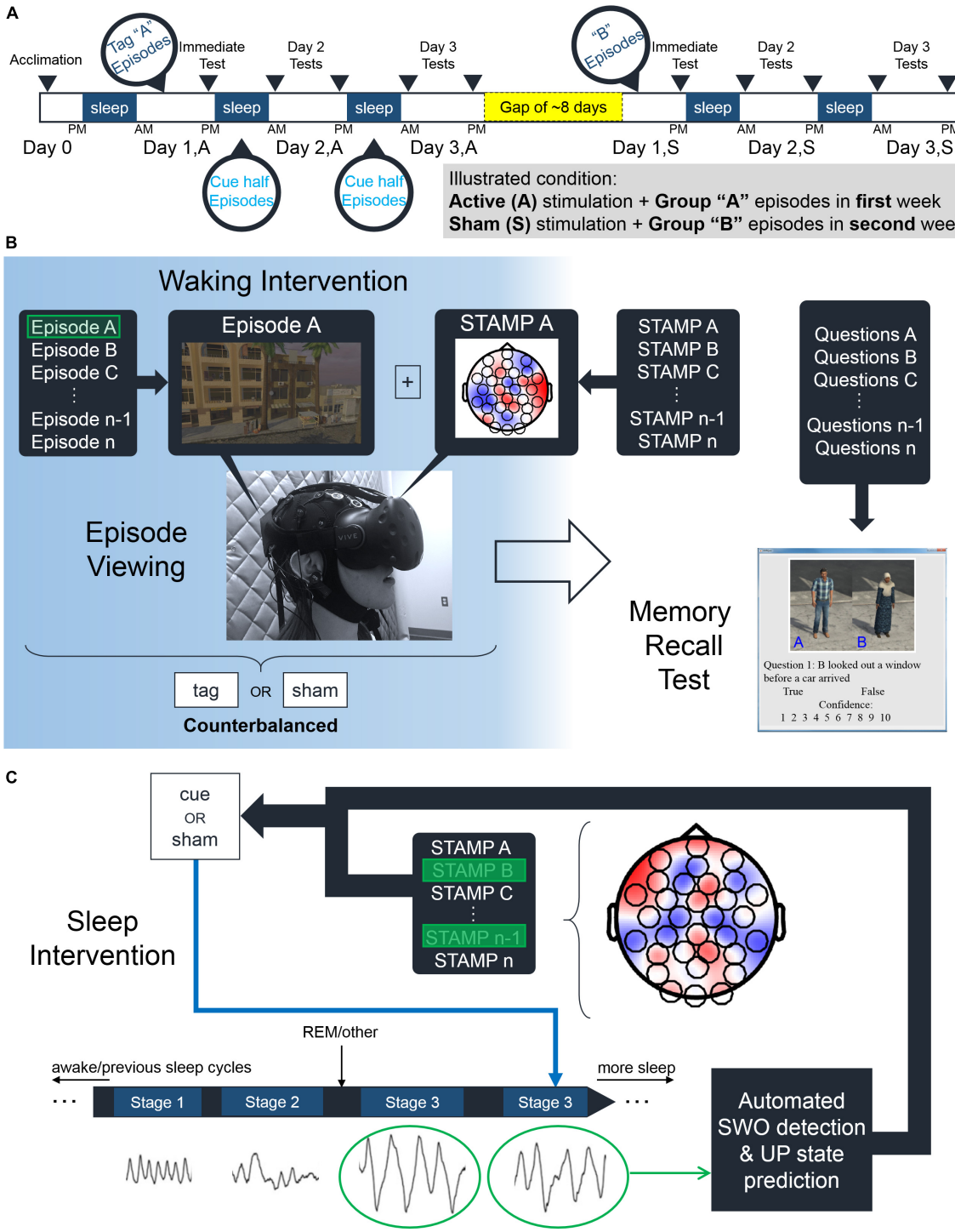

FIGURE 1 | Experimental paradigm. **(A)** Subjects participated in a within-subjects counterbalanced study over 2 weeks. After an initial acclimation night, subjects viewed various episodes belonging to either "Group A" or "Group B" episodes in an immersive virtual reality environment. These episodes were accompanied by either "Active" or "Sham" STAMPs with half of those repeating during sleep the following two nights. After a gap of about 8 days, subjects viewed the episodes from the remaining Group (e.g., "Group B" if they viewed "Group A" before) and received the other stimulation condition (e.g., "Sham" if they received "Active" before). Memory recall of the episodes was assessed in five tests over the course of the 48 h of each stimulation condition before and after the gap. **(B)** Illustration of the experimental procedures during waking. For the "Active" stimulation condition, subjects were stimulated with a randomly chosen STAMP (from the library of 14) to temporally coincide with the viewing of each episode from their assigned group. Subjects in the "Sham" stimulation condition did not receive any currents as such. **(C)** Illustration of the experimental procedures during sleep. For the "Active" stimulation condition, half of the STAMPs used to tag episodes during viewing were re-applied to temporally coincide with predicted UP states of automatically detected SWOs.

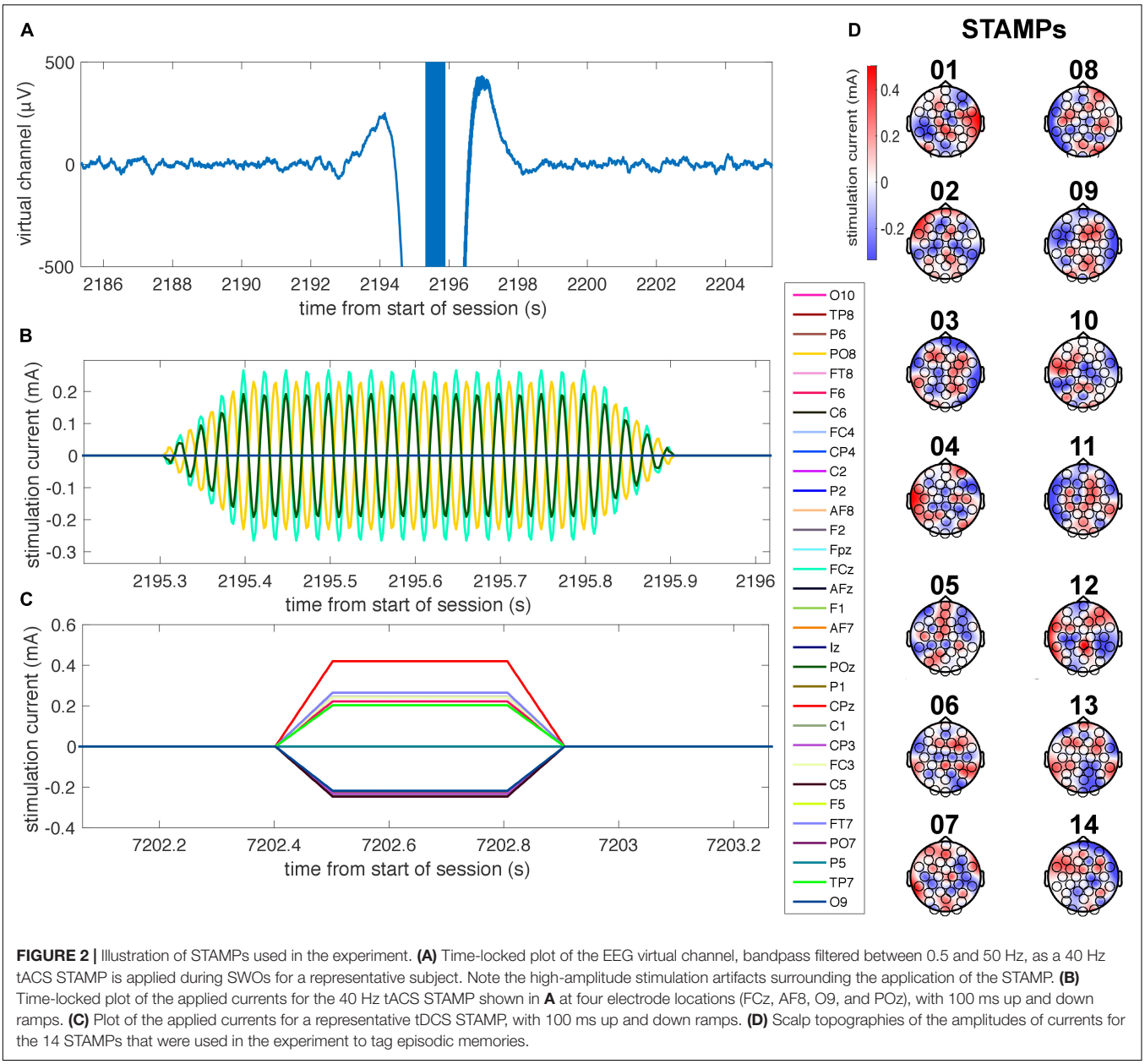

FIGURE 2 | Illustration of STAMPs used in the experiment. **(A)** Time-locked plot of the EEG virtual channel, bandpass filtered between 0.5 and 50 Hz, as a 40 Hz tACS STAMP is applied during SWOs for a representative subject. Note the high-amplitude stimulation artifacts surrounding the application of the STAMP. **(B)** Time-locked plot of the applied currents for the 40 Hz tACS STAMP shown in **A** at four electrode locations (FCz, AF8, O9, and POz), with 100 ms up and down ramps. **(C)** Plot of the applied currents for a representative tDCS STAMP, with 100 ms up and down ramps. **(D)** Scalp topographies of the amplitudes of currents for the 14 STAMPs that were used in the experiment to tag episodic memories.

was performed at the experiment outset such that every subject received questions in the same order for a given episode group.

Memory recall was assessed via a custom graphical user interface (GUI) coded in MATLAB and administered in the sleep laboratory on the same computer used for the VR episode viewing. The GUI was a single application window that cycled through three sections as the subject answered questions. The first section the subject encountered for an individual question contained a textual prompt that described the episode this question pertained to and a button labeled "View Question" that the subject pressed when they were ready to proceed to the next section. The second section was divided into two panels. The first panel contained the same textual prompt from the previous screen, a list of the two to four characters from the episode presented in a pre-randomized order with a name (e.g., "Character B") and a 99 × 142 pixel image in a neutral location and position, a question pertaining to a specific detail of the episode, and two radio buttons for "True" or "False" selection. The second panel contained 10 radio buttons for the subject to rate their confidence in the answer they provided in the first panel with 1 being "Least Confident" and 10 being "Most Confident." There was no deadline for these responses. Finally, a button labeled "Next Question" became active once the subject had answered the question and provided a confidence rating. This button led to a third screen that enforced a 4 s interval between questions and then automatically loaded the prompt screen of the next question. This process repeated until all questions for the session had been answered. No feedback on the accuracy of

their answers was provided to the subjects at any time during the experiment. Subjects were instructed to respond as quickly as possible without sacrificing accuracy.

Data were automatically collected from the GUI during user interaction and saved for later analysis. Five data points were captured for each question: the "True"/"False" response, the confidence rating, the prompt screen viewing duration, the interval from the question screen presentation to the selection of a "True"/"False" response, and the interval from the question screen presentation to the selection of a confidence rating. **Supplementary Movie S2** demonstrates the GUI used to assess the memory recall.

Type-2 ROC Curve Analysis

Metamemory was calculated empirically from correct and incorrect recalls and the corresponding confidence ratings using standard procedure (Galvin et al., 2003; MacMillan and Creelman, 2005; Fleming and Lau, 2014). In each memory recall trial, the textual prompt and pictures of characters would help retrieve the corresponding episode. The declarative statement would then be matched with the retrieved episode to determine its veracity. The stronger the memory recall, the greater is the ability to correctly recall the events from the episode without confabulating any details. A correctly answered declarative statement (irrespective of the response category) was considered a Type-2 true positive, and an incorrectly answered declarative statement (irrespective of the response category) a Type-2 false positive. Probability density functions of confidence ratings (on the scale from 1 to 10) with 10 bins were computed for Type-2 true positives (i.e., correct recalls) and for Type-2 false positives (i.e., error recalls) separately. Next, the cumulative distribution functions were calculated for each in reverse direction (from end to beginning). The data points of the cumulative distribution function for Type-2 true positives were plotted against the corresponding data points of the cumulative distribution function for Type-2 false positives to obtain the Type-2 ROC curve. The area under the Type-2 ROC curve was employed as the metric of metamemory for the episodic memory recall (see **Figure 3**). The metric is essentially the probability that a randomly chosen correct recall has a higher confidence rating than a randomly chosen incorrect recall. As the ROC curve analysis is based on the computation of probability density functions, the data from morning and evening tests were combined for Days 2 and 3 to maximize the accuracy of the estimate of metamemory.

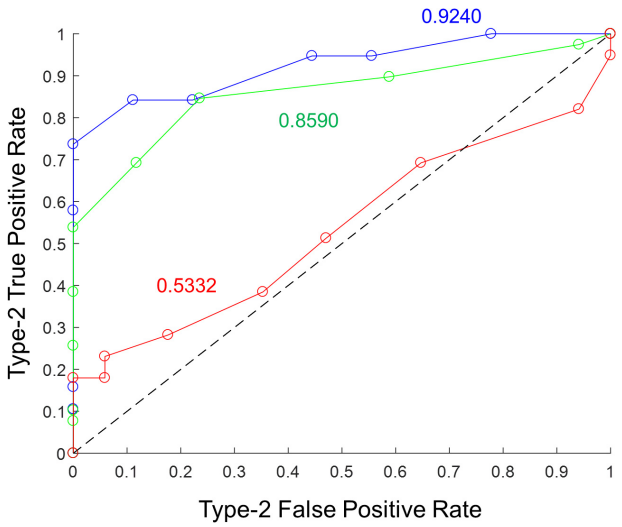

FIGURE 3 | Illustration of Type-2 ROC curve analysis to assess episodic metamemory. Type-2 ROC curves from the 3 days of testing are shown for a representative subject in the "Sham" stimulation condition. Blue corresponds to "Day 1," green to "Day 2," and red to "Day 3." The corresponding metamemory score (calculated as the area under the curve) is shown in the matching color.

Experimental Procedure

At the orientation session before the experiment began, subjects were invited to provide informed consent. Head measurements were also made (circumference, nasion to inion, and pre-auricular to pre-auricular) to fit a neoprene head cap. Subjects were next given a tour of the sleep laboratories and an explanation of the electroencephalography (EEG)/tES equipment and experimental procedures.

For the acclimation night, subjects were prepped and fitted with a neoprene head cap for polysomnographic (PSG) recording during sleep. EEG electrode locations were digitized using Polhemus FASTRAK System (Polhemus, Inc.) for data analysis purposes as well as to measure how much the cap may have shifted during the subsequent sleep session. Subjects were instructed to lie down in a supine position at approximately 22:00, when biocalibrations were performed to help identify sources of noise in later EEG acquisition. This included EEG data collection of eyes open for 1 min, closed for 1 min, looking up, down, right, and left, blinking slowly five times, clenching the jaw, and finally moving into a comfortable sleeping position. Lights out for the subjects occurred between 22:00–23:00, and they slept for up to 8 uninterrupted hours before being awoken. Upon waking, subjects could use the restroom and were offered water and snacks. They were then disconnected from the EEG/tES hardware and released.

In the evening of the acclimation night, subjects were familiarized with the VR environment and task procedures via a short practice session. During this session, subjects viewed one 3.5-min long example episode in the virtual world and then completed a 10-question sample memory recall test on a personal computer. Apart from acclimatizing the subjects to sleeping in the laboratory, the acclimation night was also leveraged for a pilot study to assess the effects of closed-loop tACS on a paired associates task, unrelated to the main experiment. Note that including this as a covariate did not change any of the findings reported in this paper.

The main experiment began the following evening. For the first experimental night, subjects arrived at the laboratory at approximately 19:00 and were immediately prepped for EEG data collection and STAMP stimulation. The subjects then sat in front of the computer, put on the HTC Vive® headset, and heard the task instructions. They viewed 14 episodes from either Group A

or B, depending on their assignment, in a random order within the VR environment. Following episode viewing, subjects rated three different types of sensations (itching, heat/burning, and tingling) on a 0–10 Likert scale, where 0 indicated no sensation at all and 10 indicated the most intense possible sensation. Any report of 7 or above would have resulted in immediate termination of the experiment without penalty to the subject. No subjects were lost due to this reason.

Next, subjects completed a test to assess their baseline memory recall. They were then prepped for PSG recording during sleep at roughly 21:00. Lights out occurred between 22:00 and 23:00, and rise time was between 06:00 and 07:00. During sleep, a trained research assistant monitored EEG data and started the cueing algorithm after observing 4 min of continuous "N2/N3" sleep, which was then allowed to run through the remainder of the night. Subjects either received "Active" (2.5 mA) or "Sham" (no current) STAMPs during predicted UP states for the entire duration of sleep. Stimulation was paused if the subject showed signs of waking and resumed after the subject was again in "N2/N3" sleep. Upon waking, subjects completed another test to assess the effect of sleep stimulation on memory recall. They were then disconnected from the EEG/tES hardware and released.

For the second experimental night, the PSG setup and STAMP stimulation procedures were identical to the first experimental night. However, subjects did not view the episodes from the previous evening again, but they completed two memory recall tests – one prior to sleep and the other upon waking. For the follow-up to the second experimental night, subjects arrived approximately 24 h after their previous day arrival (19:00), were prepped for EEG data collection, and completed a final test to assess the effect of sleep stimulation on more long-term memory recall.

After about 8 days, subjects returned to the laboratory for their third and fourth experiment nights, succeeded by the final follow-up. The timeline and procedures were identical to the first and second experimental nights and their follow-up, the only differences being the group of episodes viewed in the VR ("A," "B") and the stimulation condition ("Active," "Sham") were opposite of their assignments for the first and second experimental nights. Upon completion of the follow-up to the fourth experimental night, the subjects were debriefed about the experiment.

Only two subjects dropped out of the study, both of whom received "Active" stimulation in the first week. Only one of those opted out due to stimulation (in the last evening test for the "Active" stimulation condition); the other stopped due to unspecified reasons (in the first evening test for the "Active" stimulation condition).

Waking Electroencephalographic (EEG) Data Collection

32-channel physiological data collection and simultaneous 32-channel stimulation were conducted using the StarStim64 device (Neuroelectrics, Inc.). The 64 electrodes were held in place using a neoprene head cap, according to the international 10-10 system (recording: *P7*, T7, *CP5*, *FC5*, *F7*, F3, *C3*, *P3*, *FC1*, *CP1*, *Pz*, PO4, *O2*, Oz, *O1*, PO3, *CP2*, *Cz*, *FC2*, *Fz*, AF3, *FP1*, *FP2,* AF4, *P8*, T8, *CP6*, *FC6*, *F8*, F4, *C4*, *P4*; stimulation: O10, TP8, P6, PO8, FT8, F6, C6, FC4, CP4, C2, P2, AF8, F2, FPz, FCz, AFz, F1, AF7, Iz, POz, P1, CPz, C1, CP3, FC3, C5, F5, FT7, PO7, P5, TP7, O9). Solidgeltrodes (NE028, Neuroelectrics, Inc.) and pistim electrodes (NE024, Neuroelectrics, Inc.) were used for physiological data collection and stimulation, respectively. EEG data were collected from 23 of these 32 sites (marked in italics above). The remaining electrodes (PO3, PO4, Oz, AF3, AF4, F3, F4, T7, T8) were repurposed to record electrocardiogram (ECG), electrooculogram (EOG), and electromyogram (EMG) to allow for the detection of artifacts and sleep stages. An ECG lead (PO3) was placed under the left collarbone, and both vertical (AF3) and horizontal (AF4) EOG were collected: one lead placed superior and lateral to the right outer canthus, and another lead inferior and lateral to the left outer canthus. The physiological data were sampled at 500 Hz. Common Mode Signal (CMS) and Driving Right Leg (DRL) reference electrodes (stricktrodes: NE025, Neuroelectrics, Inc.) were placed on the right preauricular. No online hardware filtering, except for line noise (60 Hz), was applied during collection.

Polysomnographic (PSG) Data Collection

For PSG data collection during sleep, the setup was nearly identical to wake, with a few exceptions. First, two EMG electrodes were placed on and under the chin in accordance with PSG recording guidelines set forth by the American Academy for Sleep Medicine (Berry et al., 2012) to help with sleep scoring. Second, data were collected from 25 EEG electrodes, of which C3, C4, O1, O2, F3, and F4 were used for sleep staging.

Waking STAMP Stimulation

For the "Active" stimulation condition, STAMP montages were delivered via the StarStim64 device (Neuroelectrics, Inc.) during the one-shot viewing of episodes in the VR. For all subjects, each episode was randomly assigned a unique STAMP from the set of 14 montages. A given STAMP was applied for the entire duration of the corresponding episode (about a minute long) with ramp up and ramp down times of 100 ms. Inter-episode interval was randomly sampled between 6 and 8 s. We employed tDCS STAMPs for eight subjects and 40 Hz tACS STAMPs for the remaining 16 subjects to demonstrate the generality of the concept of using spatiotemporal stimulation patterns for memory tagging and cueing.

Stimulation During Slow-Wave Oscillations

Our stimulation algorithm was automatically triggered through the whole night to transiently apply "Tag & Cue" STAMPs during putative UP states of SWOs. The algorithm first detects the presence of SWOs, which consist of low-frequency synchronized upward and downward deflections of EEG. It next attempts to determine the frequency and phase of ongoing endogenous SWOs. For robust SWO detection, a virtual channel is computed by averaging 13 fronto-parieto-central EEG channels (Cz, FC1, FC2, CP1, CP2, Fz, C4, Pz, C3, F3, F4, P3, P4 in the international

10-10 system) to determine the overall synchronous activity of EEG recorded during sleep. The virtual channel allows the observation of moments of relatively high SW power, referred to as SW events, while averaging out activity of lesser magnitudes on individual channels unrelated to the pattern of SWOs. The included channels are stored in a running 5 s buffer. They undergo moving average subtraction with a 1 s window (to mean center the signals at 0 μV), and noisy channels exceeding 500 μV min-to-max amplitude across the 5 s are rejected before the virtual channel is computed. The buffer is updated with each discrete data fetch operation that gets the new latest data up to the point of data request. By the time the buffer is updated, there is a random transmission delay, which needs to be accounted for to plan and precisely time the stimulation in the near future.

The virtual channel data in the buffer are further processed to detect the presence of SWOs and predict a putative UP state. The algorithm applies a fast Fourier transform (FFT) to the buffered data to determine the power spectrum. Stimulation is planned when the ratio of the cumulative power in the SW band (0.5–1.2 Hz) is more than 30% of the total cumulative power from 0.1 to 250 Hz. If this SW relative power threshold is crossed, the data are bandpass filtered in the SW band with a second-order zero-lag Butterworth filter. The Hilbert transform is then applied to the filtered signal to obtain the analytic signal, and the phase of the analytic signal is shifted back by 90° to align it with the SWOs. Next a sine wave is fit to the imaginary component of this signal by optimizing the amplitude, offset, and phase parameter values and using the dominant frequency in the SW band from the power spectrum. The sine wave is then projected into the future, identifying the temporal targets that would synchronize STAMPs to the predicted endogenous SWOs. Throughout this process, the dynamic latency associated with data processing is timed using the system clock. Together with distributions of calibrated latencies for data fetch and stimulation commands (mean = 5 ms, standard deviation = 2 ms), which were measured offline, the algorithm estimates the correct time point to communicate with the hardware to initiate the stimulation. As an example, suppose that at a given moment the algorithm initiates data fetch to populate the buffer with the last 5 s of EEG data. The data then become available for processing a few ms (say, 6 ms) into the future based on sampling from the distribution for data fetch latency. Assume it then takes 100 ms for data processing to predict that the next putative UP state will occur 600 ms in the future from the starting time point. If it takes a few ms (say, 7 ms) to physically initiate stimulation based on sampling from the distribution for stimulation command latency, the algorithm will wait 487 ms (600 – 100 – 7 – 6 ms) after the EEG processing step to send the stimulation command to the device.

During "Active" nights, STAMPs assigned to "Tag & Cue" episodes were administered during SWOs through the sleep period to boost the probability of specific memory replays. Sometimes, due to hardware and/or processing delays, the targeted start of the stimulation was not possible. In these cases, the algorithm compared the current time to the (now deprecated) stimulation start time, and checked if at least 300 ms of stimulation was still possible within the putative UP state. If so, the stimulation was initiated immediately and continued through the remainder of the putative UP state. If this was not possible, the algorithm started stimulation at the next putative UP state based on further projection of the sine wave fit from the buffer. Once STAMP delivery was completed (i.e., after stimulation offset), the system idled for 3 s to avoid the collection of high-amplitude stimulation artifacts in the data buffer, then resumed the cycle of data update in the buffer in search of the next SW event, at which point another STAMP was administered, and so on. STAMPs had ramp up and ramp down times of 100 ms during sleep as well. A minimum interval of 8 s was imposed between two consecutive SW events. Further, the seven STAMPs for the "Tag & Cue" episodes were always applied sequentially in a batch of seven consecutive SW events, with their order randomized across batches through the sleep period. For the "Sham" stimulation condition, the same algorithm was applied to mark the potential stimulation times without any currents being actually applied.

Post hoc Sleep EEG Analyses

For sleep staging, EEG data of electrodes C3, C4, O1, O2, Fp1, and Fp2 were bandpass filtered between 0.5 and 35 Hz, together with EMG data between 10 and 100 Hz. Each 30 s epoch was visually inspected by an experienced technician and assigned a stage of "Wake," "N1," "N2," "N3/SWS," "REM," or "Movement" according to guidelines by the American Academy for Sleep Medicine (Berry et al., 2012). Time in each sleep stage was directly derived by summing up all epochs determined to belong to that sleep stage. Sleep efficiency was computed as the percentage of the sleep period that was spent in any sleep stage other than "Wake." Note that analyses of sleep stage distributions and sleep efficiency did not include a subset of subjects from each experimental night for whom more than 15% of their sleep period was not scorable.

For sleep EEG biomarker analyses, the data were analyzed with custom-built scripts implemented in Matlab R2016a (The MathWorks) utilizing FieldTrip (Oostenveld et al., 2011) and EEGLab (Delorme and Makeig, 2004) functions. The data were epoched into pre- and post-SW event windows: pre-SW event windows captured −6.4 to −0 s before the onset of SW events, and post-SW event windows captured 0 to 12.8 s after the offset of SW events. For each epoch, a first-pass artifact correction procedure that identified large amplitude artifacts was performed by searching for peak-to-peak voltage changes of 500 μV within each channel in 200 ms sliding windows, and interpolating any segment that crossed this threshold using non-artifact time points before and after the segment. If more than 25% of segments of a time series of a channel was marked for correction, then the entire epoch for that channel was interpolated using data from neighboring channels. If 80% or more of the channels exceeded the 25% segment threshold, then the epoch was discarded entirely. A second-pass artifact correction was then performed such that any channel that exceeded the 500 μV (peak-to-peak voltage change) threshold across the time series within a trial was reconstructed by interpolation of its neighbors.

Following artifact correction, trials were selected with the constraint that each trial had enough usable data both pre- and post-SW event to have good time-frequency estimates of the lowest frequency of interest (i.e., 0.5 Hz); otherwise, they were

rejected. All epochs were then truncated to −6.4 to −1 s before the SW event and 3 to 12.8 s after the SW event in order to avoid high-amplitude stimulation artifacts. This same truncation was applied to data from the "Sham" nights. Finally, all epochs were mean centered, bandpass filtered with a Butterworth filter between 0.1 and 125 Hz, and bandstop filtered between 59 and 61 Hz, and all channels were re-referenced to the global average across channels.

Time-frequency decomposition of the data was performed in FieldTrip. Prior to decomposition, symmetric (mirror) padding was applied to extend the pre- and post-SW event time series to reduce edge artifacts. EEG epochs were then convolved with Morlet wavelets starting with a width of 4 at the center frequency of 0.5 Hz and increasing in width logarithmically up to a maximum width of 7 in order to minimize the combined uncertainty in time and frequency domains. Simultaneously, subsequent center frequencies were chosen such that each wavelet was one standard deviation in frequency domain from the previous wavelet. This process resulted in a time-frequency representation of roughly 35 log-spaced frequency bins from 0.5 to 50 Hz and equally-spaced time bins of 20 ms. Once time-frequency data were calculated, pre-SW event data from −3.5 to −3 s in each frequency bin were concatenated across trials and used to estimate a mean and standard deviation. These values were then used as a baseline to z-score both the pre- and post-SW event power for each trial and within each frequency bin to compute spectral power changes without single-trial bias (Ciuparu and Mureşan, 2016). These values were then averaged across trials within "Active" and "Sham" nights to yield a single channel × time × frequency matrix per condition for each subject. Subject averages were created using a random subset of trials such that trial numbers were matched between the "Active" and "Sham" nights. Note that sleep EEG biomarker analyses could not be run on a subset of the subjects due of the lack of usable data from "Sham" nights despite artifact correction.

Significant differences in spectral power changes and correlations with behavior were assessed statistically using non-parametric cluster-based permutation tests to correct for multiple comparisons in the channel x time space (Maris and Oostenveld, 2007). Average spectral power changes were calculated within pre-defined frequency bands: SW (0.5–1.2 Hz), delta (1–4 Hz), theta (4–8 Hz), slow-spindle (8–12 Hz), and fast-spindle (12–15 Hz). For each frequency band, a paired-sample t-test was performed at each channel × time bin between 3 and 10 s from the offset of SW events, and clusters were created by grouping adjacent channels and time bins that had a P-value < 0.05. Each cluster was then characterized by the sum of its t-values, and cluster-level statistics were evaluated using a permutation distribution created by shuffling the subject labels and repeating the clustering procedure 2000 times to correct for multiple comparisons. Thus, a clusterwise significance value can be attributed to each observed cluster in reference to its position in the permutation-based surrogate distribution. Any cluster with a clusterwise P-value < 0.05 after a further application of Bonferroni correction for the five additional frequency band comparisons was considered significant.

Significant clusters from the first analysis (called "contrast clusters") were then used as a mask to perform a second cluster-based permutation test on the correlation between the differences in overnight metamemory changes for "Tag & Cue" and "Sham" episodes and the corresponding differences in average spectral power change following SW events. This effectively limited the second cluster-based analysis to the channel × time bins that showed an *a priori* significant difference between the "Active" and "Sham" nights. For each "contrast cluster," a correlation coefficient and the related P-value were calculated at each constituent channel × time bin. The same non-parametric cluster-based permutation test was then performed to group adjacent channel × time bins with P-values < 0.05 into so-called "correlation clusters" with a clusterwise P-value < 0.05.

RESULTS

Sleep Architecture

We first analyzed the potential effects of STAMPs on the sleep architecture (i.e., time spent in various sleep stages) during the experimental nights using a linear mixed-effects model with subject as a random factor and with fixed factors for stimulation condition ("Active," "Sham"), experimental night ("Night 1," "Night 2"), sleep stage ("Wake," "N1," "N2," "N3/SWS," "REM," "Movement"), all possible interactions among them, and covariates of stimulation condition order ("Active First," "Sham First") and STAMP type ("tDCS," "tACS"). We only found a marginally significant effect of stimulation condition [$F(1,394) = 3.66$, $p = 0.056$] and a significant effect of sleep stage [$F(5,394) = 1506.97$, $p <$ 2e-16]. All other effects were not significant. Importantly, there were no interactions involving stimulation condition and sleep stage. We also examined the potential effects of STAMPs on sleep efficiency using a similar linear mixed-effects model with subject as a random factor and with fixed factors for stimulation condition ("Active," "Sham"), experimental night ("Night 1," "Night 2"), an interaction between them, and covariates of stimulation condition order ("Active First," "Sham First") and STAMP type ("tDCS," "tACS"). We did not find any significant effects. These results suggest that STAMPs did not modulate the sleep stage distributions or sleep efficiency (see **Table 1**).

Further, we analyzed the number of SW events during sleep using a linear mixed-effects model with subject as a random factor and with fixed factors for stimulation condition ("Active," "Sham"), experimental night ("Night 1," "Night 2"), sleep stage ("Wake," "N1," "N2," "N3/SWS," "REM," "Movement"), all possible interactions among them, and covariates of stimulation condition order ("Active First," "Sham First") and STAMP type ("tDCS," "tACS"). We only found a significant effect of sleep stage [$F(5,337.03) = 171.71$, $p <$ 2e-16]. All other effects were not significant. As SWOs occur predominantly during NREM sleep stages 2 and 3 (Rasch and Born, 2013), we re-ran the above linear mixed-effects model with the sum for "N2" and "N3/SWS" contrasted with the sum for all the other sleep stages. We found only a significant effect of the lumped sleep stage [$F(1,116) = 230.97$, $p <$ 2e-16], with the number of SW events

about 7× more likely to occur during "N2" and "N3/SWS" compared to all other stages combined. These results verify that the automated SWO detection was sufficiently accurate for the application of STAMPs (see **Table 2**).

Waking Sensations

We next investigated the effects of STAMPs on sensations during episode viewing using a repeated measures ANOVA with two within-subjects factors (sensation type: "itching," "heat/burning," "tingling"; stimulation condition: "Active," "Sham") and two between-subjects factors (STAMP type: "tDCS," "tACS"; stimulation condition order: "Active First," "Sham First"). We found a significant effect of stimulation condition [$F(1,20) = 28.50$, $p = 0.000032$], with the sensations during "Active" stimulation rated higher by 1.58 compared to "Sham" when collapsed across sensation types. All other effects were not significant, including between tDCS and tACS STAMPs. Numerically tACS STAMP sensations were rated on average lower than tDCS STAMP sensations when collapsed across within-subject factors. The overall mean values for sensations were below 2.5 out of 10 in the "Active" stimulation condition and below 1 out of 10 in the "Sham" stimulation condition, which are much less than the threshold score of 7 on the 0–10 Likert scale for an intense sensation, suggesting that STAMPs were well tolerated.

Further, we ran a series of chi-squared tests to investigate whether subjects were blind to the stimulation conditions. Due to the within-subjects nature of the design, we assessed if subjects were able to guess both stimulation conditions successfully, which was not the case [$\chi^2(1) = 0.053$, $p = 0.82$]. We then looked at each stimulation condition separately, regardless of order. For the "Active" stimulation condition, subjects were not able to guess their condition successfully [$\chi^2(1) = 0.18$, $p = 0.67$]. For the "Sham" stimulation condition, however, all subjects guessed their condition successfully; so a chi-squared test could not be performed. Because of this, we looked at stimulation condition order effects ("Active First" vs. "Sham First"). "Active First" subjects were not able to guess their stimulation conditions successfully [$\chi^2(1) = 1.60$, $p = 0.21$], whereas "Sham First" subjects were able to do so at a trend level [$\chi^2(1) = 2.78$, $p = 0.096$]. Overall these results suggest that the subjects were sufficiently blind to the stimulation condition and order assignments.

TABLE 1 | Sleep scoring statistics.

	Night 1		Night 2	
	Active (*N* = 16)	**Sham (*N* = 18)**	**Active (*N* = 16)**	**Sham (*N* = 20)**
Wake	14.75 (4.59)	27.89 (8.60)	29 (6.25)	27.1 (4.79)
N1	13.75 (1.98)	18.92 (1.57)	15.31 (1.98)	20 (1.73)
N2	303.22 (8.54)	291.72 (8.92)	290.88 (8.60)	291.3 (7.23)
N3/SWS	89.28 (5.88)	92.75 (5.97)	80.03 (6.02)	85.68 (3.81)
REM	59.91 (6.65)	69.64 (6.73)	57.41 (6.64)	80.75 (3.30)
Movement	2.88 (0.95)	2.72 (0.52)	2.31 (0.63)	3.3 (0.63)
Sleep efficiency	97.05% (0.87%)	94.43% (1.74%)	93.92% (1.33%)	94.63% (0.99%)

Mean and standard error of mean of the amount of time (in minutes) spent in various sleep stages and of sleep efficiency (%) for the two experimental nights and the two stimulation conditions across subjects.

TABLE 2 | Validation of the application of STAMPs during SWOs in NREM sleep stages 2 and 3.

Sleep stage	**Night 1**		**Night 2**	
	Active	**Sham**	**Active**	**Sham**
Wake	7.71 (4.74)	58.31 (20.42)	54.67 (28.16)	76.22 (24.37)
N1	29.79 (7.17)	51.13 (11.67)	39.93 (8.30)	48.78 (7.31)
N2	997.43 (122.34)	800.38 (89.70)	859.47 (110.65)	813.78 (53.93)
N3/SWS	668.93 (114.61)	597.56 (82.77)	537.33 (71.76)	538.67 (52.59)
REM	183.71 (59)	94.75 (21.075)	122.87 (34.85)	114.78 (25.43)
Movement	8.43 (4.40)	9.75 (3.18)	5.2 (1.83)	11.44 (2.24)

Mean and standard error of mean of the number of SW events in various sleep stages for the two experimental nights and the two stimulation conditions across subjects.

Absolute Accuracy

For behavior, we first examined absolute accuracy scores using a linear mixed-effects model with subject as a random factor. Fixed effects included intervention type ("Tag & Cue," "Tag & No Cue," "Sham"), day ("Day 2," "Day 3"), the interaction of intervention type and day, and covariates of baseline performance ("Day 1"), STAMP type ("tDCS," "tACS"), stimulation condition order ("Active First," "Sham First"), episode group ("Group A," "Group B") in the first week, and episode subgroup that was tagged and cued ("Subgroup 1," "Subgroup 2"). We only found a significant effect of baseline performance [$F(1,79.92) = 25.33$, $p = 2.92e\text{-}6$] and a marginally significant effect of intervention type [$F(2,104.015) = 2.77$, $p = 0.067$]. All other effects were not significant. Given the marginally significant effect of intervention type, we performed two-tailed paired-sample *t*-tests on absolute accuracy scores averaged over Day 2 and Day 3. The measures for "Tag & Cue" episodes were not significantly different from those for both "Tag & No Cue" [$t(23) = -0.69$, adjusted $p = 0.50$, Holm–Bonferroni correction for two comparisons] and "Sham" [$t(23) = -1.77$, adjusted $p = 0.18$, Holm–Bonferroni correction for two comparisons] episodes. While not significant, the absolute accuracy for "Tag & No Cue" and "Sham" episodes averaged over Day 2 and Day 3 and across subjects was numerically higher than that for "Tag & Cue" episodes by 1.83 and 4.58%, respectively. Overall these results suggest that STAMPs did not selectively modulate the absolute accuracy of memory recall as such.

Metamemory

We next analyzed the metamemory scores (see **Figure 4A** and **Table 3**) using a linear mixed-effects model with the same fixed and random effects as above. Similar to absolute accuracy, we found marginally significant effects of baseline performance [$F(1,129.69) = 2.75$, $p = 0.10$] and intervention type [$F(2,113.18) = 2.90$, $p = 0.059$]. But unlike absolute accuracy, metamemory significantly differed between

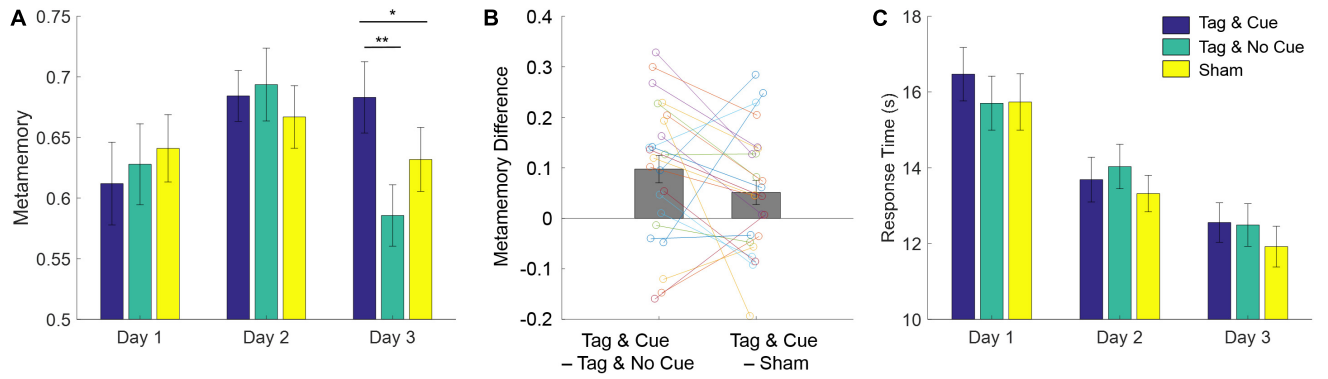

FIGURE 4 | STAMP tagging and cueing enhances episodic metamemory without a speed–accuracy trade-off. **(A)** Metamemory performance on the episodic memory task is reported across the 3 days of testing. Blue bars show the metamemory scores for "Tag & Cue" episodes, green for "Tag & No Cue" episodes, and yellow for "Sham" episodes. As shown in **Figure 3**, metamemory is computed as the area under the Type-2 ROC curve (0-1). Metamemory scores for "Tag & Cue" episodes are significantly higher than those for "Tag & No Cue" by 19.43% (p = 3.796e-3, corrected; paired-sample Cohen's d = 0.72) or "Sham" episodes by 10.01% (p = 0.048, corrected; paired-sample Cohen's d = 0.43) on Day 3. The markers correspond to data from individual subjects for Day 3. **(B)** Paired differences in metamemory on Day 3 from individual subjects with respect to "Tag & Cue" episodes. **(C)** Response time (RT) decreased across the 3 days of testing, but there were no significant differences among the intervention types. Error bars represent ± 1 SEM (N = 24).

TABLE 3 | Results of the linear mixed-effects model for the effects of STAMPs on metamemory.

Effect	NumDF	DenDF	*F*-value	*P*-value
Baseline performance	1	129.69	2.75	0.10
STAMP type	1	17.97	0.63	0.44
Stimulation condition order	1	18.011	0.19	0.67
Episode group	1	18.089	0.38	0.54
Episode subgroup	1	18.023	0.022	0.88
Intervention type	2	113.18	2.90	0.059
Day	1	113.091	8.51	**0.0043**
Intervention type × day	2	113.091	3.66	**0.029**

The P-values for the significant effects are highlighted in bold.

days [F(1,113.091) = 8.51, p = 0.0043], and there was a significant interaction between intervention type and day [F(2,113.091) = 3.66, p = 0.029]. Based on the significant interaction between intervention type and day, we ran follow-up linear mixed-effects models for each day separately with intervention type and subject as fixed and random factors, respectively. For Day 2, there were no significant effects. However, for Day 3, we found a significant effect of intervention type [F(2,46) = 6.35, p = 0.0037]. Thus, the metamemory scores differed significantly across the intervention types by Day 3 following the application of "Tag & Cue" STAMPs during two consecutive nights.

Our main hypotheses of interest were the performance for "Tag & Cue" episodes would be better than that for either "Tag & No Cue" or "Sham" episodes following the sleep intervention with "Tag & Cue" STAMPs. Given the significant effect of intervention type on Day 3, we performed two-tailed paired-sample t-tests on metamemory scores from Day 3. "Tag & Cue" metamemory scores were significantly greater than both "Tag & No Cue" [t(23) = 3.51, adjusted p = 3.79e-3, Holm–Bonferroni correction for two comparisons; paired-sample Cohen's d = 0.72] and "Sham" [t(23) = 2.089, adjusted p = 0.048, Holm–Bonferroni correction for two comparisons; paired-sample Cohen's d = 0.43] metamemory scores (see **Figure 4B**). And it turned out that "Tag & No Cue" metamemory scores were not significantly different from "Sham" metamemory scores [t(23) = −1.56, uncorrected p = 0.13]. Thus, the application of STAMPs during SWOs in the two nights following one-shot viewing led to specific enhancement of metamemory for the episodes that were both tagged and cued. The long-term benefit in metamemory for the "Tag & Cue" episodes is remarkable, considering that the episodes were only tagged once during viewing.

We also checked if mere tagging of episodes with STAMPs modulated their immediate metamemory following encoding. In particular, the baseline performance ("Day 1") was assessed with a linear mixed-effects model with intervention type ("Tag & Cue," "Tag & No Cue," "Sham") and subject as fixed and random factors, respectively. There was no significant effect of intervention type [F(2,118) = 0.56, p = 0.58], confirming that STAMP-based tagging during episode viewing did neither improve nor impair the baseline performance. To further understand the primary result, we also analyzed response times (RTs) using a linear mixed-effects model with subject as a random factor (see **Figure 4C**). Fixed effects included intervention type ("Tag & Cue," "Tag & No Cue," "Sham"), day ("Day 2," "Day 3"), the interaction of intervention type and day, and a covariate of baseline performance ("Day 1"). We found significant effects of day [F(1,108.95) = 32.11, p = 1.21e-7] and baseline performance [F(1,137) = 11.75, p = 0.00080], and a marginally significant effect of intervention type [F(2,109.54) = 2.45, p = 0.091]. Importantly, the interaction of intervention type and day was not significant [F(2,108.95) = 0.25, p = 0.78], suggesting that the subjects responded with similar speeds across the three intervention types. This demonstrates that the benefit to metamemory on Day 3 from STAMP-based tagging and cueing was not simply due to a speed-accuracy trade-off.

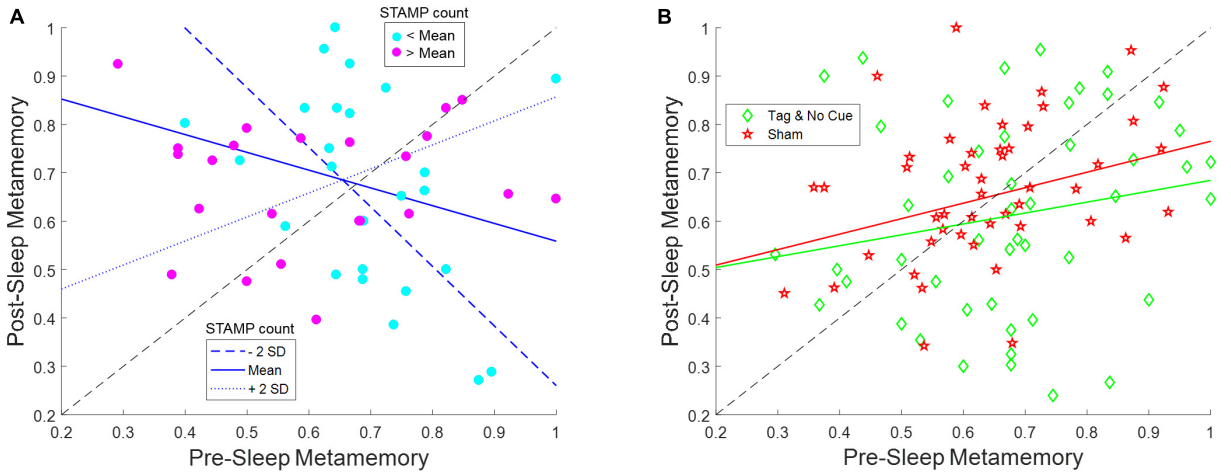

FIGURE 5 | STAMP tagging and cueing on metamemory is modulated by an interaction between pre-sleep metamemory and the number of STAMP applications. **(A)** Post-sleep metamemory for "Tag & Cue" episodes depends on the interaction between the covariates of pre-sleep metamemory and STAMP count for both experimental nights. The three lines represent the linear mixed-effects model predictions for different STAMP counts (ranging from two standard deviations below the mean to two standard deviations above the mean). The markers correspond to data for "Tag & Cue" episodes from individual subjects for both experimental nights (i.e., two per night per subject), with color coding based on whether the overnight STAMP dose was lower (cyan) or greater (magenta) than the mean. **(B)** The interactions of pre-sleep metamemory with STAMP count for "Tag & No Cue" episodes, and with the number of SW events for "Sham" episodes, are not significant for both experimental nights. The lines represent the linear fits to the pertinent data. The markers correspond to data for "Tag & No Cue" (green) and "Sham" (red) episodes from individual subjects for both experimental nights (i.e., two per night per subject).

Interaction Between Pre-Sleep Metamemory and Overnight STAMPs

The evening pre-sleep metamemory and the number of STAMP applications in each "Active" night varied widely across the subjects, with the latter depending on the number of SW events detected. We therefore analyzed the effects and interactions of these covariate variables on the morning post-sleep metamemory for "Tag & Cue" and "Tag & No Cue" episodes within the "Active" stimulation condition using a linear mixed-effects model with subject as a random factor (see **Figure 5** and **Table 4**). Fixed effects of this model included categorical variables of intervention type ("Tag & Cue," "Tag & No Cue") and experimental night ("Night 1," "Night 2"), continuous variables of pre-sleep metamemory and the number of STAMP applications, and all possible interactions among them. We found a marginally significant effect of pre-sleep metamemory [$F(1,79.009) = 3.61$, $p = 0.061$], significant effects of intervention type [$F(1,69.77) = 10.83$, $p = 0.0016$], a marginally significant two-way interaction of pre-sleep metamemory and STAMP count [$F(1,78.008) = 3.24$, $p = 0.076$], significant two-way interactions of intervention type and STAMP count [$F(1,68.19) = 6.17$, $p = 0.015$] and of intervention type and pre-sleep metamemory [$F(1,70.43) = 9.33$, $p = 0.0032$], and a significant three-way interaction of intervention type, pre-sleep metamemory, and STAMP count [$F(1,68.90) = 5.73$, $p = 0.019$]. All other effects were not significant. In particular, post-sleep metamemory was not modulated by experimental night.

Based on these results, we ran follow-up linear mixed-effects models for "Tag & Cue" and "Tag & No Cue" episodes separately with subject as a random factor and with pre-sleep metamemory, STAMP count, and the interaction of pre-sleep metamemory and STAMP count as fixed effects. There were no significant effects for "Tag & No Cue" episodes (see **Figure 5B**). However, for "Tag

TABLE 4 | Results of the linear mixed-effects model for the interaction between pre-sleep metamemory and the number of STAMP applications on post-sleep metamemory.

Effect	NumDF	DenDF	*F*-value	*P*-value
Intervention type	1	69.77	10.83	**0.0016**
Night	1	66.64	0.81	0.37
Pre-sleep metamemory	1	79.009	3.61	0.061
STAMP count	1	79.69	2.44	0.12
Intervention type × night	1	65.92	0.28	0.60
Intervention type × pre-sleep metamemory	1	70.43	9.33	**0.0032**
Intervention type × STAMP count	1	68.19	6.17	**0.015**
Night × pre-sleep metamemory	1	66.79	0.46	0.50
Night × STAMP count	1	67.34	1.06	0.31
Pre-sleep metamemory × STAMP count	1	78.008	3.24	0.076
Intervention type × night × pre-sleep metamemory	1	66.31	0.38	0.54
Intervention type × night × STAMP count	1	69.49	0.0003	0.99
Intervention type × pre-sleep metamemory × STAMP count	1	68.90	5.73	**0.019**
Night × pre-sleep metamemory × STAMP count	1	67.75	0.30	0.59
Intervention type × night × pre-sleep metamemory × STAMP count	1	70.21	0.066	0.80

The P-values for the significant effects are highlighted in bold.

& Cue" episodes, we found significant effects of both pre-sleep metamemory [$F(1,42.24) = 8.40$, $p = 0.0059$] and STAMP count [$F(1,39.72) = 6.86$, $p = 0.012$], and a significant interaction of pre-sleep metamemory and STAMP count [$F(1,38.68) = 7.14$, $p = 0.011$]. Given that the application of STAMPs occurred during SWOs, we considered if the effects involving the STAMP count for the "Tag & Cue" episodes were confounded by the number of concomitant SW events. To resolve this, we analyzed post-sleep metamemory for the "Sham" episodes using a linear mixed-effects model with subject as a random factor and with pre-sleep metamemory, the number of SW events, and the interaction between them as fixed effects. We did not find any significant effects (see **Figure 5B**). These results provide further evidence for the specific modulation of episodic memories that were both tagged during waking and cued during sleep.

For "Tag & Cue" episodes, subjects with weak pre-sleep metamemory who received more than the mean dose of STAMP cueing during sleep had a lower overnight increase in metamemory than those who received less than the mean dose. On the other hand, subjects with strong pre-sleep metamemory who received more than the mean dose of STAMP cueing had less of an overnight decrease in metamemory compared to those who received less than the mean dose (see **Figure 5A**). It is worth noting that the overall boost in metamemory for "Tag & Cue" episodes on Day 3 (see **Figures 4A,B**) occurred despite the presence of this significant interaction between pre-sleep metamemory and the number of STAMP applications on post-sleep metamemory, suggesting that the effect size can be further enhanced by regulating the number of STAMP applications based on pre-sleep metamemory.

Sleep Biomarkers

Finally, we investigated the neurophysiological effects of "Tag & Cue" STAMPs during Night 2 owing to significant differences between "Tag & Cue" episode and other intervention types on Day 3. First, we contrasted average post-SW event changes in spectral power between "Active" and "Sham" Night 2 using non-parametric cluster-based permutation tests for five frequency bands (SW: 0.5–1.2 Hz, delta: 1–4 Hz, theta: 4–8 Hz, slow-spindle: 8–12 Hz, fast-spindle: 12–15 Hz) of relevance to memory consolidation (Mölle et al., 2011; Cox et al., 2014). Note high-amplitude stimulation artifacts preclude the inspection of EEG data during the application of STAMPs and up to 3 s following their offset. Significant "contrast clusters" of channel × time bins that differed in spectral power changes between "Active" and "Sham" Night 2 within 3–10 s following the offset of SW events were determined for each frequency band using a non-parametric permutation test to correct for multiple comparisons in the channel × time space (Maris and Oostenveld, 2007). A similar non-parametric cluster-based permutation test was then carried out for correlations of differences in overnight changes in metamemory between "Tag & Cue" and "Sham" episodes with the corresponding differences in spectral power changes following SW events to obtain "correlation clusters." This analysis was restricted to the channel × time bins in the "contrast clusters" in order to relate overnight metamemory changes with specific spectral power modulations induced by STAMPs.

The analysis revealed a "contrast cluster" only in the slow-spindle band (8–12 Hz), such that the average post-SW event change in spectral power was lower (and negative) in the "Sham" Night 2 compared to the "Active" Night 2 (see **Figure 6A** and **Supplementary Figure S2**). This "contrast cluster" temporally extended from 6.18 to 6.7 s relative to the offset of SW events, and had a clusterwise *P*-value of 0.025 after the additional Bonferroni correction for the five frequency bands ($p = 0.005$, uncorrected). Scalp topography of *t*-values for the spectral power changes in the cluster indicated an early distribution over pre-frontal, left frontal, and left temporal areas, which then widened to include occipital and parietal regions (see **Figure 6B** and **Supplementary Figure S2**). These areas are consistent with the known involvement of dorsolateral prefrontal and parietal cortices (Chua et al., 2009) in the neural mechanisms of metamemory. Next, we correlated the differences in overnight metamemory changes between "Tag & Cue" and "Sham" episodes with the differences in average spectral power change within this "contrast cluster" between "Active" and "Sham" Night 2. We found a positive "correlation cluster" within the slow-spindle band between 6.56 and 6.64 s relative to the offset of SW events, with a clusterwise *P*-value of 0.013 (see **Figure 6C**), such that there was a positive correlation between the average STAMP-induced increase in slow-spindle power and the overnight improvement in metamemory ($r = 0.73$; see **Figure 6D**). Scalp topography of the summed *t*-values for the spectral power changes in this "correlation cluster" indicated a concentration on the left temporal region.

DISCUSSION

Applied neuroscience aims to develop technologies to affect behavior by modulating brain activity at the right spatiotemporal scale. It has been suggested that an intervention to enhance specific episodic memories needs to operate with high spatiotemporal resolution in the hippocampus (Suthana and Fried, 2014; Hampson et al., 2018). Contrary to this conventional wisdom, we have demonstrated a novel form of tES in healthy humans to boost the metamemory of specific episodes that were viewed only once in immersive VR. In particular, we discovered that unique spatiotemporal patterns (namely, STAMPs) of tES can be used for one-shot tagging of naturalistic episodes during waking and subsequent cueing during SWOs in sleep, and that those STAMPs when re-applied during SWOs can not only boost but also impair the metamemory of individual episodes depending on an interaction between pre-sleep metamemory and the number of STAMP applications through the night. Moreover, we found that post-stimulation increases in slow-spindle (8–12 Hz) power for left temporal areas in scalp EEG during sleep serve as a STAMP-induced biomarker of overnight metamemory improvements.

Spatiotemporal amplitude-modulated patterns did not modulate either the sleep architecture or the sleep efficiency of the subjects. In particular, there was no difference in the amount of time they were awake during the nights between the "Active" and "Sham" stimulation conditions. We therefore can conclude

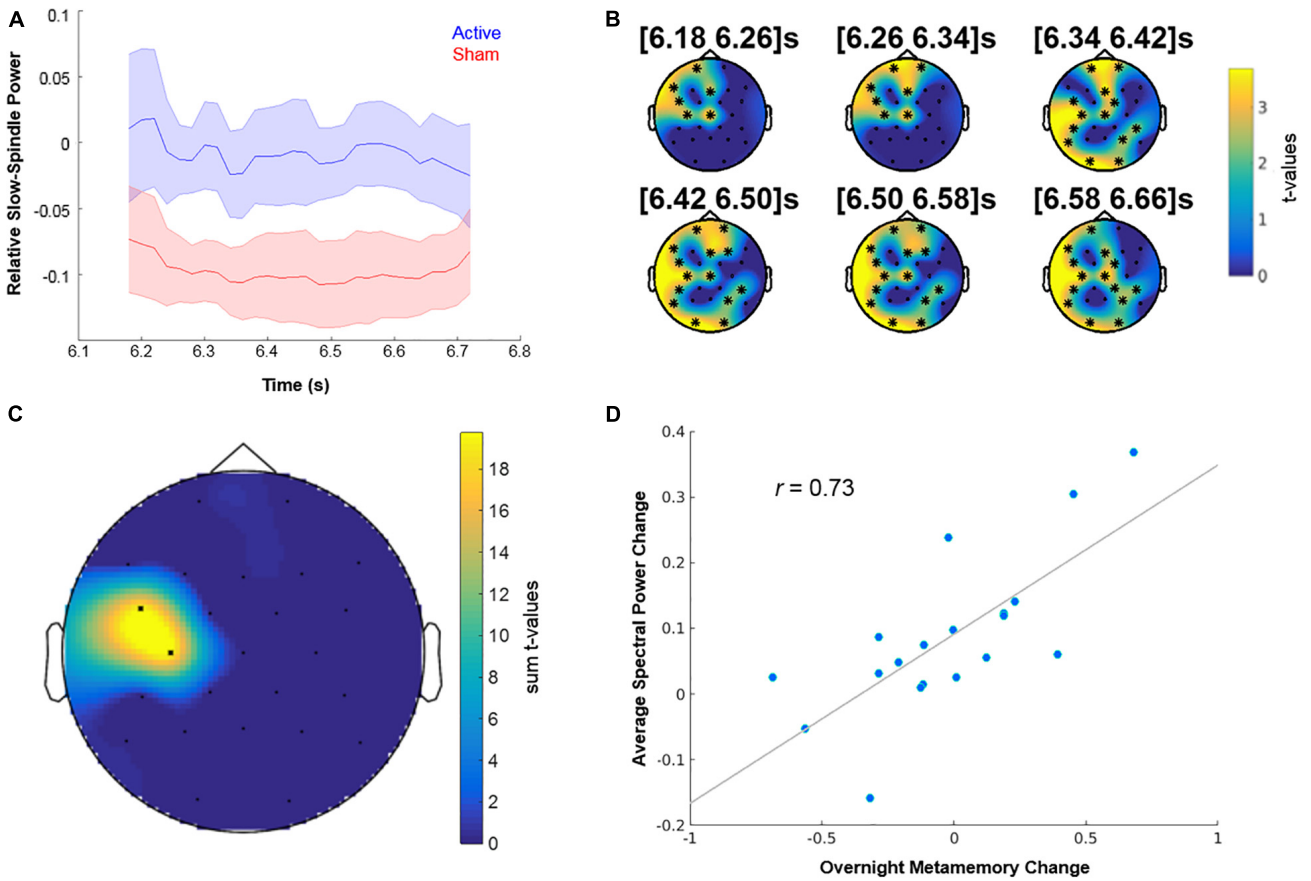

FIGURE 6 | Neurophysiological and behavioral effects of STAMPs. **(A)** Dynamics of spectral power changes for the slow-spindle (8–12 Hz) "contrast cluster," relative to the offset of SW events, showing significant differences between "Active" and "Sham" Night 2. **(B)** Scalp topography of *t*-values for the slow-spindle "contrast cluster" (clusterwise $p = 0.025$, additionally corrected for five frequency band comparisons) at six time points within the significant window (6.18–6.7 s following the offset of SW events). EEG channels participating in the cluster are marked by asterisks. **(C)** Scalp topography of summed *t*-values for the slow-spindle "correlation cluster" (clusterwise $p = 0.013$) from significant time bins. **(D)** Correlation of the differences in average spectral power change between "Active" and "Sham" Night 2 from "correlation cluster" bins and the differences in overnight metamemory change between "Tag & Cue" and "Sham" episodes ($r = 0.73$). Dots correspond to data from individual subjects ($N = 19$).

that subjects were able to sleep normally, without any disruption, despite the application of STAMPs. Moreover, we found that cueing with "Tag & Cue" STAMPs during sleep did not boost the long-term metamemory of "Tag & No Cue" episodes. This implies that the mere application of STAMP cues during SWOs does not have a non-specific effect on the metamemory of all recently viewed episodes.

There was a significant effect of stimulation condition on sensations during episode viewing with higher sensation ratings for the "Active" stimulation condition. This does not necessarily indicate a failure in blinding the subjects to the stimulation conditions. Even though the "Sham First" subjects were able to guess their stimulation conditions at a trend level, we did not find an effect of stimulation condition order on sensation ratings. Further, the significant difference in the metamemory of "Tag & Cue" and "Tag & No Cue" episodes on Day 3 within the "Active" stimulation condition cannot be accounted for by the potential confound of blinding. Nonetheless, blinding is an important concern in within-subjects designs, and in future studies we would suggest adding an additional control condition that employs one STAMP to tag an episode during waking and a different STAMP to cue that episode during sleep.

The STAMPs for this study were designed to induce different electric fields in different brain regions. Similar to sensory cue-based TMR studies (e.g., Rasch et al., 2007; Rudoy et al., 2009; Antony et al., 2012), our paradigm is based on the co-occurrence of STAMP-induced electric fields (and consequent neural effects) in various brain regions and the distributed neural activity evoked by the encoding of an episode. Previous TMR studies can be argued to take advantage of existing memory pathways from the pertinent sensory cortices to the medial temporal regions. Because STAMPs induce a wide range of effects in distributed regions, it can be argued that STAMPs may be stimulating these exact pathways along with other unknown pathways that can influence memory processes. We intentionally make no claims about the specific pathways that are stimulated, but rather suggest that the mechanism is related to the distributed pattern across many potential pathways. Further work

is necessary to understand the degree to which any particular STAMP influences memory performance and the mechanisms related to those STAMPs.

We postulate that one-shot tagging is feasible owing to what appears to be the rapid associations that are formed between the STAMP-induced neural effects and the distributed memory traces. Just as in sensory cue-based TMR studies, these functional associations are then subsequently leveraged to potentially cue the reactivation of the memory traces during offline periods using the STAMPs alone for improved likelihood of consolidation. Memory traces are understood to be re-generated (or replayed) in response to partial or associated cues due to the pattern completion property of dense recurrent networks in the hippocampus. It is important to note that we are not employing STAMPs to selectively enhance the distributed neural activity of a memory trace during encoding as such. Indeed, in our experiment, the pairing between the 14 STAMPs and episodes in the "Active" stimulation condition was arbitrary and randomly chosen for each subject.

Absolute accuracy is a function of both memory sensitivity and response bias and is hence not considered a good metric for episodic memory recall. We found that STAMPs did not modulate the absolute accuracy of memory recall, but we are not able to draw any conclusions regarding whether STAMPs can instead modulate more sensitive bias-free metrics of episodic memory such as those that use Type-1 ROC curve analysis of confidence ratings on a scale from "Definitely False" to "Definitely True" for the declarative statements about the episodes (MacMillan and Creelman, 2005; Mickes et al., 2012). Our experimental design only supports Type-2 ROC curve analysis (which measures metamemory) owing to the two-level responses – one for whether a declarative statement was "True" or "False," and the other to rate the correctness of the response on a scale from "Least Confident" to "Most Confident." Though pseudo confidence rating distributions for Type-1 true positives and false positives can be theoretically constructed by spanning the range from "Definitely False" to "Definitely True" using highest confidence "False" and "True" responses, respectively (Gombos et al., 2012), the subjects' Type-1 responses can only be predicted (with certain assumptions) rather than empirically measured (Galvin et al., 2003).

While it remains an open question if STAMPs also modulate episodic memory in a targeted manner, previous studies have suggested that memory and metamemory are likely correlated (Sacher et al., 2009; Yacoby et al., 2015). Broadly speaking, it has been proposed that metamemory is driven by either the familiarity of the recall cue, or the accessibility of any available pertinent information including that retrieved from memory in response to the cue (Koriat and Levy-Sadot, 2001). In either case, judgments about memories likely leverage the same neural representations of memory traces as the memory recall itself (Fleming and Dolan, 2012). The interaction between pre-sleep metamemory and STAMP count during sleep for "Tag & Cue" episodes on post-sleep metamemory can be understood with the framework of complementary learning systems (McClelland et al., 1995). According to this theory, episodic experiences are rapidly encoded in the hippocampus during waking for the short term. Before the hippocampal memory traces fade out, episodic memories are consolidated into long-term storage in the slow-learning neocortex during sleep through replays of pertinent neural activity patterns. The lack of an effect on metamemory on Day 2 could be due to the presence of sufficiently strong memory traces in the hippocampus for the episodes across the three intervention types, which will likely fade out by Day 3. Subjects with weak metamemory prior to sleep benefit from STAMP-based cueing because the sequential structure of the episodes can be strengthened in the hippocampus as well as consolidated in the cortex. We speculate that an excessive number of STAMPs can, however, roll back this benefit by learning remote, higher order links between events within the episodes. Subjects with strong metamemory prior to sleep do not benefit from STAMP cueing, on average, due to the same reason. So, the prescription for boosting the metamemory of episodic experiences is to apply an optimal number of STAMPs during sleep for subjects with weaker pre-sleep metamemory, and to not intervene for subjects with stronger pre-sleep metamemory (cf., Schapiro et al., 2018).

Our study has many potential extensions. First, we need to ascertain if STAMPs can also boost the memory of targeted episodic experiences by measuring Type-1 confidence ratings, which can be used to compute both memory and metamemory using ROC curve analyses (Galvin et al., 2003). Second, the neural effects of STAMPs in scalp EEG underlying the one-shot tagging of episodes during wake need to be investigated (similar to the analyses of sleep biomarkers). Third, we need to validate whether STAMPs can indeed tag distributed neural representations in a single trial by altering the functional connectivity as well as the spike timing within the brain in unique ways. This can be done using simultaneous multi-site intracranial recordings of local field potential, multi-unit activity, and single-neuron activity during wake and sleep in non-human primates and clinical human populations (cf., Krause et al., 2017, 2019b). Fourth, we need to assess the longevity of preservation of episodic metamemory with a longer longitudinal study and whether there would be any adverse effects in other aspects of behavior. Fifth, the library of mutually orthogonal STAMPs can be personalized for each individual user's head as well as optimized for particular brain areas that are pertinent to a given task to further boost the efficacy of STAMPs to tag and cue memories. Sixth, new sleep studies are in order that aim to maximize the benefits of STAMPs during sleep by regulating the number of STAMP applications based on pre-sleep metamemory (see **Figure 5**), as well as the intensity and frequency of particular STAMPs based on post-stimulation biomarkers of metamemory (see **Figure 6**). Seventh, the application of STAMPs was limited to the presence of SWOs during sleep, and so the optimal dose may not be deliverable to a subject due to impoverished SW activity. A potential strategy is to employ SW tACS to boost SWOs (Jones et al., 2018; Ketz et al., 2018) in alternating blocks with STAMPs. However, our recent attempt at this strategy failed to boost the consolidation of individual sequential experiences (Lerner et al., 2019). Potential reasons for the failure include a much smaller sample size for a between-subjects design (N = 12), the usage of a hybrid task with both procedural and declarative memory elements, the presence of a hidden temporal regularity shared across

all sequence types, and mutual interference between specific STAMPs and non-specific SW tACS. Finally, we can perform a control experiment to rule out the potential but unlikely possibility that the behavioral effects of tES STAMPs are mediated indirectly via tactile sensations on the scalp, instead of directly through electric fields induced in the brain volume. In this regard, the spatial and frequency specificity of tACS to entrain single neurons in the hippocampus of awake macaque monkeys (Krause et al., 2019b; see also Johnson et al., 2019) has been shown to be preserved even when the somatosensory afferents in the scalp are blocked using topical anesthesia (Vieira et al., 2019; see also Krause et al., 2019a).

The effect of STAMPs on overnight metamemory improvements was correlated with an increase in slow-spindle (8–12 Hz) power for left temporal areas following STAMPs during sleep. Spindles are demonstrably a critical component of sleep-dependent memory consolidation (Fogel and Smith, 2011) as shown in rodents (Eschenko et al., 2006) as well as humans (Cox et al., 2012). Recent optogenetic work in rats demonstrated a causal role for sleep spindles in coupling SWOs and hippocampal sharp wave ripples for effective consolidation to long-term memory storage (Latchoumane et al., 2017). Spindles reverberate in circular wave-like patterns across temporal, parietal, and frontal regions repeatedly throughout the night, regulating the process of memory re-organization over time and space (Muller et al., 2016). To the best of our knowledge, there have been no studies on the hemispheric differences in the sleep-dependent consolidation of episodic memory and/or metamemory. In this regard, our results suggest that the left temporal lobe may play a key role in boosting the consolidation of episodic metamemory. However, given the limited spatial resolution of EEG measurements, further work will be necessary to localize the specific neural sources contributing to the observed left temporal slow-spindle cluster. Also, volume conduction effects may influence the non-parametric cluster analysis, but the only impact would be on the spatial specificity and not the false positive rate of the presence of an effect. We therefore cannot make any conclusive statements on the cortical source of the observed effects.

CONCLUSION

In summary, we have developed a novel non-sensory non-invasive method to tag naturalistic episodic experiences in one shot and cue them during offline periods to boost their metamemory in a targeted manner. We overcome the limitations of previous TMR studies (e.g., Rasch et al., 2007; Rudoy et al., 2009; Antony et al., 2012) by demonstrating one-shot tagging during wake and cueing during sleep with tES STAMPs, which are not only scalable but also do not suffer interference from ambient environmental cues in real-world settings. Our results suggest that, unlike relatively localized brain circuits responsible for regulating mood (Rao et al., 2018) and movement (Follett et al., 2010), episodic memories are processed by a much more widespread network of brain areas. We believe that our study will pave the way for next-generation transcranial brain–machine interfaces that can boost learning and memory in healthy humans for real-world tasks. Such a non-invasive approach can also potentially benefit a majority of patients with learning and memory deficits at much lower cost and risk than required for implanting intracranial electrode arrays. It could also be possible to enhance the efficacy of exposure behavioral therapy with immersive VR using STAMP-based tagging and cueing for the treatment of post-traumatic stress disorder.

DATA AVAILABILITY STATEMENT

The datasets generated for this study are available on request to the corresponding author.

ETHICS STATEMENT

This study involving human subjects was reviewed and approved by the Chesapeake Institutional Review Board. The subjects provided their written informed consent to participate in this study.

AUTHOR CONTRIBUTIONS

PP and MH designed the research. PP, SS, NK, SR, IL, AJ, BR, NB, AH, TM, JC, VC, and MH performed the research. PP, RH, NK, AJ, BR, and TM analyzed the data. PP wrote the manuscript.

FUNDING

This material is based upon work supported by the DARPA and the Army Research Office under Contract No. W911NF-16-C-0018 (RAM Replay program). The views, opinions, and/or findings expressed are those of the authors and should not be interpreted as representing the official views or policies of the Department of Defense or the U.S. Government.

ACKNOWLEDGMENTS

We would like to thank Neuroelectrics, Inc., for contributions to the generation of STAMPs and for building the prototype StarStim 64 device, Drs. Albert Rizzo and John Wixted for contributions to the design of the behavioral paradigm, Aashish Patel for contribution to the behavioral analysis, Barry Aneda for sleep scoring, and Drs. Mark Gluck and Penelope Lewis for useful discussions through the course of this study.

SUPPLEMENTARY MATERIAL

The Supplementary Material for this article can be found online at: https://www.frontiersin.org/articles/10.3389/fnins.2019.01416/full#supplementary-material

REFERENCES

Antony, J. W., Gobel, E. W., O'Hare, J. K., Reber, P. J., and Paller, K. A. (2012). Cued memory reactivation during sleep influences skill learning. *Nat. Neurosci.* 15:1114. doi: 10.1038/nn.3152

Bendor, D., and Wilson, M. A. (2012). Biasing the content of hippocampal replay during sleep. *Nat. Neurosci.* 15, 1439–1444. doi: 10.1038/nn.3203

Berry, R. B., Brooks, R., Gamaldo, C. E., Harding, S. M., Marcus, C. L., and Vaughn, B. V. (2012). *The AASM Manual for the Scoring of Sleep and Associated Events. Rules, Terminology and Technical Specifications, Version 2.0*. Darien, IL: American Academy of Sleep Medicine.

Buzsáki, G. (1996). The hippocampo-neocortical dialogue. *Cereb. Cortex* 6, 81–92. doi: 10.1093/cercor/6.2.81

Chua, E. F., Schacter, D. L., and Sperling, R. A. (2009). Neural correlates of metamemory: a comparison of feeling-of-knowing and retrospective confidence judgments. *J. Cogn. Neurosci.* 21, 1751–1765. doi: 10.1162/jocn.2009.21123

Ciuparu, A., and Mureşan, R. C. (2016). Sources of bias in single-trial normalization procedures. *Eur. J. Neurosci.* 43, 861–869. doi: 10.1111/ejn.13179

Cox, R., Hofman, W. F., and Talamini, L. M. (2012). Involvement of spindles in memory consolidation is slow wave sleep-specific. *Learn Mem.* 19, 264–267. doi: 10.1101/lm.026252.112

Cox, R., Korjoukov, I., de Boer, M., and Talamini, L. M. (2014). Sound asleep: processing and retention of slow oscillation phase-targeted stimuli. *PLoS One* 9:e101567. doi: 10.1371/journal.pone.0101567

Crowley, R., and Javadi, A. (2019). The Modulatory Effect of Oscillatory Reinstatement During Slow-wave Sleep on declarative Memory Consolidation. *OSF Preprints*. doi: 10.31219/osf.io/8yxge.

Delorme, A., and Makeig, S. (2004). EEGLab: an open source toolbox for analysis of single-trial EEG dynamics including independent component analysis. *J. Neurosci. Methods* 134, 9–21. doi: 10.1016/j.jneumeth.2003.10.009

Eschenko, O., Mölle, M., Born, J., and Sara, S. J. (2006). Elevated sleep spindle density after learning or after retrieval in rats. *J. Neurosci.* 26, 12914–12920. doi: 10.1523/jneurosci.3175-06.2006

Fleming, S. M., and Dolan, R. J. (2012). The neural basis of metacognitive ability. *Philos. Trans. R. Soc. B* 367, 1338–1349. doi: 10.1098/rstb.2011.0417

Fleming, S. M., and Lau, H. C. (2014). How to measure metacognition. *Front. Hum. Neurosci.* 8:443. doi: 10.3389/fnhum.2014.00443

Fogel, S. M., and Smith, C. T. (2011). The function of the sleep spindle: a physiological index of intelligence and a mechanism for sleep-dependent memory consolidation. *Neurosci. Biobehav. R* 35, 1154–1165. doi: 10.1016/j.neubiorev.2010.12.003

Follett, K. A., Weaver, F. M., Stern, M., Hur, K., Harris, C. L., Luo, P., et al. (2010). Pallidal versus subthalamic deep-brain stimulation for Parkinson's disease. *New Engl. J. Med.* 362, 2077–2091. doi: 10.1056/NEJMoa0907083

Galvin, S. J., Podd, J. V., Drga, V., and Whitmore, J. (2003). Type 2 tasks in the theory of signal detectability: discrimination between correct and incorrect decisions. *Psychon. Bull. Rev.* 10, 843–876. doi: 10.3758/bf03196546

Gombos, V., Pezdek, K., and Haymond, K. (2012). Forced confabulation affects memory sensitivity as well as response bias. *Mem. Cogn.* 40, 127–134. doi: 10.3758/s13421-011-0129-5

Hampson, R. E., Song, D., Robinson, B. S., Fetterhoff, D., Dakos, A. S., Roeder, B. M., et al. (2018). Developing a hippocampal neural prosthetic to facilitate human memory encoding and recall. *J. Neural Eng.* 15:036014. doi: 10.1088/1741-2552/aaaed7

Javadi, A.-H., Glen, J. C., Halkiopoulos, S., Schulz, M., and Spiers, H. J. (2017). Oscillatory reinstatement enhances declarative memory. *J. Neurosci.* 37, 9939–9944. doi: 10.1523/jneurosci.0265-17.2017

Ji, D., and Wilson, M. A. (2007). Coordinated memory replay in the visual cortex and hippocampus during sleep. *Nat. Neurosci.* 10, 100–107. doi: 10.1038/nn1825

Johnson, L., Alekseichuk, I., Krieg, J., Doyle, A., Yu, Y., Vitek, J., et al. (2019). Dose-dependent effects of transcranial alternating current stimulation on spike timing in awake nonhuman primates. *bioRxiv [Preprint]*.

Jones, A. P., Choe, J., Bryant, N. B., Robinson, C. S. H., Ketz, N. A., Skorheim, S. W., et al. (2018). Dose-dependent effects of closed-loop tACS delivered during slow-wave oscillations on memory consolidation. *Front. Neurosci.* 12:867. doi: 10.3389/fnins.2018.00867

Ketz, N. A., Jones, A. P., Bryant, N. B., Clark, V. P., and Pilly, P. K. (2018). Closed-loop slow-wave tACS improves sleep dependent long-term memory generalization by modulating endogenous oscillations. *J. Neurosci.* 38, 7314–7326. doi: 10.1523/JNEUROSCI.0273-18.2018

Koriat, A., and Levy-Sadot, R. (2001). The combined contributions of the cue-familiarity and accessibility heuristics to feelings of knowing. *J. Exp. Psychol. Learn. Mem. Cogn.* 27, 34–53. doi: 10.1037/0278-7393.27.1.34

Krause, M. R., Vieira, P. G., Csorba, B. A., Pilly, P. K., and Pack, C. C. (2019a). Reply to Khatoun et al.: speculation about brain stimulation must be constrained by observation. *Proc. Natl. Acad. Sci. U.S.A.* 116, 22440–22441. doi: 10.1073/pnas.1914483116

Krause, M. R., Vieira, P. G., Csorba, B. A., Pilly, P. K., and Pack, C. C. (2019b). Transcranial alternating current stimulation entrains single-neuron activity in the primate brain. *Proc. Natl. Acad. Sci. U.S.A.* 116, 5747–5755. doi: 10.1073/pnas.1815958116

Krause, M. R., Zanos, T. P., Csorba, B. A., Pilly, P. K., Choe, J., Phillips, M. E., et al. (2017). Transcranial direct current stimulation facilitates associative learning and alters functional connectivity in the primate brain. *Curr. Biol.* 27, 3086–3096. doi: 10.1016/j.cub.2017.09.020

Latchoumane, C. F. V., Ngo, H. V. V., Born, J., and Shin, H. S. (2017). Thalamic spindles promote memory formation during sleep through triple phase-locking of cortical, thalamic, and hippocampal rhythms. *Neuron* 95, 424–435. doi: 10.1016/j.neuron.2017.06.025

Lerner, I., Ketz, N. A., Jones, A. P., Bryant, N. B., Robert, B., Skorheim, S. W., et al. (2019). Transcranial current stimulation during sleep facilitates insight into temporal rules, but does not consolidate memories of individual sequential experiences. *Sci. Rep.* 9:1516. doi: 10.1038/s41598-018-36107-7

Liao, H. I., Wu, D. A., Halelamien, N., and Shimojo, S. (2013). Cortical stimulation consolidates and reactivates visual experience: neural plasticity from magnetic entrainment of visual activity. *Sci. Rep.* 3:2228. doi: 10.1038/srep02228

MacMillan, N. A., and Creelman, C. D. (2005). *Detection Theory: A user's Guide*, 2nd Edn. Mahwah, NJ: Erlbaum Press.

Maris, E., and Oostenveld, R. (2007). Nonparametric statistical testing of EEG-and MEG-data. *J. Neurosci. Methods* 164, 177–190. doi: 10.1016/j.jneumeth.2007.03.024

McClelland, J. L., McNaughton, B. L., and O'Reilly, R. C. (1995). Why there are complementary learning systems in the hippocampus and neocortex: insights from the successes and failures of connectionist models of learning and memory. *Psychol. Rev.* 102:419. doi: 10.1037/0033-295X.102.3.419

Mickes, L., Flowe, H. D., and Wixted, J. T. (2012). Receiver operating characteristic analysis of eyewitness memory: comparing the diagnostic accuracy of simultaneous versus sequential lineups. *J. Exp. Psychol.* 18, 361. doi: 10.1037/a0030609

Mölle, M., Bergmann, T. O., Marshall, L., and Born, J. (2011). Fast and slow spindles during the sleep slow oscillation: disparate coalescence and engagement in memory processing. *Sleep* 34, 1411–1421. doi: 10.5665/SLEEP.1290

Muller, L., Piantoni, G., Koller, D., Cash, S. S., Halgren, E., and Sejnowski, T. J. (2016). Rotating waves during human sleep spindles organize global patterns of activity that repeat precisely through the night. *eLife* 5:e17267. doi: 10.7554/eLife.17267

Nelson, T. O., and Narens, L. (1990). Metamemory: a theoretical framework and new findings. *Psychol. Learn. Motiv.* 26, 125–173. doi: 10.1016/s0079-7421(08)60053-5

Oldfield, R. C. (1971). The assessment and analysis of handedness: the Edinburgh inventory. *Neuropsychologia* 9, 97–113. doi: 10.1016/0028-3932(71)90067-4

Oostenveld, R., Fries, P., Maris, E., and Schoffelen, J. M. (2011). FieldTrip: open source software for advanced analysis of MEG, EEG, and invasive electrophysiological data. *Comp. Intel. Neurosci.* 2011:1. doi: 10.1155/2011/156869

Rao, V. R., Sellers, K. K., Wallace, D. L., Lee, M. B., Bijanzadeh, M., Sani, O. G., et al. (2018). Direct electrical stimulation of lateral orbitofrontal cortex acutely improves mood in individuals with symptoms of depression. *Curr. Biol.* 28, 3893–3902. doi: 10.1016/j.cub.2018.10.026

Rasch, B., and Born, J. (2013). About sleep's role in memory. *Physiol. Rev.* 93, 681–766.

Rasch, B., Buchel, C., Gais, S., and Born, J. (2007). Odor cues during slow-wave sleep prompt declarative memory consolidation. *Science* 315, 1426–1429. doi: 10.1126/science.1138581

Rothschild, G., Eban, E., and Frank, L. M. (2017). A cortical–hippocampal–cortical loop of information processing during memory consolidation. *Nat. Neurosci.* 20:251. doi: 10.1038/nn.4457

Rudoy, J. D., Voss, J. L., Westerberg, C. E., and Paller, K. A. (2009). Strengthening individual memories by reactivating them during sleep. *Science* 326, 1079–1079. doi: 10.1126/science.1179013

Sacher, M., Taconnat, L., Souchay, C., and Isingrini, M. (2009). Divided attention at encoding: effect on feeling-of-knowing. *Conscious. Cogn.* 18, 754–761. doi: 10.1016/j.concog.2009.04.001

Schapiro, A. C., McDevitt, E. A., Rogers, T. T., Mednick, S. C., and Norman, K. A. (2018). Human hippocampal replay during rest prioritizes weakly learned information and predicts memory performance. *Nat. Commun.* 9:3920. doi: 10.1038/s41467-018-06213-1

Suthana, N., and Fried, I. (2014). Deep brain stimulation for enhancement of learning and memory. *Neuroimage* 85, 996–1002. doi: 10.1016/j.neuroimage.2013.07.066

Vieira, P. G., Krause, M. R., and Pack, C. C. (2019). tACS entrains neural activity while somatosensory input is blocked. *bioRxiv [Preprint]*.

Yacoby, A., Dudai, Y., and Mendelsohn, A. (2015). Metamemory ratings predict long-term changes in reactivated episodic memories. *Front. Behav. Neurosci.* 9:20. doi: 10.3389/fnbeh.2015.00020

Conflict of Interest: PP, SS, RH, NK, SR, JC, and MH were employed by HRL Laboratories, LLC. PP, JC, and MH have a patent on using tES for targeted memory reactivation (US Patent No. 10,307,592).

The remaining authors declare that the research was conducted in the absence of any commercial or financial relationships that could be construed as a potential conflict of interest.

frontiers in Neuroscience

ORIGINAL RESEARCH
published: 02 March 2020
doi: 10.3389/fnins.2020.00087

Latent Factor Decoding of Multi-Channel EEG for Emotion Recognition Through Autoencoder-Like Neural Networks

Xiang Li[1], Zhigang Zhao[1]*, Dawei Song[2]*, Yazhou Zhang[3], Jingshan Pan[1], Lu Wu[1], Jidong Huo[1], Chunyang Niu[1] and Di Wang[1]*

[1] *Key Laboratory of Medical Artificial Intelligence, Shandong Computer Science Center (National Supercomputer Center in Jinan), Qilu University of Technology (Shandong Academy of Sciences), Jinan, China,* [2] *School of Computer Science and Technology, Beijing Institute of Technology, Beijing, China,* [3] *Software Engineering College, Zhengzhou University of Light Industry, Zhengzhou, China*

OPEN ACCESS

Edited by:
Davide Valeriani, Massachusetts Eye and Ear Infirmary, Harvard Medical School, United States

Reviewed by:
Wei-Long Zheng, Massachusetts General Hospital and Harvard Medical School, United States
Matthias Treder, Cardiff University, United Kingdom

***Correspondence:**
Zhigang Zhao
zhaozhg@sdas.org
Dawei Song
dwsong@bit.edu.cn
Xiang Li
xiangli@sdas.org

Specialty section:
This article was submitted to Neural Technology, a section of the journal Frontiers in Neuroscience

Received: *10 September 2019*
Accepted: *21 January 2020*
Published: *02 March 2020*

Citation:
Li X, Zhao Z, Song D, Zhang Y, Pan J, Wu L, Huo J, Niu C and Wang D (2020) Latent Factor Decoding of Multi-Channel EEG for Emotion Recognition Through Autoencoder-Like Neural Networks. Front. Neurosci. 14:87. doi: 10.3389/fnins.2020.00087

Robust cross-subject emotion recognition based on multichannel EEG has always been hard work. In this work, we hypothesize that there exist default brain variables across subjects in emotional processes. Hence, the states of the latent variables that relate to emotional processing must contribute to building robust recognition models. Specifically, we propose to utilize an unsupervised deep generative model (e.g., variational autoencoder) to determine the latent factors from the multichannel EEG. Through a sequence modeling method, we examine the emotion recognition performance based on the learnt latent factors. The performance of the proposed methodology is verified on two public datasets (DEAP and SEED) and compared with traditional matrix factorization-based (ICA) and autoencoder-based approaches. Experimental results demonstrate that autoencoder-like neural networks are suitable for unsupervised EEG modeling, and our proposed emotion recognition framework achieves an inspiring performance. As far as we know, it is the first work that introduces variational autoencoder into multichannel EEG decoding for emotion recognition. We think the approach proposed in this work is not only feasible in emotion recognition but also promising in diagnosing depression, Alzheimer's disease, mild cognitive impairment, etc., whose specific latent processes may be altered or aberrant compared with the normal healthy control.

Keywords: latent factor decoding, emotion recognition, EEG, deep learning, variational autoencoder

1. INTRODUCTION

In recent years, affective computing has started to become an active research topic in fields of pattern recognition, signal processing, cognitive neuropsychology, etc. Its main objective is exploring effective computer-aided approaches in recognizing a person's emotions automatically by utilizing explicit or implicit body information, e.g., through facial expressions or voices. It has wide application prospects within the field of human-computer interaction (e.g., intelligent assistants and computer games) (O'Regan, 2003; Moshfeghi, 2012) and psychological health care (Sourina et al., 2012) the WHO estimates that depression, as an emotional disorder, will soon be the second leading cause of the global burden of disease (WHO, 2017).

Considering that facial or vocal muscle activity can be deliberately controlled or suppressed, researchers are currently starting to explore this question through implicit neural activities, particularly through the multichannel EEG (electroencephalograph). The neural oscillations revealed by the EEG are highly correlated with various dynamic cognitive processes (Ward, 2004), including the emotional processes. Hence, its multichannel monitoring and high temporal resolution provide us with possibilities in exploring robust indicators and computational methods for EEG-based emotion recognition.

Nevertheless, there exist some major problems with regards to multichannel EEG-based emotion recognition that need to deal with, such as the poor generalization of data across subjects and the limitations in designing and extracting handcrafted emotion-related EEG features. Further, in medical data-mining tasks, acquiring enough manually labeled data for training supervised models remains a problem. How to fully utilize the limited data to enhance the model performance is worthy of exploration. Hence, unsupervised and handcrafted featured non-dependent modeling methods are worth in-depth exploration.

In this work, we have utilized the findings of prior related works (Adolphs et al., 1994; Vytal and Hamann, 2014) and raised the hypothesis that, though differences exist between individuals, there exist also intrinsic default variables (e.g., brain networks or intracranial current sources) that take part in emotional processes. Then, the characteristics of these intrinsic variables can be utilized for analyzing different emotional states. Specifically, in this work, three unsupervised autoencoder-like neural network models have been utilized to model the multichannel EEGs and infer the state space of the latent factors. Based on the state sequences of the factors, the participants' emotional status can be estimated by applying a contextual modeling method. According to the experimental results, the unsupervised neural network models are effective and feasible in modeling multichannel EEG, and the inferred factors indeed contain emotion-related information that are beneficial for further emotion recognition.

2. MATERIALS AND METHODS

2.1. An Overview of the Framework

Emotional processes are higher-order cognitive processes that are produced by the collaborative involvement of various latent brain factors, including different brain areas and physical or functional brain networks. The status information of the latent factors contains emotion-related information that contribute to estimating the emotional status. Hence, how to effectively and precisely infer the latent factors is the core issue that we have been concerned with in this work. As the EEG is the external manifestation of the latent brain factors' activities, the recorded EEGs of different scalp locations having internal associations, it has provided us with a way to infer the latent factors from the external multichannel EEGs.

In this work, we have studied and compared three kinds of autoencoder-form neural network models, including the traditional autoencoder (AE), the variational autoencoder (VAE), and the restricted Boltzmann machine (RBM) to determine the latent factors from the multichannel EEG data. Furthermore, for estimating the emotional status, after training, the state sequences of the latent factors were modeled by contextual learning models (e.g., the LSTM unit-based recurrent neural network); at the same time, the emotional status can be estimated based on the contextual information. The entire method framework is illustrated in the flow chart as in **Figure 1**.

2.2. Neural Network-Based Latent Factor Decoding Models

Latent factor decoding from a brain activity signal is a key tool for studying cognitive task performance and impairment (Calhoun and Adali, 2012). The decoded factors can be further utilized to locate the intracranial current sources or identify intrinsic brain networks. Most of the popular methods for inferring latent factors have the core assumption of the existence of hidden factors that are mixed to produce the observed data (Calhoun et al., 2010).

Traditionally, in order to model latent factors, we first need to determine the independent components (ICs) from the multichannel brain signals by solving a blind source separation (BSS)/single matrix factorization (SMF) problem, among which the independent component analysis (ICA) is the most commonly used method (Chen et al., 2013). Specifically, the multichannel EEGs are expressed as a channels-by-time data matrix $\boldsymbol{E}^{n\times t}$, where the t is the number of measured time points of a signal, and the n is the number of electrodes (channels). Solving the BSS/SMF problem is to discover the underling latent source factors $\boldsymbol{S}^{m\times t}$ from the external multichannel EEG signals, where the m is the number of hypothesized factors, and t is the number of data points in one source signal. The relationship between the multichannel EEGs and the latent source factors is expressed in Formula 1:

$$\boldsymbol{E}^{n\times t} \approx \boldsymbol{M}^{n\times m}\boldsymbol{S}^{m\times t}, \tag{1}$$

where the channels-by-sources matrix $\boldsymbol{M}$ is the unknown "mixing" matrix. Hence, for determining the latent factors, we need to find the "demixing" matrix $\boldsymbol{D}$, which is the inverse of the matrix $\boldsymbol{M}$ that satisfies $\boldsymbol{S} \approx \boldsymbol{DE}$.

In the above latent factor decoding studies, the "demixing" matrix $\boldsymbol{D}$ and the ICs are determined through some methods based on matrix factorization (e.g., the ICA). However, the utilization of ICA has been limited by its flexibility and representation ability (Choudrey, 2002). Hence, its effectiveness in the scenario of cross-subject decoding and recognition is questionable. Currently, various deep learning (DL) models have been applied to solve supervised or unsupervised learning problems in fields of computer vision and natural language processing. Besides, DL-based approaches can learn intermediate concepts, which could yield better transfer across source and target domains (Glorot et al., 2011). Recent works have verified that the fMRI volume-based DL approach can identify comparable latent factors to the ICA-based approach (Huang et al., 2016). Hence, this inspires us to introduce neural network models to solve the problem of latent factor decoding from emotional EEG data.

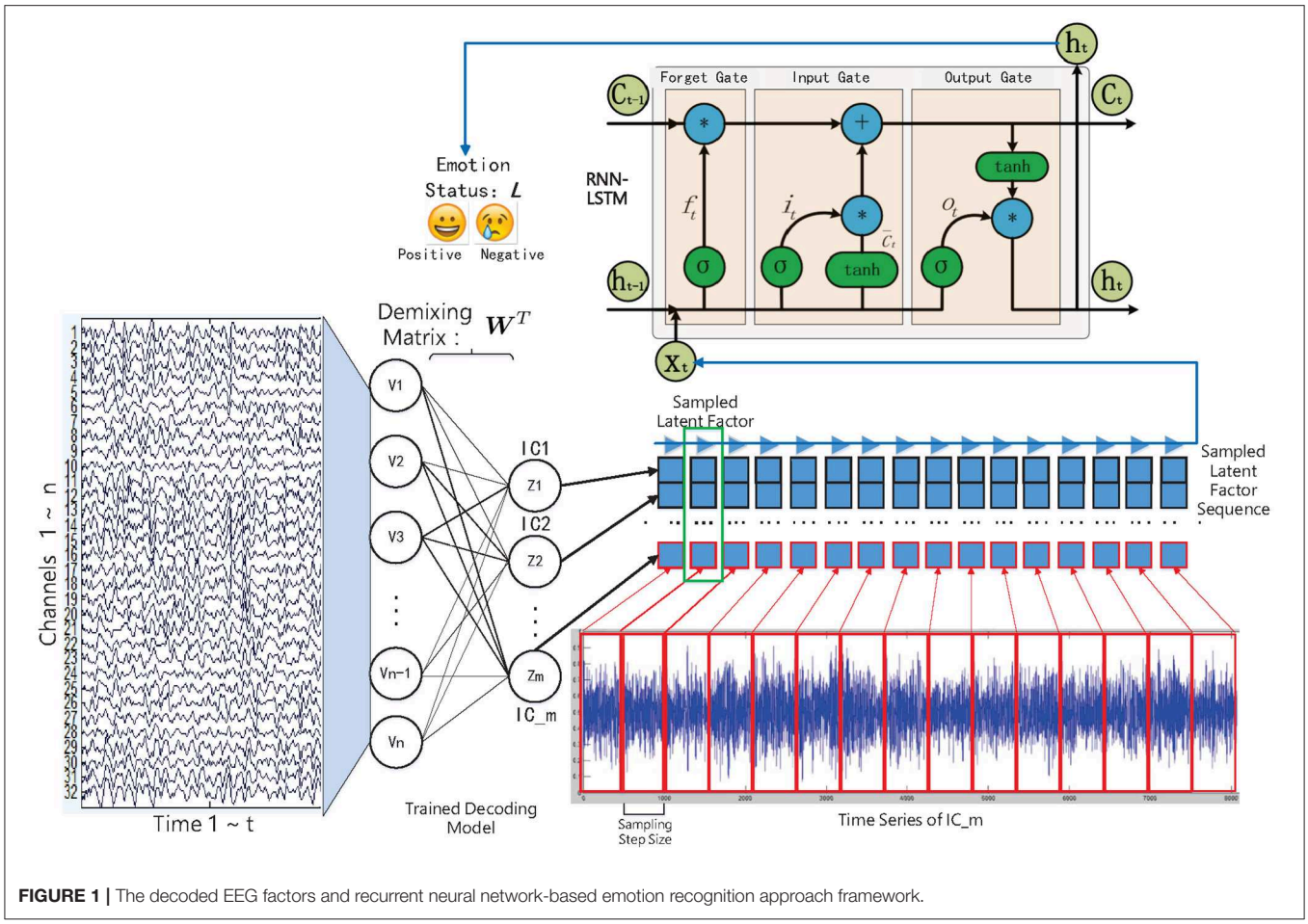

FIGURE 1 | The decoded EEG factors and recurrent neural network-based emotion recognition approach framework.

2.2.1. Traditional Autoencoder-Based Decoding Approach

The basic autoencoder model is a feedforward neural network that consists of symmetrical network structures: the "encoder" and "decoder." To be more specific, consider one dataset $\mathcal{X} = \{x^{(t)}\}_{t=1}^{N}$ of variable x. As in Formula 2, the encoder is responsible for encoding the input into a higher-level (and generally compressed) representation, which we call the "bottleneck." Then, as in Formula 3, the decoder is responsible for reconstructing the input data based on the hidden representation. The parameters of the AE are optimized by minimizing the difference (reconstruction error) between the output data and input data, as in Formula 4.

$$h_j^{(t)} = f(\sum_i W_{ij}^1 x_i^{(t)} + b_1) \tag{2}$$

$$\overline{x_i^{(t)}} = f(\sum_j W_{ij}^2 h_j^{(t)} + b_2) \tag{3}$$

$$\mathcal{L}(W^1, W^2, b_1, b_2; \mathcal{X}) = \sum_{x^{(t)} \in X} \| x^{(t)} - \overline{x^{(t)}} \| \tag{4}$$

The AE is generally trained through a back propagation (BP) method. As we can see, the AE shares some practical similarities with the SMF models. To some extent, the weight matrices $\boldsymbol{W}_1$ and $\boldsymbol{W}_2$ can also been regarded as "demixing" and "mixing" secret keys, respectively. Then, the relationship between the observed EEGs and the latent factors can be determined by them.

2.2.2. Restricted Boltzmann Machine-Based Decoding Approach

A restricted Boltzmann machine (RBM) is a kind of undirected probabilistic graph model with no connections between units of the same layer. It provides the possibility of constructing and training deeper neural networks (Hinton and Salakhutdinov, 2006). From a probabilistic modeling perspective, the latent factors learned in an RBM give a description of the distribution over the observed data. Specifically, an RBM specifies the distribution over the joint space $[x, h]$ via the Boltzmann distribution, as in Formula 5:

$$p(x, h; \theta) = \frac{1}{Z_\theta} exp(-\varepsilon_\theta^{RBM}(x, h)) \tag{5}$$

in which Z_θ is the normalization term, and $\varepsilon_\theta^{RBM}(x, h)$ is the system energy function, namely:

$$\varepsilon_\theta^{RBM}(x, h) = -x^T W h - a^T x - b^T h \tag{6}$$

where $\theta = \{W, a, b\}$ are the model parameters that respectively encode the visible-to-hidden interactions (W), the visible self-connections (a), and the hidden self-connections (b). The visible and hidden nodes of RBM are typically binary statistic units. Nevertheless, for EEG data, the visible nodes need to model a distribution that is an approximately real value and Gaussian. Hence, the RBM adopted here is the Gaussian RBM, where the conditional distribution of a single hidden and visible node is given by:

$$P(h_j = 1|x) = \sigma(\sum_i W_{ij}x_i + b_j) \tag{7}$$

and

$$x_i \sim \mathcal{N}(\sigma_i \sum_i W_{ij}h_j + a_i, \sigma_i) \tag{8}$$

where $\sigma(.)$ is the logistic function and $\mathcal{N}(\mu, \sigma)$ is the normal distribution with mean μ and standard deviation σ. Further, we make a corresponding modification for the energy function, as in Formula 9:

$$\varepsilon_\theta^{RBM}(x, h) = -\sum_{ij} \frac{x_i}{\sigma_i} W_{ij}h_j - \sum_i \frac{(a_i - x_i)^2}{\sigma^2} - \sum_j b_j h_j \tag{9}$$

The parameters $\theta = \{W, a, b\}$ are optimized by training the RBM to maximize the likelihood of the observed data: $\sum_{t=1}^{N} P(x^{(t)}; \theta)$. The traditional gradient descent-based method to maximize the likelihood is intractable in the RBM based approach. This problem is solved by approximating the gradient through Markov Chain Monte Carlo (MCMC) where contrastive divergence (CD) with truncated Gibbs sampling is applied to improve computational efficiency (Hinton, 2002). The model is further unrolled to a symmetrical auto-encoder structure, whose parameters, as was discovered in the CD process, are fine-tuned with a back-propagation (BP) process, much like the traditional auto-encoders.

2.2.3. Variational Autoencoder-Based Decoding Approach

Very recently, the variational autoencoder (VAE) was introduced as a powerful DL model for some problem scenarios that needed modeling of the data's probability distribution (Kingma and Welling, 2014). The objective function of traditional AE only measures the value difference between the input and output vector. The difference in distribution cannot be reflected and controlled. Compared with the traditional AE model, the VAE model provides a closed-form representation of the distribution underling the input data, which is quite suitable for unsupervised learning of the latent factors.

It hypothesizes that all the data are generated by one random process that involves an unobservable latent variable z. The latent variable is generated from one prior distribution $p_\theta(z)$, and the x is determined by the conditional distribution $p_\theta(x|z)$. Both the parameters θ and the latent variable z are unknown to us. The direct inference of the latent variable $p_\theta(z|x)$ is intractable. Hence, in the design of the VAE, one recognition model $q_\phi(z|x)$ is introduced to approximate the true posterior $p_\theta(z|x)$. The VAE utilizes the probabilistic encoder structure to encode the input into latent variables ($q_\phi(z|x)$), and it further utilizes the probabilistic decoder structure to map the latent variables to reconstructed input ($p_\theta(x|z)$). The optimization objective of the VAE is expressed in Formula 10:

$$\max \mathbb{E}_{q_\phi(z|x)}[\log p_\theta(x|z)] - D_{KL}(q_\phi(z|x)||p_\theta(z)) \tag{10}$$

This is also referred to as the variational lower bound.

The first term $\mathbb{E}_{q_\phi(z|x)}[\log p_\theta(x|z)]$ is the expectation of the logarithmic likelihood with regard to the approximate posterior $q_\phi(z|x)$. It can be obtained through Monte Carlo estimate, namely through sampling L times, as in Formula 11:

$$\frac{1}{L}\sum_{l=1}^{L} \log p_\theta(x^{(t)}|z_l^{(t)}) \tag{11}$$

The second term $-D_{KL}(q_\phi(z|x)||p_\theta(z))$ is the KL divergence of the approximate posterior $q_\phi(z|x)$ from the true prior $p_\theta(z)$. It is computed through Formula 12:

$$\frac{1}{2}\sum_{j=1}^{J}(1 + \log(\sigma_j^{(t)2}) - \mu_j^{(t)2} - \sigma_j^{(t)2}) \tag{12}$$

Let J be the dimensionality of z.

To sum up, the prior variational lower bound can be further transformed into the following form in Formula 13:

$$\begin{aligned}\mathcal{L}(\theta, \phi; x^{(t)}) \simeq & \frac{1}{2}\sum_{j=1}^{J}(1 + \log(\sigma_j^{(t)2}) - \mu_j^{(t)2} - \sigma_j^{(t)2}) \\ & + \frac{1}{L}\sum_{l=1}^{L} \log p_\theta(x^{(t)}|z_l^{(t)})\end{aligned} \tag{13}$$

where the z is sampled with a reparameterization trick, namely $z_l^{(t)} = \mu^{(t)} + \sigma^{(t)} \odot \epsilon_l$ and $\epsilon_l \sim \mathcal{N}(0, I)$, and the $\odot$ refers to the element-wise product. Both the $q_\phi(z|x)$ and $p_\theta(z)$ are assumed to obey the centered isotropic multivariate Gaussian, namely $q_\phi(z|x^{(t)}) = \mathcal{N}(z; \mu^{(t)}, \sigma^{(t)2}I)$, where the mean $\mu^{(t)}$ and standard deviation $\sigma^{(t)}$ are the computation outputs of the encoder network with respect to the input $x^{(t)}$ and the variational parameter ϕ. The VAE is trained through stochastic gradient descent and back-propagation (BP) method. Compared with the traditional matrix factorization-based approach, the VAE is formulated as a density estimation problem. The structure and mechanism of the three autoencoder-like neural network models are illustrated in **Figure 2**.

2.3. Contextual Learning From Latent Factors for Emotion Recognition

According to some studies, the generation of the emotional experience generally lags behind the activity of the brain neural systems (Krumhansl, 1997). The recurrent neural network (RNN), meanwhile, has the ability to accumulate useful

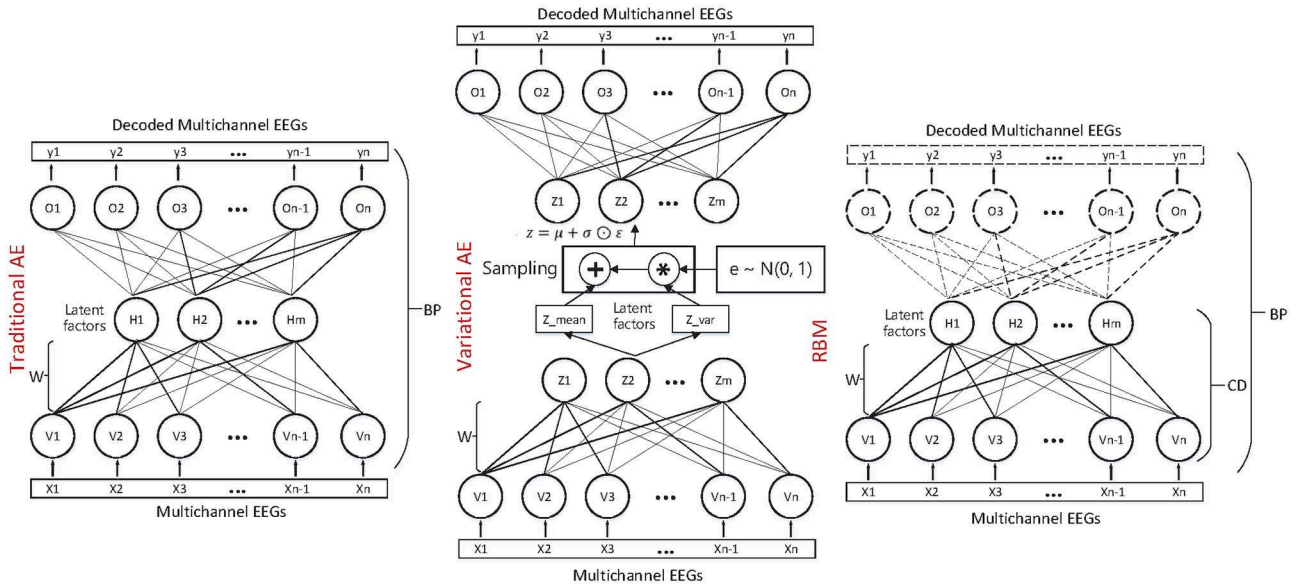

FIGURE 2 | The neural network-based multichannel EEG fusion and latent factor decoding method.

information at each time step, by which the influence of the lag-effect can be eliminated. This is important when we do not know which moment plays the most important role in the subject's final evaluation of the specific emotion they experienced in a trial. In view of this, we have considered adopting the RNN model to perform sequence modeling on the decoded latent factor sequences; meanwhile, the subjects' emotional status can be estimated, as shown in **Figure 1**, whereas traditional RNN's practical application is limited by the "gradient vanish" in back-propagation when its dependencies is too long. Some rectified recurrent units have been adopted in the RNN model, in which the LSTM unit that contains a "gate" structure has gained great success in various sequence-modeling tasks, such as speech recognition (Graves et al., 2013). The popular LSTM unit-based RNN model was therefore selected in this work.

Specifically, in this work, we have fed the multichannel EEGs into the "encoder" part of the trained models to obtain the corresponding latent factor sequences, namely the independent components (ICs): $\mathcal{IC} = \{IC^{(t)}\}_{t=1}^{N}$. The high sampling rate EEG signal also corresponds to the high sampling rate ICs, which will lead to the high computational cost in sequence modeling. Here we need sampling from the entire ICs to construct samples for LSTM training. For the m sampled elements from the entire ICs, the mechanism of the recognition model can be formulated as:

$$< IC^{(1)}, ..., IC^{(t)}, ..., IC^{(m)} > \mapsto L^{(m)} \mapsto \boldsymbol{L} \tag{14}$$

which follows the "many-to-one" mode.

2.4. Experimental Dataset

We examined the proposed approach on two publicly accessible datasets, including **DEAP** (Koelstra et al., 2011) and **SEED** (Zheng and Lu, 2015). DEAP included 32-channel EEG data collected from 32 subjects, and the subjects rated their emotional experience on a two-dimensional emotional scale, namely Arousal (which ranges from relaxed to aroused) and Valence (which ranges from unpleasant to pleasant). The higher the specific rating was, the more intense the emotion was in a specific dimension. SEED included 62-channel EEG data collected from 15 subjects. After data acquisition, some basic preprocessing processes were conducted, such as removing the electrooculogram (EOG) and electromyogram (EMG) artifacts.

The samples of DEAP were divided into positive and negative samples according to the ratings on the Valence and Arousal emotional dimensions. A sample with score over five points was considered to be a positive class, while a sample with a score below five points was considered a negative class. The SEED dataset had pre-defined negative and positive emotional classes for the samples that we did not need to conduct label processing.

3. RESULTS AND DISCUSSION

3.1. EEG Decoding Method Settings

In addition to removing EEG artifacts, we conducted z-score method-based normalization for each subject's channel data. For comparison, we built a one-hidden-layer structure for the neural network models, and the number of hidden nodes was set according to the number of latent factors we set in advance (DEAP: 2–16, SEED: 2–31). Both of the two datasets were acquired with high sampling rate. Take the DEAP dataset for example; the number of samples of one subject was over 320,000. Hence, considering the training speed, we set the batch size for unsupervised latent factor learning as 500. The loss functions were selected and set according to the descriptions in section 2.2. We selected the Adam and RMSprop method for AE and VAE training, respectively. According to the experiments, the

loss function can converge to the minimum within 20 training epoches. The RBM model-based approach was realized through the Matlab DeeBNet V3.0 deep belief network toolbox, whereas the AE- and VAE-based approaches were realized through the deep learning framework–Keras based on Tensorflow backend. More experimental setting details can be accessed in the source codes located in the following repository: https://github.com/muzixiang/LatentFactorDecodingEEG.

TABLE 1 | Three main categories of EEG features that we extracted for baseline methods.

Feature Type	Extracted Features
Time-frequency domain features	1. Peak-Peak Mean. 2. Mean Square Value. 3. Variance. 4. Hjorth Parameter:Activity. 5. Hjorth Parameter: Mobility. 6. Hjorth Parameter: Complexity. 7. Maximum Power Spectral Frequency. 8. Maximum Power Spectral Density. 9. Power Sum.
Non-linear dynamical system features	1. Approximate Entropy. 2. C0 Complexity. 3. Correlation Dimension. 4. Kolmogorov Entropy. 5. Lyapunov Exponent. 6. Permutation Entropy. 7. Singular Entropy. 8. Shannon Entropy. 9. Spectral Entropy.
Asynchronous brain activity features	1. Fp1-Fp2. 2. AF3-AF4. 3. F3-F4. 4. F7-F8. 5. FC5-FC6. 6. FC1-FC2. 7. C3-C4. 8. T7-T8. 9. CP5-CP6. 10. CP1-CP2. 11. P3-P4. 12. P7-P8. 13. PO3-PO4. 14. O1-O2.

For comparison, we also set an experiment of an ICA-based decoding approach, and selected FastICA as the implementation method, which is most widely used and accepted in the resolution of EEG source localization and blind source separation problems. This is due to the fact that the ICA-based approach has problems in determining the specific order of the latent components as well as the reconstructed multi-channel EEGs. In this work, we also took this problem into consideration. Specifically, for each original channel EEG, we measured the correlation between it and each reconstructed signal. We supposed that the reconstructed signal with the highest correlation was the counterpart of the specific original EEG, and the highest correlation was adopted here to measure the reconstructed performance of the ICA-based approach. Besides, the reconstruction experiment and performance measurement were conducted 10 times to increase the reliability of the results, and the average performance was reported in this paper. Though we know this is a crude approach, and there may be some mistakes in determining the counterpart for the original EEG, the reported results here were indeed the best estimation and constituted the performed upper bound for ICA.

Besides, the performance of the PCA-based approach was also presented. Nevertheless, the PCA and ICA were totally different in theory and application scenarios. The PCA-based approach was generally used as a dimension reduction method, which is not to mine the underling random processing but try to extract the most important information that can best represent the original data. In this work, we were interested in the EEG latent factors-based approaches. Anyway, as a classic method, the PCA was also worth exploring, and we also added experiments when the PCA approach was adopted.

3.2. Emotion Recognition Method Settings

Although LSTM unit-based RNN has the ability to process long-term sequences, in the case of high-sampling rate EEG signals,

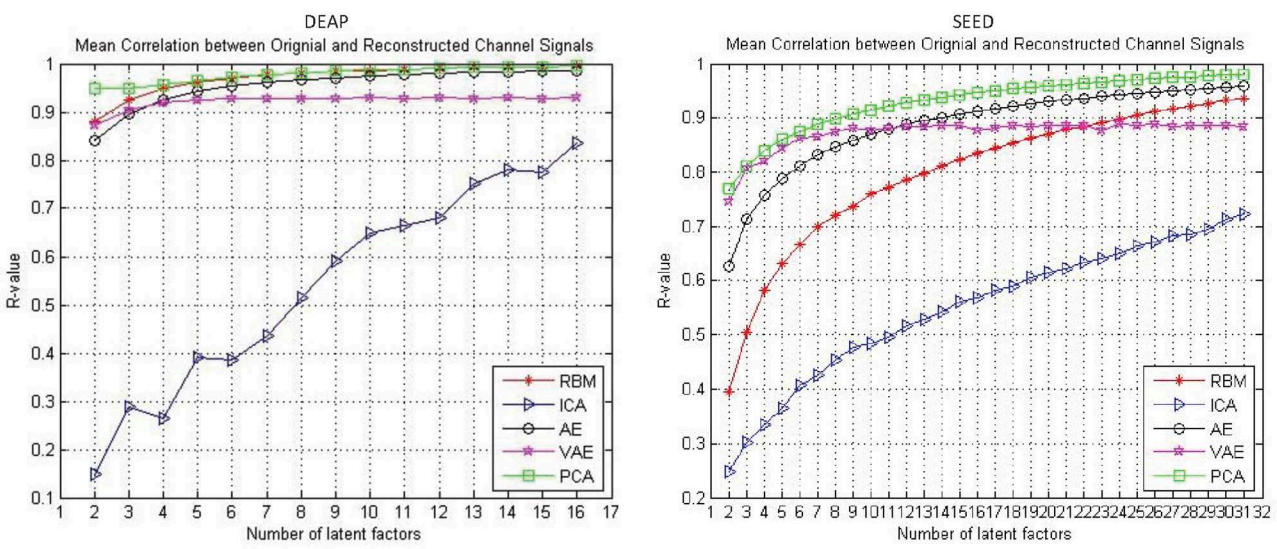

FIGURE 3 | The reconstruction performance (mean Pearson correlation coefficient) of different decoding models when assuming a different number of latent factors.

signal sequences with hundreds of thousands of data points can introduce significant time overhead in sequence learning. Hence, as shown in **Figure 1**, the training sequences were constructed based on the sampling step size, and the data were sampled from the sequence at equal intervals according to the step size. This strategy was good for quickly verifying the experimental results. In the experiment, we set the sampling step size as 0.25 s. The number of input layer nodes of the LSTM unit were determined by the number of latent factors. The number of output hidden layer nodes was set to 200, and the output nodes were fully connected with one hidden layer containing 100 Relu-type nodes. At the end of the model, a decision-making layer with Softmax-type nodes that represent different emotional state was connected. Besides, the Dropout operation was set for the last two fully connected layers. The model loss function was set to binary cross entropy, the batch size was set to 50, and the RMSprop algorithm was selected as the optimization method.

We also set baseline methods based on handcrafted features for comparison with our framework. We choose the support vector machine (SVM) combined with the L1-norm penalty-based feature selection method (SVM-L1). Besides, random forests (RF), K-nearest neighbors (KNN), logistic regression (LR), naive bayes (NB), and the feed-forward deep neural network (DNN) were also examined. As listed in **Table 1**, three main categories of EEG features were extracted for Theta rhythm, Alpha rhythm, Beta rhythm, and Gamma rhythm, including nine kinds of time-frequency domain features (TFD features), nine kinds of non-linear dynamical system features (NDS features), and 14 pairs of brain hemisphere asynchronous activity features (BHAA features). Hence, For the DEAP dataset, the total number of feature dimensions for one trial was 2360 ($4\_rhythms \times 32\_channels \times (9\_TFfeatures + 9\_NDSfeatures) + 4\_rhythms \times 14\_BHAAfeatures$). For the SEED dataset, the total number of features extracted for one trial was 4520 ($4\_rhythms \times 62\_channels \times (9\_TFfeatures + 9\_NDSfeatures) + 4\_rhythms \times 14\_BHAAfeatures$). Besides, several related representative works in recent years are also compared.

3.3. Evaluation Metrics

For evaluating the reconstruction performance, we adopted the Pearson correlation coefficient as the metric to measure the difference between the input original channel signal and the output reconstructed signal, as in Formula 15. In other words, high r-value indicated the model has good ability in

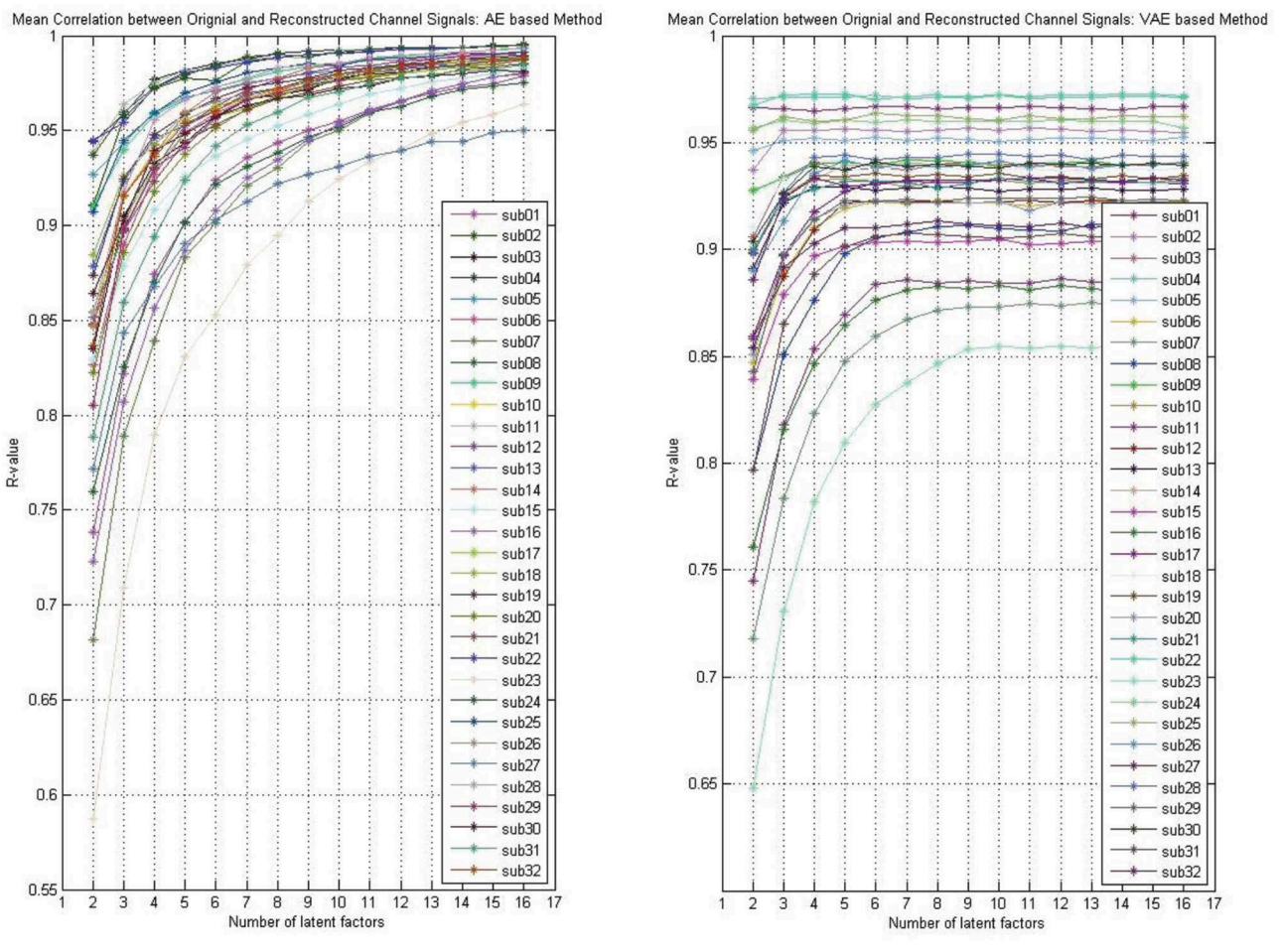

FIGURE 4 | The reconstruction performance (mean Pearson correlation coefficient) of different subjects when assuming a different number of latent factors (take the DEAP for example).

reconstructing the time series. This metric gave us a general view of the feasibility and effectiveness of the model in modeling the multichannel EEG data.

$$r_{x_{in}x_{out}} = \frac{\sum_{t=1}^{n}(x_{in}^{(t)} - \overline{x_{in}})(x_{out}^{(t)} - \overline{x_{out}})}{\sqrt{\sum_{t=1}^{n}(x_{in}^{(t)} - \overline{x_{in}})^2}\sqrt{\sum_{t=1}^{n}(x_{out}^{(t)} - \overline{x_{out}})^2}} \quad (15)$$

For evaluating the emotion recognition performance, we chose to leave one subject's data out of the cross-validation method to compare our framework with the baseline methods. Every time, we left one subject's data out as the test set and adopt the other subjects' data as the training set. Considering the problem of unbalanced classes, the model performance was evaluated on the test set based on the F1-score metric, as in Formula 16. This procedure iterates until each subject's data has been tested.

$$P_{f1} = 2 \cdot \frac{Precision \cdot Recall}{Precision + Recall} \quad (16)$$

3.4. Evaluation on EEG Modeling and Reconstruction

The reconstruction performance under different assumed number of latent factors was of interest. In this work, we examined the reconstruction performance with varying number of latent factors. Specifically, considering the experimental cost, we only examined the number of latent factors from two to half the number of EEG channels. As shown in **Figure 3**, the performance was gradually improved with the increased number of latent factors for all the approaches. It can be found that, with the increase of the number of latent factors, the AE and RBM even obtained an approximate 100% reconstruction performance on the DEAP dataset. Nevertheless, it should be noted that the VAE-based modeling method was special, and its reconstruction performance did not always improve with the increase of the number of latent factors. The mean correlation coefficient gradually stabilized at around 0.9. Besides, when tested on the SEED dataset, the VAE-based method could achieve a better reconstruction performance than other methods with fewer hidden layer node settings, which indicated that the method had the ability to mine the most important latent factors from multichannel EEGs. The PCA performed well on both datasets, as expected; however, the PCA-based approach was a kind of dimension reduction method, which was not to mine the underling random process. We still need to examine their effectiveness in recognizing subjects' emotions by further utilizing the pattern recognition methods.

Whether the reconstruction performance was consistent across subjects when assuming different latent factors is worth exploring. As shown in **Figure 4**, we presented the AE model- and VAE model-based reconstruction performance with varying number of latent factors on each subject's data. The experimental results indicated that, for each subject's data, the performance improves gradually with the increase of the number of latent factors, and we obtain relatively smooth curves on each of the subjects'data. Though, for the VAE model, there was a little fluctuation, the performance on all subjects' data eventually stabilized.

As shown in **Figure 3**, the reconstruction performance of the ICA-based method was always much lower than the neural network-based modeling method. This suggested that neural network based approaches are more suitable for modeling and decoding brain neural signals than ICA based method. According to the Universal Approximation Theorem, a neural

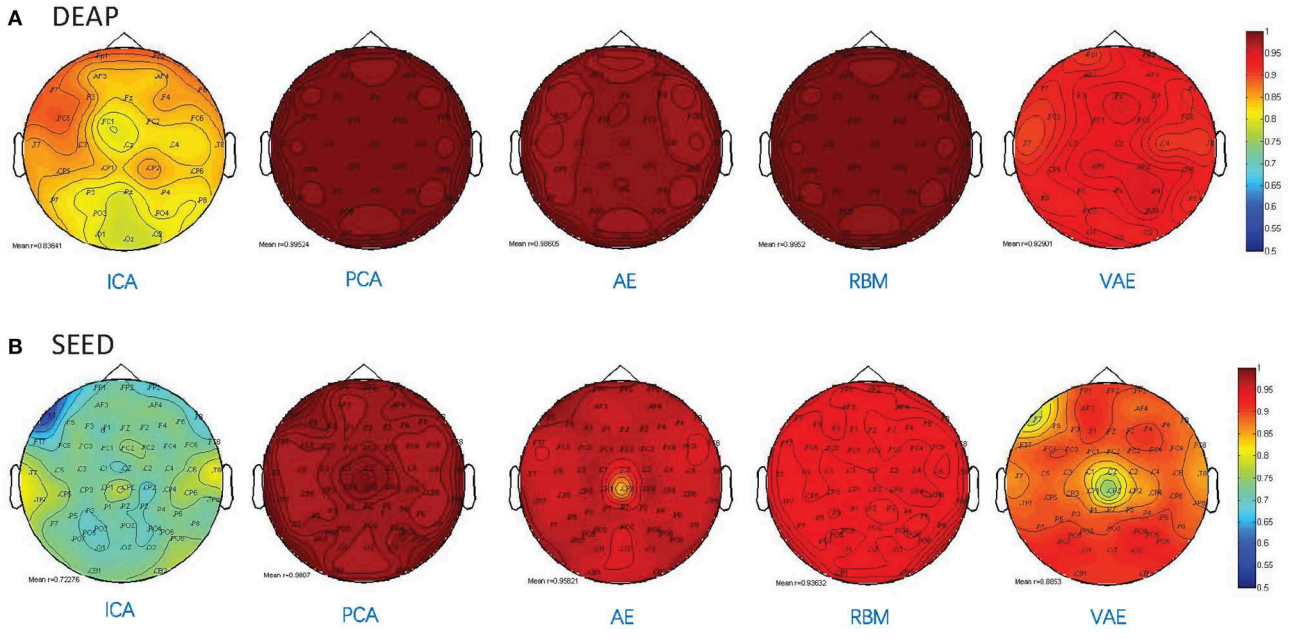

FIGURE 5 | Pearson correlation coefficient between the reconstructed EEG signal and the original EEG signal for each channel. **(A)** The reconstruction performance of different methods on DEAP dataset. **(B)** The reconstruction performance of different methods on SEED dataset.

network structure with a single hidden layer can approximate any function. In other words, even if we restrict our networks to have just a single layer intermediate between the input and the output neurons–a so-called single-hidden-layer network–such a simple network architecture can be extremely powerful. Hence, it is not surprising that the neural networks adopted in this work can achieve a good reconstruction performance. As illustrated in **Figure 4**, the neural network obtained a relatively stable reconstruction performance on each subject's data. The performance increased gradually and achieved a sufficiently good performance when setting proper number of latent factors. It also indicated the effectiveness and robustness of the neural networks in decoding and reconstructing multichannel EEGs.

Besides, as shown in **Figure 5**, we illustrated the performance of each method in reconstructing the multichannel EEGs through a channel layout heatmap format. The mean Pearson correlation coefficient over all the subjects is presented. The greater the value, the darker the color. Specifically, the figure shows the reconstructed performance when the number of latent factors is set as half the number of electrode channels (DEAP: 16 latent factors, SEED: 31 latent factors), which achieve the best reconstruction performance, as shown in **Figure 3**, and the averaged r-values are presented. It can be seen that the AE- and RBM-based methods on both datasets achieved the best reconstruction effect. Nevertheless, the frequently used ICA-based method was obviously inferior to other methods on the whole, and there existed significant performance imbalance in different brain regions. It indicated that the ICA-based EEG modeling approach was not robust compared to the neural network-based approaches.

TABLE 2 | Recognition performance on subject data of DEAP dataset (Valence).

Subject No.	ICA+LSTM	PCA+LSTM	AE+LSTM	RBM+LSTM	VAE+LSTM
s01	0.5818	0.6296	0.6207	0.6296	0.6552
s02	0.5882	0.6897	0.6885	0.7018	0.7213
s03	0.7097	0.6897	0.7241	0.7097	0.7097
s04	0.4444	0.5455	0.5490	0.5000	0.5818
s05	0.5965	0.7000	0.7302	0.7500	0.7541
s06	0.7241	0.7500	0.7419	0.8529	0.8182
s07	0.7368	0.7619	0.7586	0.8065	0.8125
s08	0.6071	0.6415	0.6545	0.6780	0.7213
s09	0.5217	0.4898	0.5926	0.6545	0.6552
s10	0.6207	0.6182	0.6441	0.6441	0.7059
s11	0.6909	0.6552	0.7097	0.7419	0.7500
s12	0.6667	0.6909	0.6552	0.6885	0.7000
s13	0.4186	0.5714	0.6182	0.5882	0.6182
s14	0.4444	0.5926	0.6182	0.6429	0.6780
s15	0.5200	0.6143	0.6667	0.6441	0.6667
s16	0.4706	0.5217	0.5306	0.5385	0.5660
s17	0.6786	0.6552	0.6885	0.6897	0.7097
s18	0.6667	0.6983	0.7407	0.7213	0.7500
s19	0.7059	0.6697	0.7302	0.7302	0.7419
s20	0.7018	0.7119	0.7097	0.7302	0.7719
s21	0.6667	0.6600	0.6441	0.6780	0.6667
s22	0.5306	0.5333	0.5965	0.6207	0.6207
s23	0.7000	0.7170	0.7119	0.7241	0.8000
s24	0.5106	0.5714	0.6207	0.5714	0.6316
s25	0.4889	0.5532	0.6441	0.6441	0.6441
s26	0.6415	0.7619	0.7333	0.7692	0.7813
s27	0.8060	0.8309	0.8125	0.8235	0.8529
s28	0.6786	0.7070	0.7241	0.7692	0.7619
s29	0.6667	0.6667	0.7097	0.7143	0.7541
s30	0.7742	0.7241	0.7813	0.8125	0.8182
s31	0.6667	0.6897	0.7018	0.7302	0.7213
s32	0.6441	0.5769	0.6538	0.6667	0.6897
Mean P_{f1}	0.6303	0.6528	0.6783	0.6927	0.7167

[1]*number of latent factors: 16.*

TABLE 3 | Recognition performance on subject data of DEAP dataset (Arousal).

Subject No.	ICA+LSTM	PCA+LSTM	AE+LSTM	RBM+LSTM	VAE+LSTM
s01	0.6545	0.7241	0.7419	0.7419	0.7500
s02	0.7119	0.7018	0.7458	0.7500	0.7619
s03	0.2791	0.3182	0.3043	0.3111	0.3478
s04	0.4138	0.5714	0.5106	0.5660	0.5714
s05	0.5600	0.6441	0.6316	0.6316	0.6441
s06	0.5200	0.6182	0.5818	0.5818	0.6275
s07	0.7213	0.7338	0.7541	0.7500	0.7869
s08	0.6667	0.6667	0.7213	0.7018	0.7333
s09	0.6885	0.7302	0.7419	0.7213	0.7636
s10	0.5660	0.6154	0.6667	0.6667	0.7097
s11	0.5217	0.4898	0.5455	0.5306	0.5556
s12	0.8000	0.8732	0.8889	0.8889	0.9041
s13	0.5385	0.7125	0.7419	0.9041	0.8889
s14	0.7241	0.7385	0.7619	0.7937	0.8060
s15	0.5882	0.6316	0.6545	0.6552	0.6667
s16	0.6273	0.6296	0.6545	0.6667	0.6667
s17	0.6667	0.7302	0.7241	0.7333	0.7869
s18	0.7541	0.7500	0.7692	0.7500	0.7742
s19	0.7213	0.7213	0.8060	0.7097	0.8065
s20	0.7879	0.8060	0.8235	0.8657	0.8732
s21	0.8529	0.8406	0.8732	0.8696	0.9014
s22	0.7241	0.7458	0.7500	0.7500	0.7500
s23	0.3673	0.3404	0.3750	0.4000	0.4000
s24	0.8358	0.8889	0.8696	0.8732	0.9041
s25	0.7500	0.7458	0.8182	0.8406	0.8406
s26	0.5714	0.5769	0.5769	0.5965	0.6071
s27	0.6780	0.7797	0.8060	0.7879	0.8060
s28	0.6071	0.6071	0.6154	0.6207	0.6545
s29	0.7018	0.7000	0.7458	0.7419	0.7586
s30	0.6182	0.5769	0.6207	0.6207	0.6441
s31	0.5769	0.6182	0.6316	0.6316	0.6552
s32	0.7213	0.7419	0.7692	0.7541	0.8148
Mean P_{f1}	0.6418	0.6741	0.6944	0.7002	0.7243

[1]*number of latent factors: 16.*

TABLE 4 | Recognition performance on subject data of SEED dataset.

Subject No.	ICA+LSTM	PCA+LSTM	AE+LSTM	RBM+LSTM	VAE+LSTM
s01	0.6753	0.7195	0.7368	0.7677	0.8308
s02	0.6897	0.7636	0.7386	0.7721	0.8504
s03	0.7255	0.7259	0.7674	0.8018	0.8741
s04	0.6434	0.6495	0.6677	0.6915	0.7012
s05	0.6683	0.7221	0.7323	0.7552	0.8027
s06	0.7321	0.7333	0.7733	0.8054	0.8904
s07	0.7143	0.7713	0.7525	0.7953	0.8600
s08	0.7053	0.7479	0.7488	0.7897	0.8571
s09	0.6912	0.7080	0.7430	0.7759	0.8538
s10	0.6677	0.7599	0.7264	0.7452	0.7931
s11	0.7295	0.7548	0.7696	0.8026	0.8827
s12	0.6776	0.7095	0.7373	0.7718	0.8320
s13	0.7168	0.7894	0.7560	0.7962	0.8676
s14	0.6939	0.7586	0.7442	0.7876	0.8565
s15	0.7608	0.7699	0.7844	0.8079	0.8908
Mean P_{f1}	0.6994	0.7389	0.7452	0.7777	0.8429

[1]*number of latent factors: 31.*

TABLE 5 | Performance comparison between this work and the baseline methods.

Approach/Model	Performance (P_{f1})		
	DEAP		SEED
	Valence	Arousal	
L1-SVM (kernel="linear") + handcrafted features	0.7134	0.7154	0.8234
RF (n_estimators=100) + handcrafted features	0.5870	0.5754	0.7680
KNN (n_neighbors=7) + handcrafted features	0.6406	0.5890	0.6763
LR + handcrafted features	0.5757	0.5614	0.7649
NB + handcrafted features	0.6903	0.6989	0.6666
DNN (hidden_layer_sizes={100, 100, 100}) + handcrafted features	0.6183	0.6593	0.7219
ICA+LSTM	0.6303	0.6418	0.6994
PCA+LSTM	0.6528	0.6741	0.7389
AE+LSTM	0.6783	0.6944	0.7452
RBM+LSTM	0.6927	0.7002	0.7777
VAE+LSTM	0.7167	0.7243	0.8429

3.5. Evaluation on Latent Factor-Based Emotion Recognition

As mentioned above, the performance of each unsupervised modeling method on EEG reconstruction cannot be used as a criterion for judging whether the model successfully deciphers latent factors that contribute to emotion recognition. It is necessary to apply pattern recognition methods on those mined factors, and conduct a comparison based on the recognition performance. Specifically, the LSTM takes charge of modeling the latent factor sequence decoded by the ICA-, AE-, RBM-, and VAE-based approaches and also inferred the emotional state. Besides, the performance, when applying the LSTM to the principle components mined by the PCA method, has also been reported.

The classification performance is evaluated when the number of the latent factor is set as half of the number of total electrodes. Namely, for the DEAP dataset, the number of latent factors used for sequence modeling and classification was 16, whereas, for the SEED dataset, the number of latent factors was set as 31. We think the emotion recognition performance must closely related to the EEG reconstruction performance. In other words, the latent factors with low reconstruction performance were not an accurate reflection of the latent EEG process and could not lead to an ideal emotion classification result. Hence, the emotion recognition experiments on both datasets were conducted on the latent factors with the high reconstruction performance, namely 16 and 31. Besides, the datasets were recorded with very high sampling rate; take the DEAP dataset for example, the total number of EEG samples of just one subject was over 320,000 the experimental cost for training, evaluating the models, and storing the decoded latent factors are high. Evaluating on more parameter settings is somewhat impractical in our current experimental conditions, e.g., for the SEED dataset, a total of 5 methods × 62 factors × 15 subjects = 4,650 different experimental settings were needed. Furthermore, the purpose of this work was to verify the effectiveness of the EEG latent factor-based emotion recognition method and was not to find the best parameter settings; the reconstruction performance achieved when the number of latent factor was half of the number of electrodes was good enough to test our idea.

We adopted a "leave one subject's data out" cross-validation method. For the DEAP dataset, **Tables 2**, **3** summarize the recognition performance on the emotional dimension of Valence and Arousal, respectively. **Table 4** summarizes the recognition performance on SEED dataset. Considering the problem of unbalanced classes, the recognition performance was measured and compared with each other using the F1 score.

It is found from the table that the ICA-LSTM-based method on both datasets exceeds 0.5, indicating that the traditional ICA-based method can still decipher emotion-related information from the multichannel EEG. It also indicates that the latent factor decoding combined with sequence modeling-based approach is suitable for emotion recognition from multichannel EEG. In general, the ICA-based approach did not perform as well as other neural network-based approaches, confirming the conclusion that ICA has limitations in representation ability (Choudrey, 2002). The RBM- and VAE-based approaches are better than the ICA- and AE-based approaches. This indicates that the generative models are more suitable in the current scenario.

$$\min_{\omega_0,\omega} \sum_{i=1}^{n} [1 - y_i(\omega_0 + \sum_{j=1}^{q} \omega_j x_{i,j})] + C\|\omega\|_1 \tag{17}$$

Table 5 lists the performance comparison between the baseline methods and the proposed approaches in this paper. Among the several baseline methods, the SVM combined with the L1-norm penalty-based feature selection method (L1-SVM) achieved the best performance when applying the optimum parameter. As shown in Formula 17, this method introduced the L1-norm regularization term $\|\omega\|_1$ into the objective function to induce sparsity by shrinking the weights toward zero. It is natural for

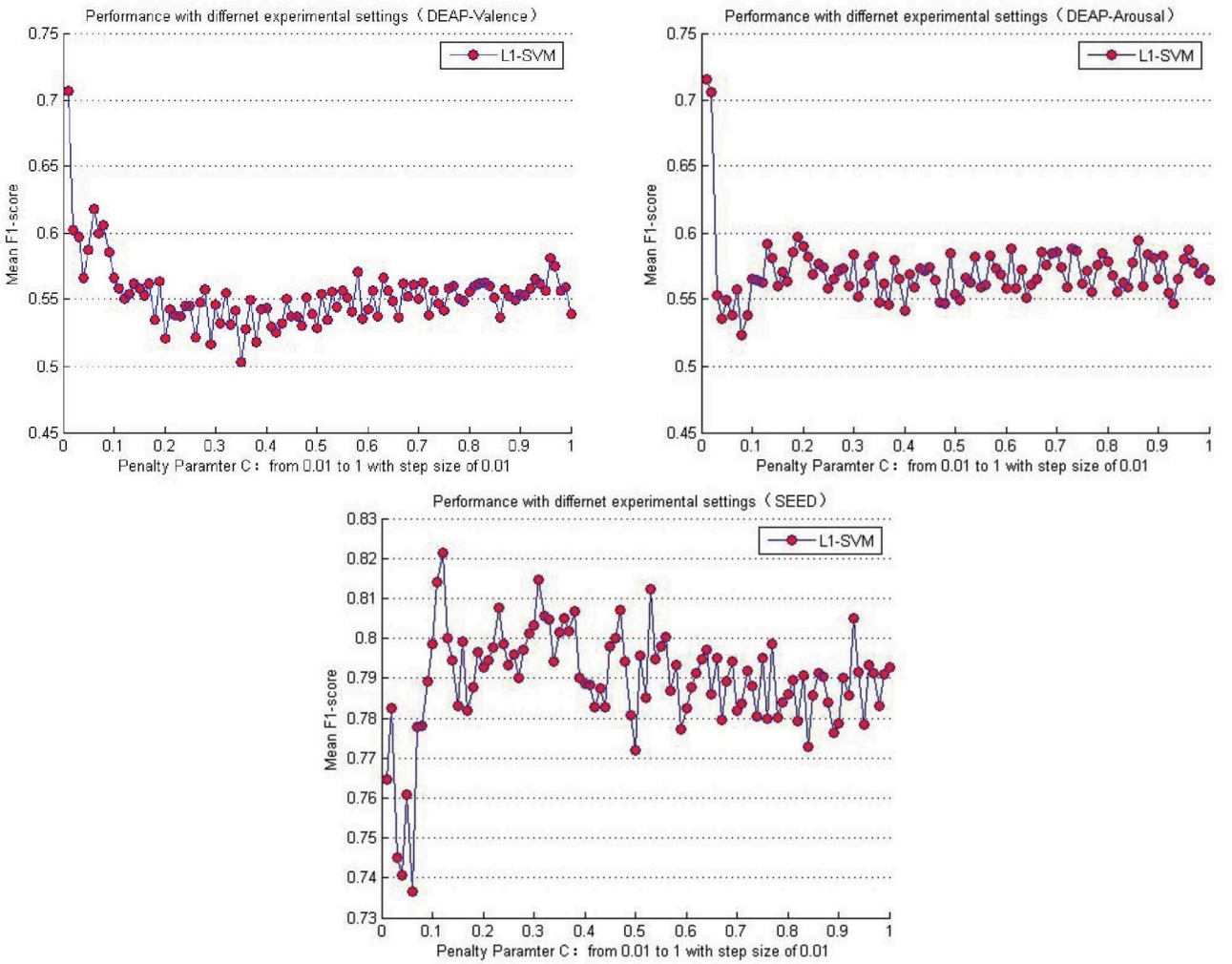

FIGURE 6 | Mean cross-subject recognition performance with different settings when L1-SVM based approach is applied.

features with 0 weights to be eliminated from the candidate set. The parameter "C" controls the trade-off between the loss and penalty. Hence, the results of the performance when a different penalty parameter "C" was tested are shown in **Figure 6**. Then the best performances on DEAP and SEED datasets are reported in **Table 5**.

Compared to the baseline methods, the VAE-based approach achieved higher performance on both datasets. It should be pointed out that, though the performance shown here was not good enough compared with the L1-SVM method, it avoided the problems of high computational cost when calculating the handcraft features, especially for the Non-linear Dynamical System Features (e.g., the Lyapunov exponent). Besides, the effectiveness of the features highly depends on the parameter settings (e.g., the setting of the number of the embedding dimension when calculating the Lyapunov exponent). When extracting the features from multichannel EEGs, the cost will multiply. This issue hampers the practical usage of the EEG-based emotion recognition. Hence, compared to the traditional handcraft feature-based methods, the proposed neural network-based approach was advantageous in terms of data-processing speed when the trained network was provided in advance. The process of latent factor decoding, sequence modeling, and classification can be conducted and completed at a very fast speed. In addition, the experimental settings and parameters of our approach were not fully tested. On the whole, the approach proposed in this paper is also valuable and has great potential in this field. The AE has shown excellent ability in reconstructing the multichannel EEG; however, according to the recognition performance, its decoded factors were not an accurate reflection of the brain cognitive state compared to the RBM- and VAE-based approaches. Hence, in cognition research-oriented neural signal computing, the generative model-based approaches are more advisable. Finally, despite the excellent performance the PCA obtained in reconstructing the multichannel EEGs, the principle components mined by it do not contribute to promoting the performance in recognizing subjects' emotions.

TABLE 6 | List of related works in recent years and the corresponding performance obtained.

	Approach/Model	Performance			
		Valence		Arousal	
		P_{acc}	P_{f1}	P_{acc}	P_{f1}
DEAP	Ontology-based storage and representation, feature selection and decision tree based recognition method (Chen et al., 2015)	0.6783	N/A	0.6896	N/A
	Minimum-redundancy-maximum-relevance (MRMR) based feature selection combined with the statistical features, band power features, Hjorth parameters and fractal dimension (Atkinson and Campos, 2016)	0.7314	N/A	0.7306	N/A
	Integrated classifier based on multi-layer stacking autoencoder combined with time domain features and PSD features (Yin et al., 2017)	0.7617	0.7243	0.7719	0.6901
	Multivariate empirical mode decomposition (MEMD) based feature extraction combined with ANN (Mert and Akan, 2018)	0.7287	N/A	0.7500	N/A
	Generative adversarial network (WGANDA) based transfer learning combined with differential entropy feature (Luo et al., 2018)	0.6799	N/A	0.6685	N/A
	The VAE based approach proposed in this work	0.7623	0.7167	0.7989	0.7243
SEED		P_{acc}		P_{f1}	
	Dynamical graph CNN (DGCNN) learns from the DE, PSD, DASM, RASM and DCAU features based adjacency matrix representation (Song et al., 2018)	0.7995		N/A	
	Extracting differential entropy features to construct 2D sparse graph representation, then combining CNN for classification (Li et al., 2018)	0.8820		N/A	
	Transfer learning methods combined with differential entropy features and logistic regression based classification (Lan et al., 2018)	0.7247		N/A	
	Generative adversarial network (WGANDA) based transfer learning combined with differential entropy feature (Luo et al., 2018)	0.8707		N/A	
	Spatial-temporal recurrent neural network (STRNN) combined with differential entropy feature (Zhang et al., 2018)	0.8950		N/A	
	The VAE based approach proposed in this work	0.8581		0.8429	

As shown in **Table 6**, we furthermore list the highly cited related works in recent years and the corresponding performance obtained. Though the performance obtained in this work was slightly inferior to some related works, it verified the effectiveness of the proposed approach and inspires us to do further research, such as finding the best model parameters and studying the brain functions based on the decoded latent factors.

4. CONCLUSION

This paper explored EEG-based emotion identification methods that were not restricted to handcrafted features. Brain cognition research finds that "there exists cross-user, default intra-brain variables involved in the emotional process." Hence, the status of the brain hidden variables is closely related with the emotional psychophysiological processes and can be utilized to infer the emotional state. In this work, artificial neural networks are used for unsupervised modeling of the state space of the latent factors from the multichannel EEGs, and LSTM-based supervised sequence modeling is further performed on the decoded latent factor sequences to mine the emotion related information, which is used for inferring the emotional states. It has been verified that the neural network models are more suitable for modeling and decoding brain neural signals than the independent component analysis (ICA) method, which is widely used in brain cognitive research. Although, from the perspective of data reconstruction, the VAE cannot achieve the same performance as that of the traditional AE, we obtained a better recognition performance on the latent factors decoded by the VAE. It indicated that VAE, as a kind of generative model, can truly model the hidden state space of the brain in cognitive processes. The decoded latent factors contain the relevant and effective information for emotional state inference. This approach is also promising in diagnosing depression, Alzheimer's disease, mild cognitive impairment, etc., whose specific brain functional networks may have been altered or could be aberrant compared with the normal healthy control. In future work, we will study the influence of a different sampling step size in latent factor sequence modeling and emotion recognition. Other directions deserving of exploration in future works include source localization and functional network analysis based on the decoded latent factors.

DATA AVAILABILITY STATEMENT

The DEAP dataset analyzed for this study can be found in the following link: http://www.eecs.qmul.ac.uk/mmv/datasets/deap/index.html. The SEED dataset analyzed for this study can be found in the following link: http://bcmi.sjtu.edu.cn/~seed/index.html.

AUTHOR CONTRIBUTIONS

XL proposed the idea, realized the proposed approach, conducted experiments and wrote the manuscript. ZZ provided advice on the research approaches, guided the experiments, checked, polished the manuscript and provided the experimental environment. DS proposed the idea, reviewed the related works,

analyzed the results and polished the manuscript. YZ realized the proposed methods, conducted experiments, analyzed the results and provided revision suggestions. JP and LW analyzed the experimental results, checked this work and provided revision suggestions. JH conducted experiments of the baseline methods for comparison and summarized the results. CN and DW acquired, pre-processed the experimental dataset and extracted the handcraft EEG features.

FUNDING

This work was supported in part by the Innovative Public Service Platform Project of Shandong Province (grant No. 2018JGX109), the Major Science and Technology Innovation Projects of Shandong Province (grant No. 2019JZZY010108), and the Natural Science Foundation of China (grant Nos. U1636203, U1736103).

ACKNOWLEDGMENTS

We thank Prof. Bin Hu and his research group in Lanzhou University for inspiring our research. We thank Dr. Junwei Zhang, Prof. Peng Zhang for taking care of our research work. Finally, we would also like to thank the editors, reviewers, editorial staffs who take part in the publication process of this paper.

REFERENCES

Adolphs, R., Tranel, D., Damasio, H., and Damasio, A. (1994). Impaired recognition of emotion in facial expressions following bilateral damage to the human amygdala. *Nature* 372, 669–672. doi: 10.1038/372669a0

Atkinson, J., and Campos, D. (2016). Improving bci-based emotion recognition by combining eeg feature selection and kernel classifiers. *Expert Syst. Appl.* 47, 35–41. doi: 10.1016/j.eswa.2015.10.049

Calhoun, V. D., and Adali, T. (2012). Multisubject independent component analysis of fmri: a decade of intrinsic networks, default mode, and neurodiagnostic discovery. *IEEE Rev. Biomed. Eng.* 5, 60–73. doi: 10.1109/RBME.2012.2211076

Calhoun, V. D., Adali, T., Pearlson, G. D., and Pekar, J. J. (2010). A method for making group inferences from functional mri data using independent component analysis. *Human Brain Mapp.* 14:140. doi: 10.1002/hbm.1048

Chen, J., Hu, B., Moore, P., Zhang, X., and Ma, X. (2015). Electroencephalogram-based emotion assessment system using ontology and data mining techniques. *Appl. Soft Comput.* 30, 663–674. doi: 10.1016/j.asoc.2015.01.007

Chen, J. L., Ros, T., and Gruzelier, J. H. (2013). Dynamic changes of ica-derived eeg functional connectivity in the resting state. *Human Brain Mapp.* 34, 852–868. doi: 10.1002/hbm.21475

Choudrey, R. A. (2002). *Variational Methods for Bayesian Independent Component Analysis*. Oxford, UK: University of Oxford.

Glorot, X., Bordes, A., and Bengio, Y. (2011). "Domain adaptation for large-scale sentiment classification: a deep learning approach," in *International Conference on International Conference on Machine Learning* (Bellevue, WA), 513–520.

Graves, A., Mohamed, A.-r., and Hinton, G. (2013). "Speech recognition with deep recurrent neural networks," in *2013 IEEE International Conference on Acoustics, Speech and Signal Processing* (Vancouver, BC: ICASSP), 6645–6649.

Hinton, G. E. (2002). Training products of experts by minimizing contrastive divergence. *Neural Comput.* 14, 1771–1800. doi: 10.1162/089976602760128018

Hinton, G. E., and Salakhutdinov, R. R. (2006). Reducing the dimensionality of data with neural networks. *science* 313, 504–507. doi: 10.1126/science.1127647

Huang, H., Hu, X., Han, J., Lv, J., Liu, N., Guo, L., and Liu, T. (2016). "Latent source mining in fmri data via deep neural network," in *IEEE International Symposium on Biomedical Imaging* (Prague), 638–641. doi: 10.1109/ISBI.2016.7493348

Kingma, D. P., and Welling, M. (2014). "Auto-encoding variational bayes," *International Conference on Learning Representations*. Banff, AB.

Koelstra, S., Muhl, C., Soleymani, M., Lee, J.-S., Yazdani, A., Ebrahimi, T., et al. (2011). Deap: a database for emotion analysis; using physiological signals. *IEEE Trans. Affect. Comput.* 3, 18–31. doi: 10.1109/T-AFFC.2011.15

Krumhansl, C. L. (1997). An exploratory study of musical emotions and psychophysiology. *Can. J. Exp. Psychol.* 51, 336–353. doi: 10.1037/1196-1961.51.4.336

Lan, Z., Sourina, O., Wang, L., Scherer, R., and Müller-Putz, G. R. (2018). Domain adaptation techniques for eeg-based emotion recognition: a comparative study on two public datasets. *IEEE Trans. Cogn. Dev. Syst.* 11, 85–94. doi: 10.1109/TCDS.2018.2826840

Li, J., Zhang, Z., and He, H. (2018). Hierarchical convolutional neural networks for eeg-based emotion recognition. *Cognit. Comput.* 10, 368–380. doi: 10.1007/s12559-017-9533-x

Luo, Y., Zhang, S.-Y., Zheng, W.-L., and Lu, B.-L. (2018). "Wgan domain adaptation for eeg-based emotion recognition," in *International Conference on Neural Information Processing* (Siem Reap: Springer), 275–286. doi: 10.1007/978-3-030-04221-9-25

Mert, A., and Akan, A. (2018). Emotion recognition from eeg signals by using multivariate empirical mode decomposition. *Patt. Analy. Appl.* 21, 81–89. doi: 10.1007/s10044-016-0567-6

Moshfeghi, Y. (2012). *Role of emotion in information retrieval*. Ph.D. thesis, University of Glasgow, Glasgow, UK.

O'Regan, K. (2003). Emotion and e-learning. *J. Asynchron. Learn. Netw.* 7, 78–92. Available online at: https://digital.library.adelaide.edu.au/dspace/handle/2440/45646

Song, T., Zheng, W., Song, P., and Cui, Z. (2018). Eeg emotion recognition using dynamical graph convolutional neural networks. *IEEE Trans. Affect. Comput.* doi: 10.1109/TAFFC.2018.2817622. [Epub ahead of print].

Sourina, O., Liu, Y., and Nguyen, M. K. (2012). Real-time eeg-based emotion recognition for music therapy. *J. Multimodal User Interf.* 5, 27–35. doi: 10.1007/s12193-011-0080-6

Vytal, K., and Hamann, S. (2014). Neuroimaging support for discrete neural correlates of basic emotions: a voxel-based meta-analysis. *J. Cogn. Neurosci.* 22, 2864–2885. doi: 10.1162/jocn.2009.21366

Ward, L. M. (2004). Synchronous neural oscillations and cognitive processes. *Trends Cogn. Sci.* 7, 553–559. doi: 10.1016/j.tics.2003.10.012

WHO (2017). *Depression and Other Common Mental Disorders: Global Health Estimates*. Geneva: WHO.

Yin, Z., Zhao, M., Wang, Y., Yang, J., and Zhang, J. (2017). Recognition of emotions using multimodal physiological signals and an ensemble deep learning model. *Comput. Methods Programs Biomed.* 140, 93–110. doi: 10.1016/j.cmpb.2016.12.005

Zhang, T., Zheng, W., Cui, Z., Zong, Y., and Li, Y. (2018). Spatial–temporal recurrent neural network for emotion recognition. *IEEE Trans. Cybernet.* 49, 839–847. doi: 10.1109/TCYB.2017.2788081

Zheng, W.-L., and Lu, B.-L. (2015). Investigating critical frequency bands and channels for eeg-based emotion recognition with deep neural networks. *IEEE Trans. Autonom. Mental Dev.* 7, 162–175. doi: 10.1109/TAMD.2015.2431497

Conflict of Interest: The authors declare that the research was conducted in the absence of any commercial or financial relationships that could be construed as a potential conflict of interest.

frontiers in Neuroscience

ORIGINAL RESEARCH
published: 07 April 2020
doi: 10.3389/fnins.2020.00290

Decoding Imagined and Spoken Phrases From Non-invasive Neural (MEG) Signals

Debadatta Dash[1,2], *Paul Ferrari*[3,4] *and Jun Wang*[2,5]*

[1] Department of Electrical and Computer Engineering, University of Texas at Austin, Austin, TX, United States, [2] Department of Neurology, Dell Medical School, University of Texas at Austin, Austin, TX, United States, [3] MEG Lab, Dell Children's Medical Center, Austin, TX, United States, [4] Department of Psychology, University of Texas at Austin, Austin, TX, United States, [5] Department of Communication Sciences and Disorders, University of Texas at Austin, Austin, TX, United States

Speech production is a hierarchical mechanism involving the synchronization of the brain and the oral articulators, where the intention of linguistic concepts is transformed into meaningful sounds. Individuals with locked-in syndrome (fully paralyzed but aware) lose their motor ability completely including articulation and even eyeball movement. The neural pathway may be the only option to resume a certain level of communication for these patients. Current brain-computer interfaces (BCIs) use patients' visual and attentional correlates to build communication, resulting in a slow communication rate (a few words per minute). Direct decoding of imagined speech from the neural signals (and then driving a speech synthesizer) has the potential for a higher communication rate. In this study, we investigated the decoding of five imagined and spoken phrases from single-trial, non-invasive magnetoencephalography (MEG) signals collected from eight adult subjects. Two machine learning algorithms were used. One was an artificial neural network (ANN) with statistical features as the baseline approach. The other was convolutional neural networks (CNNs) applied on the spatial, spectral and temporal features extracted from the MEG signals. Experimental results indicated the possibility to decode imagined and spoken phrases directly from neuromagnetic signals. CNNs were found to be highly effective with an average decoding accuracy of up to 93% for the imagined and 96% for the spoken phrases.

Keywords: MEG, speech, brain-computer interface, wavelet, convolutional neural network, neural technology

Edited by:
Hasan Ayaz,
Drexel University, United States

Reviewed by:
Damien Coyle,
Ulster University, United Kingdom
Masayuki Hirata,
Osaka University, Japan

***Correspondence:**
Jun Wang
jun.wang@austin.utexas.edu

Specialty section:
This article was submitted to Neural Technology, a section of the journal Frontiers in Neuroscience

Received: *11 August 2019*
Accepted: *13 March 2020*
Published: *07 April 2020*

Citation:
Dash D, Ferrari P and Wang J (2020) Decoding Imagined and Spoken Phrases From Non-invasive Neural (MEG) Signals. Front. Neurosci. 14:290. doi: 10.3389/fnins.2020.00290

1. INTRODUCTION

Speech is an essential attribute of humans, with the execution of verbal communication being underpinned by a very complex—yet poorly understood—relationship between neural processing and articulation. Speech centers of the brain including primary motor regions in synchrony with the articulators guide the mechanism of speech production where thoughts are transformed into meaningful words in the form of acoustics (Levelt, 1999; Ackermann, 2008). Brain damage or late-stage neurodegenerative diseases such as amyotrophic lateral sclerosis (ALS) leads to a state called locked-in syndrome, where patients are cognitively intact but motorically "locked-in" (Smith and Delargy, 2005; Kiernan et al., 2011). There is a population incidence of about 0.7/10,000 for the locked-in syndrome (Kohnen et al., 2013). Communication assistance is critical for these patients to resume a meaningful life. Since the whole body, including the articulators, fingers, and eyes are

paralyzed, a motoric bypass directly utilizing brain activity might be the only option to reestablish their communication. Electroencephalography (EEG) is the standard modality from which cortical potentials, P300, or sensory-motor rhythm (SMR) oscillations are used for assessing the brain dynamics in brain-computer interfaces (BCIs) (Brumberg et al., 2010). EEG is a reasonable choice for brain-based communication for patients with debilitating neurodegenerative diseases, primarily because of its non-invasiveness, low cost, and satisfactory temporal resolution (Birbaumer, 2006). However, the major disadvantage of current EEG-BCIs is the slow word synthesis rate which is about a few words ($<$ 10) per minute (Birbaumer, 2006). This is mostly due to the passive letter selection paradigm of the EEG-BCI designs where subjects are required to select control characters randomly displayed on a screen prompted with visual or attention correlates. A direct neural speech decoding approach may improve efficacy by providing a faster communication rate than the current BCIs. In this framework, once the imagined- or intended-speech is generated internally, these signals are then decoded to text or speech parameters, and then a text-to-speech synthesizer (Cao et al., 2017) or a vocoder (Akbari et al., 2019) can be used to construct speech immediately.

While a number of speech decoding studies have been conducted using EEG recently such as for classification of imagined syllables (D'Zmura et al., 2009; Brigham and Vijaya Kumar, 2010; Deng et al., 2010), isolated phonemes (Chi and John, 2011; Leuthardt et al., 2011; Zhao and Rudzicz, 2015; Yoshimura et al., 2016), alphabets (Wang et al., 2018), or words (Porbadnigk et al., 2009; Nguyen et al., 2017; Rezazadeh Sereshkeh et al., 2017), the decoding performances have been intermediate, e.g., 63.45% for a binary (yes/no) classification (Rezazadeh Sereshkeh et al., 2017) or 35.68% for five vowel classification (Cooney et al., 2019a). There are inherent disadvantages in using EEG that may have contributed to the difficulty in attaining high decoding performance. For example, EEG recorded signals are distorted by neural tissue boundaries, skull, and scalp. Additionally, EEG is reference-based and has a relatively lower spatial resolution. Functional magnetic resonance imaging (fMRI), which has a high spatial resolution, has also been used for speech decoding but only during speech perception, speech categorization, and speaker recognition (Formisano et al., 2008). Although these studies are important for understanding the neural speech perception mechanism, decoding speech perception is not adequate to drive a speech-BCI for intended/imagined speech production. Furthermore, fMRI has a low temporal resolution (Dash et al., 2018a,b) and hence is not suitable for decoding speech production. Very recently, Electrocorticography (ECoG) has shown great potential for direct neural speech decoding of spoken, isolated phonemes (Ramsey et al., 2018), words (Kellis et al., 2010; Martin et al., 2016), and even of continuous speech (open set phrases) (Herff et al., 2015). Direct synthesis of speech from neural signals has also been shown to be possible with ECoG (Angrick et al., 2019; Anumanchipalli et al., 2019). However, ECoG requires a craniotomy and surgical placement of electrodes into the brain, which presents a challenge for establishing bio-compatibility between the device and the brain for long-term use. In addition, with ECoG, only a part of the brain (usually speech centers) is utilized as it is extremely impractical, if not impossible, to implant electrodes across the whole brain. Thus, a non-invasive, high temporal resolution, whole-head neuroimaging modality holds the potential for the development of future BCIs with a faster communication rate.

The current focus of neural decoding has been on either overt speech (Dash et al., 2018d; Livezey et al., 2019) or imagined (covert) speech, which corresponds to imagining speech pronunciation in the absence of articulatory and acoustic output (D'Zmura et al., 2009; Yoshimura et al., 2016; Rezazadeh Sereshkeh et al., 2017; Cooney et al., 2018). Considering the behavioral difficulty in investigating imagined speech, it is understandable that the majority of the speech-BCI research is dominated by overt speech decoding studies. Overt speech performance can be verified with the produced acoustic output whereas the verification of imagined speech production is ambiguous, indefinite, and subjective. In fact, the current decoding studies involving open-set brain to text (Herff et al., 2015; Moses et al., 2019) or brain to speech (Angrick et al., 2019; Anumanchipalli et al., 2019) decoding are on overt speech. Current neural decoding of imagined or intended speech is still limited to closed-set classifications (Guenther et al., 2009; Brumberg et al., 2011; Ikeda et al., 2014; Nguyen et al., 2017; Cooney et al., 2018). For instance, using EEG, researchers have successfully performed imagined speech decoding by classifying various short speech units, e.g., two syllables (D'Zmura et al., 2009), five phonemes (Chi and John, 2011), two vowels (Iqbal et al., 2015; Yoshimura et al., 2016), seven phonemes (Zhao and Rudzicz, 2015), and even words (Porbadnigk et al., 2009; Nguyen et al., 2017; Rezazadeh Sereshkeh et al., 2017; Hashim et al., 2018). Studies using ECoG have also shown the possibility of decoding imagined speech (Ikeda et al., 2014; Martin et al., 2016). However, there is still room for improvement in the accuracies obtained in all of these imagined speech decoding studies. There is some evidence from fMRI that imagined speech produces lower levels of brain activity compared to overt speech (Palmer et al., 2001; Shuster and Lemieux, 2005), which may explain the lower decoding performance of the former in literature. In short, there is a need for improved performance of decoding imagined speech.

In this study, we performed decoding of both imagined and overt speech production. Instead of using isolated phonemes or syllables, we collected neural data during the imagination and production of phrases (e.g., how are you?), with the eventual goal of open-vocabulary decoding (decoding phonemes within phrases) for naturalistic communication (Iljina et al., 2017). Here, we classified whole phrases, as a starting point. The neurolinguistics underpinnings supporting phrase-level covert or overt articulation is widely studied topic, but has not yet been explored in a decoding experiment (Memarian et al., 2012). Furthermore, acknowledging the difficulty in verifying the behavioral compliance of imagined speech production (Cooney et al., 2018), in contrast to the data acquisition paradigm of current literature for separately collecting data for overt and imagined speech, we collected the neural signals corresponding to imagined and overt speech consecutively, within the same

trial, where the timing of this paradigm constrained the subjects to imagining/preparing the same phrase he/she is expected to articulate for the trial.

We used magnetoencephalography (MEG) to record the neuromagnetic signals corresponding to speech imagination and production. Magnetoencephalography (MEG) is a non-invasive, whole-head neuroimaging modality that uses highly sensitive magnetometers and gradiometers to record the magnetic fields associated with intracellular post-synaptic neuronal currents in the brain (Cohen and Cuffin, 1983). Unlike the electric signals measured with EEG and ECoG, the magnetic field signals measured by MEG pass through the dura, skull, and scalp relatively undistorted, and thus provide a more accurate representation of the underlying brain activities. MEG has a higher spatial resolution than EEG while maintaining a very high temporal resolution (1 ms or even lower). These unique benefits make MEG a great fit for the investigation of speech decoding. Recent MEG based speech studies suggest the efficacy of MEG in capturing the fast temporal dynamics of the speech signal (Simos et al., 1998; Memarian et al., 2012; Wang et al., 2017; Dash et al., 2018d, 2019b), and provide further evidence in support of the use of neuromagnetic signals to be used in speech decoding. Although current MEG machines are non-portable and costly, a recent study on wearable MEG (Boto et al., 2018) showed the potential of building next-generation, portable MEG devices. Further, unlike SQUID based measurement system, it uses optically pumped magnetometers (OPMs) which can reduce the cost dramatically. These recent advances in technology hold great promise for suitable MEG mediated speech-BCI applications in the near future.

Three decoding approaches were tested in this experiment. First, we used an artificial neural network (ANN) trained on the root mean square (RMS) features of the neural signals. We considered this approach as our baseline, which was used in our pilot studies (Dash et al., 2018c,d). Considering the difficulty in collecting lots of neural signal data, previously, researchers have employed simpler decoders for classification equivalent to our baseline approach such as matched filter on Hilbert envelope features (D'Zmura et al., 2009), Bayesian classifier based on multi-class linear discriminant analysis (LDA) on Hilbert envelope features (Deng et al., 2010), or spectral features (Chi and John, 2011), nearest neighbor classification on the features extracted with Euclidian distance of the coefficients from autoregressive models (Brigham and Vijaya Kumar, 2010), support vector machine on statistical features (Zhao and Rudzicz, 2015), and Euclidian distance feature (Martin et al., 2016), relevance vector machine on Riemannian manifold features (Nguyen et al., 2017), hidden Markov model on temporal neural signals (Porbadnigk et al., 2009), artificial neural network on Wavelet-transform based statistical features (root mean square and standard deviation) (Rezazadeh Sereshkeh et al., 2017), etc. Among all, ANN with wavelet-transform based statistical features (Rezazadeh Sereshkeh et al., 2017) has shown comparatively better decoding performance which inspired our pilot studies and baseline of this study for exploring with statistical features and using ANN as the decoder. Second, we employed convolutional neural networks (CNNs) trained on spectral-temporal features in terms of scalograms of the neuromagnetic signals. Third, to further utilize the neural information, we added spatial dimension on top of the second approach. In other words, CNNs were trained using spatial-spectral-temporal features in the third approach. CNNs have recently shown great potential in a wide variety of application in computer vision, and acoustic speech decoding, which outperform ANNs. CNNs are inspired by visual cortex architecture of the brain where the cortical neurons work on a restricted area of the visual domain (called receptive field) by partial overlapping with each other to cover the whole visual space. CNNs are functionally very similar to the traditional neural networks as it operates as a variation of multilayer perceptions, but are modeled to require minimal processing (Cireşan et al., 2011). In Roy et al. (2019), it is reported that a total of 40% studies amongst all research involving deep learning applications to EEG have used CNNs, but none of them were for speech decoding. Nevertheless, the efficacy of CNN for neural data analysis can be translated for neural speech decoding which we experimented within this study. Moreover, a few recent studies have shown the efficacy of using CNN to analyze MEG (Hasasneh et al., 2018; Dash et al., 2019a; Huang and Yu, 2019) or EEG data (Cooney et al., 2019a,b), which further strengthens our motivation for this approach. To our knowledge, this is the first study using CNNs to explore neural speech decoding with MEG.

2. DATASET AND FEATURE EXTRACTION

2.1. Data Collection

Eight right-handed subjects (five males and three females) with a mean age of 41 years (standard deviation = 14 years) participated in the data collection. The subjects had normal or corrected to normal vision. No speech/language/hearing or cognitive history was reported from the subjects. All the subjects were English speakers. Written consent was obtained from each subject prior to the experiment. This study has been approved by the local ethics committees at the University of Texas at Dallas, the University of Texas at Austin, Dell Children's Medical Center (Austin, TX), and Cook Children's Hospital (Fort Worth, TX).

The data acquisition was performed at two places, one at the MEG Lab, Cook Children's Hospital where the data were collected from four subjects. The data for the other four subjects were collected at the MEG lab, Dell Children's Medical Center. The two hospitals have identical Elekta Neuromag Triux MEG devices as shown in **Figure 1**, which were used to record the brain activity signals. The machine consists of 306 channels with 204 planar gradiometers and 102 magnetometer sensors. It is housed within a magnetically shielded room (MSR) to discard any unwanted environmental magnetic field interferences. Prior to recording, the coordinate system based on three fiducial points (the left and right pre-auricular points and one at the nasion) was created for the subjects. For coregistration of the subjects within the MEG system, five head-position-coils were fixed to their head and digitalized using a Polhemus Fastrak, and then localized in the MEG at the start of each experimental run. The brain activity signals were acquired via MEG with 4 kHz sampling frequency which were then band-pass filtered and

FIGURE 1 | A MEG unit. The picture represents the Neuromag Eleckta Ltd. MEG machine situated within a magnetically shielded room at the Cook Children's Hospital, Texas. A subject is seated comfortably in the unit. The projected display is for showing the stimuli (text) in a pseudo-randomized order.

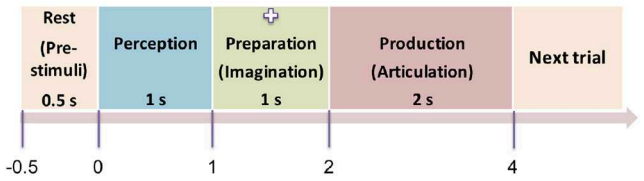

FIGURE 2 | Protocol of the time-locked experiment. The four time-locked stages of the experiment (*rest* → *perception* → *preparation* → *articulation*) are shown here. The numbers represent the initial onset time of the stages. Next trial starts with a non-movement baseline of 1 s. The screen was blank in dark background during the pre-stimuli stage. A stimulus (text) was displayed on the screen during the perception segment, then replaced by a cross sign during the preparation stage. The cross disappeared (blank display) again during the production stage.

resampled to 1 kHz. Eye-blinking artifacts were collected through electrooculography (EOG) by two integrated sensors placed at the upper and lower aspect of the outer-canthi. The cardiac signal was recorded by two bipolar integrated electrocardiograph (ECG) sensors placed on top of the collarbone areas. Acoustic output during the speech production stage was recorded through a standard built-in microphone connected to a transducer placed outside the MSR. To record the jaw movement, a custom-made air bladder was used which was connected to an air pressure sensor. By recording the depression in that bladder jaw motion data during articulation was acquired. Both speech and jaw movement analog signals were then digitized by feeding into the MEG ADC in real-time as separate channels. All the sensors were checked for noise and calibrated prior to data collection. Subjects sat upright in the MEG with their hands resting on a platform in front of them. In order to reduce head movements, subjects underwent a few minutes of adjustments and training about slouching. Visual stimuli were generated by a computer running the STIM2 software (Compumedics, Ltd.), and presented via a DLP projector situated at 90 cm from the subjects'.

2.2. Experimental Protocol

The experiment was designed as a delayed overt reading task, with four segments within each trial: pre-stimulus (rest), perception, preparation (imagination), and production (articulation) as shown in **Figure 2**. The pre-stimuli segment was designated as a period of 0.5 s prior to the stimulus onset. The perception segment was initiated by a single stimulus (phrase) being displayed on the screen for the subjects to covertly read. The stimulus was on the screen for 1 s after which it was replaced by a fixation cross (+). The duration of the fixation was 1 s which corresponded to the imagination (preparation) segment. For this segment, the subjects were previously instructed to think or imagine, and be prepared to speak. The removal of the fixation cross prompted the subjects to overtly articulate the previously viewed phrase at their natural speaking rate (production). The average time for production/articulation segment was 2 s (for one subject it was 1.5 s; for other two subjects it was 2 s, and for the rest of the 5 subjects it was 2.5 s) based on the natural speaking rate of the subjects. There was a 1 − 1.5 s of non-movement baseline prior to the next stimulus trial. This 4-stage procedure was repeated for 100 trials for each of the 5 stimuli. Five commonly used English phrases were used as stimuli, selected from the phrase lists that are used in alternative augmented communication (AAC) devices. They are: *phrase 1: Do you understand me, phrase 2: That's perfect, phrase 3: How are you, phrase 4: Good-bye, and phrase 5: I need help*. The presentation order of the stimuli was pseudo-randomized to avoid response suppression to repeated exposure (Grill-Spector et al., 2006; Cheyne and Ferrari, 2013). Subjects were trained on some sample stimuli before the experiment to ensure compliance. The whole experiment lasted approximately 45 min per subject.

2.3. Data Preprocessing

The recorded data of each stimulus type was then epoched into trials from −0.5 to +4 s centered on stimulus onset. Through visual inspection, trials containing high amplitude recorded artifacts were then removed from the MEG data. Trials in which the subject did not comply with the paradigm timing e.g., "subject spoke before the cue to articulate," were also discarded. After data preprocessing a total of 3,046 valid trials were retained out of 4,000 (8 *subjects* × 5 *phrases* × 100 *trials*) recorded trials with an average of 75 trials per phrase per subject. These valid trials were then low-pass filtered below 250 Hz with a 4th order Butterworth filter for further analysis. For this study, only gradiometer sensors were considered for decoding considering their effectiveness in noise reduction and representation of the stimuli based activation. Out of 204 gradiometer sensors, four sensors showed high channel noise during data collection from different subjects. Further, in case of some subjects, one or two more sensors showed artifact like irregularities. In total, data from eight sensors were excluded. In other words, data from 196 sensors were used for analysis.

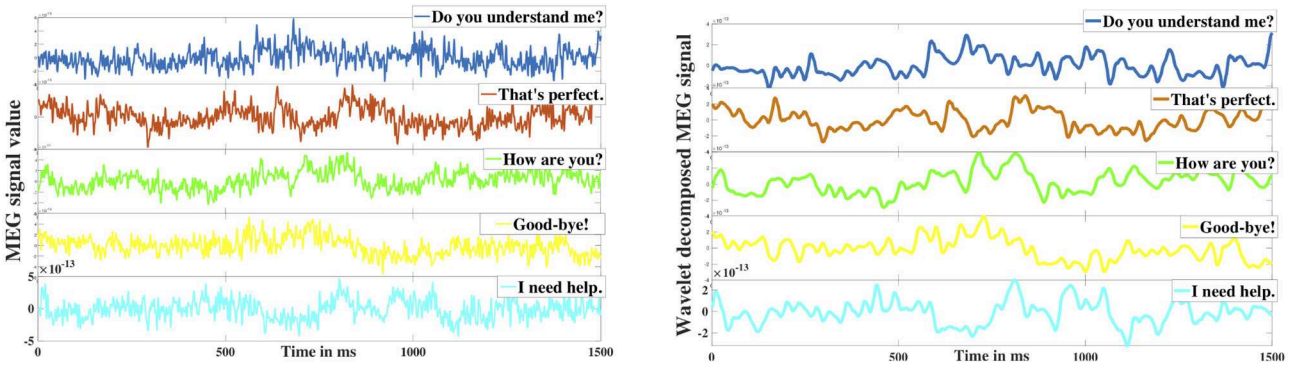

FIGURE 3 | Wavelet denoising. The left image represents the 5 raw MEG signals obtained from a sensor corresponding to the five different phrases. The right image represents the corresponding denoised signals.

2.4. Wavelet Analysis

Even though the signals were checked rigorously for artifacts, further presence of noise would hamper the characteristics of true brain oscillations. To address this issue, researchers typically employ one or several denoising algorithms (Haumann et al., 2016) including short-time Fourier transform, temporal signal source separation (t-SSS), principal component analysis (PCA), independent component analysis (ICA), and wavelet transform, etc. In particular, wavelets have been widely used for the denoising of bio-signals including MEG (Dash et al., 2018c). Wavelets express a signal as a linear combination of a distinct set of functions, obtained by shifting and scaling a single function (mother wavelet). Although the preprocessed MEG signals were in 1 kHz sampling frequency range, functional brain oscillations are believed to exist up to the high-gamma frequency range ($<\sim$ 125 Hz) (Ahnaou et al., 2017). Thus, we employed the Daubechies (db)-4 wavelet with a 7 level decomposition to perform discrete wavelet transform (DWT) for denoising and decomposing the MEG signals to specific neural oscillations. Mathematically, a signal s with a seven level wavelet decomposition can be represented as:

$$s = d_1 + d_2 + d_3 + d_4 + d_5 + d_6 + d_7 + a_7 \quad (1)$$

Here, d_{1-7} are the detail coefficients whereas a_7 is the low-frequency approximation coefficient. The signal is decomposed in such a way that in each level the signal disintegrates into two components (details and approximation) such that the detail component carries the high-frequency (upper half) element whereas the approximation component contains the low-frequency (lower half) oscillations. In this case, d_1 and d_2 are the high-frequency signals with the frequency range $250 - 500$ and $125 - 250$ Hz respectively which were discarded as noise. The effectiveness of the proposed db-4 based denoising can be observed in **Figure 3** which shows the comparison of raw signal vs. denoised signal after reconstruction (<125 Hz), Since it has been repeatedly shown that the neural information is encoded up to high gamma frequency bandwidth, removal of high-frequency components (>125 Hz) was necessary. After removing d_1 and d_2, the reconstructed signals from the remaining detail frequency components d_{3-7} represented the high-gamma (62–125 Hz), gamma (31–58 Hz), beta (16–30 Hz), alpha (8–16 Hz), and theta (4–8 Hz) frequency bands of the neural signal. The reconstructed approximation signal from a_7 was the low-frequency delta band oscillation (0.1–4 Hz).

3. DECODING APPROACHES

In this study, we performed a five-class classification task where each class corresponded to one phrase. Considering the tremendous cognitive variance across subjects (Dash et al., 2019c), only subject dependent decoding was performed, where training and testing data were from the same speakers (but unique). The classification task was performed on each of the four whole data segments (i.e., pre-stimuli, perception, preparation/imagination, and production/articulation). We leveraged two machine learning algorithms including a classic ANN as the baseline and the latest CNNs (i.e., AlexNet, ResNet, Inception-ResNet). The input to ANN was the root mean square (RMS) features of the denoised and decomposed MEG signals from each data segment. The input to CNNs was scalogram images generated from the denoised MEG signals of the whole data segments. Each of these methods is briefly described below.

3.1. Artificial Neural Network (ANN)

ANNs have been widely used for pattern classification problems to model a set of inputs leading to corresponding target outputs. The architecture of ANN is characterized by multiple connected nodes or neurons for functional processing. Considering its robust and efficient non-linear computational modeling, we used a shallow ANN as our baseline approach to classify the MEG acquired neural responses of the brain for the five respective stimuli. The input to the ANN classifier was the concatenated RMS features obtained from each of the six neural oscillation signals, high-gamma, gamma, beta, alpha, theta, and delta. A total of 196 gradiometer sensors (204 gradiometers—8 discarded due to noise) were considered for analysis. Thus, the input feature dimension of the ANN was 1,176 (6 frequency bands $\times$196 sensors). A variety of statistical features (mean, median,

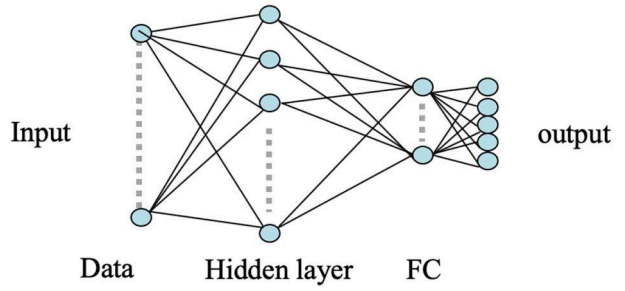

FIGURE 4 | ANN architecture. Here the circles represent the nodes whereas the arrows represent the connections between the nodes. The input layer is an 1, 176 dimensional feature vector. The hidden layer consists of 256 nodes and the remaining layers are of 5 nodes.

standard deviation, quartiles, tertiles, energy, windowed energy, cross-correlation matrix) were first extracted and examined for the statistically significant difference across the 5 classes. RMS turned out to be the best feature which was significantly different across classes (1-way ANOVA, followed by Tukey; $P < 0.001$). Feature combination was not explored since the dimension of a single type of feature was already very large (1, 176). A single hidden layer consisting of 256 number of hidden nodes with randomized weights was used during the initialization of the ANN model. A five-dimensional sigmoid activation function was connected after the hidden layer to transform the learned weights into a non-linear hyper-dimensional space. A five-dimensional fully connected softmax layer was used after sigmoid which was further connected to a five-dimensional fully-connected (FC) output classification layer to represent the cross-entropy of the five phrases. The weights of the nodes in the hidden layer of the ANN were updated via back-propagation using the stochastic gradient descent algorithm. The architecture of the used shallow ANN model is shown in **Figure 4**.

We used a coarse-to-fine hypermeter tuning strategy for tuning the learning rate with the range of values: 0.1, 0.01, 0.001, and 0.0001 on validation data, where 0.01 yielded the best performance and was used in the experiment. The data was divided into three parts as train, validation, and test such that train data consisted of 70% of the whole data whereas the test and validation data consisted of 15% each of the whole data. Our previous finding on determining the optimal number of trials for speech decoding with ANN (Dash et al., 2018c) has suggested that a total of 40 trials are sufficient for speech decoding after which the performance saturates. Hence, the traditional data split (70% − 15% − 15%) of train-validation-test was performed. Further, to avoid biased split, we performed ANN training on three separate random splits to find the average performance. Data overfitting was checked with the validation data by ensuring the early stopping of the training when the model started to generalize the data. A continuous increase in validation loss for more than 6 epochs was considered as the threshold for data overfitting. Although the maximum number of epochs were set to 100, as the data size was small, data overfitting started to occur even after an average of 35 epochs. Further, we have experimented with various combinations of hidden layer nodes to train the model to find the optimal number of nodes to train the MEG data. We tuned with various 64× nodes (i.e., 64, 128, 192, 256, 320, 384, 448, 512, 640, and 1, 024 nodes) and observed an increase in validation accuracy from 64 to 256 and then the validation accuracy saturated after 256 nodes until 512 nodes. Early data over-fitting resulted while training with more than 512 nodes in the hidden layer.

3.2. Convolutional Neural Networks (CNNs)

CNNs operate on the data by applying convolution operation on a selected receptive field. CNN makes the implicit assumption of the inputs to be images, which allows for encoding of certain properties into the architecture. CNNs are scale and shift-invariant based on their shared weight and translation invariance characteristics. Typically, a CNN architecture is formed by a stack of distinct layers (convolution, pooling, and activation) that transform the input data to an output volume with relevant class scores through a differentiable function. Here, we have used three recent deep convolutional neural networks namely AlexNet (Krizhevsky et al., 2017), ResNet101 (Wu et al., 2018), and Inception-ResNet-v2 (Szegedy et al., 2016) to evaluate the effectiveness of CNN for speech decoding (**Figure 5**). Each of the three architectures has been popularly used as classifiers for their high-performance achievement. These deep ConvNets are pre-trained with more than a million images of 1, 000 categories from the ImageNet database (Russakovsky et al., 2015) to learn rich features from the images.

3.2.1. AlexNet

AlexNet was the first deep CNN to be introduced which increased the accuracy with a very high stride compared to the then traditional approaches. It consists of five convolution layers and three fully connected (FC) layers. The kernels (filters) employed in this CNN architecture are of 11 × 11, 5 × 5, and 3 × 3 sizes and has rectified linear unit (ReLU) activation function after each convolution operation. ReLU along with dropouts were first introduced in this architecture which make AlexNet significantly faster and over-fit voided. Further, with dropouts, neurons are randomly chosen and are switched off. This restricts the neurons to coadapt and hence they learn meaningful features, independent of other neurons.

3.2.2. ResNet

ResNets introduced residual modules in the architecture which solved the degradation problem (naive addition of deeper layers leading to high training error) during the training of deeper networks. These modules create a direct pathway between input and output and learn the features on top of the available input. The residual networks were shown to be easily optimized and can gain accuracy with a significantly deeper architecture. In other words, residual modules can be thought of as shortcut connections for identity mapping. This architecture consists of 101 layers with largely 3 × 3 filters. The other attribute of this architecture is the use of global average pooling which is discussed to contribute to better accuracy since it's more native

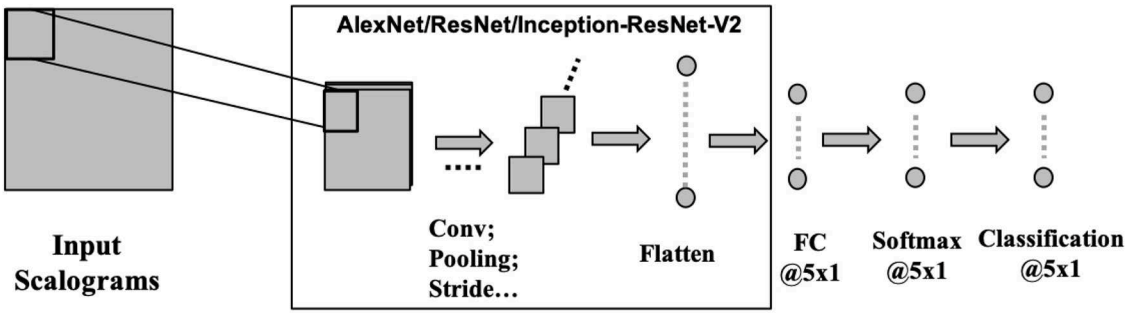

FIGURE 5 | CNN architecture. Three pre-trained deep CNNs were used with the final layers replaced by fully connected, softmax, and classification layer each with 5 nodes to suit for a 5-phrase classification problem.

to the convolutional structure and more robust to the spatial translations of the input.

3.2.3. Inception-ResNet-v2

Inception-ResNet-v2 is the second version of the combined Inception and ResNet architecture based on the idea of Microsoft ResNet to integrate residual modules on top of Inception architecture. This network has achieved one of the best performances in the ILSVRC classification task (Russakovsky et al., 2015). This ConvNet is 164 layers deep consisting of one Inception-v4 with three residual networks. The advantage of the Inception network is that here the inputs go through 1×1, 3×3, and 5×5 kernels simultaneously with max-pooling which are then concatenated to form the output. Hence, there is no need of deciding on the filter size at different layers. Further, the addition of residual networks accelerates the training of the Inception-v4 network.

3.2.4. Features for CNNs

In this experiment, two types of features were used to validate the efficacy of CNN in speech decoding. The first of these were spectral-temporal features extracted from the MEG signals, that were the scalogram images of the gradiometer signals which consist of the multi-scale variation of spectral and temporal features. The second was spatial-spectral-temporal features where we embedded the spatial information (sensors) of the corresponding gradiometers in the images. Color scalogram images were generated from the two types of features and were used as the input to the three CNN architectures.

3.2.4.1. Spectral-temporal features

Spectral features of neural signals carry important latent attributes of neural response (Halme and Parkkonen, 2016). To benefit from the frequency information of the brain activity signals we computed the wavelet scalograms of the denoised MEG signals by performing continuous wavelet transform (CWT) with Morlet wavelets. For this, the db-4 decomposed signals were first reconstructed back up to the 2nd level to accommodate all the neural oscillations (up to high-gamma frequency bandwidth). CWT generates an overcomplete representation of the signal under analysis by convolving the input data with a set of functions obtained by scaling and translating the mother wavelet (here Morlet wavelet) across various scales. The energy values of the CWT coefficients are represented as scalogram images which are extremely useful in conveying the spectral-temporal characteristics of a signal (Lilly and Olhede, 2009). Morlet wavelet has been shown to be highly effective in characterizing the MEG signal features (Tadel et al., 2011), hence we used this wavelet to compute the scalograms. **Figure 6** gives an exemplary scalogram image of the neural signal corresponding to a sensor approximately near to Broca's area while a subject is articulating "do you understand me." The scalogram images for each sensor signal during each stage were generated for all the valid trials and then resized to the specific size based on the requirement of the corresponding CNN architecture (AlexNet, ResNet, and Inception-ResNet-v2) and trained with each scalogram image as a sample. The evaluation of classification accuracy with this feature was done on single-trial level by computing the average cross-entropy score obtained from the scalogram images of all 196 sensors within a single-trial.

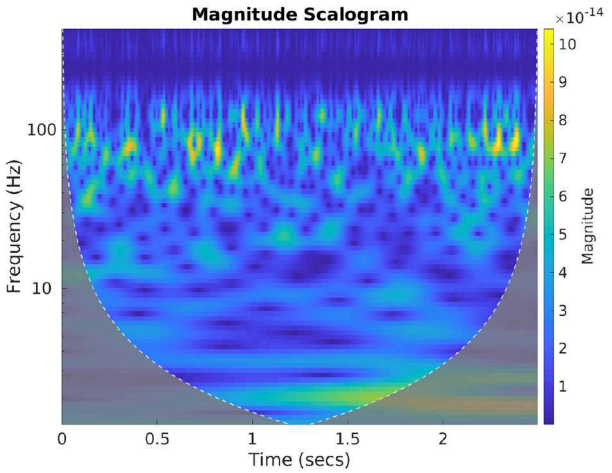

FIGURE 6 | Scalogram plot of neural signal. The image represents the cone of influence (COI) plot of the scalogram representation of the brain signal obtained from a sensor near Broca's area. This is when the subject was speaking "Do you understand me." The color bar represents the change in energy of various CWT coefficients obtained with Morlet wavelet.

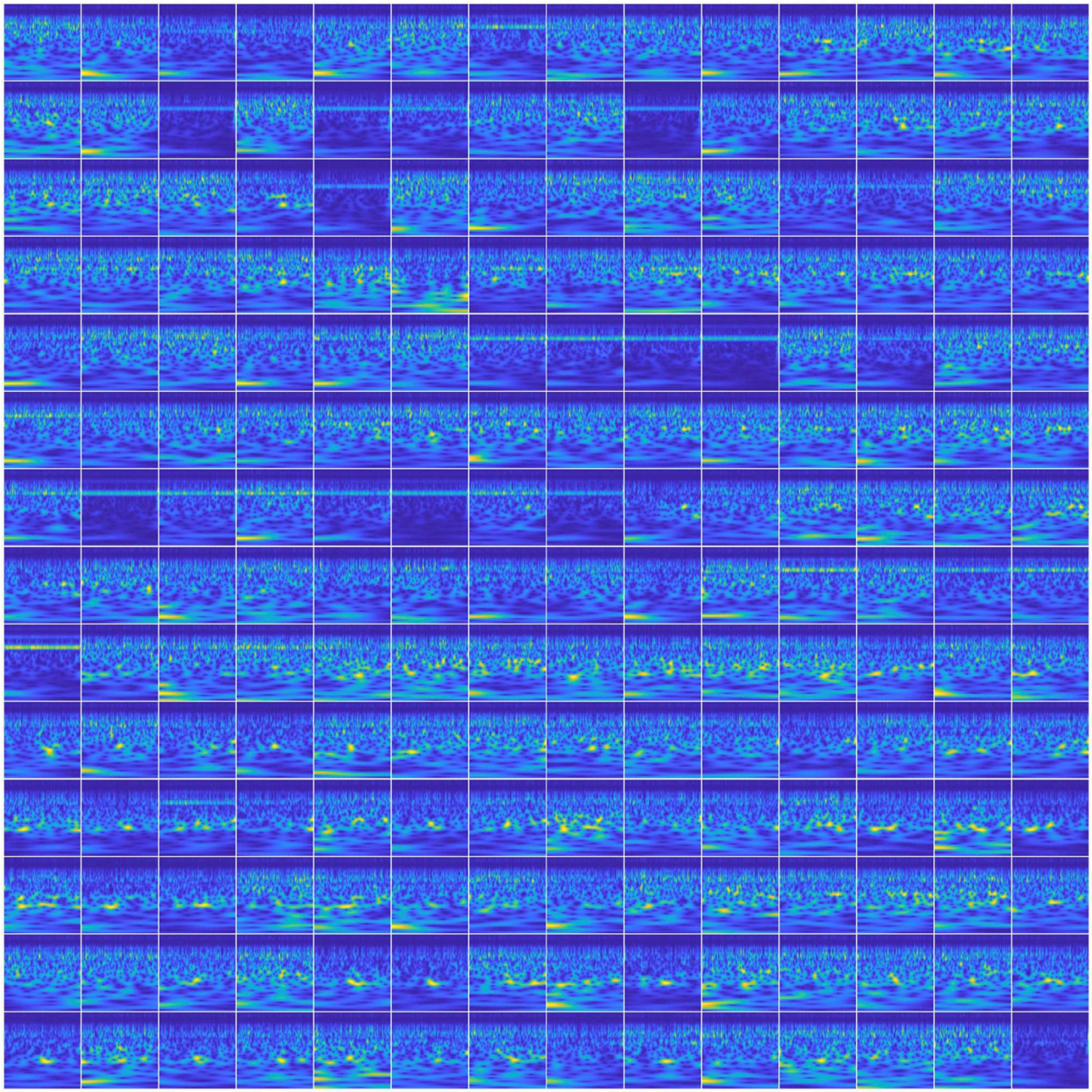

FIGURE 7 | Scalogram matrix of neural signal. The image represents a 14 × 14 matrix of scalogram images to represent the whole brain dynamics in a single image. This is when the subject was speaking "Do you understand me" for a single trial.

3.2.4.2. Spatial-spectral-temporal features

To utilize the spatial information of the MEG signals in the input images, we created a 14 × 14 matrix of scalogram images (obtained from 196 sensors) within a single image (see **Figure 7**). With this representation, for a single trial, the spatial (location) information of all the sensors was encoded within a single image. With this feature representation, the number of input images to be trained with the networks became the same as the number of trials which is about 50 per phrase per subject. Training these deep ConvNets requires a considerably higher number of inputs for proper training. Hence, we leveraged a commonly-used data augmentation approach to address this issue. Data augmentation as a self-regularizer has been demonstrated to be effective in machine learning (Shorten and Khoshgoftaar, 2019) particularly for small-data size problems. A linear positive shift of both 100 and 200 ms was performed on the signals and then their scalogram images were generated. Since the average reaction time of the subjects for speech production was about 250 ms,

this linear shift mechanism also helped in compensating for the changes in the articulation onset along with inducing variability in the input images. With this, the data size was increased to three times larger than the original and was sufficient for the training of the same three CNNs described above. To avoid possible false positives, data augmentation was implemented within each set (training, validation, or testing). In other words, a trial and its augmented versions were always under the same group (training, validation, or testing). Data augmentation for the other CNN approach (with spectral-temporal features) and the baseline approach was not needed since the training data was sufficient as observed with low variance error. Further, for ANN analysis, we have previously shown that after 40 trials, the decoding performance saturates (Dash et al., 2018c), hence, data augmentation was not necessary.

3.2.5. Experimental Setup for CNNs

As per the input requirement, for AlexNet the images were resized to $227 \times 227 \times 3$, for ResNet101 to $224 \times 224 \times 3$ and then for Inception-ResNet-v2 the input images were of size $299 \times 299 \times 3$. The third dimension (3) represents the three (RGB) colored channels. Since, these networks have been trained for a 1,000 class image classification problem, to tune these networks for our 5 class classification, the last few layers were modified, keeping the initial layers untouched. For AlexNet, the last three layers were replaced by an FC layer, a softmax layer, and a classification layer each with five nodes. Similarly, we used this five-dimensional FC layer and softmax layer to replace the last two layers of ResNet101 (fc1000 and classificationLayer-Predictions) and of Inception-ResNet-v2 (Predictions and ClassificationLayer-predictions).

Figure 5 shows the architecture for implementing the deep CNNs. For unbiased comparison, the learning rate for these three networks was fixed at 0.0001. The weight-learn-rate-factor and the bias-learn-rate-factor in the final fully-connected (FC) layer were increased to 20 for faster learning in the new layers than the transferred layers. For all the networks, Adam optimizer, a minibatch size of 64, validation frequency and validation patience of 6, a maximum epoch of 60 and gradient clipping was used. The rest of the hyperparameters were kept at their default values of the respective architectures. The same data partitioning (70%-training, 15%-validation, and 15%-testing) approach was employed here as well. The testing data were completely unseen (without containing any augmented version of the training or validation trials) and hence were new to the model. Only validation data were used for hyperparameter tuning and overfitting checking in the training stage. The CNNs were trained on a 7-GPU parallel computing server running on Linux (Ubuntu 16.04) platform using Keras imported to Matlab 2018b.

4. RESULTS

4.1. Performances of the Decoding Approaches

The classification accuracy was computed during each stage for each subject and the average classification accuracy across the eight subjects with each method can be seen in **Figure 8**. The decoding performances during all the four stages (pre-stimuli, perception, preparation/imagination, articulation) obtained with ANN or CNNs were significantly higher than the chance level accuracy (30%) (1-tail t-test, $p < 0.05$ for all). With the shallow ANN (the baseline approach), the average classification accuracy during the articulation stage was satisfactorily high ($90.55 \pm 2.11\%$), but not for perception ($71.95 \pm 3.97\%$) and imagination stage ($80.83 \pm 3.00\%$) (**Figure 8**). Both of the approaches using CNN classifier [spectral-temporal CNN (ST-CNN) and spatial-spectral-temporal CNN (SST-CNN)] outperformed the baseline (ANN) in terms of the average decoding accuracy during perception, imagination, and articulation. The average classification accuracies obtained with ST-CNN during perception, preparation, and production were $86.83 \pm 2.93\%$, $91.71 \pm 1.67\%$, and $93.56 \pm 1.92\%$, respectively, whereas, with SST-CNN the accuracies were $90.38 \pm 2.28\%$, $93.24 \pm 2.87\%$, and $96.65 \pm 2.88\%$. The differences between the decoding performances of ANN and CNN were statistically significant, which was observed via the pairwise comparison of the decoding performances with ANN, ST-CNN, and SST-CNN (2-tail t-test, $p < 0.05$, for all possible pairs). The highest p-value among all pairwise comparisons was 0.0099 when the decoding performance of ANN and ST-CNN was compared during the production stage. Among the two approaches involving CNN, spatial-spectral-temporal-CNN (SST-CNN) performed better than the spectral-temporal-CNN (ST-CNN) in terms of average decoding accuracies. A 2-tail t-test comparison of decoding performances between these two methods resulted in a significant difference between all pairs ($p < 0.05$), except between spectral-temporal and spatial-spectral-temporal features with CNN during the preparation stage ($p = 0.2135$). For the pre-stimuli stage there was no significant difference between the performances of all the three methods (2-tail t-test, $p > 0.05$).

Table 1 shows a comparison of the three specific CNN architectures, where AlexNet slightly outperformed ResNet101 and Inception-ResNet-v2 in terms of decoding accuracy. Although it has been shown that Inception-ResNet-v2 performs better with the ImageNet database, in case of MEG scalograms it was slightly different. We believe that the choice of higher initial kernel size (11×11) in the AlexNet architecture might have contributed to better performance. In the scalogram images, the features are represented with energy blobs, thus a higher initial kernel size might have helped produce better feature extraction. Nevertheless, the performances of the three ConvNets were quite similar with a standard deviation of <3% (**Table 1**). This further strengthens the efficacy of CNNs for neural speech decoding. To illustrate the details of the classification performance via the best decoder (AlexNet), **Table 2** gives the confusion matrix obtained by combining the results from all the test sets across all subjects during articulation, where the primary diagonal numbers are the correctly classified sample. The average number of misclassified samples per phrase was about 12 in the combined test set (1,382) of 8 subjects, i.e., 0.9% misclassification per phrase. Further, the receiver operating characteristics was plotted for each classification to observe the variation of true positive rate (sensitivity) with false positive rate (1-specificity) (**Figure 9**:

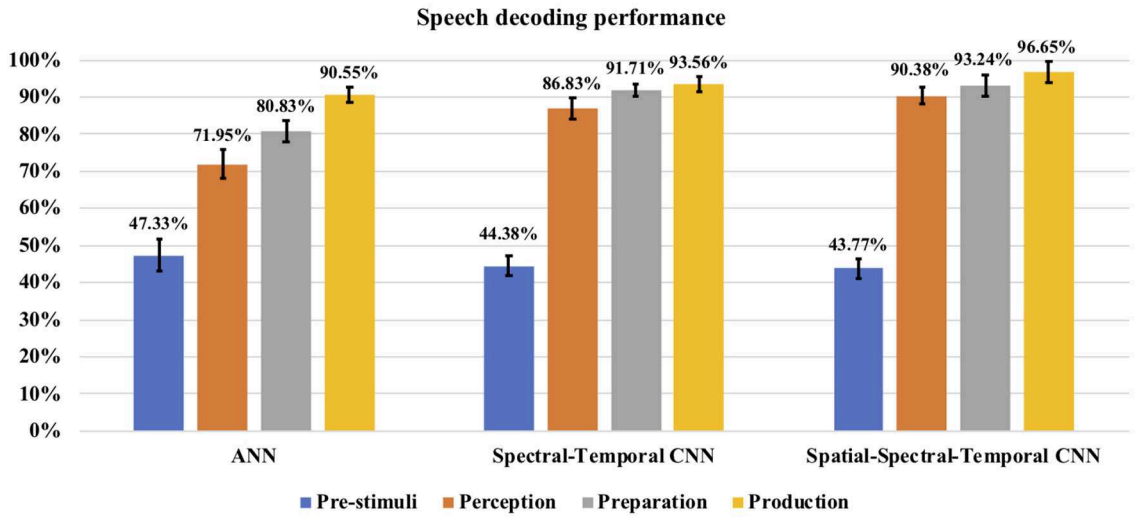

FIGURE 8 | Speech decoding accuracy. The bar graph represents the speech decoding accuracy obtained with different classifiers. For CNN the results with AlexNet are reported. The error bars represent the standard deviation in decoding accuracy across subjects.

TABLE 1 | Performance comparison of AlexNet, ResNet101, and Inception-ResNet-v2 in terms of decoding accuracies with spatial-spectral-temporal features.

CNN architecture	Pre-stimuli (%)	Perception (%)	Preparation (%)	Production (%)
AlexNet	43.77	90.38	93.24	96.65
ResNet101	42.61	84.75	87.78	92.36
Inception-ResNet-v2	42.52	87.98	91.66	94.49
Mean	42.96	87.70	90.89	94.50
STD	0.70	2.82	2.81	2.14

The test accuracies are averaged over 3 independent runs across subjects.

Exemplary ROC curve for overt speech decoding with SST-CNN using AlexNet during training and testing) to validate the classification. **Figure 9** clearly shows the validation of the classification performance across classes with a very high area under the curve (AUC).

4.2. Performances During Pre-stimuli, Perception, Imagination, and Production

Among the four stages (i.e., pre-stimuli, perception, imagination, and production), best classification accuracy was always during production, then imagination, followed by perception. Comparing classification accuracies of all the four stages (i.e., pre-stimuli, perception, preparation/imagination, production; in pairs), irrespective of classifiers, all the results were significantly different (2-tail t-test, $p < 0.05$), except in one case, where no significant difference was observed while comparing between preparation and production stage using spectral-temporal CNN. A slightly higher p-value than the desired confidence ($p = 0.0589$) was observed. During imagination, the accuracy of average speech decoding was above 91% in both cases of feature representations (ST-CNN and SST-CNN), which indicates that the information processing in the brain occurs prior to articulation. Also, with the speech perception segment, a high level (around 87–90%) accuracy was obtained, which is not surprising. This provides further evidence in the literature that decoding speech perception from the MEG signal is viable. Theoretically, the decoding accuracy for the pre-stimuli segment should be at the chance level which is about 30% for N $=\sim$ 300 ($\sim$ 60 trials $\times$ 5 classes) (Combrisson and Jerbi, 2015) (20% is for ideal population size), as there was no stimulus or task during this stage. However, the speech decoding accuracy obtained in this stage with all the classifiers were significantly higher than the chance level (1-tail t-test, $p = 0.00013$).

5. DISCUSSION

5.1. Comparison of Decoding Approaches

Overall, we found that CNNs with spatial-spectral-temporal features performed better than CNNs using only the spectral-temporal features, and that both CNN approaches outperformed the ANN classifier. We used only a single value (RMS) feature from one sensor for the ANN classifier. Temporal information was not well represented here, which may explain the lower accuracy compared to the CNNs and indicate the usefulness of temporal information for decoding. In the current experiment, the ANN feature dimension was 1,176 which was higher than the number of samples for training (about 250 per subject across 5 phrases). A dimension reduction strategy prior to the ANN training may improve the performance. There has long been evidence regarding the role of neural oscillations in brain function (Buzsáki and Draguhn, 2004; Formisano et al., 2008), and spectral features of the brain activity signals almost certainty carry more information than the integrated energy of MEG signals. Thus, it is not surprising that we found better classification accuracy using the spectral-temporal features (scalograms) based CNN classifier compared to the ANN classifier. However, a clear interpretation of what aspects

TABLE 2 | Test confusion matrix for speech decoding accumulated across all subjects during articulation stage.

		Predicted					
		Do you understand me	**That's perfect**	**How are you**	**Good bye**	**I need help**	**Accuracy (%)**
	Do you understand me	1,332	12	19	11	8	96.38
	That's perfect	10	1,338	14	11	9	96.82
	How are you	21	8	1,331	12	10	96.31
	Good bye	12	15	12	1,337	6	96.74
True	I need help	7	12	14	7	1,342	97.11
			Average:				96.67

A total of 1,382 test trials have been taken (combined across 8 subjects).

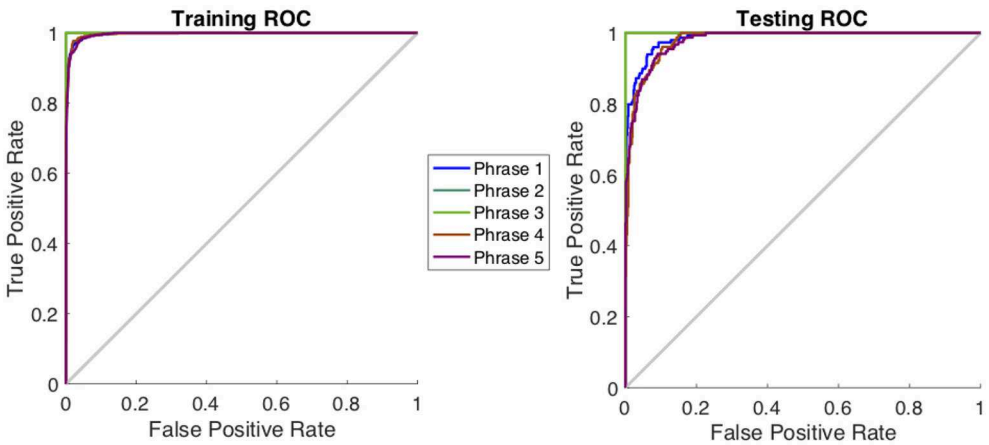

FIGURE 9 | Receiver operating characteristics curve for one subject during the classification of phrases in the articulation stage using AlexNet. The plot represents the variation between true positive rate (sensitivity) and true negative rate (1-specificity) to indicate the classification performance. For this curve average AUC >0.96 indicating a very high classification performance.

of the scalograms led to better performance is not straight forward, because of the inherent differences in the feature sets, in content and dimension. For our third approach, we added spatial information on top of spectral-temporal features by combining the scalograms of all the sensors into one image, thereby representing the neural dynamics across the whole brain. The improved results obtained with this approach (SST-CNN) indicate that CNNs were indeed able to better utilize the spatial, spectral, and temporal information from the MEG signals and for learning the appropriate feature set for the decoding tasks. The use of the scalogram images to represent the whole brain dynamics is a novel strategy to leverage the efficiency of CNNs. The same strategy can be applied while decoding with EEG or ECoG channels as well. It is possible that the data augmentation used in the SST-CNN approach might have contributed to better performance by inducing variability in the data besides increased data size for better CNN training. As mentioned previously, we did not use data augmentation for the other CNN approach (ST-CNN), because the data were sufficient for training it. We believe that using data augmentation in ST-CNN might also increase its performance. However, the training would be extremely time-consuming.

One approach may be to transform the RMS features of 1, 176 dimension to a matrix (of size $14 \times 28 \times 3$ or equivalent) and then feed to the 2D-CNNs for classification. However, there are numerous possible ways to construct such a matrix. The other way of transforming the images into vectors to be used as input to ANN is also not ideal as the feature vector dimension would be huge. Thus, here we did not intend to compare the features rather we compared the approaches used for decoding. It should be noted that this study evaluated subject-dependent classification performance, where training and testing data were from the same subjects (but unique). Hence, the features learned via CNN might be subject-specific and may not generalize across the population. Performing speaker-independent decoding is extremely challenging considering the cognitive variance across subjects. Subject normalization/adaptation based strategies are needed to be assessed to address the subject-independent decoding problem in the future (Dash et al., 2019d).

5.2. Contribution of Wavelets in Decoding

In the current study, we used discrete (DWT) and continuous (CWT) wavelet transforms as a means to both reduce the influence of noise and extract neural features from the

neuromagnetic signals. There are numerous studies showing wavelet decomposition to be an effective method for noise and artifact reduction, including those generated by muscles signals (Vialatte et al., 2008; Klados et al., 2009; Safieddine et al., 2012; Harender and Sharma, 2017). Indeed, in a previous study using a subset of the current data, we observed an increase in SNR of the neural signals after DWT (Dash et al., 2018c).

Likewise, decomposing the signal into discrete neural brainwaves may have assisted in producing robust feature representations. Comparing the current ANN decoding results—for three subjects—with an earlier pilot study (Dash et al., 2018d), we observed that wavelet decomposition accounts for an average decoding accuracy improvement of roughly 2%. While this may a be modest improvement, our ANN feature (RMS) integrates over the temporal domain effectively, removing temporal information that is well known to reflect specific functional processes (Andreou et al., 2015). Specific frequencies have been used in the past for decoding (Chi and John, 2011), so it stands to reason that the temporal information in our novel scalogram approach may have significantly contributed to decoding efficiency in the present work.

5.3. Comparisons in Decoding Imagination and Articulation

The observation that spoken information can be more efficiently retrieved directly from the brain during articulation than perception and preparation (imagination) could be because of the involvement of motor cortex (for the movement of articulators) and auditory cortex (for auditory feedback). One may argue that the articulatory (jaw) motion artifact that remained in the brain signals after denoising also contributed to the higher decoding accuracy during speech production than imagination. However, our previous study has suggested that MEG signals have more information than just jaw motion signal itself in speech decoding (Dash et al., 2018d). We found that by combining MEG and jaw motion signals, better decoding performance can be achieved than using each of them separately. Of note is that our current protocol has 1–1.5 s delay after articulation ends (before the next trial starts). However, the effect of speech processing may continue in the brain (carryover) even many seconds after the articulation ends. From the decoding perspective, however, we considered this to be a challenge since previous trials could possibly corrupt the current trial's signals at least during the pre-stimuli and possibly the perceptual phase. We interpret our results to be robust despite the possible interference, and in support of a hypothesis that it is possible to decode spoken phrases from non-invasive signals.

Another concern may be that the phrase duration information might contribute to the decoding of spoken phrases, for example, "good-bye" and "do you understand me" have considerably different lengths. While we think this is a caveat of our experimental design, there is reason to be optimistic that the main contribution is from phrase information, not just duration. As shown in **Table 2**, the decoding error (mislabeling) between "Do you understand me?" and "Good-bye" (11) was not considerably different from the mislabeling between "I need help" and "Good-bye" (7), which are of similar duration. In fact, all the mislabeling across the five phrases were similar. On the other hand, duration is an important feature for speech recognition and is commonly used in decoders for phonemes. In future studies, we plan to control the phrase duration to better understand the role of duration in phrase/phoneme decoding.

High imagined phrase decoding performance opens up the possibility of direct brain to text mapping applications for completely paralyzed patients by retrieving the intended speech from the brain without needing articulation. Although, it can be argued that, participants could have already activated vocal muscles during imagination, the inherent time-locked experimental design prevents this before the start of the articulation stage. Our experimental protocol was designed to collect both imagined and overt speech consecutively within a trial. After prompting the subject with the stimulus, only 1 s was given for the subject to imagine the pronunciation of the phrase, after which the subject articulated the phrase. This limited 1 s duration attempted to ensure the behavioral compliance of the subject to imagine only that phrase. It is extremely difficult to verify whether the subjects actually performed the task of imagination in the traditional setting of imagined speech data acquisition (Cooney et al., 2018). Hence, we collected both imagined and overt speech in a single trial with a limited duration for the imagination segment for behavioral control. In our design, 1 s may be sufficient for imagination because the average production time of the longest phrase (Do you understand me?) was 0.97 ± 0.08 s across trials, and considering that imagined speech may be faster than overt speech (Indefrey and Levelt, 2004; Oppenheim and Dell, 2008). Nevertheless, our paradigm may have a combination of both preparation and imagination within the 1 s duration. Based on the extant literature, phonological representation is shown to be activated during orthographical language processing and the preparation (pre-speech) (Cooney et al., 2018). The extent to which these phonological processes are existing in our preparation/imagination stage is not clear and would require specifically designed studies to dissociate them, if possible. Nonetheless, the high accuracy obtained during the imagined phrase segment is encouraging and provides strong support of the existence of sufficient information for fast decoding of intended speech for real-time BCI.

5.4. Toward a Next-Generation Speech-BCI

The objective of this study was to demonstrate the possibility of direct speech decoding from neural signals, which is to support the development of the next generation, more efficient, speech decoding-based BCIs. Our results have shown the feasibility to decode speech directly from MEG signals. Although we focused on a small set of stimuli (five phrases) in the early stage of this study, future studies will focus on decoding an open vocabulary set (any phrases). Another barrier for the development of a speech-BCI is that MEG is currently not suitable for this application due to its high cost, size, and immobility. Encouraging recent work on wearable, OPM-based MEG systems (Boto et al., 2018; Roberts et al., 2019; Zetter et al., 2019) has shown that it is possible to build

portable MEG machines with a significantly reduced cost and size (equivalent to the size of a helmet). This technological advance opens the possibility for utilizing OPM-based MEG as a speech-BCI to potentially restore communication for locked-in patients.

6. CONCLUSIONS

In this study, we demonstrated the possibility of decoding imagined and spoken phrase directly from non-invasive neural (MEG) signals using ANN and CNNs. We observed that speech decoding accuracy was the best during the speech production stage over other stages. However, even during the speech preparation (imagination) stage, the accuracies were very high, which suggests the feasibility for decoding intended or covert speech for the next-generation BCIs. Three state-of-the-art CNN architectures were used to provide evidence in support of the efficacy of CNNs in speech decoding over ANN. In addition, a unique representation of spatial, spectral and temporal features to represent the whole brain dynamics was found to be crucial in this neural speech decoding experiment. This study was only performed on healthy subjects. A further investigation on neural speech decoding from locked-in/ALS patients is needed to establish MEG as a potential device for the development of next generation, faster BCIs.

DATA AVAILABILITY STATEMENT

The data is currently not ready for distribution but is under the plan to be ready in the future. Codes can be obtained from the corresponding authors upon request.

ETHICS STATEMENT

The study involving human participants was reviewed and approved by The University of Texas at Dallas (IRB# 15-92), which covered the data collection at the Cook Childrenï£¡s Hospital (Fort Worth, TX) through a service, and by The University of Texas at Austin (IRB# 2015-09-0042). All participants provided their written informed consent before participating in this study.

AUTHOR CONTRIBUTIONS

DD implemented the algorithms and drafted the manuscript. PF and JW designed the experimental paradigm for data collection. DD, PF, and JW interpreted the results and performed subsequent editing.

FUNDING

This work was supported by the University of Texas System through a UT Brain grant under award number 362221 and partly by the National Institutes of Health (NIH) under award numbers R03DC013990 and R01DC016621.

ACKNOWLEDGMENTS

We thank Drs. Angel W. Hernandez-Mulero and Saleem Malik for their help on the data collection at Cook Children's Hospital, Fort Worth, TX. We also thank Dr. Ted Mau, Dr. Myungjong Kim, Dr. Mark McManis, Dr. Daragh Heitzman, Kristin Teplansky, Saara Raja, and the volunteering participants.

REFERENCES

Ackermann, H. (2008). Cerebellar contributions to speech production and speech perception: psycholinguistic and neurobiological perspectives. *Trends Neurosci.* 31, 265–272. doi: 10.1016/j.tins.2008.02.011

Ahnaou, A., Huysmans, H., Casteele, T. V. D., and Drinkenburg, W. H. I. M. (2017). Cortical high gamma network oscillations and connectivity: a translational index for antipsychotics to normalize aberrant neurophysiological activity. *Transl. Psychiatry* 7, 1–14. doi: 10.1038/s41398-017-0002-9

Akbari, H., Khalighinejad, B., Herrero, J. L., Mehta, A. D., and Mesgarani, N. (2019). Towards reconstructing intelligible speech from the human auditory cortex. *Sci. Rep.* 9:874. doi: 10.1038/s41598-018-37359-z

Andreou, L.-V., Griffiths, T. D., and Chait, M. (2015). Sensitivity to the temporal structure of rapid sound sequences—An MEG study. *NeuroImage* 110, 194–204. doi: 10.1016/j.neuroimage.2015.01.052

Angrick, M., Herff, C., Mugler, E., Tate, M. C., Slutzky, M. W., Krusienski, D. J., et al. (2019). Speech synthesis from ECoG using densely connected 3D convolutional neural networks. *J. Neural Eng.* 16:036019. doi: 10.1088/1741-2552/ab0c59

Anumanchipalli, G., Chartier, J., and F. Chang, E. (2019). Speech synthesis from neural decoding of spoken sentences. *Nature* 568, 493–498. doi: 10.1038/s41586-019-1119-1

Birbaumer, N. (2006). Brain-computer-interface research: coming of age. *Clin. Neurophysiol.* 117, 479–483. doi: 10.1016/j.clinph.2005.11.002

Boto, E., Holmes, N., Leggett, J., Roberts, G., Shah, V., Meyer, S. S., et al. (2018). Moving magnetoencephalography towards real-world applications with a wearable system. *Nature* 555, 657–661. doi: 10.1038/nature26147

Brigham, K., and Vijaya Kumar, B. V. K. (2010). "Imagined speech classification with EEG signals for silent communication: a preliminary investigation into synthetic telepathy," in *2010 4th International Conference on Bioinformatics and Biomedical Engineering* (Chengdu), 1–4.

Brumberg, J., Wright, E., Andreasen, D., Guenther, F., and Kennedy, P. (2011). Classification of intended phoneme production from chronic intracortical microelectrode recordings in speech motor cortex. *Front. Neurosci.* 5:65. doi: 10.3389/fnins.2011.00065

Brumberg, J. S., Nieto-Castanon, A., Kennedy, P. R., and Guenther, F. H. (2010). Brain-computer interfaces for speech communication. *Speech Commun.* 52, 367–379. doi: 10.1016/j.specom.2010.01.001

Buzsáki, G., and Draguhn, A. (2004). Neuronal oscillations in cortical networks. *Science* 304, 1926–1929. doi: 10.1126/science.1099745

Cao, B., Kim, M., van Santen, J., Mau, T., and Wang, J. (2017). "Integrating articulatory information in deep learning-based text-to-speech synthesis," in *Proceedings of Interspeech 2017* (Stockholm), 254–258.

Cheyne, D., and Ferrari, P. (2013). MEG studies of motor cortex gamma oscillations: evidence for a gamma "fingerprint" in the brain? *Front. Hum. Neurosci.* 7:575. doi: 10.3389/fnhum.2013.00575

Chi, X., and John, H. (2011). EEG-based discrimination of imagined speech phonemes. *Int. J. Bioelectromagn.* 13, 201–206. Available online at: http://www.ijbem.org/volume13/number4/201-206.pdf

Cireşan, D. C., Meier, U., Masci, J., Gambardella, L. M., and Schmidhuber, J. (2011). "Flexible, high performance convolutional neural networks for image classification," in *Proceedings of the Twenty-Second International Joint Conference on Artificial Intelligence - Vol. 2, IJCAI'11* (Barcelona: AAAI Press), 1237–1242.

Cohen, D., and Cuffin, B. (1983). Demonstration of useful differences between magnetoencephalogram and electroencephalogram. *Electroencephalogr. Clin. Neurophysiol.* 56, 38–51. doi: 10.1016/0013-4694(83)90005-6

Combrisson, E., and Jerbi, K. (2015). Exceeding chance level by chance: the caveat of theoretical chance levels in brain signal classification and statistical assessment of decoding accuracy. *J. Neurosci. Methods* 250, 126–136. doi: 10.1016/j.jneumeth.2015.01.010

Cooney, C., Folli, R., and Coyle, D. (2018). Neurolinguistics research advancing development of a direct-speech brain-computer interface. *iScience* 8, 103–125. doi: 10.1016/j.isci.2018.09.016

Cooney, C., Folli, R., and Coyle, D. (2019a). "Optimizing layers improves cnn generalization and transfer learning for imagined speech decoding from EEG," in *2019 IEEE International Conference on Systems, Man and Cybernetics (SMC)* (Bari), 1311–1316.

Cooney, C., Korik, A., Raffaella, F., and Coyle, D. (2019b). "Classification of imagined spoken word-pairs using convolutional neural networks," in *Proceedings of the 8th Graz Brain Computer Interface Conference 2019* (Graz: Graz University of Technology), 338–343.

Dash, D., Abrol, V., Sao, A. K., and Biswal, B. (2018a). "The model order limit: deep sparse factorization for resting brain," in *2018 IEEE 15th International Symposium on Biomedical Imaging (ISBI 2018)* (Washington, DC), 1244–1247.

Dash, D., Biswal, B., Sao, A. K., and Wang, J. (2018b). "Automatic recognition of resting state fMRI networks with dictionary learning," in *Brain Informatics*, eds S. Wang, V. Yamamoto, J. Su, Y. Yang, E. Jones, L. Iasemidis, and T. Mitchell (Cham: Springer International Publishing), 249–259.

Dash, D., Ferrari, P., Heitzman, D., and Wang, J. (2019a). "Decoding speech from single trial MEG signals using convolutional neural networks and transfer learning," in *2019 41st Annual International Conference of the IEEE Engineering in Medicine and Biology Society (EMBC)* (Berlin), 5531–5535.

Dash, D., Ferrari, P., Malik, S., Montillo, A., Maldjian, J. A., and Wang, J. (2018c). "Determining the optimal number of MEG trials: a machine learning and speech decoding perspective," in *Brain Informatics*, eds S. Wang, V. Yamamoto, J. Su, Y. Yang, E. Jones, L. Iasemidis, and T. Mitchell (Cham: Springer International Publishing), 163–172.

Dash, D., Ferrari, P., Malik, S., and Wang, J. (2018d). "Overt speech retrieval from neuromagnetic signals using wavelets and artificial neural networks," in *2018 IEEE Global Conference on Signal and Information Processing (GlobalSIP)* (Anaheim, CA), 489–493.

Dash, D., Ferrari, P., Malik, S., and Wang, J. (2019b). "Automatic speech activity recognition from MEG signals using Seq2Seq learning," in *2019 9th International IEEE/EMBS Conference on Neural Engineering (NER)* (San Francisco, CA), 340–343.

Dash, D., Ferrari, P., and Wang, J. (2019c). "Spatial and spectral fingerprint in the brain: speaker identification from single trial MEG signals," in *Proceedings of Interspeech 2019* (Graz), 1203–1207.

Dash, D., Wisler, A., Ferrari, P., and Wang, J. (2019d). "Towards a speaker independent speech-BCI using speaker adaptation," in *Proceedings Interspeech 2019* (Graz), 864–868.

Deng, S., Srinivasan, R., Lappas, T., and D'Zmura, M. (2010). EEG classification of imagined syllable rhythm using hilbert spectrum methods. *J. Neural Eng.* 7:046006. doi: 10.1088/1741-2560/7/4/046006

D'Zmura, M., Deng, S., Lappas, T., Thorpe, S., and Srinivasan, R. (2009). "Toward EEG sensing of imagined speech," in *Human-Computer Interaction. New Trends*, ed J. A. Jacko (Berlin; Heidelberg: Springer Berlin Heidelberg), 40–48.

Formisano, E., De Martino, F., Bonte, M., and Goebel, R. (2008). "Who" is saying "what"? Brain-based decoding of human voice and speech. *Science* 322, 970–973. doi: 10.1126/science.1164318

Grill-Spector, K., Henson, R., and Martin, A. (2006). Repetition and the brain: neural models of stimulus-specific effects. *Trends Cogn. Sci.* 10, 14–23. doi: 10.1016/j.tics.2005.11.006

Guenther, F. H., Brumberg, J. S., Wright, E. J., Nieto-Castanon, A., Tourville, J. A., Panko, M., et al. (2009). A wireless brain-machine interface for real-time speech synthesis. *PLoS ONE* 4:e08218. doi: 10.1371/journal.pone.0008218

Halme, H.-L., and Parkkonen, L. (2016). Comparing features for classification of MEG responses to motor imagery. *PLoS ONE* 11:168766. doi: 10.1371/journal.pone.0168766

Harender and Sharma, R. K. (2017). "EEG signal denoising based on wavelet transform," in *2017 International Conference of Electronics, Communication and Aerospace Technology (ICECA), Vol. 1* (Coimbatore, TN), 758–761.

Hasasneh, A., Kampel, N., Sripad, P., Shah, N., and Dammers, J. (2018). Deep learning approach for automatic classification of ocular and cardiac artifacts in MEG data. *J. Eng.* 2018:1350692. doi: 10.1155/2018/1350692

Hashim, N., Ali, A., and Mohd-Isa, W.-N. (2018). Word-based classification of imagined speech using EEG," in *Computational Science and Technology,* eds R. Alfred, H. Iida, A. Asri, A. Ibrahim, and Y. Lim (Kuala Lumpur: Springer), 195–204.

Haumann, N. T., Parkkonen, L., Kliuchko, M., Vuust, P., and Brattico, E. (2016). Comparing the performance of popular MEG/EEG artifact correction methods in an evoked-response study. *Intell. Neurosci.* 2016:7489108. doi: 10.1155/2016/7489108

Herff, C., Heger, D., de Pesters, A., Telaar, D., Brunner, P., Schalk, G., et al. (2015). Brain-to-text: decoding spoken phrases from phone representations in the brain. *Front. Neurosci.* 9:217. doi: 10.3389/fnins.2015.00217

Huang, Z., and Yu, T. (2019). "Cross-subject MEG decoding using 3D convolutional neural networks," in *2019 WRC Symposium on Advanced Robotics and Automation (WRC SARA)* (Beijing), 354–359.

Ikeda, S., Shibata, T., Nakano, N., Okada, R., Tsuyuguchi, N., Ikeda, K., et al. (2014). Neural decoding of single vowels during covert articulation using electrocorticography. *Front. Hum. Neurosci.* 8:125. doi: 10.3389/fnhum.2014.00125

Iljina, O., Derix, J., Schirrmeister, R. T., Schulze-Bonhage, A., Auer, P., Aertsen, A., et al. (2017). Neurolinguistic and machine-learning perspectives on direct speech BCIs for restoration of naturalistic communication. *Brain Comput. Interfaces* 4, 186–199. doi: 10.1080/2326263X.2017.1330611

Indefrey, P., and Levelt, W. (2004). The spatial and temporal signatures of word production components. *Cognition* 92, 101–144. doi: 10.1016/j.cognition.2002.06.001

Iqbal, S., Khan, Y. U., and Farooq, O. (2015). "EEG based classification of imagined vowel sounds," in *2015 2nd International Conference on Computing for Sustainable Global Development (INDIACom)* (New Delhi), 1591–1594.

Kellis, S., Miller, K., Thomson, K., Brown, R., House, P., and Greger, B. (2010). Decoding spoken words using local field potentials recorded from the cortical surface. *J. Neural Eng.* 7:056007. doi: 10.1088/1741-2560/7/5/056007

Kiernan, M. C., Vucic, S., Cheah, B. C., Turner, M. R., Eisen, A., Hardiman, O., et al. (2011). Amyotrophic lateral sclerosis. *Lancet* 377, 942–955. doi: 10.1016/S0140-6736(10)61156-7

Klados, M. A., Papadelis, C., Lithari, C. D., and Bamidis, P. D. (2009). "The removal of ocular artifacts from EEG signals: a comparison of performances for different methods," in *4th European Conference of the International Federation for Medical and Biological Engineering*, eds J. Vander Sloten, P. Verdonck, M. Nyssen, and J. Haueisen (Berlin; Heidelberg: Springer Berlin Heidelberg), 1259–1263.

Kohnen, R. F., Lavrijsen, J. C. M., Bor, J. H. J., and Koopmans, R. T. C. M. (2013). The prevalence and characteristics of patients with classic locked-in syndrome in dutch nursing homes. *J. Neurol.* 260, 1527–1534. doi: 10.1007/s00415-012-6821-y

Krizhevsky, A., Sutskever, I., and Hinton, G. E. (2017). ImageNet classification with deep convolutional neural networks. *Commun. ACM* 60, 84–90. doi: 10.1145/3065386

Leuthardt, E. C., Gaona, C. M., Sharma, M., Szrama, N. P., Roland, J. L., Freudenberg, Z., et al. (2011). Using the electrocorticographic speech network to control a brain-computer interface in humans. *J. Neural Eng.* 83:036004. doi: 10.1088/1741-2560/8/3/036004

Levelt, W. J. (1999). Models of word production. *Trends Cogn. Sci.* 3, 223–232. doi: 10.1016/S1364-6613(99)01319-4

Lilly, J. M., and Olhede, S. C. (2009). Higher-order properties of analytic wavelets. *IEEE Trans. Signal Process.* 57, 146–160. doi: 10.1109/TSP.2008.2007607

Livezey, J. A., Bouchard, K. E., and Chang, E. F. (2019). Deep learning as a tool for neural data analysis: speech classification and cross-frequency coupling in human sensorimotor cortex. *PLoS Comput. Biol.* 15:e1007091. doi: 10.1371/journal.pcbi.1007091

Martin, S. F., Brunner, P., Iturrate, I., Millán, J., Schalk, G., Knight, R. T., et al. (2016). Corrigendum: word pair classification during imagined speech using direct brain recordings. *Sci. Rep.* 7:44509. doi: 10.1038/srep44509

Memarian, N., Ferrari, P., Macdonald, M. J., Cheyne, D., Nil, L. F. D., and Pang, E. W. (2012). Cortical activity during speech and non-speech oromotor tasks: a magnetoencephalography (MEG) study. *Neurosci. Lett.* 527, 34–39. doi: 10.1016/j.neulet.2012.08.030

Moses, D., Leonard, M., Makin, J., and Chang, E. (2019). Real-time decoding of question-and-answer speech dialogue using human cortical activity. *Nat. Commun.* 10:3096. doi: 10.1038/s41467-019-10994-4

Nguyen, C. H., Karavas, G. K., and Artemiadis, P. (2017). Inferring imagined speech using EEG signals: a new approach using Riemannian manifold features. *J. Neural Eng.* 15:016002. doi: 10.1088/1741-2552/aa8235

Oppenheim, G. M., and Dell, G. S. (2008). Inner speech slips exhibit lexical bias, but not the phonemic similarity effect. *Cognition* 106, 528–537. doi: 10.1016/j.cognition.2007.02.006

Palmer, E. D., Rosen, H. J., Ojemann, J. G., Buckner, R. L., Kelley, W. M., and Petersen, S. E. (2001). An event-related fMRI study of overt and covert word stem completion. *NeuroImage* 14, 182–193. doi: 10.1006/nimg.2001.0779

Porbadnigk, A., Wester, M., Calliess, J., and Schultz, T. (2009). "EEG-based speech recognition - impact of temporal effects," in *Biosignals* eds P. Encarnação and A. Veloso (Porto: SciTePress), 376–381.

Ramsey, N., Salari, E., Aarnoutse, E., Vansteensel, M., Bleichner, M., and Freudenburg, Z. (2018). Decoding spoken phonemes from sensorimotor cortex with high-density ECoG grids. *NeuroImage* 180, 301–311. doi: 10.1016/j.neuroimage.2017.10.011

Rezazadeh Sereshkeh, A., Trott, R., Bricout, A., and Chau, T. (2017). EEG classification of covert speech using regularized neural networks. *IEEE/ACM Trans. Audio Speech Lang. Process.* 25, 2292–2300. doi: 10.1109/TASLP.2017.2758164

Roberts, G., Holmes, N., Alexander, N., Boto, E., Leggett, J., Hill, R. M., et al. (2019). Towards OPM-MEG in a virtual reality environment. *NeuroImage* 199, 408–417. doi: 10.1016/j.neuroimage.2019.06.010

Roy, Y., Banville, H., Albuquerque, I., Gramfort, A., Falk, T. H., and Faubert, J. (2019). Deep learning-based electroencephalography analysis: a systematic review. *J. Neural Eng.* 16:051001. doi: 10.1088/1741-2552/ab260c

Russakovsky, O., Deng, J., Su, H., Krause, J., Satheesh, S., Ma, S., et al. (2015). ImageNet large scale visual recognition challenge. *Int. J. Comput. Vision (IJCV)* 115, 211–252. doi: 10.1007/s11263-015-0816-y

Safieddine, D., Kachenoura, A., Albera, L., Birot, G., Karfoul, A., Pasnicu, A., et al. (2012). Removal of muscle artifact from EEG data: comparison between stochastic (ICA and CCA) and deterministic (EMD and wavelet-based) approaches. *EURASIP J. Appl. Signal Process.* 2012:127. doi: 10.1186/1687-6180-2012-127

Shorten, C., and Khoshgoftaar, T. M. (2019). A survey on image data augmentation for deep learning. *J. Big Data* 6, 1–48. doi: 10.1186/s40537-019-0197-0

Shuster, L. I., and Lemieux, S. K. (2005). An fMRI investigation of covertly and overtly produced mono- and multisyllabic words. *Brain Lang.* 93, 20–31. doi: 10.1016/j.bandl.2004.07.007

Simos, P. G., Breier, J. I., Zouridakis, G., and Papanicolaou, A. (1998). Identification of language-specific brain activity using magnetoencephalography. *J. Clin. Exp. Neuropsychol.* 20, 706–722. doi: 10.1076/jcen.20.5.706.1127

Smith, E., and Delargy, M. (2005). Locked-in syndrome. *BMJ* 330, 406–409. doi: 10.1136/bmj.330.7488.40

Szegedy, C., Ioffe, S., and Vanhoucke, V. (2016). "Inception-v4, Inception-ResNet and the impact of residual connections on learning," in *AAAI* (Phoenix, AZ), 4278–4284.

Tadel, F., Baillet, S., Mosher, J. C., Pantazis, D., and Leahy, R. M. (2011). Brainstorm: a user-friendly application for MEG/EEG analysis. *Intell. Neurosci.* 2011:8797. doi: 10.1155/2011/879716

Vialatte, F.-B., Solé-Casals, J., and Cichocki, A. (2008). EEG windowed statistical wavelet scoring for evaluation and discrimination of muscular artifacts. *Physiol. Meas.* 29, 1435–1452. doi: 10.1088/0967-3334/29/12/007

Wang, J., Kim, M., Hernandez-Mulero, A. W., Heitzman, D., and Ferrari, P. (2017). "Towards decoding speech production from single-trial magnetoencephalography (MEG) signals," in *2017 IEEE International Conference on Acoustics, Speech and Signal Processing (ICASSP)* (New Orleans, LA), 3036–3040.

Wang, Y., Wang, P., and Yu, Y. (2018). Decoding english alphabet letters using EEG phase information. *Front. Neurosci.* 12:62. doi: 10.3389/fnins.2018.00062

Wu, S., Zhong, S., and Liu, Y. (2018). Deep residual learning for image steganalysis. *Multimedia Tools Appl.* 77, 10437–10453. doi: 10.1007/s11042-017-4440-4

Yoshimura, N., Nishimoto, A., Belkacem, A. N., Shin, D., Kambara, H., Hanakawa, T., et al. (2016). Decoding of covert vowel articulation using electroencephalography cortical currents. *Front. Neurosci.* 10:175. doi: 10.3389/fnins.2016.00175

Zetter, R., Iivanainen, J., and Parkkonen, L. (2019). Optical co-registration of MRI and on-scalp MEG. *Sci. Rep.* 9:5490. doi: 10.1038/s41598-019-41763-4

Zhao, S., and Rudzicz, F. (2015). "Classifying phonological categories in imagined and articulated speech," in *2015 IEEE International Conference on Acoustics, Speech and Signal Processing (ICASSP)* (Brisbane, QLD), 992–996.

Conflict of Interest: The authors declare that the research was conducted in the absence of any commercial or financial relationships that could be construed as a potential conflict of interest.

frontiers in Neuroscience

REVIEW
published: 07 April 2020
doi: 10.3389/fnins.2020.00268

A Neuroergonomics Approach to Mental Workload, Engagement and Human Performance

Frédéric Dehais[1,2], Alex Lafont[1], Raphaëlle Roy[1] and Stephen Fairclough[3]*

[1] ISAE-SUPAERO, Université de Toulouse, Toulouse, France, [2] School of Biomedical Engineering, Science and Health Systems, Drexel University, Philadelphia, PA, United States, [3] School of Psychology, Liverpool John Moores University, Liverpool, United Kingdom

The assessment and prediction of cognitive performance is a key issue for any discipline concerned with human operators in the context of safety-critical behavior. Most of the research has focused on the measurement of mental workload but this construct remains difficult to operationalize despite decades of research on the topic. Recent advances in Neuroergonomics have expanded our understanding of neurocognitive processes across different operational domains. We provide a framework to disentangle those neural mechanisms that underpin the relationship between task demand, arousal, mental workload and human performance. This approach advocates targeting those specific mental states that precede a reduction of performance efficacy. A number of undesirable neurocognitive states (mind wandering, effort withdrawal, perseveration, inattentional phenomena) are identified and mapped within a two-dimensional conceptual space encompassing task engagement and arousal. We argue that monitoring the prefrontal cortex and its deactivation can index a generic shift from a nominal operational state to an impaired one where performance is likely to degrade. Neurophysiological, physiological and behavioral markers that specifically account for these states are identified. We then propose a typology of neuroadaptive countermeasures to mitigate these undesirable mental states.

Keywords: neuroergonomics, performance prediction, degraded attentional and executive mental states, task engagement, mental workload

OPEN ACCESS

Edited by:
Riccardo Poli,
University of Essex, United Kingdom

Reviewed by:
Ranjana K. Mehta,
Texas A&M University, United States
Ryan McKendrick,
Northrop Grumman Corporation, United States

****Correspondence:***
Frédéric Dehais
frederic.dehais@isae-suapero.fr;
frederic.dehais@isae.fr

Specialty section:
This article was submitted to Neural Technology, a section of the journal Frontiers in Neuroscience

Received: *11 December 2019*
Accepted: *10 March 2020*
Published: *07 April 2020*

Citation:
Dehais F, Lafont A, Roy R and Fairclough S (2020) A Neuroergonomics Approach to Mental Workload, Engagement and Human Performance. Front. Neurosci. 14:268. doi: 10.3389/fnins.2020.00268

INTRODUCTION

A study of mental workload is fundamental to understanding the intrinsic limitations of the human information processing system. This area of research is also crucial for investigation of complex teaming relationships especially when interaction with technology necessitates multitasking or a degree of cognitive complexity.

The Growth of Mental Workload

Mental workload has a long association with human factors research into safety-critical performance (Moray, 1979; O'Donnell and Eggemeier, 1986; Hancock and Meshkati, 1988; Hancock and Desmond, 2001; Wickens and Tsang, 2014; Young et al., 2015). Forty years have passed since the publication of the seminal collection edited by Moray (1979) and the study of mental workload remains an active topic in contemporary human factors research; a keyword

search based on Google Scholar listed more than 200,000 articles published on the topic since 2000, see also Table 1 in Young et al. (2015). The significance of human mental workload for those technological trends that are forecast during the second machine age (Brynjolfsson and McAfee, 2014) guarantees its importance for human factors research in future decades.

The lineage of mental workload incorporates a number of theoretical perspectives, some of which precede the formalization of the concept itself. Early work linking physiological activation to the prediction of performance (Yerkes and Dodson, 1908; Duffy, 1962) was formalized into an energetical model of attentional resources (Kahneman, 1973) that emphasized a dynamic relationship between finite information processing capacity and variable cognitive demands (Norman and Bobrow, 1975; Navon and Gopher, 1979; Wickens, 1980). The descriptive quality of the early work on attentional resources was sharpened by cognitive models of control (Broadbent, 1971; Schneider et al., 1984; Shallice and Burgess, 1993). Hybrid frameworks that place cognitive processes within a resource framework have been hugely influential in the field, such as the multiple resource model (Wickens, 1984, 2002, 2008; Wickens and Liu, 1988) whereas others introduced agentic features, such as dynamic self-regulation and adaptation, within models of human performance (Hockey et al., 1986; Hockey, 1997). For instance, Hancock and Warm (1989)'s dynamic adaptive theory (DAT) postulates that the brain seeks resource homeostasis and cognitive comfort. However, environmental stressors can progressively shift individual's adaptive abilities from stability to instability depending on one's cognitive and psychological resources. The DAT is an extension of the Yerkes and Dodson inverted-U law, in a sense that very low (hypostress) and very high (hyperstress) task demands can both degrade the adaptability and consequently impair performance. All these perspectives are united by a characterization of the human information processing system as a finite resource with limited capacity (Kramer and Spinks, 1991).

Mental Workload Measurement

Research into the measurement of mental workload has outstripped the development of theoretical frameworks. Measures of mental workload can be categorized as performance-based, or linked to the process of subjective self-assessment, or associated with psychophysiology or neurophysiology. Each category has specific strengths and weaknesses (O'Donnell and Eggemeier, 1986; Wierwille and Eggemeier, 1993) and the sensitivity of each measurement type can vary depending on the level of workload experienced by the operator (De Waard, 1996). The development of multidimensional measures led inevitably to an inclusive framework for mental workload. The cost of this integration is dissociation between different measures of mental workload, e.g., Yeh and Wickens (1988), and an integrated workload concept that remains poorly defined from a psychometric perspective (Matthews et al., 2015).

There are a number of reasons that explain why mental workload is easy to quantify but difficult to operationalize. The absence of a unified framework for human mental workload, its antecedents, processes and measures has generated a highly abstract concept, loosely operationalized and supported by a growing database of inconsistent findings (Van Acker et al., 2018). The absence of a general explanatory model is complicated by the fact that mental workload, like stress and fatigue (Matthews, 2002), is a transactional concept representing an interaction between the capacities of the individual and the specific demands of a particular task. Within this transactional framework, mental workload represents a confluence between inter-individual sources of trait variability (e.g., skill, IQ, personality), intra-individual variation (e.g., emotional states, motivation, fatigue), and the specific configuration of the task under investigation (see also Table 2 in Van Acker et al., 2018).

For the discipline of human factors, the study of mental workload serves two primary functions: (a) to quantify the transaction between operators and a range of task demands or technological systems or operational protocols, and (b) to predict the probability of performance impairment during operational scenarios, which may be safety-critical. One challenge facing the field is delineating a consistent relationship between mental workload measurement and performance quality on the basis of complex interactions between the person and the task. The second challenge pertains to the legacy and utility of limited capacity of resources as a framework for understanding those interactions.

In the following sections, we detail some limitations of mental resources and advocate the adoption of a neuroergonomic approach (Sarter and Sarter, 2003; Parasuraman and Rizzo, 2008; Parasuraman and Wilson, 2008; Mehta and Parasuraman, 2013; Ayaz and Dehais, 2018) for the study of mental workload and human performance. The neuroergonomic framework emphasizes a shift from limited cognitive resources to characterizing impaired human performance and associated states with respect to neurobiological mechanisms.

Toward a Limit of the Theory of Limited Resources

The concept of resources represents a foundational challenge to the development of a unified framework for mental workload and prediction of human performance. The conception of a limited capacity for information processing is an intuitive one and has been embedded within several successful models, e.g., multiple resources (Wickens, 2002). But this notion has always been problematic because resources are a general-purpose metaphor with limited explanatory powers (Navon, 1984) that incorporate both cognitive processes (e.g., attention, memory) and energetical constructs (e.g., mental effort) in ways that are difficult to delineate or operationalize. The allegorical basis of resources almost guarantees an abstract level of explanation (Van Acker et al., 2018) that is accompanied by divergent (Matthews et al., 2015), and sometimes contradictory operationalizations (Yeh and Wickens, 1988; Annett, 2002).

For example, the theory of limited cognitive resources predicts that exposure to task demands that are sustained and demanding can impair performance due to resource depletion via self-regulation mechanisms at the neuron-level (i.e., local-sleep state theory, see Van Dongen et al., 2011) or compromise access to

resources mechanisms (Borragan Pedraz and Peigneux, 2016). However, this type of explanation fails to clarify why non-challenging tasks, such as passive monitoring (Matthews et al., 2002, 2010) can promote episodes of mind wandering whereby attention drifts from task-related to task-irrelevant thoughts (Smallwood et al., 2008; Durantin et al., 2015; Smallwood and Schooler, 2015). Although some propositions, such as the theory of "malleable resources" (Young and Stanton, 2002), have intuited this paradox, this theory is at a highly descriptive level and remains difficult to operationalize.

Similarly, the occurrence of stressful and unexpected operational scenarios is known to impair executive functioning and provoke perseveration, see Dehais et al. (2019) for review. Perseveration is defined as a tendency to continue an action after cessation of the original stimulation, which is no longer relevant to the goal at hand (Sandson and Albert, 1984). For example, several studies conducted on emergency evacuation situations reported irrational and perseverative behaviors even when tasks were simple and undemanding (Proulx, 2001; Kobes et al., 2010). A paradigmatic situation is the one in which people fail to escape from fire because they push the door instead of pulling it. Perseveration can also have devastating consequences during safety-critical tasks, such as aviation (O'Hare and Smitheram, 1995; Orasanu et al., 1998; Reynal et al., 2017) and in the medical domain (Bromiley, 2008). This category of performance impairment cannot be explained solely through the prism of limited mental resources. Operators who persist with an erroneous strategy, such as an aircrew who attempt to land their craft at all costs despite bad weather conditions, are generally capable of performing the required actions and tend to invest greater effort even as their task goal becomes difficult or even impossible to achieve (Dehais et al., 2010, 2012).

The concept of limited cognitive resources could explain failures of attention such as inattentional blindness (Brand-D'Abrescia and Lavie, 2008) or deafness (Raveh and Lavie, 2015). Both categories describe an inability to detect unexpected stimuli, such as alarms from the interface (Dehais et al., 2011, 2014), and represent breakdown of selective attention due to the presence of competing demands on the human information processing system. It has been demonstrated that individuals with greater information processing capacity (i.e., higher working memory span) exhibit superior ability with respect to divided and sustained attention (Colflesh and Conway, 2007; Unsworth and Engle, 2007), and therefore, should be less susceptible to the effects of inattention during the performance of demanding tasks. However, this hypothesis is contradicted by the absence of any correlation between individual differences in processing capacity and the occurrence of inattentional blindness (Bredemeier and Simons, 2012; Beanland and Chan, 2016; Kreitz et al., 2016a) or deafness (Kreitz et al., 2016b; Dehais et al., 2019).

This research suggests that the limited resource model cannot account for critical lapses of attention and executive functioning that are observed under conditions of high mental workload. Therefore, we must go beyond the limitations of the resource concept as an explanatory model of mental workload and turn our attention to the neural underpinnings of attention and behavior (Parasuraman et al., 1999).

RESOURCES: A NEUROERGONOMIC PERSPECTIVE

The last three decades have witnessed a revolution in our understanding of neural mechanisms that are fundamental to attention and human performance. Progress in the field has been driven by the development of advanced and portable neuroimaging techniques, which permit non-invasive examination of the "brain at work." Neuroergonomics is a multidisciplinary field born from these technical innovations that is broadly defined as the study of the human brain in relation to performance at work and in everyday settings (Parasuraman and Rizzo, 2008). The goal of this field is to integrate both theories and principles from ergonomics, neuroscience and human factors in order to provide insights into the relationship between brain function and behavioral outcomes in the context of work and everyday life (Rizzo et al., 2007; Parasuraman and Rizzo, 2008; Parasuraman and Wilson, 2008; Lees et al., 2010; Ayaz and Dehais, 2018).

The Multiple Biological Substrates of Mental Resources

The incorporation of neurophysiological measures of mental workload offers a reductive pathway to the reification of resources and those neurobiological states associated with impaired performance. At a fundamental level, the functioning of neurons within the brain is a form of limited resource (Beatty, 1986), requiring oxygen and glycose to generate cellular energy in the form of adenosine triphosphate (ATP) while having a very limited capacity to store these energy substrates (Saravini, 1999). The same logic holds for ions (e.g., potassium, calcium, sodium) that play a key role in nerve impulses. It is also reasonable to consider neural networks as resources with respect to their supporting glial cells (e.g., astrocytes), which ensure the processing of information (Mandrick et al., 2016). Understanding the interactions between neurobiological resources with reference to fundamental processes in brain physiology represents a crucial approach within neuroergonomic analysis of mental workload (Parasuraman and Rizzo, 2008; Ayaz and Dehais, 2018).

Brain and Inhibitory Mechanisms

The brain must be considered to be a "noisy" organ, whereby assembly of neurons are constantly responsive to environmental stimulations, see Pandemonium architecture as an early example, such as Selfridge (1959). Inhibitory mechanisms are implemented to cancel out cerebral noise by mitigating the activation of distracting neuronal assemblies (Polich, 2007). This process may occur at a local level via lateral inhibition, whereby groups of neurons can attenuate the activity of their neighbors in order to be "better heard" (Coultrip et al., 1992). The same mechanism can also take place via top-down regulation, known as inhibitory control, wherein high-level cortical areas (e.g., prefrontal cortex) reduce task- or stimulus-irrelevant neural activities (Munakata et al., 2011). However, these inhibitory mechanisms can also curtail the capacity of the brain to consider new or alternative information, thus leading to perseveration (Dehais et al., 2019).

An appropriate metaphor is to consider a group led by an authoritarian leader who is totally engaged with one specific goal or strategy and does not listen to alternative viewpoints of other members of the group. Within this metaphor, information processing resources are present (i.e., group members) but are disregarded in the presence of an overriding directive (i.e., the leader). In other words, high mental workload leads to impaired performance, not because of limited resources *per se*, but because of those neurological mechanisms designed to prioritize a specific goal or directive.

The Non-linear Effects of Neuromodulation

The prefrontal cortex (PFC) is a brain structure often identified as the neurophysiological source of limited resources (Posner and Petersen, 1990; Parasuraman, 2003; Ramsey et al., 2004; Modi et al., 2017). The PFC serves a control function during routine cognitive operations, such as: action selection, retrieval/updating in working memory, monitoring and inhibition (Ramnani and Owen, 2004; Ridderinkhof et al., 2004). It is often activated during high levels of cognitive demand (Ayaz et al., 2012; Herff et al., 2014; Racz et al., 2017; Gateau et al., 2018; Fairclough et al., 2019) and dysfunction of this structure is known to degrade performance (Sandson and Albert, 1984; Dolcos and McCarthy, 2006). However, the PFC is complex and its function is subject to the quadratic influence of neuromodulation via the influence of noradrenaline and dopamine (Arnsten, 2009; Arnsten et al., 2012). Noradrenaline is associated with the mediation of arousal (Chrousos, 2009) whereas dopamine is involved in the processing of reward with regard to the ongoing tasks (Schultz, 2002). Both catecholamines exert an inverted-U relationship with the PFC neurons (Vijayraghavan et al., 2007; Robbins and Arnsten, 2009), a reduction of these neurochemicals will depress the firing rate of noradrenergic and dopaminergic PFC neurons (see **Figure 1**). This mechanism may explain why unstimulating and non-rewarding tasks (e.g., passive supervisory control over a sustained period) can inhibit executive functioning and induce mind wandering. Conversely, excessive levels can also have a deleterious effect by suppressing PFC neuron firing rate (Birnbaum et al., 1999). In addition to decreasing the activity of the PFC, dopamine and noradrenaline activate subcortical areas, such as basal ganglia, that trigger automated schemes and initiate automatic responses (Wickens et al., 2007). These automated behaviors have an advantage of speed compared to flexible but slower behaviors generated by the prefrontal cortex (Dolan, 2002). This neurological switch from prefrontal to subcortical areas, is presumed to derive from the early age of humanity to ensure survival (Arnsten, 2009). In modern times, it manifests itself as a process of defaulting to well-learned behaviors, which are effective for only operational situations that are simple and familiar. This is the mechanism that promotes perseveration (Dehais et al., 2019) in task scenarios that are complex and novel (Staal, 2004; Ellenbogen et al., 2006) or offer intrinsic, short-term rewards, e.g., landing at all costs after a long transatlantic flight (Causse et al., 2013). These fundamental neurological mechanisms illustrate that impaired operational performance cannot be simply explained in terms of limited resources, such as a concentration of dopamine, but must be viewed from a neuroergonomic perspective that emphasizes the complexity of interactions between brain areas that evolved over thousands of years.

Attentional Dynamics and Dominance Effects

The existence of information processing resources can also be conceptualized as functional attentional networks in the brain. Michael Posner was the first to pioneer a network approach to the operationalization of resources in the early days of neuroimaging (Posner and Tudela, 1997). His influential analysis (Posner and Petersen, 1990; Posner and Dehaene, 1994; Petersen and Posner, 2012; Posner, 2012) described how specific networks were dedicated to the particular functions of attentional regulation, e.g., alerting, orientation, focus. This conceptualization developed into the delineation of a dorsal fronto-parietal network (e.g., intraparietal cortex, superior frontal cortex) that supports focused attention on specific task-relevant stimuli and a corresponding ventral fronto-parietal network (e.g., temporo-parietal cortex, inferior frontal cortex) in the right hemisphere, which activates in a bottom-up fashion to reorientate attention to interruptive stimuli (Corbetta and Shulman, 2002; Corbetta et al., 2008). Under nominal conditions, interaction between the dorsal and the ventral pathways ensure optimal trade-off between those attentional strategies associated with exploitation and exploration. However, under conditions of high task demand or stress or fatigue, this mechanism may become biased toward dominance of the dorsal over the ventral network, leading to attentional phenomena associated with inflexibility (Todd et al., 2005; Durantin et al., 2017; Edworthy et al., 2018; Dehais et al., 2019a). A similar dynamic of bias and dominance is apparent in the relationship between the dorsal and ventral pathways and the default mode network (Andrews-Hanna et al., 2014), which is associated with mind-wandering, spontaneous thoughts and disengagement from task-related stimuli (Fox et al., 2015).

Performance Monitoring and Effort Withdrawal

The capacity of the brain to monitor performance quality and progress toward task goals is another important function of the PFC during operational performance. The posterior medial frontal cortex (pMFC) is a central hub in a wider network devoted to performance monitoring, action selection and adaptive behavior (Ullsperger et al., 2014; Ninomiya et al., 2018). The pMFC is sensitive to error and failure to achieve a task goal (Ullsperger et al., 2007); the detection of failure represents an important cue for compensatory strategies, such as increased investment of mental effort (Hockey, 1997). This network is particularly important when the level of task demand experienced by the operator is associated with a high rate of error and increased probability of failure. The model of motivational intensity (Richter et al., 2016) predicts that effort is withdrawn from task performance if success likelihood is appraised to be

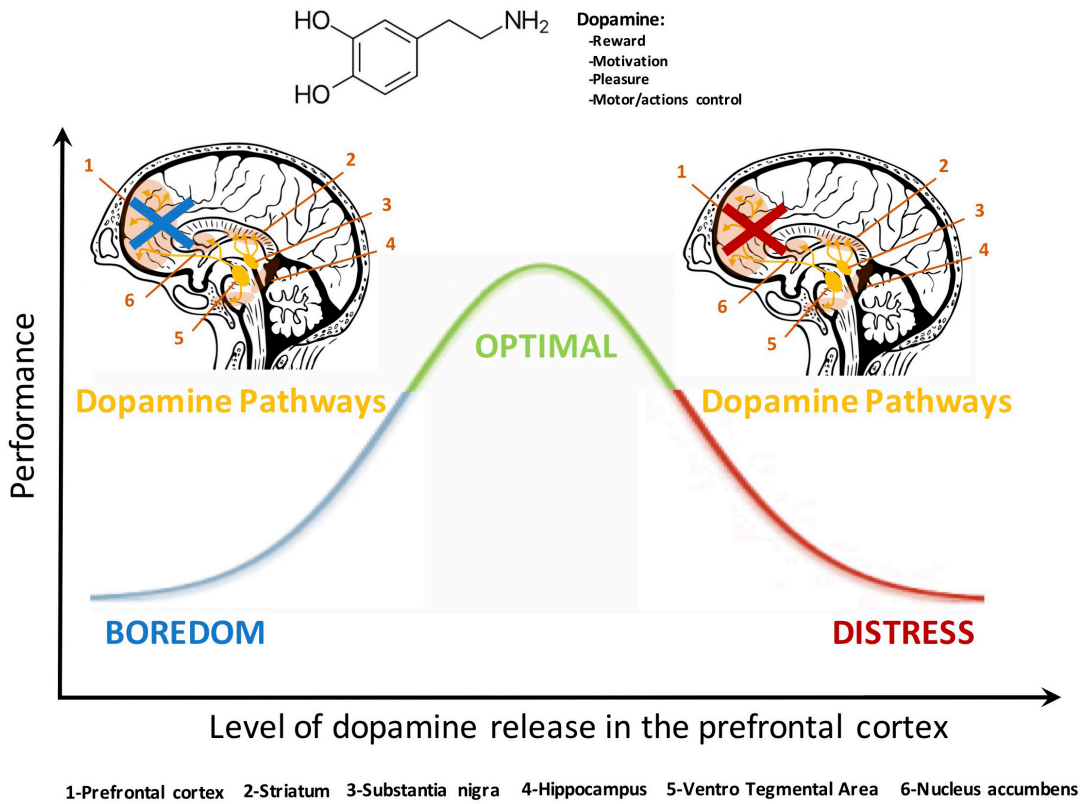

FIGURE 1 | The dopamine pathway exerts a quadratic control over the PFC. A low or a high release of this neurochemical depresses PFC activation whereas an adequate concentration ensures optimal executive functioning (Vijayraghavan et al., 2007; Robbins and Arnsten, 2009). These neurobiological considerations bring interesting highlights to understand the mechanisms underlying the Yerkes and Dodson inverted-U law and the dynamic adaptability theory (Hancock and Warm, 1989). They also provide a relevant prospect to relate motivational aspects to behavioral responses. The noradrenaline pathway mediates the PFC activity and executive functioning in a similar fashion (see Aston-Jones and Cohen, 2005).

very low (Hopstaken et al., 2015); similarly, models of behavioral self-regulation (Carver and Scheier, 2000) argue that task goals can be adjusted downward (i.e., lower levels of performance are tolerated as acceptable) or even abandoned if goal attainment is perceived to be impossible. There is evidence that increased likelihood of failure is associated with deactivation of the PFC (Durantin et al., 2014; Ewing et al., 2016; Fairclough et al., 2019), for operational performance where failure can often jeopardize the safety of oneself and others, increased likelihood of failure can also provoke strong emotional responses that are associated with stress and cognitive interference (Sarason et al., 1990), which can function as distractors from task activity in their own right (Dolcos and McCarthy, 2006; Qin et al., 2009; Gärtner et al., 2014).

This neuroergonomic approach provides a biological basis upon which to develop a concept of limited human information processing, with respect to competing neurological mechanisms, the influence of neuromodulation in the prefrontal cortex and antagonist directives between different functional networks in the brain. The prominence of inhibitory control coupled with competition between these neural networks delineate a different category of performance limitations during extremes of low vs. high mental workload, i.e., simultaneous activation of functional networks with biases toward mutually exclusive stimuli (external vs. internal) or contradictory directives (focal attention vs. reorientation of attention).

UNDERSTANDING PERFORMANCE RELATED MENTAL STATES

The previous sections have highlighted the complexity of those brain dynamics and networks that can introduce inherent limitations on human information processing. On the basis of this analysis, it is reasonable to target neurophysiological states and their associated mechanisms that account for impaired human performance (see Prinzel, 2002). This review has identified a number of suboptimal neurocognitive states that are predictive of degraded performance such as: mind wandering, effort withdrawal, perseveration, inattentional blindness and deafness. These states may be conceptually mapped along orthogonal dimensions of task engagement and arousal (**Figure 2**). Engagement is defined as an effortful investment in the service of task/cognitive goals (Pope et al., 1995; Matthews et al., 2002; Stephens et al., 2018), whereas

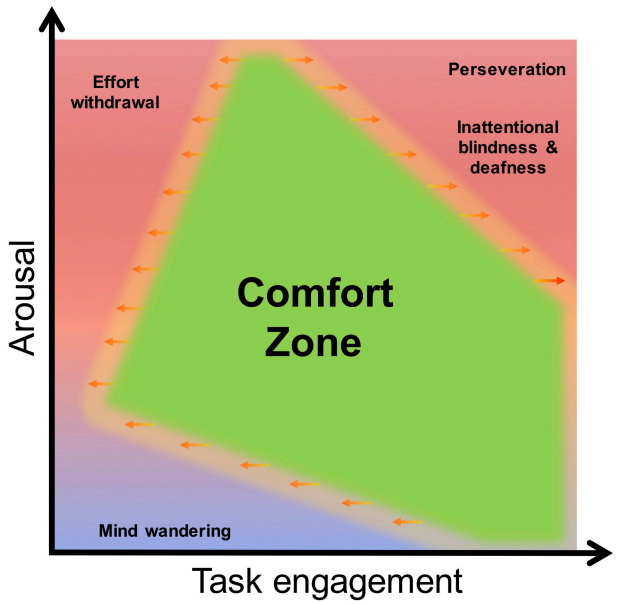

FIGURE 2 | Performance, arousal and task engagement: the green zone conceptually describes the operator's "comfort zone" where performance is optimal. The degraded mental states are mapped across a "task engagement" axis and an "arousal" axis. Interestingly, this point of view makes it possible to link the notion of engagement and degraded behavior in a simple way.

arousal represents a state of physiological readiness to respond to external contingencies (Pribram and McGuinness, 1975).

The Transactional Dimensions of Engagement and Arousal

The rationale for considering the dimension of task engagement is that performance is driven by goals and motivation (Bedny and Karwowski, 2004; Fairclough et al., 2013; Leontiev, 2014). Goal-oriented cognition theorists argue for the existence of mechanisms dedicated to maintain engagement (Atkinson and Cartwright, 1964), which are associated with an activation of an executive (Baddeley and Hitch, 1974) or task-positive network (Harrivel et al., 2013) within which the dorsolateral prefrontal cortex (DLPFC) exerts a crucial role (Goldman-Rakic, 1987; Curtis and D'Esposito, 2003). This structure plays a key role in the maintenance and updating of information that is relevant for ongoing task performance. The same structure interacts with dorsal and ventral attentional pathways to shift and focus attention to the most relevant stream of task-related information (Johnson and Zatorre, 2006). It is argued that human performance can be assessed in the context of a continuum of task engagement, ranging from disengagement (effort withdrawal, mind wandering) to high-engagement (perseveration, inattentional phenomena Lee, 2014).

Arousal makes an important contribution to the conceptual space illustrated in **Figure 2** because it modulates the homeostasis of the executive (see Arnsten, 2009 for a review) and attentional networks (see Coull, 1998 and Aston-Jones and Cohen, 2005 for review) via the dopaminergic and noradrenergic pathways. For instance, both extremes of low (Harrivel et al., 2013; Durantin et al., 2015) and high arousal can disengage the DLPFC (Goldberg et al., 1998; Arnsten, 2009; Qin et al., 2009; Causse et al., 2013; Durantin et al., 2014; Fairclough et al., 2019) and impair performance (see **Figure 3** for summary). Similarly, low (Dehais et al., 2018) and high levels of arousal (Hancock and Warm, 1989; Tracy et al., 2000; Pecher et al., 2011) can alter the interactions between the dorsal and ventral attentional networks and indistinctly that lead either to inattentional phenomena (Molloy et al., 2015; Todd et al., 2005) or effort withdrawal (Oei et al., 2012; Dehais et al., 2015).

Monitoring Performance Through Degraded Mental States

Table 1 presents a mapping between extremes of high and low engagement and arousal, their related neurocognitive states and how these states may be operationalized using neurophysiological

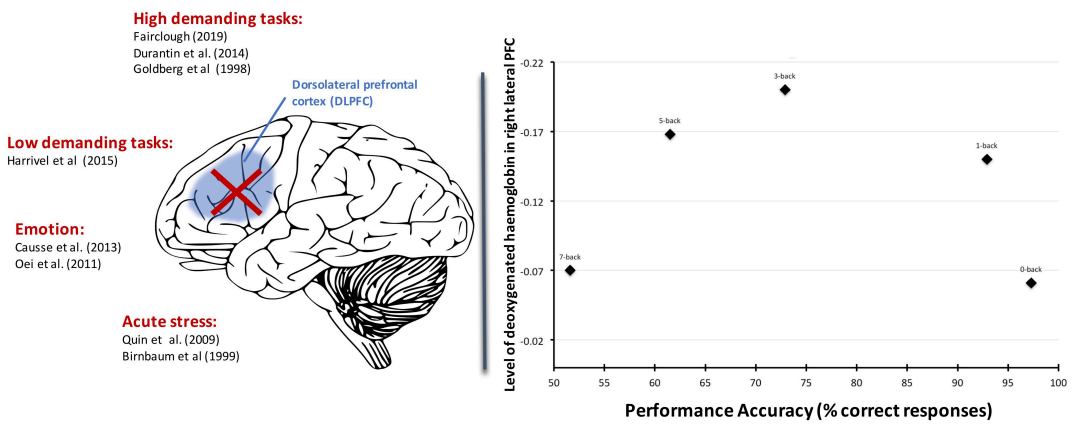

FIGURE 3 | Left part: Several types of stressors can yield to the deactivation of the DLPFC and in return drastically induce collapse of performance. Right part: An illustration with the N-Back task: the right-DLPFC deactivates when the task demands exceed mental capacity (7-Back condition) and is associated with reduced performance efficacy and effort withdrawal (from Fairclough et al., 2019).

measures in the laboratory and the field. Monitoring the activation and deactivation of the DLPFC represents a promising generic avenue to predict impaired performance across diverse states such as: mind wandering (Christoff et al., 2009; Harrivel et al., 2013), effort withdrawal (Ayaz et al., 2007; Izzetoglu et al., 2007; Durantin et al., 2014; Modi et al., 2018; Fairclough et al., 2018, 2019) and perseveration (Dehais et al., 2019). However, other neurological networks and sites should be considered as part of this analysis. Mind wandering is characterized by the concomitant activation of the default network, which includes the median prefrontal cortex (Christoff et al., 2009; Harrivel et al., 2013) and areas of the parietal cortex (Christoff et al., 2009).

Secondly, attentional states, such as inattentional deafness and blindness, result from the activation of an attentional network involving the inferior frontal gyrus, the insula and the superior medial frontal cortex (Tombu et al., 2011; Callan et al., 2018; Dehais et al., 2019). These regions represent potential candidates upon which to identify attentional failures that can be complemented by monitoring dedicated primary perceptual (see Hutchinson, 2019, for a review) and integrative cortices (Molloy et al., 2015), as well as performing connectivity analyses (Callan et al., 2018). In addition, inattentional phenomena may result from the suppression of activity in the right temporo-parietal junction (TPJ), a part of the ventral network, which also blocks reorientation of attention and the processing of unexpected stimuli (Marois et al., 2004; Todd et al., 2005).

Thirdly, measures of arousal are used to characterize high engagement and delineate distinct mental states within the category of low task engagement (**Figure 2**). Heart rate (HR) and heart rate variability (HRV) can be used to assess the activation or co-activation of the two branches of the autonomous nervous system (i.e., sympathetic or parasympathetic) (Fairclough, 2008; Qin et al., 2009; Kreibig, 2010). For instance, fluctuations in HR are commonly observed during high task engagement and high arousal (De Rivecourt et al., 2008; Qin et al., 2009; Dehais et al., 2011). Moreover, spectral analyses computed over the EEG signal revealed that shifts in parietal alpha [8–12] Hz and frontal theta [4–8] Hz are relevant markers of arousal (see Borghini et al., 2014, for a review, Senoussi et al., 2017).

Finally, behavioral metrics such as ocular behavior can complement the detection of low and high levels of engagement (**Table 1**). Hence, eye tracking metrics (e.g., fixation and dwell times, saccadic activity, blink rate) can be used to characterize mind wandering (He et al., 2011; Pepin et al., 2016), inattentional blindness (Thomas and Wickens, 2004; Wickens, 2005), perseveration (Régis et al., 2014), focal vs. diffused attention (Goldberg and Kotval, 1999; Regis et al., 2012; Dehais et al., 2015), and to characterize the level of attentional engagement in a visual task (Cowen et al., 2002; Tsai et al., 2007).

These metrics provide some relevant prospects to identify the targeted deleterious mental states for especially for field studies as long as portable devices are concerned. It is worth noting that the extraction of several features (e.g., time and frequency domains) and the use of several devices is a way for robust diagnosis. Moreover, contextual information (e.g., time of the day, time on task) should be considered as well as actions on the user interface and system parameters (e.g., flight parameters) if available so as to better quantify the user's mental state.

SOLUTIONS TO MITIGATE DEGRADED PERFORMANCE

This review has identified some undesired mental states that account for degraded performance (see section "Understanding Performance Related Mental States" and "Solutions to Mitigate Degraded Performance"). A crucial step is to design cognitive countermeasures to prevent the occurrence of these phenomena. The formal framework that we proposed (see **Table 1**) paves the way to design neuro-adaptive technology for augmented cognition and enhanced human-machine teaming (Peysakhovich et al., 2018; Krol et al., 2019; Stamp et al., 2019). The implementation of such neuro-adaptive technology relies on a pipeline that consists of a signal acquisition step, a preprocessing step to improve the signal-to-noise ratio, a feature extraction step, a classification step to diagnose the current mental states, and lastly an adaptation step (Zander and Kothe, 2011; Roy and Frey, 2016). This last step implies the implementation of formal decisional unit (Gateau et al., 2018) that dynamically close the loop by triggering the most appropriate cognitive countermeasures (May and Baldwin, 2009). There are currently three types of mitigating solutions to instigate a change in behaviors via: (1) adaptation of the user interface, (2) adaptation of the task and of the level automation, and the (3) "neuro-adaptation" of the end-users.

Adaptation of the User Interface

The first category of neuroadaptive countermeasure consists of triggering new types of notifications via the user interface to alert of impeding hazards. The design of these countermeasures is generally grounded on neuroergonomics basis so that these warning can reach awareness when other means have failed. Following this perspective, Dehais et al. (2010, 2012), Imbert et al. (2014) and Saint Lot et al. (2020) have demonstrated that very brief (∼200 *ms*) and located information removal was an efficient mean to mitigate perseveration by forcing disengagement from non-relevant tasks. Souza et al. (2016) demonstrated that digital nudging (see Weinmann et al., 2016) could be used to mitigate poor decision making and cognitive bias associated with perseveration. Imbert et al. (2014) designed attention-grabbing stimuli grounded on vision research and demonstrated that yellow chevrons pulsing at a cycle of 1 Hz can re-orientate attention and mitigate inattentional blindness. Jahanpour et al. (2018) has explored the design of pop-up videos that display the gestures to be performed by exploiting the property of mirror neurons. This visual "motor cue" approach was tested and drastically reduced reaction time to alerts during complex situations and appears to be a promising method to prevent effort withdrawal (Causse et al., 2012). In a similar fashion, Navarro et al. (2010) implemented a force-feedback steering wheel to prime the motor response from the driver. This device was found to optimize drivers' behavior during demanding driving scenario. This latter study demonstrated

TABLE 1 | Psycho-physiological and behavioral markers of different mental states related to engagement.

	Disengagement		Over-Engagement		
	Mind wandering	**Effort withdrawal**	**Perseveration**	**Inattentional blindness**	**Inattentional deafness**
Brain activity					
MEG				↘ N400 (area V3) (Scholte et al., 2006)	↘ N100 in STG and STS (Molloy et al., 2015)
*f*MRI	↗ MPFC and PCC (Mason et al., 2007; Christoff et al., 2009; Fox et al., 2015) ↗ PTPC (Christoff et al., 2009) ↗ dorsal ACC and DLPFC (Christoff et al., 2009) ↗ RPFC, DACC, insula, TPC, SSC & LG (Fox et al., 2015) ↗ MTL (Fox et al., 2015)	↘ DLPFC (Birnbaum et al., 1999; Qin et al., 2009), ↗ IFG and amygdala (Oei et al., 2012)	↘ DLPFC (Nagahama et al., 2005; Causse et al., 2013) ↘ ACC (Lie et al., 2006; Causse et al., 2013) ↘ bilateral temporo-parietal junction (Lie et al., 2006)	↘ fronto-parietal network (including DLPFC) (Beck et al., 2001; Pessoa and Ungerleider, 2004) temporo-parietal junction (Marois et al., 2004; Todd et al., 2005) ↗ activation of DMN (Weissman et al., 2006)	↗ IFG and SMFC, ↘ IFG-STG connectivity (Durantin et al., 2017)
*f*NIRS	↗ MPFC (Harrivel et al., 2013; Durantin et al., 2015) ↘ DLPFC (Harrivel et al., 2013)	↘ DLPFC (Durantin et al., 2014; Fairclough et al., 2019)	↘ Left PFC (Kalia et al., 2018)	↘ occipital lobe (Kojima and Suzuki, 2010)	
EEG	↗ α power over occipital sites (Gouraud et al., 2018) ↘ (α and (β power (auditory stimuli) (Braboszcz and Delorme, 2011) ↗ (θ power (auditory stimuli) (Braboszcz and Delorme, 2011) ↘ N1 (Kam et al., 2011) ↘ N4 (O'Connell et al., 2009) ↘ P1 (Kam et al., 2011) ↗ P2 (Braboszcz and Delorme, 2011) ↘ P3 (Schooler et al., 2011)	↘frontal θ power (Gärtner et al., 2014) ↘ P3 (Dierolf et al., 2017) ↘ frontal (θ power and ↘ parietal (α power (Ewing et al., 2016; Fairclough and Ewing, 2017)	↘ Event Related Coherence between midfrontal and right-frontal electrodes (Carrillo-De-La-Pena and García-Larrea, 2007)	↗ (α band power (Mathewson et al., 2009) ↘ P1 (Pourtois et al., 2006; Mathewson et al., 2009) ↘ P2 (Mathewson et al., 2009) ↗ N170 (Pourtois et al., 2006) ↘ P3 (Pourtois et al., 2006; Mathewson et al., 2009)	↘ N1 (Callan et al., 2018; Dehais et al., 2019a,b) ↘ P3 (Puschmann et al., 2013; Scannella et al., 2013; Giraudet et al., 2015b; Dehais et al., 2019a,b) ↘ (α power in IFG (Dehais et al., 2019a) ↘ phase synchony in (α and (θ frequencies (Callan et al., 2018) ↗ engagement ratio (Dehais et al., 2017)
ANS activity					
ECG	↗ heart rate variability (Smith, 1981) ↗ heart rate (Smith, 1981)	↘minimum LF/HF ratio (Durantin et al., 2014) ↘ minimum pre-ejection period (Mallat et al., 2019)	↗ heart rate (Dehais et al., 2011)		↗ heart rate (Dehais et al., 2014)
Skin conductance	↘ skin conductance (Smith, 1981)				
Ocular activity					
Eye-tracking	↗ number of blinks (Uzzaman and Joordens, 2011) ↘ pupil diameter (Grandchamp et al., 2014) ↗ gaze fixity (He et al., 2011; Pepin et al., 2016)	↗ maximum pupil diameter (Peavler, 1974) ↗ explore/exploit ratio (Dehais et al., 2015)	↘ switching rate between areas of interest (Régis et al., 2014) ↗ fixation duration on irrelevant areas of interest (Régis et al., 2014)	↘ saccades ↗ fixation duration (Cowen et al., 2002; Tsai et al., 2007; Regis et al., 2012) ↘ fixated areas of interest (Thomas and Wickens, 2004)	↘ pupil diameter (Causse et al., 2016)

The blue and pink color-code respectively tags states induced by low and high task demand. RIFG, right inferior frontal gyrus; DMN, default mode network, MFG, middle frontal gyrus; ACC, anterior cingulate cortex; LFC, lateral frontal cortex; STC, superior temporal cortex; PFC, prefrontal cortex; PCC, posterior cingulate cortex; MPFC, medial prefrontal cortex; PTPC, posterior temporoparietal cortex; DLPFC, dorsolateral prefrontal cortex; RPFC, rostrolateral prefrontal cortex; DACC, dorsal anterior cingulate cortex; TPC, temporopolar cortex; SSC, secondary somatosensory cortex; LG, lingual gyrus; MTL, medial temporal lobe; SMFC, superior medial frontal cortex; IFG, inferior frontal gyrus; STS, superior temporal sulcus, STG, superior temporal gyrus.

how tactile notifications can alert human operators of impeding hazards (Lewis et al., 2014; Russell et al., 2016), especially when other sensory channels of information (e.g., visual stream) are saturated (Elliott et al., 2011). However, there are potential limits to the effectiveness of these types of notifications and stimulation (Murphy and Dalton, 2016; Riggs and Sarter, 2019).

Other research indicates that multimodal alerts (Giraudet et al., 2015a; Gaspar et al., 2017) increase the likelihood of attentional capture. In addition, Lee et al. (2018) designed a motion seat that modifies the driver's seat position and posture across time to diminish the potential deleterious effect of mind wandering. Similar concepts have been applied to aviation (Zaneboni and Saint-Jalmes, 2016).

Task and Automation Adaptation

The second category of neuroadaptive countermeasure is the dynamic reallocation of tasks between humans and automation to maintain the performance efficacy of the operators (Freeman et al., 1999; Parasuraman et al., 1999; Prinzel et al., 2000; Scerbo, 2008; Stephens et al., 2018). The underlying concept in this case is to optimize human-human or human(s)-system(s) cooperation according to criteria of availability and skills of human and artificial agents (Gateau et al., 2016). For instance, Prinzel et al. (2000) utilized the continuous monitoring of brain waves that could be used to drive the level of automation and optimize the user's level of task engagement. Similarly, some authors managed to optimize air traffic controllers' task demand by triggering different levels of assistance (Aricò et al., 2016; Di Flumeri et al., 2019). These latter studies reported better human performance when neuro-adaptive automation was switched on compared to other conditions. Gateau et al. (2016) implemented an online attentional state estimator coupled with a stochastic decision framework to dynamically adapt authority sharing between human and robots in a search and rescue scenario to prevent effort withdrawal on the part of the human. In a more extreme fashion, Callan et al. (2016) revealed that it is possible to decode user motor intention so automation can perform on behalf of the user to drastically reduce the response time in emergency situations (e.g., collision with terrain). In the future, it is assumed that aircraft designers will implement adaptive automation technology that takes over from the pilots by either inhibiting their inputs on the flight deck or performing automated evasive actions (e.g., automatic pull-up) to prevent from perseveration. A complementary approach is to modulate task difficulty to maintain the task challenging but achievable while preventing the occurrence of task withdrawal (Ewing et al., 2016) or mind wandering (Freeman et al., 2004; Ewing et al., 2016). The online modulation of the tasks does not necessarily reduce the difficulty of the task. For instance, Verwey and colleagues demonstrated that the addition of an entertaining task while driving improved the operator's ability to maintain their level of task engagement over long period of time (Verwey and Zaidel, 1999). Similarly, it has been suggested that switching the types of tasks presented to the user can prevent the deleterious effect of fatigue and disengagement (Hockey, 2011).

Neuro-Adaptation of the End-User(s)

The third and final category aims to warn the users of their mental state and "stimulate" neurological activity in order to augment performance. One of the most promising approach relies on the implementation of Neurofeedback (see Gruzelier, 2014; Enriquez-Geppert et al., 2017 for reviews). The principle of the latter technique is to provide feedback in real-time to the users of their mental states in the form of a visual, tactile or auditory stimulus. The users can utilize these signals learn to regulate their brain activity and in return improve their executive (Enriquez-Geppert et al., 2013), mental flexibility (Enriquez-Geppert et al., 2014), and attentional abilities (Egner and Gruzelier, 2001) as well as enhance their task engagement (Egner and Gruzelier, 2004). However, the effects of this approach on mind wandering remain unclear (Gonçalves et al., 2018). Transcranial direct current stimulation (tDCS) represents a technique of neuromodulation that can be used to boost executive functioning (see Callan and Perrey, 2019; Cinel et al., 2019). This portable device can be combined with EEG and fNIRS and used in the context of real-life task performance for the purpose of on-line neuromodulation (McKendrick et al., 2015; Gateau et al., 2018). For example, a number of studies support the position that neurostimulation can: enhance mental flexibility and mitigate perseveration (Leite et al., 2011; Jeon and Han, 2012), improve visual attention (Falcone et al., 2012; Nelson et al., 2015), improve executive functioning in multitasking situations (Nelson et al., 2016) and increase alertness (McIntire et al., 2014; Nelson et al., 2014). There are other types of environmental stimulation such as vivid light exposure, especially during night flights, which can promote an optimal level of alertness (see Anund et al., 2015) without altering flight crew performance (see Caldwell et al., 2009). Promising results have also been highlighted by using light exposure in cars (Taillard et al., 2012). The use of light exposure and tDCS should be considered with caution as there is a need to investigate the very long-term efficiency and potential side effects. Alternatively, some authors proposed to use cold-air jet to decrease hypovigilance (Reyner and Horne, 1998), but with contradictory findings.

Synthesis of Neuro-Adaptive Solutions

The following illustration (see **Figure 4**) depicts the three families of neuro-adaptive based solutions to mitigate performance impairment.

The three types of neuroadaptive solutions offer promising prospects to mitigate the onset and likelihood of undesirable neurocognitive states. However, they should be delivered in a transparent, meaningful, and timely manner (i.e., when needed) so they are relevant and understood (Dorneich et al., 2016; Sebok et al., 2017), otherwise these types of intervention have the potential for undesirable consequences, such as performance impairment and reduced trust in technology; this point is particularly true for adaptive automation solutions that take over from humans, especially under critical scenarios (see Dorneich et al., 2016; Dehais et al., 2019). One solution is to combine different families of neuroadaptive cognitive countermeasures to maximize their efficiency. Ideally, we would argue to use a gradient of solutions such as (1) the continuous display of the users' mental states via neurofeedback techniques to give them the opportunity to regulate their brain activity; (2) using notifications to suggest to the users to delegate some tasks to automation in case they don't manage to modulate their mental states; (3) adapting the user interface (e.g., information

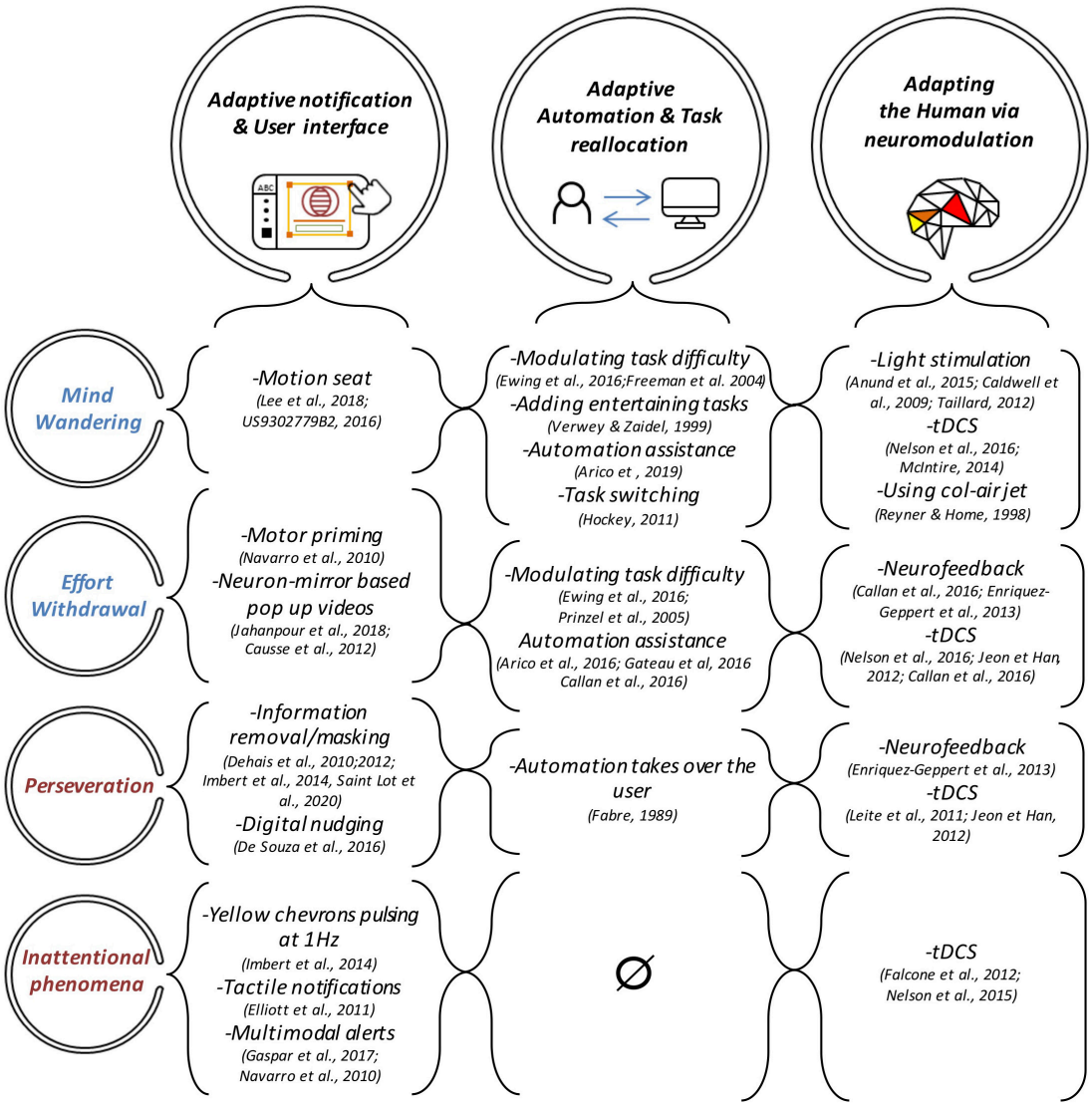

FIGURE 4 | The three types of Neuroadaptive countermeasures dedicated to mitigate the undesirable mental states. Inattentional deafness and Inattentional blindness mental states were merged into "Inattentional phenomena" as no neuroadaptive countermeasure were implemented to explicitly address failure of auditory attention to the exception of multimodal alerts. Moreover, no adaptive automation-based solutions were designed to prevent from inattentional states. This demonstrates the need to conduct more research in this direction.

removal, flashing yellow chevrons) in case of a critical situation is detected and the previous solutions were inefficient; and (4) taking over if the users do not respond to any of the previous countermeasures.

CONCLUSION

This paper has argued that the concept of a limited resource provides a limited explanation for the breakdown of operational performance. Our neurophysiological analysis describes a number of additional mechanisms, such as perseveration and effort withdrawal, which do not represent finite resources *per se*. In both cases, explanations for performance breakdown are based upon neurological processes, such as dominance of specific neural networks or the heightened activity of specific mechanisms. We propose a two-dimensional framework of engagement and arousal that captures the importance of specific degraded mental sates associated with poor performance. The rationale for including the transactional concept of engagement in this scheme is to account for the goal-oriented aspect of cognition. The benefit of including the transactional concept of arousal is to make a distinction between two categories of disengagement, one that is accompanied by high arousal (effort withdrawal) and low arousal (mind wandering) – and to link this conceptual distinction to known neurophysiological effects (see **Figure 1**). Nonetheless, this approach remains at the conceptual level and minimizes connections to the complexity of brain

functioning. To that end, we reviewed and identified several markers at the neurophysiological, physiological and behavioral level of undesirable mental states linked to poor performance.

This neuroergonomic framework encompasses operationalizations of these undesirable states that can be monitored continuously in an objective fashion. Such considerations eventually lead to propose a typology of neuroadaptive countermeasures and open promising perspectives to mitigate the degradation of human performance. However, to the authors' very best knowledge, most of the neuroadaptive experimental studies have focused on human-machine dyad situations. We believe that recent research on hyperscanning (Babiloni and Astolfi, 2014), physiological synchrony (Palumbo et al., 2017) and collaborative BCIs (Cinel et al., 2019) have opened promising prospects to improve teaming such as human-human, human(s)-machine(s) interactions. Future research should involve more complex teaming scenarios and enrich the different neuroadaptive solutions. We sincerely hope that this review will encourage research efforts to identify additional degraded mental states and associated neurophysiological markers as well as to implement neuroadaptive solutions for safer and efficient human-human and human(s)-machine(s) interactions.

AUTHOR CONTRIBUTIONS

All authors have made a substantial and intellectual contribution to this review.

FUNDING

This work was supported by ANITI ANR-19-PI3A-0004 (Neuroadaptive technology for mixed initiative interactions Chair).

REFERENCES

Andrews-Hanna, J. R., Smallwood, J., and Spreng, R. N. (2014). The default network and self-generated thought: component processes, dynamic control, and clinical relevance. *Ann. N. Y. Acad. Sci.* 1316:29. doi: 10.1111/nyas.12360

Annett, J. (2002). Subjective rating scales: science or art? *Ergonomics* 45, 966–987. doi: 10.1080/00140130210166951

Anund, A., Fors, C., Kecklund, G., Leeuwen, W. V., and Åkerstedt, T. (2015). *Countermeasures for Fatigue in Transportation: A Review of Existing Methods for Drivers on Road, Rail, Sea And In Aviation*. Linköping: Statens vägoch transportforskningsinstitut.

Aricò, P., Borghini, G., Di Flumeri, G., Colosimo, A., Bonelli, S., Golfetti, A., et al. (2016). Adaptive automation triggered by EEG-based mental workload index: a passive brain-computer interface application in realistic air traffic control environment. *Front. Hum. Neurosci.* 10:539. doi: 10.3389/fnhum.2016.00539

Arnsten, A. F. (2009). Stress signalling pathways that impair prefrontal cortex structure and function. *Nat. Rev. Neurosci.* 10:410. doi: 10.1038/nrn2648

Arnsten, A. F., Wang, M. J., and Paspalas, C. D. (2012). Neuromodulation of thought: flexibilities and vulnerabilities in prefrontal cortical network synapses. *Neuron* 76, 223–239. doi: 10.1016/j.neuron.2012.08.038

Aston-Jones, G., and Cohen, J. D. (2005). An integrative theory of locus coeruleus-norepinephrine function: adaptive gain and optimal performance. *Annu. Rev. Neurosci.* 28, 403–450. doi: 10.1146/annurev.neuro.28.061604.135709

Atkinson, J. W., and Cartwright, D. (1964). Some neglected variables in contemporary conceptions of decision and performance. *Psychol. Rep.* 14, 575–590. doi: 10.2466/pr0.1964.14.2.575

Ayaz, H., and Dehais, F. (eds) (2018). *Neuroergonomics: The Brain at Work and in Everyday Life*. Cambridge, MA: Academic Press.

Ayaz, H., Izzetoglu, M., Bunce, S., Heiman-Patterson, T., and Onaral, B. (2007). "Detecting cognitive activity related hemodynamic signal for brain computer interface using functional near infrared spectroscopy," in *Proceedins of the 3rd International IEEE EMBS conference: CNE'07*, Hawaii, 342–345.

Ayaz, H., Shewokis, P. A., Bunce, S., Izzetoglu, K., Willems, B., and Onaral, B. (2012). Optical brain monitoring for operator training and mental workload assessment. *Neuroimage* 59, 36–47. doi: 10.1016/j.neuroimage.2011.06.023

Babiloni, F., and Astolfi, L. (2014). Social neuroscience and hyperscanning techniques: past, present and future. *Neurosci. Biobehav. Rev.* 44, 76–93. doi: 10.1016/j.neubiorev.2012.07.006

Baddeley, A. D., and Hitch, G. (1974). "Working memory," in *The Psychology of Learning and Motivation: Advances in Research and Theory*, Vol. 8, eds G. H. Bower (New York, NY: Academic Press), 47–89. doi: 10.1016/S0079-7421(08)60452-1

Beanland, V., and Chan, E. H. C. (2016). The relationship between sustained inattentional blindness and working memory capacity. *Attent. Percept. Psychophys.* 78, 808–817. doi: 10.3758/s13414-015-1027-x

Beatty, J. (1986). "Computation, control and energetics: a biological perspective," in *Energetics and Human Information Processing*, ed. G. R. J. Hockey (Dordrecht: Springer).

Beck, D. M., Rees, G., Frith, C. D., and et Lavie, N. (2001). Neural correlates of change detection and change blindness. *Nat. Neurosci.* 4, 645–650. doi: 10.1038/88477

Bedny, G. Z., and Karwowski, W. (2004). Activity theory as a basis for the study of work. *Ergonomics* 47, 134–153. doi: 10.1080/00140130310001617921

Birnbaum, S., Gobeske, K. T., Auerbach, J., Taylor, J. R., and Arnsten, A. F. (1999). A role for norepinephrine in stress-induced cognitive deficits: α-1-adrenoceptor mediation in the prefrontal cortex. *Biol. Psychiatry* 46, 1266–1274. doi: 10.1016/s0006-3223(99)00138-9

Borghini, G., Astolfi, L., Vecchiato, G., Mattia, D., and Babiloni, F. (2014). Measuring neurophysiological signals in aircraft pilots and car drivers for the assessment of mental work- load, fatigue and drowsiness. *Neurosci. Biobehav. Rev.* 44, 58–75. doi: 10.1016/j.neubiorev.2012.10.003

Borragan Pedraz, G., and Peigneux, P. (2016). *Behavioural Bases and Functional Dynamics of Cognitive Fatigue,* Doctorat. Sciences psychologiques et de l'éducation, Louvain.

Braboszcz, C., and Delorme, A. (2011). Lost in thoughts: neural markers of low alertness during mind wandering. *Neuroimage* 54, 3040–3047. doi: 10.1016/j.neuroimage.2010.10.008

Brand-D'Abrescia, M., and Lavie, N. (2008). Task coordination between and within sensory modalities: effects on distraction. *Percept. Psychophys.* 70, 508–515. doi: 10.3758/pp.70.3.508

Bredemeier, K., and Simons, D. J. (2012). Working memory and inattentional blindness. *Psychon. Bull. Rev.* 19, 239–244. doi: 10.3758/s13423-011-0204-8

Broadbent, D. E. (1971). *Decision and Stress*. Oxford: Academic Press.

Bromiley, M. (2008). Have you ever made a mistake? *RCoA Bull.* 48, 2442–2445.

Brynjolfsson, E., and McAfee, A. (2014). *The Second Machine Age: Work, Progress, and Prosperity in a Time of Brilliant Technologies*, 1st Edn. New York, NY: W. W. Norton & Company.

Caldwell, J. A., Mallis, M. M., Caldwell, J. L., Paul, M. A., Miller, J. C., and Neri, D. F. (2009). Fatigue countermeasures in aviation. *Aviat. Space Environ. Med.* 80, 29–59. doi: 10.3357/asem.2435.2009

Callan, D., and Perrey, S. (2019). "The use of tDCS and rTMS methods in neuroergonomics," in *Neuroergonomics*, eds H. Ayaz and F. Dehais (Cambridge, MA: Academic Press), 31–33. doi: 10.1016/b978-0-12-811926-6.00005-1

Callan, D. E., Gateau, T., Durantin, G., Gonthier, N., and De-Hais, F. (2018). Disruption in neural phase synchrony is related to identification of inattentional

deafness in real-world setting. *Hum. Brain Mapp.* 39, 2596–2608. doi: 10.1002/hbm.24026

Callan, D. E., Terzibas, C., Cassel, D. B., Sato, M. A., and Parasuraman, R. (2016). The brain is faster than the hand in split-second intentions to respond to an impending hazard: a simulation of neuroadaptive automation to speed recovery to perturbation in flight attitude. *Front. Hum. Neurosci.* 10:187. doi: 10.3389/fnhum.2016.00187

Carrillo-De-La-Pena, M. T., and García-Larrea, L. (2007). Right frontal event related EEG coherence (ERCoh) differentiates good from bad performers of the Wisconsin Card Sorting Test (WCST). *Clin. Neurophysiol.* 37, 63–75. doi: 10.1016/j.neucli.2007.02.002

Carver, C. S., and Scheier, M. F. (2000). "On the structure of behavioural self-regulation," in *Handbook of Self-Regulation*, eds M. Boekaerts, P. R. Pintrich, and M. Zeidner (San Diego, CA: Academic Press), 41–84. doi: 10.1016/b978-012109890-2/50032-9

Causse, M., Imbert, J. P., Giraudet, L., Jouffrais, C., and Tremblay, S. (2016). The role of cognitive and perceptual loads in inattentional deafness. *Front. Hum. Neurosci.* 10:344. doi: 10.3389/fnhum.2016.00344

Causse, M., Péran, P., Dehais, F., Caravasso, C. F., Zeffiro, T., Sabatini, U., et al. (2013). Affective decision making under uncertainty during a plausible aviation task: an fMRI study. *NeuroImage* 71, 19–29. doi: 10.1016/j.neuroimage.2012.12.060

Causse, M., Phan, J., Ségonzac, T., and Dehais, F. (2012). Mirror neuron based alerts for control flight into terrain avoidance. *Adv. Cognit. Eng. Neuroergon.* 16, 157–166.

Christoff, K., Gordon, A. M., Smallwood, J., Smith, R., and Schooler, J. W. (2009). Experience sampling during fmri reveals default network and executive system contributions to mind wandering. *Proc. Natl. Acad. Sci. U.S.A.* 106, 8719–8724. doi: 10.1073/pnas.0900234106

Chrousos, G. P. (2009). Stress and disorders of the stress system. *Nat. Rev. Endocrinol.* 5:374. doi: 10.1038/nrendo.2009.106

Cinel, C., Valeriani, D., and Poli, R. (2019). Neurotechnologies for human cognitive augmentation: current state of the art and future prospects. *Front. Hum. Neurosci.* 13:13. doi: 10.3389/fnhum.2019.00013

Colflesh, G. J., and Conway, A. R. (2007). Individual differences in working memory capacity and divided attention in dichotic listening. *Psychon. Bull. Rev.* 14, 699–703. doi: 10.3758/bf03196824

Corbetta, M., Patel, G., and Shulman, G. L. (2008). The reorienting system of the human brain: from environment to theory of mind. *Neuron* 58, 306–324. doi: 10.1016/j.neuron.2008.04.017

Corbetta, M., and Shulman, G. L. (2002). Control of goal-directed and stimulus-driven attention in the brain. *Nat. Rev. Neurosci.* 3:201. doi: 10.1038/nrn755

Coull, J. T. (1998). Neural correlates of attention and arousal: insights from electrophysiology, functional neuroimaging and psychopharmacology. *Prog. Neurobiol.* 55, 343–361. doi: 10.1016/s0301-0082(98)00011-2

Coultrip, R., Granger, R., and Lynch, G. (1992). A cortical model of winner-take-all competition via lateral inhibition. *Neural Netw.* 5, 47–54. doi: 10.1016/s0893-6080(05)80006-1

Cowen, L., Ball, L. J., and Delin, J. (2002). "An eye movement analysis of web page usability," in *People and Computers Xvi-memorable Yet Invisible*, eds X. Faulkner, J. Finlay, and F. Détienne (Berlin: Springer), 317–335. doi: 10.1007/978-1-4471-0105-5_19

Curtis, C. E., and D'Esposito, M. (2003). Persistent activity in the prefrontal cortex during working memory. *Trends Cognit. Sci.* 7, 415–423. doi: 10.1016/s1364-6613(03)00197-9

De Rivecourt, M., Kuperus, M. N., Post, W. J., and Mulder, L. J. M. (2008). Cardiovascular and eye activity measures as indices for momentary changes in mental effort during simulated flight. *Ergonomics* 51, 1295–1319. doi: 10.1080/00140130802120267

De Waard, D. (1996). *The Measurement of Driver Mental Workload,* PhD Thesis., Groningen: Rijksuniversiteit Groningen.

Dehais, F., Causse, M., and Tremblay, S. (2011). Mitigation of conflicts with automation: use of cognitive countermeasures. *Hum. Fact.* 53, 448–460. doi: 10.1177/0018720811418635

Dehais, F., Causse, M., Vachon, F., Régis, N., Menant, E., and Tremblay, S. (2014). Failure to detect critical auditory alerts in the cockpit: evidence for inattentional deafness. *Hum. Fact.* 56, 631–644. doi: 10.1177/0018720813510735

Dehais, F., Causse, M., Vachon, F., and Tremblay, S. (2012). Cognitive conflict in human–automation interactions: a psychophysiological study. *Appl. Ergon.* 43, 588–595. doi: 10.1016/j.apergo.2011.09.004

Dehais, F., Duprès, A., Di Flumeri, G., Verdière, K. J., Borghini, G., Babiloni, F., et al. (2018). *Monitoring Pilots Cognitive Fatigue with Engagement Features in Simulated and actual Flight Conditions Using an Hybrid fNIRS-EEG Passive BCI. IEEE SMC.* Availale at: https://hal.archives-ouvertes.fr/hal-01959452.

Dehais, F., Hodgetts, H. M., Causse, M., Behrend, J., Durantin, G., and Tremblay, S. (2019). Momentary lapse of control: a cognitive continuum approach to understanding and mitigating perseveration in human error. *Neurosci. Biobehav. Rev.* 100, 252–262. doi: 10.1016/j.neubiorev.2019.03.006

Dehais, F., Peysakhovich, V., Scannella, S., Fongue, J., and Gateau, T. (2015). "Automation surprise in aviation: real- time solutions," in *Proceedings of the 33rd annual ACM conference on human factors in computing systems*, New York, NY, 2525–2534.

Dehais, F., Rida, I., Roy, R., Iversen, J., Mullen, T., and Callan, D. (2019a). "A pBCI to predict attentional error before it happens in real flight conditions," in *Proceedins of the Conference: 2019 IEEE International Conference on Systems, Man and Cybernetics (SMC)*, Bari.

Dehais, F., Roy, R. N., and Scannella, S. (2019b). Inattentional deafness to auditory alarms: inter-individual differences, electrophysiological signature and single trial classification. *Behav. Brain Res.* 360, 51–59. doi: 10.1016/j.bbr.2018.11.045

Dehais, F., Roy, R. N., Durantin, G., Gateau, T., and Callan, D. (2017). "EEG-engagement index and auditory alarm misperception: an inattentional deafness study in actual flight condition," in *Proceedins of the International Conference on Applied Human Factors and Ergonomics*, Washington D.C., 227–234. doi: 10.1007/978-3-319-60642-2_21

Dehais, F., Tessier, C., Christophe, L., and Reuzeau, F. (2010). "The perseveration syndrome in the pilots' activity: guide- lines and cognitive countermeasures," in *Human Error, Safety and Systems Development*, eds P. Palanque, J. Vanderdonckt, and M. Winkler (Berlin: Springer), 68–80. doi: 10.1007/978-3-642-11750-3_6

Di Flumeri, G., De Crescenzio, F., Berberian, B., Ohneiser, O., Kramer, J., Aricò, P., et al. (2019). Brain–computer interface-based adaptive automation to prevent out-of-the-loop phenomenon in air traffic controllers dealing with highly automated systems. *Front. Hum. Neurosci.* 13:296. doi: 10.3389/fnhum.2019.00296

Dierolf, A. M., Fechtner, J., Böhnke, R., Wolf, O. T., and Naumann, E. (2017). Influence of acute stress on response inhibition in healthy men: an ERP study. *Psychophysiology* 54, 684–695. doi: 10.1111/psyp.12826

Dolan, R. J. (2002). Emotion, cognition, and behavior. *Science* 298, 1191–1194.

Dolcos, F., and McCarthy, G. (2006). Brain systems mediating cognitive interference by emotional distraction. *J. Neurosci.* 26, 2072–2079. doi: 10.1523/jneurosci.5042-05.2006

Dorneich, M. C., Rogers, W., Whitlow, S. D., and DeMers, R. (2016). Human performance risks and benefits of adaptive systems on the flight deck. *Int. J. Aviat. Psychol.* 26, 15–35. doi: 10.1080/10508414.2016.1226834

Duffy, E. (1962). *Activation and Behaviour*. New York, NY: Wiley.

Durantin, G., Dehais, F., and Delorme, A. (2015). Characterization of mind wandering using fNIRS. *Front. Syst. Neurosci.* 9:45. doi: 10.3389/fnsys.2015.00045

Durantin, G., Dehais, F., Gonthier, N., Terzibas, C., and Callan, D. E. (2017). Neural signature of inattentional deafness. *Hum. Brain Mapp.* 38, 5440–5455. doi: 10.1002/hbm.23735

Durantin, G., Gagnon, J.-F., Tremblay, S., and Dehais, F. (2014). Using near infrared spectroscopy and heart rate variability to detect mental overload. *Behav. Brain Res.* 259, 16–23. doi: 10.1016/j.bbr.2013.10.042

Edworthy, J., Reid, S., Peel, K., Lock, S., Williams, J., Newbury, C., et al. (2018). The impact of workload on the ability to localize audible alarms. *Appl. Ergon.* 72, 88–93. doi: 10.1016/j.apergo.2018.05.006

Egner, T., and Gruzelier, J. H. (2001). Learned self-regulation of EEG frequency components affects attention and event-related brain potentials in humans. *Neuroreport* 12, 4155–4159. doi: 10.1097/00001756-200112210-00058

Egner, T., and Gruzelier, J. H. (2004). EEG biofeedback of low beta band components: frequency-specific effects on variables of attention and event-related brain potentials. *Clin. Neurophysiol.* 115, 131–139. doi: 10.1016/s1388-2457(03)00353-5

Ellenbogen, M. A., Schwartzman, A. E., Stewart, J., and Walker, C.-D. (2006). Automatic and effortful emotional informa- tion processing regulates different aspects of the stress response. *Psychoneuroendocrinology* 31, 373–387. doi: 10.1016/j.psyneuen.2005.09.001

Elliott, L. R., Schmeisser, E. T., and Redden, E. S. (2011). "Development of tactile and haptic systems for US infantry navigation and communication," in *Proceedins of the Symposium on Human Interface* (Berlin: Springer), 399–407. doi: 10.1007/978-3-642-21793-7_45

Enriquez-Geppert, S., Huster, R. J., Figge, C., and Herrmann, C. S. (2014). Self-regulation of frontal-midline theta facilitates memory updating and mental set shifting. *Front. Behav. Neurosci.* 8:420. doi: 10.3389/fnbeh.2014.00420

Enriquez-Geppert, S., Huster, R. J., and Herrmann, C. S. (2013). Boosting brain functions: improving executive functions with behavioral training, neurostimulation, and neurofeedback. *Int. J. Psychophysiol.* 88, 1–16. doi: 10.1016/j.ijpsycho.2013.02.001

Enriquez-Geppert, S., Huster, R. J., and Herrmann, C. S. (2017). EEG-neurofeedback as a tool to modulate cognition and behavior: a review tutorial. *Front. Hum. Neurosci.* 11:51. doi: 10.3389/fnhum.2017.00051

Ewing, K. C., Fairclough, S. H., and Gilleade, K. (2016). Evaluation of an adaptive game that uses EEG measures validated during the design process as inputs to a biocybernetic loop. *Front. Hum. Neurosci.* 10:223. doi: 10.3389/fnhum.2016.00223

Fairclough, S., Ewing, K., Burns, C., and Kreplin, U. (2019). "Neural efficiency and mental workload: locating the red line," in *Neuroergonomics*, eds A. Johnson and R. W. Proctor (Cambridge, MA: Academic Press), 73–77. doi: 10.1016/b978-0-12-811926-6.00012-9

Fairclough, S. H. (2008). Fundamentals of physiological computing. *Interact. Comput.* 21, 133–145. doi: 10.1016/j.intcom.2008.10.011

Fairclough, S. H., Burns, C., and Kreplin, U. (2018). FNIRS activity in the prefrontal cortex and motivational intensity: impact of working memory load, financial reward, and correlation-based signal improvement. *Neurophotonics* 5, 1–10.

Fairclough, S. H., and Ewing, K. (2017). The effect of task demand and incentive on neurophysiological and cardiovascular markers of effort. *Int. J. Psychophysiol.* 119, 58–66. doi: 10.1016/j.ijpsycho.2017.01.007

Fairclough, S. H., Gilleade, K., Ewing, K. C., and Roberts, J. (2013). Capturing user engagement via psychophysiology: measures and mechanisms for biocybernetic adaptation. *Int. J. Auton. Adapt. Commun. Syst.* 6, 63–79.

Falcone, B., Coffman, B. A., Clark, V. P., and Parasuraman, R. (2012). Transcranial direct current stimulation augments perceptual sensitivity and 24-hour retention in a complex threat detection task. *PLoS ONE* 7:e34993. doi: 10.1371/journal.pone.0034993

Fox, K. C., Spreng, R. N., Ellamil, M., Andrews-Hanna, J. R., and Christoff, K. (2015). The wandering brain: meta-analysis of functional neuroimaging studies of mind-wandering and related spontaneous thought processes. *Neuroimage* 111, 611–621. doi: 10.1016/j.neuroimage.2015.02.039

Freeman, F. G., Mikulka, P. J., Prinzel, L. J., and Scerbo, M. W. (1999). Evaluation of an adaptive automation system using three EEG indices with a visual tracking task. *Biol. Psychol.* 50, 61–76. doi: 10.1016/s0301-0511(99)00002-2

Freeman, F. G., Mikulka, P. J., Scerbo, M. W., and Scott, L. (2004). An evaluation of an adaptive automation system using a cognitive vigilance task. *Biol. Psychol.* 67, 283–297. doi: 10.1016/j.biopsycho.2004.01.002

Gärtner, M., Rohde-Liebenau, L., Grimm, S., and Bajbouj, M. (2014). Working memory-related frontal theta activity is decreased under acute stress. *Psychoneuroendocrinology* 43, 105–113. doi: 10.1016/j.psyneuen.2014.02.009

Gaspar, J. G., Brown, T. L., Schwarz, C. W., Lee, J. D., Kang, J., and Higgins, J. S. (2017). Evaluating driver drowsiness countermeasures. *Traff. Inj. Prevent.* 18, S58–S63.

Gateau, T., Ayaz, H., and Dehais, F. (2018). In silico versus over the clouds: on-the-fly mental state estimation of aircraft pilots, using a functional near infrared spectroscopy based passive-BCI. *Front. Hum. Neurosci.* 12:187. doi: 10.3389/fnhum.2018.00187

Gateau, T., Chanel, C. P. C., Le, M. H., and Dehais, F. (2016). "Considering human's non-deterministic behavior and his availability state when designing a collaborative human-robots system," in *Proceedings of the 2016 IEEE/RSJ International Conference on Intelligent Robots and Systems (IROS)*, Las Vegas, NV, 4391–4397.

Giraudet, L., Imbert, J. P., Bérenger, M., Tremblay, S., and Causse, M. (2015a). The Neuroergonomic evaluation of human machine interface design in air traffic control using behavioral and EEG/ERP measures. *Behav. Brain Res.* 294, 246–253. doi: 10.1016/j.bbr.2015.07.041

Giraudet, L., St-Louis, M.-E., Scannella, S., and Causse, M. (2015b). P300 event-related potential as an indicator of inat- tentional deafness? *PLoS ONE* 10:e0118556. doi: 10.1371/journal.pone.0118556

Goldberg, J. H., and Kotval, X. P. (1999). Computer interface evaluation using eye movements: methods and constructs. *Int. J. Ind. Ergon.* 24, 631–645. doi: 10.1016/s0169-8141(98)00068-7

Goldberg, T. E., Berman, K. F., Fleming, K., Ostrem, J., Van Horn, J. D., Esposito, G., et al. (1998). Uncoupling cognitive workload and prefrontal cortical physiology: a PER rCBF study. *Neuroimage* 7, 296–303. doi: 10.1006/nimg.1998.0338

Goldman-Rakic, P. (1987). *Handbook of Physiology. The Nervous System*. Bethesda, MD: American Physiological Society, 373417.

Gonçalves, ÓF., Carvalho, S., Mendes, A. J., Leite, J., and Boggio, P. S. (2018). Neuromodulating attention and mind-wandering processes with a single session real time EEG. *Appl. Psychophysiol. Biofeedback* 43, 143–151. doi: 10.1007/s10484-018-9394-4

Gouraud, J., Delorme, A., and Berberian, B. (2018). Out of the loop, in your bubble: mind wandering is independent from automation reliability, but influences task engagement. *Front. Hum. Neurosci.* 12:383. doi: 10.3389/fnhum.2018.00383

Grandchamp, R., Braboszcz, C., and Delorme, A. (2014). Oculometric variations during mind wandering. *Front. Psychol.* 5:31. doi: 10.3389/fpsyg.2014.00031

Gruzelier, J. H. (2014). EEG-neurofeedback for optimising performance. I: a review of cognitive and affective outcome in healthy participants. *Neurosci. Biobehav. Rev.* 44, 124–141. doi: 10.1016/j.neubiorev.2013.09.015

Hancock, P. A., and Desmond, P. A. (2001). *Stress, Workload, and Fatigue*. Mahwah, NJ: Erlbaum.

Hancock, P. A., and Meshkati, N. (1988). *Human Mental Workload*. Amsterdam: North-Holland.

Hancock, P. A., and Warm, J. S. (1989). A dynamic model of stress and sustained attention. *Hum. Fact.* 31, 519–537. doi: 10.1177/001872088903100503

Harrivel, A. R., Weissman, D. H., Noll, D. C., and Peltier, S. J. (2013). Monitoring attentional state with fnirs. *Front. Human Neurosci.* 7:861. doi: 10.3389/fnhum.2013.00861

He, J., Becic, E., Lee, Y.-C., and McCarley, J. S. (2011). Mind wandering behind the wheel: performance and oculomotor correlates. *Human Factors* 53, 13–21. doi: 10.1177/0018720810391530

Herff, C., Heger, D., Fortmann, O., Hennrich, J., Putze, F., and Schultz, T. (2014). Mental workload during n-back task—quantified in the prefrontal cortex using fNIRS. *Front. Hum. Neurosci.* 7:935. doi: 10.3389/fnhum.2013.00935

Hockey, G. R. J. (1997). Compensatory control in the regulation of human performance under stress and high workload: a cognitive-energetical framework. *Biol. Psychol.* 45, 73–93. doi: 10.1016/s0301-0511(96)05223-4

Hockey, G. R. J. (2011). "A motivational control theory of cognitive fatigue," in *Cognitive Fatigue: Multidisciplinary Perspectives on Current Research and Future Applications*, ed. P. L. Ackerman (Washington, DC: American Psychological Association).

Hockey, G. R. J., Coles, M. G., and Gaillard, A. W. (1986). "Energetical issues in research on human information processing," in *Energetics and Human Information Processing*, eds G. M. Hockey, A. W. K. Gaillard, and M. Coles (Berlin: Springer), 3–21. doi: 10.1007/978-94-009-4448-0_1

Hopstaken, J. F., Van Der Linden, D., Bakker, A. B., and Kompier, M. A. (2015). A multifaceted investigation of the link between mental fatigue and task disengagement. *Psychophysiology* 52, 305–315. doi: 10.1111/psyp.12339

Hutchinson, B. T. (2019). Toward a theory of consciousness: a review of the neural correlates of inattentional blindness. *Neurosci. Biobehav. Rev.* 104, 87–99. doi: 10.1016/j.neubiorev.2019.06.003

Imbert, J. P., Hodgetts, H. M., Parise, R., Vachon, F., Dehais, F., and Tremblay, S. (2014). Attentional costs and failures in air traffic control notifications. *Ergonomics* 57, 1817–1832. doi: 10.1080/00140139.2014.952680

Izzetoglu, M., Bunce, S. C., Izzetoglu, K., Onaral, B., and Pour-rezaei, K. (2007). Functional brain imaging using near- infrared technology. *IEEE Eng. Med. Biol. Mag.* 26:38. doi: 10.1109/memb.2007.384094

Jahanpour, E., Fabre, E., Dehais, F., and Causse, M. (2018). "Giving a hand to pilots with animated alarms based on mirror system functioning," in *Proceedings of the 2nd International Neuroergonomics Conference*, Philadelphia, PA.

Jeon, S. Y., and Han, S. J. (2012). Improvement of the working memory and naming by transcranial direct current stimulation. *Ann. Rehabil. Med.* 36, 585–595.

Johnson, J. A., and Zatorre, R. J. (2006). Neural substrates for dividing and focusing attention between simultaneous auditory and visual events. *NeuroImage* 31, 1673–1681. doi: 10.1016/j.neuroimage.2006.02.026

Kahneman, D. (1973). *Attention and Effort*, Vol. 1063. Englewood Cliffs, NJ: Prentice-Hall.

Kalia, V., Vishwanath, K., Knauft, K., Vellen, B. V. D., Luebbe, A., and Williams, A. (2018). Acute stress attenuates cognitive flexibility in males only: an fNIRS examination. *Front. Psychol.* 9:2084. doi: 10.3389/fpsyg.2018.02084

Kam, J. W., Dao, E., Farley, J., Fitzpatrick, K., Smallwood, J., Schooler, J. W., et al. (2011). Slow fluctuations in attentional control of sensory cortex. *J. Cognit. Neurosci.* 23, 460–470. doi: 10.1162/jocn.2010.21443

Kobes, M., Helsloot, I., De Vries, B., and Post, J. G. (2010). Building safety and human behaviour in fire: a literature review. *Fire Saf. J.* 45, 1–11. doi: 10.1016/j.firesaf.2009.08.005

Kojima, H., and Suzuki, T. (2010). Hemodynamic change in occipital lobe during visual search: visual attention allocation measured with NIRS. *Neuropsychologia* 48, 349–352. doi: 10.1016/j.neuropsychologia.2009.09.028

Kramer, A., and Spinks, J. (1991). "Capacity views of human information processing," in *Handbook of Cognitive Psychophysiology: Central and Nervous Systems Approaches*, eds J. R. Jennings and M. G. H. Coles (New York: Wiley), 179–249.

Kreibig, S. D. (2010). Autonomic nervous system activity in emotion: a review. *Biol. Psychol.* 84, 394–421. doi: 10.1016/j.biopsycho.2010.03.010

Kreitz, C., Furley, P., Memmert, D., and Simons, D. J. (2016a). The influence of attention set, working memory capacity, and expectations on inattentional blindness. *Perception* 45, 386–399. doi: 10.1177/0301006615614465

Kreitz, C., Furley, P., Simons, D. J., and Memmert, D. (2016b). Does working memory capacity predict cross-modally induced failures of awareness? *Conscious. Cognit.* 39, 18–27. doi: 10.1016/j.concog.2015.11.010

Krol, L. R., Haselager, P., and Zander, T. O. (2019). Cognitive and affective probing: a tutorial and review of active learning for neuroadaptive technology. *J. Neural Eng.* 17:012001. doi: 10.1088/1741-2552/ab5bb5

Lee, J. D. (2014). Dynamics of driver distraction: the process of engaging and disengaging. *Ann. Adv. Automot. Med.* 58:24.

Lee, S., Kim, M., Choi, S., and You, H. (2018). Evaluation of a motion seat system for reduction of a driver's passive task-related (tr) fatigue. *Proc. Hum. Factors Ergon. Soc. Annu. Meet.* 62, 1843–1847. doi: 10.1177/1541931218621420

Lees, M. N., Cosman, J. D., Lee, J. D., Rizzo, M., and Fricke, N. (2010). Translating cognitive neuroscience to the driver's operational environment: a neuroergonomics approach. *Am. J. Psychol.* 123:391. doi: 10.5406/amerjpsyc.124.4.0391

Leite, J., Carvalho, S., Fregni, F., and Gonçalves, O. F. (2011). Task-specific effects of tDCS-induced cortical excitability changes on cognitive and motor sequence set shifting performance. *PLoS ONE* 6:e24140. doi: 10.1371/journal.pone.0024140

Leontiev, A. N. (2014). *Activity and Consciousness*. Moscow: Progress Publishers.

Lewis, B. A., Eisert, J. L., and Baldwin, C. L. (2014). Effect of tactile location, pulse duration, and interpulse interval on perceived urgency. *Transport. Res. Rec.* 2423, 10–14. doi: 10.3141/2423-02

Lie, C. H., Specht, K., Marshall, J. C., and Fink, G. R. (2006). Using fMRI to decompose the neural processes underlying the Wisconsin Card Sorting Test. *Neuroimage* 30, 1038–1049. doi: 10.1016/j.neuroimage.2005.10.031

Mallat, C., Cegarra, J., Calmettes, C., and Capa, R. L. (2019). A curvilinear effect of mental workload on mental effort and behavioral adaptability: an approach with the pre-ejection period. *Hum. Fact.* [Epub ahead of print].

Mandrick, K., Chua, Z., Causse, M., Perrey, S., and Dehais, F. (2016). Why a comprehensive understanding of mental workload through the measurement of neurovascular coupling is a key issue for neuroergonomics? *Front. Hum. Neurosci.* 10:250. doi: 10.3389/fnhum.2016.00250

Marois, R., Yi, D. J., and Chun, M. M. (2004). The neural fate of consciously perceived and missed events in the attentional blink. *Neuron* 41, 465–472. doi: 10.1016/s0896-6273(04)00012-1

Mason, M. F., Norton, M. I., Van Horn, J. D., Wegner, D. M., Grafton, S. T., and Macrae, C. N. (2007). Wandering minds: the default network and stimulus-independent thought. *Science* 315, 393–395. doi: 10.1126/science.1131295

Mathewson, K. E., Gratton, G., Fabiani, M., Beck, D. M., and Ro, T. (2009). To see or not to see: prestimulus α phase predicts visual awareness. *J. Neurosci.* 29, 2725–2732. doi: 10.1523/jneurosci.3963-08.2009

Matthews, G. (2002). Towards a transactional ergonomics for driver stress and fatigue. *Theor. Issues Ergon. Sci.* 3, 195–211. doi: 10.1080/14639220210124120

Matthews, G., Campbell, S. E., Falconer, S., Joyner, L. A., Huggins, J., Gilliland, K., et al. (2002). Fundamental dimensions of subjective state in performance settings: task engagement, distress, and worry. *Emotion* 2, 315. doi: 10.1037/1528-3542.2.4.315

Matthews, G., Reinerman-Jones, L. E., Barber, D. J., and Abich, J. IV (2015). The psychometrics of mental work- load: multiple measures are sensitive but divergent. *Hum. Fact.* 57, 125–143. doi: 10.1177/0018720814539505

Matthews, G., Warm, J. S., Reinerman, L. E., Langheim, L. K., and Saxby, D. J. (2010). "Task engagement, attention, and executive control," in *Handbook of Individual Differences in Cognition*, eds A. Gruszka, G. Matthews, and B. Szymura (Berlin: Springer), 205–230. doi: 10.1007/978-1-4419-1210-7_13

May, J. F., and Baldwin, C. L. (2009). Driver fatigue: the importance of identifying causal factors of fatigue when considering detection and countermeasure technologies. *Transport. Res. Part F Traff. Psychol. Behav.* 12, 218–224. doi: 10.1016/j.trf.2008.11.005

McIntire, L. K., McKinley, R. A., Goodyear, C., and Nelson, J. (2014). A comparison of the effects of transcranial direct current stimulation and caffeine on vigilance and cognitive performance during extended wakefulness. *Brain Stimul.* 7, 499–507. doi: 10.1016/j.brs.2014.04.008

McKendrick, R., Parasuraman, R., and Ayaz, H. (2015). Wearable functional near infrared spectroscopy (fNIRS) and transcranial direct current stimulation (tDCS): expanding vistas for neurocognitive augmentation. *Front. Syst. Neurosci.* 9:27. doi: 10.3389/fnsys.2015.00027

Mehta, R. K., and Parasuraman, R. (2013). Neuroergonomics: a review of applications to physical and cognitive work. *Front. Hum. Neurosci.* 7:889. doi: 10.3389/fnhum.2013.00889

Modi, H. N., Singh, H., Orihuela-Espina, F., Athanasiou, T., Fiorentino, F., Yang, G. Z., et al. (2018). Temporal stress in the operating room: brain engagement promotes "coping" and disengagement prompts "choking". *Ann. Surg.* 267, 683–691. doi: 10.1097/sla.0000000000002289

Modi, H. N., Singh, H., Yang, G. Z., Darzi, A., and Leff, D. R. (2017). A decade of imaging surgeons' brain function (part I): terminology, techniques, and clinical translation. *Surgery* 162, 1121–1130. doi: 10.1016/j.surg.2017.05.021

Molloy, K., Griffiths, T. D., Chait, M., and Lavie, N. (2015). Inattentional deafness: visual load leads to time-specific suppression of auditory evoked responses. *J. Neurosci.* 35, 16046–16054. doi: 10.1523/jneurosci.2931-15.2015

Moray, N. (1979). *Mental Workload: Its Theory and Measurement*. New York, NY: Plenum.

Munakata, Y., Herd, S. A., Chatham, C. H., Depue, B. E., Banich, M. T., and O'Reilly, R. C. (2011). A unified framework for inhibitory control. *Trends Cognit. Sci.* 15, 453–459. doi: 10.1016/j.tics.2011.07.011

Murphy, S., and Dalton, P. (2016). Out of touch? Visual load induces inattentional numbness. *J. Exp. Psychol.* 42, 761. doi: 10.1037/xhp0000218

Nagahama, Y., Okina, T., Suzuki, N., Nabatame, H., and Matsuda, M. (2005). The cerebral correlates of different types of perseveration in the Wisconsin Card Sorting Test. *J. Neurol. Neurosurg. Psychiatry* 76, 169–175. doi: 10.1136/jnnp.2004.039818

Navarro, J., Mars, F., Forzy, J. F., El-Jaafari, M., and Hoc, J. M. (2010). Objective and subjective evaluation of motor priming and warning systems applied to lateral control assistance. *Accident Anal. Prevent.* 42, 904–912. doi: 10.1016/j.aap.2009.07.008

Navon, D. (1984). Resources - a theoretical soupstone? *Psychol. Rev.* 91, 216–234.

Navon, D., and Gopher, D. (1979). On the economy of the human-processing system. *Psychol. Rev.* 86, 214–225.

Nelson, J., McKinley, R. A., Phillips, C., McIntire, L., Goodyear, C., Kreiner, A., et al. (2016). The effects of transcranial direct current stimulation (tDCS) on multitasking throughput capacity. *Front. Hum. Neurosci.* 10:589.

Nelson, J. M., McKinley, R. A., McIntire, L. K., Goodyear, C., and Walters, C. (2015). Augmenting visual search performance with transcranial direct

current stimulation (tDCS). *Milit. Psychol.* 27, 335–347. doi: 10.1037/mil0000085

Nelson, J. T., McKinley, R. A., Golob, E. J., Warm, J. S., and Parasuraman, R. (2014). Enhancing vigilance in operators with prefrontal cortex transcranial direct current stimulation (tDCS). *Neuroimage* 85, 909–917. doi: 10.1016/j.neuroimage.2012.11.061

Ninomiya, T., Noritake, A., Ullsperger, M., and Isoda, M. (2018). Performance monitoring in the medial frontal cortex and related neural networks: from monitoring self actions to understanding others' actions. *Neurosci. Res.* 137, 1–10. doi: 10.1016/j.neures.2018.04.004

Norman, D. A., and Bobrow, D. G. (1975). On data-limited and resource-limited processes. *Cognit. Psychol.* 7, 44–64. doi: 10.1016/0010-0285(75)90004-3

O'Connell, R. G., Dockree, P. M., Robertson, I. H., Bellgrove, M. A., Foxe, J. J., and Kelly, S. P. (2009). Uncovering the neural signature of lapsing attention: electrophysiological signals predict errors up to 20 s before they occur. *J. Neurosci.* 29, 8604–8611. doi: 10.1523/jneurosci.5967-08.2009

O'Donnell, R. D., and Eggemeier, F. T. (1986). "Workload assessment methodology," in *Handbook of Human Perception and Performance*, Vol. 2, eds K. Boff, L. Kaufman, and J. P. Thomas (New York, NY: Wiley), 42.1–42.49.

Oei, N. Y., Veer, I. M., Wolf, O. T., Spinhoven, P., Rombouts, S. A., and Elzinga, B. M. (2012). Stress shifts brain activation towards ventral 'affective'areas during emotional distraction. *Soc. Cognit. Affect. Neurosci.* 7, 403–412. doi: 10.1093/scan/nsr024

O'Hare, D., and Smitheram, T. (1995). Pressing-on into deteriorating conditions: an application of behavioral decision theory to pilot decision making. *Int. J. Aviat. Psychol.* 5, 351–370. doi: 10.1207/s15327108ijap0504_2

Orasanu, J., Martin, L., Davison, J., and Null, C. H. (1998). *Errors in Aviation Decision Making: Bad Decisions or Bad Luck?* Moffett Field, CA: NASA Ames Research Center.

Palumbo, R. V., Marraccini, M. E., Weyandt, L. L., Wilder-Smith, O., McGee, H. A., Liu, S., et al. (2017). Interpersonal autonomic physiology : a systematic review of the literature. *Personal. Soc. Psychol. Rev.* 21, 99–141. doi: 10.1177/1088868316628405

Parasuraman, R. (2003). Neuroergonomics: research and practice. *Theor. Issues Ergon. Sci.* 4, 5–20. doi: 10.1080/14639220210199753

Parasuraman, R., and Rizzo, M. (2008). *Neuroergonomics: The Brain at Work*, 1st Edn. New York, NY: Oxford University Press, Inc.

Parasuraman, R., and Wilson, G. F. (2008). Putting the brain to work: neuroergonomics past, present, and future. *Hum. Fact.* 50, 468–474. doi: 10.1518/001872008X288349

Parasuraman, R., Mouloua, M., and Hilburn, B. (1999). "Adaptive aiding and adaptive task allocation enhance human-machine interaction," in *Automation Technology and Human Performance: Current Research and Trends* (Mahwah, NJ: Erlbaum), 119–123.

Peavler, W. S. (1974). Pupil size, information overload, and performance differences. *Psychophysiology* 11, 559–566. doi: 10.1111/j.1469-8986.1974.tb01114.x

Pecher, C., Quaireau, C., Lemercier, C., and Cellier, J.-M. (2011). The effects of inattention on selective attention: how sad- ness and ruminations alter attention functions evaluated with the attention network test. *Rev. Eur. Psychol. Appl. Eur. Rev. Appl. Psychol.* 61, 43–50. doi: 10.1016/j.erap.2010.10.003

Pepin, G., Malin, S., Navarro, J., Fort, A., Jallaiz, C., Moreau, F., et al. (2016). "Detection of mind-wandering in driving: contributions of cardiac measurement and eye movements," in *Proceedings of the 1st International Neuroergonomics Conference*: *The Brain at Work and in Everyday Life*, Amsterdam: Elsevier.

Pessoa, L., and Ungerleider, L. G. (2004). Neuroimaging studies of attention and the processing of emotion-laden stimuli. *Prog. Brain Res.* 144, 171–182. doi: 10.1016/s0079-6123(03)14412-3

Petersen, S. E., and Posner, M. I. (2012). The attention system of the human brain: 20 years after. *Ann. Rev. Neurosci.* 35, 73–89. doi: 10.1146/annurev-neuro-062111-150525

Peysakhovich, V., Lefrançois, O., Dehais, F., and Causse, M. (2018). The neuroergonomics of aircraft cockpits: the four stages of eye-tracking integration to enhance flight safety. *Safety* 4:8. doi: 10.3390/safety4010008

Polich, J. (2007). Updating P300: an integrative theory of P3a and P3b. *Clin. Neurophysiol.* 118, 2128–2148. doi: 10.1016/j.clinph.2007.04.019

Pope, A. T., Bogart, E. H., and Bartolome, D. S. (1995). Biocybernetic system evaluates indices of operator engagement in automated task. *Biol. Psychol.* 40, 187–195. doi: 10.1016/0301-0511(95)05116-3

Posner, M. I. (2012). Imaging attention networks. *Neuroimage* 61, 450–456. doi: 10.1016/j.neuroimage.2011.12.040

Posner, M. I., and Dehaene, S. (1994). Attentional networks. *Trends Neurosci.* 17, 75–79.

Posner, M. I., and Petersen, S. E. (1990). The attention system of the human brain. *Annu. Rev. Neurosci.* 13, 25–42.

Posner, M. I., and Tudela, P. (1997). Imaging resources. *Biol. Psychol.* 45, 95–107.

Pourtois, G., De Pretto, M., Hauert, C. A., and Vuilleumier, P. (2006). Time course of brain activity during change blindness and change awareness: performance is predicted by neural events before change onset. *J. Cognit. Neurosci.* 18, 2108–2129. doi: 10.1162/jocn.2006.18.12.2108

Pribram, K. H., and McGuinness, D. (1975). Arousal, activation, and effort in the control of attention. *Psychol. Review* 82:116. doi: 10.1037/h0076780

Prinzel, L. J. III (2002). *Research on Hazardous States of Awareness and Physiological Factors in Aerospace Operations. Report No. NASA/ TM*-2002-211444. Washington, DC: NASA.

Prinzel, L. J., Freeman, F. G., Scerbo, M. W., Mikulka, P. J., and Pope, A. T. (2000). A closed-loop system for examining psychophysiological measures for adaptive task allocation. *Int. J. Aviat. Psychol.* 10, 393–410. doi: 10.1207/s15327108ijap1004_6

Proulx, G. (2001). "Occupant behaviour and evacuation," in *Proceedings of the 9th International Fire Protection Symposium* (Iceland: Iceland Fire Authority), 219–232.

Puschmann, S., Sandmann, P., Ahrens, J., Thorne, J., Weerda, R., Klump, G., et al. (2013). Electrophysiological correlates of auditory change detection and change deafness in complex auditory scenes. *Neuroimage* 75, 155–164. doi: 10.1016/j.neuroimage.2013.02.037

Qin, S., Hermans, E. J., van Marle, H. J., Luo, J., and Fernandez, G. (2009). Acute psychological stress reduces working memory-related activity in the dorsolateral prefrontal cortex. *Biol. Psychiatry* 66, 25–32. doi: 10.1016/j.biopsych.2009.03.006

Racz, F. S., Mukli, P., Nagy, Z., and Eke, A. (2017). Increased prefrontal cortex connectivity during cognitive challenge assessed by fNIRS imaging. *Biomed. Opt. Exp.* 8, 3842–3855.

Ramnani, N., and Owen, A. M. (2004). Anterior prefrontal cortex: insights into function from anatomy and neuroimaging. *Nat. Rev. Neurosci.* 5:184. doi: 10.1038/nrn1343

Ramsey, N. F., Jansma, J. M., Jager, G., Van Raalten, T., and Kahn, R. S. (2004). Neurophysiological factors in human information processing capacity. *Brain* 127, 517–525. doi: 10.1093/brain/awh060

Raveh, D., and Lavie, N. (2015). Load-induced inattentional deafness. *Attent. Percept. Psychophys.* 77, 483–492. doi: 10.3758/s13414-014-0776-2

Régis, N., Dehais, F., Rachelson, E., Thooris, C., Pizziol, S., Causse, M., et al. (2014). Formal detection of atten- tional tunneling in human operator–automation interactions. *IEEE Trans. Hum. Mach. Syst.* 44, 326–336. doi: 10.1109/thms.2014.2307258

Regis, N., Dehais, F., Tessier, C., and Gagnon, J.-F. (2012). "Human Factors: a view from an integrative perspective," in *Proceedings HFES Europe Chapter Conference Toulouse 2012*, eds D. De Waard, K. Brookhuis, F. Dehais, C. Weikert, S. Röttger, D. Manzey, et al. (Toulouse: HFES). Available online at: http://hfes-europe.org

Reynal, M., Rister, F., Scannella, S., Wickens, C., and Dehais, F. (2017). "Investigating pilots decision making when facing an unstabilized approach: an eye-tracking study," in *Proceedings of the 19th International Symposium on Aviation Psychology*, Dayton, OH, 335.

Reyner, L. A., and Horne, J. A. (1998). Evaluation of 'in-car'countermeasures to sleepiness: cold air and radio. *Sleep* 21, 46–51.

Richter, M., Gendolla, G. H. E., and Wright, R. A. (2016). "Three decades of research on motivational intensity theory: what we have learned about effort and what we still don't know," in *Advances in Motivation Science*, ed. A. J. Elliot (Cambridge, MA: Academic Press), 149–186.

Ridderinkhof, K. R., Van Den Wildenberg, W. P., Segalowitz, S. J., and Carter, C. S. (2004). Neurocognitive mechanisms of cognitive control: the role of prefrontal cortex in action se- lection, response inhibition, performance monitoring, and

reward-based learning. *Brain Cognit.* 56, 129–140. doi: 10.1016/j.bandc.2004.09.016

Riggs, S. L., and Sarter, N. (2019). Tactile, visual, and crossmodal visual-tactile change blindness: the effect of transient type and task demands. *Hum. Fact.* 61, 5–24. doi: 10.1177/0018720818818028

Rizzo, M., Robinson, S., and Neale, V. (2007). "The brain in the wild: tracking human behavior in natural and naturalistic settings," in *Neuroergonomics: The Brain at Work*, eds R. Parasuraman and M. Rizzo (New York, NY: Oxford), 113–130.

Robbins, T. W., and Arnsten, A. F. (2009). The neuropsychopharmacology of fronto-executive function: monoaminergic modulation. *Annu. Rev. Neurosci.* 32, 267–287. doi: 10.1146/annurev.neuro.051508.135535

Roy, R. N., and Frey, J. (2016). "Neurophysiological markers for passive brain–computer interfaces," in *Brain–Computer Interfaces 1: Foundations and Methods* eds M. Clerc, L. Bougrain, and F. Lotte (Hoboken, NJ: John Wiley & Sons), 85–100. doi: 10.1002/9781119144977.ch5

Russell, D., Statz, J. K., Ramiccio, J., Henderson, M., Still, D., Temme, L., et al. (2016). *Pilot Cueing Synergies for Degraded Visual Environments (No. USAARL-2016-10)*. Fort Rucker, AL: US Army Aeromedical Research Laboratory Fort Rucker United States.

Saint Lot, J., Imbert, J.-P., and Dehais, F. (2020). "Red Altert: a cognitive countermeasure to mitigate attentional tunneling," in *Proceedings CHI 2020, April 25–30* (Honolulu, HI). doi: 10.1145/3313831.3376709

Sandson, J., and Albert, M. L. (1984). Varieties of perseveration. *Neuropsychologia* 22, 715–732. doi: 10.1016/0028-3932(84)90098-8

Sarason, I. G., Sarason, B. R., and Pierce, G. R. (1990). Anxiety, cognitive interference and performance. *J. Soc. Behav. Personal.* 5, 1–18.

Saravini, F. (1999). "Energy and the brain: facts and fantasies," in *Mind Myths*, ed. E. Della Salla (Chichester: Wiley), 43–58.

Sarter, N., and Sarter, M. (2003). Neuroergonomics: opportunities and challenges of merging cognitive neuroscience with cognitive ergonomics. *Theor. Issues Ergon. Sci.* 4, 142–150. doi: 10.1080/1463922021000020882

Scannella, S., Causse, M., Chauveau, N., Pastor, J., and Dehais, F. (2013). Effects of the audiovisual conflict on auditory early processes. *Int. J. Psychophysiol.* 89, 115–122. doi: 10.1016/j.ijpsycho.2013.06.009

Scerbo, M. W. (2008). "Adaptive automation," in *Neuroergonomics: The Brain at Work*, eds R. Parasuraman and M. Rizzo (New York, NY: Oxford), 239–252. doi: 10.1093/acprof:oso/9780195177619.003.0016

Schneider, W., Dumais, S. T., and Shiffen, R. M. (1984). "Automatic and control processing and attention," in *Varieties of Attention*, eds R. Parasuraman and D. R. Davies (Orlando: Academic Press), 1–27.

Scholte, H. S., Witteveen, S. C., Spekreijse, H., and Lamme, V. A. (2006). The influence of inattention on the neural correlates of scene segmentation. *Brain Res.* 1076, 106–115. doi: 10.1016/j.brainres.2005.10.051

Schooler, J. W., Smallwood, J., Christoff, K., Handy, T. C., Reichle, E. D., and Sayette, M. A. (2011). Meta-awareness, perceptual decoupling and the wandering mind. *Trends Cognit. Sci.* 15, 319–326.

Schultz, W. (2002). Getting formal with dopamine and reward. *Neuron* 36, 241–263. doi: 10.1016/s0896-6273(02)00967-4

Sebok, A., Wickens, C. D., Walters, B., and Fennell, K. (2017). "Alerts on the nextgen flight deck," in *Proceedings of the 19th International Symposium on Aviation Psychology*, Dayton, OH, 293.

Selfridge, O. G. (1959). "Pandemonium: a paradigm for learning," in *Mechanisation of Thought Processes* (London: H.M. Stationery Office), 511–526.

Senoussi, M., Verdière, K. J., Bovo, A., Ponzoni Carvalho, Chanel, C., Dehais, F., et al. (2017). "Pre- stimulus antero-posterior EEG connectivity predicts performance in a UAV monitoring task," in *Proceedings of 2016 International Conference on Systems, Man, and Cybernetics* (Canada: IEEE SMC, 1167–1172.

Shallice, T., and Burgess, P. (1993). "Supervisory control of action and thought selection," in *Attention: Selection, Awareness and Control*, eds A. Baddeley and L. Weiskrantz (Oxford: Clarendon Press), 171–187.

Smallwood, J., Beach, E., Schooler, J. W., and Handy, T. C. (2008). Going awol in the brain: mind wandering reduces cortical analysis of external events. *J. Cognit. Neurosci.* 20, 458–469. doi: 10.1162/jocn.2008.20037

Smallwood, J., and Schooler, J. W. (2015). The science of mind wandering: empirically navigating the stream of consciousness. *Annu. Rev. Psychol.* 66, 487–518. doi: 10.1146/annurev-psych-010814-015331

Smith, R. P. (1981). Boredom: a review. *Hum. Fact.* 23, 329–340.

Souza, P. E., Chanel, C. P. C., Dehais, F., and Givigi, S. (2016). "Towards human-robot interaction: a framing effect experiment," in *IEEE International Conference on Systems, Man, and Cybernetics*, (Budapest: IEEE SMC), 001929–001934.

Staal, M. A. (2004). Stress, cognition, and human performance: a literature review and conceptual framework.

Stamp, K., Fairclough, S., Dobbins, C., and Poole, H. (2019). "A neuroadaptive approach to analgesic gaming," in *The Second Neuroadaptive Technology Conference*, Liverpool, 19.

Stephens, C., Dehais, F., Roy, R. N., Harrivel, A., Last, M. C., Kennedy, K., et al. (2018). "Biocybernetic adaptation strategies: machine awareness of human engagement for improved operational performance," in *International Conference on Augmented Cognition*, Copenhagen, 89–98. doi: 10.1007/978-3-319-91470-1_9

Taillard, J., Capelli, A., Sagaspe, P., Anund, A., Akerstedt, T., and Philip, P. (2012). In-car nocturnal blue light exposure improves motorway driving: a randomized controlled trial. *PLoS ONE* 7:e46750. doi: 10.1371/journal.pone.0046750

Thomas, L. C., and Wickens, C. D. (2004). Eye-tracking and individual differences in off-normal event detection when flying with a synthetic vision system display. *Proc. Hum. Fact. Ergon. Soc. Annu. Meet.* 48, 223–227. doi: 10.1177/154193120404800148

Todd, J. J., Fougnie, D., and Marois, R. (2005). Visual short-term memory load suppresses temporo-parietal junction activity and induces inattentional blindness. *Psychol. Sci.* 16, 965–972. doi: 10.1111/j.1467-9280.2005.01645.x

Tombu, M. N., Asplund, C. L., Dux, P. E., Godwin, D., Martin, J. W., and Marois, R. (2011). A unified attentional bottleneck in the human brain. *Proc. Natl. Acad. Sci. U.S.A.* 108, 13426–13431. doi: 10.1073/pnas.1103583108

Tracy, J. I., Mohamed, F., Faro, S., Tiver, R., Pinus, A., Bloomer, C., et al. (2000). The effect of autonomic arousal on attentional focus. *Neuroreport* 11, 4037–4042. doi: 10.1097/00001756-200012180-00027

Tsai, Y.-F., Viirre, E., Strychacz, C., Chase, B., and Jung, T.-P. (2007). Task performance and eye activity: predicting be- havior relating to cognitive workload. *Aviat. Space Environ. Med.* 78, B176–B185.

Ullsperger, M., Danielmeier, C., and Jocham, G. (2014). Neurophysiology of performance monitoring and adaptive behavior. *Physiol. Rev.* 94, 35–79. doi: 10.1152/physrev.00041.2012

Ullsperger, M., Nittono, H., and von Cramon, D. Y. (2007). When goals are missed: dealing with self-generated and externally induced failure. *NeuroImage* 35, 1356–1364. doi: 10.1016/j.neuroimage.2007.01.026

Unsworth, N., and Engle, R. W. (2007). The nature of individ- ual differences in working memory capacity: active main- tenance in primary memory and controlled search from secondary memory. *Psychol. Rev.* 114, 104. doi: 10.1037/0033-295x.114.1.104

Uzzaman, S., and Joordens, S. (2011). The eyes know what you are thinking: eye movements as an objective measure of mind wandering. *Conscious. Cognit.* 20, 1882–1886. doi: 10.1016/j.concog.2011.09.010

Van Acker, B. B., Parmentier, D. D., Vlerick, P., and Saldien, J. (2018). Understanding mental workload: from a clarifying concept analysis toward an implementable framework. *Cognit. Technol. Work* 20, 351–365. doi: 10.1007/s10111-018-0481-3

Van Dongen, H., Belenky, G., and Krueger, J. M. (2011). A local, bottom-up perspective on sleep deprivation and neurobehavioral performance. *Curr. Top. Med. Chem.* 11, 2414–2422. doi: 10.2174/156802611797470286

Verwey, W. B., and Zaidel, D. M. (1999). Preventing drowsiness accidents by an alertness maintenance device. *Accident Anal. Prevent.* 31, 199–211. doi: 10.1016/s0001-4575(98)00062-1

Vijayraghavan, S., Wang, M., Birnbaum, S. G., Williams, G. V., and Arnsten, A. F. (2007). Inverted-U dopamine D1 receptor actions on prefrontal neurons engaged in working memory. *Nat. Neurosci.* 10:376. doi: 10.1038/nn1846

Weinmann, M., Schneider, C., and vom Brocke, J. (2016). Digital nudging. *Bus. Inform. Syst. Eng.* 58, 433–436. doi: 10.1007/s12599-016-0453-1

Weissman, D. H., Roberts, K. C., Visscher, K. M., and Woldorff, M. G. (2006). The neural bases of momentary lapses in attention. *Nat. Neurosci.* 9:971. doi: 10.1038/nn1727

Wickens, C. D. (1980). The structure of attentional resources. *Attent. Perform. VIII* 8, 239–257.

Wickens, C. D. (1984). "Processing resources in attention," in *Varieties of Attention*, eds R. Parasuraman and D. R. Davies (London: Academic Press), 63–101.

Wickens, C. D. (2002). Multiple resources and performance prediction. *Theor. Issues Ergon. Sci.* 3, 150–177.

Wickens, C. D. (2005). Attentional tunneling and task management. *Int. Symp. Aviat. Psychol.* 812–817.

Wickens, C. D. (2008). Multiple resources and mental work-load. *Hum. Fact.* 50, 449–455.

Wickens, C. D., and Liu, Y. (1988). Codes and modalities in multiple resources: a success and a qualification. *Hum. Fact.* 30, 599–616. doi: 10.1177/001872088803000505

Wickens, C. D., and Tsang, P. (2014). "Workload," in *Handbook of Human-Systems Integration*, ed. F. Durso (Washington, DC: APA).

Wickens, J. R., Horvitz, J. C., Costa, R. M., and Killcross, S. (2007). Dopaminergic mechanisms in actions and habits. *J. Neurosci.* 27, 8181–8183. doi: 10.1523/jneurosci.1671-07.2007

Wierwille, W. W., and Eggemeier, F. T. (1993). Recommendation for mental workload measurement in a test and evaluation environment. *Hum. Fact.* 35, 263–281. doi: 10.1177/001872089303500205

Yeh, Y. Y., and Wickens, C. D. (1988). Dissociation of performance and subjective measures of workload. *Hum. Fact.* 30, 111–120. doi: 10.1177/001872088803000110

Yerkes, R. M., and Dodson, J. D. (1908). The relation of strength of stimulus to rapidity of habit formation. *J. Compar. Physiol. Psychol.* 18, 459–482. doi: 10.1002/cne.920180503

Young, M. S., Brookhuis, K. A., Wickens, C. D., and Hancock, P. A. (2015). State of science: mental workload in ergonomics. *Ergonomics* 58, 1–17. doi: 10.1080/00140139.2014.956151

Young, M. S., and Stanton, N. A. (2002). Malleable attentional resources theory: a new explanation for the effects of mental underload on performance. *Hum. Fact.* 44, 365–375. doi: 10.1518/0018720024497709

Zander, T. O., and Kothe, C. (2011). Towards passive brain–computer interfaces: applying brain–computer interface technology to human–machine systems in general. *J. Neural Eng.* 8:025005. doi: 10.1088/1741-2560/8/2/025005

Zaneboni, J., and Saint-Jalmes, B. (2016). *U.S. Patent No.* 9,302,779. Washington, DC: U.S. Patent and Trademark Office.

Conflict of Interest: The authors declare that the research was conducted in the absence of any commercial or financial relationships that could be construed as a potential conflict of interest.

frontiers in Neuroscience

CLINICAL TRIAL
published: 19 May 2020
doi: 10.3389/fnins.2020.00464

Transcranial Static Magnetic Field Stimulation of the Motor Cortex in Children

*Asha Hollis[1], Ephrem Zewdie[2], Alberto Nettel-Aguirre[2], Alicia Hilderley[3], Hsing-Ching Kuo[2], Helen L. Carlson[2] and Adam Kirton[2]**

[1] Cumming School of Medicine, University of Calgary, Calgary, AB, Canada, [2] Department of Pediatrics, Cumming School of Medicine, University of Calgary, Calgary, AB, Canada, [3] Hotchkiss Brain Institute, Cumming School of Medicine, University of Calgary, Calgary, AB, Canada

OPEN ACCESS

Edited by:
Davide Valeriani, Harvard Medical School, United States

Reviewed by:
Wei-Peng Teo, Nanyang Technological University, Singapore
Isabelle Buard, University of Colorado Denver, United States

***Correspondence:**
Adam Kirton
adam.kirton@albertahealthservices.ca

Specialty section:
This article was submitted to Neural Technology, a section of the journal Frontiers in Neuroscience

Received: *10 September 2019*
Accepted: *15 April 2020*
Published: *19 May 2020*

Citation:
Hollis A, Zewdie E, Nettel-Aguirre A, Hilderley A, Kuo H-C, Carlson HL and Kirton A (2020) Transcranial Static Magnetic Field Stimulation of the Motor Cortex in Children. Front. Neurosci. 14:464. doi: 10.3389/fnins.2020.00464

Background: Non-invasive neuromodulation is an emerging therapy for children with early brain injury but is difficult to apply to preschoolers when windows of developmental plasticity are optimal. Transcranial static magnetic field stimulation (tSMS) decreases primary motor cortex (M1) excitability in adults but effects on the developing brain are unstudied.

Objective/Hypothesis: We aimed to determine the effects of tSMS on cortical excitability and motor learning in healthy children. We hypothesized that tSMS over right M1 would reduce cortical excitability and inhibit contralateral motor learning.

Methods: This randomized, sham-controlled, double-blinded, three-arm, cross-over trial enrolled 24 healthy children aged 10–18 years. Transcranial Magnetic Stimulation (TMS) assessed cortical excitability via motor-evoked potential (MEP) amplitude and paired pulse measures. Motor learning was assessed via the Purdue Pegboard Test (PPT). A tSMS magnet (677 Newtons) or sham was held over left or right M1 for 30 min while participants trained the non-dominant hand. A linear mixed effect model was used to examine intervention effects.

Results: All 72 tSMS sessions were well tolerated without serious adverse effects. Neither cortical excitability as measured by MEPs nor paired-pulse intracortical neurophysiology was altered by tSMS. Possible behavioral effects included contralateral tSMS inhibiting early motor learning ($p < 0.01$) and ipsilateral tSMS facilitating later stages of motor learning ($p < 0.01$) in the trained non-dominant hand.

Conclusion: tSMS is feasible in pediatric populations. Unlike adults, tSMS did not produce measurable changes in MEP amplitude. Possible effects of M1 tSMS on motor learning require further study. Our findings support further exploration of tSMS neuromodulation in young children with cerebral palsy.

Keywords: non-invasive brain stimulation, neurophysiology, pediatrics, neuromodulation, motor learning, tSMS

INTRODUCTION

Early brain injury can result in cerebral palsy (CP) and lifelong disability for millions (A Kirton, 2013a; Oskoui et al., 2016). Perinatal stroke (PS) is brain damage due to a focal disruption in cerebral blood flow occurring between 20 weeks gestation and 28 days postpartum (Dunbar and Kirton, 2018). PS causes most hemiparetic cerebral palsy (HCP) with disabling weakness on one side of the body. With no known treatment or prevention strategies, improving outcomes and quality of life in PS is focused on neurorehabilitation.

Non-invasive brain stimulation (NIBS) is an encouraging but understudied potential therapy for children with CP. Randomized trials suggest that repetitive transcranial magnetic stimulation (rTMS) (Gillick et al., 2015; Kirton et al., 2016) and transcranial direct current stimulation (tDCS) (Kirton et al., 2017; Gillick et al., 2018) may enhance motor learning in hemiparetic children. Proof-of-principle studies have demonstrated that the enhancement of motor learning seen in adults with tDCS of the primary motor cortex (M1) (Reis et al., 2009) also occurs in children (Ciechanski and Kirton, 2017; Cole et al., 2018). Although the safety of pediatric neurostimulation is becoming well established (Bikson et al., 2016; Friel et al., 2016), both rTMS and tDCS can have side effects, potentially limiting applications in younger children.

These neuromodulation approaches are based on evolving human and animal models of how the motor system develops following early unilateral injury (Eyre et al., 2007; Staudt, 2007a; Kirton, 2013b; Wen et al., 2018). Excessive preservation of motor control of the affected limb by the contralesional, ipsilateral hemisphere has led to trials trying "inhibitory" stimulation targeting contralesional M1. Animal models have also confirmed the optimal windows during which developmental motor plasticity occurs, with human equivalents occurring in infancy (Martin et al., 2011). Accordingly, a major limitation of existing neuromodulation approaches is difficulty of application in infants and toddlers, during the window in which one might expect the greatest potential therapeutic gains. There is therefore a need to find alternative forms of neuromodulation applicable at earlier stages of development.

Transcranial static magnetic field stimulation (tSMS) offers a potential solution. In tSMS, a strong magnet is held over the skull to generate a static magnetic field within functional cortical targets such as M1 (Oliviero et al., 2011; Kirimoto et al., 2016). Short-term application from 10 to 30 min in adults can decrease M1 excitability as assessed by the amplitude of transcranial magnetic stimulation (TMS)-generated motor-evoked potentials (MEPs). Original tSMS results have since been replicated (Silbert et al., 2013; Nojima et al., 2015; Nojima et al., 2016; Dileone et al., 2018) with only one study reporting no physiological changes (Kufner et al., 2017). tSMS effects have also been described in the cerebellum and parietal cortex (Carrasco-López et al., 2017; Matsugi and Okada, 2017). The effects of tSMS in the developing brain are unstudied.

Previous studies in the field have identified that use of south or north polarity did not alter the measured impact on cortical excitability, although most literature in the field still indicates use of south polarity by convention (Oliviero et al., 2011). Unlike polarity, magnet strength and duration of application are significant factors: stronger magnets (e.g. 45 × 30 mm versus 30 × 15 mm in size) and application for longer time periods (e.g. 30 min versus 10 min) have been shown to have a stronger and longer-lasting effect on cortical excitability.

Few investigations have explored the behavioral effects of tSMS. Two adult studies found that visual cortex tSMS could inhibit visual search performance and reduce experimental photophobia (Gonzalez-Rosa et al., 2015; Lozano-Soto et al., 2017). One study of tSMS over M1 suggested inhibitory effects on pinch force (Nakagawa and Nakazawa, 2018) while another found improved reaction times in an implicit motor learning task (Nojima et al., 2019). Studies support favorable safety and tolerability when tSMS was administered for up to 120 min (Oliviero et al., 2015). The safety, tolerability, and behavioral effects of tSMS have not been explored in children. However, a large volume of safety evidence comes from decades of MRI use where millions of patients have been exposed to much higher doses (1-8T) and durations (hours of exposure) of static magnetic fields (to much larger areas of tissue) with no significant adverse effects (van Osch and Webb, 2014). Furthermore, guidelines on safety of static magnetic field exposure conclude the evidence does not indicate the presence of serious health effects given acute exposure to up to 8T fields (International Commission on Non-Ionizing Radiation Protection, 2009).

Given its potential ease of application in young children and therapeutically relevant effects on M1 excitability, we aimed to evaluate whether tSMS could alter M1 excitability and motor learning in typically developing children. To the best of our knowledge, this is the first study of tSMS in a pediatric population. We conducted a randomized, sham-controlled, double-blinded, cross-over trial, hypothesizing that contralateral (right) M1 tSMS would decrease MEP amplitude and inhibit motor learning in the left hand.

MATERIALS AND METHODS

Trial Design

The Pediatric Transcranial Static Magnetic Field Stimulation to Improve Motor Learning (PSTIM) trial was a randomized, double-blinded, sham-controlled, three-arm, cross-over interventional trial. Methods complied with the consolidated standards of reporting trials (CONSORT) guidelines including pediatric considerations (Schulz et al., 2010). The trial was registered with www.clinicaltrials.gov (NCT03949712). Methods were approved by the University of Calgary Research Ethics Board (REB 18-0178).

Population

School-aged children were recruited through the population-based, volunteer Healthy Infants and Children Clinical Research Program (HICCUP[1]). Inclusion criteria were (a) written informed consent/assent, (b) age 8–18 years, (c) right-handed by

[1]www.hiccupkids.ca

self-report, and (d) typical development. Potential participants with any of the following were excluded: (a) diagnosis of any neurological, psychiatric or developmental disorder, (b) taking any neuroactive medications, (c) any contraindication to brain stimulation, and (d) pregnancy.

Randomization, Blinding, and Concealment

Participants were computer-randomized into three groups which determined intervention order: (A) Sham, Right tSMS, Left tSMS; (B) Left tSMS, Sham, Right tSMS; and (C) Right tSMS, Left tSMS, Sham. A second randomization assigned the sham stimulation side, such that half of the participants in each group had sham on the left and half on the right. Participants, parents and the primary researcher conducting tSMS and analysis were blinded to randomizations. Only a research assistant was unblinded in order to apply the correct intervention. Participants were asked to guess if they received real or sham tSMS. The randomization code was broken to the primary researcher only after the final outcome and initial analysis was completed.

Outcome Measures

Neurophysiological

The primary outcome of this study (and the main neurophysiological outcome) was right M1 excitability as measured by mean MEP amplitude generated in the left first dorsal interosseous (FDI) muscle. This was chosen to enable comparison of M1 excitability before and after application of the tSMS intervention. TMS is an established, safe and well tolerated method in children (Zewdie and Kirton, 2016). Previously described single and paired-pulse TMS methods were applied to assess motor system neurophysiology (Zewdie and Kirton, 2016). All experiments took place in the Alberta Children's Hospital Pediatric Neurostimulation Laboratory where children had opportunity to test procedures beforehand and watch movies when possible for distraction from the TMS stimulation and to help reduce potential fatigue.

To measure MEPs, surface electromyography (EMG) was recorded by placing Ag/AgCl electrodes on the belly of the FDI muscle. A reference electrode was placed on the second phalange, with a ground on the ulnar head. EMG signals were amplified x1000 (2024F Isolated amplifier; Intronix Technologies Corp, ON, Canada), band-pass filtered (20–2000 Hertz (Hz)), and recorded (CED1401 signal analog/digital converter; Cambridge Electronic Design, Cambridge, United Kingdom).

First, single-pulse TMS (Magstim 200, Magstim, Cardiff, United Kingdom) used a flat iron Magstim TMS coil to locate the right and left M1 "hotspots", defined as the location producing the largest and most consistent MEP (Zewdie and Kirton, 2016). The coil was placed at a 45-degree angle to the midline to induce a posterior-anterior current using monophasic waveforms. The identified "hotspot" was marked using neuronavigation (Brainsight2, Rogue Research, Montreal) to facilitate accurate coil replacement for serial measurements. Single-pulse TMS was then delivered to determine resting motor threshold (RMT) defined as the lowest stimulation intensity producing a 50 microvolts (μV) MEP in 5/10 stimulations. Ten suprathreshold (120% RMT) stimulations were administered to estimate cortical excitability.

Paired-pulse TMS was then completed using two connected stimulators (Magstim bi-stim, Magstim, Cardiff, United Kingdom). Consistent with other studies, pairs of pulses were delivered, which included a conditioning stimulus (CS) (80% RMT) followed by a test stimulus (TS) (120% RMT) (Zewdie and Kirton, 2016). Interstimulus intervals (ISIs) of 2 ms and 10 ms were used to evoke short-interval intracortical inhibition (SICI) and intracortical facilitation (ICF), respectively. A total of 30 pulses were administered in random order: 10 test single pulses, 10 paired pulses (2 ms ISI), and 10 paired pulses (10 ms ISI).

MEP signal files were imported into MATLAB R2011b (Mathworks, Inc., Natick, MA, United States) for offline analysis. Visual inspection was used to identify artifacts including baseline motor activity; proportion of traces removed was less than 5%. Peak-to-peak MEP amplitude values were calculated using a custom MATLAB script, which identified maximum and minimum MEP values within 15–80 ms after TMS. Mean peak-to-peak MEP amplitudes were averaged. SICI and ICF ratios were computed by dividing the average MEP amplitude of the conditioned responses into that of the test stimuli alone.

Behavioral

The main behavioral outcome was change in the Purdue Pegboard Test (PPT) left-hand score (PPT_L). This enabled assessment of motor skill performance before, during and after application of the tSMS intervention. The PPT is a validated simple motor task that requires both gross and fine motor skills, described in detail in the cited reference (Gardner and Broman, 1979). The PPT produces consistent motor learning curves in school-aged children across multiple sessions (Tiffin and Asher, 1948; Gardner and Broman, 1979; Ciechanski and Kirton, 2017; Cole et al., 2018). The PPT consists of four tasks. For the PPT_L, the participant used their left hand to move as many metal pegs into holes in the pegboard as fast as possible in 30 s. Following a 1-min break, the same task was performed with the right hand (PPT_R). Following another 1-min break, the task was performed using both hands at the same time (PPT_{LR}). Finally, 1-min was given to assemble a pin-washer-collar-washer structure using alternating hands for each metal piece (PPT_A). All sections were repeated three times and averaged.

Intervention

The intervention was tSMS (or sham) over left M1 (ipsilateral) or right M1 (contralateral), modeled on previous adult studies (Oliviero et al., 2011; Silbert et al., 2013; Dileone et al., 2018). A strong cylindrical Neodynium magnet (S-45-30-N, Supermagnete) or a sham magnet (MAG45s, Neurek SL, Toledo, Spain) was affixed over the M1 hotspot using a custom-designed helmet (**Figure 1**). The sham magnet was identical in appearance and weight but carried no magnetic properties. The custom helmet allowed for movement in the anterior-posterior, superior-inferior and medial-lateral directions. Neuronavigation was utilized to place the magnet over the previously identified

FIGURE 1 | Custom-Engineered tSMS Helmet. Custom designed and partially 3-D printed helmet used for application of tSMS with neuronavigation.

hotspot. The magnet was applied with South polarity (determined using a compass), consistent with previous adult studies (Oliviero et al., 2011). Magnet dimensions were 30 mm tall × 45 mm wide with an estimated strength of 300–450 milliTesla (mT) at the cortex (Tharayil et al., 2018).

Study Flow

The timeline and flow of the study is diagrammed in **Figure 2**. On visit 1, all baseline behavioral and neurophysiological measures were obtained. Participants first performed the PPT_L outcome. Additional behavioral outcomes of PPT_R, PPT_{LR} and PPT_A were then performed. The M1 hotspots for FDI were mapped followed by the single and paired pulse measurements, including RMT.

Following a short break, the magnet-holding device was affixed to the participant's head. Size was adjusted for head shape and comfort. The magnet was positioned on the skull over the left or right M1 hotspot as identified by neuronavigation. The magnet was then held in place for 30 min. During this time, participants trained the non-dominant left hand by performing the PPT_L five times (minutes 7, 12, 17, 22, and 27). The non-dominant hand was targeted to enable skill growth from baseline, given the common assumption of lower skill in the non-dominant hand. TMS studies have also suggested differences in excitability between the dominant and non-dominant hemisphere (Daligadu et al., 2013) but we could only examine one. Use of the non-dominant hand is consistent with prior motor skill learning research by our team and others (Ciechanski and Kirton, 2017; Cole et al., 2018).

After completion of tSMS, the magnet and holding device were removed. The RMT of the right M1 hotspot (identified via neuronavigation) was then re-measured and the TMS neurophysiological measurements were repeated at minutes 5, 10,

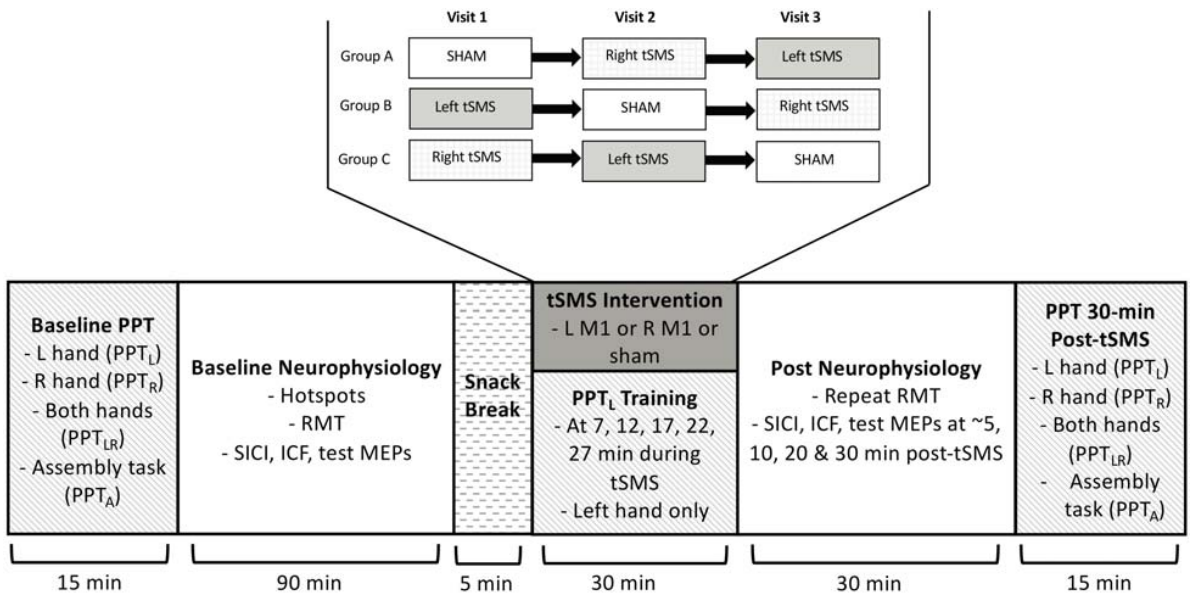

FIGURE 2 | PSTIM protocol. Participants completed baseline PPT (all tasks: PPT_L, PPT_R, PPT_{LR}, PPT_A), and then underwent baseline neurophysiology testing, including determining the "hotspot", identifying the RMT, and performing single and paired pulse protocols for test MEPs, SICI and ICF. They then received the tSMS intervention paired with motor training on the PPT_L. There were 3 treatment orders, as shown. Neurophysiology measures (single and paired pulse) and PPT (all tasks) were repeated at multiple time intervals post-tSMS.

20, and 30 post-tSMS. Finally, all PPT tasks (PPT_L, PPT_R, PPT_{LR}, and PPT_A) were repeated at approximately 35 min post-tSMS.

On visits 2 and 3, all procedures were repeated, with the exception of varying the intervention according to the randomized group. Each visit was scheduled to occur not less than two and not more than 4 weeks (+/- 4 days) from the previous one.

Safety and Tolerability

Participants completed a pediatric tSMS and TMS safety and tolerability survey at the end of each session as previously described (Garvey and Gilbert, 2004; Cole et al., 2018). Participants were asked to rank the tolerability of the tSMS or TMS session in comparison to seven common childhood experiences (e.g. birthday party, shot at the doctor). Participants were also asked to report the presence and severity of any symptoms experienced including headaches, neck pain, unpleasant tingling or itching, fatigue, nausea, and light-headedness. All procedures were performed by trained personnel. Requests for additional breaks were accommodated.

Sample Size

Sample size was determined based on the primary outcome (MEP amplitudes) using effect sizes in adults as a guide. Based on our crossover design, an expected (conservative) decrease of MEP amplitude in the stimulated M1 from approximately 1 millivolts (mV) to 0.9 mV compared to no change in sham, power of 90%, standard deviation (SD) of 0.1, and alpha of 0.05, we estimated a sample size of 24 (8 per group).

Statistical Analysis

Given our primary neurophysiological and secondary behavioral outcomes, crossover design, and aim to explore effects both between and within subjects, we employed a linear mixed effects model. Fixed effects were considered for treatment (left tSMS, right tSMS or sham), visit (1, 2 or 3), age, and an interaction between treatment and visit (visit effects were only considered for PPT). For change in PPT_L, PPT_R, PPT_{LR}, and PPT_A on visit 1 only, we also employed a simple linear regression with independent variables of treatment and age. The Shapiro–Wilks test was used to assess normality of distribution of residuals, and the Breusch-Pagan/Cook-Weisberg test was used to assess heteroskedasticity of residuals. Analyses of variance (ANOVAs) were also utilized to compare group demographics and ensure there were no significant differences in age, sex, and baseline PPT scores between groups. Analyses were performed using Stata 14.2.

RESULTS

Population

A total of 131 potential participants were approached. Thirty participants were recruited. Six were subsequently excluded due to self-withdrawal for scheduling conflicts ($n = 2$), incorrect order of intervention ($n = 1$), and high RMT that precluded the TMS protocol ($n = 3$). The final sample of participants who consented and completed the study consisted of 24 participants (13 males) with a median age of 15.9 years (range 10–18). Participant demographics and baseline motor function are summarized in **Table 1**. Groups were comparable with no differences in age, sex, or function.

TABLE 1 | Participant demographics and baseline PPT_L scores[1].

	Group A	Group B	Group C	Mean
Age	14.96 (2.60)	15.12 (2.19)	15.63 (1.92)	15.23 (2.25)
Sex (F:M)	4:4	4:4	3:5	11:13
Baseline PPT_L	14.17 (1.67)	13.67 (0.84)	14.04 (1.17)	13.96 (1.23)
Baseline PPT_R	16.79 (0.80)	15.83 (1.46)	15.25 (1.93)	15.29 (1.55)
Baseline PPT_{LR}	13.25 (1.23)	12.33 (0.78)	12.13 (0.89)	12.57 (1.07)
Baseline PPT_A	36.21 (8.38)	37.08 (5.95)	35.42 (5.82)	36.24 (6.55)

[1]*Values reported are group means (SD), with the exception of sex, reported as a ratio of females:males.*

Baseline Neurophysiology Measurements

TMS data were obtained from all participants. RMT ranged from 37% to 77% of maximum stimulus output (MSO) (mean 49.29, SD = 9.61). Baseline RMT was negatively correlated with age ($r = -0.56$, $p < 0.01$). Mean (SD) test MEP amplitude from all participants at baseline was 1.28 (1.1) mV. SICI and ICF were present with test MEP inhibited by the 2 ms subthreshold CS (0.57 (0.5) mV) and facilitated by the 10 ms CS (1.62 (1.29) mV). Raw MEP averages are shown in **Figure 3A**. Mean ratios of raw conditioned/raw test MEPs for SICI (0.47 (0.31)) and raw conditioned/raw test MEPs for ICF (1.41 (0.48)) were robust and consistent with expected SICI and ICF ratios in children (**Figure 3B**).

Effects of tSMS on M1 Neurophysiology

MEP amplitudes did not change significantly between baseline and the immediate (5 min) post-tSMS measurement regardless of treatment group. Change in individual raw test MEP amplitudes are shown in **Figure 4** by treatment group. MEP amplitudes 5 min post-left or -right tSMS and normalized to baseline did not change as compared to sham (left tSMS 95% confidence interval (CI) −0.19, 0.64; $p = 0.29$; right tSMS 95% CI −0.38, 0.44; $p = 0.89$). In addition to these results for the presumed maximal effect time at 5 min, no changes were seen at 10, 20 or 30 min post-tSMS either. RMT also did not change between baseline and follow-up for any treatment group.

Measurements of SICI and ICF ratios from baseline to immediately post-tSMS are summarized in **Figure 5**. Changes in intracortical physiology following right tSMS, left tSMS and sham tSMS and normalized to baseline did not appear different between groups (all $p > 0.24$). Although results are only shown for 5-min post-tSMS, no significant changes were observed at 10, 20 or 30 min post-tSMS either (all $p > 0.1$).

Effects of tSMS on Motor Learning Behavior

All participants demonstrated motor learning curves consistent with previous pediatric studies (Ciechanski and Kirton, 2017;

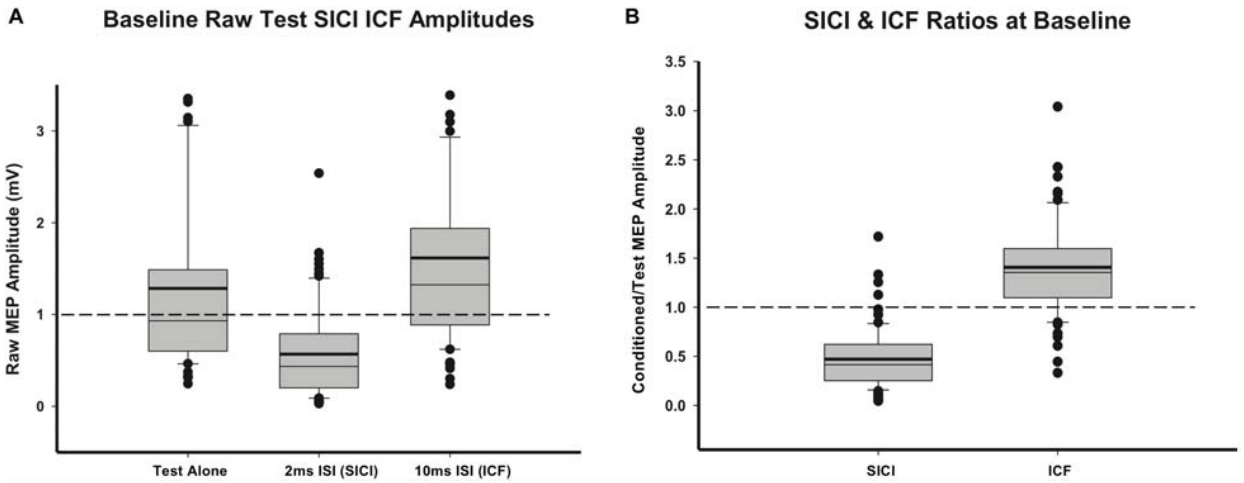

FIGURE 3 | Baseline TMS data. **(A)** Baseline raw MEP values for test-pulse MEPs and paired-pulse (SICI and ICF) MEPs. **(B)** SICI and ICF ratios at baseline, calculated as raw SICI or ICF MEPs divided by raw test MEPs. Thick lines indicate mean value.

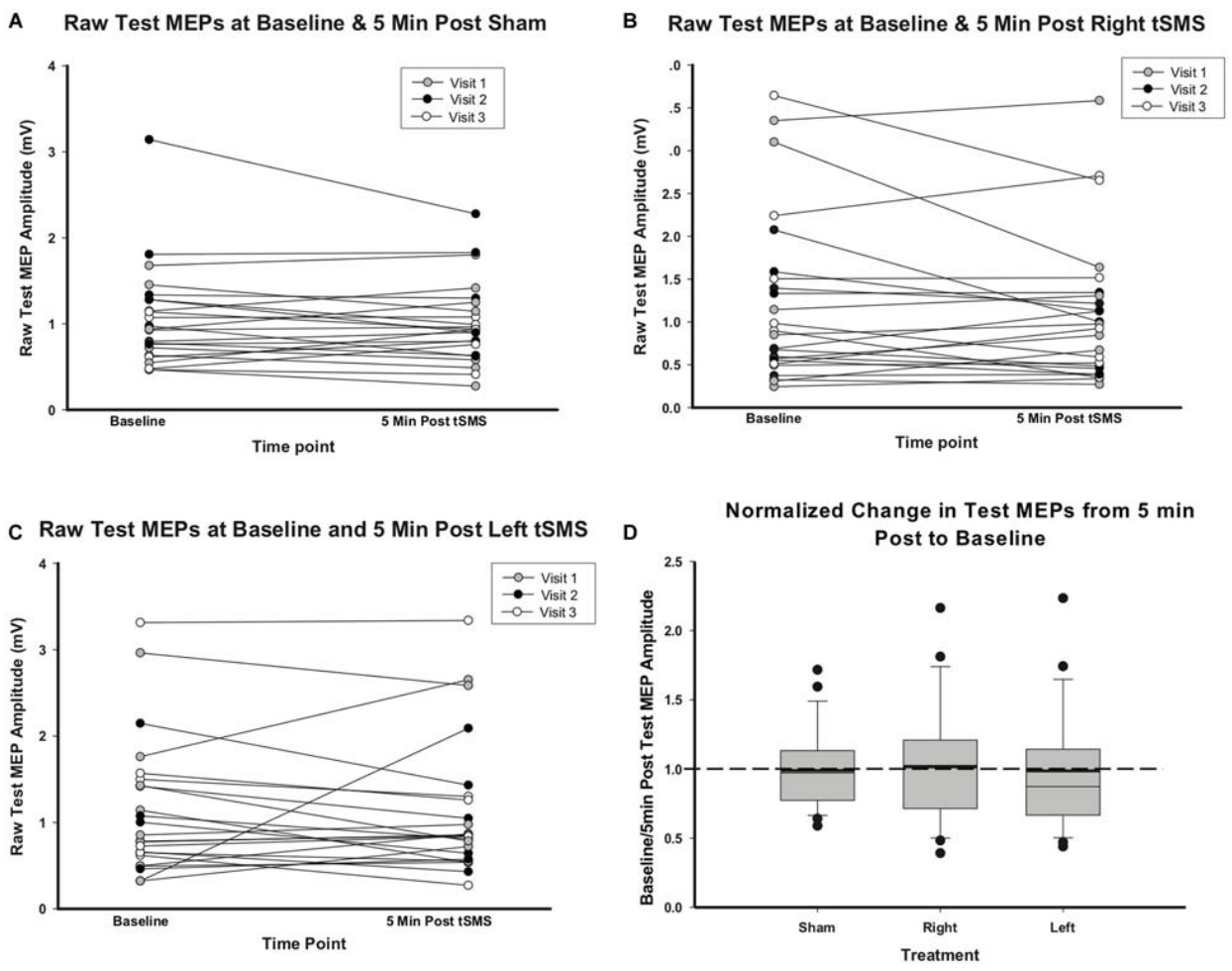

FIGURE 4 | Effect of sham, left and right tSMS on corticospinal excitability. **(A)** Raw test MEP values at baseline and 5 min post-sham tSMS. **(B)** Raw test MEP values at baseline and 5 min post-right tSMS. **(C)** Raw test MEP values at baseline and 5 min post-left tSMS. **(D)** Change in test MEPs from baseline to 5 min post-tSMS, normalized to baseline test MEPs. Thick lines indicate mean value.

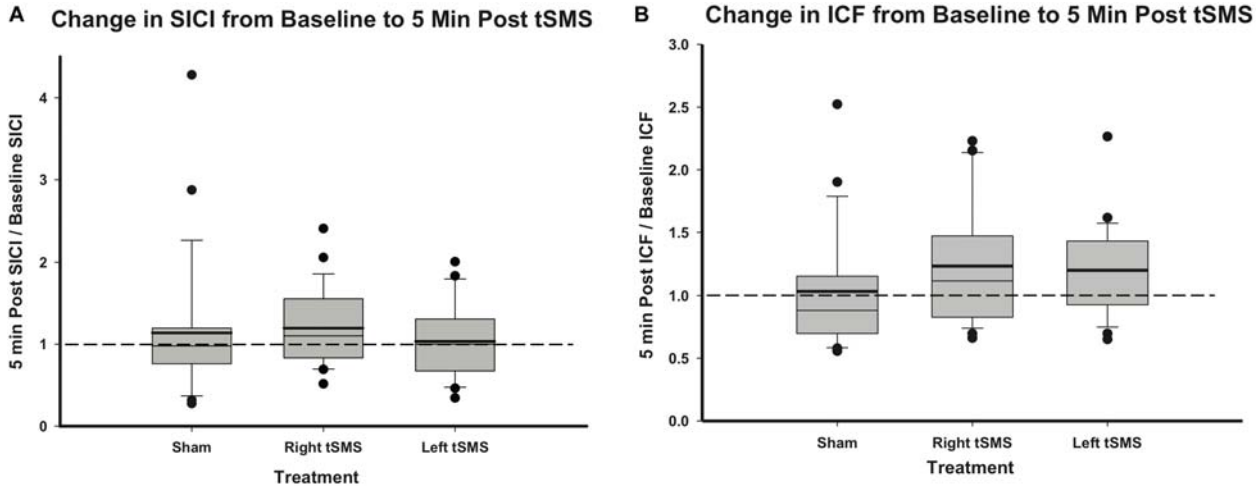

FIGURE 5 | Effect of sham, right and left tSMS on intracortical excitability. **(A)** Change in SICI ratio from baseline to 5 min post-tSMS, calculated as SICI ratio 5 min post-tSMS divided by the SICI ratio at baseline. **(B)** Change in ICF ratio from baseline to 5 min post-tSMS, calculated as ICF ratio 5 min post-tSMS divided by the ICF ratio at baseline. Thick lines indicate mean value.

Cole et al., 2018). Curves of motor learning by intervention for visit 1 are shown in **Figure 6A**. Learning differed by intervention group. On average, participants who received sham tSMS improved by 3.21(1.70) pegs by their final PPT. Those receiving left M1 tSMS improved by 2.50(1.14) pegs by their final PPT. Participants receiving right M1 tSMS improved by 1.88(0.99) pegs on their final PPT. The linear mixed effects model conditional upon age and visit suggested the effect of left tSMS compared to sham was a 0.74 *reduction* in pegs moved (95% CI −1.72, 0.25;$p = 0.14$). The effect of receiving right tSMS compared to sham was a 1.47 *reduction* in pegs moved (95% CI −2.46, −0.48;$p < 0.01$). The Cohen's *d* for sham versus right tSMS was 0.96. The same pattern of group differences was observed at the retention timepoint 30 min following completion of tSMS with a 1.36 *reduction* for right tSMS (95% CI −2.33, −0.39; $p < 0.01$) and 0.52 *reduction* (95% CI −1.48,0.45; $p = 0.26$) for left tSMS. No significant treatment group effects were seen for the other motor outcomes (**Figure 6D**). Greater variance in these other secondary motor outcomes is consistent with other similar studies. The Shapiro–Wilks test and the Breusch-Pagan/Cook-Weisberg test revealed normality and homoskedasticity of residuals could not be rejected, giving us confidence in our estimation methodology.

No significant changes were seen in the PPT_L task on visit 2 (**Figure 6B**) or any other secondary behavioral outcomes. On visit 3, treatment group specific differences were observed in motor learning curves (**Figure 6C**). Participants who received left tSMS experienced a *greater* improvement in PPT_L scores compared to the sham group. Conditional on age and visit, those who received left tSMS moved 1.47 *more* pegs than those receiving sham (95% CI −0.48, −2.46; $p < 0.01$). The Cohen's *d* for sham versus left tSMS was −1.22. The improvement with left tSMS compared to sham was consistent at the retention timepoint 30 min following tSMS (1.60 improvement, 95% CI 0.64, 2.58; $p = 0.001$). Change in pegs moved for those who received right tSMS did not differ from the other groups ($p = 0.62$). The sham group did not change from baseline on visit 3. Motor learning from original baseline for all participants by treatment group is shown in **Figure 7**.

Tolerability and Safety of tSMS

A total of 72 tSMS sessions were completed without any serious adverse events. The most common reported side effects of tSMS were headaches (Real: 19% mild, 2% moderate; Sham: 25% mild) and neck-pain (Real: 19% mild, 2% moderate; Sham: 8% mild). Other reported side effects were fatigue (Real: 8% mild, 2% moderate; Sham: 8% mild), light-headedness (Real: 2% mild; Sham 8% mild) and unpleasant tingling (Real: 2% mild; Sham 4% mild). On the pediatric brain stimulation tolerability scale, mean tSMS score was 4.06/10 (+/−1.17). This average ranked as less favorable than watching television (TV) (2.70) but more favorable than a long car ride (5.36) (**Figure 8**). The 144 TMS neurophysiology sessions were also well tolerated. The most common side effects were fatigue (24% total; 21% mild, 3% moderate) and headaches (14% total; 13% mild, 1% moderate). Others were neck pain (11% mild), unpleasant tingling (4% mild) and light-headedness (3% mild). Mean tolerability score was 4.03 (+/- 1.21), again falling between watching TV (2.07) and a long car ride (5.28) (**Figure 8**). When participants were asked if they would recommend the study to a friend, 100% said yes ($n = 21$; three participants were missed).

DISCUSSION

In this trial, we evaluated the effects of tSMS on cortical neurophysiology and motor learning in a pediatric population. We show that tSMS is feasible, well tolerated and safe in school-aged children. Our results suggest that contralateral tSMS may have inhibitory effects on motor learning while stimulation of the ipsilateral hemisphere may enhance later stages of learning, although this requires additional study. We were not able to

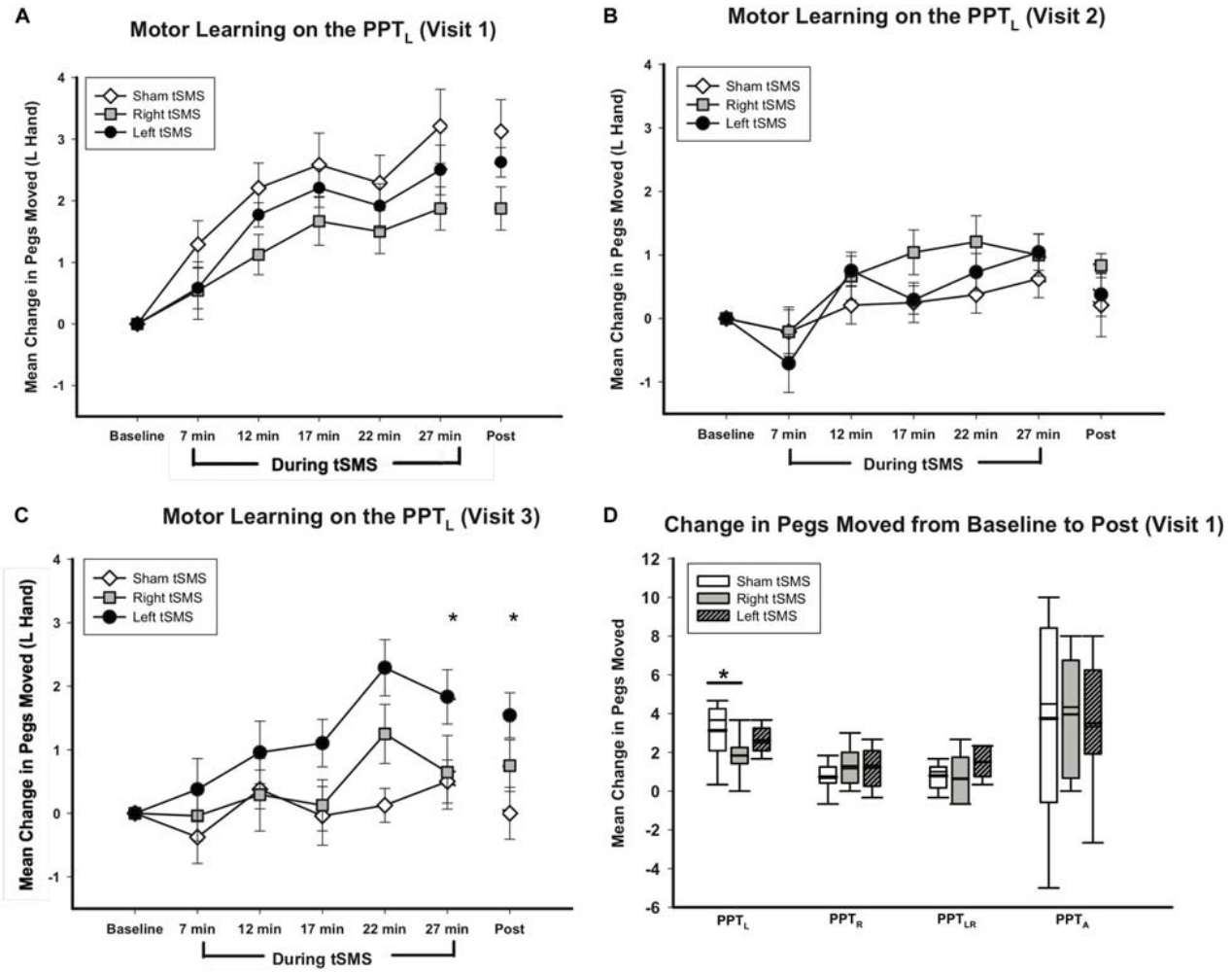

FIGURE 6 | Trained left hand motor learning by intervention. **(A–C)** Show trained left hand motor learning on PPT_L, **(D)** shows change in all PPT tasks. **(A)** Mean change in pegs moved from visit 1 baseline for PPT_L was greater for sham (white diamonds) than for left (gray squares) or right tSMS (black circles). Effects were retained for all groups 30 min post-tSMS. Error bars show standard error. $^*p < 0.01$ for right tSMS vs sham. **(B)** Mean change in pegs moved from visit 2 baseline for PPT_L were not statistically significantly different for sham (white diamonds), left (gray squares) or right tSMS (black circles) on visit 2. **(C)** Mean change in pegs moved from visit 3 baseline for PPT_L was greater for left (black circles) than for sham (white diamonds). Effects were retained 30 min post-tSMS. Error bars show standard error. $^*p < 0.01$ for left tSMS vs sham. **(D)** Mean change in pegs moved from baseline for PPT_L was greater for sham (white box) than for left (striped box) or right tSMS (gray box) at 30 min post tSMS. No statistically significant changes in pegs moved occurred for PPT_R, PPT_{LR}, or PPT_A for left or right tSMS compared to sham. Thick lines indicate mean value. Error bars show standard error. $^*p < 0.01$ for right tSMS vs sham for PPT_L on visit 1.

replicate the neurophysiological effects of tSMS reported in most adult studies.

Since the introduction of tSMS (Oliviero et al., 2011), numerous studies have tested the effect of contralateral tSMS on cortical neurophysiology over M1 and other cortical brain regions in healthy adults. The most consistent net tSMS effects have been inhibitory in nature, often demonstrating reduced excitability such as in the motor cortex where TMS-evoked MEP amplitudes are reduced (Oliviero et al., 2011; Silbert et al., 2013; Dileone et al., 2018). The mechanism behind tSMS is not yet known, but it is thought that tSMS may act by indirectly altering ion channels in cell membranes (Rosen, 2003). Surprisingly, contralateral tSMS in children did not generate similar results. Although we hypothesized there would be an inhibition of MEP amplitudes, we found no evidence of consistent effects of contralateral (or ipsilateral) tSMS on any of our neurophysiological outcomes. This included our measures of intracortical motor neurophysiology (SICI and ICF) where again no effects were observed.

Multiple potential contributing factors may account for this discrepancy from the tSMS effects described in adults. Our study tested tSMS for the first time in a pediatric population where the many known differences of the developing brain may have been a factor. Many other studies of different forms of NIBS (TMS, tDCS) have identified distinct differences in effects in children as compared to adults (Moliadze et al., 2015; Ciechanski et al., 2018). It may also be more difficult to discern changes in intracortical neurophysiology in children compared to adults.

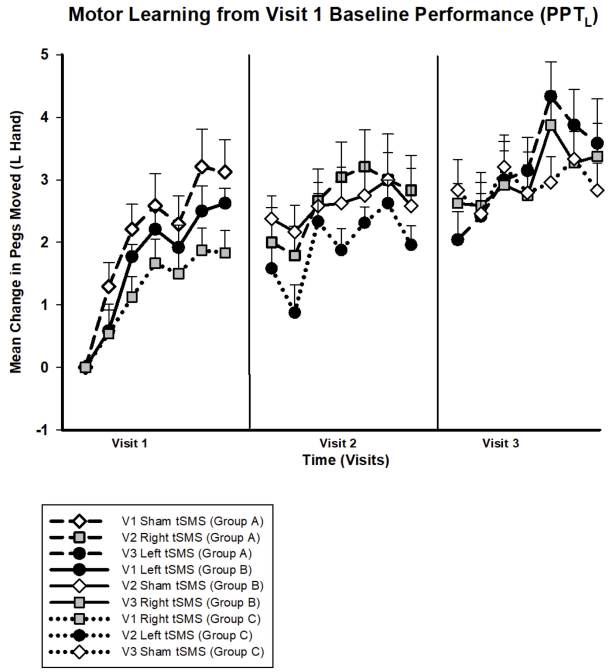

FIGURE 7 | Trained left hand motor learning by intervention for all visits. Mean change in pegs moved from visit 1 baseline for PPT$_L$. All groups experienced motor learning from baseline. Symbols indicate intervention: sham (white diamonds), right (gray squares) or left tSMS (black circles). Lines indicate participant group: group A (dashed), group B (straight), group C (dotted), for which each group contains the same participants. Error bars show standard error.

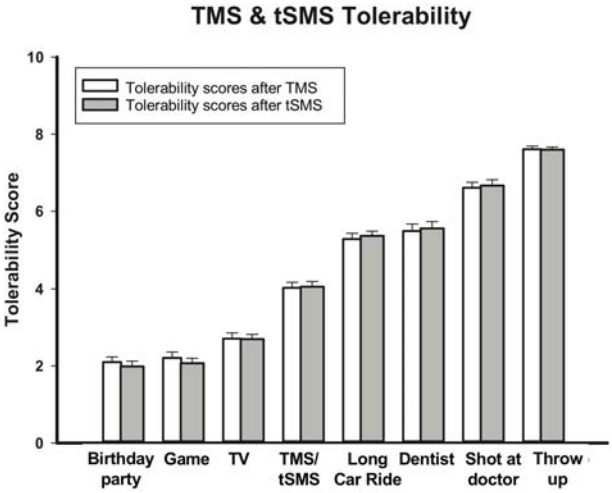

FIGURE 8 | tSMS and TMS Tolerability. Bars show tolerability score out of 8 (higher scores indicate less tolerability for various childhood experiences in comparison to TMS and tSMS. tSMS and TMS are both more tolerable than a long car ride, but less tolerable than watching TV. Error bars show standard error.

For example, SICI may be more difficult to elicit in children, and can be differentially affected by practice- or use-dependent plasticity (Garvey and Mall, 2008). The combination in our study of both a pediatric population and concomitant motor training and neuromodulation by tSMS may have further complicated our ability to detect changes in TMS measures of M1 neurophysiology.

TMS data are also intrinsically noisy. TMS neurophysiology outcomes depend on a variety of factors, such as muscle contraction, fatigue, and attention (Darling et al., 2006; Li et al., 2015). Additional factors influencing TMS neurophysiology established in adults such as gender, sleep, medications, and genetics have not been well defined in children (Ridding and Ziemann, 2010). Reliability of the measures themselves also varies. Studies of test-retest reliability in adults have established the natural variability in the data and also that this variability changes for different measures. For example, reliability of ICF and SICI measures are lower than for RMTs (Schambra et al., 2015; Hermsen et al., 2016). Even simple test stimuli demonstrate greater variability when participants are relaxed as compared to holding an active contraction (Darling et al., 2006). While the same reliability studies have not been completed in children, there are reasons to expect the same issues are at least as relevant, if not potentially more so.

Another factor unique to our study design was that TMS measures of neurophysiology had to be acquired in conjunction with the execution and measurement of motor training. This not only complicates the measurements themselves but introduces potential noise from the effects of motor learning. Previous literature assessing motor learning has shown effects on cortical neurophysiology. For example, multiple studies have shown increases in MEP amplitudes measured from hand muscles following hand motor training (Muellbacher et al., 2001; Cirillo et al., 2010). Furthermore, pharmacological studies have shown that plastic changes associated with motor learning may share mechanistic similarities with neurostimulation such as long-term potentiation (Butefisch et al., 2000). It is therefore possible that our pairing of motor training with tSMS may have altered the potential neurophysiological effects of tSMS (Foffani and Dileone, 2017). Further studies comparing tSMS alone versus tSMS combined with motor training in children would be required to determine this.

Behaviorally, we were able to demonstrate that tSMS over M1 may modulate motor learning in children. Effects appeared to be specific to both the side of stimulation and timing across multiple motor learning sessions. Consistent with our clinical hypothesis, right contralateral M1 tSMS significantly inhibited motor learning in the trained, left hand as assessed by the PPT$_L$. Effects were consistent across the learning curve which itself was comparable to previously described single day PPT learning curves in children (Ciechanski and Kirton, 2017; Cole et al., 2018). Specificity of effect to the trained hand was further suggested by the absence of other significant changes in any of the other secondary motor function outcomes (PPT$_R$, PPT$_{LR}$, PPT$_A$). While our observed behavioral effects require replication, they would appear to be of similar magnitude and effect size as described for more studied forms of M1 non-invasive neuromodulation.

In contrast to the inhibitory effects of contralateral (right) tSMS on left hand motor learning, we found that after multiple days of motor training, ipsilateral (left) tSMS had a facilitatory effect on left hand motor learning as measured by the PPT_L. This potential effect was hypothesized *a priori* based on previous studies of the effects of ipsilateral M1 rTMS and tDCS on hand motor learning. Though many exceptions are now recognized, anodal tDCS has often been suggested to increase cortical excitability while cathodal-tDCS may decrease cortical excitability (Batsikadze et al., 2013; Monte-Silva et al., 2013). In keeping with this simple model, previous adult studies have shown that anodal tDCS can facilitate motor learning when applied to the contralateral M1 (Vines et al., 2006; Reis and Fritsch, 2011). In addition, cathodal tDCS applied to the opposite, ipsilateral M1 has also been shown to facilitate motor learning (Reis and Fritsch, 2011). One study comparing these effects of M1 tDCS on motor learning directly (Vines et al., 2006) found that cathodal tDCS applied ipsilaterally improved motor learning, contralateral cathodal tDCS inhibited it, and anodal tDCS had the opposite effects (contralateral improvement, and ipsilateral inhibition). This body of adult evidence supports the concept that cathodal tDCS may improve motor learning via modulation of well-established inhibitory transcallosal pathways (interhemispheric inhibition (IHI)) which itself is associated with motor function in adults (Williams et al., 2010). Such "disinhibition" by ipsilateral cathodal stimulation might enable relative "excitation" of the opposite motor cortex, in turn facilitating motor learning (Vines et al., 2006). That TMS measures of IHI appear to be similar in school-aged children as compared to adults (Ciechanski et al., 2017) further supports this premise.

Translationally, these behavioral effects of M1 tSMS may be relevant to stroke rehabilitation. A theory of IHI imbalance has dominated early approaches to non-invasive neuromodulation of the contralesional hemisphere, though this model has more recently been questioned. Neuromodulation strategies aiming to reduce cortical excitability in the contralesional hemisphere have been associated with improved motor performance in chronic stroke (Hsu et al., 2012; Elsner et al., 2017).

Although the underlying models are different, a smaller but significant body of evidence has supported the same approach of inhibiting the contralesional motor cortex in children with PS and HCP (Kirton, 2013b). Substantial preclinical (Martin et al., 2007; Friel et al., 2013; Friel et al., 2014; Wen et al., 2018) and human (Eyre, 2007; Staudt, 2007b) evidence following early brain injury supports a negative association between the relative preservation of ipsilateral corticospinal projections from the contralesional hemisphere to the affected hand and clinical motor function. Targeting these ipsilateral tracts on the contralesional side thus has the potential to improve motor function. Multiple translational trials show both contralesional low frequency rTMS (Gillick et al., 2014; Kirton et al., 2016) and cathodal tDCS (Kirton et al., 2017; Gillick et al., 2018) may enhance therapy-induced gains in clinical function.

Our results here provide preliminary evidence that tSMS might provide an alternative application to achieve similar M1 inhibitory effects, although additional research exploring this is needed. The simplicity of tSMS, including potential ease of application to very young children, possibly paired with infant therapy in the home environment, is particularly appealing.

Our study has also established the tolerability and feasibility of tSMS in children. Rankings of tolerability were comparable with pediatric studies of motor cortex TMS and tDCS (Kirton et al., 2016; Cole et al., 2018; Zewdie et al., 2018). The most common side effects were mild headaches and neck pain. By both our observations and subject report, we believe many of these effects were largely due to the weight of the magnet itself. While our tSMS magnet weighed only 360 g (less than 1 pound), its mass was relatively highly concentrated on a small area of the skull due to its small diameter. Additional modifications to either better support the weight of the magnet (or otherwise redistribute the weight) may be helpful in improving tolerability further.

Several important limitations are noted. Our study was limited by an informed but modest sample size of 24 participants. Given the variability of TMS outcomes discussed above, larger sample sizes would certainly have been beneficial. Furthermore, with only 8 participants per treatment group, our ability to detect specific differences may have been reduced, emphasizing the need for our crossover design to be replicated in future studies. The crossover design did increase power for our neurophysiological outcomes but posed challenges for our clinical outcomes for which there may have been carry-over effects. Motor training on the PPT does not fully wash-out and can reach a plateau. As such, effect sizes on visits two and three were limited by previous motor training, and potentially by the intervention(s) received on prior visits. Therefore, potential motor learning effects of tSMS require additional studies designed primarily to assess behavioral outcomes. The 3-h study visits were tiring, especially for younger participants, although we tried to mitigate this with a snack break midway through each visit. We were not able to account for all factors that might have influenced our outcomes including fatigue, genetics, and attention (Li et al., 2015).

Ultimately, our data suggests that tSMS over M1 may modulate motor learning in children with specific effects of location and timing but this finding would benefit from further research. Our results also suggest that neurophysiological changes may differ in children compared to adults, and further research to determine neurophysiological effects of tSMS is required. Translationally, this study opens new opportunities for exploration into clinical trials of tSMS as a simple, non-invasive method to modulate motor learning in children with CP, with the ultimate goal of home-based, personalized, neuromodulation therapy during optimal windows of developmental plasticity.

DATA AVAILABILITY STATEMENT

All relevant data generated and analyzed for this study is included in the article.

ETHICS STATEMENT

The studies involving human participants were reviewed and approved by the University of Calgary Research Ethics Board.

Written informed consent to participate in this study was provided by the participants or participants' legal guardian/next of kin.

AUTHOR CONTRIBUTIONS

AHo contributed to the study design, recruitment of participants, data collection and analysis, and drafting and revising the manuscript. EZ contributed to the study design, data collection, data analysis, and revising the manuscript. HC, AHi, and H-CK contributed to the data collection, drafting and revising the manuscript. AN-A contributed to the data analysis and revising the manuscript. AK contributed to the obtaining funding, study design, and revising the manuscript. All authors reviewed and approved the final version for submission.

FUNDING

This work was supported by the Canadian Institutes of Health Research [grant number FDN-143294].

ACKNOWLEDGMENTS

Support from Adrianna Giuffre, Brandon Craig, Zahra Ofoghi, Dion Kelly, Anju Hollis, Shaelene Standing, Daria Merrikh, Julia Batycky, Tanaeem Rehman, Hana Osman and Susana Puche-Saud for their generous assistance with study sessions is gratefully acknowledged. We thank Ion Robu for all of his hard work assisting with designing and creating the helmet used to apply tSMS. We also thank Dr. Oliviero and his team for kindly supplying the sham magnet.

REFERENCES

Batsikadze, G., Moliadze, V., Paulus, W., Kuo, M.-F., and Nitsche, M. A. (2013). Partially non-linear stimulation intensity-dependent effects of direct current stimulation on motor cortex excitability in humans. *J. Physiol.* 591(Pt 7), 1987–2000. doi: 10.1113/jphysiol.2012.249730

Bikson, M., Grossman, P., Thomas, C., Zannou, A. L., Jiang, J., Adnan, T., et al. (2016). Safety of transcranial direct current stimulation: evidence based update 2016. *Brain Stimulat.* 9, 641–661. doi: 10.1016/j.brs.2017.07.001

Butefisch, C. M., Davis, B. C., Wise, S. P., Sawaki, L., Kopylev, L., Classen, J., et al. (2000). Mechanisms of use-dependent plasticity in the human motor cortex.(*Brief Article*). *Proc. Natl. Acad. Sci. U.S.A.* 97:3661. doi: 10.1073/pnas.050350297

Carrasco-López, C., Soto-León, V., Céspedes, V., Profice, P., Strange, B. A., Foffani, G., et al. (2017). Static magnetic field stimulation over parietal cortex enhances somatosensory detection in humans. *J. Neurosci.* 37:3840. doi: 10.1523/JNEUROSCI.2123-16.2017

Ciechanski, P., Carlson, H. L., Yu, S. S., and Kirton, A. (2018). Modeling transcranial direct-current stimulation-induced electric fields in children and adults. *Front. Hum. Neurosci.* 12:268. doi: 10.3389/fnhum.2018.00268

Ciechanski, P., and Kirton, A. (2017). Transcranial direct-current stimulation can enhance motor learning in children. *Cereb. Cortex* 27, 2758–2767. doi: 10.1093/cercor/bhw114

Ciechanski, P., Zewdie, E., and Kirton, A. (2017). Developmental profile of motor cortex transcallosal inhibition in children and adolescents. *J. Neurophysiol.* 118, 140–148. doi: 10.1152/jn.00076.2017

Cirillo, J., Rogasch, N., and Semmler, J. (2010). Hemispheric differences in use-dependent corticomotor plasticity in young and old adults. *Exp. Brain Res.* 205, 57–68. doi: 10.1007/s00221-010-2332-1

Cole, L., Giuffre, A., Ciechanski, P., Carlson, H. L., Zewdie, E., Kuo, H.-C., et al. (2018). Effects of high-definition and conventional transcranial direct-current stimulation on motor learning in children. *Front. Neurosci.* 12:787. doi: 10.3389/fnins.2018.00787

Daligadu, J., Murphy, B., Brown, J., Rae, B., and Yielder, P. (2013). TMS stimulus–response asymmetry in left- and right-handed individuals. *Exp. Brain Res.* 224, 411–416. doi: 10.1007/s00221-012-3320-4

Darling, W. G., Wolf, S. L., and Butler, A. J. (2006). Variability of motor potentials evoked by transcranial magnetic stimulation depends on muscle activation. *Exp. Brain Res.* 174, 376–385. doi: 10.1007/s00221-006-0468-9

Dileone, M., Mordillo-Mateos, L., Oliviero, A., and Foffani, G. (2018). Long-lasting effects of transcranial static magnetic field stimulation on motor cortex excitability. *Brain Stimul. Basic Transl. Clin. Res. Neuromodul.* 11, 676–688. doi: 10.1016/j.brs.2018.02.005

Dunbar, M., and Kirton, A. (2018). Perinatal stroke: mechanisms, management, and outcomes of early cerebrovascular brain injury. *Lancet Child Adolesc. Health* 2, 666–676. doi: 10.1016/S2352-4642(18)30173-1

Elsner, B., Kwakkel, G., Kugler, J., and Mehrholz, J. (2017). Transcranial direct current stimulation (tDCS) for improving capacity in activities and arm function after stroke: a network meta-analysis of randomised controlled trials. *J. Neuroeng. Rehabil.* 14:95. doi: 10.1186/s12984-017-0301-7

Eyre, J. A. (2007). Corticospinal tract development and its plasticity after perinatal injury. *Neurosci. Biobehav. Rev.* 31, 1136–1149. doi: 10.1016/j.neubiorev.2007.05.011

Eyre, J. A., Smith, M., Dabydeen, L., Clowry, G. J., Petacchi, E., Battini, R., et al. (2007). Is hemiplegic cerebral palsy equivalent to amblyopia of the corticospinal system? *Ann. Neurol.* 62, 493–503. doi: 10.1002/ana.21108

Foffani, G., and Dileone, M. (2017). No modulatory effects by tSMS when delivered during a cognitive task. *Brain Stimul. Basic Transl. Clin. Res. Neuromodul.* 10:867. doi: 10.1016/j.brs.2017.04.121

Friel, K. M., Chakrabarty, S., and Martin, J. H. (2013). Pathophysiological mechanisms of impaired limb use and repair strategies for motor systems after unilateral injury of the developing brain. *Dev. Med. Child Neurol.* 55, 27–31. doi: 10.1111/dmcn.12303

Friel, K. M., Gordon, A. M., Carmel, J. B., Kirton, A., and Gillick, B. T. (2016). "Pediatric issues in neuromodulation: safety, tolerability and ethical considerations," in *Pediatric Brain Stimulation: Mapping and Modulating the Developing Brain*, eds A. Kirton and D. L. Gilbert (Amsterdam: Elsevier), 475.

Friel, K. M., Williams, P. T. J. A., Serradj, N., Chakrabarty, S., and Martin, J. H. (2014). Activity-based therapies for repair of the corticospinal system injured during development. *Front. Neurol.* 5:229. doi: 10.3389/fneur.2014.00229

Gardner, R. A., and Broman, M. (1979). The purdue pegboard: normative data on 1334 school children. *J. Clin. Child Psychol.* 8, 156–162. doi: 10.1080/15374417909532912

Garvey, M. A., and Gilbert, D. L. (2004). Transcranial magnetic stimulation in children. *Eur. J. Paediatr. Neurol.* 8, 7–19.

Garvey, M. A., and Mall, V. (2008). Transcranial magnetic stimulation in children. *Clin. Neurophysiol. Off. J. Int. Fed. Clin. Neurophysiol.* 119, 973–984. doi: 10.1016/j.clinph.2007.11.048

Gillick, B., Rich, T., Nemanich, S., Chen, C.-Y., Menk, J., Mueller, B., et al. (2018). Transcranial direct current stimulation and constraint-induced therapy in cerebral palsy: a randomized, blinded, sham-controlled clinical trial. *Eur. J. Paediatr. Neurol. EJPN Off. J. Eur. Paediatr. Neurol. Soc.* 22, 358–368. doi: 10.1016/j.ejpn.2018.02.001

Gillick, B. T., Krach, L. E., Feyma, T., Rich, T. L., Moberg, K., Menk, J., et al. (2015). Safety of primed repetitive transcranial magnetic stimulation and modified constraint-induced movement therapy in a randomized controlled trial in pediatric hemiparesis. *Arch. Phys. Med. Rehabil.* 96(4 Suppl.), S104–S113. doi: 10.1016/j.apmr.2014.09.012

Gillick, B. T., Krach, L. E., Feyma, T., Rich, T. L., Moberg, K., Thomas, W., et al. (2014). Primed low-frequency repetitive transcranial magnetic stimulation and constraint-induced movement therapy in pediatric hemiparesis: a randomized

controlled trial. *Dev. Med. Child Neurol.* 56, 44–52. doi: 10.1111/dmcn.12243

Gonzalez-Rosa, J. J., Soto-Leon, V., Real, P., Carrasco-Lopez, C., Foffani, G., Strange, B. A., et al. (2015). Static magnetic field stimulation over the visual cortex increases alpha oscillations and slows visual search in humans. *J. Neurosci.* 35:9182. doi: 10.1523/JNEUROSCI.4232-14.2015

Hermsen, A. M., Haag, A., Duddek, C., Balkenhol, K., Bugiel, H., Bauer, S., et al. (2016). Test–retest reliability of single and paired pulse transcranial magnetic stimulation parameters in healthy subjects. *J. Neurol. Sci.* 362, 209–216. doi: 10.1016/j.jns.2016.01.039

Hsu, W. Y., Cheng, C. H., Liao, K. K., Lee, I. H., and Lin, Y. Y. (2012). Effects of repetitive transcranial magnetic stimulation on motor functions in patients with stroke: a meta-analysis. *Stroke* 43, 1849–1857. doi: 10.1161/STROKEAHA.111.649756

International Commission on Non-Ionizing Radiation Protection (2009). Guidelines on limits of exposure to static magnetic fields. *Health Phys.* 96, 505–511. doi: 10.1097/01.HP.0000343164.27920.4a

Kirimoto, H., Asao, A., Tamaki, H., and Onishi, H. (2016). Non-invasive modulation of somatosensory evoked potentials by the application of static magnetic fields over the primary and supplementary motor cortices. *Sci. Rep.* 6:34509. doi: 10.1038/srep34509

Kirton, A. (2013a). Life after perinatal stroke. *Stroke* 44, 3265–3271. doi: 10.1161/STROKEAHA.113.000739

Kirton, A. (2013b). Modeling developmental plasticity after perinatal stroke: defining central therapeutic targets in cerebral palsy. *Pediatr. Neurol.* 48, 81–94. doi: 10.1016/j.pediatrneurol.2012.08.001

Kirton, A., Andersen, J., Herrero, M., Nettel-Aguirre, A., Carsolio, L., Damji, O., et al. (2016). Brain stimulation and constraint for perinatal stroke hemiparesis: the PLASTIC CHAMPS trial. *Neurology* 86, 1659–1667. doi: 10.1212/WNL.0000000000002646

Kirton, A., Ciechanski, P., Zewdie, E., Andersen, J., Nettel-Aguirre, A., Carlson, H., et al. (2017). Transcranial direct current stimulation for children with perinatal stroke and hemiparesis. *Neurology* 88, 259–267. doi: 10.1212/WNL.0000000000003518

Kufner, M., Brückner, S., and Kammer, T. (2017). No modulatory effects by transcranial static magnetic field stimulation of human motor and somatosensory cortex. *Brain Stimulat.* 10, 703–710. doi: 10.1016/j.brs.2017.03.001

Li, L. M., Uehara, K., and Hanakawa, T. (2015). The contribution of interindividual factors to variability of response in transcranial direct current stimulation studies. *Front. Cell Neurosci.* 9:181. doi: 10.3389/fncel.2015.00181

Lozano-Soto, E., Soto-León, V., Sabbarese, S., Ruiz-Alvarez, L., Sanchez-del-Rio, M., Aguilar, J., et al. (2017). Transcranial static magnetic field stimulation (tSMS) of the visual cortex decreases experimental photophobia. *Cephalalgia* 38, 1493–1497. doi: 10.1177/0333102417736899

Martin, J. H., Chakrabarty, S., and Friel, K. M. (2011). Harnessing activity-dependent plasticity to repair the damaged corticospinal tract in an animal model of cerebral palsy. *Dev. Med. Child Neurol.* 53(Suppl. 4), 9–13. doi: 10.1111/j.1469-8749.2011.04055.x

Martin, J. H., Friel, K. M., Salimi, I., and Chakrabarty, S. (2007). Activity- and use-dependent plasticity of the developing corticospinal system. *Neurosci. Biobehav. Rev.* 31, 1125–1135. doi: 10.1016/j.neubiorev.2007.04.017

Matsugi, A., and Okada, Y. (2017). Cerebellar transcranial static magnetic field stimulation transiently reduces cerebellar brain inhibition. *Funct. Neurol.* 32, 77–82. doi: 10.11138/fneur/2017.32.2.077

Moliadze, V., Schmanke, T., Andreas, S., Lyzhko, E., Freitag, C. M., and Siniatchkin, M. (2015). Stimulation intensities of transcranial direct current stimulation have to be adjusted in children and adolescents. *Clin. Neurophysiol.* 126, 1392–1399. doi: 10.1016/j.clinph.2014.10.142

Monte-Silva, K., Kuo, M.-F., Hessenthaler, S., Fresnoza, S., Liebetanz, D., Paulus, W., et al. (2013). Induction of late LTP-Like plasticity in the human motor cortex by repeated non-invasive brain stimulation. *Brain Stimulat.* 6, 424–432. doi: 10.1016/j.brs.2012.04.011

Muellbacher, W., Ziemann, U., Boroojerdi, B., Cohen, L., and Hallett, M. (2001). Role of the human motor cortex in rapid motor learning. *Exp. Brain Res.* 136, 431–438. doi: 10.1007/s002210000614

Nakagawa, K., and Nakazawa, K. (2018). Static magnetic field stimulation applied over the cervical spinal cord can decrease corticospinal excitability in finger muscle. *Clin. Neurophysiol. Pract.* 3, 49–53. doi: 10.1016/j.cnp.2018.02.001

Nojima, I., Koganemaru, S., Fukuyama, H., and Mima, T. (2015). Static magnetic field can transiently alter the human intracortical inhibitory system. *Clin. Neurophysiol.* 126, 2314–2319. doi: 10.1016/j.clinph.2015.01.030

Nojima, I., Koganemaru, S., and Mima, T. (2016). Combination of static magnetic fields and peripheral nerve stimulation can alter focal cortical excitability. *Front. Hum. Neurosci.* 10:598. doi: 10.3389/fnhum.2016.00598

Nojima, I., Watanabe, T., Gyoda, T., Sugata, H., Ikeda, T., and Mima, T. (2019). Transcranial static magnetic stimulation over the primary motor cortex alters sequential implicit motor learning. *Neurosci. Lett.* 696, 33–37. doi: 10.1016/j.neulet.2018.12.010

Oliviero, A., Carrasco-López, M. C., Campolo, M., Perez-Borrego, Y. A., Soto-León, V., Gonzalez-Rosa, J. J., et al. (2015). Safety study of transcranial static magnetic field stimulation (tSMS) of the human cortex. *Brain Stimulat.* 8, 481–485. doi: 10.1016/j.brs.2014.12.002

Oliviero, A., Mordillo-Mateos, L., Arias, P., Panyavin, I., Foffani, G., and Aguilar, J. (2011). Transcranial static magnetic field stimulation of the human motor cortex. *J. Physiol.* 589(Pt 20), 4949–4958. doi: 10.1113/jphysiol.2011.211953

Oskoui, M., Messerlian, C., Blair, A., Gamache, P., and Shevell, M. (2016). Variation in cerebral palsy profile by socio-economic status. *Dev. Med. Child Neurol.* 58, 160–166. doi: 10.1111/dmcn.12808

Reis, J., and Fritsch, B. (2011). Modulation of motor performance and motor learning by transcranial direct current stimulation. *Curr. Opin. Neurol.* 24, 590–596. doi: 10.1097/WCO.0b013e32834c3db0

Reis, J., Schambra, H. M., Cohen, L. G., Buch, E. R., Fritsch, B., Zarahn, E., et al. (2009). Noninvasive cortical stimulation enhances motor skill acquisition over multiple days through an effect on consolidation. *Proc. Natl. Acad. Sci. U.S.A.* 106, 1590–1595. doi: 10.1073/pnas.0805413106

Ridding, M. C., and Ziemann, U. (2010). Determinants of the induction of cortical plasticity by non-invasive brain stimulation in healthy subjects. *J. Physiol.* 588, 2291–2304. doi: 10.1113/jphysiol.2010.190314

Rosen, A. D. (2003). Mechanism of action of moderate-intensity static magnetic fields on biological systems. *Cell Biochem. Biophys.* 39, 163–173. doi: 10.1385/CBB:39:2:163

Schambra, H. M., Ogden, R. T., Martínez-Hernández, I. E., Lin, X., Chang, Y. B., Rahman, A., et al. (2015). The reliability of repeated TMS measures in older adults and in patients with subacute and chronic stroke. *Front. Cell Neurosci.* 9:335. doi: 10.3389/fncel.2015.00335

Schulz, K. F., Altman, D. G., Moher, D., and CONSORT Group (2010). CONSORT 2010 statement: updated guidelines for reporting parallel group randomised trials. *BMJ* 340:c332. doi: 10.1016/j.ijsu.2011.09.004

Silbert, B. I., Pevcic, D. D., Patterson, H. I., Windnagel, K. A., and Thickbroom, G. W. (2013). Inverse correlation between resting motor threshold and corticomotor excitability after static magnetic stimulation of human motor cortex. *Brain Stimulat.* 6, 817–820. doi: 10.1016/j.brs.2013.03.007

Staudt, M. (2007a). Reorganization of the developing human brain after early lesions. *Dev. Med. Child Neurol.* 49:564. doi: 10.1111/j.1469-8749.2007.00564.x

Staudt, M. (2007b). (Re-)organization of the developing human brain following periventricular white matter lesions. *Neurosci. Biobehav. Rev.* 31, 1150–1156. doi: 10.1016/j.neubiorev.2007.05.005

Tharayil, J. J., Goetz, S. M., Bernabei, J. M., and Peterchev, A. V. (2018). Field distribution of transcranial static magnetic stimulation in realistic human head model. *Neuromodul. Technol. Neural Interf.* 21, 340–347. doi: 10.1111/ner.12876

Tiffin, J., and Asher, E. J. (1948). The Purdue pegboard; norms and studies of reliability and validity. *J. Appl. Psychol.* 32, 234–247.

van Osch, M. J. P., and Webb, A. G. (2014). Safety of ultra-high field mri: what are the specific risks? *Curr. Radiol. Rep.* 2:61. doi: 10.1007/s40134-014-0061-0

Vines, B. W., Nair, D. G., and Schlaug, G. (2006). Contralateral and ipsilateral motor effects after transcranial direct current stimulation. *Neuroreport* 17, 671–674. doi: 10.1097/00001756-200604240-00023

Wen, T.-C., Lall, S., Pagnotta, C., Markward, J., Gupta, D., Ratnadurai-Giridharan, S., et al. (2018). Plasticity in one hemisphere, control from two: adaptation in descending motor pathways after unilateral corticospinal injury in neonatal rats. *Front. Neural Circ.* 12:28. doi: 10.3389/fncir.2018.00080

Williams, J. A., Pascual-Leone, A., and Fregni, F. (2010). Interhemispheric modulation induced by cortical stimulation and motor training. *Phys. Ther.* 90, 398–410. doi: 10.2522/ptj.20090075

Zewdie, E., Ciechanski, P., Kuo, H.-C., Giuffre, A., Cole, L., Seeger, T., et al. (2018). F150 Non-invasive brain stimulation is safe in children: evidence from 3 million stimulations. *Clin. Neurophysiol.* 129, e123–e124. doi: 10.1016/j.clinph.2018.04.313

Zewdie, E., and Kirton, A. (2016). "TMS basics: single and paired pulse neurophysiology," in *Pediatric Brain Stimulation: Mapping and Modulating the Developing Brain*, eds A. Kirton and D. L. Gilbert (Amsterdam: Elsevier), 475.

Conflict of Interest: The authors declare that the research was conducted in the absence of any commercial or financial relationships that could be construed as a potential conflict of interest.

frontiers in Neuroscience

ORIGINAL RESEARCH
published: 23 June 2020
doi: 10.3389/fnins.2020.00584

Enhanced Accuracy for Multiclass Mental Workload Detection Using Long Short-Term Memory for Brain–Computer Interface

Umer Asgher[1], Khurram Khalil[1], Muhammad Jawad Khan[1], Riaz Ahmad[1,2], Shahid Ikramullah Butt[1], Yasar Ayaz[1,3], Noman Naseer[4] and Salman Nazir[5]*

[1] School of Mechanical and Manufacturing Engineering (SMME), National University of Sciences and Technology (NUST), Islamabad, Pakistan, [2] Directorate of Quality Assurance and International Collaboration, National University of Sciences and Technology (NUST), Islamabad, Pakistan, [3] National Center of Artificial Intelligence (NCAI) – NUST, Islamabad, Pakistan, [4] Department of Mechatronics Engineering, Air University, Islamabad, Pakistan, [5] Training and Assessment Research Group, Department of Maritime Operations, University of South-Eastern Norway, Kongsberg, Norway

Cognitive workload is one of the widely invoked human factors in the areas of human–machine interaction (HMI) and neuroergonomics. The precise assessment of cognitive and mental workload (MWL) is vital and requires accurate neuroimaging to monitor and evaluate the cognitive states of the brain. In this study, we have decoded four classes of MWL using long short-term memory (LSTM) with 89.31% average accuracy for brain–computer interface (BCI). The brain activity signals are acquired using functional near-infrared spectroscopy (fNIRS) from the prefrontal cortex (PFC) region of the brain. We performed a supervised MWL experimentation with four varying MWL levels on 15 participants (both male and female) and 10 trials of each MWL per participant. Real-time four-level MWL states are assessed using fNIRS system, and initial classification is performed using three strong machine learning (ML) techniques, support vector machine (SVM), *k*-nearest neighbor (*k*-NN), and artificial neural network (ANN) with obtained average accuracies of 54.33, 54.31, and 69.36%, respectively. In this study, novel deep learning (DL) frameworks are proposed, which utilizes convolutional neural network (CNN) and LSTM with 87.45 and 89.31% average accuracies, respectively, to solve high-dimensional four-level cognitive states classification problem. Statistical analysis, *t*-test, and one-way *F*-test (ANOVA) are also performed on accuracies obtained through ML and DL algorithms. Results show that the proposed DL (LSTM and CNN) algorithms significantly improve classification performance as compared with ML (SVM, ANN, and *k*-NN) algorithms.

Keywords: convolutional neural network, long short-term memory, functional near-infrared spectroscopy, mental workload, brain–computer interface, deep neural networks, deep learning

OPEN ACCESS

Edited by:
Hasan Ayaz,
Drexel University, United States

Reviewed by:
Brent Winslow,
Design Interactive (United States), United States
Hendrik Santosa,
University of Pittsburgh, United States

****Correspondence:***
Umer Asgher
umer.asgher@smme.nust.edu.pk

Specialty section:
This article was submitted to Neural Technology, a section of the journal Frontiers in Neuroscience

Received: *22 December 2019*
Accepted: *12 May 2020*
Published: *23 June 2020*

Citation:
Asgher U, Khalil K, Khan MJ, Ahmad R, Butt SI, Ayaz Y, Naseer N and Nazir S (2020) Enhanced Accuracy for Multiclass Mental Workload Detection Using Long Short-Term Memory for Brain–Computer Interface. Front. Neurosci. 14:584. doi: 10.3389/fnins.2020.00584

INTRODUCTION

Neuroergonomics is a research field that is focused on the estimation of the brain responses generated as a result of human behavior, physiology, emotions, and cognition; in general, it is the study of human brain and its behavior at work (Mehta and Parasuraman, 2013; Curtin and Ayaz, 2018; Ayaz and Dehais, 2019). Passive brain–computer interface (pBCI) is one of the important

research areas of neuroergonomics. pBCI is designed using the arbitrary brain signals to decode user intentions (Khan and Hong, 2015). These signals may be decoded from fatigue, mental workload (MWL), drowsiness, vigilance, stress, anxiety, and so forth. The passive brain activities are decoded for monitoring applications to ensure a reliable decision-making process. Among these passive brain activities, MWL is a complex function that involves neurophysiologic processes, perception, short-term memory (STM), long-term memory (LTM), and cognitive functions (Bergasa et al., 2018). Exceeded limits of MWL are mostly the cause for irrational decision making that can lead to errors and safety hazards (Byrne et al., 2013). Drowsiness, one of the passive brain activities, is a major cause of traffic accidents (Bioulac et al., 2017). In the present realm of human–machine interaction (HMI), modern technology requires even greater cognitive demands from users and operators for ensuring safety and maximizing the effectiveness (Saadati et al., 2019a).

There are different approaches toward estimation of MWL: subjective rating, performance, and physiological measures are the most common techniques. The performance rating method keeps track of a person's progress by using two metrics, namely, accuracy (a person's deviation from fixed procedure) and reaction time (how fast task is done), whereas the subjective rating methods use questioners that are designed by evaluators to assess the emotional and cognitive states of the subject. Also, self-reporting and opinions of the subjects during the experimentation are also considered to measure the MWL (Chen et al., 2019). Several research studies use tests like National Aeronautics and Space Administration's Task Load Index (NASA-TLX) and subjective workload assessment technique (SWAT) to measure the cognitive load (Noyes and Bruneau, 2007). A limitation of subjective method is the self-reporting protocol that is dependent on the respondent's opinion, which may be affected by self-feelings, biasedness, low motivation, ambivalence, and mistakes in interpreting environment changes (Paulhus and Vazire, 2007). In addition, these methods may not consider the physical work associated with the activities involving movement of a person's arms, legs, feet, or entire body (Cain, 2007). On the other hand, physiological methods provide a real-time assessment and higher feasibility. The physiological techniques also require a smaller sample size to estimate reliable cognitive load states (Tran et al., 2007). Physiological sensors, such as electroencephalogram (EEG), heart rate variability (HRV), eye response measurement, functional magnetic resonance imaging (fMRI), and functional near-infrared spectroscopy (fNIRS) are most commonly used for the monitoring of the MWL (Hong and Santosa, 2013; Tong et al., 2016; Curtin et al., 2019).

Electroencephalogram is commonly used modality for monitoring passive brain activities (Frey et al., 2014). In the domain of functional neuroimaging, EEG has certain robust advantages over the other techniques (J. Ph Lachaux et al., 2003; Harrison and Connolly, 2013; Wang et al., 2019) and used extensively in cognitive neuroscience and BCI applications. However, EEG has some limitations owing to its low spatial resolution and is usually constrained to measure the region-specific brain activities (Strait and Scheutz, 2014). fMRI does offer higher spatial resolution, but it limits the subject's portability and struggles in temporal resolution (Canning and Scheutz, 2013). fNIRS, on the other hand, offers balanced spatial and temporal resolution as compared with other neurophysiological modalities and is widely used for MWL estimation (İşbilir et al., 2019). fNIRS systems are described in comparison with other modalities and used as a compromise between fMRI and EEG in relation to spatial and temporal resolution, respectively. Portability requirement of fNIRS system is primarily for its use in neuroergonomic applications (MWL) in ecological environment. fNIRS is also less prone to electro-psychological artifacts, easy to wear, portable, and lightweight (Naseer and Hong, 2015; Hong and Khan, 2017). Several recent studies have used fNIRS for classification of cognitive tasks and events (Abibullaev and Jinung, 2012; Ayaz et al., 2018; Asgher et al., 2019; Wang et al., 2019). These studies include motor imagery, mental arithmetic (MA), MWL, vigilance, and motor execution-based paradigms, which have been experimentally performed to measure accuracies of system. In these studies, the most important objective is to improve classification accuracies, which lead to the exploitation of appropriate classifiers using different machine learning (ML) techniques. The challenging part in these conventional ML classification methods is feature engineering, involving feature extraction, a large number of possible features, feature selection, their combinations, and dimensionality reduction from a relatively small amount of data, which leads to overfitting and biasness (Trakoolwilaiwan et al., 2017; Wang et al., 2019). These intrinsic limitations make researchers tweak around and hence results in a lot of time consumed in data mining and preprocessing. Deep learning (DL) with deep neural networks (DNNs) has emerged as an alternative to overcome this challenge by bypassing the need for manual feature engineering, data cleaning, transformation, and reduction before feeding into learning machines (Saadati et al., 2019a).

Linear discriminant analysis (LDA), *k*-nearest neighbor (*k*-NN), and support vector machine (SVM) have been rigorously implemented and are well-studied classification algorithms in BCI and MWL analyses (Tai and Chau, 2009; Power et al., 2012; Hortal et al., 2013; Naseer and Hong, 2013; Sumantri et al., 2019). All these conventional classifiers and ML algorithms are hampered by complex feature engineering and dimensionality reduction in order to make data visible to the learning system. DNNs have recently gained popularity as highly efficient training classifiers, but limited studies are available so far (Zhang et al., 2019; Saadati et al., 2019b). Hennrich et al. (2015) and Naseer et al. (2016) used DNN and other conventional classifiers to differentiate between two and three cognitive states using brain fNIRS signals. Some studies used similar procedures for binary classification to control robot and gender classification (Ozge Mercanoglu et al., 2017; Huve et al., 2018). Saadati et al. (2019a,b) employed CNN with hybrid fNIRS–EEG for MWL classification and neurofeedback. Various studies (Abibullaev et al., 2011; Ho et al., 2019) modeled deep belief network (DBN) and CNN framework for discriminating MWL and left and right motor imagery tasks using multichannel fNIRS signals. Long short-term memory (LSTM) is one of the variants of DL–recurrent neural network (RNN) algorithms

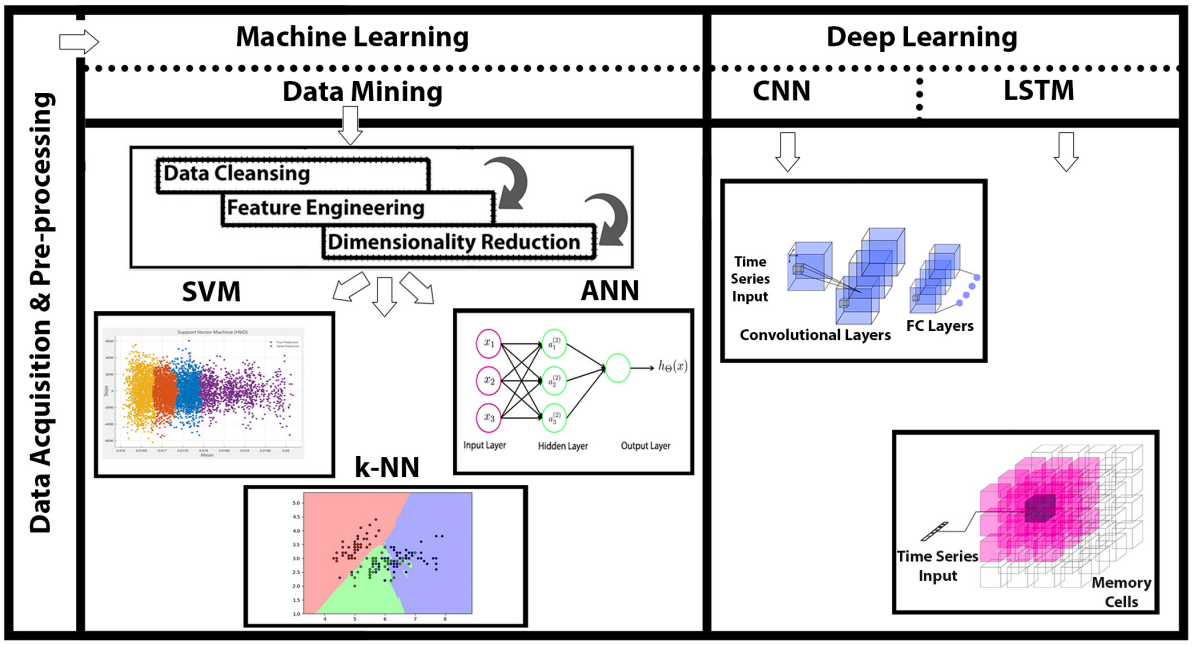

FIGURE 1 | Functional near-infrared spectroscopy (fNIRS)-based mental workload (MWL) classification using machine learning (ML) and deep learning (DL) algorithms. Data acquisition through fNIRS system (P-fNIRSSyst), data preprocessing, and detailed feature engineering followed with application of ML and DL classification.

specifically designed for time-series data (Schmidhuber and Hochreiter, 1997). The only available work on LSTM is that of Yoo et al. (2018), which is limited to only three class classifications and has not compared LSTM results with most employed CNN algorithms.

In this study, we acquired a four-level MWL with varying difficulty levels using fNIRS from 15 healthy subjects (including both male and female). Physiological noises and other high-frequency artifacts were removed using low-frequency bandpass (fourth-order Butterworth) filter (Santosa et al., 2013). Statistical significance of data is verified by *p*- and *t*-tests. Three ML classifiers [SVM, *k*-NN, and artificial neural network (ANN)] along with two DNN algorithms (CNN and LSTM) are used in the analysis and classification of four-state MWLs. The major contribution of this research is that, for the first time, LSTM is applied directly on four-class MWL-fNIRS sequential data for classification and comparison with CNN. ML classifiers couldn't perform well in comparison with DNN algorithms; and within the DL paradigm, the LSTM offers significantly better classification accuracy than does the CNN. The comprehensive summary of research is depicted in **Figure 1**.

METHODS AND METHODOLOGY

Experimental Protocol and Experimentation

Methodology

In this study, 12 channels [12 oxyhemoglobin (HbO) and 12 deoxyhemoglobin (HbR)] and two-wavelength (760 and 850 nm) continuous-wave fNIRS system, namely, "P-fNIRSSyst" is used to measure neuronal activity in form of hemodynamic concentration changes in prefrontal cortex (PFC) (Asgher et al., 2019). There is a 20-ms delay between reading channels and triggering light source, and 3 μs is employed to obtain voltage values of channels. Data samples are acquired at a rate of 8 Hz (per channel per second), which effectively translates into 192 samples per second [12 channels × 2 (both HbO and HbR) × 8 (per channel sample rate) = 192]. fNIRS optical optodes are placed in an arrangement as shown in **Figure 2**.

Experimental Conditions and Participants

Ten male and five female subjects (all right-handed; age range of 20–27 years, with a mean age 23.5 years and standard deviation of 5.5 years) participated in this experiment; they also have an educational background in engineering and technology. Before the final selection, a medical screening test is conducted with the supervision of a medical physician. None of the subjects had any mental, visual, or psychological disorder. Participants are given the details and procedures of the experiment prior to the start of the experiment. All the experiments are conducted in accordance with the Declaration of Helsinki and are approved by the Ethical Research Council of RISE at SMME—National University of Sciences and Technology (NUST). The task environment is designed such that minimum external interference and artifacts should entail in readings. The dark and quiet room is selected with a comfortable back support chair to ensure restful experience (Hong et al., 2015). After an initial relaxation period, participants are asked to put on the fNIRS forehead band on the scalp

FIGURE 2 | The functional near-infrared spectroscopy (fNIRS) (P-fNIRSSyst) system placed to measure participants' prefrontal cortex (PFC) activity. Optodes are placed according to the standard 10–20 system.

as shown in **Figure 2** and sit in front of the laptop screen. It is a supervised experiment; participants are observed with a live stream video camera placed in front of them from an adjacent room.

Data Acquisition

Experimental Tasks and Paradigm

The experiment is designed to discriminate between four levels of MWL. The participants are asked to restrict their physical and head movements as much as possible in order to avoid the artifacts. At the start of the experiment, participants are presented with Microsoft Office PowerPoint (version 16.0) slides shown on the laptop screen placed at 70 cm from nasion. The MA task is selected to evoke the brain activity and to entail a certain amount of MWL, which is prominent in case of MA problems (Power et al., 2011, 2012; Schudlo and Chau, 2013; Kosti et al., 2018). Here, the objective is to measure the mental cognition on the basis of the logic and arithmetic and to ascertain different brain activities with different difficulty levels and their classification. The participants were required to complete the task in time with accuracy. In order to set a baseline, an initial 146 (120 + 26) s are given as a rest period to settle all the brain signals at baseline. The baseline is followed by 20-s MA activity task to gauge MWL level 1 (MWL-1); next, 20 s is the relax (rest) period of the brain, and the brain attains baseline reference during the

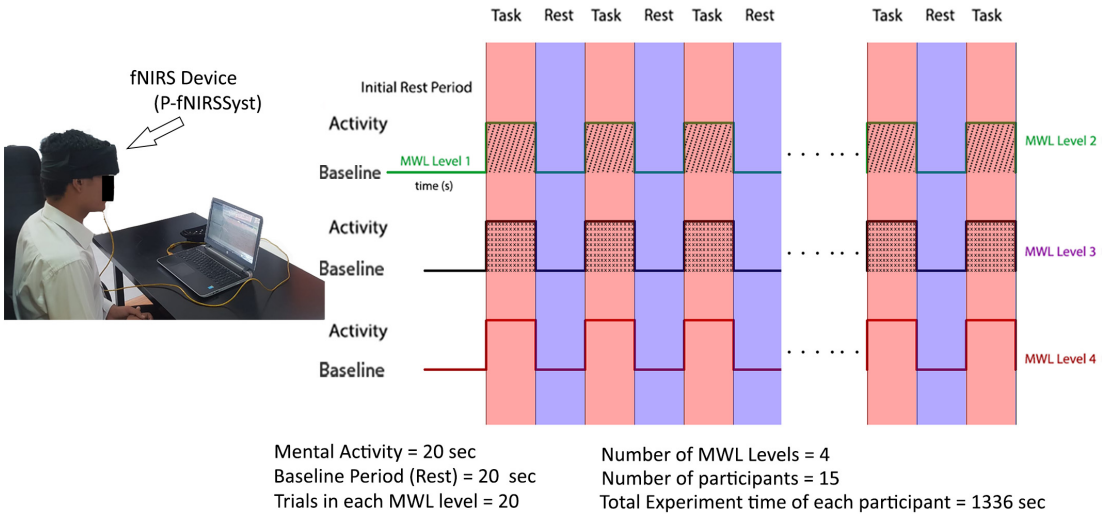

FIGURE 3 | Data acquisition and experimental paradigm with experimental trials and trial sequence diagram. After initial rest period, participants are presented through mental workload (MWL) tasks in phases with increasing difficulty order.

rest period (during the rest period, the participants are asked not to focus at any point). The first MWL-1 task is designed such that it induces a minimal amount of MWL (Galy et al., 2012). Task 1 contains a simple three-number addition such as 769 + 292 and 345 + 229 as MWL-1. Similarly, in phase I, the participants are again given consecutive second tasks to gauge MWL-1 for the same period of 20 s followed by a rest period of 20 s. During the rest period, the participants were asked to relax their mind and place mind at rest (Power et al., 2012; Naseer and Hong, 2013; Schudlo and Chau, 2013), so that no brain activity is generated during rest, whereas focusing on a point or cross in turns could generate a brain activity (Izzetoglu et al., 2011), which was not required in this study, and that could be easily differentiated from the mental math task. This pattern is repeated 10 times, with 10 trials for each participant consisting of MWL-1. After completion of MWL-1, the participants are presented with workload level 2 task in similar conditions. MWL level 2 (MWL-2) starts with a 25-s baseline (rest) period after the MWL-1 and followed the same pattern of 10 trials of MA task 2 (MWL-2) with the 20-s duration of each trail and 20-s rest period in between each MA task. MA task-2 is designed such that it creates a moderate amount of MWL-2 (Galy et al., 2012; Longo, 2018) in a fixed time window. The difficulty level is MWL-2 > MWL-1. MWL-2 has slight complex calculations as compared with MWL-1, including addition, subtraction of large numbers, and operations like multiplication and division, for example, 692 - 579, 60 × 11, and 49/29. Similarly, MWL-3 starts after a rest period of 25 s and has complex MA tasks to induce a high level of MWL. The difficulty level is MWL-3 > MWL-2. It includes arithmetic operation on equation, and the resultant answer (ANS) is utilized in the next calculations (e.g., 823 - 3, ANS × 3, ANS - 21, and ANS + 211) involving mental math task, mental logic, and memory element (Herff et al., 2013; Hosseini et al., 2018). fNIRS recording activity for MWL-1 took 546 s, MWL-2 took 405 s, and MWL-3 took also 405 s for each participant. The total time of experiment of 10 trials with the three MWLs and rest is (546 + 405 + 405) = 1336 × 15 = 2040 s. The tasks timeline sequence of three MWL levels and rest period (four cognitive states) is shown in **Figure 3**. Experimental tasks are verified using standard subjective assessment measure NASA-TLX method. Here, class is an activity (category) having a specific cognitive difficulty level (MWL), which is categorized from other classes (MWL levels) or categories using ML and DL classification. The NASA-TLX is a subjective, multidimensional assessment tool that rates perceived MWL in order to assess task, gauge cognitive workload, effectiveness, and performance. Experimental paradigm is repeated, and questionnaires are filled with subjects' input. Results show the reliability of experimental tasks and the difficulty levels (classes) of various MWLs. The TLX (index) weight is MWL-3 > MWL-2 > MWL-1. The results obtained using NASA-TLX are shown in Annexure A (**Supplementary Material**) that validate the experimental paradigm for MWL assessment and analysis.

Data Preprocessing

Brain activity is detected by measuring concentration changes of HbO and HbR molecules in the microvessels in the cortex. The modified Beer–Lambert law (MBLL) and its variants FV-MBLL are used for measuring concentration changes of HbO and HbR using the information on the intensities of detected NIR light at two different time instants (Pucci et al., 2010; Asgher et al., 2019).

$$\begin{bmatrix} \Delta C_{\mathrm{HbO}}(t_i) \\ \Delta C_{\mathrm{HbR}}(t_i) \end{bmatrix} = \frac{\begin{bmatrix} \alpha_{\mathrm{HbO}}(\lambda_1) & \alpha_{\mathrm{HbR}}(\lambda_1) \\ \alpha_{\mathrm{HbO}}(\lambda_2) & \alpha_{\mathrm{HbR}}(\lambda_2) \end{bmatrix}^{-1} \begin{bmatrix} \Delta OD(t_i;\lambda_2) \\ \Delta OD(t_i;\lambda_2) \end{bmatrix}}{1 \times \mathrm{x}\, d} \tag{1}$$

Detected raw voltage readings from fNIRS optodes of detected lights are processed through analog-to-digital converter (ADC) and are sent to the computer through Bluetooth connection,

where they are normalized by dividing with the mean value. Then signals are passed through low-passed band filter using a fourth order, with zero-phase Butterworth filter (Naseer et al., 2014) having a cutoff frequency of 0.3 Hz to remove high-frequency artifacts due to breathing (0.2–0.5 Hz), blood pressure (∼0.1 Hz), and heartbeat (1–1.5 Hz) (Franceschini et al., 2006; Huppert et al., 2009). Then relative hemodynamic concentration changes are calculated according to Naseer and Hong (2013). The time-series waveforms for different MA (MWL) tasks and MWLs are easily segregated and plotted and are included in Annexure B (**Supplementary Material**). Here, the response activities show different difficulty levels of MWL and can be easily segregated and classified as time-series data.

Statistical Significance of Functional Near-Infrared Spectroscopy Data

Functional near-infrared spectroscopy optodes are placed on the forehead (PFC) of subjects as shown in **Figure 2**. Amplitude and intensities of acquired hemodynamic signals vary from person to person and depend on various factors (Hong and Khan, 2017). The data validation and function response of the device is mentioned in Asgher et al. (2019). Further, in order to determine the integrity and validity of four-class data acquired from the fNIRS system and to make sure that each channel of the device has significant information, a statistical significance of data per channel is first calculated. Independent-samples *t*-test and *p*-test are calculated with the null hypothesis: There is no significant difference between collected fNIRS data and standard data patterns and alternate hypothesis as otherwise on each channel. Additional parameters are also considered like negative correlation between HbO and HbR and channel data comparison with MWL model. For channels having a *p*-value of less than 0.05, we rejected the null hypothesis and accepted the alternate hypothesis. For all subjects, data from only those channels that fulfill the criteria are considered, as given in **Figure 4**. The figure shows the data significance per channel. Green bars in the figure show that 89.16% of the acquired data are significant.

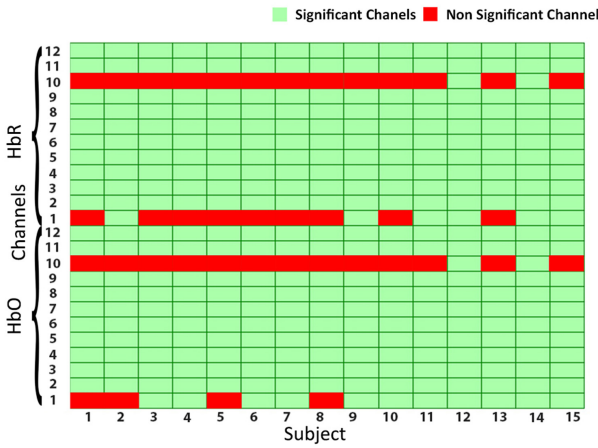

FIGURE 4 | The statistical significance of channels: green cells showing the significant channels, whereas red cells are non-significant channels.

DATA MINING AND FEATURE ENGINEERING

After the data are preprocessed and noise is removed after filtering, the features are extracted from it for classification and discrimination. Features are directly extracted from NIR intensity signals (Power et al., 2012), and the common practice is to extract features directly from acquired hemodynamic signals (HbO and HbR) in the form of changes in concentration (ΔHbO and ΔHbR) (Santosa et al., 2017; F. Wang et al., 2018) to provide improved data cleaning and feature selection. Hemodynamic activity data of the brain can be represented in various feature forms (Bashashati et al., 2007; Lotte, 2014), and different feature combinations can be effectively used for signal classification. All extracted features are normalized in the range [0, 1] before classification. Features are selected such that they have more data information and do comprise significant information that is subsequently used for precise classification (Naseer et al., 2016). The analysis and results of ML algorithms are calculated from various feature combinations: signal mean, maxima, variance, minima, slope, variance, skewness, kurtosis, and signal peak. The obtained results show slope and mean yield the best result in our study, and the best features are mentioned in **Figure 5**. These feature engineering results and findings are in line with previous studies (Abibullaev and Jinung, 2012; Khan and Hong, 2015; Naseer et al., 2016; Hong and Khan, 2017).

Feature Extraction and Selection

Selecting appropriate features for classification is vital, and most of the studies are confined to extracting optimum statistical values of hemodynamic signals. Acquiring the highest accuracy of classification depends on the number of factors such as length of the sliding window (Hong et al., 2015), choosing the best set of feature combinations (Naseer et al., 2016), wavelet functions for decomposition, and temporal and spatial resolution of modalities (Abibullaev and Jinung, 2012). After the best feature extraction techniques are mentioned, optimal features used for classification are signal mean, slope, variance, skewness, kurtosis, and signal peak (Khan and Hong, 2015; Hong and Khan, 2017). Before features are calculated, all channels were normalized between [0, 1] using the following equation:

$$x_{\text{norm}} = \frac{x - x_{\min}}{x\min_{\max}} \tag{2}$$

where x_{norm} is the normalized feature value between 0 and 1, and $x_{\min}$ and $x_{\max}$ are the smallest and largest values, respectively. To avoid the model's overfitting on training data and validating classification performance, 10-fold cross-validation is used. In 10-fold cross-validation, data are divided into 10 subsets, and one subset is used as test set while the other nine sets are used as training sets, whereas in leave-one-out cross-validation (LOOCV) is logical extreme of *k*-fold cross-validation, with *k* equal to number of total data points (*N*). For a smaller dataset, LOOCV is considered suitable, whereas for medium datasets, *k*-fold cross-validation is preferred. LOOCV is also expensive in terms of computational cost and train test time. To save the

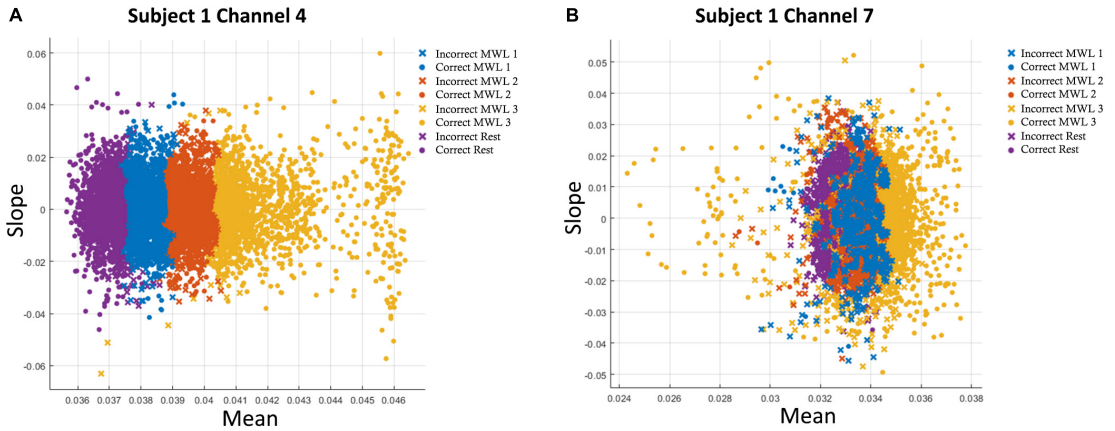

FIGURE 5 | (A) Accuracies with two-feature (mean–slope) combination in support vector machine (SVM) classification plot of oxyhemoglobin (HbO) for subject 1 on channel 4. **(B)** Accuracies with two-feature (mean–slope) combination in *k*-nearest neighbor (*k*-NN) classification plot of HbO for subject 1 on channel 7. Only statistically significant channels are considered.

computational resources and the nature of datasets lies in the medium category; therefore, *k*-fold cross-validation is employed in this study (Wong, 2015).

ANALYSIS AND CLASSIFICATION USING MACHINE LEARNING ALGORITHMS

Support Vector Machines and *k*-Nearest Neighbor Classification

Support vector machine is the most commonly used discriminative classifier in various studies for classification and pattern recognition (Thanh et al., 2013; Khan et al., 2018). In supervised learning, given a set of labeled training data, SVM outputs an optimal hyperplane that assigns new test data to one of the categories of the classification. SVM is designed such that it maximizes the distance between the closest training points and separating hyperplanes. In two dimensions, separating hyperplane feature space is given by:

$$f(x) = r \cdot x + b \tag{3}$$

where b is a scaling factor and $r, x \in R^2$. The loss function of SVM for a two-class classification problem is given in Eq. 4. For more than two classes, the one-versus-all approach is used in which class 1 is the class that we want to predict and all other classes are considered as class 2 using the same formula:

$$J(\theta) = \sum_{i=1}^{m} y^{(i)} Cost_1(\theta^T\left(x^{(i)}\right) + \left(1 - y^{(i)}\right) Cost_0(\theta^T\left(x^{(i)}\right) \tag{4}$$

In Eq. 4, m represents the total number of data points. And the cost is calculated as

$$Cost\left(h_\theta(x), y\right) = \begin{cases} \max(0, 1 - \theta^T x) & \text{if y } = 1 \\ \max(0, 1 + \theta^T x) & \text{if y } = 0 \end{cases} \tag{5}$$

The common practice to do multiclass classification with SVMs is to employ a one-versus-all classifier and predict the class with the highest margin (Manning et al., 2008).

k-Nearest neighbor is a non-parametric method, commonly used for pattern recognition, classification, and regression tasks (Sumantri et al., 2019). In the case of the classification, the output is class label assigned to the object depending on the most common class among its *k*-NNs. Weights are assigned to the test point in inverse relation to the distance, that is, $1/D$, where D is the distance to the neighbor, such that neighbors near the input are assigned more weight as the distance is less and vice versa as given in Eq. 6.

$$D(x, p) = \begin{Bmatrix} \sqrt{(x-p)^2} & \text{Euclidean} \\ (x-p)^2 & \text{Euclidean eSquared} \\ (x-p) & \text{Manhattan} \end{Bmatrix} \tag{6}$$

Training dataset in case of *k*-NN are vectors in multidimensional feature space with each class label. In the prediction phase of the algorithm, the distance of an unlabeled input is calculated using Euclidean distance. Data are in pairs like $(x_1, y_1), (x_2, y_2), ...(x_n, y_n) \in \mathbb{R}^d$ such that $\mathbb{R}^d x\{1, 2\}$ where x is the feature, y is the class label of the feature, and p is the query points. Predictions are made on the basis of *k*-NN examples by using formula (7) (Zhang et al., 2018).

$$y = \frac{1}{k} \sum_{i=1}^{k} y_i \tag{7}$$

k is a hyperparameter and its selection depends on the data. Generally, larger values of k reduce the effects of noise on the classification but make boundaries less distance between the classes. Here, SVM and *k*-NN are implemented to discriminate between four MWL levels from fNIRS datasets of 15 participants.

All algorithms were trained and tested on MSI GE62VR Apache Pro Laptop with NVIDIA GEFORCE® GTX 1060 having a 3 GB GDDR5 graphic card. SVM and *k*-NN were performed

on MATLAB 2019a Machine Learning app, whereas ANN, CNN, and LSTM were performed on Python 3.7 on Anaconda SPYDER integrated development environment (IDE). In both ML and DL algorithms, Adam optimizer is used to dynamically adjust the learning rate and is the most (Kingma and Ba, 2015). At the start of training, the weights are initialized from Xavier uniform distribution (Glorot and Bengio, 2010). For SVM and *k*-NN, we extracted nine features from the original hemodynamic HbO and HbR signals, namely, mean, median, standard deviation, variance, minima, maxima, slop, kurtosis, and skewness. These features were spatially calculated across all 12 channels with a moving overlapping window of 2 s. For two feature combinations, Signal Mean (M) and Signal Slope (S) produced the best results, which are shown in **Figures 5A,B** for Subject 1. Average accuracies across 12 channels show that average classification accuracy achieved with SVM and *k*-NN is 54.33 and 54.31%, respectively.

Artificial Neural Network Classification

An ANN has at least three layers (an input layer, a hidden layer, and an output layer), and each layer performs its computation and learning tasks, where the number of neurons in each layer depends on the number of inputs in the input layer and the number of outputs in the output layer. The hyperparameters are neurons in each layer, weights, network structure, and learning parameters that are learned by training the network again and again to get the maximum accuracy.

The output of a neuron is mathematically expressed as

$$a_i^{(j)} = g\left(\theta^{(j)} x_k\right) \tag{8}$$

where $a_i{}^{(j)}$ is the activation of unit i in a layer and g is the activation function applied, $\theta^{(j)}$ is the matrix of weights controlling function mapping from layer j to layer $j+1$, and x_k is the input from the previous layer of neurons or initial input. The recursive chain rule is implemented to calculate gradients during backpropagation. Mathematically, the chain rule is defined in Eq. 9. The cost function for ANN is given in Eq. 10.

$$\frac{dy}{dx} = \frac{dy}{du} \cdot \frac{du}{dy} \tag{9}$$

$$J(\Theta) = -\frac{1}{m}\Bigg[\sum_{i=1}^{m}\sum_{k=1}^{K} y_k^{(i)} \log h_\theta(x^{(i)})_k + \left(1 - y_k^{(i)}\right) \log(1 - h_\theta\left(x^{(i)}\right)_k)\Bigg] + \frac{\lambda}{2m}\sum_{l=1}^{L-1}\sum_{i=1}^{\delta_l}\sum_{j=1}^{\delta_{l+1}}(\Theta_j^{(l)})^2 \tag{10}$$

The proposed ANN model consists of two hidden layers along with input and output layers. The dimension of the input layer corresponds to selected features, whereas the output layer corresponds to distinguishable MWL classes, which, in our case, are 9 and 4, respectively. Each hidden layer consists of 50 neurons and is fully connected with the previous and next layers. For activation function in hidden layers, "Relu" is used, which introduces non-linearity to learn complex features, given in Eq. 11. The output layer has a "sigmoid" activation function for multiclass classification and prediction. The ANN model summary used in this study is shown in **Figure 6** with details about layers, neurons, and parameters used in this study. Every channel for each subject with nine extracted features is passed through the network, and cost is calculated through gradient descent. Loss is backpropagated through network, and weights are adjusted. This process is repeated equally to the number of epochs, that is, 100. At each epoch, accuracy is calculated; later, the accuracy is averaged out on all 12 channels and is segregated and will be discussed in section "Results".

$$f(x) = \left(x^{+}\right) = \max(0, x) \tag{11}$$

ANALYSIS WITH DEEP LEARNING CLASSIFICATION TECHNIQUES

Convolutional Neural Networks

Convolutional neural networks (CNNs) intelligently adapt the inherent properties of data by performing different operations on the data as a whole and extracting key feature before feeding it into fully connected layers (LeCun and Bengio, 1995; Dos Santos and Gatti, 2014). The acquired fNIRS dataset has specific patterns within it, which relates to the strength of mental activity with hemodynamic concentration changes (ΔHbO and ΔHbR). CNN has to learn this hidden pattern on its own (without human intervention, i.e., manual feature engineering) through end-to-end training (Ho et al., 2019; Saadati et al., 2019a). CNNs have one, two, or multiple convolutional layers with an activation function along with pooling layers to adjust the dimensions of the feed data, but these layers are not fully connected. Resultant layers formed after convolution operation are known as activation maps. These activation maps hold the features and patterns within fNIRS training data required for successful classification. The number of filters must be the same as the input data depth to perform convolution, and the output size of the resulting activation map is determined by the filter size and stride using the following formula.

$$\text{Output size (W, H)} = \frac{\text{(N-F)}}{\text{stride}} + 1 \tag{12}$$

where N is the dimension of input data; F is dimension of filter; and Stride is the step length for convolution. Convolution of the input signal and filter weights is performed as a convolution of two signals, that is, element-wise multiplication and sum of a filter and the signal (i.e., time-series fNIRS data).

$$f[x, y]^* g[x, y] = \sum_{n_1=-\infty}^{\infty}\sum_{n_2=-\infty}^{\infty} f[n_1, n_2] \cdot g[x - n_1, y - n_2] \tag{13}$$

The next important layer in the convolutional network is the pooling layer. It reduces the spatial size of the activation maps generated by the convolution operation of filters on a 12-channel data stream. The output size of volume produced as a result of pooling is determined by

$$\text{Output size (W, H)} = \frac{\text{(N-F)}}{\text{stride}} + 1 \tag{14}$$

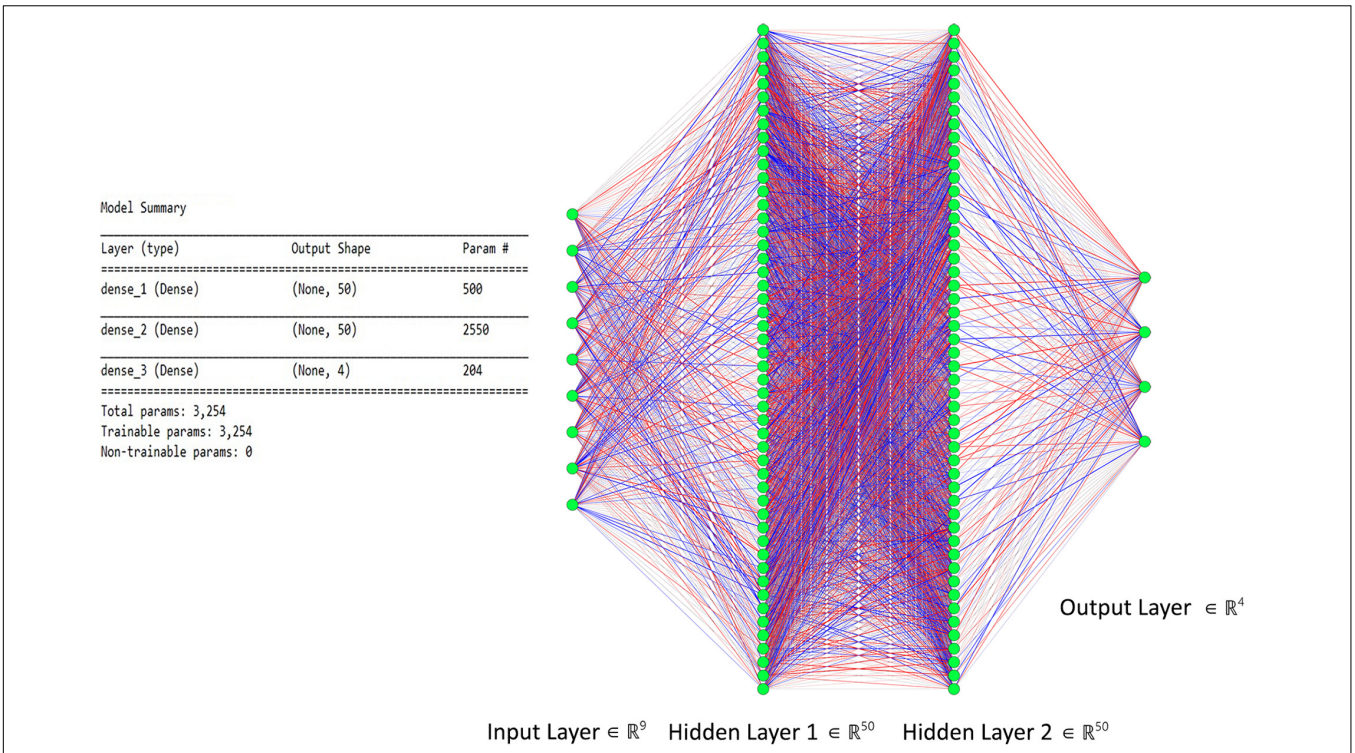

FIGURE 6 | The proposed artificial neural network (ANN) model with two hidden layers used for classification.

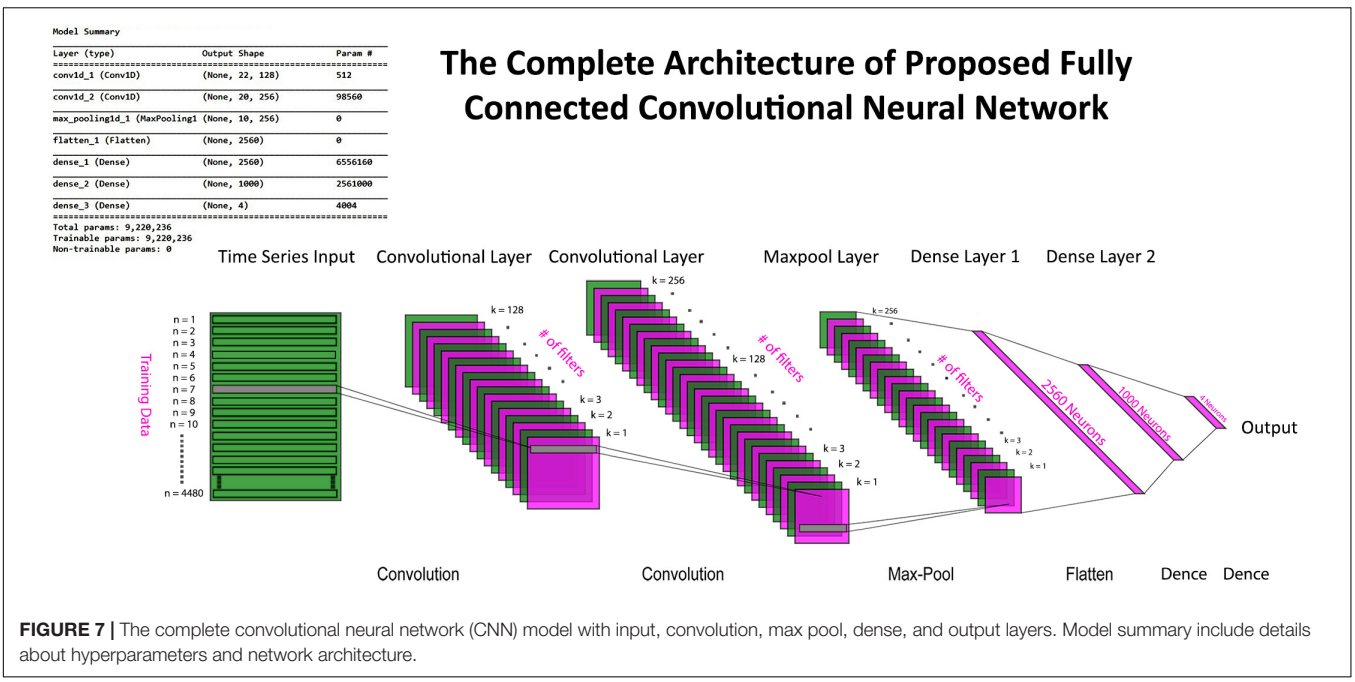

FIGURE 7 | The complete convolutional neural network (CNN) model with input, convolution, max pool, dense, and output layers. Model summary include details about hyperparameters and network architecture.

where the depth of data remains the same, whereas width and height are reduced to half in case of max pooling with a stride having a value of 2. Input data after passing through a series of convolution and pooling layers are flattened and fed into the fully connected layers to perform the classification task. The complete parameters and structure of the proposed CNN are shown in **Figure 7**. It is a fully connected feed-forward network with two convolution layers followed by one max-pooling layer, and then the output from the max-pool layer is flattened and fed into a dense layer that terminates into the final output layer

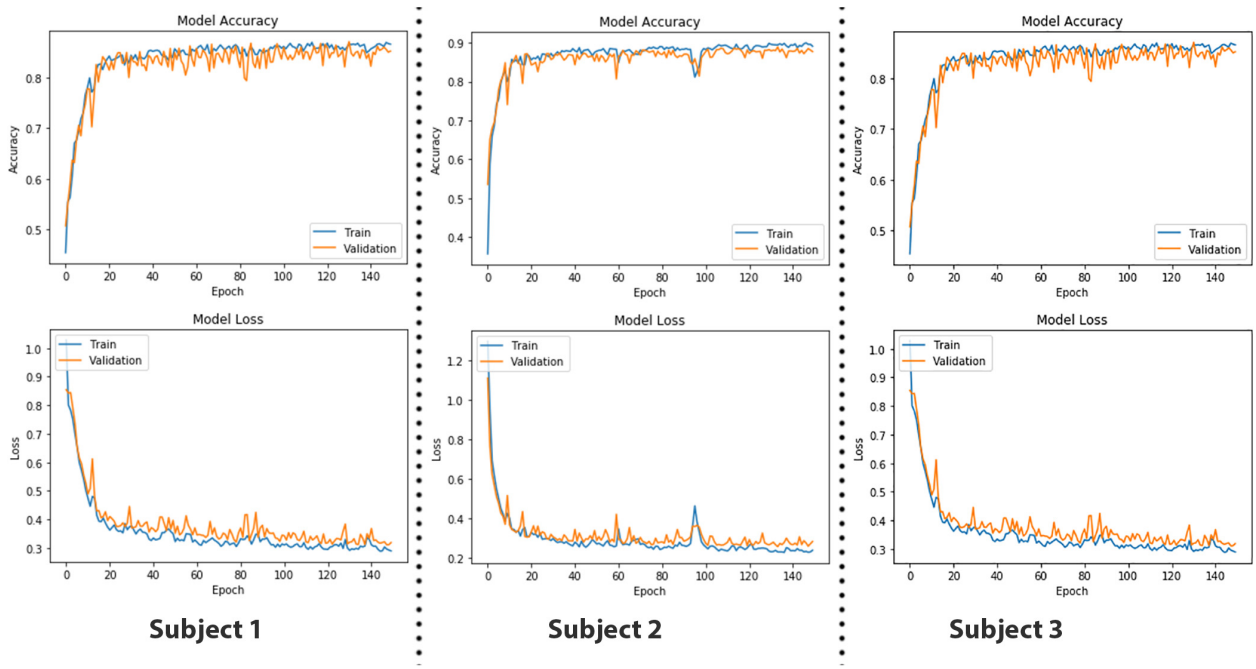

FIGURE 8 | The epoch versus accuracy and loss plots of convolutional neural network (CNN) model on train and validation datasets. Accuracy increases with number of epochs and then saturates; vice versa for the loss.

before passing through another fully connected layer. There are 24 readings vector (12 HbO + 12 HbR), which served in the "Conv1D" convolutional layer. One hundred twenty-eight filters spatially convolve with the input data stream and learn high-level features for classification in the form of activation maps. **Figure 8** represents the graphs of accuracy and loss over train and validation sessions on different subjects. A batch size of 500 is used to train the network over 150 epochs.

Long Short-Term Memory

Long short-term memory is a modification of the RNN with a feedback connection (Schmidhuber and Hochreiter, 1997). LSTM networks are well suited for time-series data classification, processing, and predictions owing to unknown time duration lag between important events in a time series. LSTM provides better classification and learning results than do conventional CNN and vanilla RNNs (Graves et al., 2009, 2013). An LSTM unit is a cell with three gates, that is, an input gate, an output gate, and a forget gate (Greff et al., 2016), as shown in **Figure 9A**. The three gates regulate the flow of information in and out of the cell, enabling it to remember values over random time intervals. The cell keeps track of the interdependencies of elements in the input sequence. Often, logistic sigmoid function is used as an activation function of LSTM gates (Gers and Schmidhuber, 2001; Gers et al., 2003). Logistic sigmoid function is given by

$$f(x) = \frac{1}{1 + e^{-k(x-x_0)}} \tag{15}$$

where e is the natural logarithm base, x_0 is the x-value of the sigmoid midpoint, and k is the logistic growth rate. There are connections between input and output gates of LSTM, usually recurrent. The weights of these connections are learned during the training to determine the operation of these gates.

The major takeaway of this study is the application of LSTM for the first time in the classification of a multiobjective task problem. First of all, data of each subject are split into train and validation sets with a 70:30 ratio. To make input data compatible with LSTM, they are reshaped such that for each time instance, we have a data stream of all 12 channels in a single row vector format of 24 units (12 HbO + 12 HbR). After initial preprocessing, time-series data are fed into the LSTM unit as vectors, labeled as lowercase variables in the following equations, with the matrices in uppercase variables. The equations for forward pass of LSTM unit with a forget gate are given below:

$$f_t = \sigma_{\text{th}}\left(W_{\text{f}}x_t + +U_{\text{f}}h_{t-1} + b_{\text{f}}\right) \tag{16}$$

$$i_t = \sigma_{\text{th}}\left(W_i x_t + +U_{\text{i}}h_{t-1} + b_{\text{i}}\right) \tag{17}$$

$$o_t = \sigma_{\text{th}}\left(W_{\text{o}}x_t + +U_{\text{o}}h_{t-1} + b_0\right) \tag{18}$$

Here, W_i, W_o, and W_f are the weight matrices of input, output, and forget gates, respectively. Each gate in the LSTM cell is a weight to control how much information can flow through that gate. The input gate controls the flow of values into the cell, the forget gate controls the values that remain in the cell, and the output gate controls the values flowing out of the cell to compute the output activation of the LSTM unit. U_i, U_o, and U_f are the weight matrices of recurrent

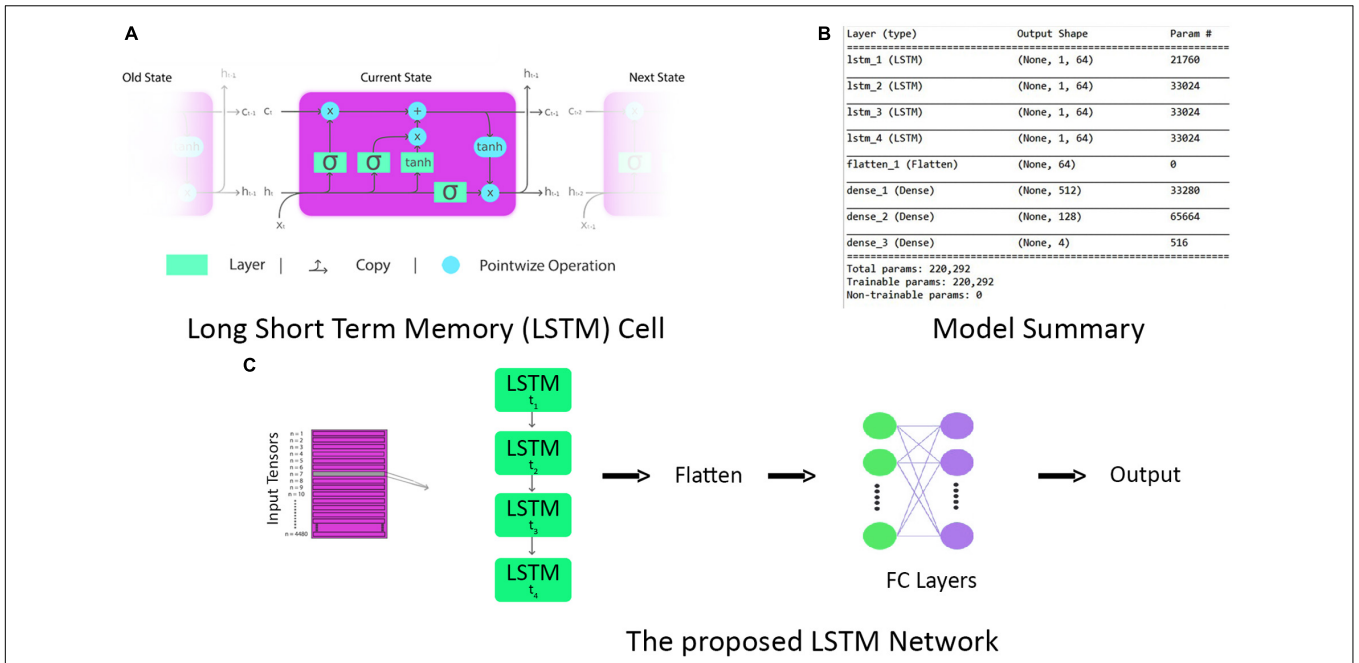

FIGURE 9 | (A) The repeating long short-term memory (LSTM) cell with input, forget, and output gates. **(B)** Complete model summary of the proposed LSTM network. **(C)** The architecture of the proposed LSTM network.

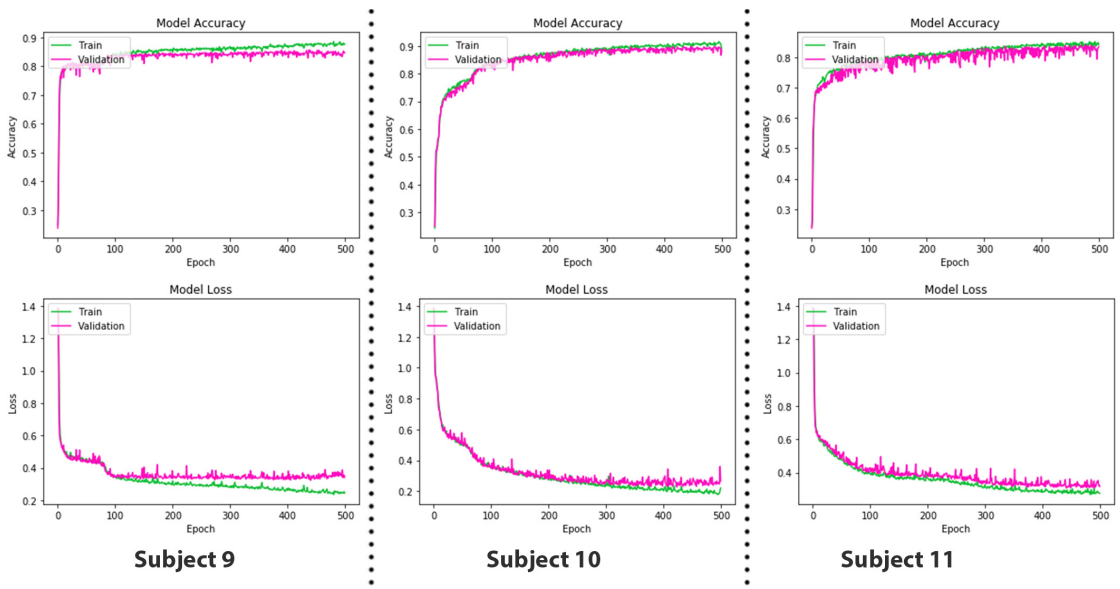

FIGURE 10 | The epoch versus accuracy and loss plots of long short-term memory (LSTM) on train and validation datasets.

connections of input, output, and forget gates, respectively.

$$c_t = f_t^{\circ} c_{t-1} + i_t^{\circ} \sigma_{\text{th}} \left(W_c x_t + U_c h_{t-1} + b_c \right) \tag{19}$$

$$h_t = o_t^{\circ} \sigma_h \left(c_t \right) \tag{20}$$

As LSTM is being used for time-series data (vector notation), in Eqs 19 and 20, $c_t \in \mathbb{R}^d$ is not a single LSTM unit but contains h LSTM unit cells. σ_{th} is the hyperbolic tangent activation function, and sigmoid function can also be used as an activation function, where x_0, f_t, i_t, o_t, h_t, and $c_t \in \mathbb{R}^d$ and are input vector of the LSTM unit; activation vector of forget gate, input gate, and output gate; output vector of LSTM unit and cell state vector, respectively. W $\mathbb{R}^{h \times d}$, U $\mathbb{R}^{h \times h}$ and b $\mathbb{R}^h$, are the weight matrices and bias vector learned during training. The initial values are $c_0 = 0$ and $h_0 = 0$. The operator denotes the element-wise product,

TABLE 1 | Artificial neural network (ANN) and convolutional neural network (CNN) accuracies, precision, and recall of all subjects (in percentage).

	S1			S2			S3		
	Accuracy	**Precision**	**Recall**	**Accuracy**	**Precision**	**Recall**	**Accuracy**	**Precision**	**Recall**
ANN	80.66	85.71	81.63	77.66	82.54	77.84	69.91	78.83	70.07
CNN	82.36	87.86	78.75	92.31	94.58	83.15	90.56	92.96	84.50
	S4			**S5**			**S6**		
	Accuracy	**Precision**	**Recall**	**Accuracy**	**Precision**	**Recall**	**Accuracy**	**Precision**	**Recall**
ANN	68.45	73.57	67.91	55.95	72.71	55.84	78.4	85.79	78.22
CNN	78.24	88.23	85.76	90.66	93.14	86.32	93.02	94.65	86.60
	S7			**S8**			**S9**		
	Accuracy	**Precision**	**Recall**	**Accuracy**	**Precision**	**Recall**	**Accuracy**	**Precision**	**Recall**
ANN	79.54	83.97	81.88	57.86	74.69	56.72	64.56	76.92	64.47
CNN	86.18	90.30	86.82	85.41	89.76	87.79	86.32	89.86	90.03
	S10			**S11**			**S12**		
	Accuracy	**Precision**	**Recall**	**Accuracy**	**Precision**	**Recall**	**Accuracy**	**Precision**	**Recall**
ANN	79.29	84.46	78.63	74.74	79.84	74.54	57.6	72.79	57.76
CNN	89.01	91.63	90.25	85.42	89.08	91.71	83.85	90.23	91.93
	S13			**S14**			**S15**		
	Accuracy	**Precision**	**Recall**	**Accuracy**	**Precision**	**Recall**	**Accuracy**	**Precision**	**Recall**
ANN	68.95	78.28	67.97	61.05	73.54	60.06	65.79	77.52	65.26
CNN	92.54	95.28	92.75	86.78	91.87	93.32	89.13	92.50	93.79

TABLE 2 | Classification accuracies, precision, and recall achieved through proposed long short-term memory (LSTM) network (in percentage).

S1			**S2**			**S3**		
Accuracy	**Precision**	**Recall**	**Accuracy**	**Precision**	**Recall**	**Accuracy**	**Precision**	**Recall**
83.11	85.34	83.84	89.09	89.53	89.12	87.52	88.68	88.51
S4			**S5**			**S6**		
Accuracy	**Precision**	**Recall**	**Accuracy**	**Precision**	**Recall**	**Accuracy**	**Precision**	**Recall**
95.51	84.03	83.86	90.85	92.16	91.84	90.42	93.38	92.44
S7			**S8**			**S9**		
Accuracy	**Precision**	**Recall**	**Accuracy**	**Precision**	**Recall**	**Accuracy**	**Precision**	**Recall**
84.29	88.25	88.37	92.97	86.65	86.40	87.27	85.66	85.49
S10			**S11**			**S12**		
Accuracy	**Precision**	**Recall**	**Accuracy**	**Precision**	**Recall**	**Accuracy**	**Precision**	**Recall**
95.05	89.76	89.28	84.94	83.68	83.72	84.79	77.88	74.63
S13			**S14**			**S15**		
Accuracy	**Precision**	**Recall**	**Accuracy**	**Precision**	**Recall**	**Accuracy**	**Precision**	**Recall**
93.40	89.79	88.68	90.77	86.81	85.06	89.78	90.95	90.12

and the subscript t indexes the time step. In Eqs 18 and 19, it can be seen that output o_t and current state vector c_t at time t not only depend on input i_t but are also related to the information at a previous time of LSTM cell. In this manner, LSTM is permitted to remember the important information in the time domain. The superscript d and h refer to the number of input features and the number of hidden units. In our study, the values of d and h are 24 and 64, respectively. The complete parameters and layer structure of the proposed LSTM network are shown in **Figure 9B**. It consists of four LSTM layers, and then the output from the last LSTM layer is flattened and fed into a dense layer that terminates into the final output layer after passing through another fully connected layer. The generalized overview of the implemented LSTM network is presented in **Figure 9C**. The epoch versus accuracy and loss plots of LSTM on train and validation datasets are shown in **Figure 10**. For training data, the batch size of 150 is used over 500 epochs for each participant. Accuracies, precision, and recall are presented in section "Results."

RESULTS

The results using different classifiers are presented in this section. For all subjects, statistical significance of data per channel is calculated, and only those channels that are employed in classification classifiers are statistically significant. The criteria used for selection of channels are discussed in section "Statistical Significance of Functional Near-Infrared Spectroscopy Data" and **Figure 4**. For two feature combinations, Signal Mean (M) and Signal Slope (S) produced the best results, which are shown in **Figures 5A,B** for Subject 1. Average accuracies across 12 channels show that the highest average classification accuracy achieved with SVM and k-NN is 54.33 and 54.31%, respectively.

Regions of interest (ROIs) represent the area of the brain that shows the increased response for a specific activity than do other areas in PFC. In this study, ROI is calculated using percentage as a criterion. The studies of Hiroyasu et al. (2015); Hong and Santosa (2016), and Hiwa et al. (2017) are referred as to benchmark studies in measuring ROI; the only difference

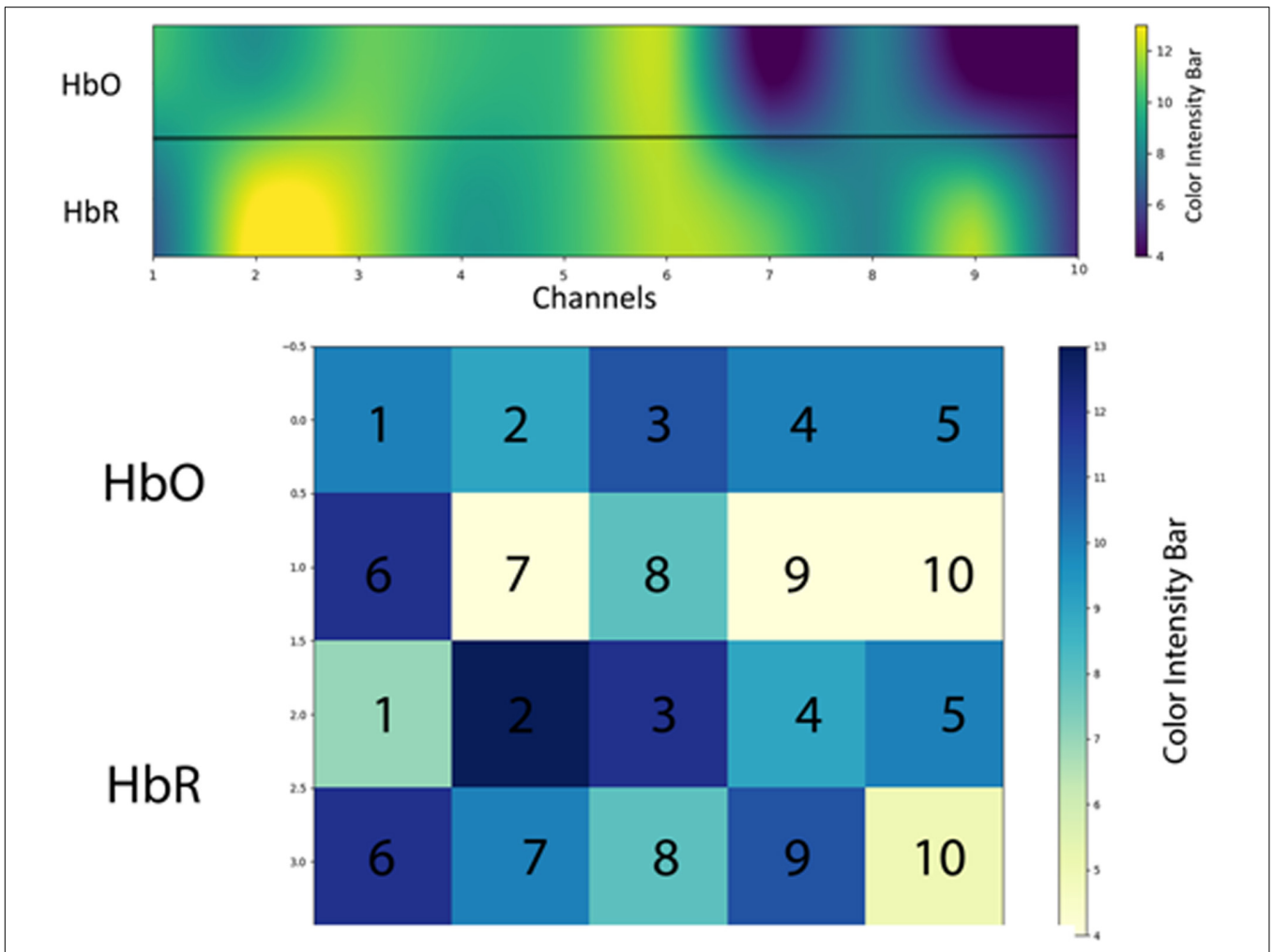

FIGURE 11 | The regions of interest (ROIs) using oxyhemoglobin (HbO) and deoxyhemoglobin (HbR)—response for a specific activity compared with the other areas in prefrontal cortex (PFC). Activation map averaged over all 15 subjects (only significant channels are considered) during activation.

is that we used a percentage instead of critical t-value (t_{crt}) in calculating ROIs. Different channel positions are highlighted in ROI with varying intensities in an activation map as mentioned in **Figure 11**. We used SVM accuracies and the color map obtained after setting critical percentage level 55% as shown in **Figure 11**.

Table 1 entails ANN in comparison with CNN averaged accuracies of 12 channels of each subject. To get a better statistical insight of data, precision and recall are also measured. The precision and recall values are also given alongside the accuracies. The average accuracy of ANN is 69.36% as mentioned in **Table 1**. Classification accuracies, precision, and recall of all participants calculated using CNN classifier are also summarized in **Table 1**, with an average accuracy of 87.45%.

We calculated the classification accurateness of model by the metric "accuracy," which is the number of correct predictions from all predictions made. To validate the model accuracies and class balance, further model precision (number of positive predictions divided by total number of positive class values predicted) and recall (number of positive predictions divided by the number of positive class values in the test data) are also calculated in **Tables 1**, **2** to assure class balance in their alignment with accuracy.

Table 2 presents classification results using LSTM classifier. The highest accuracy achieved with CNN is 93.02%, whereas the highest accuracy with LSTM is 95.51%, which shows that the classification achieved with LSTM has the highest accuracy.

Statistical analysis is performed on accuracies obtained through ANNs, CNN, and LSTM. Independent-samples t-test was performed between ANN and CNN and between CNN and LSTM accuracies. Results shows that for both statistical tests, $p < 0.05$ and the null hypothesis (with no statistical significance) is rejected. A comparison between ANN, CNN, and LSTM is obtained using one-way F-test (ANOVA) to measure inter-similarity between groups (ANN, CNN, and LSTM) on the basis of their mean similarity and f-score. Results shows that three groups at a time are also statistically significant with $p < 0.05$. The statistical analysis is coded in software Anaconda IDE with Python 3.7 used with Numpy, and Scikit library, and the software script used to calculate results is added as Annexure C (**Supplementary Material**). The comparative results between accuracies of ANN, CNN, and LSTM are presented in box plots in **Figure 12**.

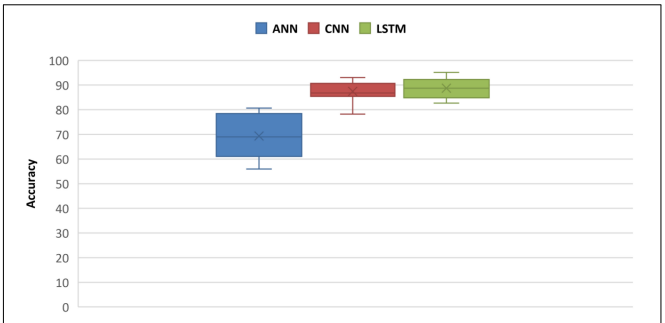

FIGURE 12 | Box plot comparison between ANN, CNN, and LSTM classification accuracies.

DISCUSSION

In various brain imaging studies, fNIRS is used to investigate the hemodynamic activities and cognitive states such as MWL, vigilance, fatigue, and stress levels (Cain, 2007; Herff et al., 2013; Ho et al., 2019). Owing to the optical nature of fNIRS, the methodology is less prone to artifacts like a heartbeat or motor, head, and eye movements, which makes it the prevalent choice over other neuroimaging modalities like EEG, PET, and fMRI (Ozge Mercanoglu et al., 2017). The primary aim of this study was to explore the optimal ML or DL algorithms that best fit the four-phase MWL assessment and classification. The cutting edge of DNN over ML is its automatic feature extraction scheme acquired brain signals that override the ML algorithms. In DL, the CNN has a powerful convolutional map to learn classifiable features, and LSTM has memory units to better keep records of time-series patterns, which in our case was the most relevant one. The major takeaway of this study is the application of LSTM for the first time in the classification of a multiobjective task problem.

Many fNIRS studies have been carried out to improve classification accuracies of different brain states by using different combinations of features using ML classifiers (Liu and Ayaz, 2018). Best-feature combinations are also shown in various studies, signal slope S (Power and Chau, 2013; Schudlo and Chau, 2013), signal mean M (Faress and Chau, 2013; Naseer and Hong, 2013), signal variance V (Tai and Chau, 2009; Holper and Wolf, 2011), signal kurtosis K (Holper and Wolf, 2011; Naseer et al., 2016), signal skewness SE (Tai and Chau, 2009; Holper and Wolf, 2011), signal peak P (Naseer and Hong, 2015), signal amplitude A (Cui et al., 2010; Stangl et al., 2013), and zero-crossing (Tai and Chau, 2009). Most commonly used features that showed sustainable results are the M, S, and P (Coyle et al., 2004; Fazli et al., 2012; Hong et al., 2015; Khan et al., 2018). In this study, we explored different combinations of two-dimensional (2D) features and concluded M (signal mean) and S (signal slope) combination as the optimal features' combinations with classification average accuracies of 54.33% (SVM) and 54.31% (k-NN), which are in accordance with previous studies and summarized in **Figure 13**.

Aside from data mining and manual feature engineering, ML classifiers struggle to generalize complex data patterns and, hence, showed poor performance in situations like higher BCI protocols with increased levels of MWL. MWL (using fNIRS) four-phase classification is not very common, and most of the studies are limited to two MWL states, and very few studies explored three MWL phases with conventional ML techniques. Hortal et al. (2013) achieved 87% accuracy on the classification of two mental tasks using SVM. Tai and Chau (2009) reported 96.6 and 94.6% as the highest accuracy of single-trial classification of NIRS signals during emotional induction tasks using LDA and SVM, respectively. Naseer and Hong (2013) reported 87.2% accuracy on two brain signals using SVM. In these studies, as the number of discriminatory phases

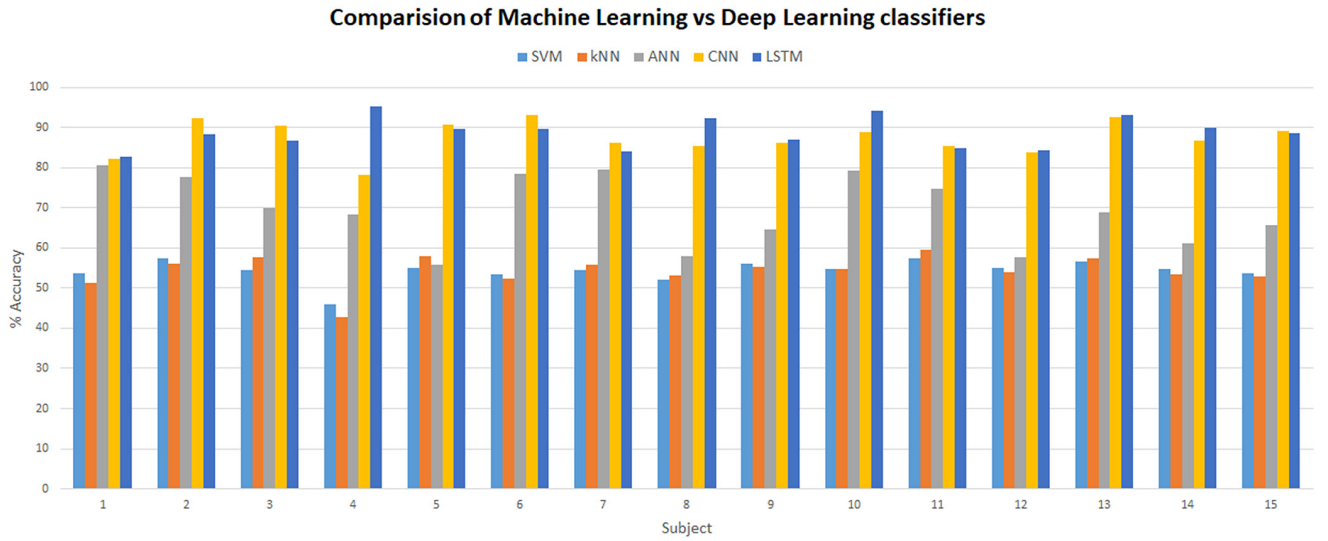

FIGURE 13 | Comparison between machine learning (SVM, *k*-NN, and ANN) and deep learning (CNN and LSTM) classifiers. SVM, support vector machine; *k*-NN, *k*-nearest neighbor; ANN, artificial neural network; CNN, convolutional neural network; LSTM, long short-term memory.

increases classification, accuracies of ML algorithms decrease. Stangl et al. (2013) classified fNIRS signals during baseline, motor imagery, and MA with an accuracy of 63%. Power et al. (2012) and Yoo et al. (2018) discriminated between three mental tasks with average accuracies of 37.96 and 62.5% using SVM and LDA, respectively. ANN has a higher generalization ability over complex patterns owing to the presence of a huge number of parameters, layers, and non-linear transfer functions. ANN shows better-improved accuracies over other conventional ML techniques. Hennrich et al. (2015) reported 84% accuracy on three mental states using neural network (NN). Abibullaev et al. (2011) managed to get a minimum 71.88% and more accuracy with different NN architectures. In this study, the average ANN accuracy is 69.36%, whereas the highest accuracy with ANN is 80.66%. ANN requires different features, and as the number of features increases, the lgorithms suffer from the curse of dimensionality. The dimensionality of ANN increases as the number of selected features times the number of channels increases, which makes dataset huge and computationally expensive. To cater this "curse of dimensionality," advance algebraic techniques like principal component analysis (PCA), independent component analysis (ICA), isomap spectral embedding, and QR matrix factorization are used in various studies (Huppert et al., 2009). Also, if data are not carefully preprocessed, over-fitting counterfeits the results on validation set, and algorithms may fail on real-time test data (Cawley and Talbot, 2010).

The trend of employing DNN for classification in BCI and MWL analysis is increasing over the past few years (Nagel and Spüler, 2019). Hennrich et al. (2015) used DNN to effectively classify brain signals. Naseer et al. (2016) analyzed the difference between two cognitive states (MA and rest) on the basis of fNIRS signals using multilayer perceptron (MLP). Huve et al. (2017) classified the fNIRS signals with three mental states including subtractions, word generation, and rest. They employed an MLP model for classification. In another study, Huve et al. (2018) repeated the same procedure for binary classification to control a robot. Hiwa et al. (2016) and Ozge Mercanoglu et al. (2017) attempted to predict the gender of the subjects through their unique fNIRS signals. Saadati et al. (2019a,b) employed CNN using hybrid fNIRS–EEG settings for three-level MWL classification. Ho et al. (2019) developed DBN and CNN for discriminating MWL levels from multichannel fNIRS signals. Left and right motor imageries were classified using DNN in the study of Thanh et al. (2013), and different mental tasks were classified by Abibullaev et al. (2011). In this study, we employed Conv1D CNN architecture, which is a variant of CNN tweaked specifically for time-varying data.

The strength of CNN lies in its self-feature extracting mechanism, which makes it not only powerful but also a preferable choice over the ML algorithms. CNN can independently be used as a full-fledged classifier (feature extraction plus classification) or as a feature extractor with ML classifiers (Tanveer et al., 2019; Zhang et al., 2019). The latter method is to use convolution layers as feature extractors, and acquired features from any fully connected layer are used by ML classifiers like SVM or *k*-NN for classification. This approach has recently been used in fNIRS BCI study (Tanveer et al., 2019) where brain heat maps are used as datasets. In this approach, the training time and computational resources required to train the CNN model increase many folds because time-series data correspond to a single vector, and the images are 2-D and 3-D matrices (2-D in case of gray scale and 3-D in case of RGB image). Matrix manipulation and operations are always expensive in terms of computation than vector operations. The same is true for the forward pass (test time) as well. Our recommendation is to use 1×1 bottleneck, and 3×3 and 5×5 filters

for increasing non-linearity and dimensionality reduction in the network instead of using separate classifiers (Lin et al., 2013). In this study, the highest accuracy achieved on any subject with CNN is 93.02%. CNN outperforms all ML algorithms including ANN with a huge margin, as presented in **Figure 13**. For the verification of experimental paradigm, MWL task difficulty validation is measured with subjective measure NASA-TLX index. In future research, SWAT analysis can also be used to gauge the strength and reliability of an experimental paradigm. Further research could be used to explore the full potential of LSTM in a multitask environment with the application of big data MWL analysis using real-time neuroergonomics and neurofeedback settings.

Long short-term memory is a variant of RNN that uses internal state (memory) to process the sequence of input (Li and Wu, 2015). LSTM shows remarkable improvement in case of time-series data like speech recognition and text-to-speech conversions (Gers and Schmidhuber, 2001; Gers et al., 2003; Graves et al., 2009, 2013; Li and Wu, 2015). So LSTMs are well suited for classifying, processing, and forecasting predictions on the basis of time-series fNIRS data. This is the first study to explore the classification capabilities of LSTM for four MWL phases on time-series fNIRS brain signals. In this study, results showed outstanding performance (highest accuracy) of LSTM over ML classifiers (highest accuracy) and even above DL-CNN (highest accuracy 93.02%). LSTM outperformed the current state-of-the-art algorithm on CNN by more than 2.51%. The highest accuracy achieved with LSTM is 95.51%. **Figure 13** shows a detailed comparison of DL (LSTM and CNN) and ML (ANN, SVM, and *k*-NN) classifiers. Being a relatively new algorithm (LSTM) in neuroscience, there is a lot of room for further research and exploration. Computational time and resources required for LSTM and other ML and DL classifiers can also be compared and analyzed in future research studies.

CONCLUSION

In this study, four-state MWLs were evaluated and classified using three ML (SVM, *k*-NN, and ANN) and two DL (CNN and LSTM) algorithms using fNIRS hemodynamics signals. Data reliability and significance are validated by *p*- and *t*-tests per channel. Nine extracted features from original hemodynamic signals were used with two feature combination arrangements for ML classification. The signal mean–slope (M–S) combination yielded the average classification accuracy of 54.33, 54.31, and 69.36% using SVM, *k*-NN, and ANN, respectively. Averaged classification accuracy achieved by CNN is 87.45%, and it outperformed all conventional classifiers by an acceptable margin. This study shows that LSTM can be effectively used for optimum classification of MWL-fNIRS brain signals with classification accuracies ranging from 83.11 to 95.51%. Classification accuracies of LSTM are compared with the accuracies achieved using SVM, ANN, KNN, and CNN methods. LSTM works better than CNN, ANN, and other conventional classifiers. The average accuracy achieved with LSTM is 89.31%, which is greater as compared with the average accuracy (87.45%) acquired using CNN. The novelties of this study are that four levels of MWL are estimated using a combination of mental logic and MA tasks and also for the first time LSTM is implemented on four-level MWL-fNIRS data with achieved optimum classification accuracies.

DATA AVAILABILITY STATEMENT

All datasets generated for this study are included in the article/**Supplementary Material**.

ETHICS STATEMENT

The studies involving human participants were reviewed and approved by the Ethical Research Council of RISE at SMME—National University of Sciences and Technology (NUST). The patients/participants provided their written informed consent to participate in this study.

AUTHOR CONTRIBUTIONS

UA, KK, and NN contributed to the conception of the study. UA and MK provided the methodology. UA, KK, and MK acquired the software, conducted the investigation, and formally analyzed the results. MK, NN, and UA validated the results. RA, YA, and SB acquired the resources and supervised the study. UA, KK, and YA wrote the original draft. UA, MK, SB, and KK revised and edited the manuscript. UA, NN, and SN provided the visualization. RA, SB, YA, and SN administered the experimentation. All authors contributed to the article and approved the submitted version.

ACKNOWLEDGMENTS

We would like to acknowledge the School of Mechanical and Manufacturing Engineering (SMME), National University of Sciences and Technology (NUST), Islamabad, Pakistan, for providing necessary support, laboratory equipment, and facilities to conduct this study. We would also like to acknowledge the EU H2020 RISE ENHANCE project (MSCA-RISE 823904).

SUPPLEMENTARY MATERIAL

The Supplementary Material for this article can be found online at: https://www.frontiersin.org/articles/10.3389/fnins.2020.00584/full#supplementary-material

REFERENCES

Abibullaev, B., and Jinung, A. (2012). Classification of frontal cortex haemodynamic responses during cognitive tasks using wavelet transforms and machine learning algorithms. *Med. Eng. Phys.* 34, 1394–1410. doi: 10.1016/j.medengphy.2012.01.002

Abibullaev, B., Jinung, A., and Moon, J. I. (2011). Neural network classification of brain hemodynamic responses from four mental tasks. *Int. J. Optomechatronics* 5, 340–359. doi: 10.1080/15599612.2011.633209

Asgher, U., Ahmad, R., Naseer, N., Ayaz, Y., Khan, M. J., and Amjad, K. A. (2019). Assessment and classification of mental workload in the prefrontal cortex (PFC) using fixed-value modified beer-lambert law. *IEEE Access.* 7, 143250–143262. doi: 10.1109/access.2019.2944965

Ayaz, H., and Dehais, F. (2019). *Neuroergonomics: The Brain at Work and Everyday Life*. Elsevier: Academic Press.

Ayaz, H., Izzetoglu, M., Izzetoglu, K., and Onaral, B. (2018). "The use of functional near-infrared spectroscopy in neuroergonomics," in *Neuroergonomics*, ed. C. S. Nam (Berlin: Springer Nature), 17–25. doi: 10.1016/b978-0-12-811926-6.00003-8

Bashashati, A., Fatourechi, M., Rabab, K. W., and Gary, E. B. (2007). A survey of signal processing algorithms in brain–computer interfaces based on electrical brain signals. *J. Neural Eng.* 4, R32–R57. doi: 10.1088/1741-2560/4/2/R03

Bergasa, L. M., Cabello, E., Arroyo, R., Romera, E., and Serrano, A. (2018). "Chapter 9 - Human Factors," in *Intelligent Vehicles*, ed. F. Jiménez (Oxford: Butterworth-Heinemann), 345–394.

Bioulac, S., Micoulaud-Franchi, J. A., Arnaud, M., Sagaspe, P., Moore, N., and Salvo, F. (2017). Risk of motor vehicle accidents related to sleepiness at the wheel: a systematic review and meta-analysis. *Sleep* 40:zsx134. doi: 10.1093/sleep/zsx134

Byrne, A., Murphy, A., McIntyre, O., and Tweed, N. (2013). The relationship between experience and mental workload in anaesthetic practice: an observational study. *Anaesthesia* 68, 1266–1272. doi: 10.1111/anae.12455

Cain, B. (2007). *A Review of the Mental Workload Literature*. Toronto, ON: Defence Research and Development.

Canning, C., and Scheutz, M. (2013). Functional near-infrared spectroscopy in human-robot interaction. *J. Hum. Robot Int.* 2, 62–84. doi: 10.5898/JHRI.2.3.Canning

Cawley, G. C., and Talbot, N. L. C. (2010). On over-fitting in model selection and subsequent selection bias in performance evaluation. *J. Mach. Learn. Res.* 11, 2079–2107.

Chen, Y., Yan, S., and Tran, C. C. (2019). Comprehensive evaluation method for user interface design in nuclear power plant based on mental workload. *Nuclear Eng. Technol.* 51, 453–462. doi: 10.1016/j.net.2018.10.010

Coyle, S., Tomás, E., Ward, T., Markham, C., and McDarby, G. (2004). On the suitability of Near-Infrared (NIR) systems for next-generation brain-computer interfaces. *Physiol. Meas.* 25, 815–822. doi: 10.1088/0967-3334/25/4/003

Cui, X., Bray, S., and Reiss, A. L. (2010). Speeded near infrared spectroscopy (NIRS) response detection. *PLoS One* 5:e15474. doi: 10.1371/journal.pone.0015474

Curtin, A., and Ayaz, H. (2018). The age of neuroergonomics: towards ubiquitous and continuous measurement of brain function with fNIRS. *Jpn Psychol. Res.* 60, 374–386. doi: 10.1111/jpr.12227

Curtin, A., Tong, S., Sun, J., Wang, J., Onaral, B., and Ayaz, H. (2019). A systematic review of integrated functional near-infrared spectroscopy (fNIRS) and transcranial magnetic stimulation (TMS) studies. *Front. Neurosci.* 13:84. doi: 10.3389/fnins.2019.00084

Dos Santos, C., and Gatti, M. (2014). "Deep convolutional neural networks for sentiment analysis of short texts," in *Proceedings of COLING 2014, the 25th International Conference on Computational Linguistics: Technical Papers*, Dublin, 69–78.

Faress, A., and Chau, T. (2013). Towards a multimodal brain-computer interface: combining FNIRS and FTCD measurements to enable higher classification accuracy. *NeuroImage* 77, 186–194. doi: 10.1016/j.neuroimage.2013.03.028

Fazli, S., Mehnert, J., Steinbrink, J., Curio, G., Villringer, A., Müller, K. R., et al. (2012). Enhanced performance by a hybrid NIRS-EEG brain computer interface. *NeuroImage* 59, 519–529. doi: 10.1016/j.neuroimage.2011.07.084

Franceschini, M. A., Joseph, D. K., Huppert, T. J., Diamond, S. G., and Boas, D. A. (2006). Diffuse optical imaging of the whole head. *J. Biomed. Opt.* 11:054007. doi: 10.1117/1.2363365

Frey, J., Mühl, C., Lotte, F., and Hachet, M. (2014). "Review of the use of electroencephalography as an evaluation method for human-computer interaction," in *PhyCS - International Conference on Physiological Computing Systems*, Lisbonne.

Galy, E., Cariou, M., and Mélan, C. (2012). What is the relationship between mental workload factors and cognitive load types? *Int. J. Psychophysiol.* 83, 269–275. doi: 10.1016/j.ijpsycho.2011.09.023

Gers, F. A., and Schmidhuber, J. (2001). LSTM recurrent networks learn simple context-free and context-sensitive languages. *IEEE Trans. Neural Netw.* 12, 1333–1340. doi: 10.1109/72.963769

Gers, F. A., Schraudolph, N. N., and Schmidhuber, J. (2003). Learning precise timing with LSTM recurrent networks. *J. Mach. Learn. Res.* 3, 115–143. doi: 10.1162/153244303768966139

Glorot, X., and Bengio, Y. (2010). *Understanding the Difficulty of Training Deep Feedforward Neural Networks*. Palermo: AISTATS.

Graves, A., Liwicki, M., Fernández, S., Bertolami, R., Bunke, H., and Schmidhuber, J. (2009). A Novel connectionist system for unconstrained handwriting recognition. *IEEE Trans. Patt. Anal. Mach. Intell.* 31, 855–868. doi: 10.1109/TPAMI.2008.137

Graves, A., Mohamed, A. R., and Hinton, G. (2013). "Speech recognition with deep recurrent neural networks," in *ICASSP, IEEE International Conference on Acoustics, Speech and Signal Processing - Proceedings*, Vancouver, BC.

Greff, K., Srivastava, R. K., Koutník, J., Steunebrink, B. R., and Schmidhuber, J. (2016). LSTM: a search space odyssey. *IEEE Trans. Neural Netw. Learn. Syst.* 28, 2222–2232. doi: 10.1109/TNNLS.2016.2582924

Harrison, A. H., and Connolly, J. F. (2013). Finding a way in: a review and practical evaluation of FMRI and EEG for detection and assessment in disorders of consciousness. *Neurosci. Biobehav. Rev.* 7, 1403–1419. doi: 10.1016/j.neubiorev.2013.05.004

Hennrich, J., Herff, C., Heger, D., and Schultz, T. (2015). Investigating deep learning for FNIRS Based BCI. *Conf. Proc. IEEE Eng. Med. Biol. Soc.* 2015, 2844–2847.

Herff, C., Heger, D., Putze, F., Hennrich, J., Fortmann, O., and Schultz, T. (2013). "Classification of mental tasks in the prefrontal cortex using fNIRS," in *2013 35th Annual International Conference of the IEEE Engineering in Medicine and Biology Society (EMBC)*, Osaka: IEEE, 2160–2163.

Hiroyasu, T., Yoshida, T., and Yamamoto, U. (2015). "Investigation of regions of interest (ROI) through the selection of optimized channels in fNIRS data," in *2015 IEEE Congress on Evolutionary Computation (CEC*, Sendai, 764–768.

Hiwa, S., Hanawa, K., Tamura, R., Hachisuka, K., and Hiroyasu, T. (2016). Analyzing brain functions by subject classification of functional near-infrared spectroscopy data using convolutional neural networks analysis. *Comput. Intell. Neurosci.* 2016:1841945. doi: 10.1155/2016/1841945

Hiwa, S., Miki, M., and Hiroyasu, T. (2017). Validity of decision mode analysis on an ROI determination problem in multichannel fNIRS data. *Artif Life Rob.* 22, 336–345. doi: 10.1007/s10015-017-0362-5

Ho, T. K. K., Gwak, J., Park, C. M., and Song, J. I. (2019). Discrimination of mental workload levels from multi-channel FNIRS using deep leaning-based approaches. *IEEE Access.* 7, 24392–24403. doi: 10.1109/ACCESS.2019.2900127

Holper, L., and Wolf, M. (2011). Single-trial classification of motor imagery differing in task complexity: a functional near-infrared spectroscopy study. *J. NeuroEng. Rehabil.* 8:34. doi: 10.1186/1743-0003-8-34

Hong, K., and Santosa, H. (2013). "Current BCI technologies in brain engineering," in *2013 International Conference on Robotics, Biomimetics, Intelligent Computational Systems*, Jogjakarta, 1–4.

Hong, K.-S., and Khan, M. J. (2017). Hybrid brain–computer interface techniques for improved classification accuracy and increased number of commands: a review. *Front. Neurorobot.* 11:35. doi: 10.3389/fnbot.2017.00035

Hong, K.-S., Naseer, N., and Kim, Y. H. (2015). Classification of prefrontal and motor cortex signals for three-class FNIRS-BCI. *Neurosci. Lett.* 587, 87–92. doi: 10.1016/j.neulet.2014.12.029

Hong, K.-S., and Santosa, H. (2016). Decoding four different sound-categories in the auditory cortex using functional near-infrared spectroscopy. *Hear. Res.* 333, 157–166. doi: 10.1016/j.heares.2016.01.009

Hortal, E., Ubeda, A., Ianez, E., Planelles, D., and Azorin, J. M. (2013). "Online Classification of Two Mental Tasks Using a SVM-Based BCI System," in *International IEEE/EMBS Conference on Neural Engineering*, San Diego, CA: NER.

Hosseini, R., Walsh, B., Tian, F., and Wang, S. (2018). An fNIRS-based feature learning and classification framework to distinguish hemodynamic patterns in children who stutter. *IEEE Trans. Neural Syst. Rehabil. Eng.* 26, 1254–1263. doi: 10.1109/TNSRE.2018.2829083

Huppert, T. J., Diamond, S. G., Franceschini, M. A., and David, A. (2009). HomER: a review of time-series analysis methods for near-infrared spectroscopy of the brain. *Appl. Opt.* 48, D280–D298. doi: 10.1364/AO.48.00D280

Huve, G., Takahashi, K., and Hashimoto, M. (2017). "Brain activity recognition with a wearable fNIRS using neural networks," *2017 IEEE International Conference on Mechatronics and Automation (ICMA)* (Takamatsu), 1573–1578. doi: 10.1109/ICMA.2017.8016051

Huve, G., Takahashi, K., and Hashimoto, M. (2018). "Brain-computer interface using deep neural network and its application to mobile robot control," in *Proceedings - 2018 IEEE 15th International Workshop on Advanced Motion Control*, Tokyo: AMC.

İşbilir, E., Çakır, M. P., Acartürk, C., and Tekerek, A. S. (2019). Towards a multimodal model of cognitive workload through synchronous optical brain imaging and eye tracking measures. *Front. Hum. Neurosci.* 13:375. doi: 10.3389/fnhum.2019.00375

Izzetoglu, K., Ayaz, H., Merzagora, A., Izzetoglu, M., Shewokis, P. A., Bunce, S. C., et al. (2011). The evolution of field deployable fNIR spectroscopy from bench to clinical settings. *J. Innovat. Opt. Health Sci.* 4, 239–250. doi: 10.1142/s1793545811001587

Khan, M. J., and Hong, K.-S. (2015). Passive BCI based on drowsiness detection: an fnirs study. *Biomed. Opt. Exp.* 6, 4063–4078. doi: 10.1364/BOE.6.004063

Khan, R. A., Naseer, N., Qureshi, N. K., Noori, F. M., Nazeer, H., and Khan, J. M. (2018). fNIRS-based neurorobotic Interface for gait rehabilitation. *J. NeuroEng. Rehabil.* 15, 7. doi: 10.1186/s12984-018-0346-2

Kingma, D. P., and Ba, J. L. (2015). "Adam: A method for stochastic optimization," in *3rd International Conference on Learning Representations, ICLR 2015 - Conference Track Proceedings*, Ithaca, NY: arXiv.org, 1–13.

Kosti, M. V., Georgiadis, K. K., Adamos, D. A., Laskaris, N., and Angelis, L. (2018). Towards an affordable brain computer interface for the assessment of programmers' mental workload. *Int. J. Hum. Comput. Stud.* 115, 52–66. doi: 10.1016/j.ijhcs.2018.03.002

Lachaux, J. P., Rudrauf, D., and Kahane, P. (2003). Intracranial EEG and human brain mapping. *J. Physiol. Paris* 97, 613–628. doi: 10.1016/j.jphysparis.2004.01.018

LeCun, Y., and Bengio, Y. (1995). "Convolutional networks for images, speech, and time series," in *The Handbook of Brain Theory and Neural Networks*, Vol 3361 ed M. A. Arbib (Cambridge, MA: MIT Press), 10.

Li, X., and Wu, X. (2015). "Constructing long short-term memory based deep recurrent neural networks for large vocabulary speech recognition," in *ICASSP, IEEE International Conference on Acoustics, Speech and Signal Processing*, Brisbane, QLD.

Lin, M., Chen, Q., and Yan, S. (2013). Network in network. *ArXiv* [Preprint] Avaliable online at: https://arxiv.org/abs/1312.4400 (accessed November 14, 2019).

Liu, Y., and Ayaz, H. (2018). Speech recognition via fnirs based brain signals. *Front. Neurosci.* 12:695. doi: 10.3389/fnins.2018.00695

Longo, L. (2018). Experienced mental workload, perception of usability, their interaction and impact on task performance. *PLoS One* 13:e0199661. doi: 10.1371/journal.pone.0199661

Lotte, F. (2014). "A tutorial on EEG signal-processing techniques for mental-state recognition in brain–computer interfaces," in *Guide to Brain-Computer Music Interfacing*, eds R. Miranda and J. Castet (Berlin: Springer), 133–161. doi: 10.1007/978-1-4471-6584-2_7

Manning, C. D., Raghavan, P., and Schütze, H. (2008). "Support vector machines and machine learning on documents," in *Introduction to Information Retrieval*, (Cambridge: Cambridge University Press), 319–348. doi: 10.1017/CBO9780511809071.016

Mehta, R. K., and Parasuraman, R. (2013). Neuroergonomics: a review of applications to physical and cognitive work. *Front. Hum. Neurosci.* 7:889. doi: 10.3389/fnhum.2013.00889

Nagel, S., and Spüler, M. (2019). World's fastest brain-computer interface: combining EEG2Code with deep learning. *PLoS One* 14:e0221909. doi: 10.1371/journal.pone.0221909

Naseer, N., and Hong, K.-S. (2013). Classification of functional near-infrared spectroscopy signals corresponding to the right- and left-wrist motor imagery for development of a brain-computer interface. *Neurosc. Lett.* 553, 84–89. doi: 10.1016/j.neulet.2013.08.021

Naseer, N., and Hong, K.-S. (2015). FNIRS-based brain-computer interfaces: a review. *Front. Hum. Neurosci.* 9:3. doi: 10.3389/fnhum.2015.00003

Naseer, N., Hong, M. J., and Hong, K.-S. (2014). Online binary decision decoding using functional near-infrared spectroscopy for the development of brain–computer interface. *Exp. Brain Res.* 232, 555–564. doi: 10.1007/s00221-013-3764-1

Naseer, N., Qureshi, N. K., Noori, F. M., and Hong, K.-S. (2016). Analysis of different classification techniques for two-class functional near-infrared spectroscopy-based brain-computer interface. *Comput. Intell. Neurosci.* 2016:5480760. doi: 10.1155/2016/5480760

Noyes, J. M., and Bruneau, D. P. J. (2007). A self-analysis of the NASA-TLX workload measure. *Ergonomics* 50, 514–519. doi: 10.1080/00140130701235232

Ozge Mercanoglu, S., Yalim Keles, H., Kır, Y., Kuşman, A., and Baskak, B. (2017). Person identification using functional near-infrared spectroscopy signals using a fully connected deep neural network. *Commun. Fac. Sci. Univ. Ank. Series A2–A3* 59, 55–67. doi: 10.1501/commua1-2_0000000104

Paulhus, D. L., and Vazire, S. (2007). "The self-report method," in *Handbook of Research Methods in Personality Psychology*, eds R. W. Robins, R. C. Fraley, and R. F. Krueger (New York, NY: The Guilford Press), 224–239.

Power, S. D., and Chau, T. (2013). Automatic single-trial classification of prefrontal hemodynamic activity in an individual with duchenne muscular dystrophy. *Dev. Neurorehabil.* 16, 67–72. doi: 10.3109/17518423.2012.718293

Power, S. D., Kushki, A., and Chau, T. (2011). Towards a system-paced near-infrared spectroscopy brain–computer interface: differentiating prefrontal activity due to mental arithmetic and mental singing from the no-control state. *J. Neural Eng.* 8:066004. doi: 10.1088/1741-2560/8/6/066004

Power, S. D., Kushki, A., and Chau, T. (2012). Automatic single-trial discrimination of mental arithmetic, mental singing and the no-control state from prefrontal activity: toward a three-State NIRS-BCI. *BMC Res. Notes* 5:14. doi: 10.1186/1756-0500-5-141

Pucci, O., Toronov, V., and St Lawrence, K. (2010). Measurement of the optical properties of a two-layer model of the human head using broadband near-infrared spectroscopy. *Appl. Opt.* 49, 6324–6332. doi: 10.1364/AO.49.006324

Saadati, M., Nelson, J., and Ayaz, H. (2019a). "Multimodal FNIRS-EEG classification using deep learning algorithms for brain-computer interfaces purposes," in *Advances in Intelligent Systems and Computing AHFE (2019)*. doi: 10.1007/978-3-030-20473-0_21

Saadati, M., Nelson, J., and Ayaz, H. (2019b). "Convolutional Neural Network for Hybrid FNIRS-EEG Mental Workload Classification," in *International Conference on Applied Human Factors and Ergonomics (AHFE 2019)*,Cham: Springer, 221–232. doi: 10.1007/978-3-030-20473-0_22

Santosa, H., Aarabi, A., Perlman, S. B., and Huppert, T. J. (2017). Characterization and correction of the false-discovery rates in resting state connectivity using functional near-infrared spectroscopy. *J. Biomed. Opt.* 22:55002. doi: 10.1117/1.jbo.22.5.055002

Santosa, H., Hong, M. J., Kim, S.-P., and Hong, K.-S. (2013). Noise reduction in functional near-infrared spectroscopy signals by independent component analysis. *Rev. Sci. Instrum.* 84:073106. doi: 10.1063/1.4812785

Schmidhuber, J., and Hochreiter, S. (1997). Long short-term memory. *Neural Comput.* 9, 1735–1780. doi: 10.1162/neco.1997.9.8.1735

Schudlo, L. C., and Chau, T. (2013). Dynamic topographical pattern classification of multichannel prefrontal NIRS signals: II. Online differentiation of mental arithmetic and rest. *J. Neural Eng.* 11:016003. doi: 10.1088/1741-2560/11/1/016003

Stangl, M., Bauernfeind, G., Kurzmann, J., and Scherer, R. (2013). A Haemodynamic brain-computer interface based on real-time classification of near infrared spectroscopy signals during motor imagery and mental arithmetic. *J. Near Infrared Spectroscopy* 21, 157–171. doi: 10.1255/jnirs.1048

Strait, M., and Scheutz, M. (2014). What we can and cannot (yet) do with functional near infrared spectroscopy. *Front. Neurosci.* 8:117. doi: 10.3389/fnins.2014.00117

Sumantri, A. F., Wijayanto, I., Patmasari, R., and Ibrahim, N. (2019). Motion artifact contaminated functional near-infrared spectroscopy signals classification using K-Nearest Neighbor (KNN). *IOP J. Phys. Conf. Ser.* 1201:012062. doi: 10.1088/1742-6596/1201/1/012062

Tai, K., and Chau, T. (2009). Single-trial classification of NIRS signals during emotional induction tasks: towards a corporeal machine interface. *J. NeuroEng. Rehabil.* 6:39. doi: 10.1186/1743-0003-6-39

Tanveer, M. A., Khan, M. J., Qureshi, M. J., and Naseer, N. (2019). Enhanced drowsiness detection using deep learning: an FNIRS study. *IEEE Access.* 7, 137920–137929. doi: 10.1109/access.2019.2942838

Thanh, H. N., Cuong, N. Q., Dang, K. T. Q., and Van, T. V. (2013). Temporal hemodynamic classification of two hands tapping using functional near—infrared spectroscopy. *Front. Hum. Neurosci.* 7:516. doi: 10.3389/fnhum.2013.00516

Tong, Y., Hocke, L. M., Lindsey, K. P., Erdoðan, S. B., Vitaliano, G., and Caine, C. E. (2016). Systemic low-frequency oscillations in BOLD signal vary with tissue type. *Front. Neurosci.* 10:313. doi: 10.3389/fnins.2016.00313

Trakoolwilaiwan, T., Behboodi, B., Lee, J., Kim, K., and Choi, J. W. (2017). Convolutional neural network for high-accuracy functional near-infrared spectroscopy in a brain–computer interface: three-class classification of rest, right-, and left-hand motor execution. *Neurophotonics* 5:011008. doi: 10.1117/1.NPh.5.1.011008

Tran, T. Q., Boring, R. L., Dudenhoeffer, D. D., Hallbert, B. P., Keller, M. D., Anderson, Y. M., et al. (2007). "Advantages and disadvantages of physiological assessment for next generation control room design," in *IEEE 8th Human Factors and Power Plants and HPRCT 13th Annual Meeting*, Monterey, CA, 259–263.

Wang, F., Mao, M., Duan, L., Huang, Y., Li, Z., and Zhu, C. (2018). Intersession Instability in fNIRS-Based emotion recognition. *IEEE Trans. Neural Syst. Rehabil. Eng.* 26, 1324–1333. doi: 10.1109/TNSRE.2018.2842464

Wang, Y., Nakanishi, M., and Zhang, D. (2019). EEG-based brain-computer interfaces. *Adv. Exp. Med. Biol.* 101, 41–65. doi: 10.1007/978-981-13-2050-7_2

Wong, T. T. (2015). Performance evaluation of classification algorithms by k-fold and leave-one-out cross validation. *Patt. Recognit.* 48, 2839–2846. doi: 10.1016/j.patcog.2015.03.009

Yoo, S.-H., Woo, S.-W., and Amad, Z. (2018). "Classification of three categories from prefrontal cortex using LSTM networks: fNIRS study," *18th International Conference on Control. Automation and Systems (ICCAS-2018)* PyeongChang, 1141–1146.

Zhang, S., Li, X., Zong, M., Zhu, X., and Wang, R., (2018). Efficient kNN classification with different numbers of nearest neighbors. *IEEE Transactions on Neural Networks and Learning Systems* 29, 1774–1785. doi: 10.1109/TNNLS.2017.2673241

Zhang, X., Yao, L., Wang, X., Monaghan, J., Mcalpine, D., and Zhang, Y. (2019). A survey on deep learning based brain computer interface: recent advances and new frontiers. *ArXiv* [Preprint] Avaliable online at: https://arxiv.org/abs/1905.04149 (accessed November 14, 2019).

Conflict of Interest: The authors declare that the research was conducted in the absence of any commercial or financial relationships that could be construed as a potential conflict of interest.

frontiers in Neuroscience

ORIGINAL RESEARCH
published: 11 August 2020
doi: 10.3389/fnins.2020.00795

Tracing Pilots' Situation Assessment by Neuroadaptive Cognitive Modeling

Oliver W. Klaproth[1,2], Christoph Vernaleken[3], Laurens R. Krol[4], Marc Halbruegge[2], Thorsten O. Zander[4,5] and Nele Russwinkel[2]*

[1] Airbus Central R&T, Hamburg, Germany, [2] Chair of Cognitive Modelling in Dynamic Systems, Department of Psychology and Ergonomics, Technische Universität Berlin, Berlin, Germany, [3] Airbus Defence and Space, Manching, Germany, [4] Zander Laboratories B.V., Amsterdam, Netherlands, [5] Chair of Neuroadaptive Human-Computer Interaction, Brandenburg University of Technology, Cottbus-Senftenberg, Germany

This study presents the integration of a passive brain-computer interface (pBCI) and cognitive modeling as a method to trace pilots' perception and processing of auditory alerts and messages during operations. Missing alerts on the flight deck can result in out-of-the-loop problems that can lead to accidents. By tracing pilots' perception and responses to alerts, cognitive assistance can be provided based on individual needs to ensure they maintain adequate situation awareness. Data from 24 participating aircrew in a simulated flight study that included multiple alerts and air traffic control messages in single pilot setup are presented. A classifier was trained to identify pilots' neurophysiological reactions to alerts and messages from participants' electroencephalogram (EEG). A neuroadaptive ACT-R model using EEG data was compared to a conventional normative model regarding accuracy in representing individual pilots. Results show that passive BCI can distinguish between alerts that are processed by the pilot as task-relevant or irrelevant in the cockpit based on the recorded EEG. The neuroadaptive model's integration of this data resulted in significantly higher performance of 87% overall accuracy in representing individual pilots' responses to alerts and messages compared to 72% accuracy of a normative model that did not consider EEG data. We conclude that neuroadaptive technology allows for implicit measurement and tracing of pilots' perception and processing of alerts on the flight deck. Careful handling of uncertainties inherent to passive BCI and cognitive modeling shows how the representation of pilot cognitive states can be improved iteratively for providing assistance.

Keywords: situation awareness, aviation, brain-computer-interfaces, ACT-R, human-automation interaction

OPEN ACCESS

Edited by:
Davide Valeriani, Massachusetts Eye and Ear Infirmary and Harvard Medical School, United States

Reviewed by:
Frederic Dehais, Institut Supérieur de l'Aéronautique et de l'Espace (ISAE-SUPAERO), France
Pietro Aricò, Sapienza University of Rome, Italy
Gianluca Di Flumeri, Sapienza University of Rome, Italy

****Correspondence:***
Oliver W. Klaproth
oliver.klaproth@airbus.com

Specialty section:
This article was submitted to Neural Technology, a section of the journal Frontiers in Neuroscience

Received: *08 May 2020*
Accepted: *07 July 2020*
Published: *11 August 2020*

Citation:
Klaproth OW, Vernaleken C, Krol LR, Halbruegge M, Zander TO and Russwinkel N (2020) Tracing Pilots' Situation Assessment by Neuroadaptive Cognitive Modeling. Front. Neurosci. 14:795. doi: 10.3389/fnins.2020.00795

INTRODUCTION

Irrespective of ubiquitous automation, current-generation commercial and business aircraft still rely on pilots to resolve critical situations caused, among others, by system malfunctions. Pilots need to maintain situational awareness (SA) so they can assume manual control or intervene when necessary. It is essential for flight safety that pilots understand the criticality of flight deck alerts, and do not accidentally miss alerts, e.g., due to high workload and cognitive tunneling (Dehais et al., 2014). Human-machine interfaces

on the flight deck therefore need to ensure messages are processed correctly to reduce the risk of out-of-the-loop problems (Endsley and Kiris, 1995; Berberian et al., 2017). Failed, delayed or otherwise inadequate response to flight deck alerts has been associated with several fatal accidents in the past (Air Accident Investigation and Aviation Safety Board, 2006; Aviation Safety Council, 2016).

Automation has transformed pilots' role from hands-on flying to monitoring system displays which is ill-matched to human cognitive capabilities (Bainbridge, 1983) and facilitates more superficial processing of information (Endsley, 2017). Furthermore, reduced-crew (e.g., single-pilot) operations can increase demands on pilots in commercial aircraft through elevated workload of remaining crew (Harris et al., 2015) and higher complexity imposed by additional automation (Bailey et al., 2017). More complex automation can impede the detection of divergence in the situation assessment by human operator and automated system, neither of which may adequately reflect reality (Rußwinkel et al., 2020). We believe that neurotechnologies can be used for cognitive enhancement and support of pilots in face of increased demands (Scerbo, 2006; Cinel et al., 2019). One way to achieve this is by monitoring the pilots' cognitive states and performance during flight deck operations in order to detect the onset of such divergence e.g., cognitive phenomena that may lead to out-of-the-loop situations. Being able to detect such cognitive states, corrective measures may be initiated to prevent or reduce risk of out-of-the-loop situations and to maintain the high level of safety in aviation.

OOTL and Situation Awareness

Out-of-the-loop problems arise when pilots lack SA (Endsley and Jones, 2011). SA is progressively developed through the levels of perception (1), comprehension (2), and projection (3) of a situation's elements. Missing critical alerts impairs situation perception and inhibits the development of higher SA levels. In a study on pilot errors, the vast majority of errors could be accounted to incorrect perception (70.3%) and comprehension (20.3%) of situations (Jones and Endsley, 1996).

Situational awareness is commonly measured by sampling with the help of probing questions. Probes can give insights into pilots' deeper understanding of a situation as well as whether or not a probed piece of information can be retrieved from memory. However, probing methods either require flight scenarios to be frozen (e.g., Endsley, 2000) or incur extra workload (Pierce, 2012) when assessing pilots' SA. Physiological (e.g., Berka et al., 2006; van Dijk et al., 2011; Di Flumeri et al., 2019) and performance-based metrics (e.g., Vidulich and McMillan, 2000) are less direct measures of memory contents, but they can be used unobtrusively in operations (see Endsley and Jones, 2011, for a summary of measures). As an example, van Dijk et al. (2011) showed how eye tracking can serve as an indicator of pilots' perceptual and attentional processes. The abundance of visual information in the cockpit, however, makes tracing visual attention very challenging and susceptible to selective ignoring and inattentional blindness (Haines, 1991; Most et al., 2005).

Alerts in the cockpit are presented both visually and acoustically, while acoustic stimuli have shown to be more effective in attracting attention (Spence and Driver, 1997). Physiological responses to alert stimuli may reveal whether or not alerts have been perceived and processed. For example, event-related potentials (ERPs) in operators' electroencephalogram (EEG) were proposed as indicators of attended and unattended stimuli in the assessment of SA (Endsley, 1995). Dehais et al. (2016) demonstrated that ERP components indeed allow to differentiate between missed and processed auditory stimuli in the cockpit, even in single trials (Dehais et al., 2019). They noted that these differences are primarily reflected in early perceptual and late attentional stages of auditory processing. According to Dehais et al. (2019), failure to adequately perceive or process an alert is likely due to excessive demand to cognitive resources in terms of attention and memory at a central executive level. In addition, deterministic modeling individual processed or missed alerts requires lots of data about the situation and the pilot's state and neurophysiological measures can help reduce uncertainty.

Thus, by monitoring what stimuli are provided when and checking for ERPs at stimulus onset, perception of a situation could be tracked in real-time (Wilson, 2000). After that, performance metrics in terms of comparing pilots' actual behavior to normative procedures can provide information on later SA stages. In contrast to product-focused measures, this process-based approach of situation assessment (Sarter and Sarter, 2003; Durso and Sethumadhavan, 2008) allows to also capture implicit components of SA (Endsley, 2000) that might be overlooked in SA probing.

Requirements for Cognitive State Assessment

As cognitive states underlying situation assessment are not directly observable, their detection and prediction in this study is approached from different angles by neurophysiological measures and cognitive modeling. Consistent monitoring of a pilot's situation assessment in flight requires tracing what elements of a situation are perceived and processed. Tracing perceptual and cognitive processing can best be done implicitly by interpreting psycho-physiological measures so as not to increase the pilots' load or otherwise interfere with operations. As we are interested in event-related cognitive processing, i.e., the processing of specific visual or auditory alerts, one requirement is that the onset of these alerts is captured accurately (Luck, 2014). This allows the timing of each alert to be synchronized with a measurement of the pilots' neuroelectric activity, which is sensitive to even slight temporal misalignments. This activity can then be analyzed relative to each alert's exact onset, allowing alert-specific cognitive states to be decoded. Such automated, non-intrusive detection of cognitive processing can be done using a passive brain-computer interface (pBCI), based on a continuous measurement of brain activity (Zander and Kothe, 2011; Krol et al., 2018).

If unprocessed alerts are detected, cognitive assistance can be offered depending on the alert's significance for the course of the operation. In order to assess the significance of a missed alert, its impact on SA and the operation can be simulated. This way, critical drops in pilot performance can be anticipated and

assistance can be provided to prevent the pilot from getting out of the loop. This simulation can be performed using cognitive models that capture the characteristics of the human cognitive system such as resource limitations.

Cognitive Pilot Models

ACT-R[1] (Anderson et al., 2004) is the most comprehensive and widely used architecture to build models that can simulate, predict, and keep track of cognitive dynamics. It is based on accumulated research about the human brain's modular architecture, where each module maps onto a different functional area of the brain. In its current 7.14 version the ACT-R architecture comprises separate modules for declarative and procedural memory, temporal, and intentional (i.e., "goal") processing and visual, aural, motor, speech modules for limited perceptual-motor capabilities. While highly interconnected within themselves, exchange of symbolic information between modules is constrained by a small number of interfaces that are modeled as buffers (Anderson, 2007)[2]. These intermodular connections meet in the procedural memory module (representing the caudate of the basal ganglia; Anderson et al., 2008), where condition-action statements (i.e., "productions") are triggered depending on buffer contents. Actions can be defined for example in terms of memory retrieval, directing attention or manipulating the outside world through speech or motor actions. Based on sub-symbolic mechanisms such as utility learning, spreading activation, memory decay, and random noise, ACT-R models can adapt to dynamic environments and represent average human behavior in non-deterministic fashion.

ACT-R has frequently been used for modeling pilots' cognitive dynamics (e.g., Byrne and Kirlik, 2005; Gluck, 2010; Somers and West, 2013). It allows for the creation of cognitive models according to specific task descriptions, e.g., a goal-directed hierarchical task analysis (HTA; Endsley, 1995; Stanton, 2006). When this task description focuses on maintaining good SA, a normative cognitive model can be developed that acts in order to optimize SA. Normative models can be compared to individual pilot behavior to detect deviations and to make inferences about individual pilots' SA. Tracing individual behavior (model-tracing; Fu et al., 2006) can suffer from epistemic uncertainty (Kiureghian and Ditlevsen, 2009), for example, when it is unknown why a pilot did not react to an alert. This uncertainty can be reduced by using physiological data alongside system inputs to build richer models of individual performance (Olofsen et al., 2010; Putze et al., 2015; Reifman et al., 2018). However, sensor data inaccuracies can introduce a different, aleatory kind of uncertainty that is hard to assign to individual observations and needs to be considered in design of adaptive models (Kiureghian and Ditlevsen, 2009).

ACT-R has gained popularity in modeling human autonomy interaction. The work of Putze et al. (2015) showed how an ACT-R model allows to modulate interface complexity according to operator workload measured in EEG. Ball et al. (2010) have developed a synthetic teammate able to pilot unmanned aerial vehicles and communicate with human teammates based on an extensive model of SA (see also Rodgers et al., 2013; Freiman et al., 2018). Both these models demonstrate how selected human capabilities such as piloting and communicating (McNeese et al., 2018) or being empathic to operators' cognitive state (Putze et al., 2015) can be allocated to an ACT-R model in human autonomy teaming.

Neuroadaptive Technology

Neuroadaptive technology refers to technology that uses cognitive state assessments as implicit input in order to enable intelligent forms of adaptation (Zander et al., 2016; Krol and Zander, 2017). One way to achieve this, is to maintain a model that is continuously updated using measures of situational parameters as well as the corresponding cognitive states of the user (e.g., Krol et al., 2020). Adaptive actions can then be initiated based on the information provided by the model. Cognitive states can be assessed in different ways. Generally, certain cognitive states result, on average, in specific patterns of brain activity, and can be inferred from brain activity if the corresponding pattern distributions are known. As patterns differ to some extent between individuals and even between sessions, it is usually necessary to record multiple samples of related brain activity in order to describe the pattern distribution of cognitive responses in an individual. Given a sufficient amount of samples of a sufficiently distinct pattern, a so-called classifier can be calibrated which is capable of detecting these patterns in real time, with typical single-trial accuracies between 65 and 95% (Lotte et al., 2007).

Importantly, since these cognitive states occur as a natural consequence of the ongoing interaction, no additional effort is required, nor task load induced, for them to be made detectable. It is thus possible to use a measure of a user's cognitive state as implicit input, referring to input that was acquired without this being deliberately communicated by the operator (Schmidt, 2000; Zander et al., 2014). Among other things, this has already been used for adaptive automation. For example, without the pilots explicitly communicating anything, a measure of their brain activity revealed indices of e.g., engagement or workload, allowing the automation to be increased or decreased accordingly (e.g., Pope et al., 1995; Bailey et al., 2003; Aricò et al., 2016).

In the cockpit, each alert can be expected to elicit specific cortical activity, e.g., an ERP. If this activity can be decoded to reveal whether or not the alert has been perceived, and potentially whether and how it was processed, it can be used as implicit input. Since such input can be obtained from an ongoing measurement of the pilots' brain activity, no additional demands are placed on the pilots. By interpreting this information alongside historic pilot responses and further operational parameters, an informed decision can be made about the current cognitive state of the pilots and recommended adaptive steps.

Current Study

The remainder of this article describes the implementation and application of a concept for tracing individual pilots' perception

[1] http://act-r.psy.cmu.edu/

[2] The "two streams hypothesis" (Milner and Goodale, 2008) is implemented for the visual and aural module, resulting in a visual- and aural-location buffer for the where-pathway and visual and aural buffers for the what-pathway in the respective modules.

and processing of aural alerts based on neuroadaptive cognitive modeling. In contrast to conventional measures of SA, this method is designed for application in operations that require unobtrusive tracing of cognitive states. The method is applied to explore how to anticipate pilot behavior and when to offer assistance according to their cognitive state. To this end, we test (1) the feasibility of distinguishing between processed and missed alerts based on pilots' brain activity, (2) whether individual pilot behavior can be anticipated using cognitive models, and (3) how the methods of pBCI and cognitive modeling can be integrated. Results are discussed regarding their implications for cognitive assistance on the flight deck and potential benefits for single pilot operations. Limitations are addressed to explore what else is needed in cognitive assistance for the anticipation and prevention of out-of-the-loop situations.

MATERIALS AND METHODS

This research complied with the American Psychological Association Code of Ethics and was approved by the Institutional Review Board at TU Berlin. Informed consent was obtained from each participant.

Participants

Twenty-four aircrew (one female) with a mean age of 49.08 years (SD = 6.08) participated in the flight simulator study. Participants were predominantly military pilots with an average experience of 3230 h of flight (SD = 2330.71), of which on average 51.21 h (SD = 90.76) were performed in the previous year. All participating aircrew had normal or corrected to normal vision, all but two were right-handed.

Procedure

Participating aircrew were asked for information on their flight experience and physical health relevant for physiological data assessment in the simulator. After application of EEG sensors, participants performed a desktop-based auditory oddball training paradigm (Debener et al., 2005). Participants performed 10 blocks during each of which a sequence of 60 auditory tones was presented. Each tone could be either a standard tone of 350 Hz occurring 70–80% of the time, a target deviant tone of 650 Hz (10–15%), or non-target deviant (2000 Hz, 10–15%). There was a variable interval between stimulus onsets of 1.5 $\pm$ 0.2 s, and a self-paced break after each block. Each tone lasted 339 ms. Participants were instructed to count the target tones in each block with eyes open, and to verbally report their count after each block to ensure they stayed attentive during the task. Thus, the standard tones represent frequent but task-irrelevant events, target tones represent rare task-relevant events, and the deviants were rare but task-irrelevant.

Following this, participants were seated in the simulator and briefed on the flying task. For the flight scenario, participants were instructed to avoid communicating with the experimenter during the scenario but were allowed to think aloud and to perform readbacks of air traffic control (ATC) messages just as they would during a normal flight. After the scenario, a debriefing session was conducted in order to collect feedback from participants.

Simulator and Scenario

Participants flew a mission in the fixed-base cockpit simulator of a mission aircraft similar to current-generation business jets certified according to EASA CS-23, which may be operated by a single pilot. The mission was implemented and simulated using the open source flight simulation software "FlightGear 3.4"[3]. Participants' task was to perform a fictitious routine VIP passenger transport from Ingolstadt-Manching (ETSI) to Kassel (EDVK) airport. To keep workload levels associated with basic flying low, the scenario started with the aircraft already airborne at cruise flight level (FL 250) with autopilot (altitude and NAV[4] mode) engaged. According to the flight management system (FMS) flight plan presented, the remaining flight time was approximately 40 min in fair weather conditions. To maintain speed, thrust had to be adjusted manually, since the aircraft was – like most business jets today – not equipped with auto-thrust. To simulate interactions with ATC and to ensure a consistent flow of the scenario for all participants, pilots were presented with pre-recorded routine ATC instructions relating to flight level and heading changes at fixed time intervals after the start of the scenario.

Also, at pre-defined times, pilots would encounter a series of flight deck alerts of varying, but generally increasing severity. First, 4 min into the scenario, the main fuel pump in the right wing tank failed, resulting in a caution level flight deck alert and, subsequently, the display of a simple recovery procedure, which was automatically presented as electronic checklist. After 6 min, a small fuel leak appeared in the right fuel tank, which had initially no salient flight deck effects and would therefore go mostly unnoticed. Contributing to this was a TCAS traffic advisory (caution level alert) after approximately 7 min, which would coincide with an ATC instruction to descend due to traffic (e.g., "F-UO[5], due to traffic, descend and maintain FL 280" or "F-UO, direct TUSOS and descend FL 200"). Moreover, to simulate the effects of an intermittent spurious alert, and to divert pilot attention from the FUEL format to decrease the chance of the pilot noticing the leak, an identical caution-level alert of an electrical bus system failure was triggered four times throughout the scenario. This alert would automatically be removed after 5 s without any pilot action, and before pilots were able to access the associated recovery procedure. When the fuel leak had caused a fuel imbalance exceeding a certain threshold, a caution-level alert relating to the imbalance would be raised. The associated procedure would then guide pilots through several steps intended to find the root cause of the fuel imbalance. The scenario ended once an in-flight fire of the left engine initiated after 16:40 min, resulting in a warning level alert, had successfully been extinguished by the pilot. To make sure that all participants encountered all events of the scenario, speed warnings were

[3]http://home.flightgear.org/

[4]NAV mode is a managed lateral navigation mode of the autoflight system in which the aircraft follows the flight plan programmed in the FMS.

[5]Abbreviated callsign, spoken FOXTROT UNIFORM OSCAR.

issued dynamically by the simulated ATC whenever airspeed did not remain within a predefined range.

Figure 1 gives an overview of events' position on the flight path while **Figure 2** shows the vertical profile including timing of events during the flight task. Normative responses to these events would result in the following respective parameter changes:

- ATC 1: Altitude-Select 280 and Speed-Select 220.
- ATC 2: Altitude-Select 300.
- Fuel Pump Failure: Right-Main-Pump Off.
- Electrical Systems Alert 1: No parameter change[6].
- ATC 3: Altitude-Select 280.
- TCAS TA-Alert: No parameter change.
- ATC 4: Altitude-Select 300.
- Electrical Systems Alert 2: No parameter change.
- ATC 5: Altitude-Select 320.
- ATC 6: Heading-Select 325.
- Electrical Systems Alert 3: No parameter change.
- Fuel Imbalance: Fuel-X-Feed True (not included in data analysis).
- ATC 7: Heading-Select 350.
- Electrical Systems Alert 4: No parameter change.

EEG

Electroencephalogram was recorded continuously at 500 Hz using a mobile, wireless LiveAmp amplifier (Brain Products, Gilching, Germany) using 32 active Ag/AgCl electrodes arranged on actiCAP caps according to the international 10–20 system and referenced to FCz. EEG was synchronized with both the desktop stimuli and the flight events using the Lab Streaming Layer (Kothe, 2014) software framework to ensure that EEG data could be related to the respective simulator events with adequate temporal resolution. In particular, FlightGear was configured to log the status of each of the alarms and send it at 100 Hz to a UDP port, where a custom Python script listened for incoming data and immediately forwarded each packet through LSL. A change in alert status could then be interpreted as the on- or offset of the alert.

ERP Classification

A windowed-means classifier (Blankertz et al., 2011) was calibrated on the EEG data recorded for each individual participant during the oddball paradigm to distinguish between their neurophysiological response to two different categories of tones. Features were the mean amplitudes of eight consecutive non-overlapping time windows of 50 ms each starting at 150 ms following onset of the auditory tone, after band-pass filtering the signal between 0.3 and 20 Hz. Shrinkage-regularized linear discriminant analysis was used to separate the classes. A fivefold cross-validation with margins of five was used to obtain estimates of the classifier's parameters and accuracy. We focused on distinguishing between standard versus target tones, i.e., task-irrelevant versus task-relevant events. The classification algorithm was implemented using BCILAB (Kothe and Makeig, 2013).

The trained classifier was optimally capable of distinguishing between the two categories of tones based solely on the participant's brain activity following each tone's onset. Having trained the classifier on detecting differences between these events in an abstract oddball task, we then applied the classifier to the data recorded during that same participant's flight. This thus allowed us to investigate to what extent flight deck alerts could be reliably identified as the comparable equivalent of "standard" (task-irrelevant, unimportant) or "target" (etc.) tones, based solely on the pilots' EEG data less than 1 second after onset of each event. For each simulated flight event, the classifier returned a number between 1 and 2, signifying that the neurophysiological response was closest to the activity following standard (1) or target (2) tones in the oddball paradigm, respectively.

Cognitive Model

A normative and a neuroadaptive cognitive model were created following a HTA performed with a subject matter expert for the flight scenario using ACT-R. For the HTA and the cognitive model, good SA level 1 was defined as perceiving and paying attention to all auditory stimuli provided in the scenario. While adequacy of responses depended on the type of alert or contents of ATC messages, the time limit for initiating a first reaction to an alert was set to 25 s for all events. As the spurious electrical bus alerts disappeared before pilots were able to react, they are not included in the analysis of this article. The interface between the models and the simulator/Flight Gear was implemented as an extended version of ACT-CV (Halbrügge, 2013), where log files of cockpit system states recorded with a sampling rate of 20 Hz served as ACT-R task environment.

Both normative and neuroadaptive model were based on a routine loop consisting of monitoring flight parameters and managing thrust accordingly in order to have comparable workload as participants in the simulator; however, cognitively plausible modeling of workload and accuracy in thrust management was beyond the focus of this study and therefore not evaluated. The routine loop was temporarily exited when an aural alert was perceived. The normative model shifted its attention to read the warning message and initiate the corresponding procedure.

In order to illustrate the model's flow of information from one module to another with respect to ACT-R's neuroanatomical assumptions, associated brain areas as described by Anderson et al. (2008) and Borst et al. (2013) will be given in parentheses behind each module. The validation of activity predicted by the model with brain imaging data was beyond the scope of this article. For example of the fuel pump failure alert the model would go through the following steps: (1) a chunk representing a sound activates the aural module (mapped to the superior temporal gyrus) by being put in the model's aural-location buffer. (2) Next, this information allows the procedural module (basal ganglia) to fire a production that starts counting seconds passed since the alert with the temporal module and that decodes the sound as an alert sound using the aural buffer. This latter information would trigger productions that (3) make the model

[6]The spurious electrical alert would vanish by itself irrespective of any flight crew action; the normative response to a TCAS TA alert is to visually acquire the intruding aircraft and to prepare for a subsequent evasive maneuver, should a so-called "Resolution Advisory (RA)" alert follow.

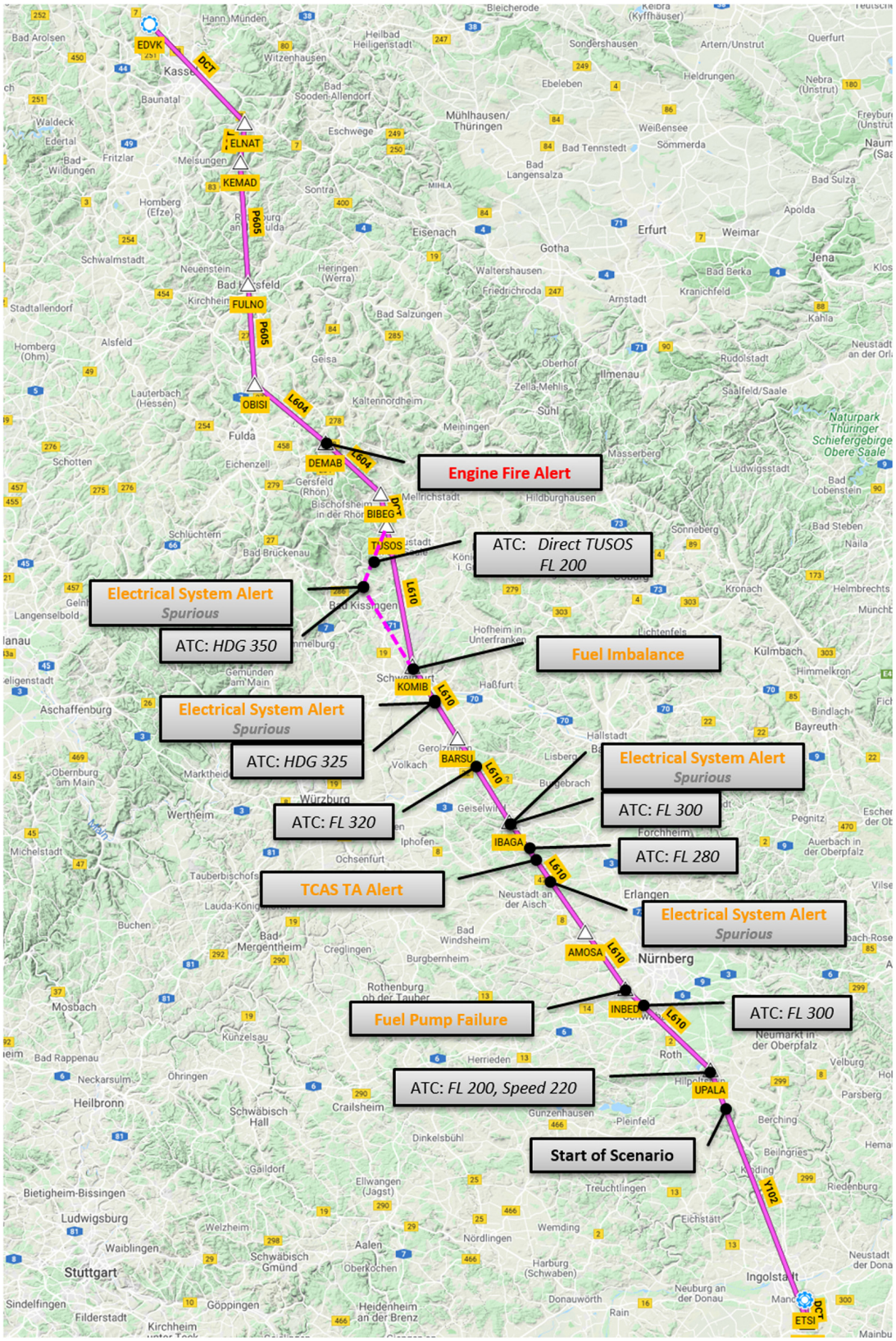

FIGURE 1 | Lateral profile of simulator task including events, waypoints, and geographic information.

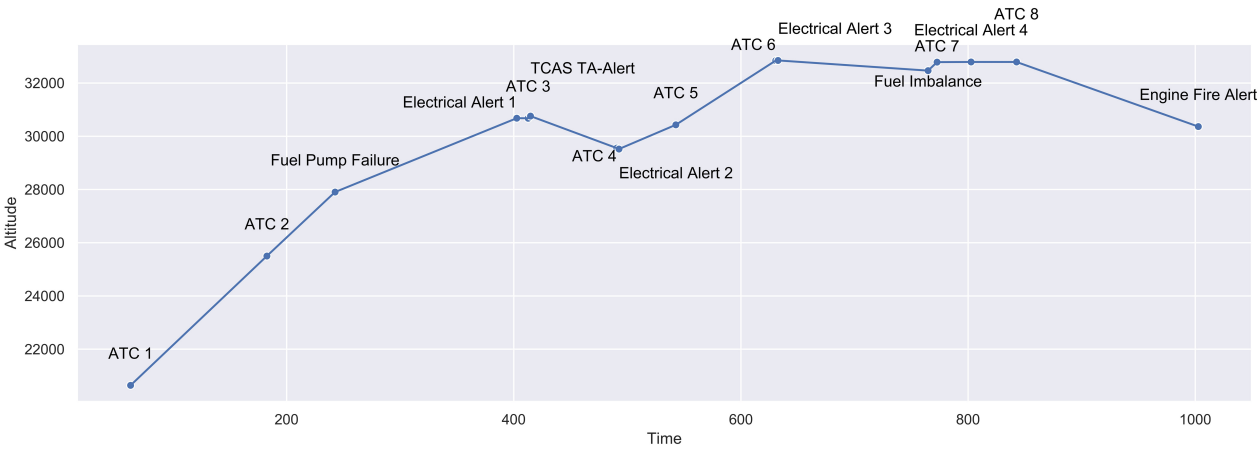

FIGURE 2 | Vertical profile of simulator task including events, altitude in meters, and timing in seconds.

shift its visual attention to the warning display by calling on the visual module's (fusiform gyrus) visual-location buffer and (4) read the written fuel pump failure message using the visual buffer. (5) The following production would result in calling up the corresponding pump failure checklist, memorizing its first item (i.e., pressing the right main fuel pump pushbutton) in the imaginal buffer (intraparietal sulcus, representing the model's short-term memory problem state). (6) Then, using its motor module (precentral gyrus), the model acts as if pressing the pump pushbutton (without changing any of the flight parameters) before (7) reading and carrying out the remaining checklist items in the same fashion while it keeps counting. (8) Finally when the count in the temporal module has reached 25 s, the module checks the flight parameters for the state of the right main fuel pump's pushbutton to verify whether the pilot has carried out the action required by the first checklist item as memorized in the model's imaginal buffer.

As the normative model assumed that pilots will correctly process each alert, adequate responses were scored as correct and inadequate (i.e., commission errors) as well as lacking and too late responses (i.e., omission errors) as incorrect classification of behavior. Adequacy and timeliness of responses were scored according to criteria assessed in the HTA with subject matter experts. For example, if an ATC message requested a flight level change to 300, entering an altitude-select of 300 in the flight control unit within a time window of 25 s was scored as good performance; all other responses such as entering an altitude-select of 280 or entering the correct altitude-select after 25 s were classified as missed ATC message. The fraction of incorrect classifications was treated as epistemic uncertainty ($\mu_{\text{Epistemic}}$) as the model had no information about why the pilot did not respond as expected.

The neuroadaptive model considered individual brain activity when classifying behavior to reduce this uncertainty. pBCI data were provided to the model along with the cockpit systems data. After each acoustic alert and message was decoded, the neuroadaptive model checked if the sound was processed as task-relevant by the participant according to pBCI data before shifting its visual attention to read the alert's or message's actual content. To build and improve on the normative model's accuracy, the neuroadaptive model assumed that alerts will be processed correctly. If pBCI data showed that a message was processed as irrelevant (classifier output <1.5), the model scored lacking or inadequate responses as correct behavior classification. If the message was processed as relevant but no adequate response can be found, the model scored its classification as incorrect and treats these cases as epistemic uncertainty.

Responses were assessed for 10 events for each of the 21 pilots whereof eight ATC messages, one amber, and one red alert. Model accuracies were computed across participants as the fraction of correct classifications in all events. Normative and neuroadaptive model were compared by a paired samples t-test. Effect size is reported as Cohen's d_{av} (Lakens, 2013). Aleatory uncertainty (μ_{Aleatory}) was defined as one minus EEG classifier accuracy. Though aleatory uncertainty affects correct and incorrect classifications, an accuracy corrected for aleatory uncertainty was computed for the neuroadaptive model. The distribution of lacking and inadequate responses was tested for a relationship with EEG classifications by a Chi-square test. A detailed description of the cognitive model including the overall approach and modeling decisions made can be found in Klaproth et al. (2020).

RESULTS

ERP Classification

Figure 3 shows the grand-average ERPs on channel Pz for the standard and target tones during the oddball experiment on three electrode sites. Note that there is a delay. We had previously estimated our stimulus presentation pipeline to contain a lag of approximately 150 ms. This would coincide with the common interpretation that the initial negative peak visible in these plots is the N100.

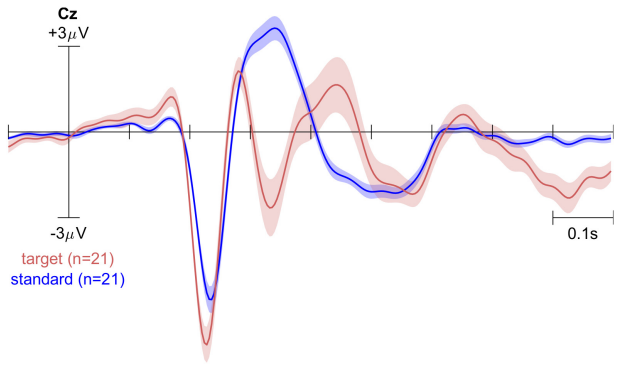

FIGURE 3 | The grand-average ERP of 21 participants showing responses to target and standard tones on channel Cz. Shaded area indicates the standard error of the mean.

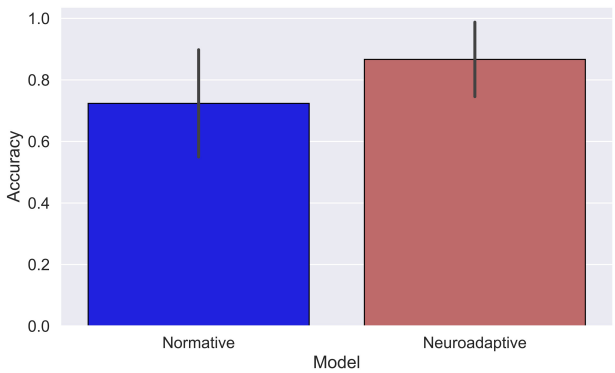

FIGURE 4 | Mean model accuracies, error bars indicate standard deviations across participants.

The classifier was trained to detect the differences between single-trial ERPs using all 32 channels and had a cross-validated averaged accuracy of 86%. Given the class imbalance between the standard deviant tones, chance level was not at 50% for this binary classifier. Instead, significant classification accuracy ($p < 0.05$) is reached at 78%. The classes could be separated with significant accuracy for all but three participants. This was in part due to technical issues with the EEG recording. These three participants were excluded from further analysis.

The classifier trained on data from the oddball paradigm was subsequently applied to data following four flight events: ATC messages, the spurious electrical bus system failure alert, the fuel imbalance alert, and the fire alert. These classification results provided information to be used in the neuroadaptive cognitive model.

Cognitive Model

The normative model correctly described participants' behavior for 162 of the total 210 observed events ($M_{\text{Normative}} = 0.72$, SD = 0.09), indicating that participants missed to respond to 48 events. The neuroadaptive model was able to simulate 182 of participant's responses correctly ($M_{\text{Neuroadaptive}} = 0.87$, SD = 0.13, see **Figure 4**), resulting in a significant added value of including pBCI data compared to the normative model [$t(20) = 5.62$, $p < 0.01$, $d_{\text{av}} = 1.3$]. **Figure 5** shows the respective models' accuracies for each of the 21 pilots.

Epistemic uncertainties for the models are $\mu_{\text{Epistemic}} = 0.28$ for the normative and $\mu_{\text{Epistemic}} = 0.13$ for the neuroadaptive model. The added value of the neuroadaptive over the normative model is 0.15, so the neuroadaptive model's accuracy corrected for EEG-classifier accuracy of 0.88 is 0.85 with $\mu_{\text{Epistemic}} = 0.15$ and $\mu_{\text{Aleatory}} = 0.02$.

Of the 58 events left unexplained by the normative model, 22 events did not show a response to the respective alert or message and 36 showed an incorrect response by the participant. Chi-square tests yielded no significant relationship between EEG classifier output (standard/target) and the event having missing or incorrect responses [$\chi^2(1, N = 58) = 1.04$, $p = 0.31$), i.e., pBCI-data do not predict whether a participant will respond incorrectly or not at all to missed alerts.

DISCUSSION

The use of increasingly complex and less traceable automation can result in out-of-the loop situations thanks to different assessment of situations by pilot and automated system. Results of this study have demonstrated the feasibility of implicitly detecting and handling of emerging divergence in situation assessment with the help of a neuroadaptive cognitive model.

Using a pBCI for real-time assessment of cognitive responses evoked by events in the cockpit provides insight into subjective situational interpretations. Such information is highly dependent on the context sensitive, individual state of the operator and can hardly, if at all, be inferred by purely behavioral or environmental measures. In general, we conclude that the combination of pBCI approaches with advanced methods of cognitive modeling, leads to an increase in the reliability and capability of the resulting cognitive model – introducing the idea of neuroadaptive cognitive modeling – as shown in this study.

Specifically, the ERP produced by the oddball paradigm shows clear differences between the different categories of tones. In particular, a P300 at Pz clearly distinguishes between target (task-relevant) and standard (task-irrelevant) tones. Based on these differences in single-trial event-related activity, the classifier was capable of distinguishing between target and standard tones with single-trial accuracies significantly higher than chance in the training session.

The improvement in the cognitive model that resulted from including the pBCI output indicates that it is possible to obtain informative cognitive state information based on a pilot's brain activity immediately following an auditory event. The fact that the classifier decoding this information was trained in a desktop setting demonstrates that no elaborate training sessions are required.

Normative model results suggest that individual pilot behavior can be traced and anticipated by a cognitive model. By comparing

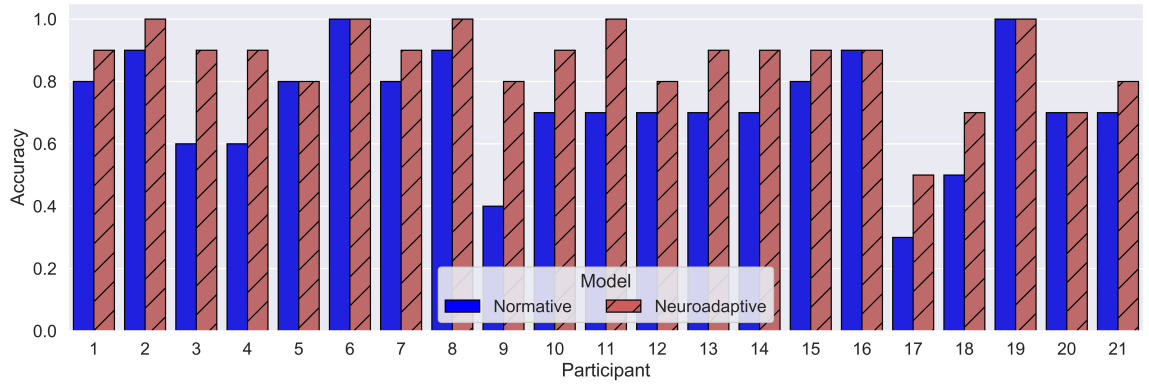

FIGURE 5 | Mean model accuracies per model and participant.

individual pilots' actions to the normative model behavior, deviations could be detected and inferences about SA could be made without intruding the task (Vidulich and McMillan, 2000). Twenty-eight percent of epistemic uncertainty, with lacking and incorrect responses evenly distributed, indicate that additional diagnostic information is required for meaningful analysis and support in cases of deviating behavior.

The improvement in accuracy for the neuroadaptive model demonstrate how individual behavior models can benefit from the integration of physiological data. Not only can top-down modeling of human cognition in a task be complemented by bottom-up integration of (neuro-) behavioral data for example to account for behavioral moderators (e.g., Ritter et al., 2004), it can also provide contextual information required for situation-dependent interpretation of EEG data. The different types of uncertainties inherent to model tracing and pBCI determined the model's systematic design: pBCI data could only be used to reduce the fraction of the normative model's unexplained behavior to deal with aleatory uncertainty.

The method's limitations are quantified in terms of uncertainty. Later SA stages need to be monitored to increase accuracy in pilot modeling. Measures of additional physiological indicators might be connected in line to further reduce both epistemic uncertainty with new types of information, and aleatory with joint probability distributions. For example, gaze data such as visual search behavior in response to alerts could be indicative of comprehension problems and reinforce or challenge pBCI classifications of alerts being perceived or not. Other indicators, for example the error-related negativity component of the ERP, could help to identify situations where operators have low comprehension or are out of the loop (Berberian et al., 2017).

Any cockpit application of passive BCI technology requires a thorough consideration regarding the intrusiveness of the measurement, the intended function(s) enabled by the BCI, as well as the safety and airworthiness implications associated with this function. The intrusiveness perceived by pilots will mainly depend on how well the (dry) EEG electrodes can be integrated for example into the interior lining of a pilot helmet or the headband of a headset. The intended cockpit (assistance) function, in turn, will mainly determine the airworthiness certification and associated validation effort required.

If the system described in this article is merely be used to enhance the efficiency of the already certified flight deck alerting system of an aircraft, the design assurance level required from an airworthiness and safety perspective could be lower compared to a solution where a passive BCI-based cockpit function is an integral part of the aircraft's safety net. In the latter case, the airworthiness effort will be substantial irrespective of whether AI and/or machine learning are used or not. Although evaluated offline after data collection, the methods presented in this paper are well-suited to be applied online without substantial modifications. While the abstract oddball task can replace more realistic alternatives to gather training data, and thus substantially shorten the amount of time required to do so, it may still be necessary to gather new training data before each flight due to the natural non-stationarity present in EEG activity. For a truly walk-up-and-use neuroadaptive solution, a subject-independent classifier would be required (e.g., Fazli et al., 2009). Monitoring pilots' ERPs in response to alerts gives diagnostic value. Detection of inattentional deafness in early, perceptual ERP components could trigger communication of the alert in alternative modalities (e.g., tactile or visual; Liu et al., 2016). For unattended alerts detected in later ERP components, cockpit automation could prioritize and choose to postpone reminders in case of minor criticality. Withholding information that is not alert-related can be effective in forcing pilots' attention onto the alert, but it may be accompanied by decrease in pilots' authority and associated risks, for example to resilience in unexpected situations and technology acceptance.

The simulator setting likely introduced biases in task engagement and density of events in the scenario. Measuring system input from pilots while they monitor instruments in real flight conditions may not provide enough data to make inferences about cognitive states. This emphasizes the need for additional behavioral measures (e.g., neurophysiological activity, speech, or gaze) to provide individual assistance.

Pilots are capable of anticipating complex system behavior but reports of automation surprises and out-of-the-loop situations

stress the importance of a shared understanding of situations by pilot and cockpit automation. Increasing complexity of automation should therefore go together with a paradigm shift toward human-autonomy teaming based on a shared understanding of the situation. This includes bi-directional communication whenever a significant divergence in the understanding of a situation occurs to provide information missing for shared awareness of the human autonomy team (Shively et al., 2017). Anticipation of divergences and understanding human information needs to ensure shared awareness remains a challenge for human autonomy teaming (McNeese et al., 2018). By addressing divergences in human and autonomy situation assessment, critical situations might be prevented or at least resolved before they result in incidents or accidents. Tracing pilots' perception of cockpit events represents a first step toward this goal.

CONCLUSION

A pBCI allows to implicitly monitor whether pilots have correctly processed alerts or messages without intruding the mission using a classifier trained in a desktop setting. The integration of pBCI data in cognitive pilot models significantly improves the accuracy in following up with pilots' situation assessment. Tracing pilots' situation assessment through neuroadaptive cognitive modeling may facilitate the early detection of divergences in situation assessment in human autonomy teams. While sensor obtrusiveness and computational limitations may obstruct application, neuroadaptive cognitive modeling could help to tracing of pilots' situation awareness and enable adaptive alerting.

DATA AVAILABILITY STATEMENT

The datasets presented in this article were mainly collected using aircrew employed by Airbus. For privacy and confidentiality reasons, they are not readily available; requests to address the datasets should be directed to oliver.klaproth@airbus.com.

ETHICS STATEMENT

The studies involving human participants were reviewed and approved by the Ethik-Kommission Fakultät V – Verkehrs – und Maschinensysteme Institut für Psychologie und Arbeitswissenschaft TU Berlin. The patients/participants provided their written informed consent to participate in this study.

AUTHOR CONTRIBUTIONS

OK, CV, LK, TZ, and NR designed the experiment. CV designed the flight task. LK and TZ designed the EEG trainings. OK and NR created the cognitive model. MH created the interface between flight simulator data and ACT-R. OK, CV, and LK performed the experiments and drafted the manuscript. OK and LK analyzed the data. OK, CV, LK, MH, TZ, and NR edited, revised, and approved the manuscript. All authors contributed to the article and approved the submitted version.

ACKNOWLEDGMENTS

The authors thank Brain Products GmbH (Gilching, Germany) for supporting this research by providing an additional LiveAmp system including electrodes. Furthermore, the authors would like to thank Dr. Daniel Dreyer, Christophe Chavagnac, and all participating air crew for their fantastic support.

REFERENCES

Air Accident Investigation and Aviation Safety Board (2006). *Aircraft Accident Report Helios Airways Flight HCY522 Boeing 737-31S at Grammitko, Hellas on 14 August 2005*. Available online at: http://www.aaiu.ie/sites/default/files/Hellenic%20Republic%20Accident%20Helios%20Airways%20B737-31S%20HCY522%20Grammatiko%20Hellas%202005-085-14.pdf (accessed December 19, 2019).

Anderson, J. R. (2007). *Oxford Series On Cognitive Models And Architectures. How Can The Human Mind Occur In The Physical Universe?*. Oxford: Oxford University Press.

Anderson, J. R., Bothell, D., Byrne, M. D., Douglass, S., Lebiere, C., and Qin, Y. (2004). An integrated theory of the mind. *Psychol. Rev.* 111, 1036–1060. doi: 10.1037/0033-295X.111.4.1036

Anderson, J. R., Fincham, J. M., Qin, Y., and Stocco, A. (2008). A central circuit of the mind. *Trends Cogn. Sci.* 12, 136–143. doi: 10.1016/j.tics.2008.01.006

Aricò, P., Borghini, G., Di Flumeri, G., Colosimo, A., Bonelli, S., Golfetti, A., et al. (2016). Adaptive automation triggered by EEG-based mental workload index: a passive brain-computer interface application in realistic air traffic control environment. *Front. Hum. Neurosci.* 10:539. doi: 10.3389/fnhum.2016.00539

Aviation Safety Council (2016). *Aviation Occurrence Report: 4 February, 2015, TransAsia Airways Flight GE235 ATR72-212A: Loss of Control and Crashed into Keelung River Three Nautical Miles East of Songshan Airport. Aviation Occurrence Report ASC-AOR-16-06-001*. Available online at: https://www.asc.gov.tw/upload/acd_att/ASC-AOR-16-06-001%20EN.pdf (accessed December 19, 2019).

Bailey, N. R., Scerbo, M. W., Freeman, F. G., Mikulka, P. J., and Scott, L. A. (2003). "A brain-based adaptive automation system and situation awareness: The role of complacency potential," in *Proceedings of the Human Factors and Ergonomics Society 47th Annual Meeting*, Santa Monica, CA.

Bailey, R. E., Kramer, L. J., Kennedy, K. D., Stephens, C. L., and Etherington, T. J. (2017). "An assessment of reduced crew and single pilot operations in commercial transport aircraft operations," in *Proceedings of the IEEE/AIAA 36th Digital Avionics Systems Conference (DASC)*, St. Petersburg, FL.

Bainbridge, L. (1983). "Ironies of automation," in *Automatica: 19.1983,6. Analysis, Design and Evaluation Of Man-Machine Systems: Control Frontiers in Knowledge Based And Man-Machine Systems*, ed. G. Johannsen (Oxford: Pergamon Press), 129–135. doi: 10.1016/B978-0-08-029348-6.50026-9

Ball, J., Myers, C., Heiberg, A., Cooke, N. J., Matessa, M., Freiman, M., et al. (2010). The synthetic teammate project. *Comput. Math. Organ. Theor.* 16, 271–299. doi: 10.1007/s10588-010-9065-3

Berberian, B., Somon, B., Sahaï, A., and Gouraud, J. (2017). The out-of-the-loop brain: a neuroergonomic approach of the human automation interaction. *Ann. Rev. Control* 44, 303–315. doi: 10.1016/j.arcontrol.2017.09.010

Berka, C., Levendowski, D. J., Davis, G., Whitmoyer, M., Hale, K., and Fuchs, K. (2006). "Objective measures of situational awareness using neurophysiology technology," in *Augmented Cognition: Past, Present and Future*, eds D. Schmorrow, K. Stanney, and L. Reeves (Arlington, VA: Strategic Analysis Inc), 145–154.

Blankertz, B., Lemm, S., Treder, M., Haufe, S., and Müller, K.-R. (2011). Single-trial analysis and classification of ERP components–a tutorial. *Neuroimage* 56, 814–825. doi: 10.1016/j.neuroimage.2010.06.048

Borst, J., Nijboer, M., Taatgen, N., and Anderson, J. R. (2013). "A data-driven mapping of five ACT-R modules on the brain," in *Proceedings of the 12th International Conference on Cognitive Modeling*, eds R. L. West and T. C. Stewart (Ottawa: Carleton University).

Byrne, M. D., and Kirlik, A. (2005). Using computational cognitive modeling to diagnose possible sources of aviation error. *Intern. J. Aviat. Psychol.* 15, 135–155. doi: 10.1207/s15327108ijap1502_2

Cinel, C., Valeriani, D., and Poli, R. (2019). Neurotechnologies for human cognitive augmentation: current state of the art and future prospects. *Front. Hum. Neurosci.* 13:13. doi: 10.3389/fnhum.2019.00013

Debener, S., Makeig, S., Delorme, A., and Engel, A. K. (2005). What is novel in the novelty oddball paradigm? Functional significance of the novelty P3 event-related potential as revealed by independent component analysis. *Cogn. Brain Res.* 22, 309–321. doi: 10.1016/j.cogbrainres.2004.09.006

Dehais, F., Causse, M., Vachon, F., Régis, N., Menant, E., and Tremblay, S. (2014). Failure to detect critical auditory alerts in the cockpit: evidence for inattentional deafness. *Hum. Fact.* 56, 631–644. doi: 10.1177/0018720813510735

Dehais, F., Roy, R. N., Gateau, T., and Scanella, S. (2016). "Auditory alarm misperceptions in the cockpit: An EEG-study of inattentional deafness," in *Proceedings of the 10th Foundations of Augmented Cognition: Neuroergonomics and Operational Neuroscience Lecture Notes In Computer Science Lecture Notes in Artificial Intelligence*, eds D. D. Schmorrow and C. M. Fidopiastis (Cham: Springer), 177–187. doi: 10.1007/978-3-319-39955-3_17

Dehais, F., Roy, R. N., and Scannella, S. (2019). Inattentional deafness to auditory alarms: Inter-individual differences, electrophysiological signature and single trial classification. *Behav. Brain Res.* 360, 51–59. doi: 10.1016/j.bbr.2018.11.045

Di Flumeri, G., De Crescenzio, F., Berberian, B., Ohneiser, O., Kramer, J., Aricò, P., et al. (2019). Brain-computer interface-based adaptive automation to prevent out-of-the-loop phenomenon in air traffic controllers dealing with highly automated systems. *Front. Hum. Neurosci.* 13:296. doi: 10.3389/fnhum.2019.00296

Durso, F. T., and Sethumadhavan, A. (2008). Situation awareness: Understanding dynamic environments. *Hum. Fact.* 50, 442–448. doi: 10.1518/001872008X288448

Endsley, M. R. (1995). Measurement of situation awareness in dynamic systems. *Hum. Fact.* 37, 65–84. doi: 10.1518/001872095779049499

Endsley, M. R. (2000). "Direct measurement of situation awareness: validity and use of SAGAT," in *Situation Awareness Analysis And Measurement*, eds M. R. Endsley and D. J. Garland (Mahwah, NJ: Lawrence Erlbaum Associates), 147–173.

Endsley, M. R. (2017). From here to autonomy. *Hum. Fact.* 59, 5–27. doi: 10.1177/0018720816681350

Endsley, M. R., and Jones, D. G. (2011). *Designing for Situation Awareness: An Approach To User-Centered Design*. Boca Raton, FL: CRC Press.

Endsley, M. R., and Kiris, E. O. (1995). The out-of-the-loop performance problem and level of control in automation. *Hum. Fact.* 37, 381–394. doi: 10.1518/001872095779064555

Fazli, S., Popescu, F., Danóczy, M., Blankertz, B., Müller, K. R., and Grozea, C. (2009). Subject-independent mental state classification in single trials. *Neural Netw.* 22, 1305–1312. doi: 10.1016/j.neunet.2009.06.003

Freiman, M., Caisse, M., Ball, J., Halverson, T., and Myers, C. (2018). "Empirically identified gaps in a situation awareness model for human-machine coordination," in *Proceedings of the 2018 IEEE International Conference on Cognitive and Computational Aspects of Situation Management (CogSIMA)*, Piscataway, NJ.

Fu, W.-T., Bothell, D., Douglass, S., Haimson, C., Sohn, M.-H., and Anderson, J. (2006). Toward a real-time model-based training system. *Interact. Comput.* 18, 1215–1241. doi: 10.1016/j.intcom.2006.07.011

Gluck, K. A. (2010). "Cognitive architectures for human factors in aviation," in *Human Factors in Aviation*, 2nd Edn, eds E. Salas and D. Maurino (New York, NY: Elsevier), 375–400. doi: 10.1016/B978-0-12-374518-7.00012-2

Haines, R. F. (1991). "A breakdown in simultaneous information processing," in *Presbyopia Research: From Molecular Biology To Visual Adaptation*, eds G. Obrecht and L. W. Stark (New York, NY: Springer), 171–175. doi: 10.1007/978-1-4757-2131-7_17

Halbrügge, M. (2013). "ACT-CV - Bridging the gap between cognitive models and the outer world," in *Grundlagen und Anwendungen der Mensch-Maschine-Interaktion: 10. Berliner Werkstatt Mensch-Maschine-Systeme = Foundations and Applications Of Human Machine Interaction*, ed. E. Brandenburg (Berlin: Springer), 205–210.

Harris, D., Stanton, N. A., and Starr, A. (2015). Spot the difference: operational event sequence diagrams as a formal method for work allocation in the development of single-pilot operations for commercial aircraft. *Ergonomics* 58, 1773–1791. doi: 10.1080/00140139.2015.1044574

Jones, D. G., and Endsley, M. R. (1996). Sources of situation awareness errors in aviation. *Aviat. Space Environ. Med.* 67, 507–512.

Kiureghian, A. D., and Ditlevsen, O. (2009). Aleatory or epistemic? Does it matter?. *Struct. Saf.* 31, 105–112. doi: 10.1016/j.strusafe.2008.06.020

Klaproth, O. W., Halbruegge, M., Krol, L. R., Vernaleken, C., Zander, T. O., and Rußwinkel, N. (2020). A neuroadaptive cognitive model for dealing with uncertainty in tracing pilots' cognitive state. *Top. Cogn. Sci.* doi: 10.1111/tops.12515

Kothe, C. A. (2014). *Lab Streaming Layer*. Available online at: https://github.com/sccn/labstreaminglayer (accessed December 19, 2019).

Kothe, C. A., and Makeig, S. (2013). BCILAB: a platform for brain-computer interface development. *Neural Eng.* 10:56014. doi: 10.1088/1741-2560/10/5/056014

Krol, L. R., Andreessen, L., and Zander, T. O. (2018). "Passive brain-computer interfaces: A perspective on increased interactivity," in *Brain-Computer Interfaces Handbook: Technological and Theoretical Advances*, eds C. S. Nam, A. Nijholt, and F. Lotte (Boca Raton, FL: CRC Press), 69–86. doi: 10.1201/9781351231954-3

Krol, L. R., Haselager, P., and Zander, T. O. (2020). Cognitive and affective probing: a tutorial and review of active learning for neuroadaptive technology. *J. Neural Eng.* 17:012001. doi: 10.1088/1741-2552/ab5bb5

Krol, L. R., and Zander, T. O. (2017). "Passive BCI-based neuroadaptive systems," in *Proceedings of the 7th Graz Brain Computer Interface Conference*, Graz.

Lakens, D. (2013). Calculating and reporting effect sizes to facilitate cumulative science: a practical primer for t-tests and ANOVAs. *Front. Psychol.* 4:863. doi: 10.3389/fpsyg.2013.00863

Liu, J., Gardi, A., Ramasamy, S., Lim, Y., and Sabatini, R. (2016). Cognitive pilot-aircraft interface for single-pilot operations. *Knowl. Based Syst.* 112, 37–53. doi: 10.1016/j.knosys.2016.08.031

Lotte, F., Congedo, M., Lécuyer, A., Lamarche, F., and Arnaldi, B. (2007). A review of classification algorithms for EEG-based brain-computer interfaces. *Neural Eng.* 4, R1–R13. doi: 10.1088/1741-2560/4/2/R01

Luck, S. J. (2014). *An Introduction to the Event-Related Potential Technique*. Cambridge: MIT Press.

McNeese, N. J., Demir, M., Cooke, N. J., and Myers, C. (2018). Teaming with a synthetic teammate: Insights into human-autonomy teaming. *Hum. Fact.* 60, 262–273. doi: 10.1177/0018720817743223

Milner, A. D., and Goodale, M. A. (2008). Two visual systems re-viewed. *Neuropsychologia* 46, 774–785. doi: 10.1016/j.neuropsychologia.2007.10.005

Most, S. B., Scholl, B. J., Clifford, E. R., and Simons, D. J. (2005). What you see is what you set: Sustained inattentional blindness and the capture of awareness. *Psychol. Rev.* 112, 217–242. doi: 10.1037/0033-295X.112.1.217

Olofsen, E., van Dongen, H. P. A., Mott, C. G., Balkin, T. J., and Terman, D. (2010). Current approaches and challenges to development of an individualized sleep and performance prediction model. *Open Sleep J.* 3, 24–43. doi: 10.2174/1874620901003010024

Pierce, R. S. (2012). The effect of SPAM administration during a dynamic simulation. *Hum. Factors* 54, 838–848. doi: 10.1177/0018720812439206

Pope, A. T., Bogart, E. H., and Bartolome, D. S. (1995). Biocybernetic system evaluates indices of operator engagement in automated task. *Biol. Psychol.* 40, 187–195. doi: 10.1016/0301-0511(95)05116-3

Putze, F., Schultz, T., and Propper, R. (2015). "Dummy model based workload modeling," in *Proceedings of the 2015 IEEE International Conference on Systems, Man, and Cybernetics*, Hong Kong.

Reifman, J., Ramakrishnan, S., Liu, J., Kapela, A., Doty, T. J., Balkin, T. J., et al. (2018). 2B-Alert App: a mobile application for real-time individualized prediction of alertness. *Sleep Res.* 2018:e12725. doi: 10.1111/jsr.12725

Ritter, F. E., Reifers, A., Klein, L. C., Quigley, K., and Schoelles, M. (2004). "Using cognitive modeling to study behavior moderators: pre-task appraisal and anxiety," in *Proceedings of the Human Factors and Ergonomics Society*, Santa Monica, CA.

Rodgers, S. M., Myers, C. W., Ball, J., and Freiman, M. D. (2013). Toward a situation model in a cognitive architecture. *Comput. Math. Organ. Theor.* 19, 313–345. doi: 10.1007/s10588-012-9134-x

Rußwinkel, N., Vernaleken, C., and Klaproth, O. W. (2020). "Towards cognitive assistance and teaming in aviation by inferring pilot's mental State," in *Proceedings of the 3rd International Conference on Intelligent Human Systems Integration*, Modena.

Sarter, N., and Sarter, M. (2003). Neuroergonomics: Opportunities and challenges of merging cognitive neuroscience with cognitive ergonomics. *Theor. Issues Ergon. Sci.* 4, 142–150. doi: 10.1080/1463922021000020882

Scerbo, M. W. (2006). "Adaptive automation," in *Neuroergonomics: The Brain At Work*, eds R. Parasuraman and M. Rizzo (New York, NY: Oxford Universtity Press), 239–252. doi: 10.1093/acprof:oso/9780195177619.003.0016

Schmidt, A. (2000). Implicit human computer interaction through context. *Pers. Technol.* 4, 191–199. doi: 10.1007/BF01324126

Shively, R. J., Lachter, J., Brandt, S. L., Matessa, M., Battiste, V., and Johnson, W. W. (2017). "Why human-autonomy teaming?," in *Advances in Neuroergonomics and Cognitive Engineering*, ed. C. Baldwin (Cham: Springer), 3–11. doi: 10.1007/978-3-319-60642-2_1

Somers, S., and West, R. (2013). "Steering control in a flight Simulator using ACT-R," in *Proceedings of the 12th International Conference on Cognitive Modeling*, eds R. L. West and T. C. Stewart (Ottawa: Carleton University).

Spence, C., and Driver, J. (1997). "Audiovisual links in attention: implications for interface design: job design and product design," in *Engineering Psychology And Cognitive Ergonomics*, ed. D. Harris (Hampshire: Ashgate), 185–192. doi: 10.4324/9781315094489-24

Stanton, N. A. (2006). Hierarchical task analysis: Developments, applications, and extensions. *Appl. Ergon.* 37, 55–79. doi: 10.1016/j.apergo.2005.06.003

van Dijk, H., van de Merwe, K., and Zon, R. (2011). A coherent impression of the pilots' situation awareness: studying relevant human factors tools. *Aviat. Psychol.* 21, 343–356. doi: 10.1080/10508414.2011.606747

Vidulich, M., and McMillan, G. (2000). "The global implicit measure: evaluation of metrics for cockpit adaptation," in *Contemporary Ergonomics 2000*, eds P. T. McCabe, M. A. Hanson, and S. A. Robertson (London: Taylor and Francis), 75–80.

Wilson, G. F. (2000). "Strategies for psychophysiological assessment of situation awareness," in *Situation Awareness Analysis And Measurement*, eds M. R. Endsley and D. J. Garland (Mahwah, NJ: Lawrence Erlbaum Associates), 175–188.

Zander, T. O., Brönstrup, J., Lorenz, R., and Krol, L. R. (2014). "Towards BCI-based implicit control in human-computer interaction," in *Human-Computer Interaction Series. Advances in Physiological Computing*, eds S. H. Fairclough and K. Gilleade (London: Springer), 67–90. doi: 10.1007/978-1-4471-6392-3_4

Zander, T. O., and Kothe, C. (2011). Towards passive brain-computer interfaces: applying brain-computer interface technology to human-machine systems in general. *Neural Eng.* 8:25005. doi: 10.1088/1741-2560/8/2/025005

Zander, T. O., Krol, L. R., Birbaumer, N. P., and Gramann, K. (2016). Neuroadaptive technology enables implicit cursor control based on medial prefrontal cortex activity. *Proc. Natl. Acad. Sci. U.S.A.* 113, 14898–14903. doi: 10.1073/pnas.1605155114

Conflict of Interest: OK was employed by Airbus Central R&T. CV was employed by Airbus Defence and Space. LK and TZ were employed by Zander Laboratories B.V.

The remaining authors declare that the research was conducted in the absence of any commercial or financial relationships that could be construed as a potential conflict of interest.

frontiers in Neuroscience

ORIGINAL RESEARCH
published: 03 December 2020
doi: 10.3389/fnins.2020.575521

Physiological Synchrony in EEG, Electrodermal Activity and Heart Rate Detects Attentionally Relevant Events in Time

Ivo V. Stuldreher[1,2], Nattapong Thammasan[2], Jan B. F. van Erp[1,2] and Anne-Marie Brouwer[1]*

[1] Perceptual and Cognitive Systems, Netherlands Organisation for Applied Scientific Research (TNO), Soesterberg, Netherlands, [2] Human Media Interaction, Faculty of Electrical Engineering, Mathematics and Computer Science, University of Twente, Enschede, Netherlands

OPEN ACCESS

Edited by:
Hasan Ayaz, Drexel University, United States

Reviewed by:
Lucas C. Parra, City College of New York (CUNY), United States
Motoaki Kawanabe, Advanced Telecommunications Research Institute International (ATR), Japan

***Correspondence:**
Ivo V. Stuldreher
ivo.stuldreher@tno.nl

Specialty section:
This article was submitted to Neural Technology, a section of the journal Frontiers in Neuroscience

Received: *23 June 2020*
Accepted: *10 November 2020*
Published: *03 December 2020*

Citation:
Stuldreher IV, Thammasan N, van Erp JBF and Brouwer A-M (2020) Physiological Synchrony in EEG, Electrodermal Activity and Heart Rate Detects Attentionally Relevant Events in Time. Front. Neurosci. 14:575521. doi: 10.3389/fnins.2020.575521

Interpersonal physiological synchrony (PS), or the similarity of physiological signals between individuals over time, may be used to detect attentionally engaging moments in time. We here investigated whether PS in the electroencephalogram (EEG), electrodermal activity (EDA), heart rate and a multimodal metric signals the occurrence of attentionally relevant events in time in two groups of participants. Both groups were presented with the same auditory stimulus, but were instructed to attend either to the narrative of an audiobook (audiobook-attending: AA group) or to interspersed emotional sounds and beeps (stimulus-attending: SA group). We hypothesized that emotional sounds could be detected in both groups as they are expected to draw attention involuntarily, in a bottom-up fashion. Indeed, we found this to be the case for PS in EDA or the multimodal metric. Beeps, that are expected to be only relevant due to specific "top-down" attentional instructions, could indeed only be detected using PS among SA participants, for EDA, EEG and the multimodal metric. We further hypothesized that moments in the audiobook accompanied by high PS in either EEG, EDA, heart rate or the multimodal metric for AA participants would be rated as more engaging by an independent group of participants compared to moments corresponding to low PS. This hypothesis was not supported. Our results show that PS can support the detection of attentionally engaging events over time. Currently, the relation between PS and engagement is only established for well-defined, interspersed stimuli, whereas the relation between PS and a more abstract self-reported metric of engagement over time has not been established. As the relation between PS and engagement is dependent on event type and physiological measure, we suggest to choose a measure matching with the stimulus of interest. When the stimulus type is unknown, a multimodal metric is most robust.

Keywords: physiological synchrony, inter-subject correlations, interpersonal physiology, EEG, electrodermal activity, heart rate, multimodal

INTRODUCTION

Knowing what events in the external environment people attend to, and how their shared attentional engagement to events varies over time, can be useful in a range of settings, from evaluating educational or entertaining material, to real time adjustment of important instructions. Unlike explicit measures, such as questionnaires in which people are asked to specify their attentional engagement, physiological signals can provide continuous and implicit information on mental state (Zander and Kothe, 2011). However, the link between mental state and physiological measures [e.g., electroencephalography (EEG), electrodermal activity (EDA) or heart rate] is not straightforward (Brouwer et al., 2015). A popular approach to uncover the complex links between physiology and mental state is the use of supervised learning algorithms. These algorithms predict mental state based on a set of features extracted from physiological variables (Hamadicharef et al., 2009; Hussain et al., 2011; Fleureau et al., 2012; Liu et al., 2013; Aliakbaryhosseinabadi et al., 2017). A disadvantage of these types of analyses is the need for labeled training data, i.e., a set of physiological data that are labeled with a known value for the mental state of interest. Not only is it time consuming to obtain such a labeled dataset, it is also very difficult to determine the 'ground truth' mental state than can be used for data labeling (Brouwer et al., 2015). A second drawback of these supervised learning approaches is that classification is often limited to a small number of discrete states. Attentional, emotional or cognitive state, however, cannot realistically be represented by a small number of discrete states, but are naturally of more continuous nature (Zehetleitner et al., 2012; Rosenberg et al., 2013).

For monitoring attentional engagement, an approach that may be suited to circumvent both of the abovementioned problems is to monitor the physiological synchrony (PS) between individuals. PS is the degree to which physiological measures of multiple people uniformly change. Studies exploring PS in functional magnetic resonance imaging data have revealed strong voxel-wise inter-subject correlations across participants exposed to a common narrative stimulus (Hasson et al., 2004, 2010; Hanson et al., 2009). In the faster EEG signals, similar results were found (Dmochowski et al., 2012, 2014). The fast-changing EEG enabled the computation of a continuous measure of PS in time and suggested that moments of high PS corresponded with emotionally arousing scenes of the movie clips (Poulsen et al., 2017). For instance, high PS was found when scenes were viewed that involved the threat of a gun. Dmochowski et al. (2014) further showed that moment-to-moment variation in the PS predicted the general expressions of interest and attention of the public as indicated by number of tweets during a popular television series. Davidesco et al. (2019) found that PS over time indicated what specific information was retained by students in a lecture. Namely, PS was higher in lecture parts that provided answers for questions that students answered incorrectly in the pre-test and correctly in the delayed post-test than for questions where students' answers did not change. The relationship between neural PS and attentional engagement was also found to be less complex than most traditional physiological metrics. Neural PS was found to be directly proportional to attentional engagement, as strong correlations were found between PS and performance on questionnaires reflective of paid attention (Cohen and Parra, 2016; Cohen et al., 2018; Stuldreher et al., 2020). This directly proportional relationship may thus be used to circumvent supervised learning approaches and the problems that come with such approaches, such as the dependency on labeled training data.

In the current work, we aim to employ the relation between PS and attentional engagement to detect the occurrence of attentionally relevant events in time. Rather than limiting the analyses to EEG, we also include PS measures of peripheral nervous system activity (EDA and heart rate), and quantify their comparative sensitivity of detecting relevant events. Up to recently, PS in peripheral physiological measures has been studied mainly as a metric of some form of affective connectedness between individuals (reviewed by Palumbo et al., 2017). Examples include peripheral PS in therapist-patient dyads as a measure of psychotherapy success (Koole et al., 2020), in couples in marital counseling as a measure of therapy outcome (Tourunen et al., 2019) and as measure of collaborative learning (Malmberg et al., 2019). Positive results found in these contexts may (partly) be driven by shared attentional engagement to external events, as connectedness between people may be strongly associated with mutual attentiveness (Tickle-Degnen and Rosenthal, 1990). Recently, it was found that PS in EDA and heart rate can indeed reflect shared attention toward narrative stimuli (Pérez et al., 2020; Stuldreher et al., 2020).

The advantage of peripheral physiological measures over EEG is that they can be recorded more easily and less obtrusively. In addition, EEG and peripheral measures may complement each other since they likely reflect different mental processes. EEG is, for example, sensitive to selective attention (Polich, 2007), whereas EDA and heart rate are sensitive to (emotional) arousal (Cacioppo et al., 2007; Boucsein, 2012).

As of yet, it is unknown whether PS in EEG, EDA and heart rate can be used to detect relevant moments in time. For EDA and heart rate, time-resolved dynamics of PS have not been investigated at all in the context of attentional engagement. For EEG, time-resolved dynamics have been explored (see for instance Dmochowski et al., 2014; Poulsen et al., 2017), but this has not been done systematically, using a-priori known cognitively or emotionally engaging stimuli for which detection performance can be evaluated. We here evaluate whether PS in EEG, EDA and heart rate can be used to detect cognitively or emotionally relevant moments in time. Our goal is not to compare detection performance directly between the different types of stimuli, but to evaluate PS for a range of events differing in terms of total duration, sound onset, mental processes addressed and more. Just as in real-world conditions, some event may capture attention in a bottom-up fashion, related to salience or emotional relevance, whereas others may only capture attention due to top-down mechanisms related to task instruction (Lang, 1995; Öhman et al., 2001; Schupp et al., 2003). We invited participants to come to our lab and listen to an audiobook that was interspersed with short auditory events, that we expected to induce emotional and cognitive load. We divided

the participants in two equal-sized groups. Participants in the audiobook-attending group (AA) were instructed to focus their attention on the audiobook and ignore the interspersed stimuli. Participants in the stimulus-attending group (SA) were instructed to focus their attention on the interspersed stimuli and ignore the audiobook. In a previous paper on this experiment (Stuldreher et al., 2020), we showed that PS can be used to correctly classify a listener as being instructed to attend to the audiobook or to the sounds. In the current paper, we use PS among individuals in the same group to predict the occurrence of interspersed stimuli over time, for each of the three physiological measures. In addition, we investigated if the PS across AA participants was predictive of the occurrence of engaging moments in the book. We aimed to answer the following research questions:

Does PS in EEG and EDA, heart rate and a multimodal metric predict the occurrence of attentionally engaging moments in time? And does this depend on the attentional instruction, type of stimuli and physiological measure?

We expect that interspersed stimulus detection performance of PS measures depends on combinations of the attentional group (AA or SA), the interspersed stimulus type (emotional sounds or beeps) and the physiological measure (EEG and EDA, heart rate or the multimodal metric). We hypothesized the following;

(1) Attentional instruction and stimulus type: (a) for the SA group, detection performance based on PS is above chance for all interspersed stimuli. (b) For the AA group, detection performance based on PS is above chance for emotional sounds, since these attract attention through bottom-up mechanisms related to salience or emotional relevance (Lang, 1995; Öhman et al., 2001; Schupp et al., 2003) irrespective of task instruction. (c) For the AA group, detection performance based on PS is not above chance for beeps, as these are expected to mainly attract attention through top-down mechanisms related to task-instructions.

(2) Physiological measure and stimulus type (a) PS based on peripheral signals (EDA and heart rate) performs better on the detection of emotional sounds than on beeps, because they primarily reflect emotional state (Cacioppo et al., 2007; Boucsein, 2012). (b) PS based on EEG performs better on the detection of beeps than on the detection of emotional sounds, because they primarily reflect top-down selective attention or mental effort (Hogervorst et al., 2014).

(3) Combining physiological measures: combining the physiological measures into a single multimodal metric of PS would result in relatively high detection accuracies when disregarding the differences between stimulus types.

While for the SA group, the timing of short stimuli serve as "ground truth" relevant events to compare to the moments of high PS, we do not know *a priori* what constitutes relevant events or engaging moments in the audiobook. We therefore investigate ratings of post-hoc determined moments of high and low PS in the audiobook by an independent group of participants. We hypothesized that;

(4) Events in audiobook: moments of the audiobook that were associated with high PS in the AA group are rated as more engaging than moments of the audiobook that were associated with low PS.

MATERIALS AND METHODS

Participants

Twenty-seven participants (17 female), between 18 and 48 years old, with an average of 31.6 years and a standard deviation of 9.8 years, were recruited through the institute's participant pool. Before performing the study, approval was obtained from the TNO Institutional Review Board (IRB). The approval is registered under the reference 2018–70. Prior to the experiment all participants signed informed consent, in accordance with the Declaration of Helsinki. After signing, all participants were randomly assigned to either the AA group or the SA group. After the experiment they received a small monetary reward for their time and traveling costs. None of the participants indicated problems in hearing or attention. Data of one participant were discarded due to failed physiological recordings, resulting in two equal-sized groups.

Materials

EEG, EDA, and electrocardiogram (ECG) were recorded at 1024 Hz using an ActiveTwo Mk II system (BioSemi, Amsterdam, Netherlands). EEG was recorded with 32 active Ag-AgCl electrodes, placed on the scalp according to the 10–20 system, together with a common mode sense active electrode and driven right leg passive electrode for referencing. The electrode impedance threshold was maintained below 20 kOhm. For EDA, two passive gelled Nihon Kohden electrodes were placed on the ventral side of the distal phalanges of the middle and index finger. For ECG, two active gelled Ag-AgCl electrodes were placed at the right clavicle and lowest floating left rib. EDA and heart rate were also recorded using wearable systems (Movisens EdaMove 4 and Wahoo Tickr, respectively). These data are discussed elsewhere (Borovac et al., 2020; Van Beers et al., 2020).

Stimuli and Design

Participants performed the experiment one by one. Each participant was presented with the exact same audio file, composed of a 66 min audiobook (a Dutch thriller "Zure koekjes," written by Corine Hartman) interspersed with other short, auditory stimuli. Half of the participants were asked to focus on the narrative of the audiobook and ignore all other stimuli or instructions (AA group); and half of the participants were asked to focus on the short, interspersed stimuli and perform accompanying tasks, and ignore the narrative (SA group). The auditory stimuli were 36 emotional sounds, 27 blocks of beeps that SA participants had to keep track of, and an auditory instruction to sing a song. The order of sounds and beeps was randomly determined but was identical for each participant. Inter-stimulus intervals varied between 35 and 55 s, with an average of 45 s and a standard deviation of 6.1 s. We selected these stimuli to evaluate PS for a broad range of events, differing in e.g., audio profile and expected effect on mental processes as a function of task instructions.

Emotional sounds were taken from the second version of the International Affective Digitized Sounds (IADS) (Bradley and Lang, 2007). The IADS is a collection of 6-s acoustic stimuli

that have been normatively rated for valence (positive or negative affect), arousal and dominance. Examples of stimuli are the sound of a crying baby or a cheering sports crowd. We selected 12 neutral sounds (IADS number 246, 262, 373, 376, 382, 627, 698, 700, 708, 720, 723, 728), 12 pleasant sounds (110, 200, 201, 202, 311, 352, 353, 365, 366, 367, 415, 717) and 12 unpleasant sounds (115, 255, 260, 276, 277, 278, 279, 285, 286, 290, 292, 422) based on their normative ratings of valence and arousal. We expected these sounds to attract attention of all participants, even those instructed to ignore the interspersed sounds.

Beeps were presented in blocks of 30 s, with every 2 s a 100 ms high (1 kHz) or low (250 Hz) pitched beep. SA participants needed to separately count the number of high and low beeps presented in a block, as in (De Dieuleveult et al., 2018). This task was practiced with them beforehand. In total, 27 blocks of beeps were presented. We expected these sounds to only attract attention of participants clearly instructed to keep track of them.

Toward the end of the audiobook, the instruction was presented to sing a song aloud after a subsequent auditory countdown reached 0. This instruction had to be followed by the SA group and was expected to induce stress and a strong increase in EDA and heart rate (Brouwer and Hogervorst, 2014). For the current analyses, data following the onset of this stimulus were discarded, because some participants started singing before the counter reached 0. This prohibited analysis of the data in terms of mental processes due to confounding movement effects and artifacts in the data recording.

In total, we consider 3,800 s of data in further analyses, out of which 1,026 s involved concurrent presentation of the audiobook and interspersed stimuli.

Analysis

Pre-processing

Data processing was done using MATLAB 2019a software (Mathworks, Natick, MA, United States). For EEG pre-processing we also used EEGLAB v14.1.2 for MATLAB (Delorme and Makeig, 2004). To remove potentials not reflecting sources of neural activity, but ocular or muscle-related artifacts, logistic infomax independent component analysis (ICA) (Bell and Sejnowski, 1995) was performed. EEG was first down sampled to 256 Hz and high-pass filtered at 1 Hz. This relatively high cut-off frequency has shown to work better for ICA compared to lower cut-off frequencies (Winkler et al., 2015). Data were then notch filtered at 50 Hz, using the standard FIR-filter implemented in EEGLAB function pop_eegfiltnew. ICA was performed and the Multiple Artifact Rejection Algorithm (MARA) (Winkler et al., 2011) was used to identify artifactual independent components, i.e., components not reflecting sources of neural activity, but ocular or muscle-related artifacts. These components were removed from re-referenced, but uncleaned data. In these data, samples whose squared amplitude magnitude exceeded the mean-squared amplitude of that channel by more than four standard deviations were marked as missing data ("NaN") in an iterative way with four repetitions. By doing so, 0.82 % of data were marked as missing.

EDA was downsampled to 32 Hz. The fast changing phasic and slowly varying tonic components of the signal were extracted using Continuous Decomposition Analysis as implemented in the Ledalab toolbox for MATLAB (Benedek and Kaernbach, 2010). In the further analyses we use the phasic component of the signal as this component of the EDA signal is mainly related to responses to external stimuli.

ECG measurements were processed to acquire the inter-beat interval (IBI – inversely proportional to heart rate). After downsampling to 256 Hz, ECG was high-pass filtered at 0.5 Hz. Peaks were detected following Pan and Tompkins (1985). The IBI semi-time series was transformed into a timeseries by interpolating consecutive intervals and resampling at 32 Hz.

Computation of Inter-Subject Correlations as Measure of Physiological Synchrony

We computed PS by measuring the inter-subject correlations of the neurophysiological signals. For EEG, rather than treating the signals from the 32 channels separately, we evaluated the inter-subject correlations in the correlated components of the EEG (Dmochowski et al., 2012, 2014). The goal of the correlated component analysis is to find underlying neural sources that are maximally correlated between participants, based on linear combinations of electrodes. Components were extracted separately from the AA group and SA group. EEG data from each participant were projected on the component vectors. Participant-to-group inter-subject correlations were then computed as the sum of correlations in the first three component projections, following (Dmochowski et al., 2012, 2014; Cohen and Parra, 2016; Ki et al., 2016; Cohen et al., 2018). Even though we used fewer participants in each attentional group than earlier work on auditory PS (e.g., Cohen and Parra, 2016; Ki et al., 2016), scalp projections of the components were very similar to those obtained in these earlier works, and our EEG PS values were in a similar range of 0.01 to 0.04. For the computation of time-resolved inter-subject correlations, correlations were computed in running 5 s windows at 1 s increments.

Inter-subject correlations in EDA and IBI were computed following (Marci et al., 2007). We computed Pearson correlations over successive, running 15 s windows at 1 s increments as measure of time-resolved inter-subject correlations. Participant-to-group correlations were computed by averaging over all correlations with all other participants in a group.

Physiological Synchrony for the Detection of Interspersed Stimuli

We designed a paradigm to detect relevant events using gradually increasing thresholds to capture the gradual nature of attentional engagement. **Figure 1** provides a visual explanation of our detection paradigm. Consider the EEG, EDA and IBI response traces that were recorded during the experiment. The timestamps of the data recordings can be separated in moments where interspersed stimuli were presented and where an event detection would thus be considered correct (True) and moments where no interspersed stimuli were presented and where an event detection would be considered incorrect (False). Rather than using the raw physiological responses, the detection paradigm is based on the

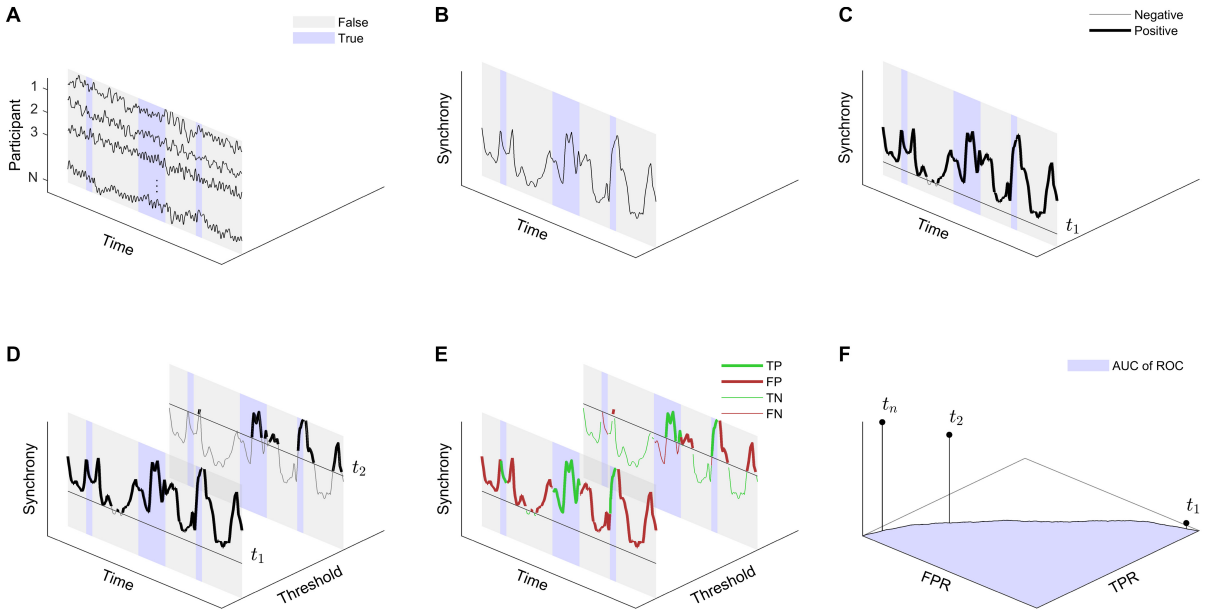

FIGURE 1 | Illustration of the event detection paradigm. **(A)** Consider the physiological response traces recorded from *N* participants who were presented with the same external stimuli at the same time. The timestamps of the data recordings can be separated in moments where events were presented and where an event detection would thus be correct (True) and moments where no events where presented and where an event detection would thus be incorrect (False). **(B)** Rather than considering the raw physiological responses, the detection paradigm is based on the PS between the participants. **(C)** Now let us define a threshold *t*. The moments in time where the synchrony is higher than *t* are marked as an event (Positive) and the moments in time where the synchrony is lower than *t* are marked as a non-event (Negative). **(D)** Rather than using a single value for *t*, we consider a gradually changing threshold t_0 to t_n, so that at t_0 all data are marked as Positive and at t_n all data are marked as Negative **(E)** For each iteration t_i, we can now define the true positives (TP), false positives (FP), true negatives (TN), and false negatives (FN) and thus compute the true-positive rate (TPR) and false-positive rate (FPR). **(F)** Plotting the FPR versus the TPR – both as a function of *t* – results in the receiver operating curve (ROC). Detection performance is defined as the standard metric of area under the ROC (AUC of ROC).

PS between the participants as a function of time. Now let us define a threshold *t*. The moments in time where the synchrony is higher than *t* are marked as an event (Positive) and the moments in time where the synchrony is lower than *t* are marked as a non-event (Negative). Rather than using a single value for *t*, we consider a gradually changing threshold *t*, ranging from the minimum inter-subject correlation value to the maximum inter-subject correlation value. For each iteration of *t*, we can now define the true positives (TP), false positives (FP), true negatives (TN) and false negatives (FN). Using this, the true-positive rate or sensitivity (TPR) is then computed as,

$$TPR = \frac{TP}{TP + FN}$$

and the false-positive rate (FPR) or specificity as,

$$FPR = \frac{FP}{FP + TN}$$

Plotting TPR against FPR provides the receiver operating curve (ROC). Detection performance was assessed using the standard metric of the area under the ROC (AUC of ROC).

Chance level performance was assessed using permutations with randomized stimulus timing. In each permutation, the timing of all interspersed stimuli was randomized between the start and the end of the experiment. The same procedure as above was then applied to obtain the AUC of ROC metric of performance with random stimuli. This procedure was performed on 1000 renditions of such randomized data.

The above-mentioned procedure was repeated 2 × 3 × 4 times, namely for:

(1) Two attentional groups; considering PS between AA participants and PS between SA participants.
(2) Three stimulus types; considering as events (True) either blocks of beeps, emotional sounds, or both of these.
(3) Four physiological measures in which PS is computed; EEG, EDA, heart rate and a multimodal metric that is composed of PS in EEG, EDA and heart rate. To compose this multimodal metric, the PS in EEG, EDA and heart rate were each *z*-scored. The multimodal PS value at each timestamp was then computed as the average of the *z*-scored PS values in EEG, EDA and heart rate at that timestamp, for all timestamps ranging from zero to the end of the experiment.

In each condition, one-tailed two-sample t-tests were conducted to test whether detection performance was higher than chance level performance.

Correspondence Between Physiological Synchrony and Reported Engagement With the Audiobook

While for the SA group, the timing of short stimuli served as "ground truth" relevant events to compare to the moments of

high PS, we did not know a priori what constituted relevant, engaging moments in the audiobook. To systematically examine whether moments of high PS were associated with moments of high relevance in the audiobook, we performed a follow-up test in which a second cohort of participants judged clips of the audiobook that were found to be associated with either high or low PS. We recruited 29 participants through the Prolific online experiment environment. All participants signed informed consent before participating. The participants received a small monetary reward for the invested time. We only included participants who indicated to be fluent in Dutch.

We selected clips based on continuous signals of PS among AA participants. We detected the positive and negative peaks in the signals using the 'findpeaks' function in MATLAB. For each measure (EEG, EDA, heart rate and the multimodal metric), the six peaks with highest positive peak-amplitude and six peaks with largest negative peak-amplitude were selected. For each detected peak, we created a 10 s sound clip, that was composed of the 10 s of audio before the detected peak. For four measures, this thus resulted in a total of 48 clips. Clips associated with peaks that were within 10 s of each other were considered to be overlapping, and were merged into one clip by using only the latest of the two clips in time. This resulted in a total of 38 clips that were presented to the participants.

The procedure of the online test was similar to the initial experiment. The participants were first presented with the same audiostream that was presented to the initial cohort of participants. The participants were instructed as participants from the AA group, i.e., to focus their attention on the narrative of the audiobook and ignore any interspersed stimuli as much as possible. After listening to the book, the participants were asked the same questions about the content of the narrative as participants in the initial cohort. We then presented the participants with the sound clips, each of them directly followed by a rating scale. Participants were instructed to rate the preceding clip using an 11-point Likert scale, ranging from 0 to 10. The lower the score, the more the participant's experience corresponded to the words on the left side of the scale (Dutch: 'verveeld', 'kalm', 'ontspannen'; Translated to English: 'bored', 'calm', 'relaxed'). The higher the score, the more the participant's experience corresponded to the words on the right side of the scale (Dutch: 'geïnteresseerd', 'geboeid', 'emotioneel', 'intens'; Translated to English: 'interested', 'fascinated', 'emotional', 'intense'). Using these words, we intended to capture mental states that are expected to be associated with perceiving relevant events, such as engagement, attention and arousal.

For each modality, we tested whether audio clips corresponding to a positive peak in PS were rated as more 'engaging' than audio clips corresponding to a negative peak in PS, using a Wilcoxon signed-rank test. Participants who answered less than three out of ten questions correctly on the questionnaire about the content of the audiobook were considered as not having participated seriously (AA participants in the main experiment answered 5.8 ± 2.0 questions correctly). This concerned three participants. Removing their data left us with data of 26 participants.

RESULTS

Detection of Interspersed Stimuli Using Physiological Synchrony

Figure 2 and **Table 1** show our measure of interspersed stimuli detection performance, the AUC of ROC as described in the methods. It is presented separately for AA and SA participants; in EEG, EDA, heart rate, and the multimodal metric; and for blocks of beeps, emotional sounds or both of these stimuli together as to-be identified events. **Figure 2** and **Table 1** also show the mean and standard deviation AUC of ROC of permutations with randomized event timing as a chance level baseline. Detection performance was largely in line with hypotheses 1 - 3. For the AA group, we found that, as expected, only the occurrence of emotional sounds could be predicted, using PS in EDA ($p < 0.001$) or the multimodal metric $(p = 0.003)$. For the SA group, occurrences of beep blocks could be detected well above chance level by PS in EEG, EDA and the multimodal metric ($p < 0.001$, $p = 0.002$ and $p < 0.001$, respectively). The occurrence of emotional sounds could be detected significantly better than chance using PS in EDA, heart rate and the multimodal combination ($p = 0.043$, $p = 0.023$, and $p = 0.011$, respectively). When stimuli were not differentiated according to stimulus type, detection performance was well above chance level for PS in EEG ($p < 0.001$), EDA ($p < 0.001$) and the multimodal metric ($p < 0.001$), but not for PS in heart rate.

Correspondence Between Physiological Synchrony and Reported Engagement

Figure 3 shows engagement ratings of audio clips corresponding to positive peaks and ratings of audio clips corresponding to negative peaks for PS in EEG, EDA, heart rate and the multimodal metric. Results did not follow our hypothesis that audio clips corresponding to positive peaks were rated as more engaging than audio clips corresponding to negative peaks. In fact, in EEG and EDA the opposite effect was found (Wilcoxon test statistic: $W = -3.06$, $p = .002$; $W = -3.44$, $p < .001$, respectively). In heart rate and the multimodal metric no significant difference between ratings corresponding to either positive or negative peaks was found ($W = 0.70$, $p = 0.486$, $W = 0.87$, $p = 0.385$).

DISCUSSION

In the sections below, the hypotheses as stated in the Introduction are discussed separately.

Hypothesis 1: Attentional Instruction and Stimulus Type

We hypothesized that interspersed stimulus detection performance would depend on the attentional group (AA or SA) and the interspersed stimulus type (emotional sounds or beeps), due to bottom-up and top-down mechanisms of attention (Lang, 1995; Öhman et al., 2001; Schupp et al., 2003). For the SA group, we hypothesized that detection performance based on PS would be above chance for all interspersed stimuli, whereas for

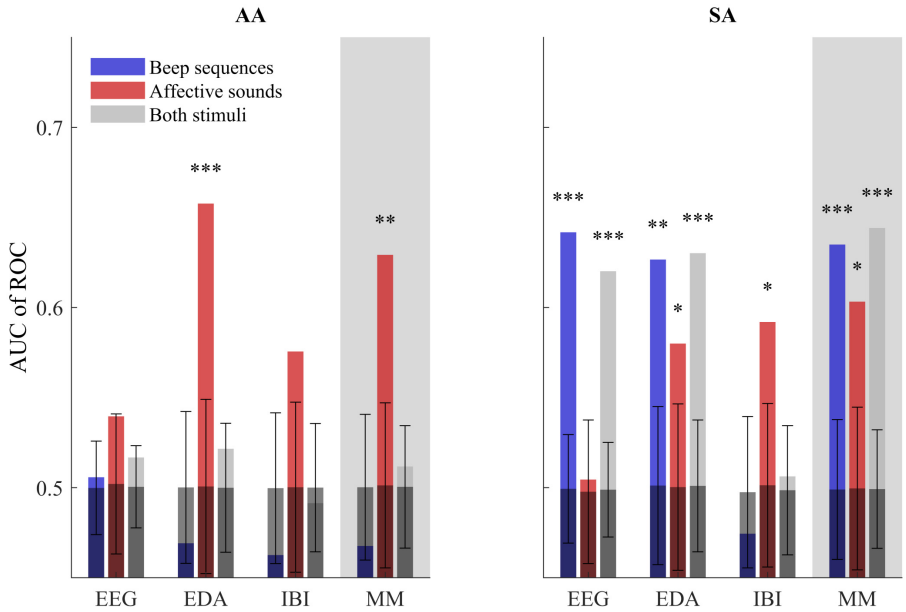

FIGURE 2 | AUC of ROC metric of stimulus detection performance using PS in EEG, EDA, IBI and a multi-modal combination of the three (MM). Performance is shown for the AA and SA groups, when considering only beep blocks or emotional sounds as true positives and when considering both types of stimuli as true positives. In addition, the mean and standard deviation chance level detection performance based on 1,000 renditions with randomized stimulus timing is shown with test results comparing detection performance to chance level (*$p < 0.05$, **$p < 0.01$, ***$p < 0.001$). Note that for the AA group, the emotional sounds but not the beeps are expected to draw (bottom-up) attention, i.e., for the AA group we expect high AUC for emotional sounds only. For the SA group, both beep sequences and emotional sounds are relevant and expected to draw attention.

the AA group we hypothesized that detection performance would be above chance only for emotional sounds, but not for beeps. Results were largely in line with this hypothesis: for the AA group only the emotional sounds were detected with an accuracy above chance level, whereas for the SA group both stimulus types could be detected with above chance level accuracy. Note again that detection performance cannot be directly compared between the different stimulus conditions. There were differences in detection performance between the used physiological measures, these are discussed in the next section.

Hypothesis 2: Physiological Measure and Stimulus Type

Besides the dependency of detection performance on the attentional group and interspersed stimulus type, we expected that detection performance would depend on the used physiological measure and stimulus type. As hypothesized, EEG worked best for the detection of blocks of beeps, while it did not work well for the detection of emotional sounds. We also found EDA to perform well for detecting blocks of beeps. For the detection of emotional sounds, we hypothesized that the peripheral measures (EDA and heart rate) would perform well relative to EEG. Indeed, for both attentional groups, PS in EDA and heart rate perform relatively well for the detection of emotional sounds. Detection performance was significantly above chance using EDA in both groups and using heart rate in the SA group, and near significance ($p = 0.055$) using heart rate in the AA group, whereas detection performance using PS in EEG was far from significant for emotional sounds in both groups. We think that the observed EEG PS differences between the types of stimuli are the result of both the difference in mental processing (top-down, effortful attention for beeps, versus bottom-up, affective processing for emotional sounds) and low level stimulus features. The beep blocks consisted of precisely-timed, repeated beep occurrences, with constant sound levels, while our emotional stimuli consisted of sounds with irregular sound profiles. The positive results obtained with peripheral measures provide further insight in the mechanisms underlying PS. Whereas previous findings on peripheral PS have been viewed in terms of social relation (Palumbo et al., 2017), we here show that PS in peripheral measures can also be explained by shared attentional engagement. It may be the case that shared attention also underlies results found in contexts of social relation.

Hypothesis 3: Combining Physiological Measures

As the three used physiological measures vary with respect to their ability to reflect different mental states, we hypothesized that combining the physiological measures into a single multimodal metric of PS would result in relatively high detection performance when differences between stimulus types are disregarded. Indeed, the multimodal metric performs best when considering both emotional sounds and beeps as relevant events. Detection accuracies are slightly higher than for the best performing unimodal measure when considering emotional sounds or

TABLE 1 | AUC of ROC metric of stimulus detection performance using PS in EEG, EDA, IBI and a multi-modal combination of the three (MM).

	AA				SA			
	EEG	**EDA**	**IBI**	**MM**	**EEG**	**EDA**	**IBI**	**MM**
Beep blocks	0.506 (0.500 ± 0.026) $p = 0.410$	0.470 (0.500 ± 0.042) $p = 0.769$	0.463 (0.500 ± 0.042) $p = 0.813$	0.468 (0.500 ± 0.040) $p = 0.790$	0.642 (0.499 ± 0.030) $p < 0.001$	0.627 (0.501 ± 0.044) $p = 0.002$	0.475 (0.498 ± 0.042) $p = 0.708$	0.635 (0.499 ± 0.039) $p < 0.001$
Emotional sounds	0.540 (0.502 ± 0.039) $p = 0.168$	0.658 (0.501 ± 0.048) $p < 0.001$.	0.576 (0.500 ± 0.047) $p = 0.055$	0.629 (0.501 ± .046) $p = 0.003$	0.505 (0.498 ± 0.040) $p = 0.433$	0.580 (0.500 ± 0.046) $p = 0.043$	0.592 (0.500 ± 0.045) $p = 0.023$	0.604 (0.500 ± 0.045) $p = 0.011$
Both stimuli	0.517 (0.501 ± 0.023) $p = 0.238$	0.522 (0.500 ± 0.036) $p = 0.273$	0.492 (0.500 ± 0.036) $p = 0.596$	0.512 (0.501 ± 0.034) $p = 0.370$	0.621 (0.499 ± 0.026) $p < 0.001$	0.631 (0.501 ± 0.036) $p < 0.001$	0.507 (0.499 ± 0.036) $p = 0.415$	0.644 (0.499 ± 0.033) $p < 0.001$

Performance is shown for the AA and SA groups, when considering only beep blocks or emotional sounds as true positives and when considering both types of stimuli as true positives. In addition, the mean and standard deviation chance level detection performance based on 1,000 renditions with randomized stimulus timing is shown plus p-values of t-tests testing whether detection performance is significantly difference from chance level. Gray cells depict conditions in which detection performance is significantly higher than chance level ($p < 0.05$).

both types of stimuli but not when considering blocks of beeps. We expect that sensor fusion is not beneficial when variables are highly correlated (Hogervorst et al., 2014) – for example for physiological variables all reflecting mental effort – but that sensor fusion can benefit from tasks involving emotional processing besides effortful attentional processing. Besides potentially higher detection performance, the main advantage of multimodal PS seems to be the robustness regarding different types of stimuli, i.e., detection performance varies less between different types of stimuli than for single physiological metrics. In previous work similar effects have been found. For example, when using sensor fusion on machine learning models to distinguish between 13 emotional states, maximum performance was not higher for the multimodal metric, but performance was more robust across the range of emotional states (Verma and Tiwary, 2014). In the end, although adding sensors does not lead to much higher performance compared to the most suitable unimodal recording, a multimodal approach seems to enable detection of relevant events when it is unknown what the best measure for certain stimulus types is. Also note that it is not always known whether certain stimuli will induce mostly effortful cognitive or emotional processing; in many practical cases such processes can co-occur and vary between individuals.

Hypothesis 4: Events in Audiobook

We hypothesized that audio clips corresponding to moments of highest PS would be post-hoc scored as more engaging than audio clips corresponding to moments of lowest PS, but our findings indicated rather the opposite. These findings may be caused by a mismatch between our index of PS and the rating scale of experienced engagement. Post-hoc qualitative analysis of the selected audio-clips revealed that part of the audio clips corresponding to very high PS in EEG coincided with short-term moments of tension or engagement, as expressed through keywords (e.g., swear words) and salient intonation (e.g., a phrase spoken in a very indignant manner). This is in line with earlier work, where moments of high PS in EEG were found to correspond to moments in video clips marked by a high level of short-term suspense, tension or surprise, such as the sight of a gun (Poulsen et al., 2017). Indeed, emotional images and sounds that are rated as highly arousing induce responses in peripheral and central physiological measures (Bradley and Lang, 2000; Lang and Bradley, 2007), which in term may lead to strong PS. In our used audiobook, the keywords that may have driven the particularly high PS contained relatively little important information about the narrative of the story. It seems that this could have been the aspect rated by participants using our engagement scale, leading to a mismatch between self-reported engagement and PS. However, this speculation would need to be investigated further, preferably without having to rely on varying engagement judgements after the fact, but for instance with systematic sentiment analysis (Wöllmer et al., 2013). It is important to further specify what types of attentional engagement can and cannot be captured by PS and how that is dependent on the psychological measure used. Attentional engagement to well-timed events will be better reflected in

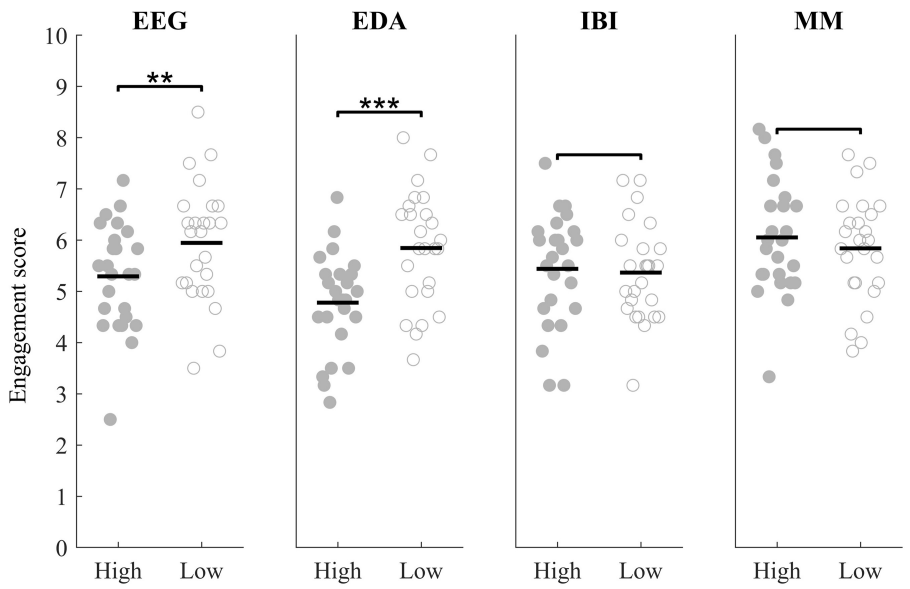

FIGURE 3 | Self-reported engagement scores for audio clips corresponding to moments in the audiobook with high PS (closed markers) or low PS (open markers) in EEG, EDA, IBI and the multimodal metric (MM) (**$p < 0.01$, ***$p < 0.001$).

PS than attentional engagement to less well-timed event on a more abstract level.

Limitations

It should be noted that the stimulus detection performance when not taking stimulus type into consideration ('both stimuli') were mainly driven by detection performance of beep blocks. These beep blocks were interspersed for a total of 810 s, whereas the emotional sounds were only interspersed for a total of 216 s. The stimuli also differed on other aspects. For instance, the beep blocks consisted of precisely timed beeps with immediate stimulus onset equal across trials, whereas the emotional sounds all differed in sound profile. For the AUC of ROC metrics when considering detection of both types of stimuli, beep blocks thus influence the performance metric more than the emotional sounds. While this can be seen as a limitation, this is exemplary for real life situations, where one is interested in detecting relevant, attentionally engaging events, without further specifying or knowing the different types of stimuli, and the proportion of in which they occur; i.e., in such a situation, the 'both stimuli' situation is the default.

We must also note that our simple multimodal approach is certainly not the optimal approach to combine data. In particular, we expect that detection performance can be enhanced by compensating for differences in response latencies across measures. To illustrate the difference in response latency, in response to the same set of emotional sounds, response peak latency ranges from a few 100 ms for EEG to multiple seconds in EDA heart rate (Bradley and Lang, 2000; Hettich et al., 2016). In this paper we simply averaged over response traces in a point-wise fashion, meaning that response-induced peaks may be spread out and their amplitude reduced. Our current results should therefore be interpreted as a first confirmation that multimodal sensor fusion can be of added value, but we expect that other approaches can greatly enhance performance. In future work we would like to explore other methods for the combination of physiological measures into a multimodal metric of PS.

CONCLUSION

We determined PS in EEG and EDA, heart rate and a multimodal fusion of these three sensors in two groups of participants, that were instructed to attend either to the narrative of an audiobook or to interspersed auditory events. We found that PS could detect the relevant interspersed stimuli with accuracies well above chance level, but also found that moments in the audiobook corresponding to high PS were not rated as more engaging than moments corresponding to low PS. Our results support the notion that PS can be valuable when interested in the course of attentional engagement over time. Currently the relation between PS and engagement is only established for well-defined, interspersed emotional or effortful cognitive stimuli, whereas the relation between PS and a more abstract self-reported metric of engagement is not yet established. We further note that obtained results vary between the used physiological measures. Interesting from a user perspective, EDA worked best overall. These results should enable researchers to monitor PS in situations where intrusive EEG measurements are not suited. However, we also note that the optimal physiological metric may be dependent on the goal of a study and suggest to choose a measure matching with the stimulus of interest. EEG works especially well for well-timed effortful cognitive stimuli, heart rate works especially well for emotional stimuli and EDA works quite well on both types of stimuli. When the stimulus type is unknown, a multimodal

metric may work best as it seems most robust across a broad range of stimuli.

DATA AVAILABILITY STATEMENT

The data presented in this study can be found on the Open Science Framework: https://osf.io/8kh36/. The code can be obtained from the corresponding author upon request.

ETHICS STATEMENT

The studies involving human participants were reviewed and approved by the TNO Institutional Review Board. The participants provided their written informed consent to participate in this study.

AUTHOR CONTRIBUTIONS

A-MB and IS conceived and designed the study. IS and NT performed the experiment. IS analyzed the data with input from A-MB, JE, and NT. IS wrote the first draft of the manuscript. All authors thoroughly reviewed and revised the manuscript drafts and approved the submitted version.

FUNDING

This work was supported by the Netherlands Organization for Scientific Research (NWA Startimpuls 400.17.602).

ACKNOWLEDGMENTS

We thank Ana Borovac for her help with performing the experiment.

REFERENCES

Aliakbaryhosseinabadi, S., Kamavuako, E. N., Jiang, N., Farina, D., and Mrachacz-Kersting, N. (2017). Classification of EEG signals to identify variations in attention during motor task execution. *J. Neurosci. Methods* 284, 27–34. doi: 10.1016/j.jneumeth.2017.04.008

Bell, A. J., and Sejnowski, T. J. (1995). An information-maximization approach to blind separation and blind deconvolution. *Neural Comput.* 7, 1129–1159. doi: 10.1162/neco.1995.7.6.1129

Benedek, M., and Kaernbach, C. (2010). A continuous measure of phasic electrodermal activity. *J. Neurosci. Methods* 190, 80–91. doi: 10.1016/j.jneumeth.2010.04.028

Borovac, A., Stuldreher, I. V., Thammasan, N., and Brouwer, A. M. (2020). "Validation of wearables for electrodermal activity (EdaMove) and heart rate (Wahoo Tickr)," in *Proceedings of 12th International Conference on Measuring Behavior 2020-21*, Kraków, 18–24.

Boucsein, W. (2012). *Electrodermal Activity*. Cham: Springer Science and Business Media.

Bradley, M. M., and Lang, P. J. (2000). Affective reactions to acoustic stimuli. *Psychophysiology* 37, 204–215. doi: 10.1111/1469-8986.3720204

Bradley, M. M., and Lang, P. J. (2007). *Emotion and Motivation*. Cham: Springer.

Brouwer, A. M., and Hogervorst, M. A. (2014). A new paradigm to induce mental stress: the sing-a-song stress test (SSST). *Front. Neurosci.* 8:224. doi: 10.3389/fnins.2014.00224

Brouwer, A. M., Zander, T. O., Van Erp, J. B., Korteling, J. E., and Bronkhorst, A. W. (2015). Using neurophysiological signals that reflect cognitive or affective state: six recommendations to avoid common pitfalls. *Front. Neurosci.* 9:136. doi: 10.3389/fnins.2015.00136

Cacioppo, J. T., Tassinary, L. G., and Berntson, G. (eds) (2007). *Handbook of Psychophysiology*. Cambridge, MA: Cambridge university press.

Cohen, S. S., Madsen, J., Touchan, G., Robles, D., Lima, S. F., Henin, S., et al. (2018). Neural engagement with online educational videos predicts learning performance for individual students. *Neurobiol. Learn. Mem.* 155, 60–64. doi: 10.1016/j.nlm.2018.06.011

Cohen, S. S., and Parra, L. C. (2016). Memorable audiovisual narratives synchronize sensory and supramodal neural responses. *ENeuro* 3:ENEURO.0203-16.2016.

Davidesco, I., Laurent, E., Valk, H., West, T., Dikker, S., Milne, C., et al. (2019). Brain-to-brain synchrony predicts long-term memory retention more accurately than individual brain measures. *BioRxiv* [Preprint]. doi: 10.1101/644047v1

De Dieuleveult, A. L., Brouwer, A. M., Siemonsma, P. C., Van Erp, J. B., and Brenner, E. (2018). Aging and sensitivity to illusory target motion with or without secondary tasks. *Multisens. Res.* 31, 227–249. doi: 10.1163/22134808-00002596

Delorme, A., and Makeig, S. (2004). EEGLAB: an open source toolbox for analysis of single-trial EEG dynamics including independent component analysis. *J. Neurosci. Methods* 134, 9–21. doi: 10.1016/j.jneumeth.2003.10.009

Dmochowski, J. P., Bezdek, M. A., Abelson, B. P., Johnson, J. S., Schumacher, E. H., and Parra, L. C. (2014). Audience preferences are predicted by temporal reliability of neural processing. *Nat. Commun.* 5:4567.

Dmochowski, J. P., Sajda, P., Dias, J., and Parra, L. C. (2012). Correlated components of ongoing EEG point to emotionally laden attention–a possible marker of engagement? *Front. Hum. Neurosci.* 6:112. doi: 10.3389/fnhum.2012.00112

Fleureau, J., Guillotel, P., and Huynh-Thu, Q. (2012). Physiological-based affect event detector for entertainment video applications. *IEEE Trans. Affect. Comput.* 3, 379–385. doi: 10.1109/t-affc.2012.2

Hamadicharef, B., Zhang, H., Guan, C., Wang, C., Phua, K. S., Tee, K. P., et al. (2009). "Learning EEG-based spectral-spatial patterns for attention level measurement," in *Proceedings of the 2009 IEEE International Symposium on Circuits and Systems*, Taipei, 1465–1468.

Hanson, S. J., Gagliardi, A. D., and Hanson, C. (2009). Solving the brain synchrony eigenvalue. problem: conversation of temporal dynamics (fMRI) over subjects doing the same task. *J. Comput. Neurosci.* 27, 103–114 doi: 10.1007/s10827-008-0129-z

Hasson, U., Malach, R., and Heeger, D. J. (2010). Reliability of cortical activity during natural stimulation. *Trends Cogn. Sci.* 14, 40–48. doi: 10.1016/j.tics.2009.10.011

Hasson, U., Nir, Y., Levy, I., Fuhrmann, G., and Malach, R. (2004). Intersubject synchronization of cortical activity during natural vision. *Science* 303, 1634–1640. doi: 10.1126/science.1089506

Hettich, D. T., Bolinger, E., Matuz, T., Birbaumer, N., Rosenstiel, W., and Spüler, M. (2016). EEG responses to auditory stimuli for automatic affect recognition. *Front. Neurosci.* 10:244. doi: 10.3389/fnins.2016.00244

Hogervorst, M. A., Brouwer, A. M., and Van Erp, J. B. (2014). Combining and comparing EEG, peripheral physiology and eye-related measures for the assessment of mental workload. *Front. Neurosci.* 8:322. doi: 10.3389/fnins.2014.00322

Hussain, M. S., AlZoubi, O., Calvo, R. A., and D'Mello, S. K. (2011). "Affect detection from multichannel physiology during learning sessions with AutoTutor," in *Proceedings of the International Conference on Artificial Intelligence in Education*, (Berlin: Springer), 131–138. doi: 10.1007/978-3-642-21869-9_19

Ki, J. J., Kelly, S. P., and Parra, L. C. (2016). Attention strongly modulates reliability of neural responses to naturalistic narrative stimuli. *J. Neurosci.* 36, 3092–3101.

Koole, S. L., Tschacher, W., Butler, E., Dikker, S., and Wilderjans, T. (2020). "In sync with your shrink," in *Applications of Social Psychology*, eds J. P. Forgas, W. D. Crano, and K. Fiedler (Milton Park: Taylor and Francis), 161–184. doi: 10.4324/9780367816407-9

Lang, P., and Bradley, M. M. (2007). The International Affective Picture System (IAPS) in the study of emotion and attention. *Handb. Emot. Elicitation Assess.* 29, 70–73.

Lang, P. J. (1995). The emotion probe: studies of motivation and attention. *Am. Psychol.* 50:372. doi: 10.1037/0003-066x.50.5.372

Liu, N. H., Chiang, C. Y., and Chu, H. C. (2013). Recognizing the degree of human attention using EEG signals from mobile sensors. *Sensors* 13, 10273–10286. doi: 10.3390/s130810273

Malmberg, J., Järvelä, S., Holappa, J., Haataja, E., Huang, X., and Siipo, A. (2019). Going beyond what is visible: What multichannel data can reveal about interaction in the context of collaborative learning? *Comput. Hum. Behav.* 96, 235–245. doi: 10.1016/j.chb.2018.06.030

Marci, C. D., Ham, J., Moran, E., and Orr, S. P. (2007). Physiologic correlates of perceived therapist empathy and social-emotional process during psychotherapy. *J. Nerv. Ment. Dis.* 195, 103–111. doi: 10.1097/01.nmd.0000253731.71025.fc

Öhman, A., Flykt, A., and Esteves, F. (2001). Emotion drives attention: detecting the snake in the grass. *J. Exp. Psychol. Gen.* 130:466. doi: 10.1037/0096-3445.130.3.466

Palumbo, R. V., Marraccini, M. E., Weyandt, L. L., Wilder-Smith, O., McGee, H. A., Liu, S., and Goodwin, M. S. (2017). Interpersonal autonomic physiology: a systematic review of the literature. *Pers. Soc. Psychol. Rev.* 21, 99–141. doi: 10.1177/1088868316628405

Pan, J., and Tompkins, W. J. (1985). A real-time QRS detection algorithm. *IEEE Trans. Biomed. Eng.* 32, 230–236. doi: 10.1109/tbme.1985.325532

Perez, P., Madsen, J., Banellis, L., Turker, B., Raimondo, F., Perlbarg, V., and Similowski, T. (2020). Conscious processing of narrative stimuli synchronizes heart rate between individuals. *bioRxiv* doi: 10.1101/2020.05.26.116079

Polich, J. (2007). Updating P300: an integrative theory of P3a and P3b. *Clin. Neurophysiol.* 118, 2128–2148. doi: 10.1016/j.clinph.2007.04.019

Poulsen, A. T., Kamronn, S., Dmochowski, J., Parra, L. C., and Hansen, L. K. (2017). EEG in the classroom: synchronised neural recordings during video presentation. *Sci. Rep.* 7:43916.

Rosenberg, M., Noonan, S., DeGutis, J., and Esterman, M. (2013). Sustaining visual attention in the face of distraction: a novel gradual-onset continuous performance task. *Attent. Percept. Psychophys.* 75, 426–439. doi: 10.3758/s13414-012-0413-x

Schupp, H. T., Junghöfer, M., Weike, A. I., and Hamm, A. O. (2003). Attention and emotion: an ERP analysis of facilitated emotional stimulus processing. *Neuroreport* 14, 1107–1110. doi: 10.1097/00001756-200306110-00002

Stuldreher, I. V., Thammasan, N., Van Erp, J. B. F., and Brouwer, A. M. (2020). Physiological synchrony in EEG, electrodermal activity and heart rate reflects shared selective auditory attention. *J. Neural Eng.* 17:046028. doi: 10.1088/1741-2552/aba87d

Tickle-Degnen, L., and Rosenthal, R. (1990). The nature of rapport and its nonverbal correlates. *Psychol. Inq.* 1, 285–293. doi: 10.1207/s15327965pli0104_1

Tourunen, A., Kykyri, V. L., Seikkula, J., Kaartinen, J., Tolvanen, A., and Penttonen, M. (2019). Sympathetic nervous system synchrony: an exploratory study of its relationship with the therapeutic alliance and outcome in couple therapy. *Psychotherapy* 57, 160–173. doi: 10.1037/pst0000198

Van Beers, J., Stuldreher, I. V., Thammasan, N., and Brouwer, A. M. (2020). "A comparison between laboratory and wearable sensors in the context of physiological synchrony," in *Proceedings of the 2020 International Conference on Multimodal Interaction (ICMI)*, Utrecht, 604–608.

Verma, G. K., and Tiwary, U. S. (2014). Multimodal fusion framework: a multiresolution approach for emotion classification and recognition from physiological signals. *NeuroImage* 102, 162–172. doi: 10.1016/j.neuroimage.2013.11.007

Winkler, I., Debener, S., Müller, K. R., and Tangermann, M. (2015). "On the influence of high-pass filtering on ICA-based artifact reduction in EEG-ERP," in *Proceedings of the 2015 37th Annual International Conference of the IEEE Engineering in Medicine and Biology Society (EMBC)*, Milan, 4101–4105.

Winkler, I., Haufe, S., and Tangermann, M. (2011). Automatic classification of artifactual ICA-components for artifact removal in EEG signals. *Behav. Brain Funct.* 7:30. doi: 10.1186/1744-9081-7-30

Wöllmer, M., Weninger, F., Knaup, T., Schuller, B., Sun, C., Sagae, K., et al. (2013). Youtube movie reviews: Sentiment analysis in an audio-visual context. *IEEE Intelligent Syst.* 28, 46–53. doi: 10.1109/mis.2013.34

Zander, T. O., and Kothe, C. (2011). Towards passive brain–computer interfaces: applying brain–computer interface technology to human–machine systems in general. *J. Neural Eng.* 8:025005. doi: 10.1088/1741-2560/8/2/025005

Zehetleitner, M., Goschy, H., and Müller, H. J. (2012). Top-down control of attention: it's gradual, practice-dependent, and hierarchically organized. *J. Exp. Psychol.* 38:941. doi: 10.1037/a0027629

Conflict of Interest: The authors declare that the research was conducted in the absence of any commercial or financial relationships that could be construed as a potential conflict of interest.

frontiers in Neuroscience

SYSTEMATIC REVIEW
published: 09 April 2021
doi: 10.3389/fnins.2021.648354

Effects of Transcranial Direct Current Stimulation Combined With Physical Training on the Excitability of the Motor Cortex, Physical Performance, and Motor Learning: A Systematic Review

Baofeng Wang[1], *Songlin Xiao*[1], *Changxiao Yu*[1], *Junhong Zhou*[2,3]* *and Weijie Fu*[1,4]*

[1] School of Kinesiology, Shanghai University of Sport, Shanghai, China, [2] The Hinda and Arthur Marcus Institute for Aging Research, Hebrew SeniorLife, Boston, MA, United States, [3] Harvard Medical School, Boston, MA, United States, [4] Key Laboratory of Exercise and Health Sciences of Ministry of Education, Shanghai University of Sport, Shanghai, China

Purpose: This systematic review aims to examine the efficacy of transcranial direct current stimulation (tDCS) combined with physical training on the excitability of the motor cortex, physical performance, and motor learning.

Methods: A systematic search was performed on PubMed, Web of Science, and EBSCO databases for relevant research published from inception to August 2020. Eligible studies included those that used a randomized controlled design and reported the effects of tDCS combined with physical training to improve motor-evoked potential (MEP), dynamic posture stability index (DPSI), reaction time, and error rate on participants without nervous system diseases. The risk of bias was assessed by the Cochrane risk of bias assessment tool.

Results: Twenty-four of an initial yield of 768 studies met the eligibility criteria. The risk of bias was considered low. Results showed that anodal tDCS combined with physical training can significantly increase MEP amplitude, decrease DPSI, increase muscle strength, and decrease reaction time and error rate in motor learning tasks. Moreover, the gain effect is significantly greater than sham tDCS combined with physical training.

Conclusion: tDCS combined with physical training can effectively improve the excitability of the motor cortex, physical performance, and motor learning. The reported results encourage further research to understand further the synergistic effects of tDCS combined with physical training.

Keywords: cortical excitability, motor learning, physical performance, physical training, transcranial direct current stimulation

OPEN ACCESS

Edited by:
Pattie Maes,
Massachusetts Institute of Technology, United States

Reviewed by:
Farheen Syeda,
United States Department of the Navy, United States
Ying Shen,
The First Affiliated Hospital of Nanjing Medical University, China

***Correspondence:**
Weijie Fu
fuweijie@sus.edu.cn
Junhong Zhou
junhongzhou@hsl.harvard.edu

Specialty section:
This article was submitted to Neural Technology, a section of the journal Frontiers in Neuroscience

Received: *31 December 2020*
Accepted: *08 March 2021*
Published: *09 April 2021*

Citation:
Wang B, Xiao S, Yu C, Zhou J and Fu W (2021) Effects of Transcranial Direct Current Stimulation Combined With Physical Training on the Excitability of the Motor Cortex, Physical Performance, and Motor Learning: A Systematic Review. Front. Neurosci. 15:648354. doi: 10.3389/fnins.2021.648354

INTRODUCTION

Transcranial direct current stimulation (tDCS) is a non-invasive brain stimulation technique that modulates the neural activities of cortical brain regions by applying a constant weak current (e.g., current intensity of one electrode is usually smaller than 2 mA) *via* the scalp electrodes (Nitsche and Paulus, 2000). More and more research using tDCS has emerged in the fields of sports and rehabilitative medicine these days (Chang et al., 2017; Xiao et al., 2020). Two types of tDCS are commonly used, that is, anodal tDCS (a-tDCS) aiming to increase the excitability of the targeting cortical regions by depolarizing the resting membrane potentials of neurons, and cathodal tDCS (c-tDCS) that often induces inhibitory effects of neural excitability in the targeted brain regions (Nitsche and Paulus, 2000, 2001; Bastani and Jaberzadeh, 2012). Recent studies in the field of sports sciences have shown that using tDCS can significantly enhance physical performance, such as the toe abduction strength (Tanaka et al., 2009) and reaction time (Tseng et al., 2020) in healthy people and the knee extensor force in patients with hemiparetic stroke. Several previous systematic reviews have also confirmed that using tDCS can induce benefits to important functionalities, such as motor control, in different populations (e.g., people with Parkinson's disease (PD) (Broeder et al., 2015) and healthy cohorts (Machado et al., 2019).

More recently, researchers have started to combine tDCS with other types of interventions, such as physical (e.g., exercise, physiotherapy, etc.) and cognitive training (Beretta et al., 2020), and explore the effects of this mixed type of intervention. Studies have shown that both tDCS and exercise (e.g., strength training) can increase the excitability of cortical (e.g., primary motor cortex, M1) as measured by the amplitude of motor-evoked potential (MEP) (Kidgell et al., 2010; Mazzoleni et al., 2019). Therefore, it is speculated that this mixed-type intervention may induce greater improvements as compared to tDCS-or exercise/training-only intervention. However, a large variance in the results of the studies exploring the effects of such mixed-type intervention was observed in previous studies. For example, Kim and Ko (2013) observed that tDCS combined with grip strength training induced a greater increase in MEP amplitude as compared to tDCS applied alone, and Jafarzadeh et al. (2019) also observed that tDCS combined with physical training induced greater improvement in dynamic stability. However, Zandvliet et al. (2018) reported that in healthy people, tDCS combined with posture training did not induce significant improvement in the center of pressure (CoP) parameters when standing quietly with eyes open or closed, including the mean and variability of the amplitude of the CoP displacement and the mean and variability of the velocity of CoP fluctuation.

Therefore, the effects of this mixed-type intervention consisting of tDCS with physical training remain unclear due to the inconsistent results of previous publications. This systematic review here thus aims to examine the efficacy of tDCS combined with physical training on the excitability of M1, physical performance and motor learning function in populations without any major neurological diseases by critically evaluating and comparing the results in the publications, which will ultimately provide important knowledge to this field and informing the design of future studies.

METHODS

Search Strategy

Literature searches were conducted up to August 2020 in electronic databases, namely, PubMed, Web of Science, and EBSCO. The following search terms were used: "transcranial direct current stimulation," "tDCS," "training," "intervention," "exercise," "physical therapy," and "motor learning." In addition, the reference lists of the included articles were investigated to detect additional relevant articles that cannot be found *via* the initial electronic search strategy.

Inclusion and Exclusion Criteria

Inclusion criteria were determined on the basis of the population, intervention, comparison, and outcome approach (PICO) (Cerqueira et al., 2020). The population included adult groups (i.e., without major neurological diseases). The type of intervention was defined as tDCS combined with physical training. The control group was designed as sham tDCS (s-tDCS) combined with physical training. The outcomes included the cortical excitability as measured by MEP, dynamic posture stability index (DPSI), muscle strength, reaction time, and error rate of motor learning tasks. Exclusion criteria were: studies published in any language other than English, open-label protocol, review papers, book chapters, conference abstract, commentaries, study protocols, or clinical trial registers. **Figure 1** depicted the flow diagram of the screening. Articles were then categorized in accordance with the methodological and assessed parameters.

Data Extraction

The articles were exported to Endnote for screening and qualitative assessment. Two authors (BW and SX) independently screened all titles and abstracts. If an abstract met the inclusion criteria, the full text of the article was then reviewed for confirmation. Discrepancies were resolved by two senior investigators (WF and JZ). Then, the two authors extracted the data into spreadsheets, which included participant demographics, sample size, tDCS characteristics (e.g., electrode position, current intensity, duration), intervention characteristics (e.g., number of sessions), and main outcomes (MEP, DPSI, muscle strength, reaction time, error rate, etc.).

Risk of Bias Assessment

We assessed the risk of bias using the Cochrane risk of bias assessment tool (Cerqueira et al., 2020). Study quality assessment included random sequence generation; allocation concealment; blinding of investigators, participants, assessors, and outcome assessors; description of losses and exclusions; selective report; and other biases. Each domain was scored as "high," "low," or "unclear" risk of bias.

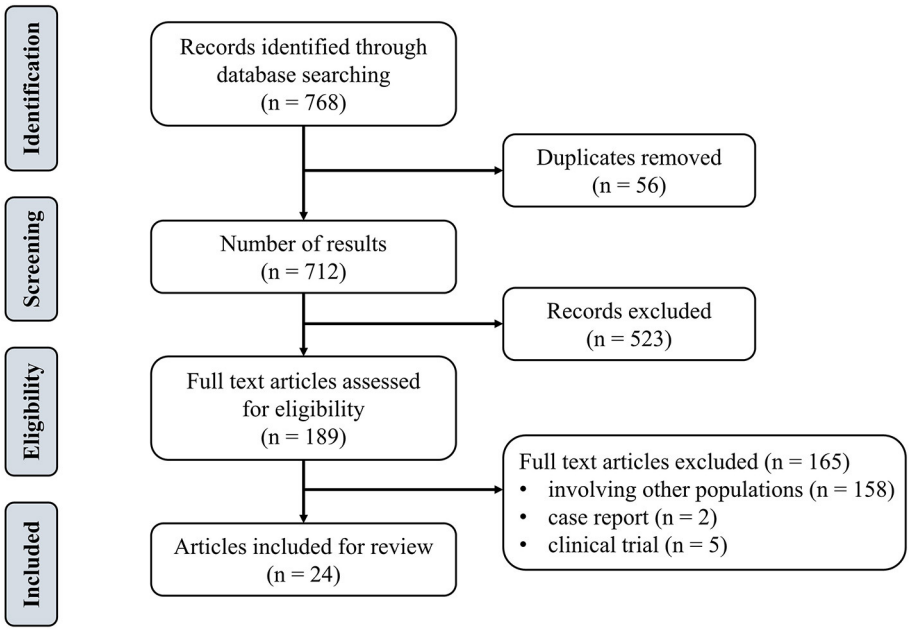

FIGURE 1 | Flowchart of the search and inclusion process.

RESULTS

We identified 768 studies, of which 24 meeting the eligibility criteria were included in this review. **Table 1** summarized eight studies on the effects of mixed-type intervention on the excitability of M1, **Table 2** summarized eight relevant studies on the effects on physical performance, and **Table 3** summarized 13 studies on the effects on motor learning.

Risk of Bias Assessment

The level of the risk of bias varied across studies, as shown in **Figure 2**. The most common potential causes of bias were inadequate description of randomization and concealment of procedures reported in studies and deemed to moderate to high risk of bias. Fifteen studies implemented a double-blinded design (Vines et al., 2008; Reis et al., 2009, 2013; Williams et al., 2010; Kang and Paik, 2011; Thirugnanasambandam et al., 2011; Goodwill et al., 2013; Hendy and Kidgell, 2013; Kim and Ko, 2013; Fujimoto et al., 2014; Steiner et al., 2016; Rumpf et al., 2017; Baltar et al., 2018; Yosephi et al., 2018; Jafarzadeh et al., 2019), in which both the study personnel and participants were not aware of the types of intervention. Five studies used a single-blinded design (Stagg et al., 2011; Naros et al., 2016; Zandvliet et al., 2018; Bruce et al., 2020; Tseng et al., 2020), and the blinding was not reported in other four studies (Karok and Witney, 2013; Looi et al., 2016; Washabaugh et al., 2016; Chen et al., 2020).

Study Characteristics

The total number of recruited participants was 784 (462 males and 322 females, age range: 18–80 years). All interventions were designed as tDCS combined with physical training [muscle strength training ($n = 153$), balance training ($n = 133$), running ($n = 12$), shaping task ($n = 20$), visuomotor tracking ($n = 239$), grating orientation task ($n = 9$), motor sequence task ($n = 218$)]. For the design of tDCS, 19 studies used tDCS to target the M1 (Vines et al., 2008; Reis et al., 2009, 2013; Williams et al., 2010; Kang and Paik, 2011; Stagg et al., 2011; Thirugnanasambandam et al., 2011; Goodwill et al., 2013; Hendy and Kidgell, 2013; Karok and Witney, 2013; Kim and Ko, 2013; Naros et al., 2016; Washabaugh et al., 2016; Rumpf et al., 2017; Baltar et al., 2018; Jafarzadeh et al., 2019; Bruce et al., 2020; Chen et al., 2020; Tseng et al., 2020), two studies targeted the cerebellum (Steiner et al., 2016; Zandvliet et al., 2018), one study targeted both the M1 and the cerebellum (Yosephi et al., 2018), one study targeted the primary somatosensory cortex (Fujimoto et al., 2014), and one study targeted the dorsolateral prefrontal cortex (Looi et al., 2016). The current intensities of tDCS were between 1.5 and 2 mA, and the duration of each stimulation session was between 15 to 20 min. The size of the electrodes was between 35 and 40 cm^2. Most studies used sham protocol as the control, in which the current was delivered only during the initial period of each session (i.e., the first 15 to 30 s) and then turned off (Vines et al., 2008; Reis et al., 2009, 2013; Williams et al., 2010; Kang and Paik, 2011; Stagg et al., 2011; Thirugnanasambandam et al., 2011; Goodwill et al., 2013; Hendy and Kidgell, 2013; Karok and Witney, 2013; Kim and Ko, 2013; Fujimoto et al., 2014; Looi et al., 2016; Naros et al., 2016; Steiner et al., 2016; Washabaugh et al., 2016; Rumpf et al., 2017; Baltar et al., 2018; Yosephi et al., 2018; Zandvliet et al., 2018; Jafarzadeh et al., 2019; Chen et al., 2020; Tseng et al., 2020); One study used the sham protocol that delivered current during the initial 120 s (Bruce et al., 2020).

TABLE 1 | The effects of tDCS combined with physical training on the excitability of the motor cortex.

References	Sample size	Intervention	Control	Protocol	tDCS site	Combine way	Outcome measure	Time of assessment	Results
Bruce et al. (2020)	26 CAI	a-tDCS + strength training	s-tDCS + strength training	10 session 18 min 1.5 mA	M1	During	MEP amplitude	Before, halfway through training (week-2), completion of training (week-4), and retention (week-6)	Cortical excitability was increased in the a-tDCS group, which lasted until the 6th week
Baltar et al. (2018)	12 YA	a-tDCS + running	c-tDCS + running s-tDCS + running	1 session 20 min 2 mA	M1	Preconditioned by tDCS	MEP amplitude	Before, immediately, 10, 20, 30, 60, and 90 min after the interventions	No significant interaction in MEP between the a-tDCS combined with running group and s-tDCS combined with running groups
Kim and Ko (2013)	44 YA	a-tDCS + grip exercise	a-tDCS s-tDCS Grip exercise	1 session 20 min 2 mA	M1	During	MEP amplitude	Before, immediately after the interventions	The combination of a-tDCS with voluntary grip exercise produced a 2-fold increase in the MEP amplitude as compared with the a-tDCS group or voluntary grip exercise group
Hendy and Kidgell (2013)	30 YA	a-tDCS + strength training	s-tDCS + strength training No intervention	9 session 20 min 2 mA	M1	During	MEP amplitude SICI	Before, immediately after the interventions	There was an increase (22.6%) in MEP amplitude for the tDCS combined with strength training group and was significantly greater than the change for the sham condition
Goodwill et al. (2013)	11 OA	Bilateral tDCS + visuomotor tracking	Unilateral tDCS + visuomotor tracking s-tDCS + visuomotor tracking	1 session 15 min 1 mA	M1	During	MEP amplitude SICI	Before, immediately and 30 min after intervention	The change from baseline to immediately after intervention for both the unilateral (38%) and bilateral (53%) conditions were significantly greater than the change for the sham condition
Karok and Witney (2013)	22 YA	Bilateral tDCS + motor sequence task	Unilateral tDCS + motor sequence task s-tDCS + motor sequence task	1 session 10 min 1.5 mA	M1	During	MEP amplitude	Before, during, immediately and 15 min after intervention	MEP amplitude of bilateral tDCS group was significantly higher than in the sham condition
Thirugnanasambandam et al. (2011)	16 YA	a-tDCS + voluntary muscle contraction	a-tDCS c-tDCS s-tDCS	1 session 20 min 1 mA	M1	Preconditioned by tDCS	MEP amplitude SICI CSP	Before, immediately after the interventions	There was no significant difference in cortical excitability between a-tDCS combined with voluntary muscle contraction group and s-tDCS group
Williams et al. (2010)	20 YA	a-tDCS + motor training	s-tDCS + motor training	1 session 40 min 1 mA	M1	During	MEP amplitude TCI	Before, immediately and 2 h after the interventions	There was a significant increase in MEP amplitude after a-tDCS combined with motor training and no significant change after sham tDCS combined with motor training

YA, young adult; OA, old adult; CAI, chronic ankle instability; tDCS, transcranial direct current stimulation; a-tDCS, anodal tDCS; c-tDCS, cathodal tDCS; s-tDCS, sham tDCS; MEP, motor-evoked potentials; SICI, short-interval intracortical inhibition, CSP, cortical silent period; TCI, transcallosal inhibition.

TABLE 2 | The effects of tDCS combined with physical training on physical performance.

References	Sample size	Intervention	Control	Protocol	tDCS site	Combine way	Outcome measure	Time of assessment	Results
Bruce et al. (2020)	26 CAI	a-tDCS + strength training	s-tDCS + strength training	4 session 18 min 1.5 mA	M1	During	DPSI Muscle activation	Before, halfway through training (week-2), completion of training (week-4), and retention (week-6)	Dynamic balance and muscle activation improved in the a-tDCS combined strength training group from baseline to week-6
Jafarzadeh et al. (2019)	38 LBP	a-tDCS + postural training	s-tDCS + postural training Postural training	6 session 20 min 2 mA	M1	During	DPSI BBS VAS	Before, immediately and 1-month after the interventions	The postural stability indices, BBS and VAS scores significantly improved immediately and one-month after the intervention in the a-tDCS combined training group, while there were significant differences between active a-tDCS and other two groups
Zandvliet et al. (2018)	10 OA	a-tDCS + postural training	s-tDCS + postural training	1 session 20 min 1.5 mA	Cerebellum	During	CoP VAS	Before, immediately after the interventions	No significant changes in CoP comp-score and performance on the tracking task
Yosephi et al. (2018)	65 OA	M1 a-tDCS + postural training Bilateral cerebellar a-tDCS + postural training	Sham a-tDCS + Postural training Cerebellar a-tDCS postural training	6 session 20 min 2 mA	M1 Cerebellum	During	DPSI BBS	Before, immediately after the interventions	Simultaneous postural training with M1 or bilateral cerebellar a-tDCS significantly improved postural stability indices and BBS scores. Moreover, two weeks postural training alone or cerebellar a-tDCS alone is not an adequate intervention to improve the postural stability indices
Washabaugh et al. (2016)	22 YA	a-tDCS + intermittent quadriceps activity	a-tDCS + resting	1 session 20 min 1.5 mA	M1	During	Knee extension torque Knee flexion torque	Before, immediately, 5 and 25 min after the interventions	The tDCS combined with training group produced greater knee extension torques when compared with the tDCS-resting group
Steiner et al. (2016)	30 YA	a-tDCS + postural training	s-tDCS + postural training	1 session 20 min 2 mA	Cerebellum	During	Balance time Platform angle	Before, immediately, and 25 h after the interventions	Cerebellar tDCS did not improve a complex whole body dynamic balance performance in young and healthy subjects
Hendy and Kidgell (2013)	30 YA	a-tDCS + strength training	s-tDCS+ strength training No intervention	9 session 20 min 2 mA	M1	During	Maximal voluntary Strength Muscle thickness	Before, immediately, after the interventions	Maximal voluntary strength increased in both the tDCS and sham groups. There was no difference in strength gain between the two groups and no change in muscle thickness
Williams et al. (2010)	20 YA	a-tDCS + motor training	s-tDCS + motor training	1 session 40 min 1 mA	M1	During	Hand function test	Before, immediately and 2 h after the interventions	There was a larger increase in motor performance for the a-tDCS group compared with the s-tDCS group

YA, young adult; OA, old adult; CAI, chronic ankle instability; LBP, low back pain; tDCS, transcranial direct current stimulation; a-tDCS, anodal tDCS; c-tDCS, cathodal tDCS; s-tDCS, sham tDCS; M1, Primary motor cortex, BBS, Berg Balance Scale; VAS, Visual Analog Scale; CoP, Center of pressure.

TABLE 3 | The effects of tDCS combined with physical training on motor learning.

References	Sample size	Intervention	Control	Protocol	tDCS site	Combine way	Outcome measure	Time of assessment	Results
Chen et al. (2020)	100 YA	a-tDCS + motor sequence task	s-tDCS + motor sequence task	1 session 15 min 1.5 mA	M1	Stimulation after motor training	RT	Before, during, 15 and 120 min after intervention	No significant interaction between anodal and sham conditions in motor sequencing task
Tseng et al. (2020)	20 YA	a-tDCS + stepping task	s-tDCS + stepping task	1 session 20 min 2 mA	M1	During	RT Movement time Step accuracy Step termination	Before, during, immediately and 30 min after intervention	A significant decrease in RT at 30 min after the intervention in the a-tDCS group
Rumpf et al. (2017)	47 OA	a-tDCS + motor sequence task	s-tDCS+ motor sequence task	1 session 15 min 1 mA	M1	Stimulation after motor training	Speed Error Performance index, PI	Before, immediately, 8 and 24 h after intervention	A-tDCS led to performance improvements at 8 h after the intervention and were maintained on the next day
Naros et al. (2016)	50 YA	Bilateral stimulation + motor task	a-tDCS + motor task s-tDCS + motor task	1 session 20 min 1 mA	M1	During	Motor performance	Before, immediately after the intervention	Only the bilateral paradigms led to an improvement of the final motor performance at the end of the training period as compared to the sham condition
Looi et al. (2016)	30 YA	a-tDCS + adaptive video game	s-tDCS + adaptive video game	1 session 30 min 2 mA	DLPFC	During	RT Accuracy	Before, during, immediately and two months after the intervention	Participants who received a-tDCS performed significantly better in the RT than the sham group and all effects associated with a-tDCS remained 2 months after-intervention
Fujimoto et al. (2014)	9 YA	Dual-Hemisphere tDCS + grating orientation task	Uni-Hemisphere tDCS + grating orientation task s-tDCS + grating orientation task	1 session 20 min 2 mA	S1	During	Percentage of the correct response	Before, immediately and 30 min after intervention	The percentage of correct responses on the task during dual-hemisphere tDCS was significantly higher than that in the uni-hemisphere or sham tDCS conditions
Reis et al. (2013)	109 YA	a-tDCS + visual isometric pinch force skill task	s-tDCS + visual isometric pinch force skill task	3 session 20 min 1 mA	M1	During	Motor skill measure	Before, 15 min, 3 and 6 h after intervention	Compared with the s-tDCS group, the a-tDCS group showed a significant skill improvement at 3 and 6 h after the intervention
Goodwill et al. (2013)	11 OA	Bilateral tDCS + visuomotor tracking	Unilateral tDCS + visuomotor tracking s-tDCS + visuomotor tracking	1 session 15 min 1 mA	M1	During	Tracking error	Before, immediately and 30 min after intervention	Unilateral and bilateral tDCS decreased tracking error by 12–22% at both time points and were significantly lower than the s-tDCS group

(Continued)

TABLE 3 | Continued

References	Sample size	Intervention	Control	Protocol	tDCS site	Combine way	Outcome measure	Time of assessment	Results
Karok and Witney (2013)	22 YA	Bilateral tDCS + motor sequence task	Unilateral tDCS + motor sequence task s-tDCS + motor sequence task	1 session 10 min 1.5 mA	M1	During	RT Mean accuracy	Before, during, immediately and 15 min after intervention	Task-concurrent stimulation with a dual M1 montage significantly reduced RTs by 23% as early as with the onset of stimulation with this effect increased to 30% at the final measurement
Stagg et al. (2011)	22 YA	a-tDCS + reaction time task	a-tDCS c-tDCS s-tDCS	1 session 10 min 1 mA	M1	During	RT	Before, immediately after the intervention	Mean RT showed a significant decrease after a-tDCS
Kang and Paik (2011)	11 YA	Bilateral tDCS + motor sequence task	Unilateral tDCS + motor sequence task s-tDCS + motor sequence task	1 session 20 min 2 mA	M1	During	RT Motor sequence task performance	Before, immediately and 24 h after intervention	Mean RT showed a significant decrease after uni-tDCS and bi-tDCS
Reis et al. (2009)	24 YA	a-tDCS + sequential visual isometric pinch task	s-tDCS + sequential visual isometric pinch task	5 session 20 min 1 mA	M1	During	Error rate Skill measure	Before, during, immediately, 8, 15, 29, 57, and 85 days after the intervention	There was greater total (online plus offline) skill acquisition with anodal tDCS compared to sham
Vines et al. (2008)	16 YA	Bilateral tDCS + motor sequence task	Unilateral tDCS + motor sequence task s-tDCS + motor sequence task	1 session 20 min 1 mA	M1	During	Percentage of change in performance Scores	Before, immediately after the intervention	Dual-hemisphere stimulation improved performance significantly more than both uni-hemisphere and sham stimulation.

YA, young adult; OA, old adult; a-tDCS, tDCS, transcranial direct current stimulation; anodal tDCS; c-tDCS, cathodal tDCS; s-tDCS, sham tDCS; M1, Primary motor cortex; S1, somatosensory cortex; DLPFC, dorsolateral prefrontal cortex; RT, reaction time.

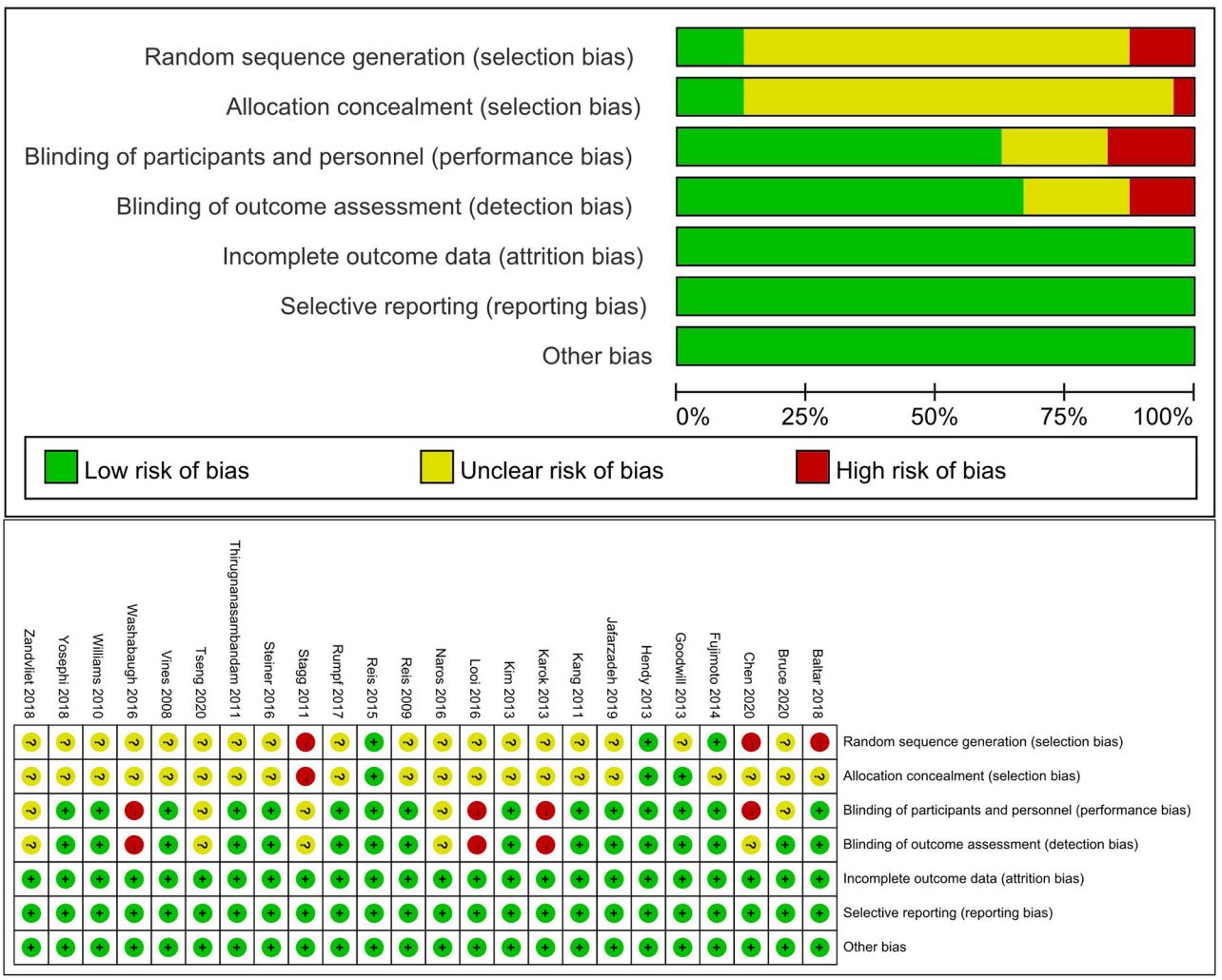

FIGURE 2 | Risk of bias assessment.

Different timing of applying tDCS was used. Two studies applied tDCS before physical training (Thirugnanasambandam et al., 2011; Baltar et al., 2018), and two studies conducted tDCS after physical training (Rumpf et al., 2017; Chen et al., 2020); The other 20 studies applied tDCS during the physical training (Vines et al., 2008; Reis et al., 2009, 2013; Williams et al., 2010; Kang and Paik, 2011; Stagg et al., 2011; Goodwill et al., 2013; Hendy and Kidgell, 2013; Karok and Witney, 2013; Kim and Ko, 2013; Fujimoto et al., 2014; Looi et al., 2016; Naros et al., 2016; Steiner et al., 2016; Washabaugh et al., 2016; Yosephi et al., 2018; Zandvliet et al., 2018; Jafarzadeh et al., 2019; Bruce et al., 2020; Tseng et al., 2020).

Eighteen studies examined the acute effects of one session of intervention (Reis et al., 2009; Williams et al., 2010; Kang and Paik, 2011; Stagg et al., 2011; Thirugnanasambandam et al., 2011; Goodwill et al., 2013; Karok and Witney, 2013; Kim and Ko, 2013; Fujimoto et al., 2014; Looi et al., 2016; Naros et al., 2016; Steiner et al., 2016; Washabaugh et al., 2016; Rumpf et al., 2017; Baltar et al., 2018; Zandvliet et al., 2018; Chen et al., 2020; Tseng et al., 2020); six studies examined the longer-term effects of multiple-session intervention, including three (Reis et al., 2013), five (Reis et al., 2009), six (Yosephi et al., 2018; Jafarzadeh et al., 2019), nine (Hendy and Kidgell, 2013), and 10 sessions of intervention (Bruce et al., 2020). Most studies observed no side effects associated with the intervention (Vines et al., 2008; Williams et al., 2010; Kang and Paik, 2011; Stagg et al., 2011; Thirugnanasambandam et al., 2011; Goodwill et al., 2013; Hendy and Kidgell, 2013; Karok and Witney, 2013; Kim and Ko, 2013; Fujimoto et al., 2014; Looi et al., 2016; Naros et al., 2016; Steiner et al., 2016; Washabaugh et al., 2016; Rumpf et al., 2017; Baltar et al., 2018; Yosephi et al., 2018; Zandvliet et al., 2018; Jafarzadeh et al., 2019; Bruce et al., 2020; Chen et al., 2020; Tseng et al., 2020), whereas two studies reported mild discomfort, which was described as a tingling sensation (Reis et al., 2009, 2013).

Effects of tDCS Combined With Physical Training on Cortical Excitability

Four out of eight studies observed the increase of MEP after one-session tDCS combined with physical training (including shaping tasks, visuomotor tracking, motor sequence task, and grip exercise) (Williams et al., 2010; Goodwill et al., 2013; Karok and Witney, 2013; Kim and Ko, 2013). Another two studies showed no significant improvements in MEP after a-tDCS combined with physical training (including voluntary muscle contraction and running) as compared to the control (Thirugnanasambandam et al., 2011; Baltar et al., 2018). Additionally, the other two studies observed the improved effects of multiple sessions of tDCS combined with physical training (including eccentric ankle strength training and wrist extensors strength training) on MEP (Hendy and Kidgell, 2013; Bruce et al., 2020). Moreover, Bruce et al. (2020) reported that such increase of MEP can last for 2 weeks (**Table 1**).

Effects of tDCS Combined With Physical Training on Physical Performance

Three out of eight studies reported beneficial effects of tDCS combined with physical training on postural control, that is, the decrease of DPSI (Yosephi et al., 2018; Jafarzadeh et al., 2019; Bruce et al., 2020). Another two studies that assessed postural control reported no significant difference between anodal and s-tDCS at post-test (Steiner et al., 2016; Zandvliet et al., 2018). One study observed the improvement in shaping task performance at post-test (Williams et al., 2010). One study reported significantly increased knee extension moment (Washabaugh et al., 2016), and another study reported no significant difference in dynamic 1RM strength between anodal and s-tDCS at post-test (Hendy and Kidgell, 2013) (**Table 2**).

Effects of tDCS Combined With Physical Training on Motor Learning

Twelve out of 13 studies observed that one session of tDCS combined with physical training improved the motor learning performance, as assessed by decreased reaction time (Stagg et al., 2011; Karok and Witney, 2013; Looi et al., 2016; Tseng et al., 2020) and error rate (Goodwill et al., 2013; Fujimoto et al., 2014), increased keystroke rate (Vines et al., 2008), and improved task performance (Reis et al., 2009, 2013; Kang and Paik, 2011; Naros et al., 2016; Rumpf et al., 2017). The other study that assessed reaction time on a motor sequence task reported no significant difference in the a-tDCS group as compared to the sham group (Chen et al., 2020).

DISCUSSION

To the best of our knowledge, this systematic review is the first to assess the effects of tDCS combined with physical training on the excitability of M1, physical performance, and motor learning performance. Our results showed that tDCS combined with physical training can induce significant increase in MEP (75%, 6 out of the 8 included studies), improvement in physical performance (62.5%, 5 of the 8 included studies), and motor learning (92.3%, 12 of the 13 included studies).

Cortical Excitability

Studies have shown tDCS itself holds great promise to improve functional performance and help in rehabilitative medicine field *via* the facilitation and modulation of cortical excitability and plasticity (Santos Ferreira et al., 2019). However, large inter-personal variability in the effects of tDCS is observed due to the variance in the protocol of using tDCS, including the electrode position, dose (current intensity and duration), and differences in the brain structure across people (e.g., skull thickness, subcutaneous fat levels, cerebrospinal fluid density, cortical surface topography, age, gender, and genetics) (Wiethoff et al., 2014). Fritsch et al. (2010) reported tDCS combined additional synaptic activation (e.g., physical training) may lead to synapse specificity as a source for changes in synaptic strength, which provides an evidence for the cellular and molecular mechanisms of tDCS combined additional synaptic activation. Therefore, researchers are expected to produce more stable and effective effects to improve cortical excitability by combining tDCS (exogenous neuromodulation) with physical training (endogenous neuronal activation) (Bliss and Cooke, 2011). Six out of the eight included studies reported that a-tDCS combined with physical training induces a greater extent in the increase of cortical excitability as compared to control (i.e., sham plus physical training). This augmentation of mix-type intervention may arise from the increased synaptic strength *via* modulating the activity of N-methyl-D-aspartic acid and γ-aminobutyric acid receptors (Samii et al., 1996; Liebetanz et al., 2002; Nitsche et al., 2012). Previous studies have also shown that compared to using physical training only, tDCS combined with physical training can induce a greater increase in synaptic strength in human (Samii et al., 1996; Bliss and Cooke, 2011). Additionally, a functional magnetic resonance imaging (*f*MRI) study that conducted a-tDCS combined with hand movements found that a-tDCS application during motor tasks enhances voxel counts, peak intensity, and cortical activation on the targeted motor cortex compared with the same motor task only without using tDCS (Kwon and Jang, 2011). Taken together, a-tDCS combined with physical training may augment the increase of cortical excitability as compared to using one type of intervention only. There is evidence that the temporary modifications in cortical function correspond with transient effects in motor behaviors (Hendy and Kidgell, 2013). Meanwhile, Fregni et al. (2006) reported a significant correlation between motor function improvement after M1 a-tDCS and MEP increase.

It should be noted that 2 out of the 8 studies observed non-significant effects of intervention on cortical excitability. This may be due to two potential reasons, that is the timing of the administration of tDCS and the intensity of the physical training. These two studies administrated tDCS before physical training (Thirugnanasambandam et al., 2011; Baltar et al., 2018). Remarkably, the two studies reported similar results: physical training reduces the enhancement effect of a-tDCS on motor cortical excitability or even decreases the cortical excitability. This phenomenon may be related to the timing of tDCS

administration. Homeostatic plasticity describes the fact that neuroplastic excitability diminutions are more easily achieved in highly active cortical networks but are more difficult to achieve in networks with low-level activity (Thirugnanasambandam et al., 2011). The application of a-tDCS enhances the level of motor cortical excitability, and the subsequent physical training may induce the depotentiation phenomenon. These specific mechanisms of depotentiation have been proven in animal experiments (Kumar et al., 2007). Regarding to the intensity of the physical training, Baltar et al. (2018) reported that high-intensity physical activity (e.g., running with a heart rate at 77–95% of the maximum) may cause fatigue and decrease cortical excitability, while moderate-intensity physical activity (e.g., running with a heart rate at 64–76% of the maximum) increases cortical excitability. This is also consistent with previous study showing that the task characteristics play a major role in determining the resulting plasticity (Bolognini et al., 2009). Therefore, the negative results of Baltar et al. (2018) and Thirugnanasambandam et al. (2011) may relate to the timing of tDCS administration and the characteristics of training protocols.

Physical Performance

Five of the eight included studies reported that a-tDCS combined with physical training improved physical performance more than the s-tDCS combined with physical training. Although the other three studies did not report that a-tDCS combined with physical training was superior to s-tDCS combined with physical training, it still showed certain positive effects. For example, Hendy and Kidgell (2013) observed that a-tDCS combined with physical training induced 14.89% increase in wrist strength. Findings from Yosephi et al. (2018) and Jafarzadeh et al. (2019) also indicated a higher effect of a-tDCS combined with physical training compared with the application of physical training alone. In the cognitive domain, a combination of tDCS and aerobic training could act synergistically to improve cognitive performance beyond the level known for each technique alone (Steinberg et al., 2018). Therefore, the combination of tDCS and physical training may play a synergistic role in improving physical performance. The reason for the improvement in physical performance may be caused by cortical excitability. Although many studies have proven that tDCS combined with physical training can increase cortical excitability and improve physical performance, none has explored the correlation between cortical excitability and physical performance. Future research should conduct a correlation analysis between cortical excitability and physical performance to clarify the relationship.

Although several studies (Hendy and Kidgell, 2013; Steiner et al., 2016; Zandvliet et al., 2018) found that a-tDCS combined with physical training could significantly improve physical performance, no significant differences in strength of wrist extensors and dynamic balance task performance were observed in comparison with s-tDCS combined with physical training. Healthy participants performed well and may experience a pronounced "ceiling effect." These individuals reached their maximum potentials after the training, leaving less room for the desired improvement in physical performance by a-tDCS combined with physical training (Chen et al., 2020). Yosephi et al. (2018) and Steiner et al. (2016) also reflected this problem. The DPSI of healthy elderly people decreased after the combination training, whereas similar results of the balance time of healthy young people were obtained for anodal and s-tDCS after the intervention (Steiner et al., 2016; Yosephi et al., 2018). This result indicates that the effect of a-tDCS combined with physical training may be disrupted by the "ceiling effect."

Motor Learning

The acquisition and consolidation of motor skills are crucial for sports or clinical areas; therefore, strategies to improve motor skill learning are important (Reis et al., 2013). In the past decade, tDCS has been frequently used to promote motor skill learning as a neuroregulatory approach. a-tDCS can promote motor skill acquisition (Vines et al., 2008; Reis et al., 2009, 2013; Kang and Paik, 2011; Stagg et al., 2011; Goodwill et al., 2013; Karok and Witney, 2013; Fujimoto et al., 2014; Looi et al., 2016; Needle et al., 2017) and improve translation into stable performance for days (Reis et al., 2009, 2013; Kang and Paik, 2011; Goodwill et al., 2013; Karok and Witney, 2013; Looi et al., 2016; Rumpf et al., 2017; Tseng et al., 2020).

tDCS may influence motor learning behavior by regulating excitability and synaptic plasticity in interest regions (Goodwill et al., 2013). A study on the motor learning network showed that converging activations are revealed in the dorsal premotor cortex, supplementary motor cortex, primary motor cortex, primary somatosensory cortex, superior parietal lobule, thalamus, putamen, and cerebellum during the movement learning process (Hardwick et al., 2013). A previous study on combining tDCS and *f*MRI showed that a-tDCS over M1 during motor skill learning leads to regional cerebral blood increase in M1 and other brain regions (e.g., the caudal portion of the anterior cingulate cortex, right parieto-occipital junction) (Lang et al., 2005). Furthermore, previous studies have reported that the functional connectivity within the motor network increases (Amadi et al., 2014), and the interhemispheric inhibition is reduced (Goodwill et al., 2013) after a-tDCS over M1. Therefore, the combination of a-tDCS with physical training promotes the acquisition and consolidation of motor skills by modulating the excitability of M1, as well as the regions that are related to the motor learning.

Limitations

Firstly, it is still challenging to determine the optimal montage of tDCS (e.g., duration, number of sessions, appropriate cortical targets) and the optimal design of the mixed-type intervention (e.g., the most appropriate type of the physical training program) for increasing cortical excitability, improving physical performance, and augmenting motor learning due to the large variance of study protocols in current publications. Second, this review focuses on the effects of the intervention on healthy cohorts, without limiting other demographic

factors (i.e., young vs. old adults), which may potentially contribute to the variance of tDCS-induced effects. Lastly, some factors limited our ability to draw more accurate conclusions about the synergistic effects of tDCS combined with physical training; for example, only a few studies assessed the effects on single-joint or multi-joint strength and endurance.

CONCLUSION

This systematic review shows that compared with s-tDCS combined with physical training, a-tDCS combined with physical training has a greater effect on the excitability of the motor cortex, physical performance, and motor learning, including increased MEP, improved dynamic balance performance, and decreased reaction time. tDCS combined with physical training may promote benefits to a great extent on synaptic intensity and brain functional connectivity beyond the level known for each technique alone. However, further studies are needed to explore the most potentially effective physical training protocol and the differences among populations at different physiological levels.

DATA AVAILABILITY STATEMENT

The original contributions presented in the study are included in the article/supplementary material, further inquiries can be directed to the corresponding author/s.

AUTHOR CONTRIBUTIONS

BW, WF, and JZ contributed to conception and design of the study. BW organized the database and wrote the first draft of the manuscript. All authors contributed to manuscript revision, read, and approved the submitted version.

FUNDING

This research was funded by the National Key Technology Research and Development Program of the Ministry of Science and Technology of China (2019YFF0302100 and 2018YFF0300500), the National Natural Science Foundation of China (11772201 and 119320131), Talent Development Fund of Shanghai Municipal (2018107), and the Dawn Program of Shanghai Education Commission, China (19SG47).

REFERENCES

Amadi, U., Ilie, A., Johansen-Berg, H., and Stagg, C. J. (2014). Polarity-specific effects of motor transcranial direct current stimulation on fMRI resting state networks. *Neuroimage* 88, 155–161. doi: 10.1016/j.neuroimage.2013.11.037

Baltar, A., Nogueira, F., Marques, D., Carneiro, M., and Monte-Silva, K. (2018). Evidence of the homeostatic regulation with the combination of transcranial direct current stimulation and physical activity. *Am. J. Phys. Med. Rehabil.* 97, 727–733. doi: 10.1097/PHM.0000000000000956

Bastani, A., and Jaberzadeh, S. (2012). Does anodal transcranial direct current stimulation enhance excitability of the motor cortex and motor function in healthy individuals and subjects with stroke: a systematic review and meta-analysis. *Clin. Neurophysiol.* 123, 644–657. doi: 10.1016/j.clinph.2011.08.029

Beretta, V. S., Conceição, N. R., Nóbrega-Sousa, P., Orcioli-Silva, D., Dantas, L., Gobbi, L. T. B., et al. (2020). Transcranial direct current stimulation combined with physical or cognitive training in people with Parkinson's disease: a systematic review. *J. Neuroeng. Rehabil.* 17:74. doi: 10.1186/s12984-020-00701-6

Bliss, T. V., and Cooke, S. F. (2011). Long-term potentiation and long-term depression: a clinical perspective. *Clinics* 66 (Suppl 1), 3–17. doi: 10.1590/S1807-59322011001300002

Bolognini, N., Pascual-Leone, A., and Fregni, F. (2009). Using non-invasive brain stimulation to augment motor training-induced plasticity. *J. Neuroeng. Rehabil.* 6:8. doi: 10.1186/1743-0003-6-8

Broeder, S., Nackaerts, E., Heremans, E., Vervoort, G., Meesen, R., Verheyden, G., et al. (2015). Transcranial direct current stimulation in Parkinson's disease: neurophysiological mechanisms and behavioral effects. *Neurosci. Biobehav. Rev.* 57, 105–117. doi: 10.1016/j.neubiorev.2015.08.010

Bruce, A. S., Howard, J. S., H, V.A. N. W., McBride, J. M., and Needle, A. R. (2020). The effects of transcranial direct current stimulation on chronic ankle instability. *Med. Sci. Sports Exerc.* 52, 335–344. doi: 10.1249/MSS.0000000000002129

Cerqueira, M. S., Do Nascimento, J. D. S., Maciel, D. G., Barboza, J. A. M., and De Brito Vieira, W. H. (2020). Effects of blood flow restriction without additional exercise on strength reductions and muscular atrophy following immobilization: a systematic review. *J. Sport Health Sci.* 9, 152–159. doi: 10.1016/j.jshs.2019.07.001

Chang, W. J., Bennell, K. L., Hodges, P. W., Hinman, R. S., Young, C. L., Buscemi, V., et al. (2017). Addition of transcranial direct current stimulation to quadriceps strengthening exercise in knee osteoarthritis: a pilot randomised controlled trial. *PLoS ONE* 12:e0180328. doi: 10.1371/journal.pone.0180328

Chen, J., McCulloch, A., Kim, H., Kim, T., Rhee, J., Verwey, W. B., et al. (2020). Application of anodal tDCS at primary motor cortex immediately after practice of a motor sequence does not improve offline gain. *Exp. Brain Res.* 238, 29–37. doi: 10.1007/s00221-019-05697-7

Fregni, F., Boggio, P. S., Santos, M. C., Lima, M., Vieira, A. L., Rigonatti, S. P., et al. (2006). Noninvasive cortical stimulation with transcranial direct current stimulation in Parkinson's disease. *Mov. Disord.* 21, 1693–1702. doi: 10.1002/mds.21012

Fritsch, B., Reis, J., Martinowich, K., Schambra, H. M., Ji, Y., Cohen, L. G., et al. (2010). Direct current stimulation promotes BDNF-dependent synaptic plasticity: potential implications for motor learning. *Neuron* 66, 198–204. doi: 10.1016/j.neuron.2010.03.035

Fujimoto, S., Yamaguchi, T., Otaka, Y., Kondo, K., and Tanaka, S. (2014). Dual-hemisphere transcranial direct current stimulation improves performance in a tactile spatial discrimination task. *Clin. Neurophysiol.* 125, 1669–1674. doi: 10.1016/j.clinph.2013.12.100

Goodwill, A. M., Reynolds, J., Daly, R. M., and Kidgell, D. J. (2013). Formation of cortical plasticity in older adults following tDCS and motor training. *Front. Aging Neurosci.* 5:87. doi: 10.3389/fnagi.2013.00087

Hardwick, R. M., Rottschy, C., Miall, R. C., and Eickhoff, S. B. (2013). A quantitative meta-analysis and review of motor learning in the human brain. *Neuroimage* 67, 283–297. doi: 10.1016/j.neuroimage.2012.11.020

Hendy, A. M., and Kidgell, D. J. (2013). Anodal tDCS applied during strength training enhances motor cortical plasticity. *Med. Sci. Sports Exerc.* 45, 1721–1729. doi: 10.1249/MSS.0b013e31828d2923

Jafarzadeh, A., Ehsani, F., Yosephi, M. H., Zoghi, M., and Jaberzadeh, S. (2019). Concurrent postural training and M1 anodal transcranial direct current stimulation improve postural impairment in patients with chronic low back pain. *J. Clin. Neurosci.* 68, 224–234. doi: 10.1016/j.jocn.2019.07.017

Kang, E. K., and Paik, N. J. (2011). Effect of a tDCS electrode montage on implicit motor sequence learning in healthy subjects. *Exp. Transl. Stroke Med.* 3:4. doi: 10.1186/2040-7378-3-4

Karok, S., and Witney, A. G. (2013). Enhanced motor learning following task-concurrent dual transcranial direct current stimulation. *PLoS ONE* 8:e85693. doi: 10.1371/journal.pone.0085693

Kidgell, D. J., Stokes, M. A., Castricum, T. J., and Pearce, A. J. (2010). Neurophysiological responses after short-term strength training of the biceps brachii muscle. *J. Strength Cond. Res.* 24, 3123–3132. doi: 10.1519/JSC.0b013e3181f56794

Kim, G. W., and Ko, M. H. (2013). Facilitation of corticospinal tract excitability by transcranial direct current stimulation combined with voluntary grip exercise. *Neurosci. Lett.* 548, 181–184. doi: 10.1016/j.neulet.2013.05.037

Kumar, A., Thinschmidt, J. S., Foster, T. C., and King, M. A. (2007). Aging effects on the limits and stability of long-term synaptic potentiation and depression in rat hippocampal area CA1. *J. Neurophysiol.* 98, 594–601. doi: 10.1152/jn.00249.2007

Kwon, Y. H., and Jang, S. H. (2011). The enhanced cortical activation induced by transcranial direct current stimulation during hand movements. *Neurosci. Lett.* 492, 105–108. doi: 10.1016/j.neulet.2011.01.066

Lang, N., Siebner, H. R., Ward, N. S., Lee, L., Nitsche, M. A., Paulus, W., et al. (2005). How does transcranial DC stimulation of the primary motor cortex alter regional neuronal activity in the human brain? *Eur. J. Neurosci.* 22, 495–504. doi: 10.1111/j.1460-9568.2005.04233.x

Liebetanz, D., Nitsche, M. A., Tergau, F., and Paulus, W. (2002). Pharmacological approach to the mechanisms of transcranial DC-stimulation-induced after-effects of human motor cortex excitability. *Brain* 125 (Pt. 10), 2238–2247. doi: 10.1093/brain/awf238

Looi, C. Y., Duta, M., Brem, A. K., Huber, S., Nuerk, H. C., and Cohen Kadosh, R. (2016). Combining brain stimulation and video game to promote long-term transfer of learning and cognitive enhancement. *Sci. Rep.* 6:22003. doi: 10.1038/srep22003

Machado, D., Unal, G., Andrade, S. M., Moreira, A., Altimari, L. R., Brunoni, A. R., et al. (2019). Effect of transcranial direct current stimulation on exercise performance: a systematic review and meta-analysis. *Brain Stimul.* 12, 593–605. doi: 10.1016/j.brs.2018.12.227

Mazzoleni, S., Tran, V. D., Dario, P., and Posteraro, F. (2019). Effects of transcranial direct current stimulation (tDCS) combined with wrist robot-assisted rehabilitation on motor recovery in subacute stroke patients: a randomized controlled trial. *IEEE Trans. Neural Syst. Rehabil. Eng.* 27, 1458–1466. doi: 10.1109/TNSRE.2019.2920576

Naros, G., Geyer, M., Koch, S., Mayr, L., Ellinger, T., Grimm, F., et al. (2016). Enhanced motor learning with bilateral transcranial direct current stimulation: impact of polarity or current flow direction? *Clin. Neurophysiol.* 127, 2119–2126. doi: 10.1016/j.clinph.2015.12.020

Needle, A. R., Lepley, A. S., and Grooms, D. R. (2017). Central nervous system adaptation after ligamentous injury: a summary of theories, evidence, and clinical interpretation. *Sports Med.* 47, 1271–1288. doi: 10.1007/s40279-016-0666-y

Nitsche, M. A., Müller-Dahlhaus, F., Paulus, W., and Ziemann, U. (2012). The pharmacology of neuroplasticity induced by non-invasive brain stimulation: building models for the clinical use of CNS active drugs. *J. Physiol.* 590, 4641–4662. doi: 10.1113/jphysiol.2012.232975

Nitsche, M. A., and Paulus, W. (2000). Excitability changes induced in the human motor cortex by weak transcranial direct current stimulation. *J. Physiol.* 527, 633–639. doi: 10.1111/j.1469-7793.2000.t01-1-00633.x

Nitsche, M. A., and Paulus, W. (2001). Sustained excitability elevations induced by transcranial DC motor cortex stimulation in humans. *Neurology* 57, 1899–1901. doi: 10.1212/WNL.57.10.1899

Reis, J., Fischer, J. T., Prichard, G., Weiller, C., Cohen, L. G., and Fritsch, B. (2013). Time- but not sleep-dependent consolidation of tDCS-enhanced visuomotor skills. *Cereb. Cortex* 25, 109–117. doi: 10.1093/cercor/bht208

Reis, J., Schambra, H. M., Cohen, L. G., Buch, E. R., Fritsch, B., Zarahn, E., et al. (2009). Noninvasive cortical stimulation enhances motor skill acquisition over multiple days through an effect on consolidation. *Proc. Natl. Acad. Sci. U.S.A.* 106, 1590–1595. doi: 10.1073/pnas.0805413106

Rumpf, J. J., Wegscheider, M., Hinselmann, K., Fricke, C., King, B. R., Weise, D., et al. (2017). Enhancement of motor consolidation by post-training transcranial direct current stimulation in older people. *Neurobiol. Aging* 49, 1–8. doi: 10.1016/j.neurobiolaging.2016.09.003

Samii, A., Wassermann, E. M., Ikoma, K., Mercuri, B., and Hallett, M. (1996). Characterization of postexercise facilitation and depression of motor evoked potentials to transcranial magnetic stimulation. *Neurology* 46, 1376–1382. doi: 10.1212/WNL.46.5.1376

Santos Ferreira, I., Teixeira Costa, B., Lima Ramos, C., Lucena, P., Thibaut, A., and Fregni, F. (2019). Searching for the optimal tDCS target for motor rehabilitation. *J. Neuroeng. Rehabil.* 16:90. doi: 10.1186/s12984-019-0561-5

Stagg, C. J., Jayaram, G., Pastor, D., Kincses, Z. T., Matthews, P. M., and Johansen-Berg, H. (2011). Polarity and timing-dependent effects of transcranial direct current stimulation in explicit motor learning. *Neuropsychologia* 49, 800–804. doi: 10.1016/j.neuropsychologia.2011.02.009

Steinberg, F., Pixa, N. H., and Fregni, F. (2018). A review of acute aerobic exercise and transcranial direct current stimulation effects on cognitive functions and their potential synergies. *Front. Hum. Neurosci.* 12, 534. doi: 10.3389/fnhum.2018.00534

Steiner, K. M., Enders, A., Thier, W., Batsikadze, G., Ludolph, N., Ilg, W., et al. (2016). Cerebellar tDCS does not improve learning in a complex whole body dynamic balance task in young healthy subjects. *PLoS ONE* 11:e0163598. doi: 10.1371/journal.pone.0163598

Tanaka, S., Hanakawa, T., Honda, M., and Watanabe, K. (2009). Enhancement of pinch force in the lower leg by anodal transcranial direct current stimulation. *Exp. Brain Res.* 196, 459–465. doi: 10.1007/s00221-009-1863-9

Thirugnanasambandam, N., Sparing, R., Dafotakis, M., Meister, I. G., Paulus, W., Nitsche, M. A., et al. (2011). Isometric contraction interferes with transcranial direct current stimulation (tDCS) induced plasticity: evidence of state-dependent neuromodulation in human motor cortex. *Restor. Neurol. Neurosci.* 29, 311–320. doi: 10.3233/RNN-2011-0601

Tseng, S. C., Chang, S. H., Hoerth, K. M., Nguyen, A. A., and Perales, D. (2020). Anodal transcranial direct current stimulation enhances retention of visuomotor stepping skills in healthy adults. *Front. Hum. Neurosci.* 14:251. doi: 10.3389/fnhum.2020.00251

Vines, B. W., Cerruti, C., and Schlaug, G. (2008). Dual-hemisphere tDCS facilitates greater improvements for healthy subjects' non-dominant hand compared to uni-hemisphere stimulation. *BMC Neurosci.* 9:103. doi: 10.1186/1471-2202-9-103

Washabaugh, E. P., Santos, L., Claflin, E. S., and Krishnan, C. (2016). Low-level intermittent quadriceps activity during transcranial direct current stimulation facilitates knee extensor force-generating capacity. *Neuroscience* 329, 93–97. doi: 10.1016/j.neuroscience.2016.04.037

Wiethoff, S., Hamada, M., and Rothwell, J. C. (2014). Variability in response to transcranial direct current stimulation of the motor cortex. *Brain Stimul* 7, 468–475. doi: 10.1016/j.brs.2014.02.003

Williams, J. A., Pascual-Leone, A., and Fregni, F. (2010). Interhemispheric modulation induced by cortical stimulation and motor training. *Phys. Ther.* 90, 398–410. doi: 10.2522/ptj.20090075

Xiao, S., Wang, B., Zhang, X., Zhou, J., and Fu, W. (2020). Acute effects of high-definition transcranial direct current stimulation on foot muscle strength, passive ankle kinesthesia, and static balance: a pilot study. *Brain Sci.* 10:246. doi: 10.3390/brainsci10040246

Yosephi, M. H., Ehsani, F., Zoghi, M., and Jaberzadeh, S. (2018). Multi-session anodal tDCS enhances the effects of postural training on balance and postural stability in older adults with high fall risk: primary motor cortex versus cerebellar stimulation. *Brain Stimul.* 11, 1239–1250. doi: 10.1016/j.brs.2018.07.044

Zandvliet, S. B., Meskers, C. G. M., Kwakkel, G., and van Wegen, E. E. H. (2018). Short-Term effects of cerebellar tDCS on standing balance performance in patients with chronic stroke and healthy age-matched elderly. *Cerebellum* 17, 575–589. doi: 10.1007/s12311-018-0939-0

Conflict of Interest: The authors declare that the research was conducted in the absence of any commercial or financial relationships that could be construed as a potential conflict of interest.

frontiers in Neuroscience

ORIGINAL RESEARCH
published: 28 May 2021
doi: 10.3389/fnins.2021.660032

Dynamics of Long-Range Temporal Correlations in Broadband EEG During Different Motor Execution and Imagery Tasks

Maitreyee Wairagkar[1,2,3]*, *Yoshikatsu Hayashi*[1] and *Slawomir J. Nasuto*[1]

[1] Brain Embodiment Laboratory, Biomedical Engineering, School of Biological Sciences, University of Reading, Reading, United Kingdom, [2] Biomechatronics Laboratory, Department of Mechanical Engineering, Imperial College London, London, United Kingdom, [3] Care Research and Technology Centre, The UK Dementia Research Institute (UK DRI), London, United Kingdom

Brain activity is composed of oscillatory and broadband arrhythmic components; however, there is more focus on oscillatory sensorimotor rhythms to study movement, but temporal dynamics of broadband arrhythmic electroencephalography (EEG) remain unexplored. We have previously demonstrated that broadband arrhythmic EEG contains both short- and long-range temporal correlations that change significantly during movement. In this study, we build upon our previous work to gain a deeper understanding of these changes in the long-range temporal correlation (LRTC) in broadband EEG and contrast them with the well-known LRTC in alpha oscillation amplitude typically found in the literature. We investigate and validate changes in LRTCs during five different types of movements and motor imagery tasks using two independent EEG datasets recorded with two different paradigms—our finger tapping dataset with single self-initiated asynchronous finger taps and publicly available EEG dataset containing cued continuous movement and motor imagery of fists and feet. We quantified instantaneous changes in broadband LRTCs by detrended fluctuation analysis on single trial 2 s EEG sliding windows. The broadband LRTC increased significantly ($p < 0.05$) during all motor tasks as compared to the resting state. In contrast, the alpha oscillation LRTC, which had to be computed on longer stitched EEG segments, decreased significantly ($p < 0.05$) consistently with the literature. This suggests the complementarity of underlying fast and slow neuronal scale-free dynamics during movement and motor imagery. The single trial broadband LRTC gave high average binary classification accuracy in the range of $70.54 \pm 10.03\%$ to $76.07 \pm 6.40\%$ for all motor execution and imagery tasks and hence can be used in brain–computer interface (BCI). Thus, we demonstrate generalizability, robustness, and reproducibility of novel motor neural correlate, the single trial broadband LRTC, during different motor execution and imagery tasks in single asynchronous and cued continuous motor-BCI paradigms and its contrasting behavior with LRTC in alpha oscillation amplitude.

Keywords: movement execution, motor imagery, electroencephalography (EEG), long-range temporal correlation (LRTC), broadband EEG, brain-computer interface (BCI), movement classification

OPEN ACCESS

Edited by:
Riccardo Poli,
University of Essex, United Kingdom

Reviewed by:
Aleksandra Dagmara Kawala-Sterniuk,
Opole University of Technology, Poland
Aritra Kundu,
University of Texas at Austin, United States

***Correspondence:**
Maitreyee Wairagkar
m.wairagkar@reading.ac.uk

Specialty section:
This article was submitted to Neural Technology, a section of the journal Frontiers in Neuroscience

Received: *28 January 2021*
Accepted: *22 March 2021*
Published: *28 May 2021*

Citation:
Wairagkar M, Hayashi Y and Nasuto SJ (2021) Dynamics of Long-Range Temporal Correlations in Broadband EEG During Different Motor Execution and Imagery Tasks. Front. Neurosci. 15:660032. doi: 10.3389/fnins.2021.660032

1. INTRODUCTION

The brain activity is composed of various complex processes that undergo changes during different tasks and brain functions. Spontaneous electroencephalography (EEG) contains rhythmic oscillatory components such as delta, theta, alpha, and beta oscillations in narrow frequency bands, and arrhythmic scale-free broadband component without a characteristic timescale or frequency that leads to a typical $1/f$ EEG spectrum (He, 2014). Additionally, EEG also contains event-related potentials that are one-off non-oscillatory and non-rhythmic responses to sensory, cognitive, or motor events. During voluntary movement, distinct changes occur in all the above three components of EEG. In the rhythmic sensorimotor oscillatory component of EEG, we observe the well-known event-related (de)synchronization (ERD/S), which quantifies increase or decrease, respectively, in band power of narrowband sensorimotor oscillations during a motor task with reference to its baseline (Pfurtscheller and Lopes Da Silva, 1999; Yuan and He, 2014; He et al., 2015). In the event-related potential component of EEG in response to a motor task, we observe non-oscillatory non-rhythmic movement-related cortical potentials (MRCP), which are characterized by an increase in slow negative potentials (Shibasaki and Hallett, 2006; Bai et al., 2011). Changes in the arrhythmic broadband component of EEG during motor task, however, are not investigated in the literature.

Rhythmic narrowband oscillatory processes and arrhythmic broadband processes co-exist in EEG, where rhythmic oscillations appear as distinct peaks (e.g., alpha peak around 10 Hz) on the arrhythmic broadband $1/f$ EEG spectrum (illustrated in Wairagkar et al., 2019). However, there is more focus on studying rhythmic oscillatory components of EEG. The broadband arrhythmic process was previously considered as background noise in brain activity. However, recent reports suggest that the broadband activity has physiological and functional relevance (He, 2014), its dynamics change with task demand and cognitive state, and it has also been associated with the excitation/inhibition balance of the neuronal populations (Chaudhary et al., 2017; Haller et al., 2018). This has rekindled the interest to investigate the broadband EEG during motor tasks. Widely used complementary neural correlates of ERD/S and MRCP do not describe the dynamical changes in the temporal dependencies in the broadband arrhythmic EEG. Hence, we propose that changes in the broadband scale-free arrhythmic component in EEG can reveal yet another complementary neural correlate of voluntary movement (Wairagkar et al., 2019).

We previously studied the temporal dynamics of broadband EEG and found that its autocorrelation decayed slower during movement intention and execution than in the resting state (Wairagkar et al., 2018). We modeled these broadband autocorrelation dynamics on single trial EEG using the autoregressive fractionally integrated moving average (ARFIMA) model, which led to the discovery that broadband EEG contains coexisting short-range and long-range temporal correlations. These short-range and long-range temporal correlations changed significantly during voluntary movement and can be used together as novel neural correlates of movement (Wairagkar et al., 2019). Several studies have approximated short-range correlations using autoregressive models to estimate movement correlates from EEG (Schlögl et al., 2005; D'Croz-Baron et al., 2012; Wang et al., 2018). However, there is limited literature on long-range temporal correlations (LRTC) in broadband EEG (Hou et al., 2017; Lombardi et al., 2020), and there are no other studies investigating long-range temporal dynamics of single trial broadband EEG during motor tasks. Hence, in this study, building upon our previous work, we delve deeper to investigate changes in broadband LRTC during movement and compare it with the well-known alpha oscillation LRTC.

Neural activity has been reported to produce long-range interactions leading to power-law scaling, suggesting that these neuronal processes are similar across different scales (Kello et al., 2010; Berthouze and Farmer, 2012; Heiney et al., 2021). The power-law scaling is observed in several cases of neuronal recordings such as neuronal firings (Hu et al., 2013), neuronal avalanches (Benayoun et al., 2010; Palva et al., 2013), intracranial recordings such as local field potentials (Benayoun et al., 2010), and electrocorticography (Chaudhary et al., 2017), and non-invasive scalp recordings of EEG and magnetoencephalography (Nikulin and Brismar, 2005; Benayoun et al., 2010; Kwok et al., 2019; Jannesari et al., 2020) in both oscillatory and non-oscillatory processes. In the surface-level brain activity such as EEG and magnetoencephalography, the power-law scaling is observed in the form of the $1/f$ power spectrum of non-oscillatory or arrhythmic scale-free neuronal activity. Spontaneous oscillatory neuronal processes also show LRTC in their amplitude envelope fluctuations (Linkenkaer-Hansen et al., 2001; Nikulin and Brismar, 2005; Berthouze et al., 2010; Hardstone et al., 2012). LRTCs are the result of power-law decay of the autocorrelation of neural activity. The LRTCs have been observed in the alpha, beta, theta oscillation amplitude envelopes (Berthouze et al., 2010), alpha oscillation phase (Botcharova et al., 2014), broadband phase synchrony (Kitzbichler et al., 2009), avalanches (Benayoun et al., 2010; Palva et al., 2013), and energy profile (Parish et al., 2004; Benayoun et al., 2010). It is commonly postulated in the literature that the power-law behavior and LRTCs occur because the brain operates at criticality (Poil et al., 2012; Massobrio et al., 2015), thus optimizing information storage capacity (Kitzbichler et al., 2009) and enabling quick adaptation to the cognitive processing demands (Ezaki et al., 2020; Ouyang et al., 2020; Zimmern, 2020). In the absence of long-range temporal correlations, correlations on shorter timescales lead to reduction in the ability to integrate information (for example, during certain stages of sleep; Meisel et al., 2017).

In EEG, LRTCs have been traditionally identified in the amplitude envelope fluctuations of narrow frequency bands corresponding to different brain oscillations (Linkenkaer-Hansen et al., 2001; Nikulin and Brismar, 2005). LRTCs have also been observed in the sensorimotor oscillations (Linkenkaer-Hansen et al., 2004; Botcharova et al., 2015). LRTCs in the alpha amplitude envelope fluctuations decrease due to the disruption caused in the long-memory process by an external stimulus (Linkenkaer-Hansen et al., 2004; Botcharova et al.,

2014; Zhigalov et al., 2016). Neurological conditions also affect LRTCs (Parish et al., 2004; Ros et al., 2014, 2016). The LRTCs can be modulated using neurofeedback where these correlations increase because of the closed-loop stimulus (Ros et al., 2014, 2016; Zhigalov et al., 2016). The scale-free dynamics are also identified in behavioral data (Palva et al., 2013). LRTCs in neuronal activity and movement patterns are correlated (Hu et al., 2004, 2013), and neural scale-free dynamics can predict the performance of motor tasks (Samek et al., 2016). There are very few studies in the literature that consider broadband LRTC such as the ones by Hou et al. (2017) that found attenuation in broadband LRTC during depression and by Lombardi et al. (2020) that characterized LRTC in the resting-state broadband EEG using neuronal avalanches. However, there have been no previous external studies investigating LRTCs in broadband arrhythmic EEG during different motor tasks and their relationship with alpha oscillatory LRTC, which is the focus of this study.

LRTCs are typically characterized in the amplitude envelope fluctuations of oscillations in brain activity. These oscillations are typically extracted using Fourier-based spectral methods. Cole and Voytek (2018) showed that the brain rhythms are non-stationary and not strictly restricted to pre-selected narrow sinusoidal frequency bands; therefore, restricting to a narrowband analysis can disregard important features present in the entire power spectrum. Hence, the LRTCs computed from narrow frequency band amplitude envelope fluctuations may not give complete information present in these brain rhythms, and there is a need for assessing LRTCs in the broadband arrhythmic brain activity as well.

The LRTC in EEG can be characterized by its scaling exponent computed from the spectral domain by estimating the slope of $1/f$ power spectrum on a log-log scale and computed from the temporal domain by fitting the power-law directly to the autocorrelation, both of which are often difficult to achieve in practice (Rangarajan and Ding, 2000; Delignieres et al., 2006). Hence, LRTCs are most preferably characterized in the temporal domain using Hurst exponent, which shows a consistent relationship with scaling exponents from autocorrelation and $1/f$ spectrum for a stationary time series (Rangarajan and Ding, 2000). A Hurst exponent between 0.5 and 1 indicates the presence of LRTC (Hardstone et al., 2012). The detrended fluctuation analysis (DFA) (Peng et al., 1995) is the most common method for estimating Hurst exponent in a non-stationary signal, which is computed from the slope of fluctuations in the signal at different timescales. The power spectrum analysis is not suitable for reliably identifying LRTC in a non-stationary time series (Linkenkaer-Hansen et al., 2001). The DFA is used for estimating Hurst exponent from EEG because it facilitates the detection of LRTC embedded in a non-stationary time series by avoiding artifactual dependencies caused by non-stationarity and trends (Peng et al., 1995; Kantelhardt et al., 2001; Linkenkaer-Hansen et al., 2001; Delignieres et al., 2006; Hardstone et al., 2012).

LRTC is considered an invariant property of brain dynamics spanning several time scales (Delignieres et al., 2006) and hence is not computed as a function of time. LRTC is traditionally estimated on an amplitude envelope of narrowband EEG oscillations, which requires long EEG segments (Linkenkaer-Hansen et al., 2001). With this approach, we cannot observe the ongoing instantaneous changes in LRTC. Detecting short movement from LRTC requires evaluating the changes in the dynamics of the LRTC continuously as a function of time. Berthouze and Farmer (2012) have previously captured the changes in LRTCs using a Kalman filter, but the timescales over which LRTCs were observed were still several seconds long. Here, we investigate the instantaneous changes occurring in the LRTCs using shorter timescales to study the fast brain dynamics during different motor tasks such that it can be applied in brain–computer interface (BCI). Continuous characterization of LRTC on short broadband EEG windows using BCI-style processing pipeline can enable detecting movement on a single-trial basis without the need of choosing participant-specific parameters. Our previous work (Wairagkar et al., 2019) has established the presence of LRTC during finger tap voluntary movement. Consistently, we obtained high classification accuracies to detect finger tap intention using broadband LRTC-related indices. In this study, we expand this investigation to explore the changes in the broadband LRTC in different types of movement and motor imagery with paradigms that are commonly used in BCI. To our knowledge, LRTCs in the broadband have not been observed before during motor imagery. Our analysis will help in understanding the functional role the broadband arrhythmic brain activity plays in motor command generation and motor imagery.

The aims of this paper are (1) to build upon our previous work to investigate further the dynamics of LRTC in single trial broadband EEG during five different types of motor tasks with different experimental paradigms including single asynchronous finger tap, and continuous fist and feet movement and motor imagery from two independent EEG datasets, validate broadband LRTC rigorously and demonstrate its generalizability, robustness, and reproducibility; (2) to compare and contrast the broadband LRTC with LRTC in the alpha oscillation amplitude envelope commonly observed in the literature during corresponding motor tasks to identify contrast in the dynamics of coexisting oscillatory and arrhythmic scale-free processes; (3) to classify movement intention, execution, and motor imagery from resting state by using broadband LRTC independently on a single-trial basis as a novel feature for applications in BCI.

2. METHODS

2.1. EEG Datasets and Participants

The first dataset is our voluntary single finger tap EEG dataset (available from Wairagkar, 2017) that we recorded from 14 healthy participants (8 female, age 26 $\pm$ 4 years, 12 right-handed). Ethical approval for the EEG experiment was obtained from the ethics committee of the University of Reading, UK. Informed written consent was obtained from all participants.

The second dataset is a publicly available EEG Motor Movement/Imagery Dataset (EEGMMI) (Schalk et al., 2004) from PhysioNet (Goldberger et al., 2000). This dataset is used to validate our novel broadband LRTC neural correlate and to

widen its scope by extrapolating its utility for broader use in different types of motor tasks. EEGMMI dataset comprises EEG recorded from 109 participants for four different types of motor tasks: (1) right and left fist continuous opening and closing, (2) motor imagery of right and left fist continuous opening and closing, (3) both feet continuous movement and both fists continuous opening and closing, and (4) motor imagery of both feet continuous movement and both fists continuous opening and closing.

Our EEG dataset has self-initiated asynchronous single finger tap in contrast to the EEGMMI dataset, which has cued continuous fist and feet movement and imagery. Thus, these datasets cover complementary paradigms and motor tasks to assess the robustness and reproducibility of our broadband LRTC neural correlate for broader applications.

2.2. Experimental Paradigm and Pre-processing

Our finger tap EEG dataset was recorded for a self-initiated single asynchronous index finger tapping task. A text instruction was shown on the screen placed 1 m from the participant to perform a right finger tap, left finger tap, or resting state (no tap) within a following 10 s window asynchronously at any random time (see **Figure 1A**). Participants were specifically asked not to react immediately to the instruction to avoid cue effect. The timing of the initiation of the movement was entirely participant's decision. Forty trials per condition were recorded with the sampling frequency of 1,024 Hz and were downsampled to 128 Hz. The exact onset of finger tap was recorded using a microcontroller device and was co-registered with the EEG. Further details of the finger tap dataset are given in Wairagkar (2017).

The EEGMMI dataset recorded four cued motor tasks described in the previous section, including continuous fist and feet movement execution and motor imagery. Each trial started with a resting state of 4 s followed by a cue to perform continuous movement/imagery for 4 s (left/right arrows for respective fists, up arrow for both fists together, and down arrow for both feet together) as shown in **Figure 1B**. A 1 min baseline EEG with eyes open is included in the dataset, which we segmented and used as neutral state trials for further processing. There were around 22 trials for each of the four motor tasks per participant recorded with the sampling frequency of 160 Hz, which were downsampled to 128 Hz.

The same artifacts removal and pre-processing pipeline was used for both datasets. Artifacts were removed with independent component analysis (Jung et al., 2000) using EEGLAB toolbox (Makeig et al., 1997; Delorme and Makeig, 2004) before trial segmentation. EEG was bandpass filtered between 0.5 and 45 Hz using a fourth-order zero-phase non-causal Butterworth filter to avoid phase distortions. We extracted 6 s EEG trials (−3 to +3 s of movement onset) from our finger tap dataset and 7 s EEG trials (−3 to +4 s of motor cue) from the EEGMMI dataset from the channels C3, Cz, and C4 over motor cortex according to the 10–20 international system. These channels were selected for the study because of their locations on sensorimotor area responsible for hand and feet movement and imagery (Resniak et al., 2020). These trials were divided into 2 s sliding Hanning windows shifted by 100 ms. Each feature at time t was causally obtained on a window from $t - 2$ s to t s. All the analysis was done offline in MATLAB (The MathWorks, Inc., Natick, MA, USA).

2.3. Detrended Fluctuation Analysis to Identify LRTC in EEG

We hypothesized that the LRTCs in the broadband EEG change during movement intention and execution. We quantified the broadband LRTC using Hurst exponent computed using DFA (Peng et al., 1995). The DFA analysis calculates root mean square (RMS) fluctuations of integrated and detrended time series at different timescales as follows:

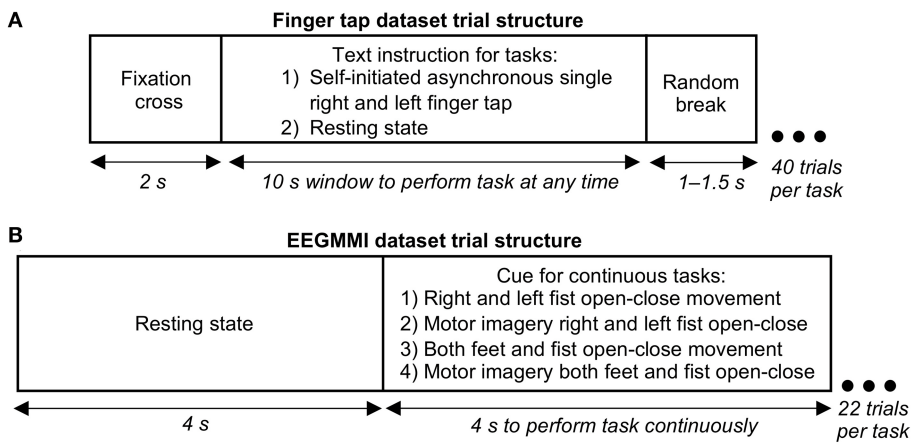

FIGURE 1 | Structure of a single electroencephalography (EEG) trial in our finger tapping dataset and EEG Motor Movement/Imagery Dataset (EEGMMI) dataset. **(A)** Trial structure for single self-initiated asynchronous finger tap. Participants were given a window of 10 s to perform a single tap any time, or if it was a resting state task, they were asked to remain still with eyes open without thinking of movement. **(B)** Trial structure for four cued EEGMMI tasks, including continuous movement or motor imagery for 4 s of single or both fists and both feet.

1. The time series x of length N is integrated according to Equation (1) where $k = 1, ..., N$ and y is the integrated time series.

$$y(k) = \sum_{i=1}^{k} x(i) - \bar{x} \quad (1)$$

2. The integrated time series y is then divided into N/n non-overlapping boxes of length n, where n is individual timescales at which we want to compute fluctuations. The box sizes have an impact on the DFA scaling exponent and are usually chosen between $n = [10, N/4]$ (Delignieres et al., 2006; Botcharova et al., 2013) to get good estimate of RMS fluctuations at each scale with $[N/10, 4]$ number of boxes. We used 25 box sizes between $n = [10, N/4]$ equidistant on log_2 scale as our number of samples was a power of 2.
3. At each scale n, for every non-overlapping segment of y of length n, trend is obtained by least square linear fit. The y_n is concatenation of trends at a scale n for all the N/n boxes and the RMS fluctuations are computed according to Equation (2).

$$F(n) = \sqrt{\frac{1}{N}\sum_{i=1}^{N}(y(i) - y_n(i))^2} \quad (2)$$

4. A log–log plot of fluctuations at each timescale n ($log_2 F(n)$ vs. $log_2 n$) was plotted and DFA scaling exponent was obtained by calculating the slope of the linear fit to this plot.

Since N is not divisible by n for each box size, fluctuations were obtained from performing the above analysis from forward and backward direction (Kantelhardt et al., 2001) of each EEG window and then averaging them at each timescale. When the log–log DFA plot is linear, the DFA scaling exponent or Hurst exponent indicates power-law in fluctuations at different timescales.

2.3.1. LRTC Using DFA in Broadband EEG and Alpha Oscillation Amplitude Fluctuations During Different Motor Tasks

We studied the changes in LRTC in the broadband EEG, and compared and contrasted them with the LRTC in the alpha oscillation amplitude envelope during movement, which is typically assessed in the literature (Linkenkaer-Hansen et al., 2004). We investigated changes in the broadband LRTC and alpha envelope LRTC during different types of motor execution and imagery from the finger tap and EEGMMI datasets using the same analysis pipeline as described in the next sections. For clarity, throughout the paper, we use H_{BB} to indicate DFA scaling exponent or Hurst exponent in the broadband and H_{alpha} to indicate Hurst exponent in the amplitude envelope of the alpha oscillations.

2.4. Broadband LRTC in Single Trials During Different Motor Tasks

We performed DFA on each 2 s sliding broadband (0.5–45 Hz) EEG window shifted by 100 ms to obtain continuous changes in the LRTC (Hurst exponent H_{BB}) throughout the trial during different motor tasks. The Hanning window was applied to each 2 s window to avoid edge effects. Note that 256 samples were available for performing DFA on a 2 s window. Delignieres et al. (2006) have shown that the DFA method can accurately estimate Hurst exponent in short time series. Our range of timescales ($[10, N/4]$ samples, i.e., [78 ms 0.5 s]) is within the range suggested by Li et al. (2018) $[max(k + 2, F_s/F_{max}), min(N/4, F_s/F_{min})]$ where $k = 1$ (linear detrending in DFA) for filtered data between F_{min}(0.5 Hz) and F_{max} (45 Hz). We used an exponential smoothing filter to smooth the H_{BB} in consecutive windows in single trials to avoid noisy estimates of H_{BB}. We rigorously validated the scaling exponents H_{BB} and the presence of LRTC in broadband using the procedure described below.

2.4.1. Validation of Broadband LRTC

We validated our results to confirm that the obtained broadband LRTCs were not artifactual. The autocorrelation of a time series decays exponentially if it has short-range dependence and slower than exponential if it has long-range dependence (Botcharova, 2014). A specific case of long-range dependence is LRTC, where the autocorrelation decays according to the power-law that is identified using the Hurst exponent. Hence, to identify LRTC, we must validate the Hurst exponent obtained using DFA. We systematically validated the LRTC in three stages as follows.

2.4.1.1. Identification of Significant Correlations in Broadband EEG Using Surrogate Test

We first identified whether significant temporal correlations are present in the broadband 2 s EEG windows, and their DFA exponents H_{BB} are significantly different from the DFA exponents of white noise obtained by randomly shuffling samples from the same EEG windows using the surrogate test as suggested in Delignieres et al. (2006) and Hausdorff et al. (1995).

2.4.1.2. Determination of Long-Range vs. Short-Range Dependence in the Broadband EEG

After establishing significant correlations in broadband EEG, we identified whether these correlations are short-range or long-range dependence by comparing the fit of corresponding ARMA(p, q) and ARFIMA(p, d, q) models to each 2 s EEG windows (Wairagkar et al., 2019) using Akaike's information criterion (AIC) (Wagenmakers et al., 2004; Delignieres et al., 2006; Clauset et al., 2009). We first estimated the orders p and q of ARFIMA and ARMA independently by comparing models of orders p=1...10 and q = 0 [this range was selected by observing the autocorrelation function and partial autocorrelation function of the EEG (Wairagkar et al., 2019) using AIC]. The ARMA model was estimated using the functions provided by the Econometrics toolbox in MATLAB (https://www.mathworks.com/help/econ/). For estimating ARFIMA, we first fractionally differentiated our EEG window with $d = H_{BB} - 0.5$ and then fitted ARMA(p, q) to it. Then, for each 2 s EEG window of each trial of each participant, AIC was computed to compare ARMA and ARFIMA models of estimated orders. Percentage of total 2 s EEG that showed better fit to ARFIMA model (indicating long-range dependence) than ARMA (indicating short-range dependence) was computed.

2.4.1.3. Identification of LRTC by Validation of Broadband DFA Scaling Exponent H_{BB} Using Maximum Likelihood DFA

After establishing the long-range dependence, we then narrowed down the type of long-range dependence. If the fluctuations in log–log DFA plot at different timescales follow a linear relationship, then this regularity can be captured by the least squared fit, and the slope of this linear fit represents a well-defined power-law scaling exponent (Botcharova et al., 2013, 2015). We used the maximum likelihood DFA (ML-DFA; Botcharova et al., 2013, 2015) method to show that the linear fit is the best fitting model to the log–log DFA fluctuation plot.

The DFA scaling exponents are valid if the linear model fitted best to the log–log DFA fluctuation plot (Botcharova et al., 2014). First, we assessed the quality of the linear fit using R^2 measure (Linkenkaer-Hansen et al., 2001). Identifying the power-law is inherently difficult (Clauset et al., 2009). Frequently used R^2 measure is insensitive (Botcharova et al., 2013) because it may yield high values even for a non-linear relationship in the data (Clauset et al., 2009); therefore, it is not sufficient to assess the quality of the linear fit. Hence, we used the ML-DFA (Botcharova et al., 2013, 2015) to compare the fits of different models.

We fitted polynomials of order 1–5, an exponential function, a logarithmic function, and a root function as suggested in Botcharova et al. (2013) to the log–log DFA fluctuations and compared them using AIC and Bayesian information criterion (BIC). If the resulting best-fitting model is linear, then we interpret it as an indicator of potential power-law and LRTC.

2.5. LRTC in Alpha Envelope and Broadband Stitched EEG During Different Motor Tasks

Traditionally, LRTCs are found in alpha amplitude fluctuations (Linkenkaer-Hansen et al., 2001, 2004; Nikulin and Brismar, 2005; Zhigalov et al., 2016). Since the alpha amplitude has a low frequency, LRTC cannot be computed reliably in short timescales within 2 s windows and require longer timescales. We bandpass filtered each EEG trial between 8 and 13 Hz and segmented it in 2 s sliding windows, then obtained their amplitude envelope by computing the analytic signal using Hilbert transform. We then stitched the corresponding EEG envelope windows from all the trials for each participant to obtain longer EEG segments. For our finger tap dataset with 40 trials per participant, the individual stitched EEG segment was 80 s, and for the EEGMMI dataset with 22 trials per participant, the individual stitched EEG segment was 44 s. Stitching of the data with the same properties does not affect DFA scaling exponent (Hu et al., 2001; Chen et al., 2002; Botcharova et al., 2015). We assume that the corresponding EEG windows from all time-locked trials at each time point during the motor task have same properties, thus ensuring that the stitching will not affect the DFA exponent. We selected the timescales between [2, 20 s] corresponding to approximately box sizes of $[2^8, 2^{11}]$ samples for the finger tap dataset and between [2, 8 s] corresponding to box sizes of $[2^8, 2^{10}]$ for EEGMMI dataset for performing DFA. Then we applied the DFA analysis to obtain scaling exponents H_{alpha} and validated them using ML-DFA. We also computed DFA exponents on the broadband EEG to verify our single-trial broadband LRTC results.

2.6. Classification of Single-Trial Broadband LRTC to Detect Movement and Motor Imagery

We used DFA exponents H_{BB} from channels C3, Cz, and C4 as three features of single trial broadband LRTC to continuously classify motor task vs. resting state throughout the course of EEG trial using single windows for binary classification of single finger tap and continuous fist movement, feet movement, fist motor imagery, and feet motor imagery from the two datasets.

For our single finger tap dataset, the H_{BB} feature vectors of each participant were classified into right tap vs. resting state and left tap vs. resting state independently using binary linear discriminant analysis (LDA) classifier. A separate LDA classifier was trained for each sliding window with the feature vectors from corresponding windows in all the movement trials and the same number of feature vectors randomly chosen from the resting state trials of that participant. Each LDA had 40 data samples with three features for each class. A 10×10 fold cross-validation was used to obtain the classification accuracies and F1 scores at the time points given by the 2 s sliding windows. The 95% confidence level for binary classification (tap or rest) was obtained from the binomial distribution with n = number of EEG trials and $p = 0.05$.

For the EEGMMI dataset, to perform binary classification of each movement/imagery task vs. resting state, we again used the LDA classifier with the single trial H_{BB} from C3, Cz, and C4 as features. Since there were not enough trials of each condition per participant (22 trials) to train the classifier for each participant individually as above, we used the leave-one-participant-out cross-validation to train the LDA classifier. Leave-one-participant-out scheme gives participant-independent classifier performance on unseen data and is commonly used by several EEG and BCI studies such as Kwon and Im (2021) and Wu et al. (2018). Thus, for each of the participants, a separate LDA classifier was trained for each sliding window as above with the feature vectors from corresponding windows from all the trials from the remaining 108 participants. The classification accuracies and F1 scores were computed along with a 95% confidence level using the binomial distribution.

2.6.1. Statistical Analysis

We used parametric t-test and non-parametric Mann–Whitney U-test for identifying the statistical significance of normally distributed data and data without normal distribution, respectively, throughout this paper. We determined the normality of the data using the one-sample Kolmogorov–Smirnov test.

3. RESULTS

We have identified the temporal dynamics of long-range dependencies in broadband EEG during different types of

movements and motor imagery with different paradigms and compared them with the corresponding temporal dynamics of alpha oscillation amplitude envelope fluctuations in the following sections.

3.1. Changes in the Broadband LRTC in Single Trials During Different Motor Tasks

The time evolution of the grand average H_{BB} obtained on a single trial basis in C3, Cz, and C4 are shown in **Figure 2** for 14 participants' right and left self-initiated asynchronous single finger tap (**Figure 2A**, for individual participants LRTC, see **Supplementary Figure 1**) and 109 participants' cued continuous tasks of right and left fist open-close movement (**Figure 2B**), both feet and fist open-close movement (**Figure 2C**), motor imagery of right and left fist open-close (**Figure 2D**), and motor imagery of both feet and fist open-close (**Figure 2E**). A clear increase in H_{BB} is seen during all motor tasks.

For the finger tap dataset, the H_{BB} increased during movement intention and execution of right and left index finger single tap and restored to its baseline level afterwards. For the EEGMMI dataset, the H_{BB} also increased during movement and imagery shortly after the cue and then restored to its baseline levels before the continuous motor task was over (the continuous motor task in this dataset lasted from 0 to 4 s). There was no such increase in the H_{BB} during the resting state in both the datasets. The H_{BB} during the motor task and resting state was between 0.5 and 1, indicating the presence of power-law decay and LRTC in the autocorrelation of broadband EEG (Berthouze and Farmer, 2012). The long-range temporal correlations in the EEG became stronger during voluntary movement and motor imagery.

The solid vertical line at 0 s marks the onset of the self-initiated asynchronous single finger-tap in **Figure 2A**, and it marks the start of cue for the continuous motor task that lasts for the next 4 s in the EEGMMI dataset in **Figures 2B–E**. The two vertical dotted gray lines show the period between which H_{BB} for motor tasks colored traces is significantly different from the resting state (black) ($p < 0.05$, Mann–Whitney U-test, $n =$ total number of trials in all participants of each dataset). The peaks of H_{BB} in the individual trials were not time-locked or aligned. Since the EEGMMI dataset had more participants, the standard deviation of H_{BB} is also larger, as indicated by the shaded area. There is no visible difference in the grand average LRTCs of different tasks in the EEGMMI database. Being able to compute the DFA exponent on a single-trial basis that shows significant changes during a range of motor execution and imagery tasks with different paradigms can allow its use as a feature for motor-based BCIs. In the case of self-initiated voluntary movements, LRTCs can also predict movement before its onset, as seen from finger tap LRTCs in **Figure 2A**.

Before validating broadband LRTC, we validated raw EEG by computing spectrograms (see **Supplementary Figure 2**). A clear attenuation of alpha band power around 10 Hz was observed, which indicates the presence of ERD. Thus, the presence of ERD, a commonly used correlated of movement validates EEG data by confirming that it contains motor-related information. Details of the relationship between ERD and broadband LRTC are given in Wairagkar et al. (2019).

3.1.1. Validation of Broadband LRTC

3.1.1.1. Identification of Significant Correlations in Broadband EEG Using Surrogate Test

The surrogate test confirmed that H_{BB} in 2 s EEG windows were significantly different from the DFA exponents of randomly shuffled samples from the same EEG windows ($p = 0$, Mann–Whitney U-test, $n =$ individual windows in all the participants). The scaling exponents of the shuffled data were close to 0.5, as shown in **Supplementary Figure 3**, confirming the presence of white noise with no correlations. Thus, there were significant correlations present in the broadband 2 s EEG.

3.1.1.2. Determination of Long-Range vs. Short-Range Dependence in the Broadband EEG

The comparison of ARMA for short-range dependence and ARFIMA for long-range dependence using AIC resulted in the selection of the ARFIMA model by AIC for about 80% of the total 2 s EEG windows compared. Hence, the ARFIMA model was a better fit for the short broadband EEG windows confirming that the long-range dependence was indeed present.

3.1.1.3. Identification of LRTC by Validation of Broadband DFA Scaling Exponent H_{BB} Using Maximum Likelihood DFA

The average R^2 measure for all the EEG windows of all the participants in all the channels was 0.96 ± 0.02 (mean $\pm$ SD), indicating that the regression line of the DFA fluctuation plot is a close fit. The ML-DFA method resulted in the selection of the linear model for 80% of the times in all the windows across all the trials, channels, and participants during all the conditions. In the remaining cases, a quadratic polynomial was chosen. We attribute this to the noise induced in computing the root mean square DFA fluctuations at the larger timescales due to short EEG segments. The distribution of the coefficient of the linear term in the linear model and the quadratic model was the same when these respective models were selected as best fitting. In the case where the quadratic model was chosen, the ratio of the coefficient of the quadratic term to that of the linear term was small (0.02), showing a significantly smaller contribution of the quadratic term than the linear term ($p < 0.05$, two-tailed t-Test, $n =$individual windows in all the participants) and hence we did not discard these EEG windows. All these factors led us to conclude that the log–log DFA fluctuation plots were linear and the H_{BB} was indeed valid.

3.2. Changes in LRTC in Alpha Envelope and Broadband Stitched EEG During Different Motor Tasks

We obtained LRTC on longer stitched EEG segments in both broadband and alpha oscillation amplitude envelope during different motor execution and imagery tasks from both datasets. We then compared the changes in the broadband LRTC and alpha amplitude envelope LRTC in the following sections.

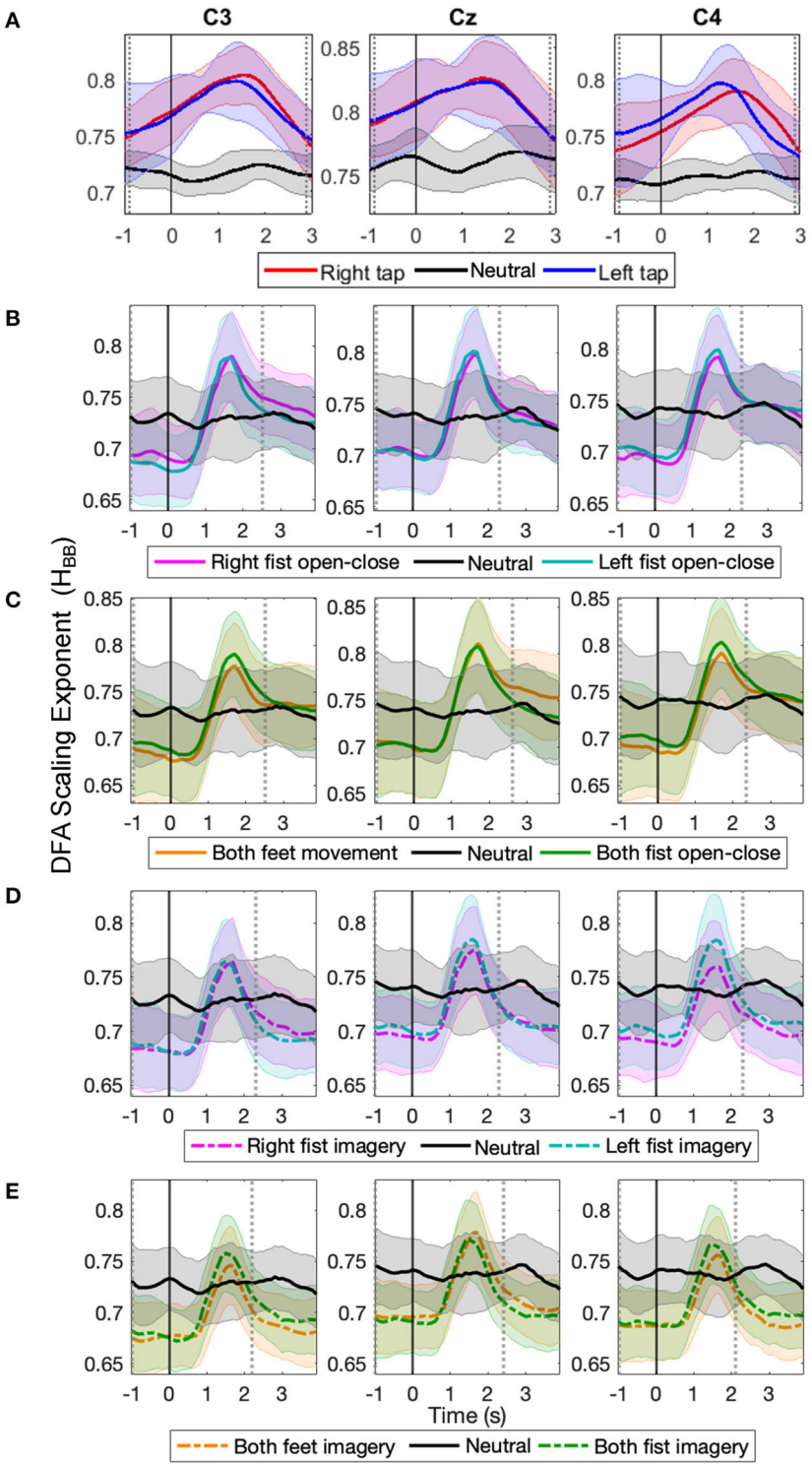

FIGURE 2 | The time evolution of grand average detrended fluctuation analysis (DFA) scaling exponents of broadband electroencephalography (EEG) (H_{BB}) in C3, Cz, and C4 during different movement and motor imagery tasks. The progression of the grand average of mean H_{BB} of all participants during **(A)** single asynchronous right (red) and left (blue) finger tap and resting state (black), **(B)** continuous right (magenta) and left (cyan) fist open-close movement, **(C)** continuous both feet (orange) and both fist (green) open-close movement, **(D)** motor imagery of continuous right (dashed magenta) and left (dashed cyan) fist open-close, **(E)** motor imagery of continuous both feet (dashed orange) and both fist (dashed green) open-close. Shaded areas show the standard deviation. Solid vertical line at 0 s marks finger tap onset in **(A)** and motor task cue in **(B–E)**. Dotted gray vertical lines show the period in which H_{BB} of motor task trials is significantly different ($p < 0.05$, Mann–Whitney U-test) from that of resting state trials. The H_{BB} shows clear increase during all motor tasks.

3.2.1. Changes in Alpha Envelope LRTC (H_{alpha}) Using Stitched EEG

The time evolution of the grand average alpha envelope LRTCs in **Figure 3** shows that H_{alpha} values decreased significantly ($p < 0.05$, Mann–Whitney U-test, $n =$ number of participants) during all the motor execution consistently with the literature (Linkenkaer-Hansen et al., 2004) and during all motor imagery tasks as well. The decrease in alpha envelope LRTC is in contrast to the increase in the broadband LRTC of the same motor tasks (**Figure 2**), indicating that different long-range dependent processes coexist during a motor task. The decrease in the alpha envelope LRTC was observed in the single asynchronous finger tap task from our finger tapping dataset (**Figure 3A**) and in cued continuous tasks of right and left fist open-close movement (**Figure 3B**), both feet and fist open-close movement (**Figure 3C**), motor imagery of right and left fist open-close (**Figure 3D**), and motor imagery of both feet and fist open-close (**Figure 3E**) from the EEGMMI dataset. The decrease in H_{alpha} is prominent in C3 and C4. We validated these DFA exponents from stitched EEG, which ranged between 0.5 and 1 using ML-DFA, and confirmed the presence of LRTCs in the fluctuations of the alpha amplitude envelope of stitched EEG.

3.2.2. Verification of Changes in Broadband LRTC (H_{BB}) During Movement Using Stitched EEG

The progression of the broadband LRTC (H_{BB}) of stitched EEG shown in **Figures 4A–E** also shows that the scaling exponents increase significantly during different motor execution and imagery tasks from our finger tap dataset and EEGMMI dataset ($p < 0.05$, Mann–Whitney U-test, $n =$number of participants). This is consistent with the changes in the single trial broadband EEG from **Figure 2**. The H_{BB} values are similar for both 2 s windows and stitched EEG and are in the range of 0.5–1. The scaling exponents of the stitched EEG were also validated using ML-DFA. The linear model was selected by AIC and BIC individually for 96% times of all the stitched EEG segments in all the windows of all the three channels in all the participants and all conditions. This confirmed the validity of the H_{BB} estimates on single 2 s windows and the presence of LRTC in the broadband EEG. ML-DFA results showed that the quadratic model was previously incorrectly selected in the single-trial DFA because of the noise in the estimation of RMS fluctuations at higher timescales due to short EEG segments.

3.2.3. Correlation Between Broadband LRTC (H_{BB}) and Alpha Envelope LRTC (H_{alpha})

The broadband LRTC and alpha envelope LRTC show changes in opposite directions during all the motor tasks. The broadband LRTCs increased (**Figures 2**, **4**), while the alpha envelope LRTCs decreased (**Figure 3**) during same motor tasks. The increase in broadband LRTC and the decrease in the corresponding alpha envelop LRTC are inversely correlated and temporally co-evolve during a motor task. However, in the resting state, broadband and alpha envelope LRTC are uncorrelated. This distinction in the behavior of the two LRTC dynamics during movement and in the resting state is shown in **Supplementary Figure 4** by the scatter plot between H_{BB} and H_{alpha} of stitched EEG during right and left finger tap and resting state, and their corresponding correlation coefficients.

3.2.4. Timescales of Broadband LRTCs and Alpha Envelope LRTCs

Figure 5A shows the grand average broadband DFA plots, and **Figure 5B** shows the grand average alpha envelope DFA plots. The broadband DFA fluctuations are linear (and thus the scaling exponent H_{BB} is valid) in the log–log plot on the shorter timescales $< 2^8$, while the alpha envelope DFA fluctuations are linear only on the longer timescales $> 2^8$. The maximum timescale of $< 2^8$ corresponds to 2 s on which the broadband DFA fluctuations are linear (i.e., the maximum possible box size can be 2 s for broadband DFA if sufficiently long EEG segment is available), however, the slope of the DFA fluctuations remains the same on shorter timescales and thus broadband DFA scaling exponent H_{BB} can be accurately estimated from shorter EEG segments. This shows that broadband LRTCs are present on the shorter timescales capturing faster changes in the dynamics and alpha envelope LRTCs are present on the longer timescales representing slower changes in the dynamics. Though both the LRTCs show change in dynamics during different motor tasks, broadband LRTCs can be used to identify these change almost instantly as opposed to the alpha envelope LRTCs, which require longer EEG segments for detection.

3.3. Classification Accuracies of Single-Trial Broadband LRTC to Detect Movement and Motor Imagery

Table 1 shows the grand average of peak binary classification accuracies of different motor tasks vs. resting state and their F1 scores. Maximum classification accuracy of 76.07 ± 6.4% was obtained for finger tap. Classification accuracies for different motor execution and imagery tasks from the EEGMMI dataset were similar to that of the finger tapping dataset. Peak classification accuracy for single finger tap was obtained around 1 s after the movement onset, which corresponds to the EEG window from −1 to +1 s, and peak classification accuracies were obtained around the same time for motor execution and imagery tasks from the EEGMMI database as well. This time of peak accuracies corresponds to the time of the maximum difference between a motor task and resting state H_{BB}, which was also approximately at 1–1.5 s (see **Figure 2**). However, all classification accuracies crossed the significance threshold ($p < 0.05$) of chance level earlier than this. In the case of a self-initiated asynchronous single finger tap, the time of movement intention was recorded as the time at which the classification accuracy crosses the significance threshold. We observed that finger tap movement can be predicted on average 0.5 s before its actual onset using the LRTCs in broadband EEG over shorter timescales.

4. DISCUSSION

The temporal dynamics of broadband EEG during voluntary movement remain mostly unexplored in the literature as opposed

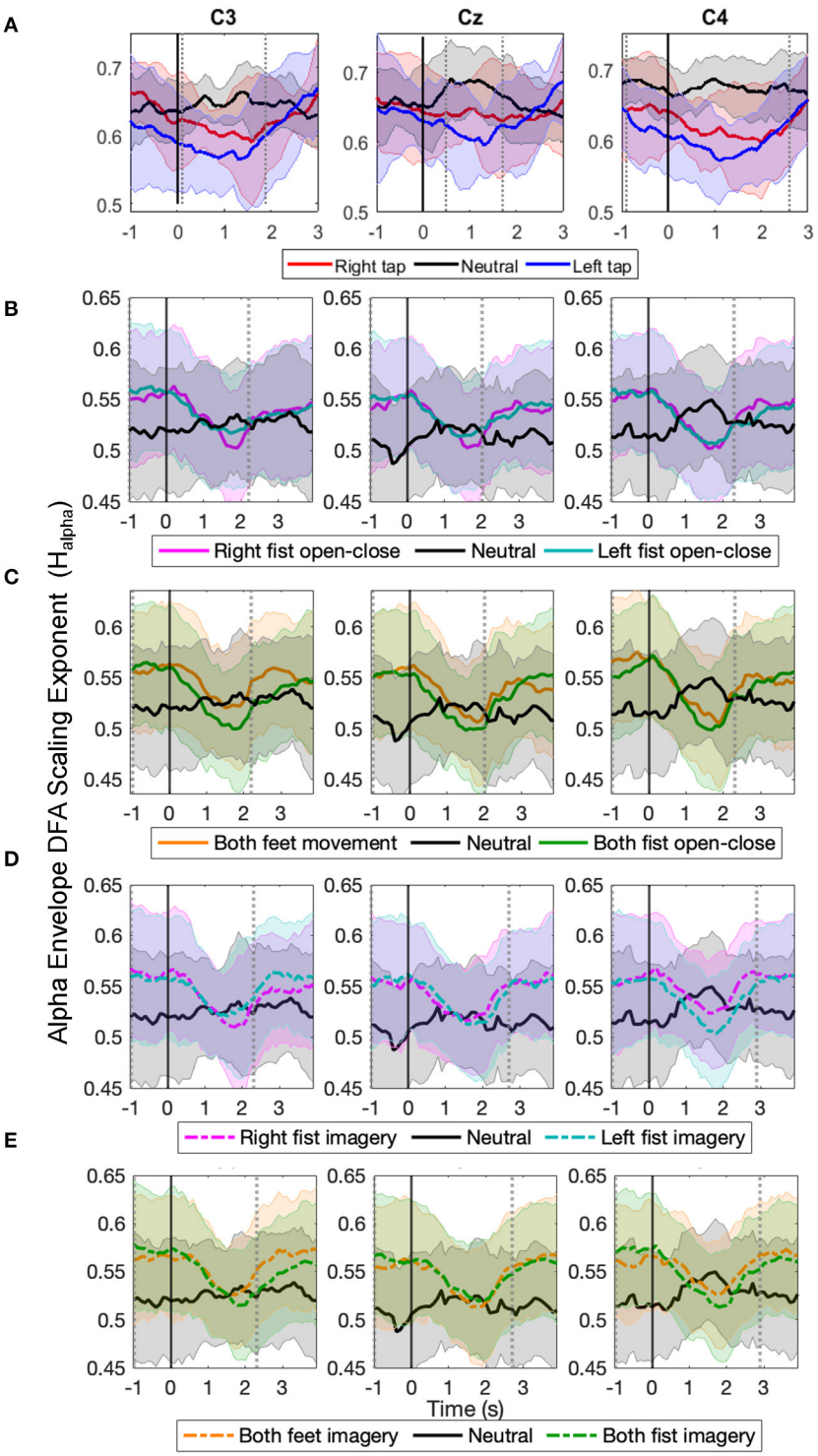

FIGURE 3 | The time evolution of grand average detrended fluctuation analysis (DFA) scaling exponents in the envelope of alpha oscillations of stitched electroencephalography (EEG) (H_{alpha}) in C3, Cz, and C4 during different movement and motor imagery tasks. The progression of the grand average of alpha oscillation amplitude envelope DFA scaling exponent H_{alpha} of all participants during **(A)** single asynchronous right (red) and left (blue) finger tap and resting state (black), **(B)** continuous right (magenta) and left (cyan) fist open-close movement, **(C)** continuous both feet (orange) and both fist (green) open-close movement, **(D)** motor imagery of continuous right (dashed magenta) and left (dashed cyan) fist open-close, **(E)** motor imagery of continuous both feet (dashed orange) and both fist (dashed green) open-close. Shaded areas show the standard deviation. Solid vertical line at 0 s marks finger tap onset in **(A)** and motor task cue in **(B–E)**. Dotted gray vertical lines show the period in which H_{alpha} of motor task trials is significantly different ($p < 0.05$, Mann–Whitney U-test) from that of resting state trials. The H_{alpha} shows clear decrease during all motor tasks.

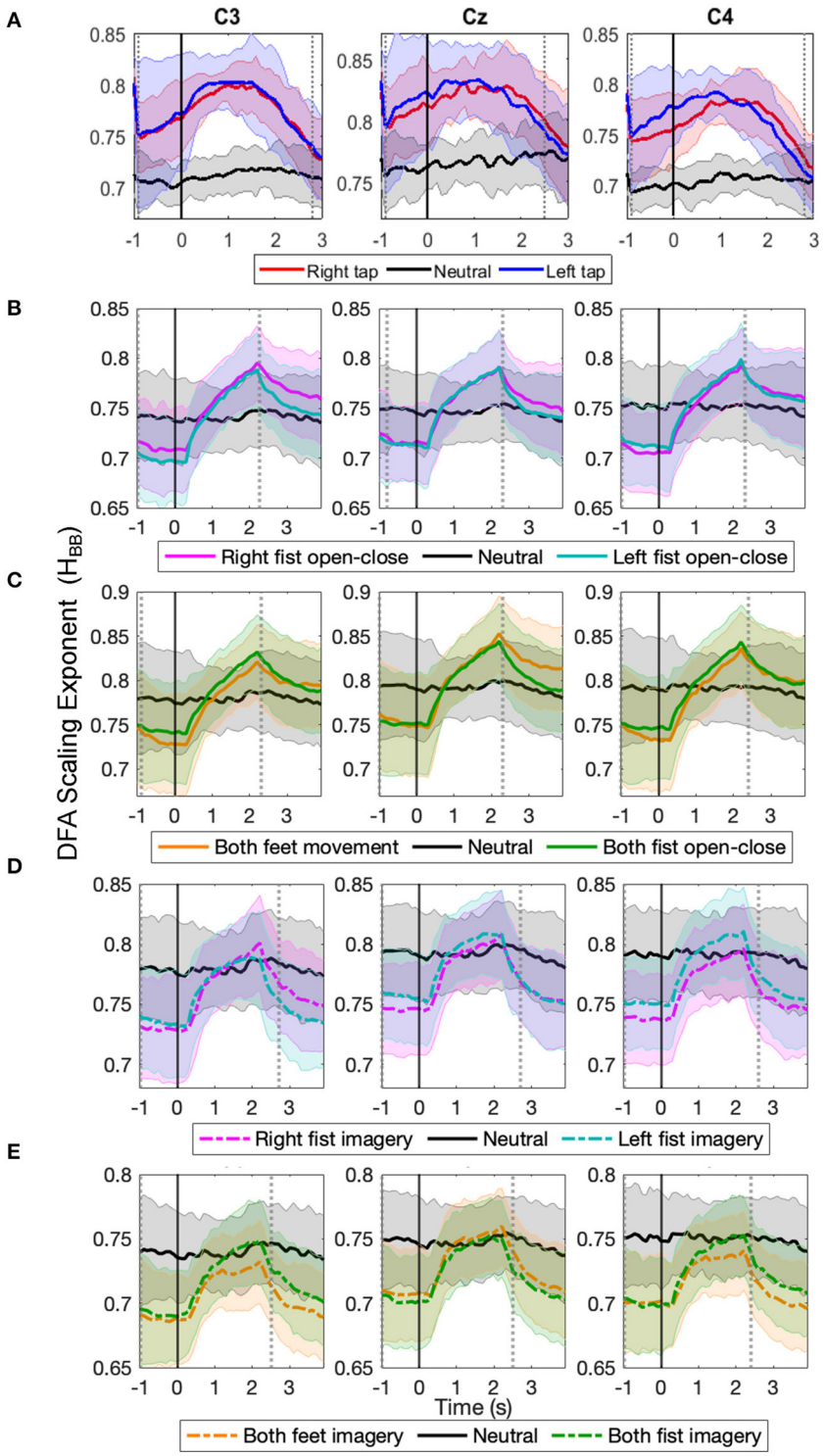

FIGURE 4 | The time evolution of grand average detrended fluctuation analysis (DFA) scaling exponents in broadband stitched electroencephalography (EEG) (H_{BB}) in C3, Cz, and C4 during different movement and motor imagery tasks. The progression of the grand average of broadband DFA scaling exponent H_{BB} from stitched EEG segments of all participants during **(A)** single asynchronous right (red) and left (blue) finger tap and resting state (black), **(B)** continuous right (magenta) and left (cyan) fist open-close movement, **(C)** continuous both feet (orange) and both fist (green) open-close movement, **(D)** motor imagery of continuous right (dashed magenta) and left (dashed cyan) fist open-close, **(E)** motor imagery of continuous both feet (dashed orange) and both fist (dashed green) open-close. Shaded areas show the standard deviation. Solid vertical line at 0 s marks finger tap onset in **(A)** and motor task cue in **(B–E)**. Dotted gray vertical lines show the period in which H_{BB} of motor task trials is significantly different ($p < 0.05$, Mann–Whitney U-test) from that of resting state trials. The H_{BB} shows clear increase during all motor tasks.

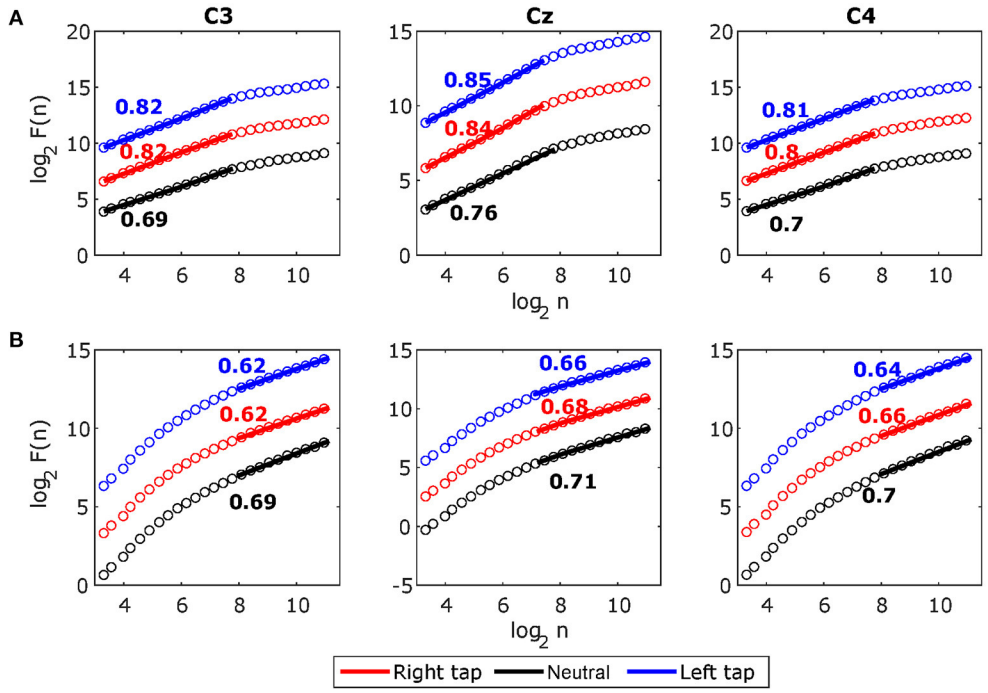

FIGURE 5 | The grand average detrended fluctuation analysis (DFA) plots for stitched broadband electroencephalography (EEG) and alpha amplitude fluctuations during movement in C3, Cz, and C4. **(A)** The grand average DFA plots for stitched broadband EEG during right tap (red), left tap (blue), and resting state (black) for all the participants. This EEG segment is extracted from −1 to +1 s of the movement onset. The Hurst exponents H_{BB} obtained from the slope of the fitted line to the DFA plots are shown. **(B)** The grand average DFA plots for stitched alpha amplitude fluctuations H_{alpha}. The broadband DFA exponents are valid over shorter scales as there is a crossover point at 8 (i.e., log_2 of 256 samples) and the alpha envelope DFA exponents are valid over longer timescales. With sampling frequency of 128 Hz, smallest DFA box size of 10 samples ($log_2 10 = 3.32$) correspond to 78 ms, crossover point at 256 samples ($log_2 256 = 8$) correspond to 2 s, and largest DFA box size of 2,241 samples ($log_2 2241 = 11.13$) correspond to 17.5 s.

TABLE 1 | The grand average of peak linear discriminant analysis (LDA) classification accuracies for different motor tasks vs. resting state of all the participants using single trial broadband long-range temporal correlation (LRTC) scaling exponents from C3, Cz, and C4 as features.

	Average classification accuracy (%)	F1 score
Right finger tap vs. neutral	76.07 (6.40)	0.76 (0.06)
Left finger tap vs. neutral	75.69 (6.77)	0.75 (0.07)
Right fist open-close vs. neutral	73.00 (8.84)	0.79 (0.08)
Left fist open-close vs. neutral	72.24 (8.50)	0.79 (0.08)
Both feet movement vs. neutral	74.41 (9.67)	0.80 (0.08)
Both fist open-close vs. neutral	73.26 (9.09)	0.80 (0.08)
Right fist imagery vs. neutral	70.54 (10.03)	0.77 (0.09)
Left fist imagery vs. neutral	72.60 (9.08)	0.79 (0.08)
Both feet imagery vs. neutral	71.51 (9.87)	0.78 (0.09)
Both fist imagery vs. neutral	73.18 (10.18)	0.80 (0.09)

Standard deviations are given in brackets. All values are significantly above chance level ($p < 0.05$).

to the commonly studied narrow band oscillatory ERD/S (Yuan and He, 2014) or slow potentials of MRCP (Bai et al., 2011; Ibáñez et al., 2014). In our previous work, we have shown that EEG is composed of coexisting broadband short- and long-range temporal correlations, which we modeled with ARFIMA, and both these processes show significant changes during finger tap movement intention and execution (Wairagkar et al., 2019). Building upon our previous work, to deepen our understanding of LRTCs during different motor tasks, we investigated the nature of changes in LRTCs further in broadband and alpha envelope EEG in this study and made the following novel contributions: (1) We demonstrated wider applications of broadband LRTC with consistent changes over different motor tasks by using two independent datasets comprising a total of 123 participants with five different motor execution and imagery tasks recorded using two different experimental paradigms (asynchronous single finger tap and cued continuous movements), thus enhancing its usability. (2) We systematically validated the presence of single trial broadband LRTC on short timescales. This ubiquitous presence of broadband LRTC in different motor tasks suggests existence of potential power-law dynamics in the temporal broadband brain activity as well. (3) We observed contrasting behavior of LRTC dynamics in broadband and alpha envelope. Broadband LRTCs increased during motor tasks (**Figure 2**). In contrast, LRTCs in the narrow band alpha oscillation envelop decreased in corresponding tasks (**Figure 3**), consistent with the literature (Botcharova

et al., 2015). Thus, two distinct fast and slow LRTC processes coexist in arrhythmic broadband EEG and oscillatory alpha wave envelop, respectively. (4) For the first time, we showed LRTC dynamics (of broadband EEG and alpha envelope) during motor imagery, which has never been studied before. (5) Single trial broadband LRTC can be used independently as a neural correlate of different motor execution and imagery tasks for robust classification.

We systematically validated LRTCs in the short 2 s broadband EEG windows by establishing first that there is a significant correlation in the EEG using surrogate test (Hausdorff et al., 1995), then identifying the nature of these correlations as long-range dependence using ARFIMA modeling (Wagenmakers et al., 2004; Torre et al., 2007; Wairagkar et al., 2019) and finally showing that these long-range dependencies are in fact LRTCs (power-law decay of autocorrelation) using ML-DFA (Botcharova et al., 2013). Clauset et al. (2009) discuss that identifying power-law is a difficult problem and linearity on the log-log plot is a necessary but not sufficient condition; the best approach for identifying the power-law is by comparing different models and determining whether the power-law is the best fitting model (which we implemented with ML-DFA). Here, we accept the assumption that the linear trend of the DFA fluctuations at different scales is an indicator of the power-law according to several studies in EEG (Linkenkaer-Hansen et al., 2001; Nikulin and Brismar, 2005; Botcharova et al., 2014). Thus, we rigorously validate the presence of LRTCs in broadband EEG in line with this suggested approach. The broadband EEG, which is non-oscillatory and arrhythmic and hence scale-free and stochastic, coexists with oscillatory processes in the brain (He, 2014). Hence, we can obtain a good estimate of the Hurst exponent (H_{BB}, **Figure 2**) using short segment (2 s) of broadband EEG with 256 samples (Delignieres et al., 2006), which we also verified using the longer stitched EEG segments (**Figure 4**). Thus, our results prove the presence of this scale-free property of the broadband EEG over small timescales (from 78 ms up to 2 s; **Figure 5**).

According to Kantelhardt (2009), the power-law is valid if it exists for at least one order of magnitude, which we obtain in the stitched broadband EEG (78 ms–2 s). The LRTC in the single-trial 2 s broadband EEG was present over a short range of 78 ms–0.5 s. The analysis of stitched broadband EEG allowed us to extrapolate that these LRTC dynamics hold up to 2 s (**Figure 5**). The range of 78 ms–0.5 s for single trials falls within the recommended range for the DFA plot of filtered data by Li et al. (2018) to avoid the effects of filtering on DFA. The study by Hu et al. (2013) also found LRTCs in the neuronal firing in a similar range of timescales as ours, which helps in confirming that LRTCs exist in the shorter timescales in the neuronal activity.

Broadband LRTC was present only in shorter timescales irrespective of the length of the EEG, and it did not extend over longer timescales (**Figure 5A**). The stitched H_{BB} DFA plots in **Figure 5A** show that there is a crossover at 2 s (2^8). This suggests that the broadband activity may be multifractal (Kantelhardt et al., 2002), in which a single power-law is valid in the range of 78 ms–2 s, beyond which there may be a different scale-free trend with a different scaling exponent. The investigation of multifractality in broadband EEG, which is often modeled by stochastic processes, will be an interesting future avenue as we have shown in our previous work that arrhythmic EEG can be modeled by stochastic ARFIMA (Wairagkar et al., 2019); however, it is beyond the scope of this paper since we do not observe these longer timescales in single short 2 s EEG windows, which are essential for application in BCI. Single trial EEG analysis not only plays an important role in BCI but also in cognitive neuroscience to study the ongoing instantaneous changes in temporal dynamics during memory task (Ratcliff et al., 2016), cognitive functions (Debener et al., 2006), and voluntary responses (Yamanaka and Yamamoto, 2010). Single trial broadband LRTC could have potential applications in studying instantaneous dynamics of other cognitive tasks as well.

The range of timescales over which H_{BB} is valid is especially interesting because it enabled monitoring of the instantaneous modulations in the broadband LRTC, facilitating the detection of movements and motor imagery in single trials. These LRTCs over short timescales characterize long-memory of the faster processes as opposed to longer timescales that contain the long-memory of slower brain processes. In the case of a motor task, the brain must switch between different cortical areas and modulate the neuronal activity selectively to produce dynamic movement; stronger LRTCs may provide favorable conditions for this (Samek et al., 2016). This might be one of the reasons for the increase in broadband LRTCs during a motor task. We infer that the broadband activity may be multifractal and more dynamic with changes happening over shorter timescales. Multifractality was also observed by Hu et al. (2013) in neuronal firing during a movement task. Consistent with our results, they also observed that the LRTCs increased during the reaching movement in neuronal firings, which correlated with the movement trajectory, and the LRTC was reset at the beginning of the next movement. There may be several different mechanisms giving rise to the power-law dynamics (Stumpf and Porter, 2012) in brain activity. Further investigation is needed to identify the mechanisms and causes for the increase in the broadband LRTC during motor tasks.

Since ERD is the most common measure of identifying movement from EEG in literature, the question arises about the relationship between ERD and our proposed broadband LRTC. Linkenkaer-Hansen et al. (2001) have specified that the power spectrum and LRTC are not equivalent. We have shown in Wairagkar et al. (2019) that ERD and broadband LRTC are indeed complementary processes and provide different information about a motor task. Removing the broadband LRTC from EEG by fractional differencing does not affect the ERD output, and removing ERD from EEG by filtering out the ERD frequency band does not affect the broadband LRTC. Becker et al. (2018) reported that the increase in power of alpha oscillations in the spontaneous activity caused a decrease in the long-range dependence in the lower frequencies (<5 Hz) of EEG. Extending their finding to a wider range of broadband frequencies in EEG, we also obtained this inverse relationship between alpha power (which decreases leading to ERD (Pfurtscheller and Lopes Da Silva, 1999) and broadband LRTC, which increased during different motor tasks. However, Becker et al. (2018) concluded the existence of this causality merely by identifying the lag at

which the maximum correlation between the alpha power and LRTCs in < 5 Hz band occurs, which may not be sufficient to establish causality. Moreover, such a causal relationship does not exist in the case of wider broadband LRTC (0.5–45 Hz), which we have shown in our previous work (Wairagkar et al., 2019).

The LRTCs in the EEG are usually detected in the amplitude fluctuations of the narrow band oscillations (Linkenkaer-Hansen et al., 2001; Nikulin and Brismar, 2005; Zhigalov et al., 2015). Such LRTCs of alpha oscillations decrease due to a sensorimotor stimulus or task (Linkenkaer-Hansen et al., 2004). We have also observed the same effect on LRTCs in the amplitude fluctuations of the alpha oscillations obtained from the stitched EEG windows (see **Figure 4**). Computing LRTCs in the alpha oscillation amplitude requires a longer EEG segment. Thus, LRTC analysis of alpha amplitude faces limitations on observing fast LRTC changes and their continuous assessment in single trials during a short event such as movement, unlike broadband EEG, which renders alpha envelop LRTCs inappropriate for use in BCI. The continuous monitoring of the ongoing changes in broadband LRTC achieved using 2 s sliding windows gives an additional dimension of movement-related information.

All motor tasks caused modulations in the broadband and oscillatory LRTC dynamics, but in opposite directions and over different timescales. The H_{BB} and H_{alpha} obtained from stitched EEG are uncorrelated during the resting state, and there is a switch in their behavior during movement when they become coupled and inversely correlated (with a strong average correlation coefficient of −0.8 as shown in **Supplementary Figure 4**). In the resting state, H_{BB} has a lower variance, and H_{alpha} has a broader range of observed values. Hence, the alpha amplitude and broadband LRTCs reflect distinct processes occurring during voluntary movement, capturing the slow processes on the macroscopic level and complementary fast processes on the microscopic level, respectively.

Both finger tapping and EEGMMI datasets showed a similar buildup of broadband LRTC (and a corresponding decrease of alpha envelope LRTC); however, the LRTC peak was narrow in case EEGMMI dataset with cued continuous movement and imagery and the increase in broadband LRTC (and the corresponding decrease in alpha envelope LRTC) started around 0.5 s after the cue (see **Figures 4B–E**). This could be because of some evoked response to a cue or because of delayed reaction time for movement or imagery initiation by participants in response to the cue. ERD was also delayed by about 0.5 s after the onset of cue in all the motor tasks from this dataset (see **Supplementary Figures 2B–E**). In the finger tapping dataset, this increase in broadband LRTC starts before the onset of single finger movement (see **Figure 4A**) because it is also capturing movement intention for initiating the finger tap movement voluntarily. Same effect was observed in ERD of finger tapping dataset where ERD started before the onset of finger tap (see **Supplementary Figure 2A**). In the EEGMMI dataset continuous motor tasks, the broadband LRTC restores to its baseline level before the continuous motor execution or imagery ends at 4 s. No such return to baseline level is observed in the ERD of this dataset (see **Supplementary Figures 2B–E**). This could be another indicator that broadband LRTC captures information about movement intention and initiation and differs from the information content of ERD.

We have shown that we can reliably detect different motor execution and imagery tasks using LRTC from 2 s single broadband EEG segments independently with average classification accuracies in the range of 70.54 ± 10.03% to 76.07 ± 6.40% (**Table 1**). We were also able to predict the single finger tap movement 0.5 s before its onset, which also had the highest classification accuracy of 76.07 ± 6.4%. Slightly lower classification accuracies for continuous fist and feet motor execution and imagery from the EEGMMI dataset can be attributed to the leave-one-participant-out LDA classifier training scheme as for each participant, the classifier was trained with the data from the remaining participants, whereas, for finger tapping dataset, the classifier was trained for each participant using their own data with 10 x 10 fold cross-validation. The classification accuracies using broadband LRTC are comparable to the accuracies obtained in the BCI literature (Ibáñez et al., 2014; Lew et al., 2014; Lopez-Larraz et al., 2014; Xu et al., 2014; Padfield et al., 2019; Zhang et al., 2021). Thus, broadband LRTCs can be used as features independently for application in BCI. In our previous work (Wairagkar et al., 2019), we showed that combining short-range and long-range temporal correlation features increases classification accuracy, thus broadband LRTC being a novel complementary process can be used in combination with motor-related features to obtain high classification accuracies for motor execution or imagery-based BCI. Though we used an offline analysis in this paper, the DFA analysis is done on a single trial basis with movement detected every 100 ms based on the 2 s EEG segment and can be easily adapted for online BCI. The successful application of broadband LRTCs as features for offline BCI serves as a robust method of validation of their dynamical changes occurring during motor tasks. Having broadband LRTC as an additional neural correlate with the capability of detecting movement may also be useful in the cases where individuals are unable to operate BCIs with common ERD and MRCP features.

5. CONCLUSIONS

We demonstrated by deeper investigation and rigorous validation of changes in the single trial broadband LRTC over short timescales that it is a robust neural correlate of movement, expanding our previous understanding. Broadband LRTC showed consistent changes and is hence generalizable over different motor tasks such as the finger, fist, and feet movements and motor imagery with different experimental paradigms including single self-initiated asynchronous movement and cued continuous motor execution and imagery. We proved the validity and reproducibility of broadband LRTC on short timescales on single trial 2 s EEG segments by applying it to two independent (our own and external) EEG datasets recorded from a total of 123 participants. LRTCs in the

broadband EEG increased significantly ($p < 0.05$) during motor tasks (**Figures 2**, **4**). In contrast, LRTCs in the alpha oscillation amplitude envelope (which we could only observe by stitching the EEG windows together) decreased during motor tasks (**Figure 3**). Thus, there are complementary fast processes from the scale-free broadband arrhythmic neuronal activity and slow processes from oscillatory neuronal activity coexisting and contributing to voluntary movement tasks. We also identified for the first time, changes in LRTC dynamics during motor imagery which has not been explored before in the literature.

The broadband LRTC has proved to be a novel neural correlate that can be used independently to detect different types of movement or imagery vs. resting state every 100 ms on a single trial basis with the classification accuracy in the range of 70.54 ± 10.03% to 76.07 ± 6.40%. It can also predict a single voluntary asynchronous finger tap 0.5 s before its onset. Hence, the broadband LRTC provides a new stream of movement-related information for application in BCI with different paradigms, including single or continuous movement and motor imagery.

DATA AVAILABILITY STATEMENT

The datasets presented in this study can be found in online repositories. The names of the repository/repositories and accession number(s) can be found at: University of Reading Research Data Archive (http://dx.doi.org/10.17864/1947.117) for the single finger tap EEG dataset that we generated, and PhysioNet (https://doi.org/10.13026/C28G6P) for the EEG Movement/Motor Imagery dataset.

ETHICS STATEMENT

The studies involving human participants were reviewed and approved by the ethics committee of the School of Systems Engineering, University of Reading, UK. The participants provided their written informed consent to participate in this study.

AUTHOR CONTRIBUTIONS

MW conceptualized the study, designed and conducted the experiments, developed the methodology, analyzed and interpreted the results, created the visualizations, and wrote the original manuscript. YH and SN supervised the study, conceptualized the methodology, validated and interpreted the results, and reviewed the manuscript. All authors contributed to the article and approved the submitted version.

FUNDING

This research was funded by the University of Reading International Research Studentship awarded to MW (reference number: GS14-46, URL: http://www.reading.ac.uk/). The funders had no role in study design, data collection and analysis, decision to publish, or preparation of the manuscript.

SUPPLEMENTARY MATERIAL

The Supplementary Material for this article can be found online at: https://www.frontiersin.org/articles/10.3389/fnins.2021.660032/full#supplementary-material

REFERENCES

Bai, O., Rathi, V., Lin, P., Huang, D., Battapady, H., Fei, D.-Y. Y., et al. (2011). Prediction of human voluntary movement before it occurs. *Clin. Neurophysiol.* 122, 364–372. doi: 10.1016/j.clinph.2010.07.010

Becker, R., Van De Ville, D., and Kleinschmidt, A. (2018). Alpha oscillations reduce temporal long-range dependence in spontaneous human brain activity. *J. Neurosci.* 38, 755–764. doi: 10.1523/JNEUROSCI.0831-17.2017

Benayoun, M., Kohrman, M., Cowan, J., and van Drongelen, W. (2010). EEG, temporal correlations, and avalanches. *J. Clin. Neurophysiol.* 27, 458–464. doi: 10.1097/WNP.0b013e3181fdf8e5

Berthouze, L., and Farmer, S. F. (2012). Adaptive time-varying detrended fluctuation analysis. *J. Neurosci. Methods* 209, 178–188. doi: 10.1016/j.jneumeth.2012.05.030

Berthouze, L., James, L. M., and Farmer, S. F. (2010). Human EEG shows long-range temporal correlations of oscillation amplitude in Theta, Alpha and Beta bands across a wide age range. *Clin. Neurophysiol.* 121, 1187–1197. doi: 10.1016/j.clinph.2010.02.163

Botcharova, M. (2014). *Modelling and analysis of amplitude, phase and synchrony in human brain activity patterns* (Ph.D. thesis). University College London, London, United Kingdom.

Botcharova, M., Berthouze, L., Brookes, M. J., Barnes, G. R., and Farmer, S. F. (2015). Resting state MEG oscillations show long-range temporal correlations of phase synchrony that break down during finger movement. *Front. Physiol.* 6:183. doi: 10.3389/fphys.2015.00183

Botcharova, M., Farmer, S. F., and Berthouze, L. (2013). A maximum likelihood based technique for validating detrended fluctuation analysis (ML-DFA). *arXiv [Preprint]. arXiv:1306.5075*.

Botcharova, M., Farmer, S. F., and Berthouze, L. (2014). Markers of criticality in phase synchronisation. *Front. Syst. Neurosci.* 8:176. doi: 10.3389/fnsys.2014.00176

Chaudhary, U., Xia, B., Silvoni, S., Cohen, L. G., and Birbaumer, N. P. (2017). Brain-computer interface-based communication in the completely locked-in state. *PLoS Biol.* 15:e1002593. doi: 10.1371/journal.pbio.1002593

Chen, Z., Ivanov, P. C., Hu, K., and Stanley, H. E. (2002). Effect of nonstationarities on detrended fluctuation analysis. *Phys. Rev. E Stat. Phys. Plasmas Fluids Relat. Interdisc. Top.* 65:15. doi: 10.1103/PhysRevE.65.041107

Clauset, A., Shalizi, C. R., and Newman, M. E. J. (2009). Power-law distributions in empirical data. *SIAM Rev.* 51, 661–703. doi: 10.1137/070710111

Cole, S. R., and Voytek, B. (2018). Cycle-by-cycle analysis of neural oscillations. *bioRxiv*. 2018:302000. doi: 10.1101/302000

D'Croz-Baron, D., Ramirez, J. M., Baker, M., Alarcon-Aquino, V., and Carrera, O. (2012). "A BCI motor imagery experiment based on parametric feature extraction and Fisher Criterion," in *CONIELECOMP 2012 - 22nd International Conference on Electronics Communications and Computing* (Cholula), 257–261.

Debener, S., Ullsperger, M., Siegel, M., and Engel, A. K. (2006). Single-trial EEG-fMRI reveals the dynamics of cognitive function. *Trends Cogn. Sci.* 10, 558–563. doi: 10.1016/j.tics.2006.09.010

Delignieres, D., Ramdani, S., Lemoine, L., Torre, K., Fortes, M., and Ninot, G. (2006). Fractal analyses for 'short' time series: a re-assessment of classical methods. *J. Math. Psychol.* 50, 525–544. doi: 10.1016/j.jmp.2006.07.004

Delorme, A., and Makeig, S. (2004). EEGLAB: An open source toolbox for analysis of single-trial EEG dynamics including independent component analysis. *J. Neurosci. Methods* 134, 9–21. doi: 10.1016/j.jneumeth.2003.10.009

Ezaki, T., Fonseca dos Reis, E., Watanabe, T., Sakaki, M., and Masuda, N. (2020). Closer to critical resting-state neural dynamics in individuals with higher fluid intelligence. *Commun. Biol.* 3, 1–9. doi: 10.1038/s42003-020-0774-y

Goldberger, A., Amaral, L., Glass, L., Hausdorff, J., Ivanov, P. C., Mark, R., et al. (2000). PhysioBank, physioToolkit, and physioNet: components of a new research resource for complex physiologic signals. *Circulation* 101, e215–e220. doi: 10.13026/C28G6P

Haller, M., Donoghue, T., Peterson, E., Varma, P., Sebastian, P., Gao, R., et al. (2018). Parameterizing neural power spectra. *bioRxiv*. 2018:299859 doi: 10.1101/299859

Hardstone, R., Poil, S.-S. S., Schiavone, G., Jansen, R., Nikulin, V. V., Mansvelder, H. D., et al. (2012). Detrended fluctuation analysis: a scale-free view on neuronal oscillations. *Front. Physiol.* 3:450. doi: 10.3389/fphys.2012.00450

Hausdorff, J. M., Peng, C. K., Ladin, Z., Wei, J. Y., and Goldberger, A. L. (1995). Is walking a random walk? Evidence for long-range correlations in stride interval of human gait. *J. Appl. Physiol.* 78, 349–358. doi: 10.1152/jappl.1995.78.1.349

He, B., Baxter, B., Edelman, B. J., Cline, C. C., and Ye, W. W. (2015). Noninvasive brain-computer interfaces based on sensorimotor rhythms. *Proc. IEEE* 103, 907–925. doi: 10.1109/JPROC.2015.2407272

He, B. J. (2014). Scale-free brain activity: past, present, and future. *Trends Cogn. Sci.* 18, 480–487. doi: 10.1016/j.tics.2014.04.003

Heiney, K., Huse Ramstad, O., Fiskum, V., Christiansen, N., Sandvig, A., Nichele, S., et al. (2021). Criticality, connectivity, and neural disorder: a multifaceted approach to neural computation. *Front. Comput. Neurosci.* 15:611183. doi: 10.3389/fncom.2021.611183

Hou, D., Wang, C., Chen, Y., Wang, W., and Du, J. (2017). Long-range temporal correlations of broadband EEG oscillations for depressed subjects following different hemispheric cerebral infarction. *Cogn. Neurodyn.* 11, 529–538. doi: 10.1007/s11571-017-9451-3

Hu, J., Zheng, Y., and Gao, J. (2013). Long-range temporal correlations, multifractality, and the causal relation between neural inputs and movements. *Front. Neurol.* 4:158. doi: 10.3389/fneur.2013.00158

Hu, K., Ivanov, P. C., Chen, Z., Carpena, P., and Stanley, H. E. (2001). Effect of trends on detrended fluctuation analysis. *Phys. Rev. E* 64:19. doi: 10.1103/PhysRevE.64.011114

Hu, K., Ivanov, P. C., Chen, Z., Hilton, M. F., Stanley, H. E., and Shea, S. A. (2004). Non-random fluctuations and multi-scale dynamics regulation of human activity. *Phys. A* 337, 307–318. doi: 10.1016/j.physa.2004.01.042

Ibáñez, J., Serrano, J. I., Del Castillo, M. D., Monge-Pereira, E., Molina-Rueda, F., Alguacil-Diego, I., et al. (2014). Detection of the onset of upper-limb movements based on the combined analysis of changes in the sensorimotor rhythms and slow cortical potentials. *J. Neural Eng.* 11:056009. doi: 10.1088/1741-2560/11/5/056009

Jannesari, M., Saeedi, A., Zare, M., Ortiz-Mantilla, S., Plenz, D., and Benasich, A. A. (2020). Stability of neuronal avalanches and long-range temporal correlations during the first year of life in human infants. *Brain Struct. Funct.* 225, 1169–1183. doi: 10.1007/s00429-019-02014-4

Jung, T. P., Makeig, S., Humphries, C., Lee, T. W., McKeown, M. J., Iragui, V., et al. (2000). Removing electroencephalographic artifacts by blind source separation. *Psychophysiology* 37, 163–178. doi: 10.1111/1469-8986.3720163

Kantelhardt, J. W. (2009). "Fractal and multifractal time series," in *Encyclopedia of Complexity and Systems Science*, ed R. A. Meyers (New York, NY: Springer), 3754–3779. doi: 10.1007/978-0-387-30440-3_221

Kantelhardt, J. W., Koscielny-Bunde, E., Rego, H. H., Havlin, S., and Bunde, A. (2001). Detecting long-range correlations with detrended fluctuation analysis. *Phys. A* 295, 441–454. doi: 10.1016/S0378-4371(01)00144-3

Kantelhardt, J. W., Zschiegner, S. A., Koscielny-Bunde, E., Havlin, S., Bunde, A., and Stanley, H. E. (2002). Multifractal detrended fluctuation analysis of nonstationary time series. *Phys. A* 316, 87–114. doi: 10.1016/S0378-4371(02)01383-3

Kello, C. T., Brown, G. D., Ferrer-i Cancho, R., Holden, J. G., Linkenkaer-Hansen, K., Rhodes, T., et al. (2010). Scaling laws in cognitive sciences. *Trends Cogn. Sci.* 14, 223–232. doi: 10.1016/j.tics.2010.02.005

Kitzbichler, M. G., Smith, M. L., Christensen, S. R., and Bullmore, E. (2009). Broadband criticality of human brain network synchronization. *PLoS Comput. Biol.* 5:e1000314. doi: 10.1371/journal.pcbi.1000314

Kwok, E. Y., Cardy, J. O., Allman, B. L., Allen, P., and Herrmann, B. (2019). Dynamics of spontaneous alpha activity correlate with language ability in young children. *Behav. Brain Res.* 359, 56–65. doi: 10.1016/j.bbr.2018.10.024

Kwon, J., and Im, C.-H. (2021). Subject-independent functional near-infrared spectroscopy-based brain-computer interfaces based on convolutional neural networks. *Front. Hum. Neurosci.* 15:646915. doi: 10.3389/fnhum.2021.646915

Lew, E. Y. L., Chavarriaga, R., Silvoni, S., and Millán, J. D. R. (2014). Single trial prediction of self-paced reaching directions from EEG signals. *Front. Neurosci.* 8:222. doi: 10.3389/fnins.2014.00222

Li, R., Wang, J., and Chen, Y. (2018). Effect of the signal filtering on detrended fluctuation analysis. *Phys. A* 494, 446–453. doi: 10.1016/j.physa.2017.12.011

Linkenkaer-Hansen, K., Nikouline, V. V., Palva, J. M., Ilmoniemi, R. J., Nikulin, V. V., Palva, J. M., et al. (2001). Long-range temporal correlations and scaling behavior in human brain oscillations. *J. Neurosci.* 21, 1370–1377. doi: 10.1002/anie.201106423

Linkenkaer-Hansen, K., Nikulin, V. V., Palva, J. M., Kaila, K., and Ilmoniemi, R. J. (2004). Stimulus-induced change in long-range temporal correlations and scaling behaviour of sensorimotor oscillations. *Eur. J. Neurosci.* 19, 203–211. doi: 10.1111/j.1460-9568.2004.03116.x

Lombardi, F., Shriki, O., Herrmann, H. J., and de Arcangelis, L. (2020). Long-range temporal correlations in the broadband resting state activity of the human brain revealed by neuronal avalanches. *bioRxiv*. doi: 10.1101/2020.02.03.930966

Lopez-Larraz, E., Montesano, L., Gil-Agudo, A., and Minguez, J. (2014). Continuous decoding of upper limb movement intention from EEG measurements on the. *J. NeuroEng. Rehabil.* 11:153. doi: 10.1186/1743-0003-11-153

Makeig, S., Jung, T.-P. P., Bell, A. J., Ghahremani, D., and Sejnowski, T. J. (1997). Blind separation of auditory event-related brain responses into independent components. *Proc. Natl. Acad. Sci. U.S.A.* 94, 10979–10984. doi: 10.1073/pnas.94.20.10979

Massobrio, P., de Arcangelis, L., Pasquale, V., Jensen, H. J., and Plenz, D. (2015). Criticality as a signature of healthy neural systems. *Front. Syst. Neurosci.* 9:22. doi: 10.3389/fnsys.2015.00022

Meisel, C., Klaus, A., Vyazovskiy, V. V., and Plenz, D. (2017). The interplay between long-and short-range temporal correlations shapes cortex dynamics across vigilance states. *J. Neurosci.* 37, 10114–10124. doi: 10.1523/JNEUROSCI.0448-17.2017

Nikulin, V. V., and Brismar, T. (2005). Long-range temporal correlations in electroencephalographic oscillations: relation to topography, frequency band, age and gender. *Neuroscience* 130, 549–558. doi: 10.1016/j.neuroscience.2004.10.007

Ouyang, G., Hildebrandt, A., Schmitz, F., and Herrmann, C. S. (2020). Decomposing alpha and 1/f brain activities reveals their differential associations with cognitive processing speed. *NeuroImage* 205:116304. doi: 10.1016/j.neuroimage.2019.116304

Padfield, N., Zabalza, J., Zhao, H., Masero, V., and Ren, J. (2019). EEG-based brain-computer interfaces using motor-imagery: techniques and challenges. *Sensors* 19:1423. doi: 10.3390/s19061423

Palva, J. M., Zhigalov, A., Hirvonen, J., Korhonen, O., Linkenkaer-Hansen, K., and Palva, S. (2013). Neuronal long-range temporal correlations and avalanche dynamics are correlated with behavioral scaling laws. *Proc. Natl. Acad. Sci. U.S.A.* 110, 3585–3590. doi: 10.1073/pnas.1216855110

Parish, L. M., Worrell, G. A., Cranstoun, S. D., Stead, S. M., Pennell, P., and Litt, B. (2004). Long-range temporal correlations in epileptogenic and non-epileptogenic human hippocampus. *Neuroscience* 125, 1069–1076. doi: 10.1016/j.neuroscience.2004.03.002

Peng, C.-K. K., Havlin, S., Stanley, H. E., and Goldberger, A. L. (1995). Quantification of scaling exponents and crossover phenomena in nonstationary heartbeat time series. *Chaos* 5, 82–87. doi: 10.1063/1.166141

Pfurtscheller, G., and Lopes Da Silva, F. H. (1999). Event-related EEG/MEG synchronization and desynchronization: basic principles. *Clin. Neurophysiol.* 110, 1842–1857. doi: 10.1016/S1388-2457(99)00141-8

Poil, S.-S. S., Hardstone, R., Mansvelder, H. D., and Linkenkaer-Hansen, K. (2012). Critical-state dynamics of avalanches and oscillations jointly emerge from balanced excitation/inhibition in neuronal networks. *J. Neurosci.* 32, 9817–9823. doi: 10.1523/JNEUROSCI.5990-11.2012

Rangarajan, G., and Ding, M. (2000). Integrated approach to the assessment of long range correlation in time series data. *Phys. Rev. E Stat. Phys.* 61, 4991–5001. doi: 10.1103/PhysRevE.61.4991

Ratcliff, R., Sederberg, P. B., Smith, T. A., and Childers, R. (2016). A single trial analysis of EEG in recognition memory: tracking the neural correlates of memory strength. *Neuropsychologia* 93, 128–141. doi: 10.1016/j.neuropsychologia.2016.09.026

Resniak, A., Poling, B., and Maloney, L. (2020). *SENSORY MOTOR (C3, CZ, AND C4). Practical Neurocounseling: Connecting Brain Functions to Real Therapy Interventions*. Routledge.

Ros, T., Frewen, P., Théberge, J., Michela, A., Kluetsch, R., Mueller, A., et al. (2016). Neurofeedback tunes scale-free dynamics in spontaneous brain activity. *Cereb. Cortex* 27, 4911–4922. doi: 10.1093/cercor/bhw285

Ros, T., J. Baars, B., Lanius, R. A., and Vuilleumier, P. (2014). Tuning pathological brain oscillations with neurofeedback: a systems neuroscience framework. *Front. Hum. Neurosci.* 8:1008. doi: 10.3389/fnhum.2014.01008

Samek, W., Blythe, D. A., Curio, G., Müller, K. R., Blankertz, B., and Nikulin, V. V. (2016). Multiscale temporal neural dynamics predict performance in a complex sensorimotor task. *NeuroImage* 141, 291–303. doi: 10.1016/j.neuroimage.2016.06.056

Schalk, G., McFarland, D. J., Hinterberger, T., Birbaumer, N., and Wolpaw, J. R. (2004). BCI2000: A general-purpose brain-computer interface (BCI) system. *IEEE Trans. Biomed. Eng.* 51, 1034–1043. doi: 10.1109/TBME.2004.827072

Schlögl, A., Lee, F., Bischof, H., and Pfurtscheller, G. (2005). Characterization of four-class motor imagery EEG data for the BCI-competition 2005. *J. Neural Eng.* 2, 14–22. doi: 10.1088/1741-2560/2/4/L02

Shibasaki, H., and Hallett, M. (2006). What is the bereitschaftspotential? *Clin. Neurophysiol.* 117, 2341–2356. doi: 10.1016/j.clinph.2006.04.025

Stumpf, M. P., and Porter, M. A. (2012). Critical truths about power laws. *Science* 335, 665–666. doi: 10.1126/science.1216142

Torre, K., Delignieres, D., and Lemoine, L. (2007). Detection of long-range dependence and estimation of fractal exponents through ARFIMA modelling. *Br. J. Math. Stat. Psychol.* 60, 85–106. doi: 10.1348/000711005X89513

Wagenmakers, E.-J., Farrell, S., and Ratcliff, R. (2004). Estimation and interpretation of 1/fα noise in human cognition. *Psychon. Bull. Rev.* 11, 579–615. doi: 10.3758/BF03196615

Wairagkar, M. (2017). *EEG Data for Voluntary Finger Tapping Movement*. University of Reading Dataset.

Wairagkar, M., Hayashi, Y., and Nasuto, S. J. (2018). Exploration of neural correlates of movement intention based on characterisation of temporal dependencies in electroencephalography. *PLoS ONE* 13:e193722. doi: 10.1371/journal.pone.0193722

Wairagkar, M., Hayashi, Y., and Nasuto, S. J. (2019). Modeling the ongoing dynamics of short and long-range temporal correlations in broadband EEG during movement. *Front. Syst. Neurosci.* 13:66. doi: 10.3389/fnsys.2019.00066

Wang, J., Feng, Z., Lu, N., and Luo, J. (2018). Toward optimal feature and time segment selection by divergence method for EEG signals classification. *Comput. Biol. Med.* 97, 161–170. doi: 10.1016/j.compbiomed.2018.04.022

Wu, C.-T., Dillon, D., Hsu, H.-C., Huang, S., Barrick, E., and Liu, Y.-H. (2018). Depression detection using relative EEG power induced by emotionally positive images and a conformal kernel support vector machine. *Appl. Sci.* 8:1244. doi: 10.3390/app8081244

Xu, R., Jiang, N., Lin, C., Mrachacz-Kersting, N., Dremstrup, K., and Farina, D. (2014). Enhanced low-latency detection of motor intention from EEG for closed-loop brain-computer interface applications. *IEEE Trans. Biomed. Eng.* 61, 288–296. doi: 10.1109/TBME.2013.2294203

Yamanaka, K., and Yamamoto, Y. (2010). Single-trial EEG power and phase dynamics associated with voluntary response inhibition. *J. Cogn. Neurosci.* 22, 714–727. doi: 10.1162/jocn.2009.21258

Yuan, H., and He, B. (2014). Brain-computer interfaces using sensorimotor rhythms: current state and future perspectives. *IEEE Trans. Biomed. Eng.* 61, 1425–1435. doi: 10.1109/TBME.2014.2312397

Zhang, K., Robinson, N., Lee, S. W., and Guan, C. (2021). Adaptive transfer learning for EEG motor imagery classification with deep Convolutional Neural Network. *Neural Netw.* 136, 1–10. doi: 10.1016/j.neunet.2020.12.013

Zhigalov, A., Arnulfo, G., Nobili, L., Palva, S., and Palva, J. M. (2015). Relationship of fast- and slow-timescale neuronal dynamics in human MEG and SEEG. *J. Neurosci.* 35, 5385–5396. doi: 10.1523/JNEUROSCI.4880-14.2015

Zhigalov, A., Kaplan, A. Y., and Palva, J. M. (2016). Modulation of critical brain dynamics using closed-loop neurofeedback stimulation. *Clin. Neurophysiol.* 127, 2882–2889. doi: 10.1016/j.clinph.2016.04.028

Zimmern, V. (2020). Why brain criticality is clinically relevant: a scoping review. *Front. Neural Circuits* 14:54. doi: 10.3389/fncir.2020.00054

Conflict of Interest: The authors declare that the research was conducted in the absence of any commercial or financial relationships that could be construed as a potential conflict of interest.

frontiers in Neuroscience

REVIEW
published: 15 November 2021
doi: 10.3389/fnins.2021.658930

Projections and the Potential Societal Impact of the Future of Neurotechnologies

Kate S. Gaudry[1], Hasan Ayaz[2,3,4,5,6†], Avery Bedows[7†], Pablo Celnik[8†], David Eagleman[9†], Pulkit Grover[10,11†], Judy Illes[12,13†], Rajesh P. N. Rao[14†], Jacob T. Robinson[15,16,17,18†], Krishnan Thyagarajan[19†] and The Working Group on Brain-Interfacing Devices in 2040[‡]*

[1] Kilpatrick Townsend & Stockton LLP, Washington, DC, United States, [2] School of Biomedical Engineering, Science and Health Systems, Drexel University, Philadelphia, PA, United States, [3] Department of Psychology, College of Arts and Sciences, Drexel University, Philadelphia, PA, United States, [4] Drexel Solutions Institute, Drexel University, Philadelphia, PA, United States, [5] Department of Family and Community Health, University of Pennsylvania, Philadelphia, PA, United States, [6] Center for Injury Research and Prevention, Children's Hospital of Philadelphia, Philadelphia, PA, United States, [7] Substrate Group, New York, NY, United States, [8] Department of Physical Medicine and Rehabilitation, Johns Hopkins, School of Medicine, Baltimore, MD, United States, [9] Department of Psychiatry, Stanford University School of Medicine, Stanford, CA, United States, [10] Center for the Neural Basis of Cognition, Carnegie Mellon University, Pittsburgh, PA, United States, [11] Department of Electrical and Computer Engineering, Carnegie Mellon University, Pittsburgh, PA, United States, [12] Department of Medicine, University of British Columbia, Vancouver, BC, Canada, [13] Neuroethics Canada, University of British Columbia, Vancouver, BC, Canada, [14] Center for Neurotechnology, Paul G. Allen School of Computer Science and Engineering, University of Washington, Seattle, DC, United States, [15] Department of Bioengineering, Rice University, Houston, TX, United States, [16] Department of Electrical and Computer Engineering, Rice University, Houston, TX, United States, [17] Applied Physics Program, Rice University, Houston, TX, United States, [18] Department of Neuroscience, Baylor College of Medicine, Houston, TX, United States, [19] Palo Alto Research Center (PARC), A Xerox Company, Palo Alto, CA, United States

OPEN ACCESS

Edited by:
Michele Giugliano, International School for Advanced Studies (SISSA), Italy

Reviewed by:
Farheen Syeda, Baton Rouge, United States
Stephanie Gauttier, Grenoble École de Management, France
Brent Winslow, Design Interactive, United States

***Correspondence:**
Kate S. Gaudry
kgaudry@kilpatricktownsend.com

[†] These authors have contributed equally to this work

[‡] Authors listed in Acknowledgments

Specialty section:
This article was submitted to Neural Technology, a section of the journal Frontiers in Neuroscience

Received: *26 January 2021*
Accepted: *04 October 2021*
Published: *15 November 2021*

Citation:
Gaudry KS, Ayaz H, Bedows A, Celnik P, Eagleman D, Grover P, Illes J, Rao RPN, Robinson JT, Thyagarajan K and The Working Group on Brain-Interfacing Devices in 2040 (2021) Projections and the Potential Societal Impact of the Future of Neurotechnologies. Front. Neurosci. 15:658930. doi: 10.3389/fnins.2021.658930

Traditionally, recording from and stimulating the brain with high spatial and temporal resolution required invasive means. However, recently, the technical capabilities of less invasive and non-invasive neuro-interfacing technology have been dramatically improving, and laboratories and funders aim to further improve these capabilities. These technologies can facilitate functions such as multi-person communication, mood regulation and memory recall. We consider a potential future where the less invasive technology is in high demand. Will this demand match that the current-day demand for a smartphone? Here, we draw upon existing research to project which particular neuroethics issues may arise in this potential future and what preparatory steps may be taken to address these issues.

Keywords: ethics, neuroethics, brain interfacing, policy, brain recording, brain stimulation, non-invasive, minutely invasive

INTRODUCTION

Capabilities of today's most powerful brain-interfacing technologies are extraordinary. Brain stimulation can alter a person's memory (Beynel et al., 2019; Reinhart and Nguyen, 2019), attentiveness (Filmer et al., 2017; Curtin et al., 2019), mood (Mayberg et al., 2005; Schlaepfer et al., 2008), and physical capabilities (Wagner F. B. et al., 2018; Barbe et al., 2020). Brain recordings can allow sensed stimuli, perceptions and motor intentions to be decoded

(Kay et al., 2008; Edelman et al., 2015; Gateau et al., 2018; Liu and Ayaz, 2018; Sani et al., 2018; Volkova et al., 2019; Krol et al., 2020; Schwarz et al., 2020). Yet, to date, the most dramatic stimulation-triggered actions and the most temporally and spatially precise recordings primarily use very invasive technologies (Lebedev and Nicolelis, 2017; Wallis, 2018). Invasive technology currently faces impediments about the potential limitations of adoption, the potential of adverse events (from implantation surgery or adverse events from usage, such as the possibility of burns), the potential reduced quality of recorded neurological signals over time, and the potential reduction in impact of stimulation over time. Development of non-invasive neurotechnologies is progressing rapidly and demonstrating potential beyond research toward everyday life (Roelfsema et al., 2018; Dehais et al., 2020). And, even today, some commercial home-use consumer devices are already on the market (Ienca et al., 2018).

Might the capabilities of brain-interfacing technology advance sufficiently to garner demand akin to the modern-day smart phone? If so, what policy issues might this technology present to society, and how might we prepare for this potential future.

Present-Day Brain-Interfacing Technology

Advances in neuroscience and engineering have facilitated development of diverse non-invasive neurotechnologies for monitoring and modulating brain activity (Roelfsema et al., 2018). Whole-brain activity monitoring modalities [e.g., functional magnetic resonance imaging (fMRI) or magnetoencephalogram] require room-size equipment but provide high spatial resolution (though portable MRI is being increasingly explored). Portable recording modalities [e.g., electroencephalography (EEG) and near-infrared spectroscopy (NIRS)] have lower spatial resolution but are widely used to study neural mechanisms underlying cognitive functioning within real-world contexts (Ayaz and Dehais, 2019). Non-invasive brain-stimulation (NIBS) [e.g., transcranial magnetic and electrical stimulation (TMS, tES)] is used for research, prognostication and treatment of many disorders (Bikson et al., 2020). Focused ultrasound (FUS) is emerging as a high-resolution and potentially portable alternative, pending safety challenges (Shen et al., 2020). Targeted indirect brain modulation even may be achieved *via* visual sensory substitution (Adaikkan and Tsai, 2020) and somatosensory senses (Novich and Eagleman, 2015).

Non-invasive neurotechnology already has been used to restore function or enhance human capabilities, including motor abilities, communication, perception, attention, mood, situational awareness, memory, problem-solving, and decision making (Cinel et al., 2019). TMS is FDA-approved to treat major depression and obsessive-compulsive disorder. Other non-invasive neurotechnologies have tracked speaker-listener communication (Liu et al., 2017) and decoded participants' mental states (Trimper et al., 2014), and supported brain-to-brain communication between multiple brains (Jiang et al., 2019).

Nonetheless, to date, invasive neurotechnology maintains the highest spatial and temporal resolution, deep-brain accessibility and performance. Established forms of such technologies include electrocorticography (ECoG); multi-unit electrode arrays and tetrodes; and emerging ultraminiature and flexible technologies, with spatial resolution reaching sub-50 micron (Neely et al., 2018). These technologies have prompted invasive-device use for augmentative applications, such as communication *via* translating cortical activity to text, mood regulation, quicker memory recall and brain co-processors (Ezzyat et al., 2018; Hampson et al., 2018; Rao, 2019; Shanechi, 2019; Makin et al., 2020). Although invasive technologies carry many risks (e.g., brain tissue damage associated with surgery, infection, implantation, and explantation) (Hendriks et al., 2019), they currently provide the fastest operation and greatest portability, in addition to the highest spatiotemporal resolution. As improved non-invasive technologies become more competitive, development focus has shifted to improving perceived benefits relative to accompanying risks.

State of the Art and Engineering

Recent engineering breakthroughs suggest that, non-invasive or minutely invasive portable wireless technologies will soon record from 50,000 to 100,000 neurons simultaneously (with minutely invasive devices being temporarily and non-surgically provided to the brain). This projection is based on prior exponential scaling (Stevenson and Kording, 2011) of the number of neurons simultaneously recorded. These interfaces likely will be able to detect dendritic/axonal level activity and record and affect neurotransmitters and ion concentrations that drive neural behavior. The feasibility of achieving these capabilities is evidenced by a recent DARPA program called the Next-Generation Non-surgical Neurotechnology (N^3) program, which seeks to develop non-invasive or minutely invasive interfaces having 50-ms temporal resolution and 1-mm^3 spatial resolution for closed-loop sensing and stimulation from each of 16 or more brain locations.

Figure 1 illustrates how different types of existing neurotechnologies vary with respect to invasiveness and performance metrics (e.g., spatial and temporal precision). As shown, minimally invasive devices (which can be used without a user having a craniotomy), and minutely invasive devices (which can be used without a user having an incision), are less invasive than surgically implanted devices but more invasive than wearable devices. Technological advances are currently and likely to continue to trend toward improved performance and reduced invasiveness. The future of brain-interfacing devices, therefore, may be sufficiently non-invasive to not require surgery, but still be capable of recording or stimulating brain areas with high temporal and spatial precision.

In our view, the goals of the DARPA N^3 grant and others similar to it will be achieved or surpassed by 2040. We project that there will be high demand for non- or minutely invasive brain-recording devices that have capabilities that include at least one of: enhancing attention, memory or learning; enhancing mood; or supporting inter-person communication. This projection of high demand is further based on a projection that having the technical capabilities of recording from and/or stimulating brain regions in a temporally and spatially precise manner will facilitate further understandings of human neuroscience, such that such

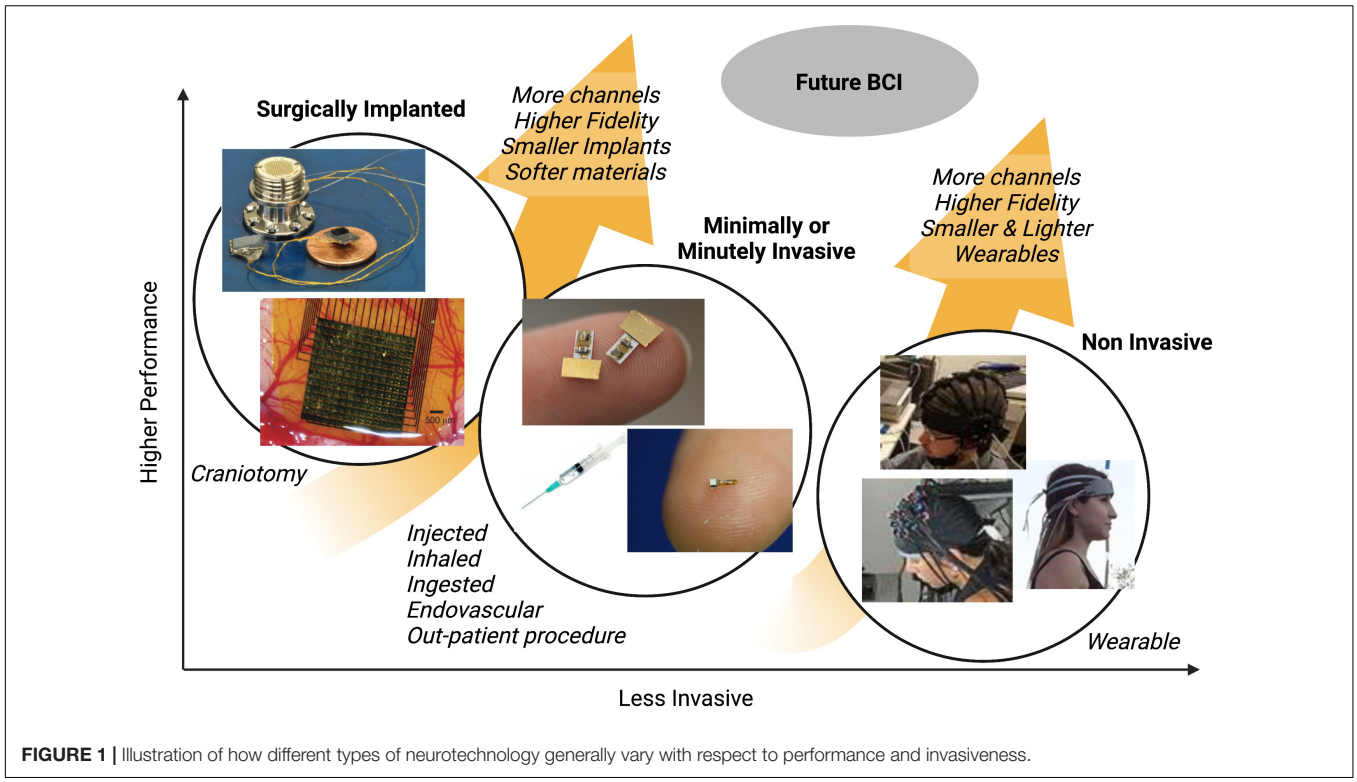

FIGURE 1 | Illustration of how different types of neurotechnology generally vary with respect to performance and invasiveness.

recordings or stimulations provide a practical use. Given these projections, we consider key ethical implications here. Some are commensurate with past discussions about neurotechnology; others are novel.

DISCUSSION OF NEUROETHICAL ISSUES OF THE POTENTIAL BRAIN-INTERFACING FUTURE

Access

Minutely invasive or non-invasive brain interfaces that safely enhance brain function could be advantageous in some academic, recreational and professional settings. Well-resourced societies may actually deem technology to be as essential to learning and job performance as computers are now. Schools and employers may routinely supply brain-interfacing devices. However, as with other health or performance enhancing products, such provisions may result in disparate access that exacerbates existing disparities. Further, if global initiatives are not established to provide equal access to brain-interfacing technology, global inequalities and instability are likely to become even more pronounced than they are today (Delegates et al., 2018). Access to technology that can alter brain function in ways that enhance productivity can further, and arguably in more significant ways, exacerbate global inequity and socioeconomic divides.

The achievability of fair access may depend on a degree to which potential users trust that recorded neural data will be secure (e.g., from the government or from being sold or availed to corporations) and stimulation will only be of a type for which a user provided informed consent. Toward this goal, we suggest three anticipatory remedies:

1. Government establishment of distributions, subsidizations, incentive programs, to facilitate access to brain-interfacing devices across populations.
2. Shaping of marketing, price points, regulation and education by technologists and policy-makers to promote, not only fair device access, but also widespread understanding of the potential value and risks of technology. Such efforts can support underprivileged individuals while also improving the productivity and well-being of societies.
3. Passing of regulations that restrict the authority of a government or corporations to receive raw or processed brain data or to control stimulation by designing networks that thwart unauthorized access, supporting watchdog entities, and publicizing these outreach efforts.
4. Evaluation of cultural meaningfulness and receptivity to brain technologies on a case-by-case basis, as traditional and biomedical understandings of brain wellness, enhancement, and disease are far from homogeneous (Delegates et al., 2018).

Despite such efforts, some potential users or populations may remain skeptical of potential unauthorized use or control and may reject the technology. Much of this process will require cultivation of scientists' and engineers' orientation toward voices

and needs of the end-user (Sullivan et al., 2017). Ultimately, decisions to reject the technology must be respected by society.

Power Asymmetries in the Workplace or Militaries

Due to the potential performance enhancements, it is conceivable that employers or governments may implement policies requiring, availing or prohibiting use of neurotechnologies. For example, many employers currently require computer-based augmentation of their employees' capabilities and offer caffeine stimulation. If neurotechnology proves to improve capabilities, this technology may conceivably become an explicit or implicit job requirement (Bard et al., 2018; Brühl et al., 2019; Dubljevic et al., 2019), and ethical considerations of the usage of human-integrated technology may be all the more important (Gauttier, 2019).

Currently, most risks of job-associated technologies are well-characterized (e.g., consider risk of factory workers vs. SWAT teams). However, very few studies have explored whether usage of a brain-interfacing device for hundreds of hours per month (particularly when used for enhancement, and not medical, purposes). For example, such usage may present health risks, confusion of users of body integrity, shifts in users' identities as individuals, and/or pressure to use neurotechnology intensely to keep with a raised society-, employer-, or individual-imposed performance bar. Therefore, we recommend that:

1. Studies be conducted that identify any biological risks of extended use of brain-interfacing devices (e.g., 50 + *hour* work-weeks for years) (Sahakian et al., 2015), which can inform the decisions of government agencies, soldiers, employers and employees as to what type of usage of brain-interfacing devices is reasonable.
2. Information-distribution campaigns be initiated to ensure that information that details any potential risks or uncertainties is availed to employees or soldiers who may be asked by their employers or superiors to use brain-interfacing devices and to employers so as to understand the potential impacts and uncertainties of requests to use brain-interfacing devices. A focus in the distribution of responsibilities that lie with an individual vs. an institution (e.g., school or military) may further help individuals understand how to plan for (e.g., train for and/or deliberate about) particular potential circumstances that may arise and to assess risk of the technology's use (Binnendijk et al., 2020).

Consent/Assent

If non-invasive or minutely invasive brain-interfacing technology advances in its capabilities (in a manner where significant side effects are not observed), parents may believe that brain-interfacing technology will promote their children's success. For example, conceivably, non-invasive or minutely invasive brain-interfacing technology may be used to help to establish sleep routines, deliver personalized education, and even provide the opportunity to control toddlers' outbursts, However, brain-recording data may reflect mere contemplations or self-identifications that may correspond to most-personal data, and parents and children may be at odds about what degree of stimulation-based enhancement is desirable (Maslen et al., 2014). Further, long-term impacts of the use of brain-interfacing technology on the pediatric population may be inadvertently overlooked.

Therefore, we suggest:

1. Child advocates be intensively engaged when determining what types of brain-interfacing usage is permitted or required for children.
2. Standards or laws be established that define limits on parental access and control of neural data and stimulation.
3. Long-term pediatric studies also be performed to alert society of whether and how stimulation affects brain plasticity, induces addiction, and alters neural development, and long-term risks. Depending on studies' outcomes, society may choose to restrict pediatric use (e.g., as prescriptions are now) or may largely rely on sound parental judgment (e.g., consider the accessibility of coffee).

Assessments relating to the pediatric population and the potential of future non- or minutely invasive brain-interfacing technology extends beyond consent and assent issues (e.g., potential for discrimination, potential for evading best interests of a child, etc.) (Dubljevi, 2019; Committee on the Rights of the Child [CRC], 2021). At least some of the suggested approaches above may facilitate informed decision-making on multiple issues relating to the intersection of the pediatric population and the potential future of non- or minutely invasive brain-interfacing technology.

Data Privacy, Security, and Liability

Currently, laws, professional standards, and regulations. Exist to ensure that medical data is protected and that informed consent it obtained before performing medical procedures. For example, the U.S. Health Insurance Portability and Accountability Act (HIPAA) includes a Privacy Rule that includes restriction of when protected health information can be released to a party. However, many of these laws, standards, and regulations (e.g., HIPAA) are focused on medical or investigational use cases and may not pertain to uses of non-medical uses of brain-interfacing technology. Some other laws, professional standards, and regulations [e.g., the European General Data Protection Regulation (GDPR)] focus on protecting individuals' personal data, though various criteria still differentially pertain to health data and other data. For example, while "explicit consent" is required for use of health data, only "consent" is required for other data.

Brain-interfacing devices are unique in that this recorded data may well be considered not to be medical or health data (and may thus may not qualify for protections offered by some current laws); scientists may learn to extract more brain-signal information post-recording than originally identified for a specific use; and brain stimulation may alter users' behavior or personalities (Minielly et al., 2020a; Naufel and Klein, 2020).

Recording

Storing neural data can provide value both to the subject and to a larger population by enabling post-collection analysis of the data. However, the longer that the data are stored (and the larger a collective data is) the higher the risk is for unauthorized data access. In view of this risk, we recommend:

1. Signal processing and deletion of the raw brain data be performed expediently. These practices can drastically reduce risks of hacking and unauthorized data use.
2. Data sharing be performed only after informed consent has been received and be limited in content (e.g., restricted to specific brain-region channels, time periods and higher-level variables established by standards). This approach is particularly valuable because expedient data processing and deletion becomes more complicated if a first entity controls neural data initially collected from a device and other entities develop applications to process the brain recordings. Informed consent and imposed limitations of data sharing may result in brain-app developers then sharing in the obligation of expediently processing signals and deleting underlying data.
3. Data-restriction standards and regulations can constructively formally establish which entities own data in which contexts (veering largely to the recorded individual) (Minielly et al., 2020b). Given that device functionalities may well be dependent on knowledge of neural representations of external stimuli and meaningful translations of various types of brain stimuli, we recommend establishing standards that further promote (or require) sharing of raw or processed data. This sharing may avoid the necessity to re-learn user-specific information upon device transfer and may promote efficient data-collection/processing pipelines.

Stimulation

In many contexts, legal systems are structured to allow users to choose to take calculated risk. However, these systems are largely premised on the understanding that the users are aware of the potential risks. If non-invasive or minutely invasive brain-interfacing technology will become increasingly common, it is possible that conveying risks to users will require more effort and more explicit warnings. Therefore, we recommend:

1. Guidelines and laws be established to ensure that suppliers of stimulation devices fully inform (Suthana et al., 2018; Wexler and Reiner, 2019) users of stimulation sites, intensity, duration, purposes and onset conditions that are being used for clinical and non-clinical applications.
2. Disclosures clearly convey potential side effects, including long-term use risks (Minielly et al., 2020a).

Opt-in Default

How can companies obtain informed consent to store neural signatures, and mine, share or sell brain data? Best practices from genetic sequencing companies offer guidance, although brain data presents new challenges. For example, brain data are arguably a closer representation of who a person is than the genome, as it represents not just genetics but also experience (Purcell and Rommelfanger, 2015; Ienca et al., 2018). Additionally, the brain may be quicker to adapt to dynamic changes than even the epigenome. Data from a previous time point might be of questionable relevance to later situations (Eagleman, 2020).

Accordingly, we recommend:

1. Manufacturers and sellers err toward providing and emphasizing potential risks, and government agencies err toward requiring risk disclosure. Risks may involve health risks (e.g., associated with stimulation), identity risks, and the potential of unauthorized data access (e.g., *via* hacking). Given that it may be appropriate to disclose a sizable number of risks, we recommend that risks that are of higher potential magnitude be particularly emphasized.
2. When possible, data controllers (and stimulation controllers) use opt-in instead of opt-out techniques. Requiring opt-in authorization can facilitate ensuring that users understand the potential risks of a given action.

Regulations, Laws, and Standards

The breadth of possible brain-interfacing devices poses a challenge for government oversight of this technology (Coates McCall et al., 2019). For example, the U.S. Food and Drug Administration (FDA) currently regulates medical devices but not low-risk devices used for entertainment or wellness (e.g., mental acuity or relaxation). The FDA frequently turns to marketing materials for devices to characterize intended use. Currently, many non-invasive brain-interfacing devices used by the general public are not FDA-regulated. Even if they were, they may be exempt from the agency's premarket notification requirement that assesses safety and efficacy, as demonstrated by the current exemption for EEG devices. Unlike drugs, devices highly similar to pre-approved devices enjoy a low bar of approval.

As the brain interfaces industry grows, we recommend that standards for a variety of neurotechnologies be established to ensure operational performance, conformity, and safety of new systems. New laws will be needed to identify liability: e.g., when is a manufacturer, employer, or user liable for unintended consequences of brain stimulation? Is the user or device manufacturer liable for actions resulting from a brain interface and user co-adapting to each other? If brain signals from a first person's brain generate stimulation of a second person's brain, when might the second person be liable for the second person's actions and when might the first person be liable for the second person's actions (Maslen et al., 2014).

Historical data from developmental trajectories of many other domains (e.g., ranging wireless communications to equal opportunity in employment) demonstrate that standards and laws catalyze innovation and industry growth. Currently, no existing standards or guidelines exist for brain interfacing products and their system-level function, but a new IEEE Standards Association effort reported a roadmap for brain-machine interfacing standards (The Group on Neurotechnologies for Brain-Machine Interfacing, 2020).

However, all stakeholders must participate to converge toward standards that facilitate transparency, interoperability, interpretability, reproducibility, safety, and efficacy.

ADDITIONAL ISSUES AND PERSPECTIVES

While this work identifies exemplary non- and minutely invasive brain-interfacing technology currently in existence, exemplary research efforts in this field, exemplary neuroethical considerations, and exemplary potential strategies for addressing these considerations, it will be appreciated that the description in each of these areas is incomplete. For example, this publication emphasizes potential neuroethical considerations and strategies that may pertain to a future where the potential neurotechnology identified in the DARPA N^3 grant (non- or minutely invasive brain-interfacing technology that can record and stimulate the brain in many different areas with fine spatial and temporal resolution). However, the neuroethical issues and potential tactics for addressing such issues overlap significantly with other spaces (that may encompass this technology or may be tangential to this technology). For example, recent attention to human-centered artificial intelligence has considered potential future scenarios and ethical considerations the overlap with and expand upon some of the concepts identified here (Shneiderman, 2020a,b).

Similarly, many of the ethical concerns and potential approaches involving human enhancement technology apply to the target neurotechnology of the DARPA N^3 grant. To illustrate, the Sienna Project's State-of-the-Art Review of Human Enhancement (Jensen et al., 2018), as well as other studies (e.g., Wagner N.-F. et al., 2018) considers Human Enhancement Technology more generally and considers the potential impacts on many different types of parties affected by the technology. However, even the Sienna Project's Review concludes by setting forth a recommendation that acknowledges a "need for a greater and refreshed dialogue on impacts [of human enhancement technology]., particularly one that looks at specific applications in specific contexts". While providing projections and potential strategy pertaining to a higher level class of technology can facilitate prudently advancing many technologies, focusing this assessment on a more specific type of potential technology may support more specific analysis of issues and more pertinent potential strategies to employ.

CONCLUSION

Just as smart phones and the Internet transformed the way we conduct our lives compared to 20 years ago, brain interfaces 20 years from now may foster more intimate and direct collaborations between brains and technology, allowing augmentation of sensory, motor, communication, and cognitive capabilities. These capabilities may become most utilized across a population when they can be achieved using non-invasive or minutely invasive brain-interfacing technology, and recent research and funding priorities suggest that these types of technology will substantially advance over the next two decades. While previous research has already identified many neuroethical issues that may arise in the future, here we consider a particular hypothetical scenario where there is a high demand in 20 years for non- or minutely invasive brain-recording devices that have capabilities that include at least one of: enhancing attention, memory or learning; enhancing mood; or supporting inter-person communication. We can nonetheless draw from the insightful past work to identify neuroethics issues that may pertain to this potential context and to further identify particular recommendations to address these issues in advance and in real-time. The issues and potential proactive and responsive measures identified here are certainly incomplete, and manufacturer, seller, or user entities may well independently establish anticipatory measures to address potential risks. However, we propose that enacting appropriate ethical frameworks for standards, government programs, oversight, and liabilities will enable the design of ethically guided neurotechnologies that propel humanity to new heights in the near future.

AUTHOR CONTRIBUTIONS

KG initiated and supervised the project and coordinated the collection of expert opinions summarized in the figure. HA, KT, PG, JR, PC, and RR led efforts to characterize current capabilities and ongoing research aims of non-invasive and minutely invasive brain-interfacing technology. JI, PC, DE, KG, and AB led efforts to synthesize neuroethics issues and tactics pertaining to non/minutely invasive brain-interfacing technology and to draft the ethical sections. HA and KG led drafting efforts of the regulations and standards section. PG provided expertise in ongoing research aims of non/minutely invasive brain-interfacing technology. DE and AB provided expertise in market forces and business strategies that may influence how brain-interfacing technology develops and is used. All authors contributed to the article and approved the submitted version.

FUNDING

This work was supported by the National Science Foundation (HA, PG, JR), the National Institutes of Health (Grant Nos.: R01HD053793, R01NS072171, R37NS090610, R21AG059184, R01MH119086, R01HD097619 to PC; R01NS115233 to CK), the Defense Advanced Research Projects Agency (Grant No. NESD to CK; JR, PG, CK, KT), the National Institute of Mental Health (JI), the US Department of Defense (Grant No. N66001-10-C-4056 to PC), the National Institute of Drug Abuse (HA), the National Institute of Nursing Research (HA), the National Institute of Child Health and Human Development (HA), the Air Force Office of Scientific Research (HA), the Canadian Institutes of Health Research (JI), the Kavli

Foundation (KR), the Chuck Noll Foundation (PG), the NIH BRAIN Initiative (JR), the NIH HEAL (JR), Welch Foundation (JR), and the Pennsylvania Department of Health (HA).

ACKNOWLEDGMENTS

Contributions were received from The Working Group on Brain-Interfacing Devices in 2040, which included: Nena Bains (Kilpatrick Townsend & Stockton LLP), John Brigagliano (Kilpatrick Townsend & Stockton LLP), Robert Carter (Avalere Health), Caleb Kemere (Rice University), Mark P. Mathison (Kilpatrick Townsend & Stockton LLP), Jon Neiditz (Kilpatrick Townsend & Stockton LLP), Karen Rommelfanger (Emory University Center for Ethics, Neuroethics Progam), and Joseph Snyder (Kilpatrick Townsend & Stockton LLP). JB and JN provided expertise in data privacy and security law and industry efforts that pertain to brain-interfacing technology. CK and MM contributed to and coordinated discussions pertaining to neuroethical issues summarized in this work. NB and JS contributed and coordinated discussions pertaining to existing brain-interfacing technology and research efforts summarized in this work. RC provided expertise in market forces and business strategies that may influence how brain-interfacing technology develops and is used. KR provided expertise in neuroethics and pertinent analyses and issues previously studied and discussed in the field and contributed to editing and writing. RC was employed by Avalere Health. DE was employed by Neurosensory, Inc. and BrainCheck. NB, JB, MM, JN, and JS were employed by Kilpatrick Townsend & Stockton LLP.

REFERENCES

Adaikkan, C., and Tsai, L.-H. (2020). Gamma entrainment: impact on neurocircuits, glia, and therapeutic opportunities. *Trends Neurosci.* 43, 24–41. doi: 10.1016/j.tins.2019.11.001

Ayaz, H., and Dehais, F. (2019). *Neuroergonomics: the Brain at Work and Everyday Life (1st ed.)*. United States: Elsevier Academic Press.

Barbe, M. T., Tonder, L., Krack, P., Debû, B., Schüpbach, M., Paschen, S., et al. (2020). Deep Brain Stimulation for Freezing of Gait in Parkinson's Disease With Early Motor Complications. *Mov. Disord.* 35, 82–90. doi: 10.1002/mds.27892

Bard, I., Gaskell, G., Allansdottir, A., de Cunha, R. V., Eduard, P., Hampel, J., et al. (2018). Bottom up ethics – neuroenhancement in education and employment. *Neuroethics* 11, 309–322. doi: 10.1007/s12152-018-9366-7

Beynel, L., Davis, S. W., Crowell, C. A., Hilbig, S. A., and Lim, W. (2019). Online repetitive transcranial magnetic stimulation during working memory in younger and older adults: a randomized within-subject comparison. *PLoS One* 14:e0213707. doi: 10.1371/journal.pone.0213707

Bikson, M., Hanlon, C. A., Woods, A. J., Gillick, B. T., Charvet, L., Lamm, C., et al. (2020). Guidelines for TMS/tES clinical services and research through the COVID-19 pandemic. *Brain Stimul.* 13, 1124–1149. doi: 10.1016/j.brs.2020.05.010

Binnendijk, A., Marler, T., and Bartels, E. M. (2020). *Brain-Computer Interfaces: U.S. Military Applications and Implications, An Initial Assessment*. United States: RAND Corporation.

Brühl, B., d'Angelo, C., and Sahakian, B. J. (2019). Neuroethical issue in cognitive enhancement: modafinil as the example of a workplace drug? *Brain Neurosci. Adv.* 3, 2398212818816018. doi: 10.1177/2398212818816018

Cinel, C., Valeriani, D., and Poli, R. (2019). Neurotechnologies for human cognitive augmentation: current state of the art and future prospects. *Front. Hum. Neurosci.* 13:13. doi: 10.3389/fnhum.2019.00013

Coates McCall, I., Lou, H., Lau, C., and Illes, J. (2019). Owning ethical innovation: claims about commercial brain wearable technologies. *Neuron* 102, 728–731. doi: 10.1016/j.neuron.2019.03.026

Committee on the Rights of the Child [CRC], (2021). *General Comment No. 25 (2021) on Children's Rights in Relation to the Digital Environment*. UN: United Nations Convention on the Rights of the Child.

Curtin, A., Ayaz, H., Tang, Y., Sun, J., Wang, J., and Tong, S. (2019). Enhancing neural efficiency of cognitive processing speed *via* training and neurostimulation: an fNIRS and TMS study. *NeuroImage* 198, 73–82. doi: 10.1016/j.neuroimage.2019.05.020

Dehais, F., Karwowski, W., and Ayaz, H. (2020). Brain at work and in everyday life as the next frontier: grand field challenges for neuroergonomics. *Front. Neuroergonomics* 1:583733. doi: 10.3389/fnrgo.2020.583733

Delegates, G. N. S., Rommelfanger, K. S., Jeong, S., Ema, A., Fukushi, T., Kasai, K., et al. (2018). Neuroethics questions to guide ethical research in the international brain initiatives. *Neuron* 100, 19–36. doi: 10.1016/j.neuron.2018.09.021

Dubljevi, V. (2019). "Pediatriic neuro-enhancement, best interest, and autonomy: a case for normative reversal" in *Shaping Children*. ed. S. Nagel (Germany: Springer). 199–212. doi: 10.1007/978-3-030-10677-5

Dubljevic, V. C., McCall, I., and Illes, J. (2019). "Neuroenhancement at work: addressing the ethical, legal, and social implications" in *Organizational Neuroethics*. ed. E. Racine (New York: Springer). 87–103.

Eagleman, D. (2020). *Livewired*. New York, NY.

Edelman, B. J., Baxter, B., and He, B. (2015). EEG Source Imaging Enhances the Decoding of Complex Right-Hand Motor Imagery Tasks. *IEEE Transac. Biomed. Eng.* 63, 4–14. doi: 10.1109/TBME.2015.2467312

Ezzyat, Y., Wanda, P. A., Fevy, D. F., Kadel, A., Aka, A., Pedisich, I., et al. (2018). Closed-loop stimulation of temporal cortex rescues functional networks and improves memory. *Nat. Commun.* 9:365. doi: 10.1038/s41467-017-02753-0

Filmer, H. L., Varghese, E., Hawkins, G. E., Mattingley, J. B., and Dux, P. E. (2017). Improvements in attention and decision-making following combined behavioral training and brain stimulation. *Cereb. Cortex.* 27, 3675–3682. doi: 10.1093/cercor/bhw189

Gateau, T., Ayaz, H., and Dehais, F. (2018). *In silico* vs. Over the clouds: on-the-fly mental state estimation of aircraft pilots, using a functional Near Infrared Spectroscopy based passive-BCI. *Front. Hum. Neurosci.* 12:187. doi: 10.3389/fnhum.2018.00187

Gauttier, S. (2019). 'I've got you under my skin' – The role of ethical consideration in the (non-) acceptance of insideables in the workplace. *Technol. Soc.* 56, 93–108.

Hampson, R. E., Song, D., Robinson, B. S., Fetterhoff, D., Dakos, A. S., Roeder, B. M., et al. (2018). Developing a hippocampal neural prosthetic to facilitate human memory encoding and recall. *J. Neural. Eng.* 15:036014. doi: 10.1088/1741-2552/aaaed7

Hendriks, S., Grady, C., Ramos, K. M., Chiong, W., Fins, J. J., Ford, P., et al. (2019). Ethical challenges of risk, informed consent, and posttrial responsibilities in human research with neural devices: a review. *JAMA Neurol.* 76, 1506–1514. doi: 10.1001/jamaneurol.2019.3523

Ienca, M., Haselager, P., and Emanuel, E. J. (2018). Brain leaks and consumer neurotechnology. *Nat. Biotechnol.* 36, 805–810. doi: 10.1038/nbt.4240

Jensen, S. R., Nagel, S., Brey, P., Ditzel, T., Rodrigues, R., Broadhead, S., et al. (2018). *SIENNA D3.1: state-of-the-art Review: human Enhancement (V1.1)*. European Commission: Zenodo. doi: 10.5281/zenodo.4066557

Jiang, L., Stocco, A., Losey, D. M., Abernethy, J. A., Prat, C. S., and Rao, R. P. N. (2019). BrainNet: a multi-person brain-to-brain interface for direct collaboration between brains. *Sci. Rep.* 9:6115. doi: 10.1038/s41598-019-41895-7

Kay, K. N., Naselaris, T., Prenger, R. J., and Gallant, J. L. (2008). Identifying natural images from human brain activity. *Nature* 452, 352–355. doi: 10.1038/nature06713

Krol, L. R., Haselager, P., and Zander, T. (2020). Cognitive and affective probing: a tutorial and review of active learning for neuroadaptive technology. *J. Neural. Eng.* 17:012001. doi: 10.1088/1741-2552/ab5bb5

Lebedev, M., and Nicolelis, M. A. L. (2017). Brain-machine interfaces: from basic science to neuroprostheses and neurorehabilitation. *Physiol. Rev.* 97, 767–837. doi: 10.1152/physrev.00027.2016

Liu, Y., Piazza, E. A., Simony, E., Shewokis, P. A., Onaral, B., Hasson, U., et al. (2017). Measuring speaker-listener neural coupling with functional near infrared spectroscopy. *Sci. Rep.* 7:43293. doi: 10.1038/srep43293

Liu, Y., and Ayaz, H. (2018). Speech recognition *via* fNIRS based brain signals. *Front. Neurosci.* 12:695. doi: 10.3389/fnins.2018.00695

Makin, J. G., Moses, D. A., and Chang, E. F. (2020). Machine translation of cortical activity to text with an encoder-decoder framework. *Nat. Neurosci.* 23, 575–582. doi: 10.1038/s41593-020-0608-8

Maslen, H., Earp, B. D., Kadosh, R. C., and Savulescu, J. (2014). Brain stimulation for treatment and enhancement in children: an ethical analysis. *Front. Hum. Neurosci.* 8:953. doi: 10.3389/fnhum.2014.00953

Mayberg, H. S., Lozano, A. M., Voon, V., McNeely, H. E., Seminowicz, D., Hamani, C., et al. (2005). Deep brain stimulation for treatment-resistant depression. *Neuron* 45, 651–660. doi: 10.1016/j.neuron.2005.02.014

Minielly, N., Hrincu, V. M., and Illes, J. (2020a). "A view on incidental findings and adverse events associated with neurowearables in the consumer marketplace" in *Developments in Neuroethics and Bioethics*. eds I. Bard and E. Hildt (United States: Academic Press). 267–277. doi: 10.1016/bs.dnb.2020.03.010

Minielly, N., Hrincu, V. M., and Illes, J. (2020b). Privacy challenges to the democratization of brain data. *Iscience* 23:101134. doi: 10.1016/j.isci.2020.101134

Naufel, S., and Klein, E. (2020). Brain-computer interface (BCI) researcher perspectives on neural data ownership and privacy. *J. Neural Eng.* 17:016039. doi: 10.1088/1741-2552/ab5b7f

Neely, R. M., Piech, D. K., Santacruz, S. R., Maharbiz, M. M., and Carmena, J. M. (2018). Recent advances in neural dust: towards a neural interface platform. *Curr. Opin. Neurobiol.* 50, 64–71. doi: 10.1016/j.conb.2017.12.010

Novich, S. D., and Eagleman, D. M. (2015). Using space and time to encode vibrotactile information: toward an estimate of the skin's achievable throughput. *Exp. Brain Res.* 233, 2777–2788. doi: 10.1007/s00221-015-4346-1

Purcell, R. H., and Rommelfanger, K. S. (2015). Internet-based brain training games, citizen scientists, and big data: ethical issues in unprecedented virtual territories. *Neuron* 86, 356–359. doi: 10.1016/j.neuron.2015.03.044

Rao, R. P. N. (2019). Towards neural co-processors for the brain: combining decoding and encoding in brain-computer interfaces. *Curr. Opin. Neurobiol.* 55, 142–151. doi: 10.1016/j.conb.2019.03.008

Reinhart, R. M. G., and Nguyen, J. A. (2019). Working memory revived in older adults by synchronizing rhythmic brain circuits. *Nat. Neurosci.* 22, 820–827. doi: 10.1038/s41593-019-0371-x

Roelfsema, P. R., Denys, D., and Klink, P. C. (2018). Mind reading and writing: the future of neurotechnology. *Trends Cogn. Sci.* 22, 598–610. doi: 10.1016/j.tics.2018.04.001

Sahakian, J., Bruhl, A. B., Cook, J., Killikelly, C., Savulich, G., Piercy, T., et al. (2015). The impact of neuroscience on society: cognitive enhancement in neuropsychiatric disorders in healthy people. *Philos. Trans. R. Soc. Lond. B. Biol. Sci.* 370:20140214. doi: 10.1098/rstb.2014.0214

Sani, O. G., Yang, Y., Lee, M. B., Dawes, H. E., Chang, E. F., and Shanechi, M. M. (2018). Mood variations decoded from multi-site intracranial human brain activity. *Nat. Biotechnol.* 36, 954–961.

Schlaepfer, T. E., Cohen, M. X., Frick, C., Kosel, M., Brodesser, D., Axmacher, N., et al. (2008). Deep brain stimulation to reward circuitry alleviates anhedonia in refractory major depression. *Neuropsychopharmacology* 33, 368–377. doi: 10.1038/sj.npp.1301408

Schwarz, A., Escolano, C., Montesano, L., and Muller-Putz, G. R. (2020). Analyzing and decoding natural reach-and-grasp actions using gel, water and dry EEG systems. *Front. Neurosci.* 14:849. doi: 10.3389/fnins.2020.00849

Shanechi, M. M. (2019). Brain-machine interfaces from motor to mood. *Nat. Neurosci.* 22, 1554–1564. doi: 10.1038/s41593-019-0488-y

Shen, F. X., Shen, Wolf, S. M., Gonzalez, R. G., and Garwood, M. (2020). Ethical issues posed by field research using highly portable and cloud-enabled neuroimaging. *Neuron* 105, 771–775. doi: 10.1016/j.neuron.2020.01.041

Shneiderman, B. (2020a). Bridging the gap between ethics and practice: guidelines for reliable, safe, and trustworthy human-centered AI systems. *ACM Transac. Interac. Intell. Syst.* 10, 1–31. doi: 10.1145/3419764

Shneiderman, B. (2020b). Human-centered artificial intelligence: three fresh ideas. *AIS Transac. Hum. Comput. Interact.* 12, 109–124. doi: 10.17705/1thci.00131

Stevenson, I. H., and Kording, K. P. (2011). How advances in neural recording affect data analysis. *Nat. Neurosci.* 14, 139–142. doi: 10.1038/nn.2731

Sullivan, L. E., Klein, E., Brown, T., Sample, M., Pham, M., Tubig, P., et al. (2017). Keeping disability in mind: a qualitative study of BCI research perspectives. *Sci. Eng. Ethics* 24, 479–504. doi: 10.1007/s11948-017-9928-9

Suthana, N., Aghaian, Z. M., Mankin, E. A., and Lin, A. (2018). Reporting guidelines and issues to consider for using intracranial brain stimulation in studies of human declarative memory. *Front. Neurosci.* 12:905. doi: 10.3389/fnins.2018.00905

The Group on Neurotechnologies for Brain-Machine Interfacing (2020). "Standards roadmap: neurotechnologies for brain-machine interfacing" in *Neurotechnologies Consortium, IEEE Industry Connections Report*. (United States: Institute of Electrical and Electronics Engineers).

Trimper, J. B., Wolpe, P. R., and Rommelfanger, K. S. (2014). When "I" becomes "we": ethical implications of emerging brain-to-brain interfacing technologies. *Front. Neuroeng.* 7:4. doi: 10.3389/fneng.2014.00004

Volkova, K., Lebedev, M. A., Kaplan, A., and Ossadtchi, A. (2019). Decoding Movement From Electrocorticographic Activity: a Review. *Front. Neuroinform.* 13:74. doi: 10.3389/fninf.2019.00074

Wagner, F. B., Mignardot, J. B., Le Goff-Mignardot, C. G., Demesmaeker, R., Komi, S., Capogrosso, M., et al. (2018). Targeted neurotechnology restores walking in humans with spinal cord injury. *Nature* 563, 65–71. doi: 10.1038/s41586-018-0649-2

Wagner, N.-F., Robinson, J., and Wiebking, C. (2018). "The Societal Hazards of Neuroenhancement Technologies." in *The Changing Scope of Technoethics in Contemporary Society*. ed. L. Rocci (United States: IGI Global), 163–196. doi: 10.4018/978-1-5225-5094-5.ch010

Wallis, J. D. (2018). Decoding Cognitive Processes from Neural Ensembles. *Trends Cogn. Sci.* 22, 1091–1102. doi: 10.1016/j.tics.2018.09.002

Wexler, A., and Reiner, P. B. (2019). Oversight of direct-to-consumer neurotechnologies. *Science* 363, 234–235. doi: 10.1126/science.aav0223

Conflict of Interest: DE was employed by Neurosensory, Inc. and Braincheck. KG was employed by Kilpatrick Townsend and Stockton LLP. AB was employed by The Substrate Group. KT was employed by Palo Alto Research Center (PARC), A Xerox Company.

The remaining authors declare that the research was conducted in the absence of any commercial or financial relationships that could be construed as a potential conflict of interest.

Advantages of publishing in Frontiers

OPEN ACCESS
Articles are free to read for greatest visibility and readership

FAST PUBLICATION
Around 90 days from submission to decision

HIGH QUALITY PEER-REVIEW
Rigorous, collaborative, and constructive peer-review

TRANSPARENT PEER-REVIEW
Editors and reviewers acknowledged by name on published articles

Frontiers
Avenue du Tribunal-Fédéral 34
1005 Lausanne | Switzerland

Visit us: www.frontiersin.org
Contact us: frontiersin.org/about/contact

REPRODUCIBILITY OF RESEARCH
Support open data and methods to enhance research reproducibility

DIGITAL PUBLISHING
Articles designed for optimal readership across devices

FOLLOW US
@frontiersin

IMPACT METRICS
Advanced article metrics track visibility across digital media

EXTENSIVE PROMOTION
Marketing and promotion of impactful research

LOOP RESEARCH NETWORK
Our network increases your article's readership